NASA
Computational
Fluid Dynamics
Conference
Volume 2: Sessions VII - XII

NASA

NASA Computational Fluid Dynamics Conference

Volume 2 : Sessions VII - XII

*Proceedings of a conference
sponsored by the Aerodynamics Division,
Office of Aeronautics
and Space Technology, NASA,
held at Ames Research Center
Moffett Field, California
March 7-9, 1989*

NASA

National Aeronautics and
Space Administration

Ames Research Center
Moffett Field, California

1989

TABLE OF CONTENTS — VOLUME 2

TABLE OF CONTENTS — VOLUME 1

VOLUME 1 (Concluded)

PREFACE

This publication is a collection of the presentations given at the NASA Computational Fluid Dynamics (CFD) Conference held at NASA Ames Research Center, Moffett Field, California, March 7-9, 1989. The objectives of the conference were to disseminate CFD research results to industry and university CFD researchers, to promote synergy among NASA CFD researchers, and to permit feedback from researchers outside NASA on issues pacing the discipline of CFD. The focus of the conference was on the application of CFD technology but also included fundamental activities. The conference was sponsored by the Aerodynamics Division, Office of Aeronautics and Space Technology (OAST), NASA Headquarters, Washington, DC 20546.

The conference consisted of twelve sessions of papers representative of CFD research conducted within NASA and three non-NASA panel sessions. For each panel session, the panel membership consisted of industry and university CFD researchers. A summary of the comments made during the panel sessions have been included in this publication.

The conference proceedings are published in two volumes. Volume 1 contains the papers presented in Sessions I-VI; Volume 2 contains those given in Sessions VII-XII. Each volume contains the same front matter, and each contains a list of attendees as an appendix.

PANEL SESSION SUMMARY

NASA CFD Conference
NASA Ames Research Center
March 7-9, 1989

Panel Sessions Summary

The NASA CFD Conference was held at Ames Research Center on March 7-9, 1989. To conclude each day's presentations, a panel session with participation from the audience furnished a great deal of excellent feedback from the industry and academic communities. During the conference it was evident that the panel members proffered comments only after having spent considerable time in preparing them.

The members of the panel sessions are listed below:

March 7   P. Rubbert - Boeing Commercial Airplanes
           R. Melnik - Grumman Aerospace Corporation
           D. Whitfield - Mississippi State University

March 8   I. Bhateley - General Dynamics - Fort Worth Division
           R. Agarwal - McDonnell Douglas Research Laboratories
           R. MacCormack - Stanford University

March 9   V. Shankar - Rockwell International Science Center
           J. Carter - United Technologies Research Center
           A. Jameson - Princeton University

The crucial comments from the three panel sessions have been combined and are summarized as follows:

- NASA's CFD program is now too heavily focused on applications: program balance has swung from fundamentals (1970's) to applications (1980's)

- Three critical "needs" emerged:

    (1) More algorithm research is needed; especially for Navier-Stokes solvers with unstructured grids

    (2) More research is required on geometric modelling; need rapid, accurate, and effective surface definition techniques

    (3) More research is needed on grid generation methods with the focus on speed, efficiency, and grid quality to reduce set up time and complexity

- Developers of CFD need to understand the needs of the users; designers of aerospace vehicles have requirements that are different than the CFD researchers perceptions

- Industry needs more reliable and cost effective CFD tools

Additional detail comments from the three panel sessions are listed below:

- CFD has matured during the last decade and is being used to solve real problems; however, industry lacks confidence in Navier-Stokes solutions

- Industry needs codes that have been validated to increase confidence in CFD technology

- Improved communality between codes would increase usability; standards are needed

- Improved data storage, networking, data transfer, and graphics required to assimilate information provided by CFD

- Improved turbulence modeling for separated flows

- Accurate prediction of drag for complete powered aerospace vehicles

- Develop multidisciplinary CFD technology with optimization capability

- NASA must maintain focus on technology development and high risk research

- Technology transfer is not complete until design engineers are using CFD codes successfully

- Industry needs NASA to improve CFD technology for codes simpler than Navier-Stokes solvers

- NAS program has been extremely helpful to industry in transferring CFD technology

- Industry needs to be more aggressive in their use of CFD

- Improved understanding of CFD by design engineers required; cooperative programs or workshops were suggested to bring CFD researchers and designers together

- Design cycle time needs to be reduced with CFD; codes must be cost effective, reliable, and useable, and robust to work at flight Reynolds Numbers

- Improved coordination/reduced overlap of CFD applications between NASA centers

Organizing Committee

General Chairman ....Dale Satran
Administrative Chairman ....Paul Kutler
Deputy Administrative Chairman .... Anthony R. Gross
Conference Coordinator...Lyz Dunham
Administrative Associate .... Linda Callison
Publications... Betty Rogers
Budget ....Karl Talarico
Secretary & Consultant ....Aggie Ernst

Center Focal Points

Ames Research Center .... Terry Holst
Langley Research Center ....Jerry South
Lewis Research Center..Robert Stubbs
Marshall Space Flight Center..Luke Schutzenhofer
Johnson Space Center...C. P. Li
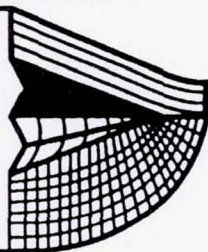
PROGRAM

NASA CFD Conference
NASA Ames Research Center
March 7-9, 1989

Tuesday, March 7

7:30 am   Registration

8:00 am   Welcome
                D. Satran - Conference Chairman
                K. Szalai - Ames Acting Associate Director
                R. Graves - OAST Aerodynamics Division Director

Session I (Center Overviews) Chairman: R. Graves

8:30 am   Ames Research Center CFD Overview
                by T. Holst

9:10 am   Langley Research Center CFD Overview
                by J. South, Jr.

9:50 am   Lewis Research Center CFD Overview
                by R. Stubbs

10:30 am   Break

Session II (Center Overviews Continued) Chairman: P. Kutler

10:50 am   Marshall Space Flight Center CFD Overview
                by L. Schutzenhofer

11:20 am   Johnson Space Center CFD Overview
                by C. Li

11:50 am   CFD Validation Program Overview
                by D. Satran

12:10 pm   Lunch

NASA CFD CONFERENCE PROGRAM

Session III (Transition and Turbulence) Chairman: T. Pulliam

1:10 pm	Understanding Transition and Turbulence Through Direct Simulations by P. Spalart and J. Kim
1:30 pm	Direct Simulation of Compressible Turbulence by T. Zang, G. Erlebacher, and M. Hussaini
1:50 pm	Nonlinear Evolution of a Second Mode Wave in Supersonic Boundary Layers by G. Erlebacher and M. Hussaini
2:10 pm	Numerical Simulation of Nonlinear Development of Instability Waves by R. Mankbadi
2:30 pm	More Accurate Predictions with Transonic Navier-Stokes Methods Through Improved Turbulence Modeling by D. Johnson
2:50 pm	Break

Session IV (CFD Codes) Chairman: J. South

3:10 pm	Recent Advances in Runge-Kutta Schemes for Solving 3-D Navier-Stokes Equations by V. Vatsa, B. Wedan, and R. Abid
3:30 pm	Computations of Three-Dimensional Steady and Unsteady Viscous Incompressible Flows by D. Kwak, S. Rogers, S. Yoon, M. Rosenfeld, and L. Chang
3:50 pm	SAGE - A Self-Adaptive Grid Evolution Code and Its Application in Computational Fluid Dynamics by C. Davies, E. Venkatapathy, and G. Deiwert
4:10 pm	Time Dependent Viscous Incompressible Navier-Stokes Equations by J. Goodrich
4:30 pm	CFD for Applications to Aircraft Aeroelasticity by G. Guruswamy
4:50 pm	Application of Unstructured Grid Methods to Steady and Unsteady Aerodynamic Problems by J. Batina
5:10 pm	Break
5:20 pm	**Panel Session Chairman: P. Rubbert - Boeing Commercial** R. Melnick - Grumman Aerospace D. Whitfield - Mississippi State
6:20 pm	Adjourn to Officer's Club
6:30 pm	Cocktail Party at Moffet Field Officer's Club

NASA CFD CONFERENCE PROGRAM

Wednesday, March 8

    7:50 am   Administrative Announcements

Session V (Fighter Aircraft) Chairman: T. Holst
    8:00 am   Grid Generation and Inviscid Flow Computation about Fighter Airplanes
                     by R. Smith

    8:20 am   A Zonal Navier-Stokes Methodology for Flow Simulation about a Complete Aircraft
                     by J. Flores

    8:40 am   Numerical Simulation of F-18 Fuselage Forebody Flows at High Angles of Attack
                     by L. Schiff, R. Cummings, R. Sorenson, and Y. Rizk

    9:00 am   Navier-Stokes Solutions about the F-18 Forebody-Strake Configuration
                     by F. Ghaffari, J. Luckring, and J. Thomas

    9:20 am   Navier-Stokes Solutions for Store Separation and Related Problems
                     by O. Baysal, R. Stallings, Jr., and E. Plentovich

    9:40 am   TRANAIR: Recent Advances and Applications
                     by M. Madison

    10:00 am   Break

Session VI (Rotorcraft) Chairman: W. McCroskey
    10:20 am   Computations of Airloads and Acoustics of Rotorcraft
                     by W. McCroskey, J. Baeder, C. Chen, E. Duque, and G. Srinivasan

    10:40 am   Calculation of Rotor Induced Download on Airfoils
                     by C. Lee

    11:00 am   Three-Dimensional Viscous Drag Prediction for Rotor Blades
                     by C. Chen

    11:20 am   Progress Toward the Development of an Airfoil Icing Analysis Capability
                     by M. Potapczuk, C. Bidwell, B. Berkowitz

    11:40 am   The Breakup of Trailing-Line Vortices
                     by D. Jacqmin

    12:00 pm   Lunch

NASA CFD CONFERENCE PROGRAM

Session VII (Hypersonics/NASP) Chairman: D. Dwoyer

1:00 pm   A Comparative Study of Navier-Stokes Codes for High-Speed Flows
             by D. Rudy, J. Thomas, A. Kumar, P. Gnoffo, and S. Chakravarthy

1:20 pm   Modeling of High Speed Chemically Reacting Flow Fields
             by J. Drummond, M. Carpenter, and H. Kamath

1:40 pm   Three-Dimensional Simulation of Supersonic Reacting Flows with Finite Rate
             Chemistry
             by S. Yu, J. Shuen, and P. Tsai

2:00 pm   Progress in Computing Nozzle/Plume Flowfields
             by S. Ruffin, E. Venkatapathy, W. Feiereisen, and S. Lee

2:20 pm   Application of CFD Codes for the Simulation of Scramjet Combustor Flow Fields
             by T. Chitsomboon and G. Northam

2:40 pm   Hypersonic CFD Applications at NASA Langley Using CFL3D and CFL3DE
             by P. Richardson

3:00 pm   Break

Session VIII (Space Shuttle) Chairman: L. Schutzenhofer

3:20 pm   Comparison of the ARC Shuttle Ascent Simulations with Wind Tunnel and Flight Data
             by J. Slotnick and F. Martin, Jr.

3:40 pm   Computational Fluid Dynamics Analysis of Space Shuttle Main Propulsion Feed
             Line 17-Inch Disconnect Valves
             by M. Kandula and D. Pearce

4:00 pm   Analysis of SSME HPOTP Bearing Inlet Cavity
             by P. McConnaughey

4:20 pm   A Combined Eulerian-Lagrangian Two-Phase Analysis of the SSME HPOTP
             Nozzle Plug Trajectories
             by R. Garcia, P. McConnaughey, F. de Jong, J. Sabnis, and D. Pribik

4:40 pm   Conjugate (Solid/Fluid) Computational Fluid Dynamics Analysis of the Space
             Shuttle Solid Rocket Motor Nozzle-to-Case and Case-to-Field Joints
             by D. Doran, L. Keeton, P. Dionne, and A. Singhal

5:00 pm   Break

5:10 pm   **Panel Session Chairman: I. Bhateley - General Dynamics**
             R. Agarwal - McDonnell Douglas
             R. MacCormack - Stanford University

6:10 pm   Adjourn to Banquet at Santa Clara Marriott Hotel

7:00 pm   Banquet at Marriott Hotel

NASA CFD CONFERENCE PROGRAM

Thursday, March 9

    7:50 am   Administrative Announcements

Session IX (Turbomachinery) Chairman: R. Stubbs
    8:00 am   Simulation of Turbomachinery Flows
                    by J. Adamczyk

    8:20 am   Prediction of Turbine Rotor-Stator Interaction Using Navier-Stokes Methods
                    by N. Madavan, M. Rai, and S. Gavali

    8:40 am   Turbine Stage Aerodynamics and Heat Transfer Prediction
                    by L. Griffin and H. McConnaughey

    9:00 am   Automated Design of Controlled Diffusion Blades
                    by J. Sanz

    9:20 am   Numerical Analysis of Flow Through Oscillating Cascade Sections
                    by D. Huff

    9:40 am   Numerical Analysis of Three-Dimensional Viscous Internal Flows
                    by R. Chima and J. Yokota

   10:00 am   Break

Session X (STOVL) Chairman: M. Liou
   10:20 am   Simulators of PoweredLift Flows
                    by W. Van Dalsem, K. Chawla, M. Smith, K. Rao, and T. Blum

   10:40 am   A Numerical Study of the Hot Gas Environment Around a STOVL Aircraft in Ground Proximity
                    by T. Van Overbeke and J. Holdeman

   11:00 am   CFD Analysis for High Speed Inlets
                    by T. Benson

   11:20 am   The Use of a Navier-Stokes Code in the Wing Design Process
                    by S. McMillin

   11:40 am   Application of a Transonic Wing Design Method
                    by R. Campbell and L. Smith

   12:00 pm   Lunch

NASA CFD CONFERENCE PROGRAM

Session XI (Algorithms and Tools) Chairman: J. Steger

1:00 pm   An Embedded Grid Formulation Applied to Delta Wings
            by J. Thomas and S. Taylor

1:20 pm   Unstructured Mesh Solution of the Euler and Navier-Stokes Equations
            by T. Barth

1:40 pm   3-D Unstructured Grids for the Solution of the Euler Equations
            by C. Gumbert, P. Parikh, S. Pirzadeh, and R. Lohner

2:00 pm   Flux Splitting Algorithms for Two-Dimensional Real Gas Flows
            by J. Shuen and M. Liou

2:20 pm   Visualization of Fluid Dynamics at NASA Ames
            by V. Watson

2:40 pm   Computational Fluid Dynamics on a Massively Parallel Computer
            by D. Jespersen and C. Levit

3:00 pm   Break

Session XII (Hypersonics/AFE) Chairman: C. Li

3:20 pm   Conservation Equations and Physical Models for Hypersonic Air Flows Over the
            Aeroassist Flight Experiment Vehicle
            by P. Gnoffo

3:40 pm   The Computation of Thermo-Chemical Nonequilibrium Hypersonic Flows
            by G. Candler

4:00 pm   Aerodynamic Heating and Stability Analyses for Aeroassist Flight Experiment
            Vehicle
            by J. McGary and C. Li

4:20 pm   Aeroassist Flight Experiment Aerodynamics and Aerothermodynamics
            by E. Brewer

4:40 pm   Direct Simulation of Rarefied Hypersonic Flows
            by J. Moss

5:00 pm   Break

5:10 pm   **Panel Session Chairman: V. Shankar - Rockwell**
            J. Carter - United Technology
            A. Jameson - Princeton University

6:10 pm   Conference Adjourned

SESSION VII

HYPERSONICS/NASP

Chairman:
Douglas L. Dwoyer
Chief, Facilities Planning Office
NASA Langley Research Center

A COMPARATIVE STUDY OF NAVIER-STOKES CODES FOR HIGH-SPEED FLOWS

David H. Rudy, James L. Thomas, Ajay Kumar, Peter Gnoffo
NASA Langley Research Center

and

Sukumar R. Chakravarthy
Rockwell International Science Center

A comparative study has been made with four different codes for solving the compressible Navier-Stokes equations using three different test problems. The first of these cases was hypersonic flow through the P8 inlet, which represents inlet configurations typical of a hypersonic airbreathing vehicle. The free-stream Mach number in this case was 7.4. This 2-D inlet was designed to provide an internal compression ratio of 8. Initial calculations were made using two state-of-the-art finite-volume upwind codes, CFL3D and USA-PG2, as well as NASCRIN, a code which uses the unsplit finite-difference technique of MacCormack. All of these codes used the same algebraic eddy-viscosity turbulence model. In the experiment, the cowl lip was slightly blunted; however, for the computations, a sharp cowl leading edge was used to simplify the construction of the grid. Although the overall features of the inlet flow field were predicted reasonably well, discrepancies between the computed and experimental profiles of pitot pressure and total temperature were found for all of the codes. Calculations were then made with the two finite-volume upwind codes using a patched-grid approach which allowed the use of a blunt cowl tip. This produced a more accurate location for the cowl leading-edge shock and thus an improvement in the location of the resultant shock reflections within the inlet.

The second test problem was the supersonic (Mach 3.0) flow in a three-dimensional corner formed by the intersection of two wedges with equal wedge angles of 9.48 degrees. The flow in such a corner is representative of the flow in the corners of a scramjet inlet. Calculations were made for both laminar and turbulent flow and compared with experimental data. The three-dimensional versions of the three codes used for the inlet study (CFL3D, USA-PG3, and SCRAMIN, respectively) were used for this case. For the laminar corner flow, a fourth code, LAURA, which also uses recently-developed upwind technology, was also utilized. It was found that the complex flow structure was qualitatively predicted by all of the codes. Furthermore, with a sufficiently-refined grid, all four codes gave identical results for the laminar case.

The final test case is the two-dimensional hypersonic flow over a compression ramp. In this case, the flow is laminar with a free-stream Mach number of 14.1. In the experiment, the ramp angle was varied to change the strength of the ramp shock and the extent of the viscous-inviscid interaction. Calculations have been made for the 24-degree ramp configuration which produces a large separated-flow region that extends upstream of the corner. All of the codes predicted the strong-interaction structure observed experimentally. However, a wide variation in the predicted extent of separation was found for the grid that was used.

DESCRIPTION OF CODES

- CFL3D

  - Written by James L. Thomas

  - Upwind-biased Roe scheme for pressure and convective terms

  - Central-difference treatment of viscous terms

  - Approximate-factorization time differencing

- USA-PG3

  - Written by Sukumar Chakravarthy

  - Roe scheme for convective and pressure terms

  - Central-difference treatment of viscous terms

 - Approximate-factorization time differencing

4

DESCRIPTION OF CODES

- LAURA

    - Written by Peter A. Gnoffo

    - Symmetric TVD scheme with Roe averaging

    - Alternating directional-sweep Gauss-Seidel relaxation

    - Laminar flow only at present time

- NASCRIN and SCRAMIN

    - Written by Ajay Kumar

    - Explicit unsplit MacCormack scheme

TEST PROBLEMS

- P8 Inlet

    - 2-D, transitional

    - Experimental data: Gnos et al.

- Symmetric-wedge corner

    - 3-D, laminar and turbulent

    - Experimental data: West and Korkegi

- Hypersonic compression corner

    - 2-D, laminar

    - Experimental data: Holden and Moselle

P8 INLET
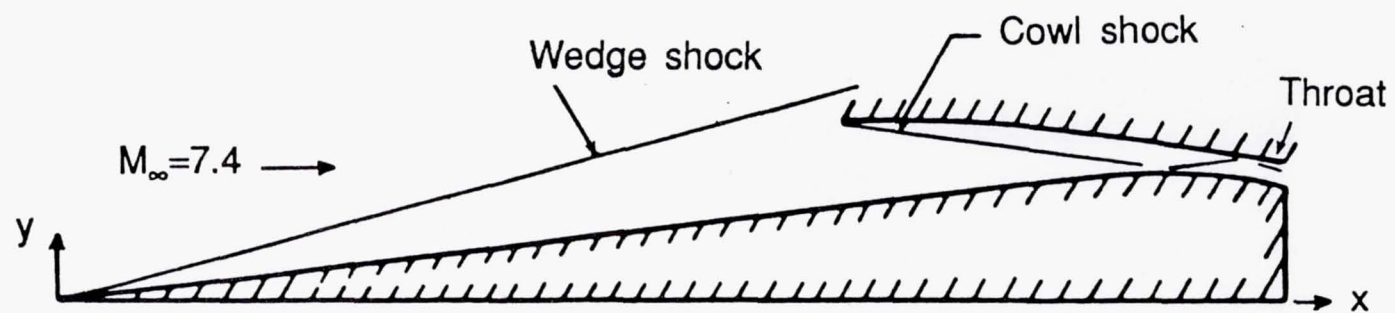
GRIDS NEAR INLET ENTRANCE

Patched-grid computations
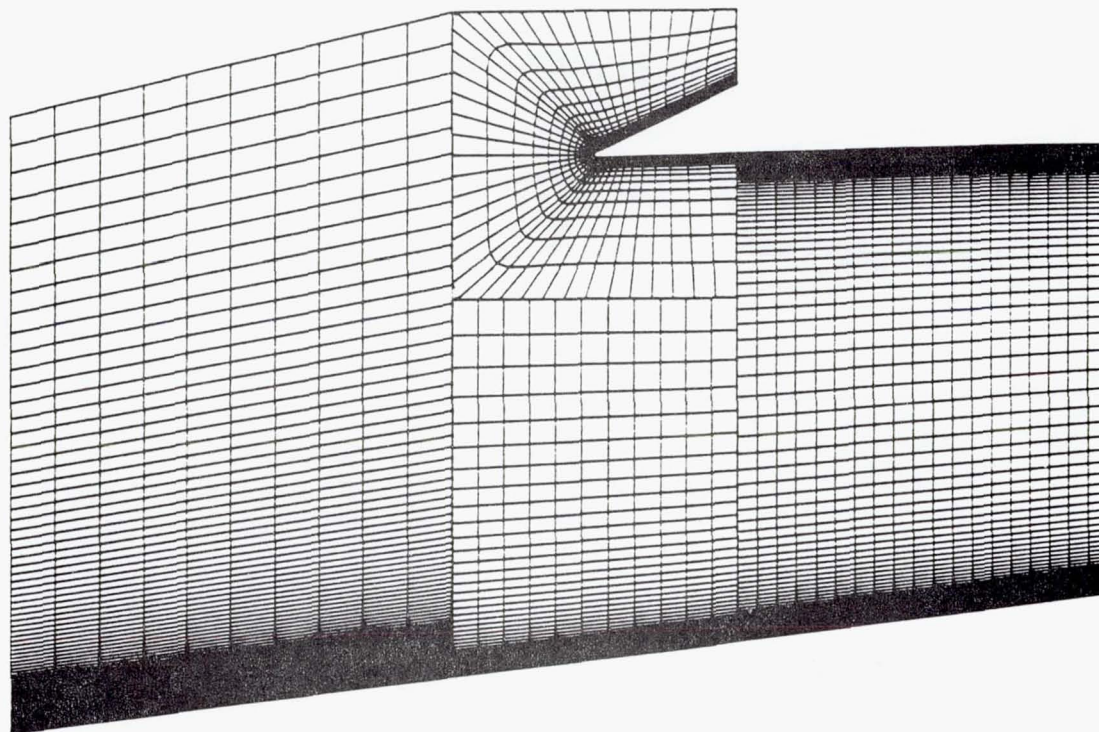
COMPUTED INLET PRESSURE

USA-PG2
Transitional computation
Sharp cowl leading edge
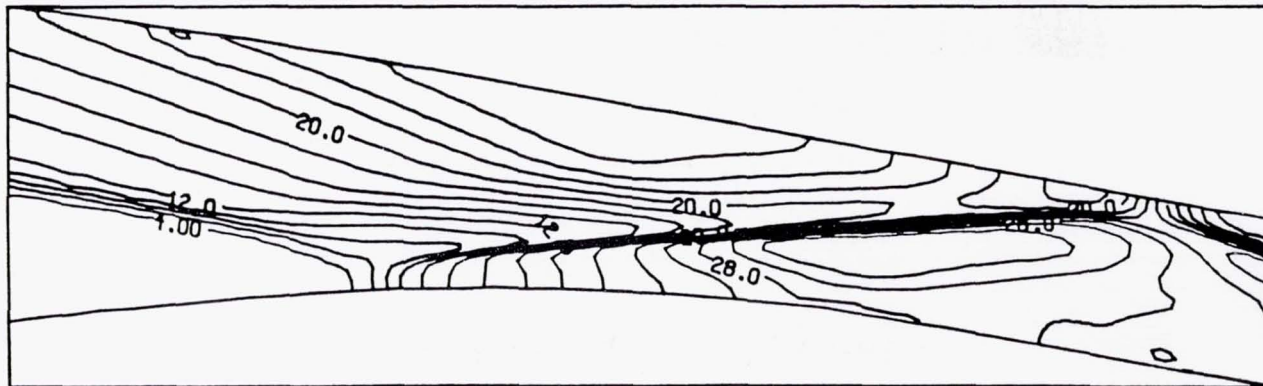
CENTERBODY PRESSURE

Blunt cowl leading edge
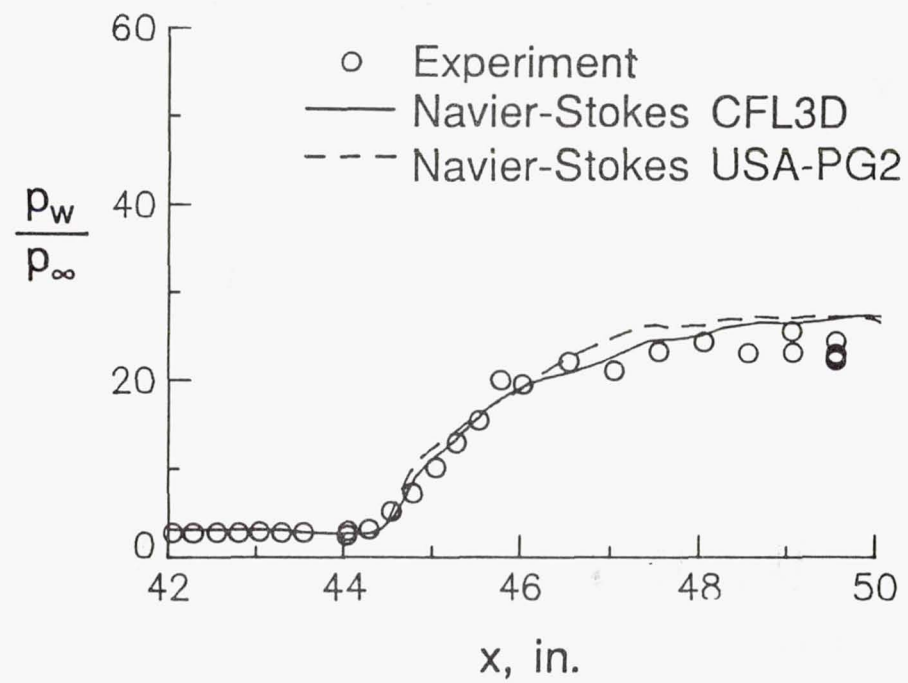
PITOT PRESSURE PROFILE

x = 40.9 in.
Blunt cowl leading edge
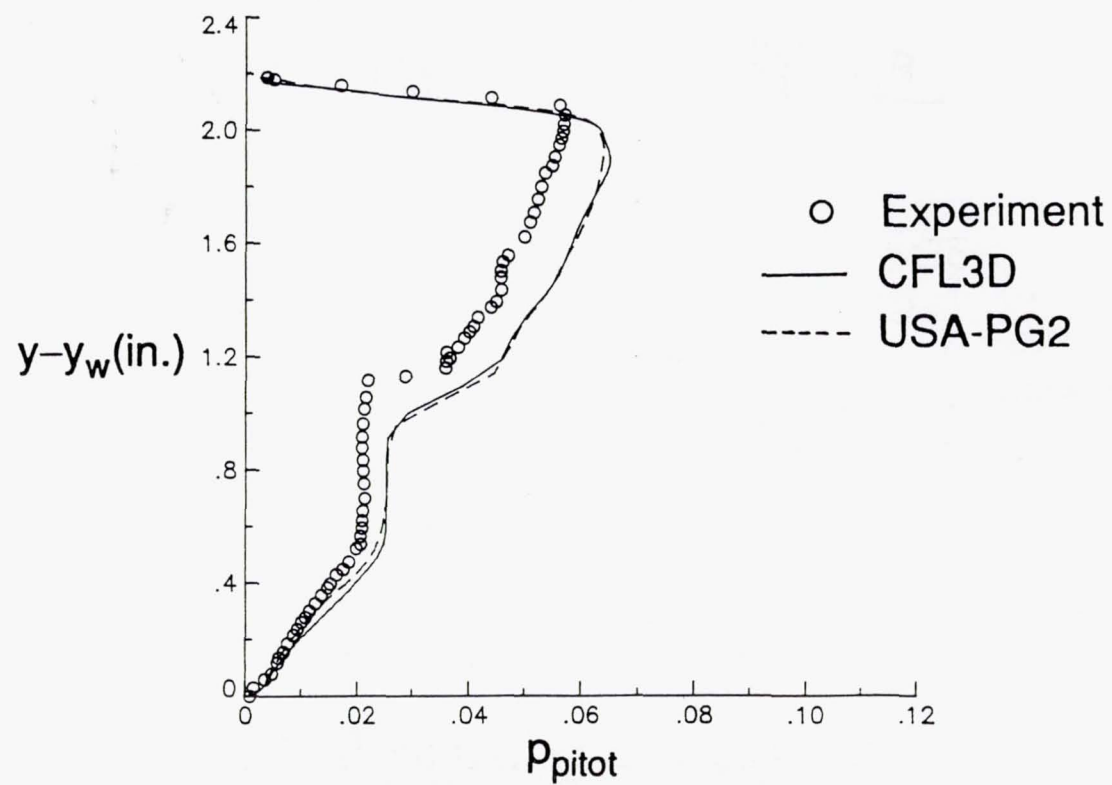
CORNER FLOW

$M_\infty = 3.0$

1 Corner shock
2 Internal shock
3 Slip line
4 Wall shock

12
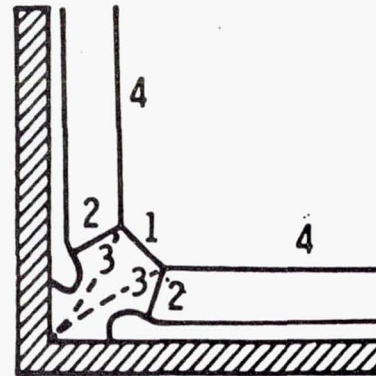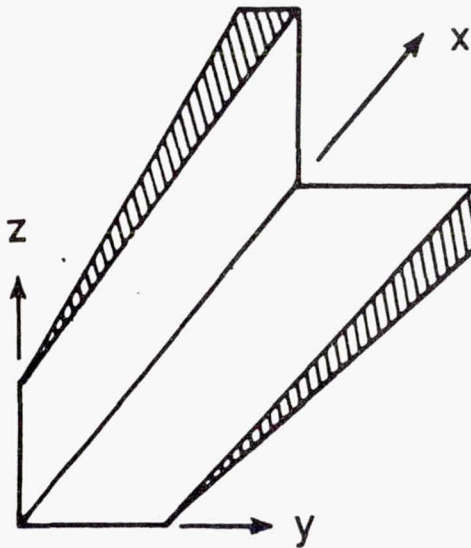
LAMINAR CORNER FLOW

x = 0.0733 m.
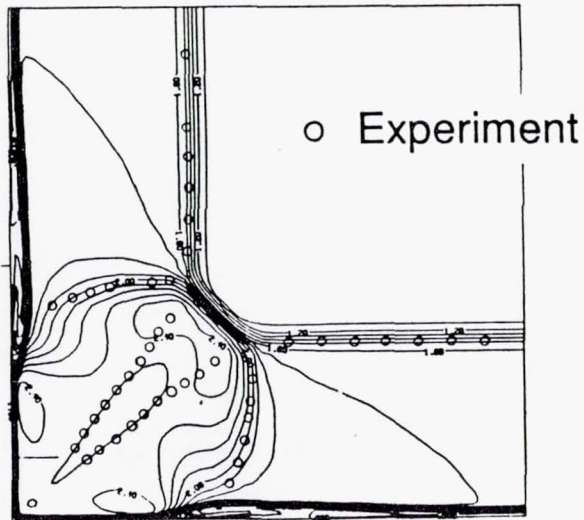
Density contours
USA-PG3
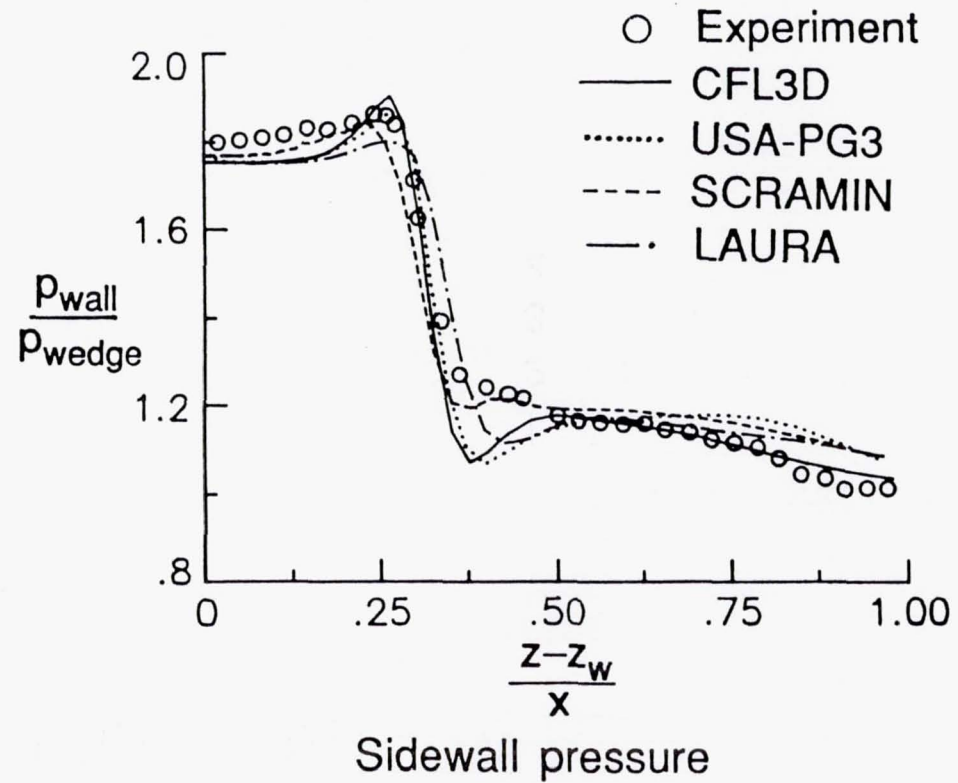
Sidewall pressure

LAMINAR CORNER FLOW

Sidewall pressure

x = 0.0733 m.

Conical flow

121 x 121 grid
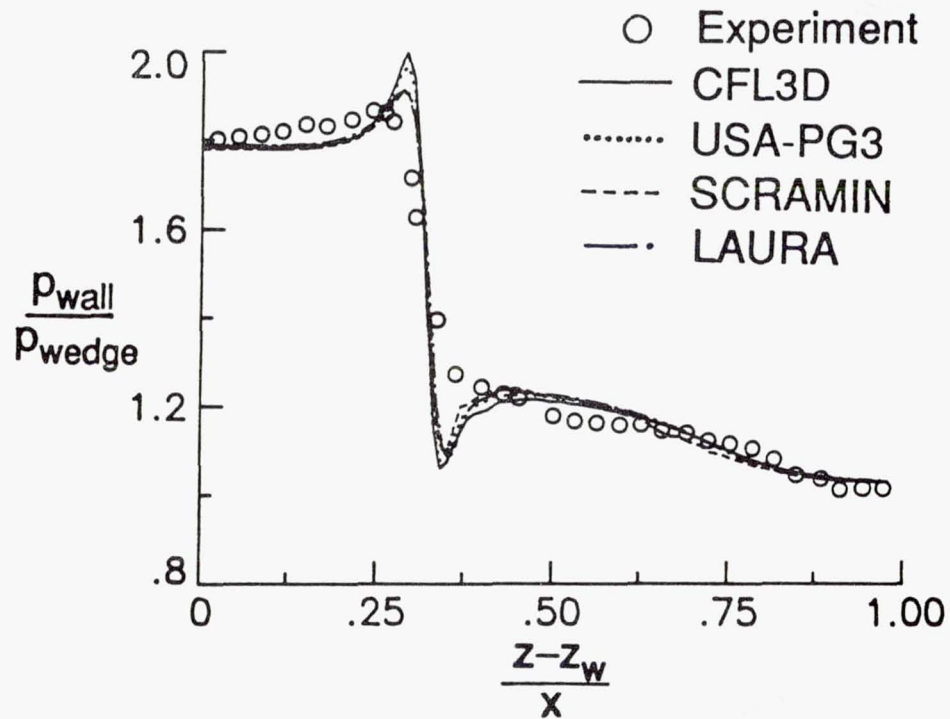
HYPERSONIC COMPRESSION CORNER

Streamlines
24-degree ramp

USA-PG2
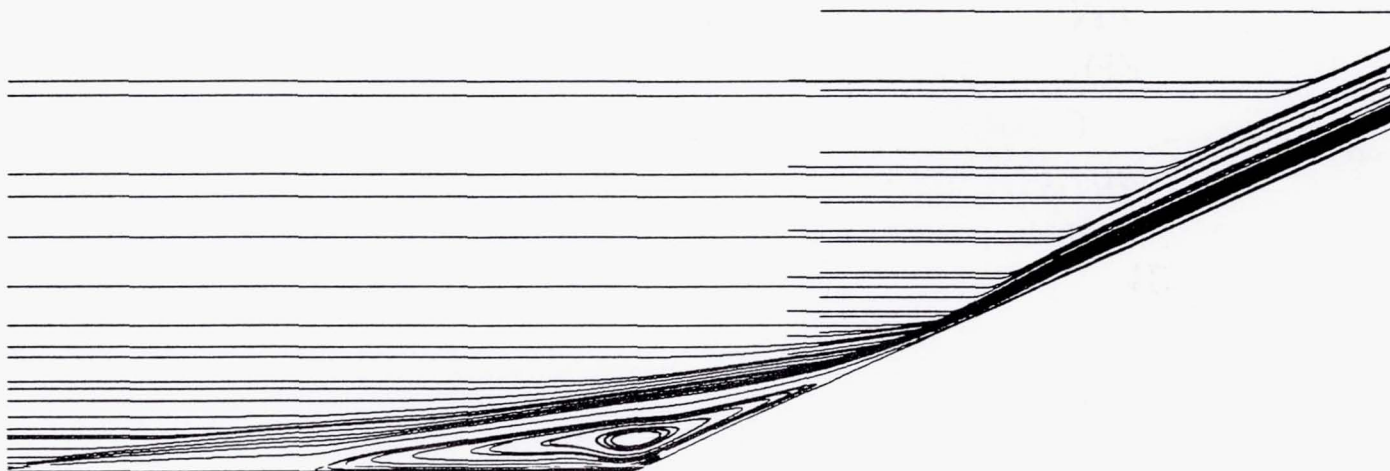
SURFACE PRESSURE

24° ramp
201 x 60 grid
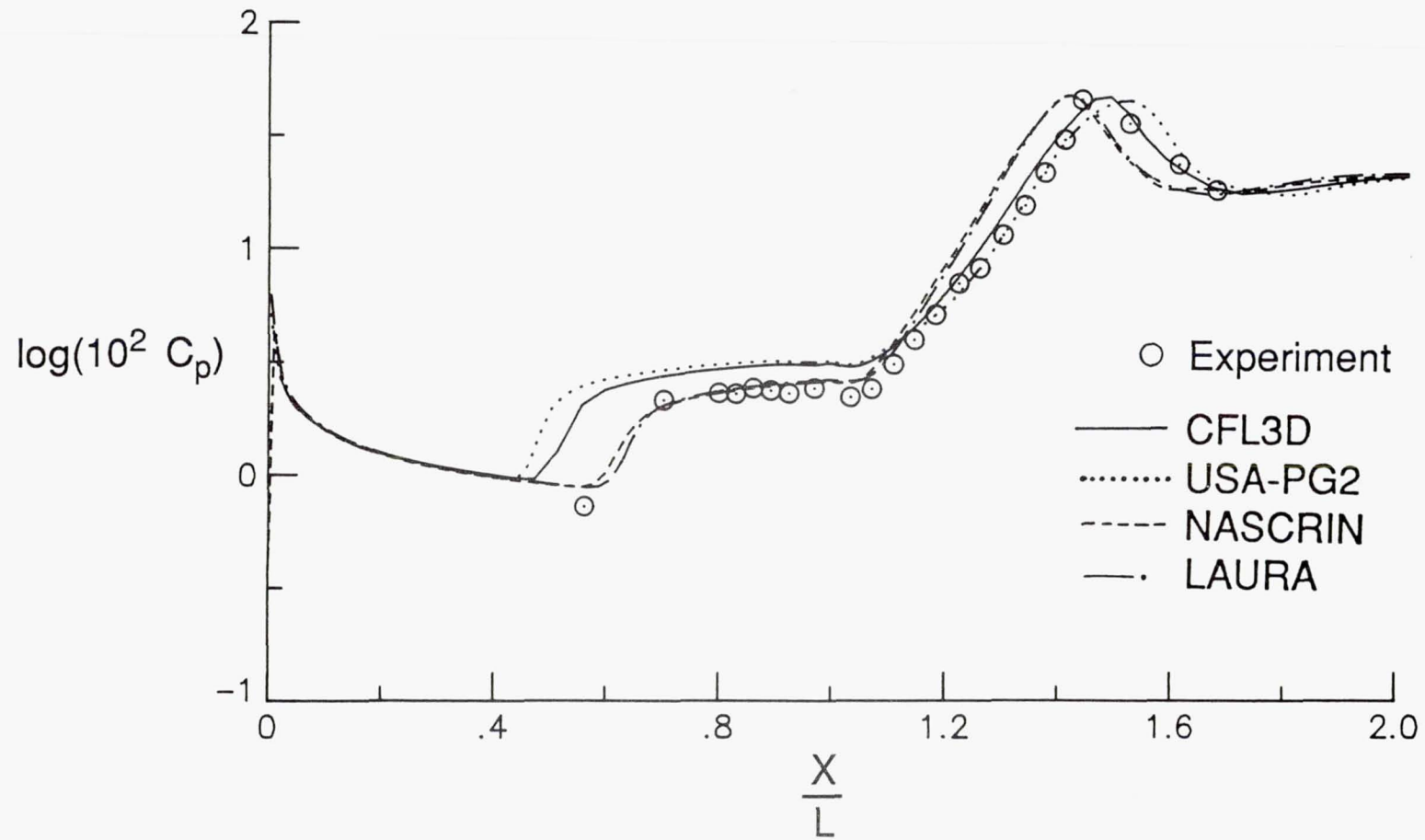
SKIN FRICTION

24° ramp
201 x 60 grid
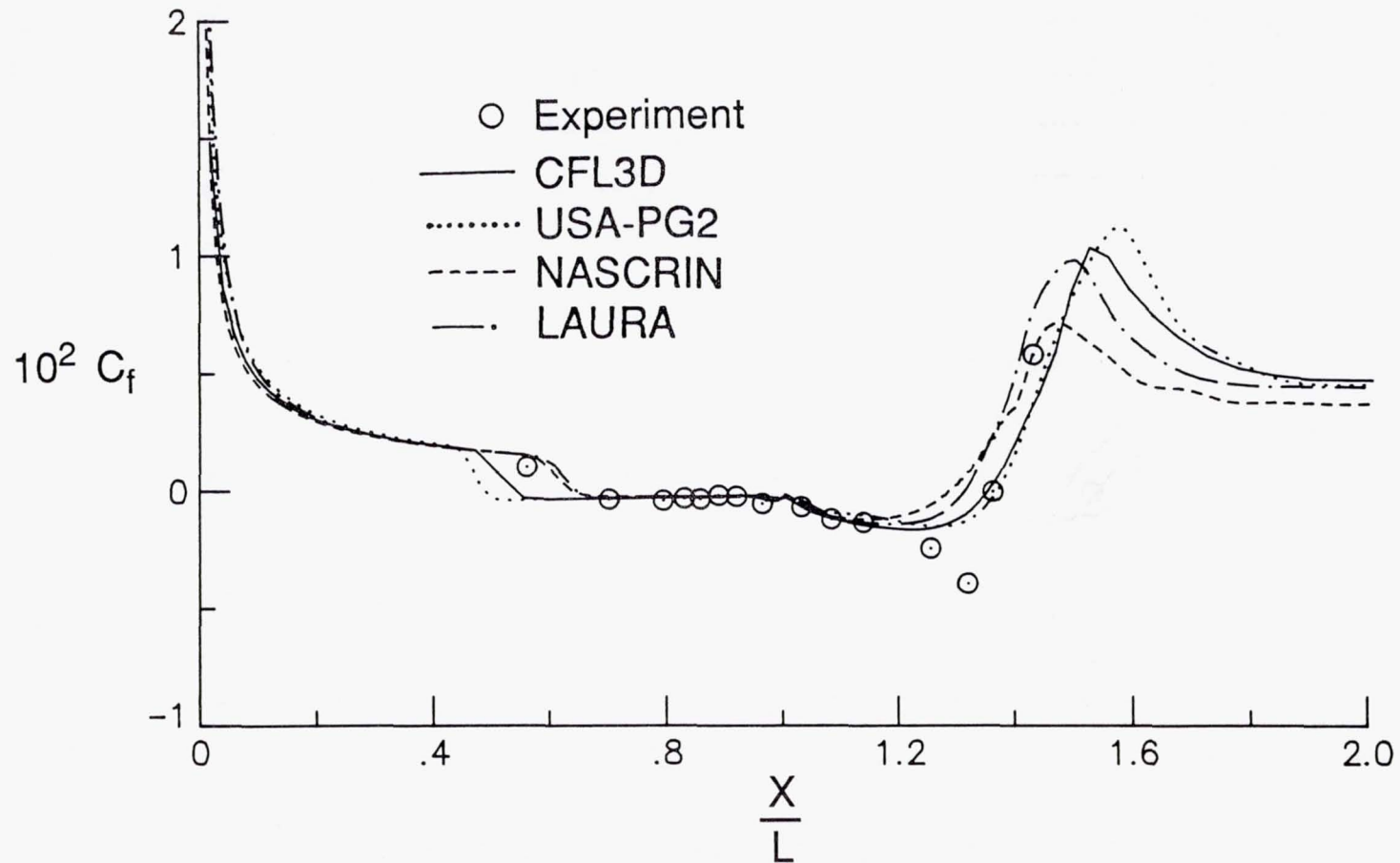
SUMMARY AND CONCLUSIONS

- A comparative study of four computer codes for the Navier-Stokes equations was performed using three test problems for high-speed flow.

- For the P8 inlet, good agreement was found between the codes. Differences between computation and experiment were possibly due to experimental effects not included.

- Flow structure in 3-D corner was predicted well by all of the codes. Good agreement was found between the solutions for all four codes.

- For the hypersonic compression ramp, the codes predicted the strong interaction structure observed experimentally. A wide variation in the predicted extent of separation was found.

18

MODELING OF HIGH SPEED CHEMICALLY REACTING FLOW-FIELDS

J. P. Drummond, M. H. Carpenter* and H. Kamath*
NASA Langley Research Center
Hampton, VA 23665

ABSTRACT

The SPARK3D and SPARK3D-PNS computer programs have been developed to model 3-D supersonic, chemically reacting flow-fields. The SPARK3D code is a full Navier-Stokes solver, and is suitable for use in scramjet combustors and other regions where recirculation may be present. The SPARK3D-PNS is a parabolized Navier-Stokes solver and provides an efficient means of calculating steady-state combustor far-fields and nozzles. Each code has a generalized chemistry package, making modeling of any chemically reacting flow possible.

Research activities by the Langley group range from addressing fundamental theoretical issues to simulating problems of practical importance. Algorithmic development includes work on higher order and upwind spatial difference schemes. Direct numerical simulations employ these algorithms to address the fundamental issues of flow stability and transition, and the chemical reaction of supersonic mixing layers and jets. It is believed that this work will lend greater insight into phenomenological model development for simulating supersonic chemically reacting flows in practical combustors. Currently, the SPARK3D and SPARK3D-PNS codes are used to study problems of engineering interest, including various injector designs and 3-D combustor-nozzle configurations. Examples, which demonstrate the capabilities of each code are presented.

*Analytical Services and Materials, Inc.

OVERVIEW

- GROUP OBJECTIVES

- DESCRIPTION OF 2 AND 3-D CODES

- 3-D FULL NAVIER-STOKES

- 3-D PARABOLIZED NAVIER-STOKES

- 2 AND 3-D MIXING ENHANCEMENT

- CONCLUSIONS AND DIRECTIONS

OBJECTIVES

- THEORETICAL ISSUES

    - NUMERICS FOR SUPERSONIC CHEMICALLY
      REACTING FLOWS

        - Numerical Efficiency
        - Numerical Accuracy
        - Robustness

    - PHYSICAL ISSUES

        - Mixing Enhancement and Combustion
        - Transition to Turbulence
        - Phenomenological Turbulence Models

- APPLICATIONS

    - 3-D COMBUSTORS AND NOZZLES

        - SPARK3D
        - SPARK3D-PNS

SPARK 3-D

- 3-D NAVIER-STOKES AND CHEMISTRY

- FULLY ELLIPTIC STRUCTURE

- VISCOUS OR INVISCID CAPABILITIES

- TIME-ACCURATE OR LOCAL RELAXATION

- GENERALIZED CHEMISTRY ROUTINES

- LOW STORAGE FORMAT

GENERALIZED CHEMISTRY ROUTINE

- REAL GAS THERMODYNAMICS MODELS

  - POLYNOMIAL FITS FOR C_p, C_v, S, G
  - KINETIC THEORY BASED DIFFUSION MODELS

    - Sutherlands Law for μ_i and k_i
    - Wilkes law for μ and k
    - Binary or multicomponent diffusion models

- CHEMISTRY MODELS

  - FROZEN
  - EQUILIBRIUM
  - FINITE RATE CHEMISTRY (NS=9, NR=18)

NUMERICAL METHODS

- TRANSFORMED COORDINATES (ξ, η, ζ)

  - GEOMETRIC CONSERVATION LAW TERMS INCLUDED

- TEMPORAL INTEGRATION (2ND ORDER)

  - EXPLICIT FORMULATION FOR HYDRO-DYNAMIC TERMS
    - Allows local time stepping

  - EXPLICIT/IMPLICIT FORMULATION FOR CHEMICAL SOURCE TERMS

- FINITE DIFFERENCE SPATIAL DISCRETIZATION

  - STANDARD MACCORMACK (2ND ORDER)
  - GOTTLIEB MACCORMACK (4TH ORDER)
  - COMPACT MACCORMACK (4TH ORDER AT S.S.)
  - UPWIND (3RD ORDER)

CORNER FLOW

1 Corner shock
2 Internal shock
3 Slip line
4 Wall shock
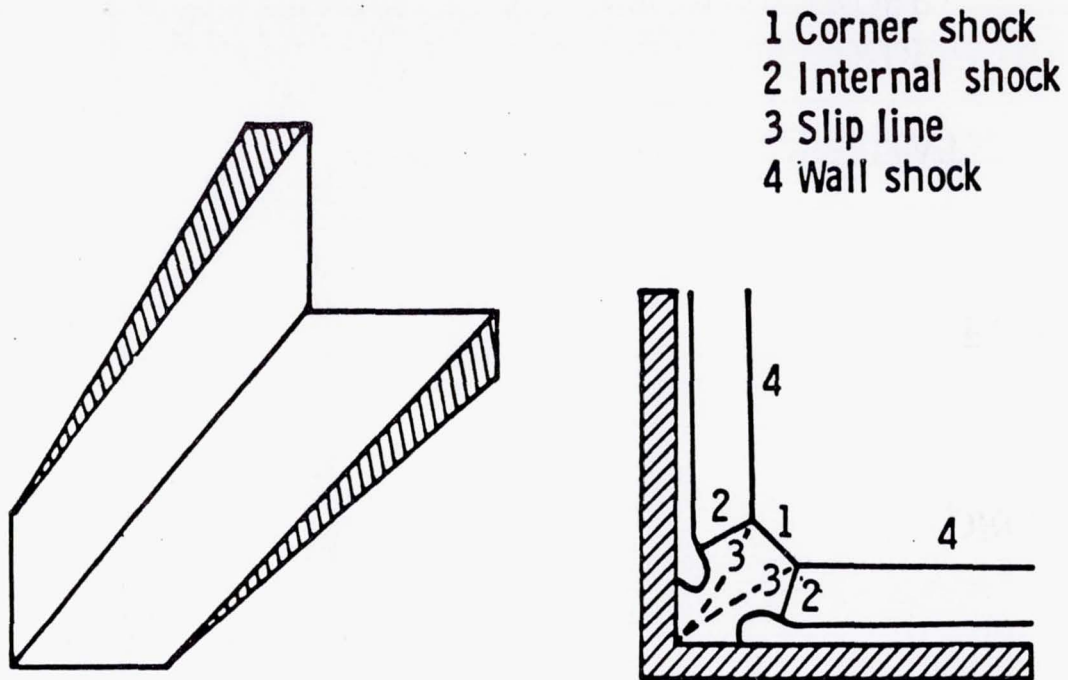
Figure 3.- Symmetric-wedge corner and schematic of corner flow.

CORNER FLOW

Symmetric-Wedge Corner
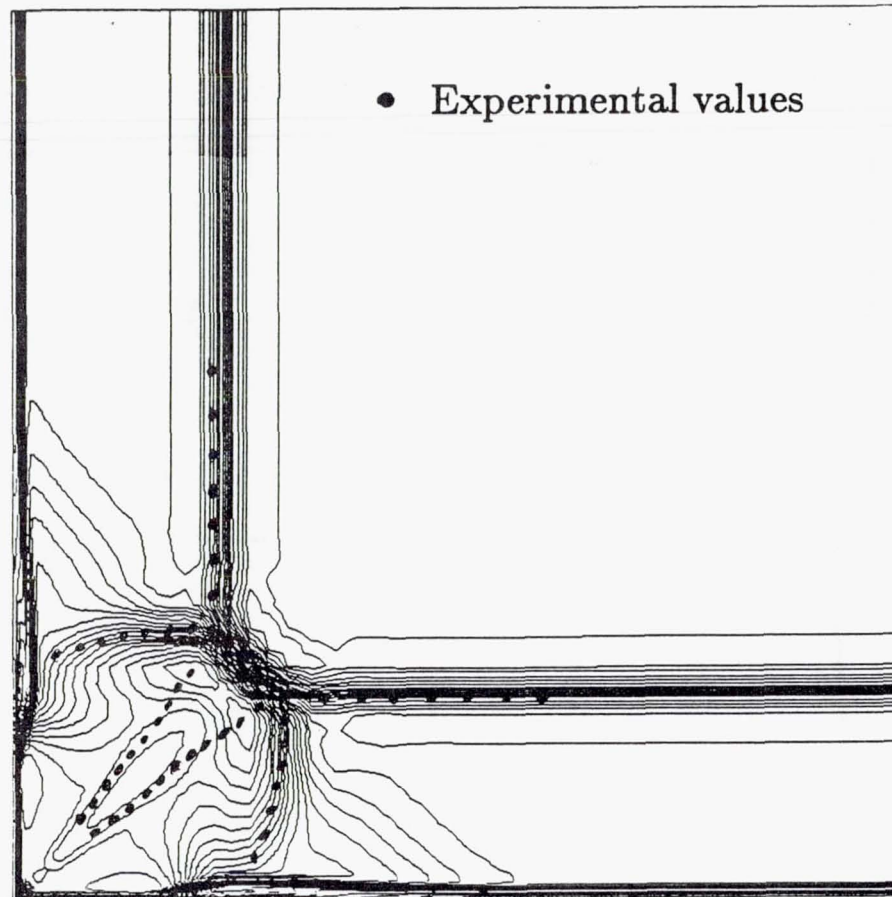
Density Contours (Laminar Flow)

REARWARD STEP
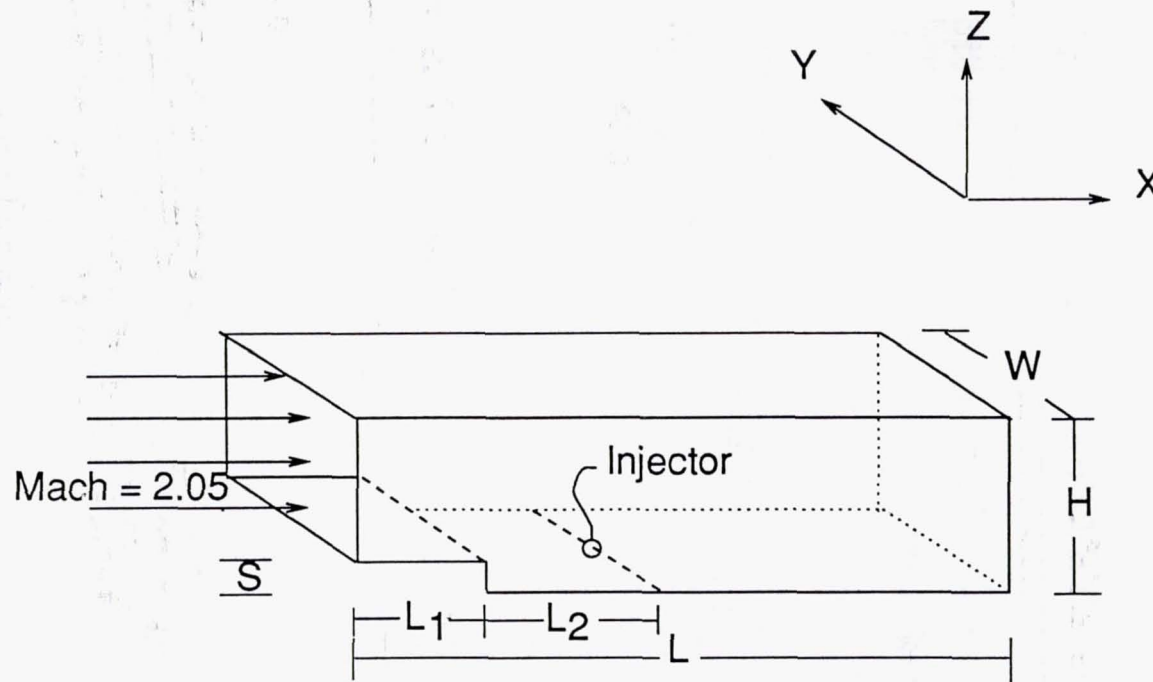
L = 7.0 cm, H = 1.8 cm, W = 2.9 cm

L_1 = 0.7 cm, L_2 = 1.2 cm, S = 0.3 cm

SPARK3D
REARWARD STEP COMPARISON

Mach = 2.05
101 x 41 x 25 GRID
Qr = 0.39

JET PENETRATION IN X-Z PLANE AT Y = $Y_{\mathcal{L}}$

o Experimental data at approximately 1 percent.
– Computed mass percent contours.

0.2┐ 0.1┐ 0.01┐

0.5┘ 0.4┘ 0.3┘
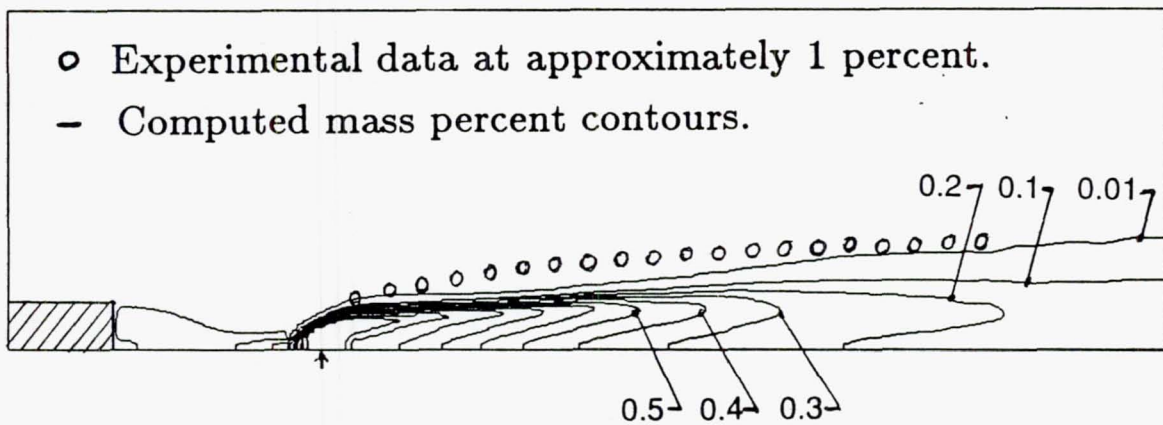
JET SPREAD IN X-Y PLANE AT Z = D
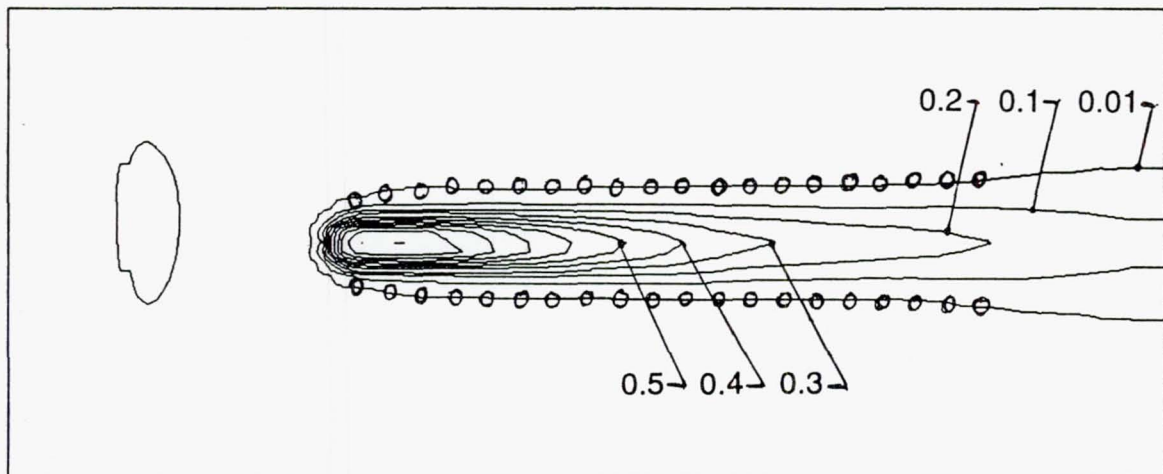
0.2┐ 0.1┐ 0.01┐

0.5┘ 0.4┘ 0.3┘

EXPERIMENTAL COMPARISON
Jet Penetration

61 x 41 x 25 GRID

Qr = 0.39

0.2 0.1 0.01

0.5 0.4 0.3

Qr = 0.78

0.2 0.1 0.01

0.5 0.4 0.3

Qr = 1.13

0.2 0.1 0.01

0.5 0.4 0.3

EXPERIMENTAL COMPARISON
Jet Penetration

## 61 x 41 x 25 GRID

30
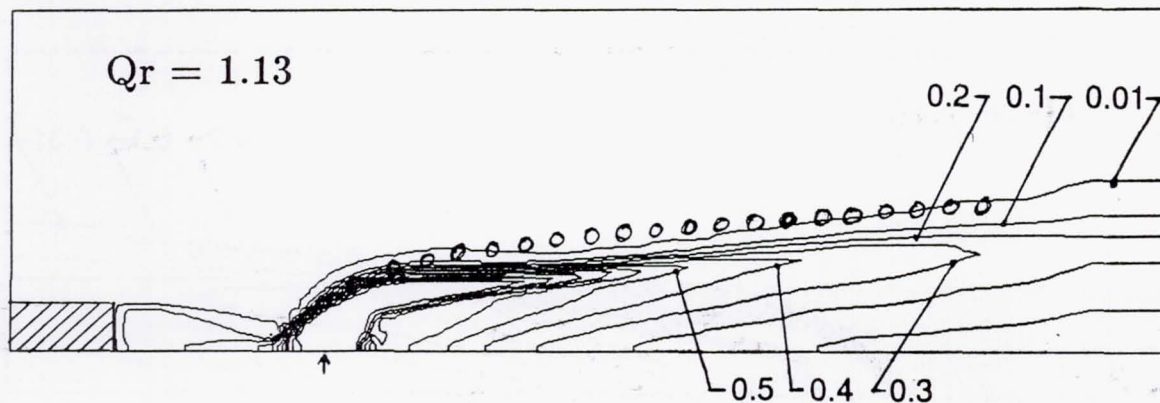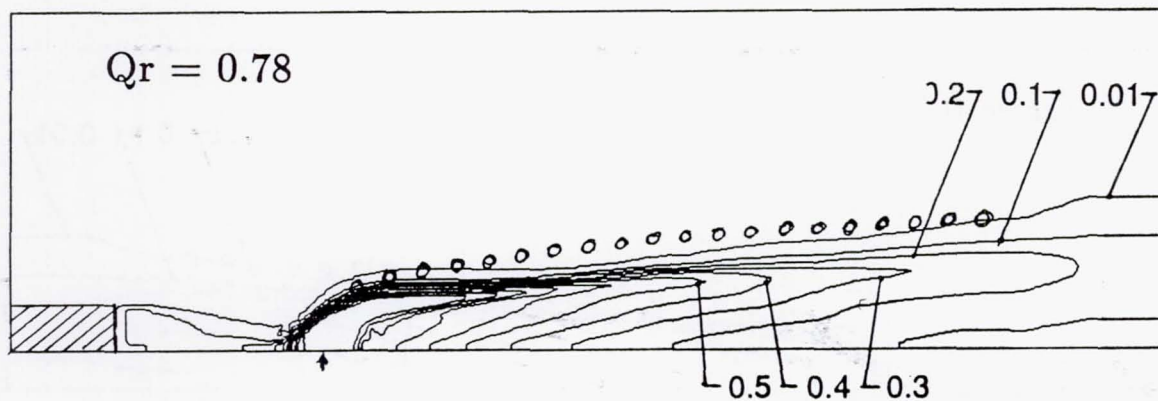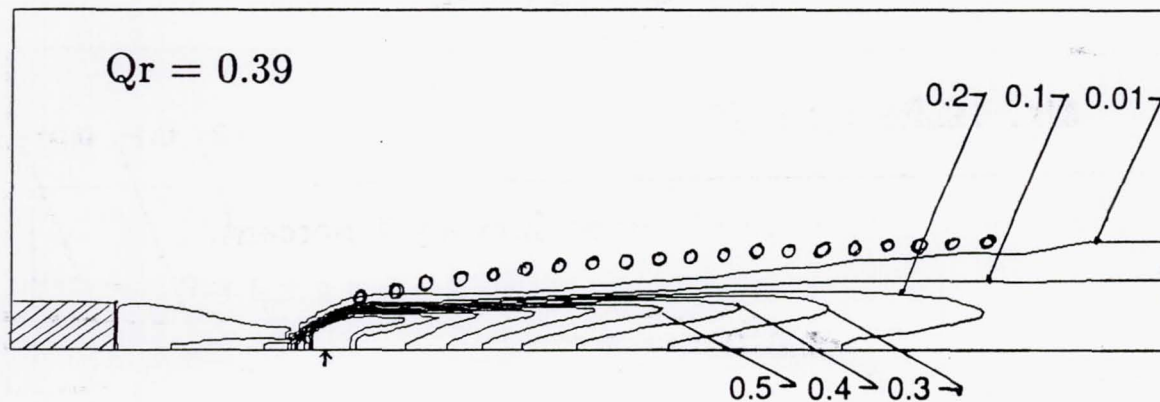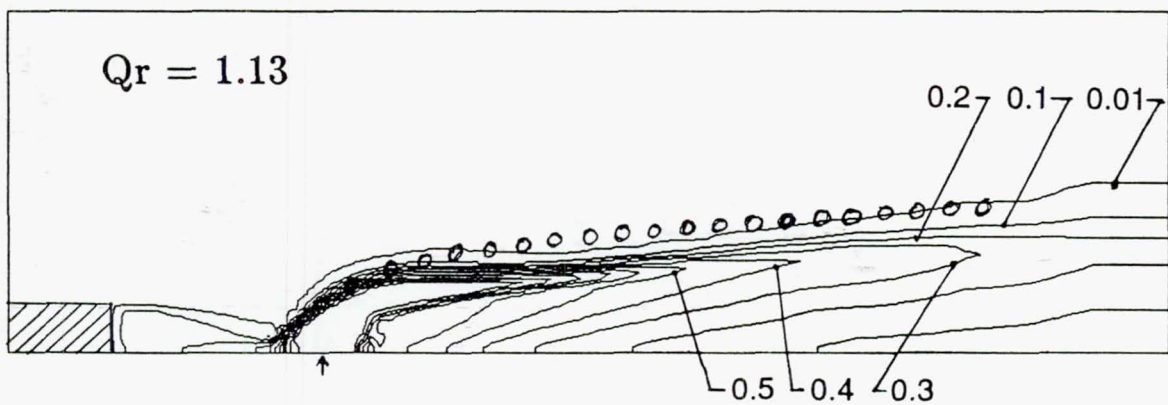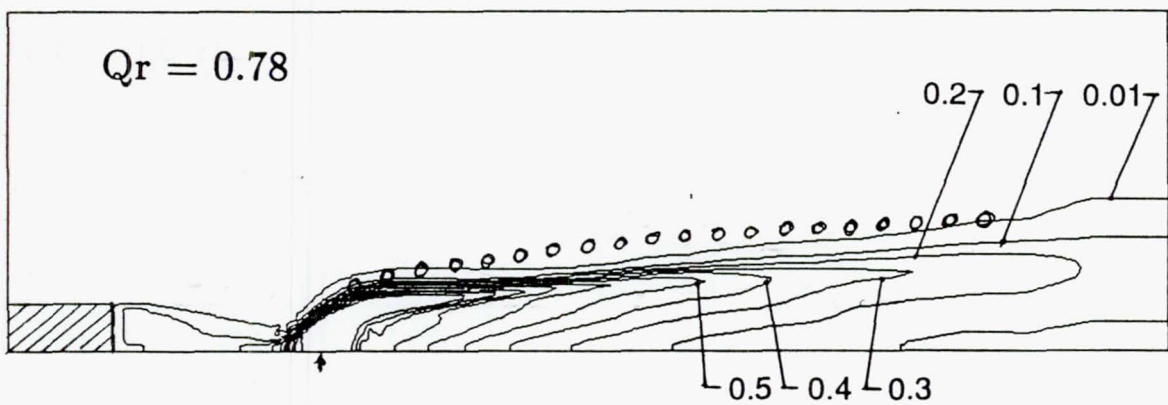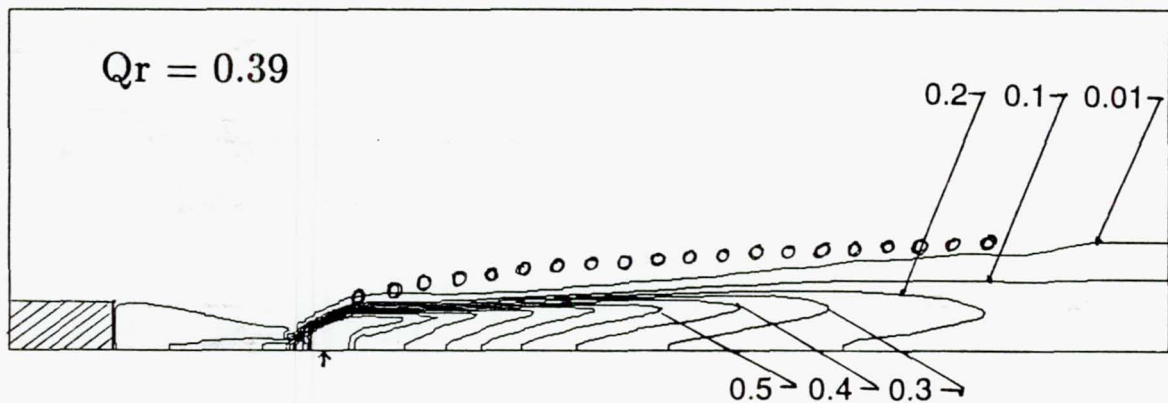
REARWARD STEP COMPARISON
Jet Spread

61 x 41 x 25 GRID

0.2 0.1 0.01

Qr = 0.39

0.5 0.4 0.3

0.2 0.1 0.01

Qr = 0.78

0.5 0.4 0.3

0.2 0.1 0.01

Qr = 1.13

0.5 0.4 0.3
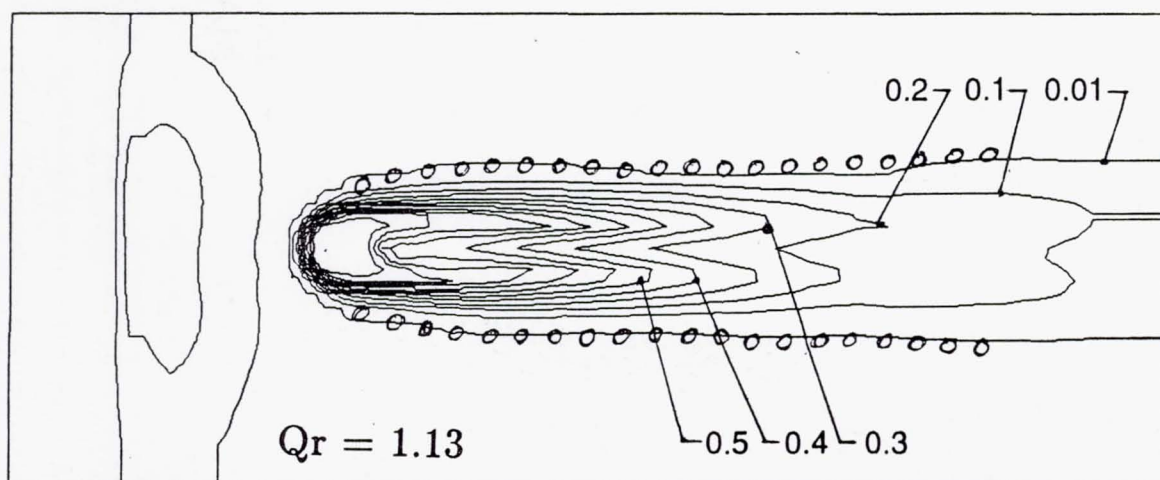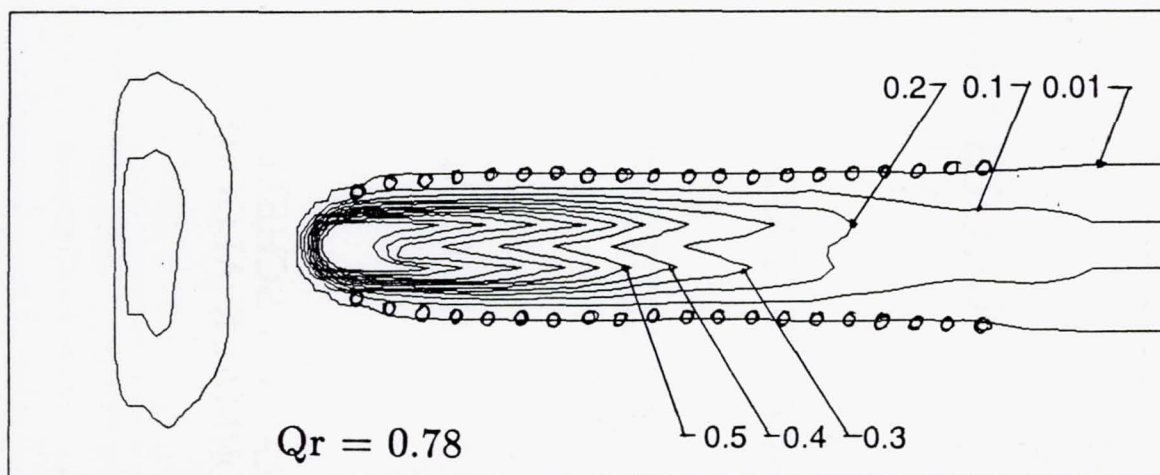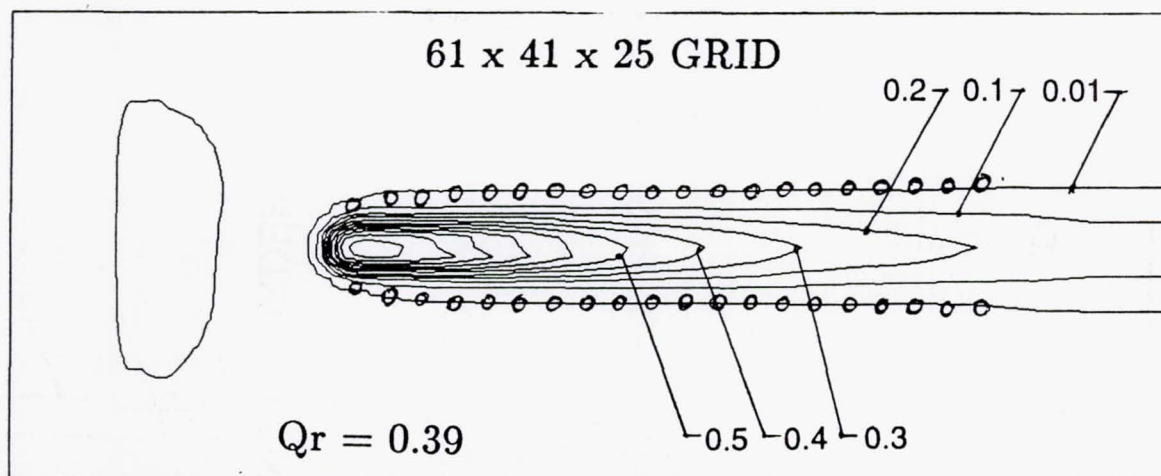
SPARK3D-PNS

- EXTENSION OF SPARK3D

- EFFICIENT SOLUTIONS OF STEADY 3-D PNS EQUATIONS

- FOR USE IN THE COMBUSTOR FAR-FIELD AND NOZZLE

- INTEGRATION SCHEME BASED ON 2ND ORDER MACCORMACK ALGORITHM

CORNER FLOW
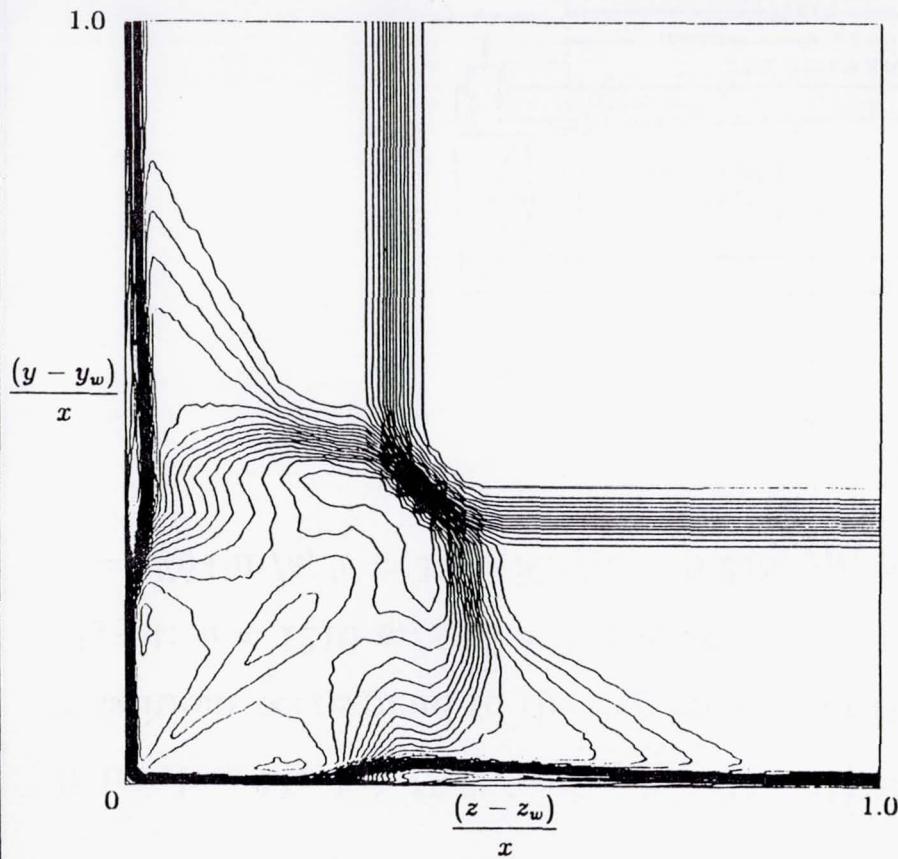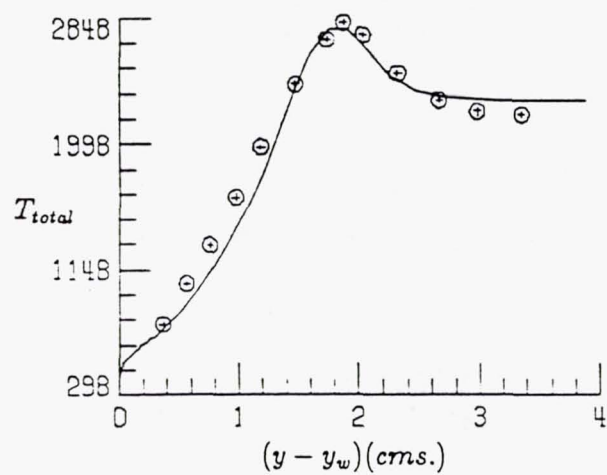

1. Computed density contours.
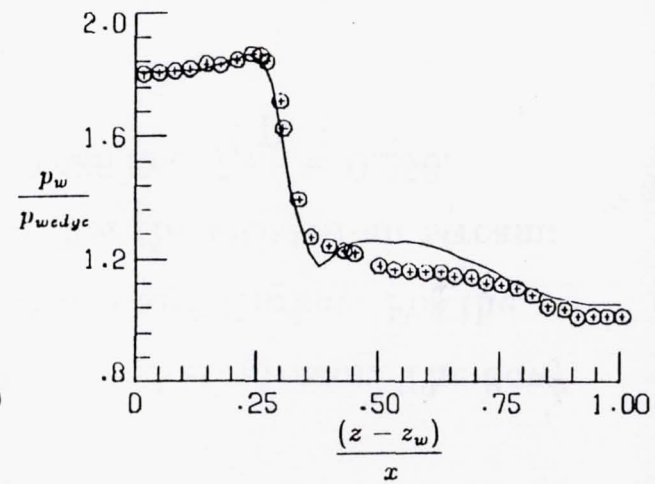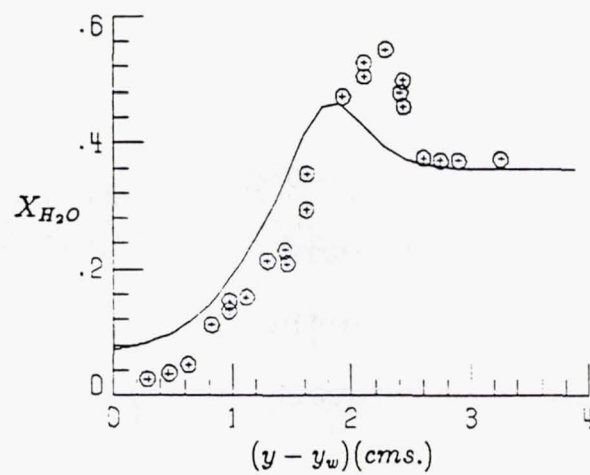

2. Wall pressure comparison.

BURROWS KURKOV

It involves Mach 1 H_2 injection in a Mach 2.44 vitiated-air stream. The flow conditions correspond to the experiments of Burrows and Kurkov. For the H_2 jet: $u = 1216$ m/s, $T = 254$ K and $f_{H_2} = 1.0$. For the vitiated-air stream: $u = 1764$ m/s, $T = 1270$ K, $f_{O_2} = 0.258$, $f_{N_2} = 0.486$ and $f_{H_2O} = 0.256$.
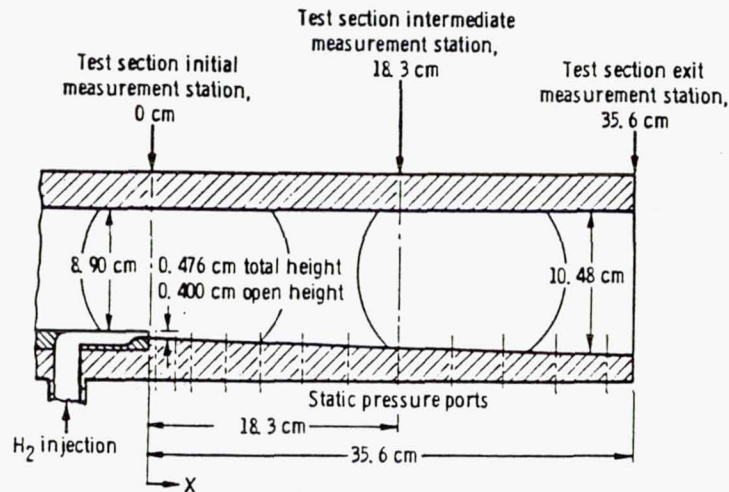
# BURROWS KURKOV

1. Total temperature comparison.

2. H_2O mole fraction comparison.

MIXING ENHANCEMENT STUDIES

- FUEL-AIR MIXING DECREASES WITH INCREAS-
  ING MACH NUMBER

- MIXING ENHANCEMENT MECHANISMS ARE
  REQUIRED AT HIGH COMBUSTOR MACH
  NUMBER

  - PLANAR SHOCKS   EXCITATION
  - CURVED SHOCKS   OF
  - SWIRL   UNSTABLE
  - ACOUSTIC FORCING   MODES

- ENHANCEMENT BY SHOCKS IS EXAMINED IN
  THIS STUDY

NASA

STRUT MODIFICATION FOR IMPROVED COMBUSTION EFFICIENCY

Air →

H₂

H₂

Air →

Conventional strut

Air →

H₂   H₂

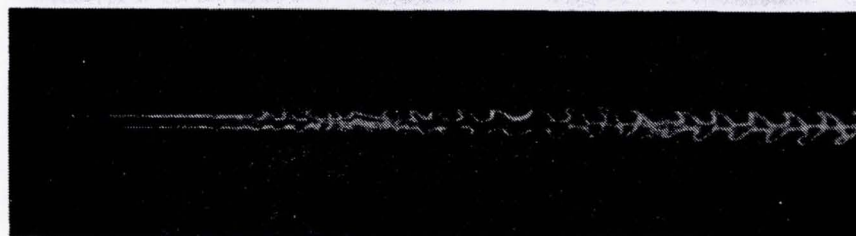Air →
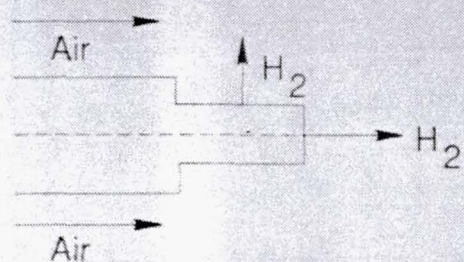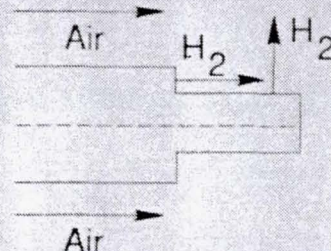
Modified strut

Water mass fraction
Conventional strut
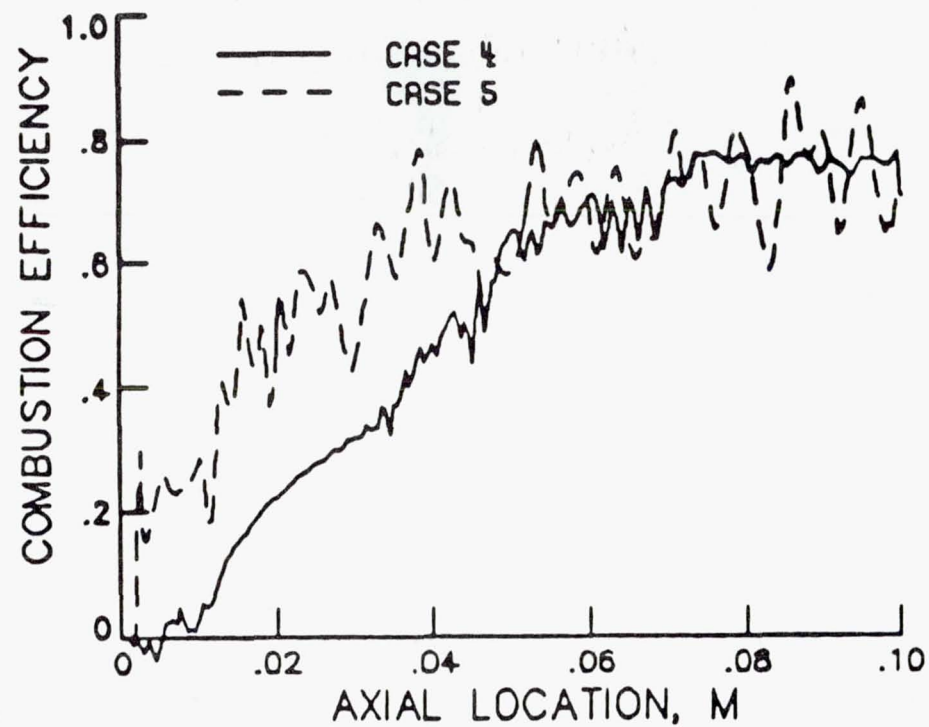
Water mass fraction
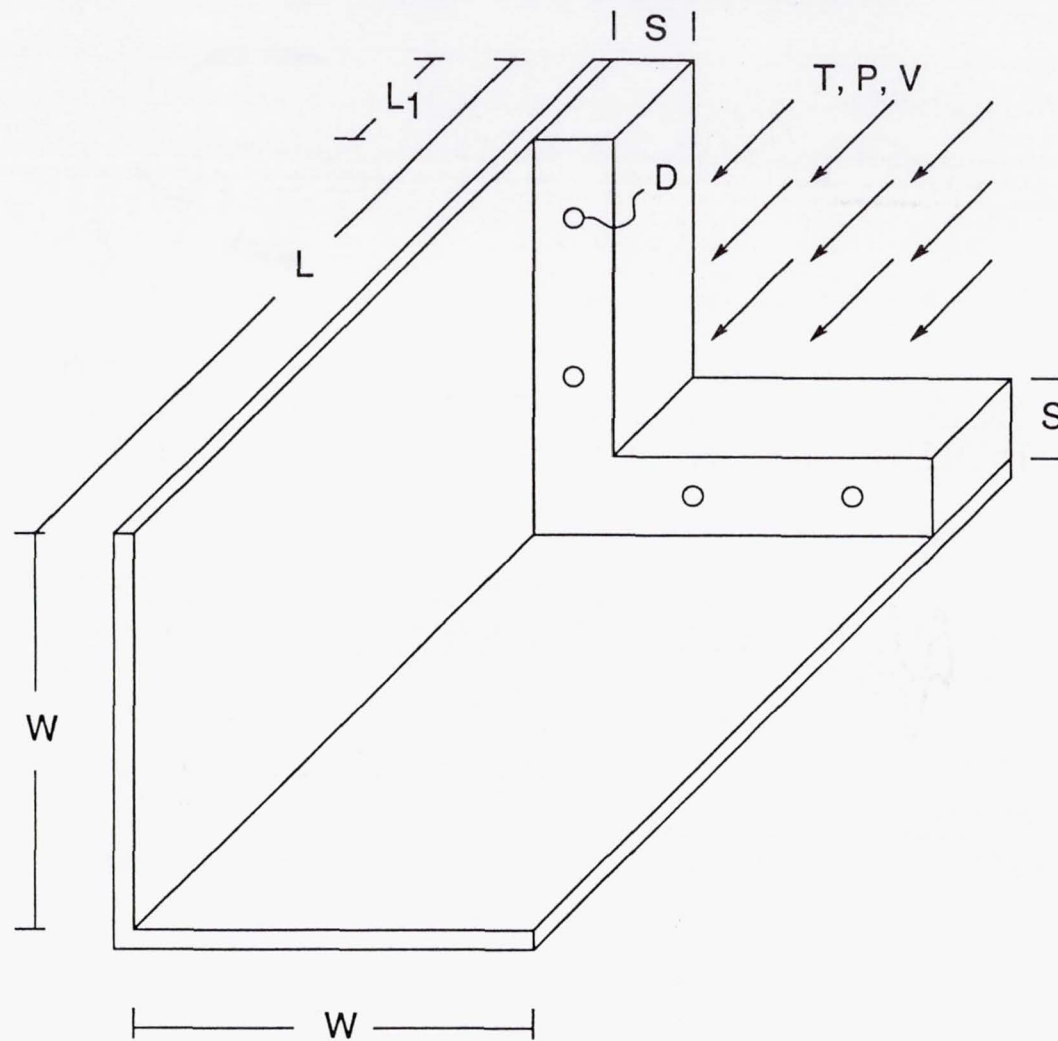Modified strut

STRUT WITH TRANSVERSE - PARALLEL JETS

MODEL COMBUSTOR

L = 20.0 cm, W = 10.0 cm
S = 2.0 cm, L_1 = 1.5 cm, D = 3.5 mm
T = 1000 K, P = 0.5 atm, V = 1500 m/s

CONCLUSIONS

- COMPUTER PROGRAMS DEVELOPED TO MODEL 3-D SUPERSONIC CHEMICALLY REACTING FLOWFIELDS.

- FAVORABLE VALIDATION AGAINST AVAILABLE EXPERIMENTAL RESULTS

- BEING USED EXTENSIVELY IN THEORETICAL STUDIES AND IN ENGINEERING ENVIRONMENTS

40

DIRECTIONS

- ALGORITHMS

  - HIGHER ORDER AND COMPACT
  - UPWINDING
  - PARALLEL COMPUTING

- TRANSITION - TURBULENCE MODELING

  - COMPARISON WITH LINEAR STABILITY CODES
  - DIRECT SIMULATIONS OF SUPERSONIC JETS AND MIXING LAYERS
  - "DATABASE" FOR PHENOMINOLOGICAL MODELS

- PRODUCTION CODE SUPPORT

Three–Dimensional Calculation of Supersonic Reacting Flows Using an LU Scheme

Sheng–Tao Yu
Y–L Peter Tsai
Jian–Shun Shuen

Sverdrup Technology, Inc.
NASA Lewis Research Center
Cleveland, Ohio

ABSTRACT

A new three-dimensional numerical program incorporated with comprehensive real gas property models has been developed to simulate supersonic reacting flows. The code employs an implicit finite volume, Lower-Upper (LU) time-marching method to solve the complete Navier-Stokes and species equations in a fully-coupled and very efficient manner. A chemistry model with nine species and eighteen reaction steps are adopted in the program to represent the chemical reaction of H_2 and air. To demonstrate the capability of the program, flow fields of underexpanded hydrogen jets transversely injected into supersonic air stream inside the combustors of scramjets are calculated. Results clearly depict the flow characteristics, including the shock structure, separated flow regions around the injector, and the distribution of the combustion products.

PREVIOUS WORK

- Develop fluid dynamic code to study the mixing and chemical reactions inside the combustors of ramjets.

- A two-dimensional computer code (RPLUS) using LU scheme to simulate chemical reacting flows has been developed:
    - Fully coupled and very efficient.
    - Finite rate chemistry.
    - A fast equilibrium chemistry package.

- Previous work done by using RPLUS 2D code:
    - Hypersonic inlet flows at Mach 10 and 13.
    - The combustion of a hydrogen jet transversely injected into a supersonic air stream.
    - Hydrogen air mixture passing a 10° ramp.

ANALYSIS

- 3D Navier-Stokes and N_s-1 species equations.

- Brabbs' finite rate chemistry model.

  - 9 species: H_2, H, OH, H_2O, O, O_2, HO_2, H_2O_2, and N_2.

  - 18 reaction steps.

- Implicit treatment of source terms in species equations.

- No source term in energy equation for either exothermic or endothermic reactions.

- Temperature and pressure are calculated iteratively from the following equations:

$$e = \sum_{i=1}^{N_s} Y_i h_i - \frac{p}{\rho} + \frac{1}{2} \left(u^2 + v^2 + w^2 \right)$$

$$h_i = h_{fi}^o + \int_{T_{ref}}^{T} C_{pi} dT$$

$$p = \rho R_u T \sum_{i=1}^{N_s} \frac{Y_i}{M_i}$$

THERMODYNAMIC AND TRANSPORT PROPERTIES

- C_p, thermal conductivity, and viscosity of individual species are obtained from fourth order polynomial of T.

- Binary mass diffusivity is calculated using the Chapman-Enskog theory with Lennard-Jones intermolecular potential energy functions.

- Wilke's mixing rule is used for the transport properties of gas mixture.

- Mass concentration weighing is used for the C_p of gas mixture.

TURBULENCE MODEL

- Baldwin-Lomax model.

- $Sc_t = Pr_t = 0.9$

NUMERICAL SCHEME

- Time-marching LU scheme.

- Implicit treatment of source terms.

$$\frac{\partial Q}{\partial t} + \frac{\partial}{\partial x}\left(E^n + A^n \Delta Q\right) + \frac{\partial}{\partial y}\left(F^n + B^n \Delta Q\right) + \frac{\partial}{\partial z}\left(G^n + C^n \Delta Q\right)$$

$$= \frac{\partial E_v^n}{\partial x} + \frac{\partial F_v^n}{\partial y} + \frac{\partial G_v^n}{\partial z} + H^n + T^n \Delta Q$$

$$A = \frac{\partial E}{\partial Q}, \quad B = \frac{\partial F}{\partial Q}, \quad C = \frac{\partial G}{\partial Q}, \quad T = \frac{\partial H}{\partial Q}$$

$$A = A^+ + A^-$$

$$B = B^+ + B^-$$

$$C = C^+ + C^-$$

$$A^+ = 0.5(A + \gamma_A I)$$

$$A^- = 0.5(A - \gamma_A I)$$

$$B^+ = 0.5(B + \gamma_B I)$$

$$B^- = 0.5(B - \gamma_B I)$$

$$C^+ = 0.5(C + \gamma_C I)$$

$$C^- = 0.5(C - \gamma_C I)$$

$$\gamma_A \geq \max(|\lambda_A|)$$

$$\gamma_B \geq \max(|\lambda_B|)$$

$$\gamma_C \geq \max(|\lambda_C|)$$

$$\left[I + \Delta t\left(D_x^- A^+ + D_x^+ A^- + D_y^- B^+ + D_y^+ B^- + D_z^- C^+ + D_z^+ C^- - T\right)\right]\Delta Q$$

$$= \Delta t RHS$$

$$RHS = -\frac{\partial E^n}{\partial x} - \frac{\partial F^n}{\partial y} - \frac{\partial G^n}{\partial z} + \frac{\partial E_v^n}{\partial x} + \frac{\partial F_v^n}{\partial y} + \frac{\partial G_v^n}{\partial z} + H^n$$

NUMERICAL SCHEME

- Two operators for 3D calculation.
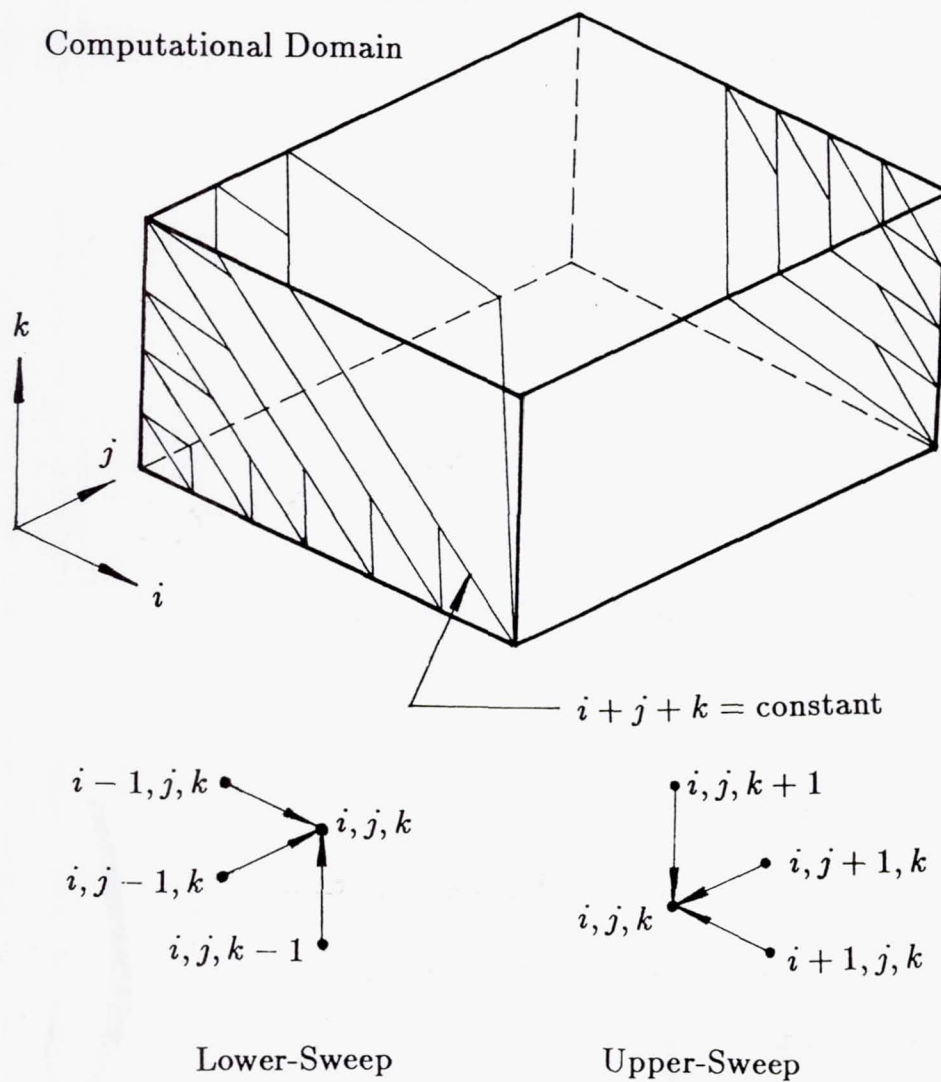
- Operation count comparable to explicit schemes.

$$N\Delta Q_{ijk} - \Delta t T_{ijk}\Delta Q_{ijk}+$$

$$\frac{\Delta t}{\Delta x}\left(A^-_{i+1,j,k}\Delta Q_{i+1,j,k} - A^+_{i-1,j,k}\Delta Q_{i-1,j,k}\right)+$$

$$\frac{\Delta t}{\Delta y}\left(B^-_{i,j+1,k}\Delta Q_{i,j+1,k} - B^+_{i,j-1,k}\Delta Q_{i,j-1,k}\right)+$$

$$\frac{\Delta t}{\Delta z}\left(C^-_{i,j,k+1}\Delta Q_{i,j,k+1} - C^+_{i,j,k-1}\Delta Q_{i,j,k-1}\right)$$

$$= \Delta t RHS$$

$$N = I + \frac{\Delta t}{\Delta x}\left(A^+_{i,j,k} - A^-_{i,j,k}\right) + \frac{\Delta t}{\Delta y}\left(B^+_{i,j,k} - B^-_{i,j,k}\right) + \frac{\Delta t}{\Delta z}\left(C^+_{i,j,k} - C^-_{i,j,k}\right)$$

$$\left[N + \frac{\Delta t}{\Delta x}\left(A^-_{i+1,j,k}\right) + \frac{\Delta t}{\Delta y}\left(B^-_{i,j+1,k}\right) + \frac{\Delta t}{\Delta z}\left(C^-_{i,j+1,k}\right)\right]N^{-1}$$

$$\left[N - \Delta t T_{i,j} - \frac{\Delta t}{\Delta x}\left(A^+_{i-1,j,k}\right) - \frac{\Delta t}{\Delta y}\left(B^+_{i,j-1,k}\right) - \frac{\Delta t}{\Delta z}\left(C^+_{i,j,k-1}\right)\right]\Delta Q$$

$$= \Delta t RHS$$

$$N = \left(1 + \frac{\Delta t}{\Delta x}\gamma_A + \frac{\Delta t}{\Delta y}\gamma_B + \frac{\Delta t}{\Delta z}\gamma_C +\right)I$$

PROGRAM VECTORIZATION

- LHS can be vectorized on planes normal to the sweeping direction.

Computational Domain

k

j

i

$i + j + k = \text{constant}$

$i-1, j, k$ i, j, k

$i, j-1, k$

$i, j, k-1$

Lower-Sweep

$i, j, k+1$

$i, j+1, k$

i, j, k

$i+1, j, k$

Upper-Sweep

CONVERGENCE HISTORY

- Coarse grid (30x25x30)
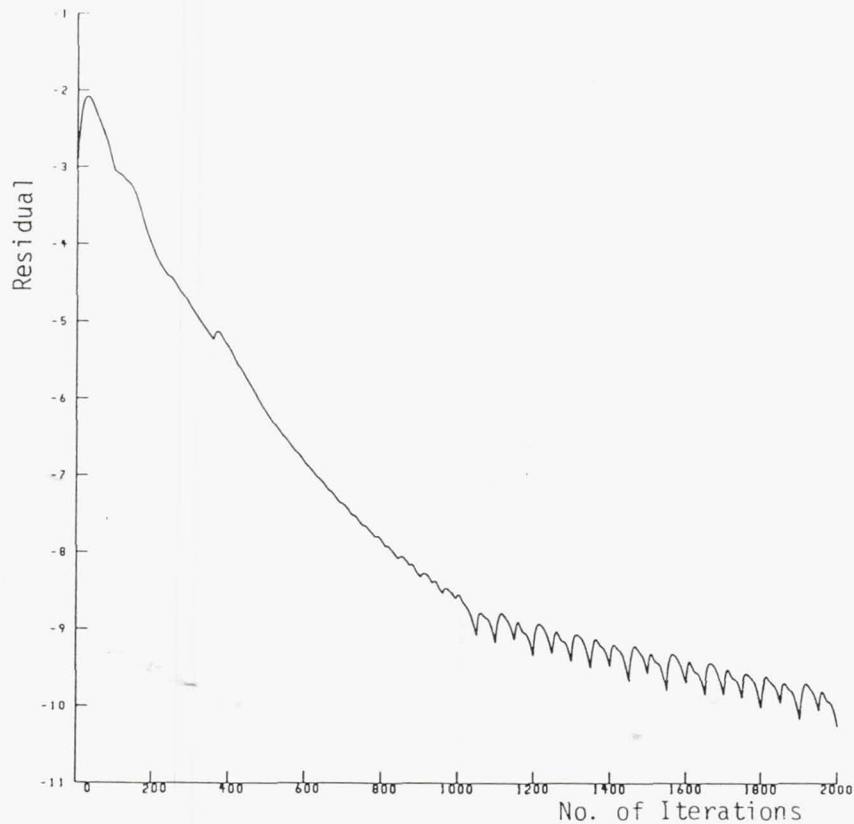
- Present calculation:

    - Residuals reduced by 4 orders of magnitude.

    - Single injection case: (61x39x43) 8 MW, 5 hrs on Cray 2.

    - Dual Injection case: (81x39x43) 11 MW, 6 hrs on Cray 2.

GEOMETRY AND FLOW CONDITION

Underexpanded Jet
$M_J = 1$

0.029 m

0.002 m

0.018 m

$M_{FS} = 2.07$

$P^o_{FS} = 310$ kPa

$T^o_{FS} = 298$ K
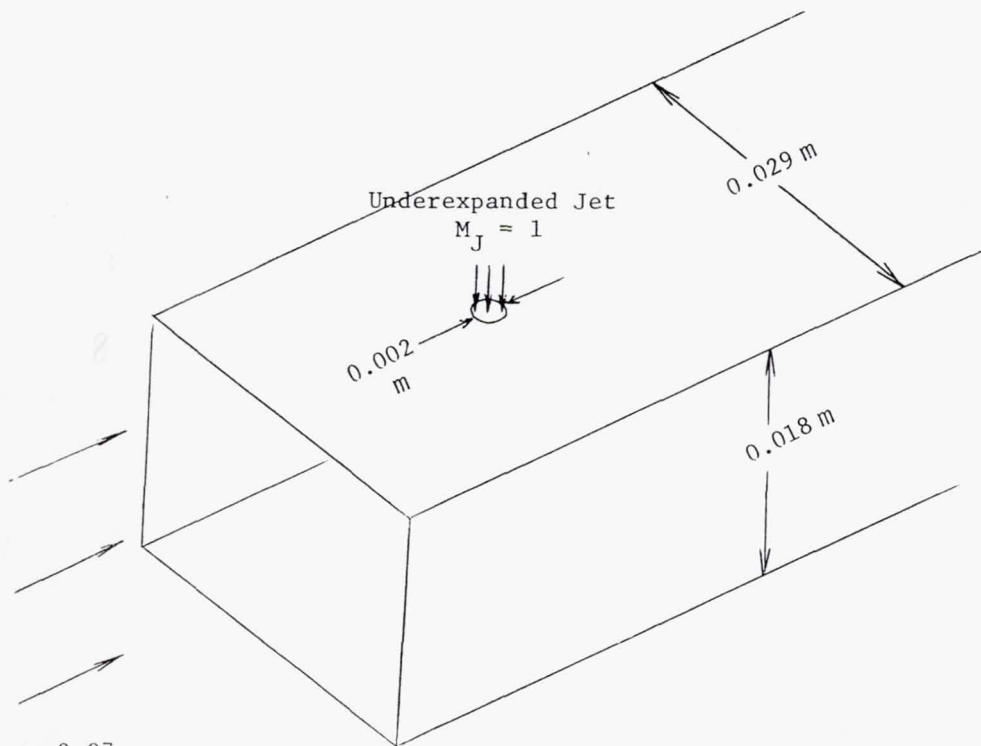
$$\bar{q} = \frac{1}{2}\rho_J u_J^2 \Big/ \frac{1}{2}\rho_{FS} u_{FS}^2$$

MASS-FRACTION CONTOUR ($\bar{Q} = 1.02, 60 \times 100 \times 50$)

Jet

y

J. C. MacDaniel
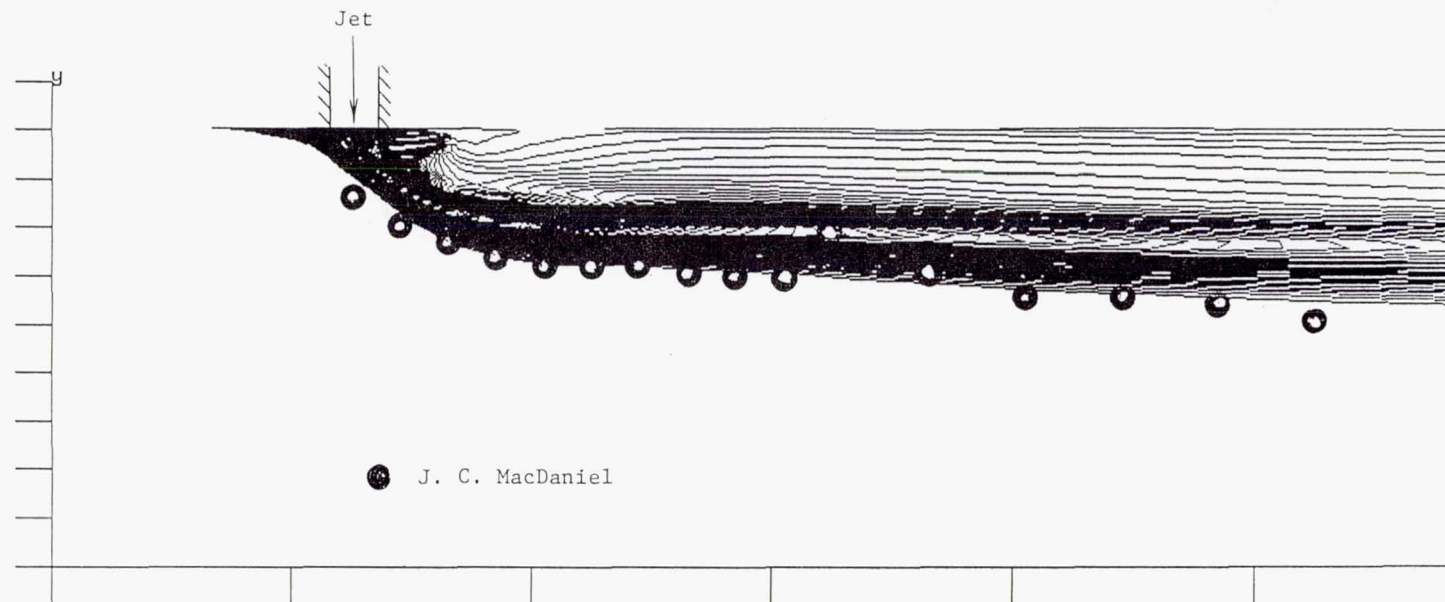
MASS-FRACTION CONTOUR (Two Ports, $\bar{Q} = 1.02$, $70 \times 100 \times 50$)

FLOW CONFIGURATION

P=8 atm
M=1

L₁

L

H

W

Z

Y

X

p = 1 atm
M = 4

L=0.024 m
H=0.01 m
W=0.01404 m
L₁=0.006 m
D=0.0012 m

P=8atm
M=1

L₂

L₁

L

H

W

p=1 atm
M=4.

L=0.03 m
H=0.01 m
W=0.01404 m
L₁=0.006 m
L₂=0.006 m
D=0.0012 m

Mach Number

3.8
3.8
3.8
3.8
3.8
3.2
3.2
3.2
1.1
1.4
1.4
x=0.615cm
x=1.16cm
x=1.61cm
x=2.19cm

Temperature

1500
1500
1500
1200
1500
1500
1500
1250
1500
1000
1750
1000
1000
750
750
x=0.615cm
x=1.16cm
x=1.61cm
x=2.19cm

H2

0.1

0.1

0.1

0.7

0.9

0.1

0.6

0.5

x=0.615cm

x=1.16cm

x=1.61cm

x=2.19cm

H2O

0.02

0.02

0.02

0.22

0.22

0.22

0.02

0.04

0.22

0.22

0.1

0.18

0.2

x=0.615cm

x=1.16cm

x=1.61cm

x=2.19cm

CONCLUDING REMARKS

- A new three-dimensional computer code for high speed reacting flows has been successfully developed.

- The code is very efficient because the LHS can be vectorized on the planes normal to the sweeping directions.

- The validity of the code is assessed by the comparison between the calculated results and MacDaniel's experimental data for non-reacting mixing flows.

- The code is applied to chemically reacting flows of H_2 jets transversely injected into hot airstream.

  - Results clearly depict the shock structure, recirculations, and species distribution due to chemical reaction.
  - Two-hole injection allows deeper penetration of the fuel jet and more complete combustion of H_2 and air.

Progress in Computing Nozzle/Plume Flow Fields

Stephen M. Ruffin
NASA Ames Research Center, Moffett Field, CA

Ethiraj Venkatapathy
Eloret Institute, Sunnyvale, CA

William J. Feiereisen
NASA Ames Research Center, Moffett Field, CA

Seung-Ho Lee
Eloret Institute, Sunnyvale, CA

Abstract

The long-term goal of this work is to develop the capability to predict chemically-reacting, multi-stream nozzle and plume flow fields. Two basic Navier-Stokes solvers, including the widely used F-3D code, are upgraded to include several upwind difference schemes and portable chemistry packages. Current computational capabilities for solving eqilibrium single-stream and multi-stream, frozen gas and finite rate chemistry problems are described. A variety of complex nozzle and plume flows have been computed. Solutions presented herein include axisymmetric plume flow for ideal and equilibrium air, 3-D NASP nozzle/afterbody flow, and an internal nozzle calculation comparing various finite-rate chemistry packages.

Motivations, Objective, and Applications

Motivations

- Flow in nozzle and propulsive plume strongly influence performance of hypersonic vehicles.

- Ground-based facilities can not fully simulate these flow fields.

- Validated, accurate and efficient flow codes are needed to design integrated propulsion systems of hypersonic vehicles.

Objective

- Develop computational ability to predict chemically reacting, multi-stream, nozzle/plume flow fields.

Applications

- NASP, Space Shuttle, general plume flows and signatures

SCHEMATIC OF AXISYMMETRIC PLUME FLOWS
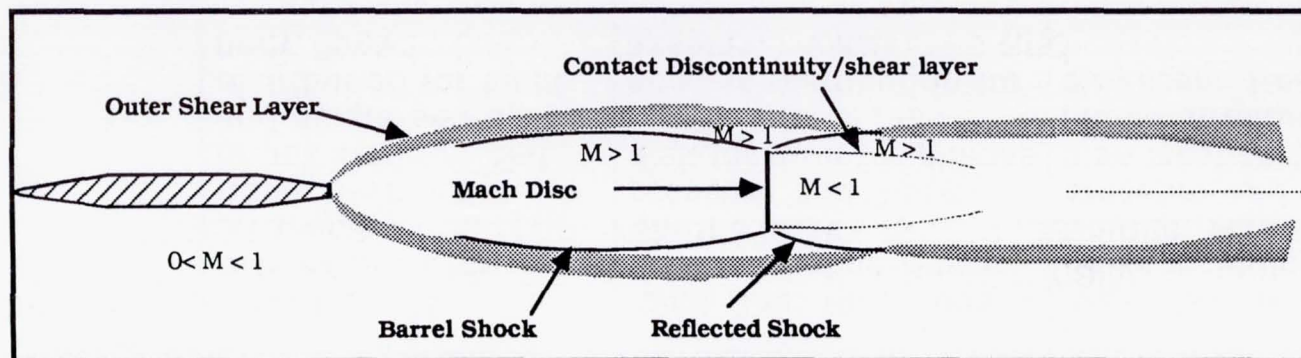
Plume Flow in Subsonic External Stream
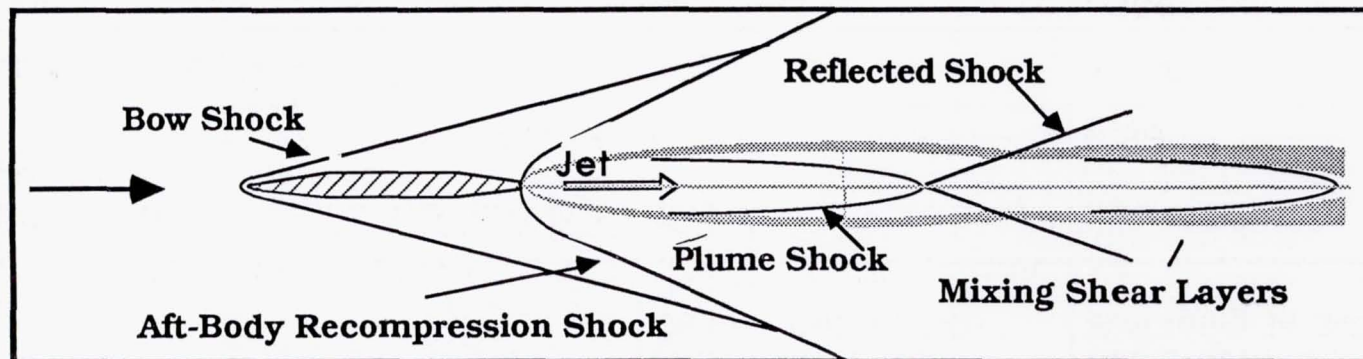
Plume Flow in Supersonic External Stream

Nozzle/Plume Flow Solvers

Difference Scheme	2-D Axisym. Eqns. Flux-Split in 2-D	3-D Eqns. Flux-Split in 1-D Central Diff. in 2-D	3-D Eqns. Roe's upwind averaging in 3-D
Implicit Soln. Algorithm	Beam & Warming in "delta form"	Two-Factor Flux-Split	LDU-ADI
Viscous Terms	in 1-D	in 1-D	in 3-D
Chemistry	Ideal Gas Equil. single-stream Equil. multi-stream Frozen	Ideal Gas Finite-Rate	Ideal Gas Equil. single-stream
Calibration	Ideal Gas: Mach disk location for jet plumes Equil. 1-stream: Shock standoff dist., and shape and species distribution for blunt body flow.	Ideal Gas: Numerous flows including Space Shuttle, Mach No., pressure and Mach disk location for plumes Finite-Rate: H_2-air species distribution for axsymm. nozzle.	Ideal Gas: Numerous flows including Space Shuttle, Mach No., pressure and Mach disk location for plumes, plume structure in quiescent freestream

62

Nozzle/Plume Flow Solvers (cont.)

- All calculations performed for laminar flow

- Adaptive grid routine used for all 2-D cases
  (3-D adaptive grid routine recently completed)

- 3-D code can handle multiple, patched-grid regions
  and generalized specification of boundary conditions

63

Equilibrium and Frozen Gas Chemistry

Constant Elemental Composition (i.e., single-stream)

- Uniform gas throughout flow field

  Equilibrium Gas
  - table look-up, curve fits
  - relatively fast
  - must be pre-calculated

Variable Elemental Composition (i.e., multi-stream)

- Solution of species partial density equations allows for convection, diffusion and mixing of multiple streams

  Equilibrium Gas
  - Gordon-McBride free energy minimization
  - arbitrary gas mixtures
  Frozen Chemistry
  - No reactions

Finite Rate Chemistry

- H_2 - air chemistry currently being used
    - JANNAF plume model (Dash and Pergament, 1980)
    - 7 Species: H, H_2, H_2O, O, OH, O_2, N_2
    - 8 Reactions

- Specific heats from curve fits (Gordon and McBride data)

- Binary diffusion
    - Fick's Law with $D_{i,j}$ given by Reid, et.al., 1977)

- Non-catalytic wall

- Chemistry Coupling
    - Fully-Coupled
        Invert large matrix of order $5 + (N_{species} - 1)$ per node
    - Loosely-Coupled
        Locally constant $\bar{\gamma}$
        P not affected by species concentration variations
        Invert two smaller matrices of order 5 and $N_{species} - 1$ per node.

Types of Nozzle/Plume Flows Computed

Cases	Main complexity is due to: Fluid Dyn. Features	Body Geom.	Flow Chem.	References
I. Axisymmetric Single-Nozzle Plume				
A. Not including afterbody				
Ideal gas, sub. freestream ◄—	X			AIAA 89-0129
Ideal gas, sup. freestream	X			AIAA 88-3158
B. Including afterbody				
Ideal Gas ◄—	X	X		AIAA 88-2636
Equil. single-stream	X	X	X	AIAA 88-2636
Equil. multi-stream	X	X	X	in preparation
Frozen	X	X	X	in preparation
II. 3-D Multiple-Nozzle Plume				
A. Not including afterbody	X			AIAA 88-3158
B. Including afterbody	X	X		AIAA 89-0129
III. Hypersonic Nozzle/Afterbody				
A. 2-D Geometry				
Subsonic freestream	X			AIAA 89-0446
Supersonic freestream	X			AIAA 89-0446
B. 3-D Geometry				
Plume region alone	X	X		AIAA 89-0446
Complete geometry ◄—	X	X		AIAA 89-0446
IV. Internal Nozzle, finite rate chem. ◄—			X	in preparation

Axisymmetric Plume Flow in Quiscent Air
Pj/Pinf = 21.9 - Mj = 1.5

Upper Half - Computed Mach Contours with Adapted Grid
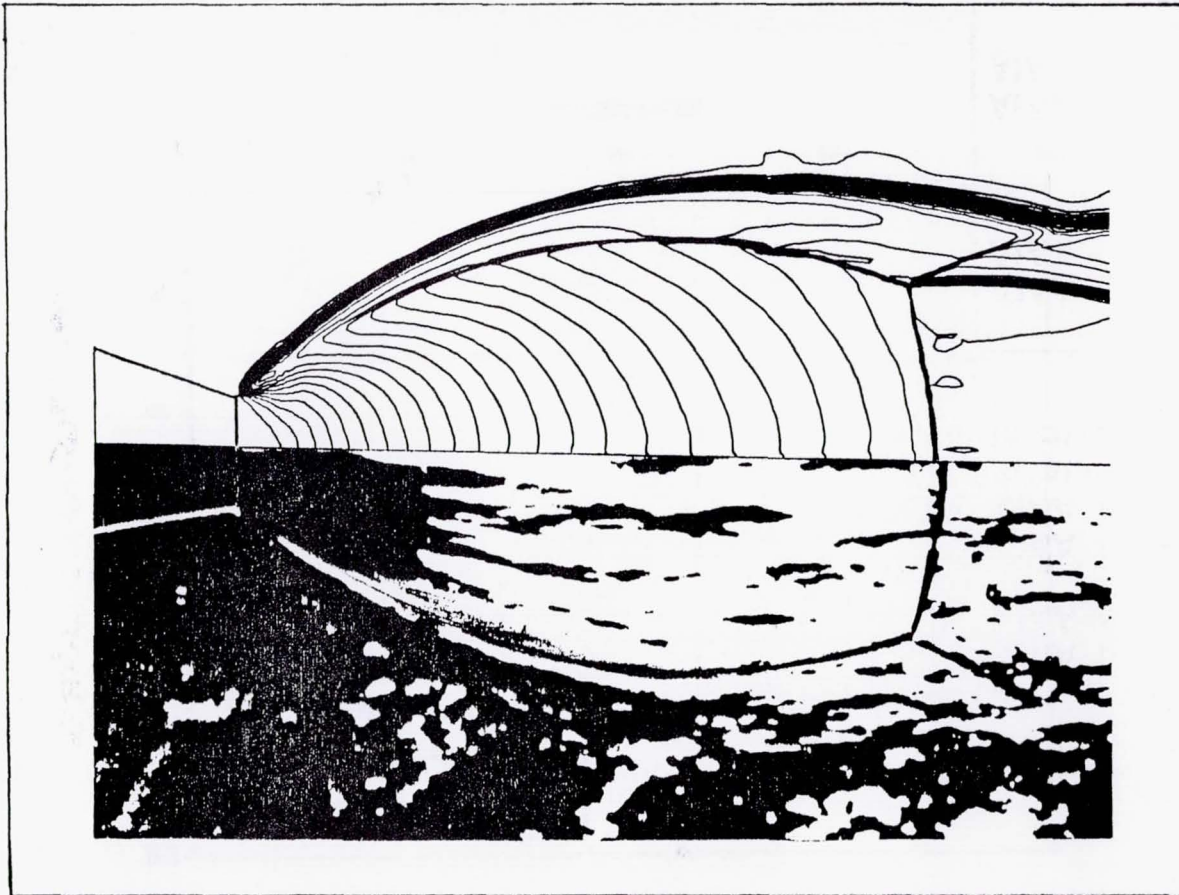
Lower Half - Experimetnal Shadowgraph - (NASA TR R 6)
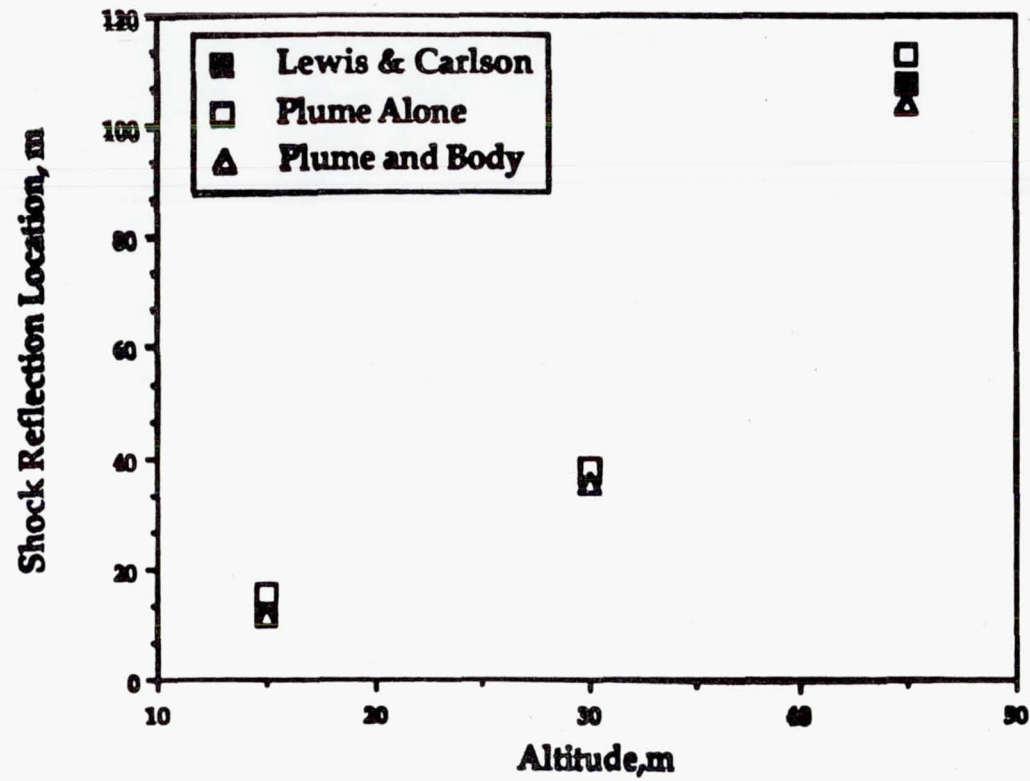
Comparison of Shock Reflection Location vs Altitude

3-D, HYPERSONIC, NOZZLE AFTER-BODY SOLUTIONS
Mach Contours — Symmetry and Cross-flow Planes
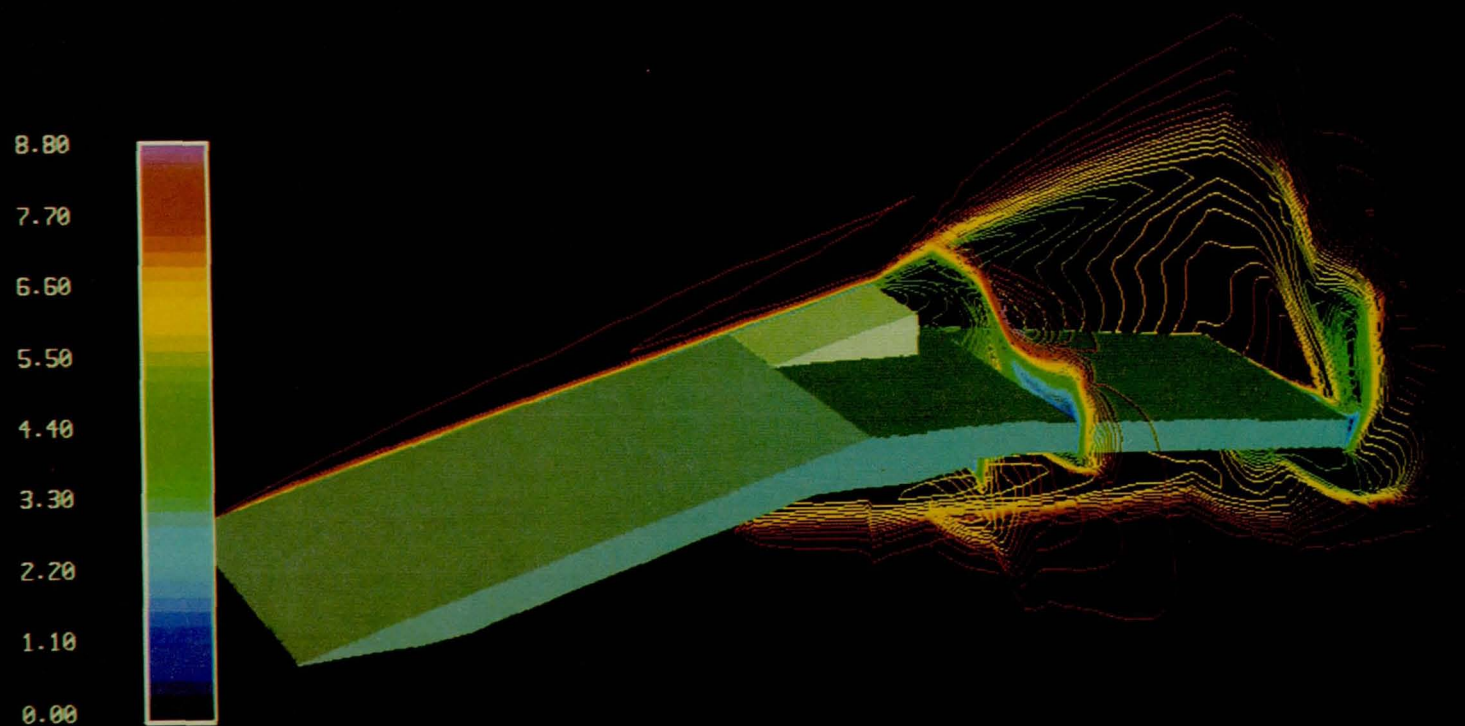
3-D, HYPERSONIC, NOZZLE AFTER-BODY SOLUTIONS
Surface Oil-flow Simulations
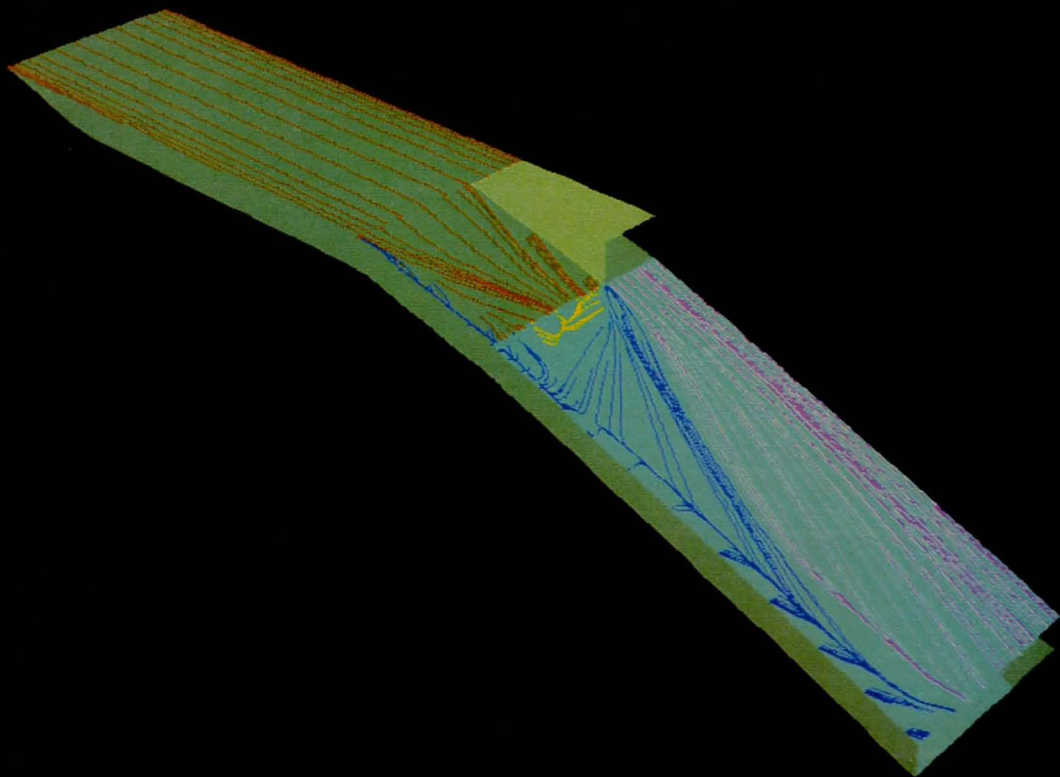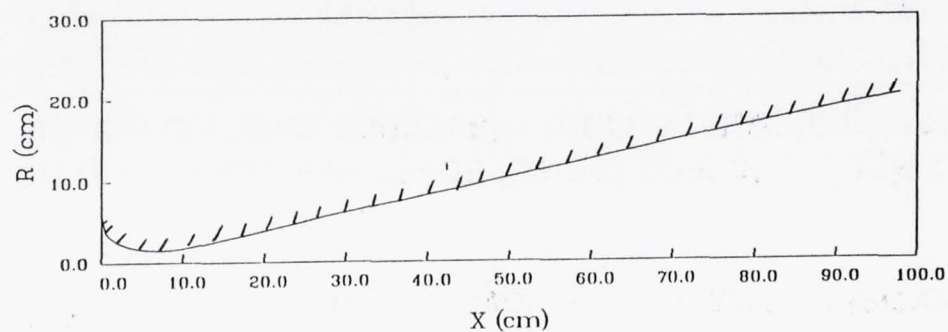
NOZZLE GEOMETRY

OH CONCENTRATIONS VERSUS DISTANCE ALONG NOZZLE AXIS
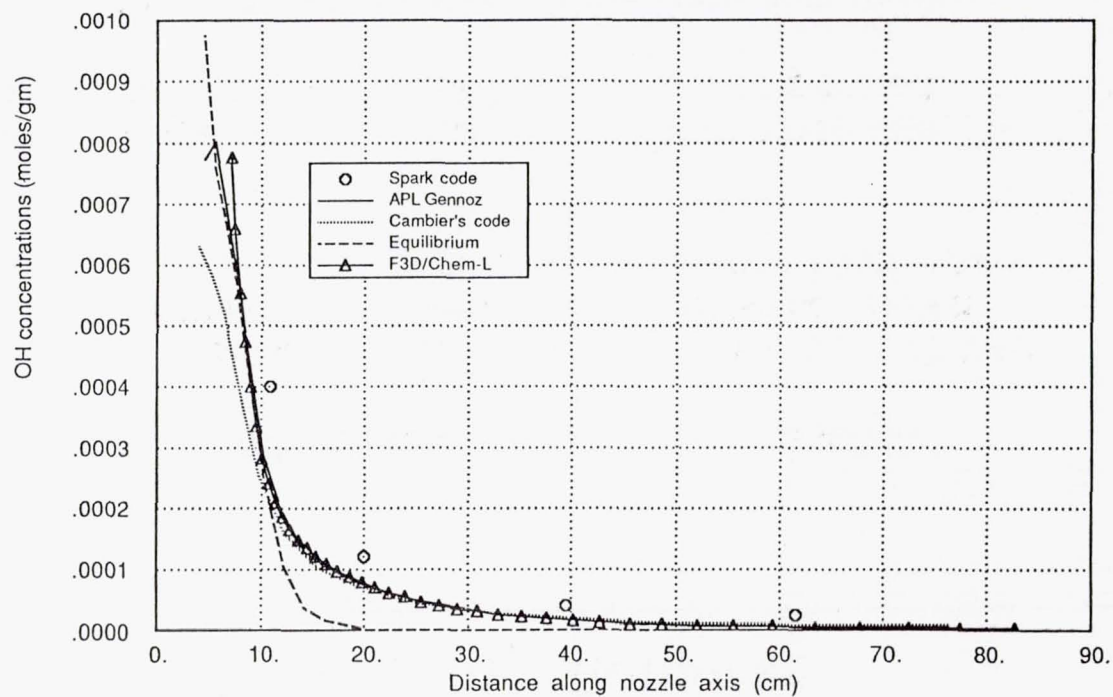
Concluding Remarks

- A variety of nozzle/plume flows have been successfully computed.
    - Complex flow structures and geometries have been studied
    - Good agreement with experimental and other computed results has been found for plume structure and Mach disk location.

- Equilibrium single-stream, equil. multi-stream, finite rate, and frozen chemistry packages have been incorporated.

- Turbulence modeling for complex plume flows is currently being studied

- 3-D code will be validated against hypersonic nozzle/afterbody experimental data

- Significant progress has been made toward goal of a single code capable of solving complex chemically reacting nozzle/plume flow fields.

APPLICATION OF CFD CODES FOR THE SIMULATION OF

SCRAMJET COMBUSTOR FLOWFIELDS

Tawit Chitsomboom
NASA Langley Research Center/Vigyan Research Associates, Inc.
Hampton, Virginia 23665-5225

and

G. Burton Northam
NASA Langley Research Center
Hampton, Virginia 23665-5225

ABSTRACT

An overview of CFD activities in the Hypersonic Propulsion Branch is
given. Elliptic and PNS codes that are being used for the simulation of
hydrogen-air combusting flowfields for scramjet applications are discussed.
Results of the computer codes are shown in comparison with those of the
experiments where applicable. Two classes of experiments will be presented:
(a) parallel injection of hydrogen into vitiated supersonic air flow; and (b)
normal injection of hydrogen into supersonic crossflow of vitiated air.

INTRODUCTION

- A number of CFD codes are being developed and
  validated at the Hypersonic Propulsion Branch,
  Fluid Mechanics Division, NASA Langley Research Center

- These CFD codes are being applied to solving flowfields
  inside hydrogen-fueled scramjet combustors

- Fully elliptic codes

  - 2D, Axisymmetric, 3D

  - Global two-step finite rate combustion model

  - Use unsplit explicit MacCormack Algorithm with point-implicit
    chemistry source terms

- PNS Codes

  - 2D, 3D

  - Global two-step finite rate combustion model

  - Implicit, coupled space marching procedure

3D-ELLIPTIC CFD CODE

- Unsplit explicit MacCormack finite-difference algorithm

- Solve 9 PDE's by finite-difference technique

  - 1   Density
  - 3   Momentum
  - 1   Energy
  - 4   Species (O_2, H_2, H_2O, OH)

- Treat chemical source terms implicitly to alleviate stiffness associated with fast chemistry

- 2D-Layer design for efficient use of memory

COMBUSTION AND TURBULENCE MODELS

- Four-species two-step finite-rate model (Rogers-Chinitz)

$$H_2 + O_2 \underset{kb1}{\overset{kf1}{\rightleftharpoons}} 2OH$$

$$2OH + H_2 \underset{kb2}{\overset{kf2}{\rightleftharpoons}} 2H_2O$$
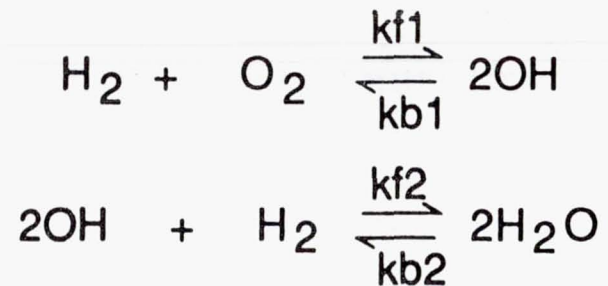
kf, kb = kf, kb (ϕ, T)

- Chemical source terms are obtained by applying the law of mass action

- Prandtl mixing length hypothesis for the jet mixing process

$$\mu_t = k\rho\omega\ell^2$$

$$k \approx 0.02$$

- Baldwin-Lomax model for near-wall turbulence

RESULTS OF 2D ELLIPTIC CODE

- Supersonic coaxial burner of hydrogen-air
- Hot vitiated outer air stream co-flowing with cold inner hydrogen fuel, exiting into a quiescent air
- Use "CARS" technique to obtain data point for oxygen, nitrogen and temperature
- Compare CARS data with CFD results
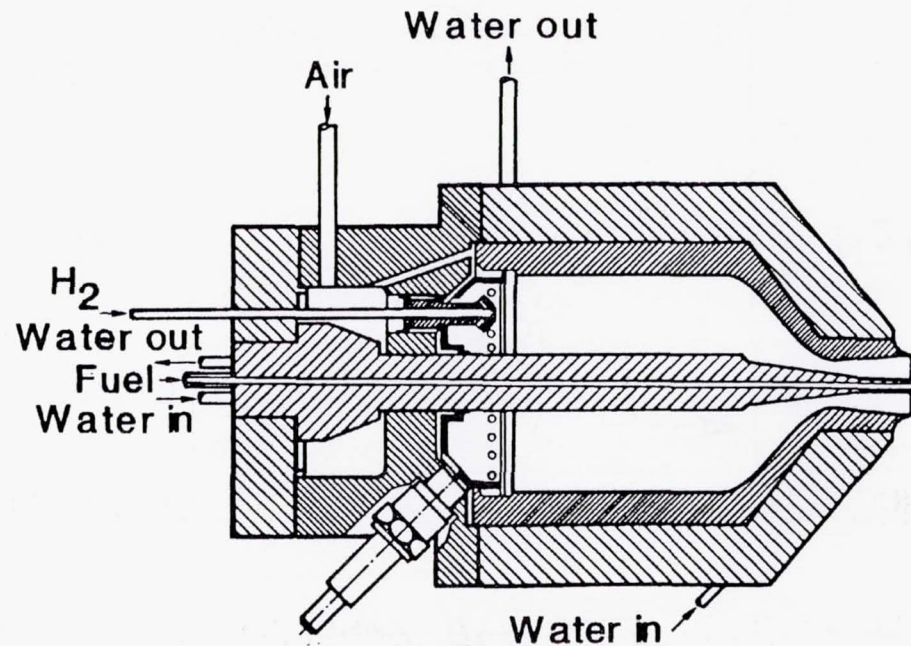
CENTERLINE DISTRIBUTION OF O_2 AND N_2 SPECIES

Symbol : CARS data
Lines : CFD data

O_2 Density x E^{-19}

N_2 Density x E^{-18}

X-inch
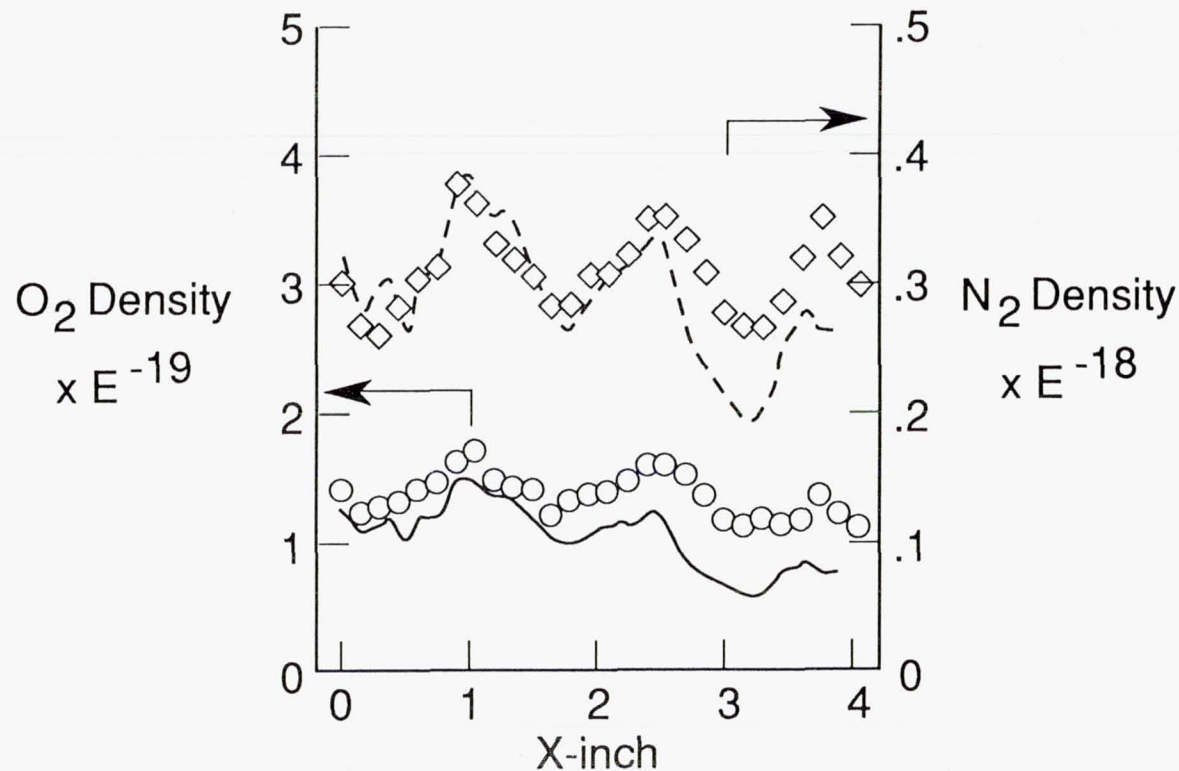
- Wavy distributions due to shock waves reflection from the free stream

- Flame was, infact, ignited by shock wave

RESULTS OF 2D ELLIPTIC CODE (CON'T)
Comparison of radial distributions at various streamwise stations

○ CARS   ——— CFD

Radius

(O_2 x E -18)

Radius

(N_2 x E -19)

Radius

(Temperature, K)

81
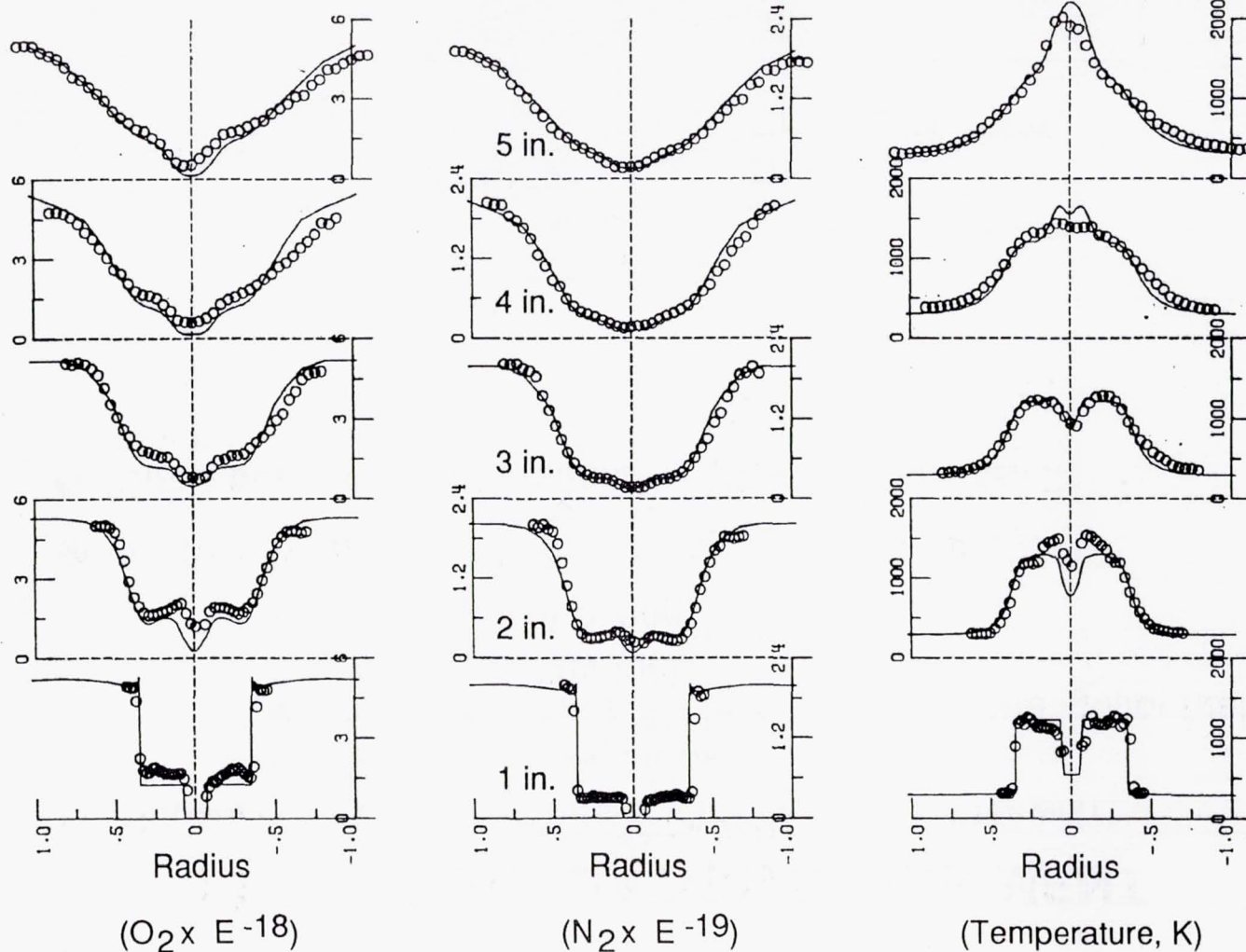
3D-CODE VALIDATION EXPERIMENT

- Subscale scramjet combustor (3.5"W, 4"L, 1.8"H) with :
    - Backward facing steps
    - Normal injections of H_2 pilot fuel, Silane ignitor fuel and H_2 primary fuel
    - 2^O, Nozzle (4 ft long)

- Inflow gas was Mach 2 vitiated air at high enthalpy.

- Static pressures were measured at various points along the surfaces

CONTOURS AND VECTORS PLOT THROUGH THE MAIN JET: NO COMBUSTION

Flow conditions: $T_S = 810K$, $P_S = 1$ atm, $M = 2; \phi = 0.43$

Pressure contours

Velocity vectors
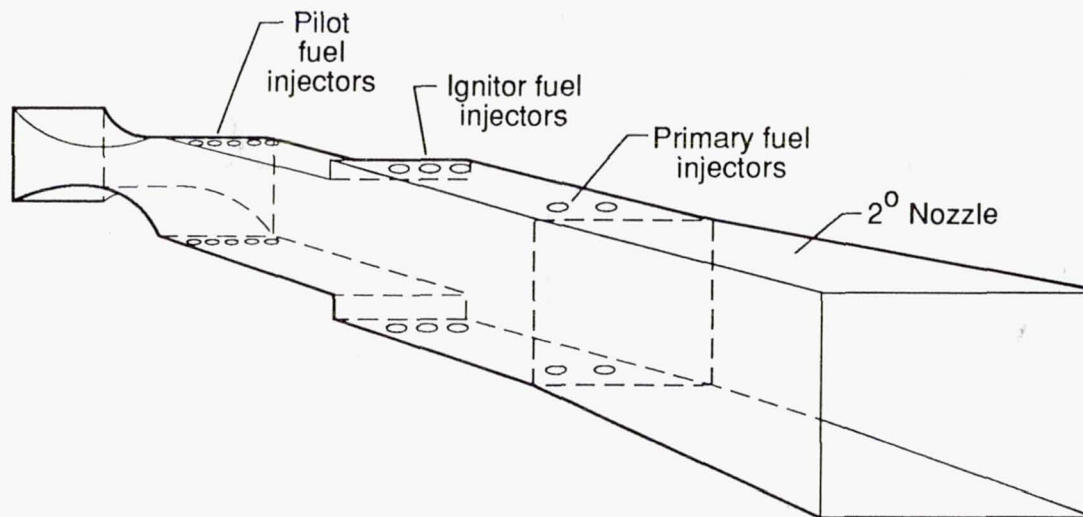
Hydrogen contours

PRESSURE DISTRIBUTIONS ALONG BOTTOM WALL
AT MIDPLANE

Flow conditions: $T_S = 1200K$, $P_S = 1$ atm, $M = 2$; $\phi = 0.48$

○   Experiment, reacting
◇   Experiment, non-reacting, no jets
——   CFD, reacting
- - -   CFD, non-reacting, with jets

Step

Jet

P-BOT

X/Gap
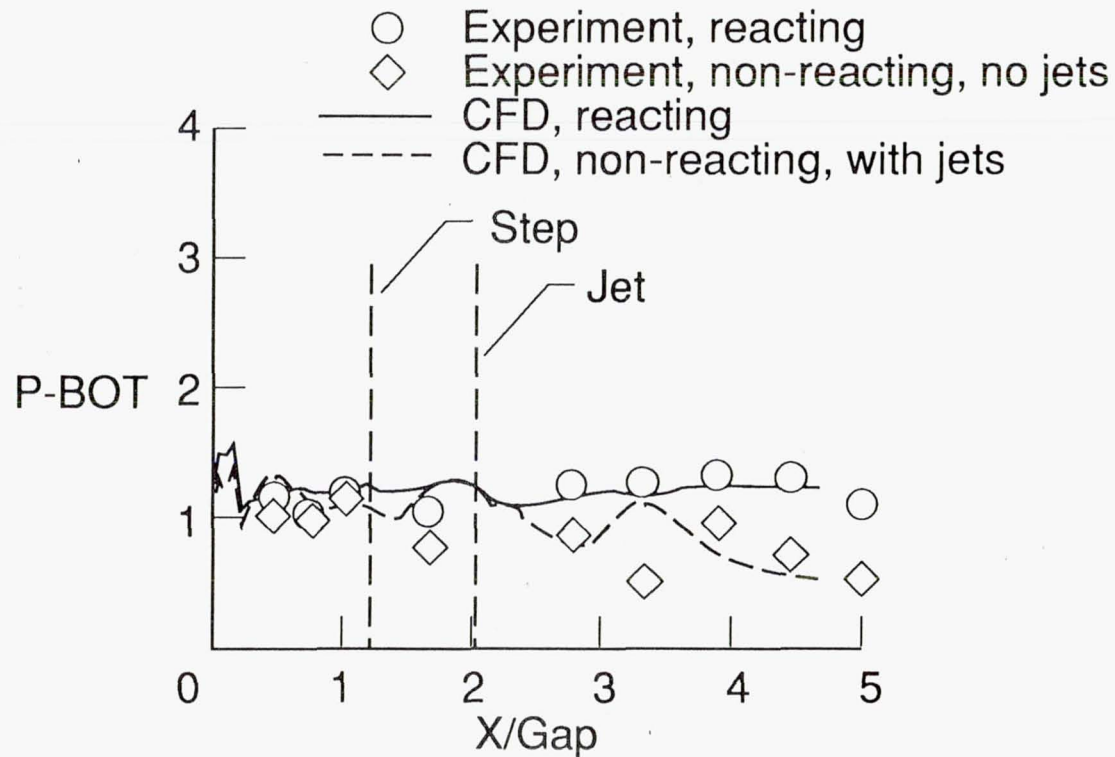
- Mixing and combustion efficiency at exit was underpredicted by 20%

- Prandtl mixing length hypothesis seems to work well

HYDROGEN CONTOURS AND VELOCITY VECTORS AT X = 1.5" DOWNSTREAM OF MAIN JET

Flow conditions: T_S = 1200K, P_S = 1 atm, M = 2; ϕ = 0.48
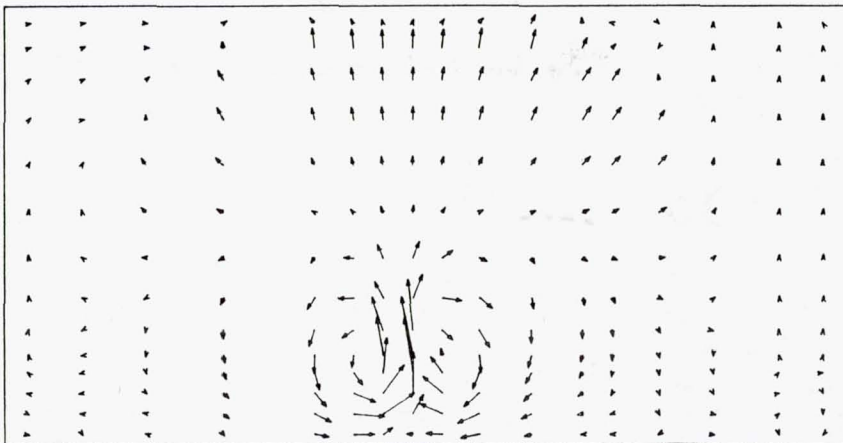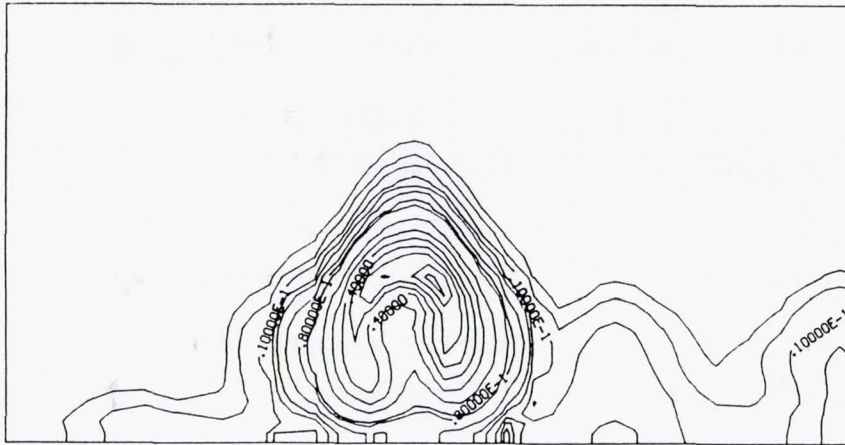
- Kidney shape profile

- Counter rotating vortices

3D-PNS CODE

- Applicable for supersonic high Reynolds number flow

- More efficient than full Navier-Stokes procedure

- Space marching technique using steady version of beam-warming algorithm (Vigneron, et al; Schiff-Steger)

- 4 Species, 2-step combustion model (Rogers-Chinitz) for hydrogen-air

- Fluid and chemical species are solved together creating block (9 x 9) tridiagonal system

- Baldwin-Lomax turbulence model

- See also AIAA Paper 84-0438

SCHEMATIC OF THE MODEL PROBLEM FOR THE 3D-PNS CODE
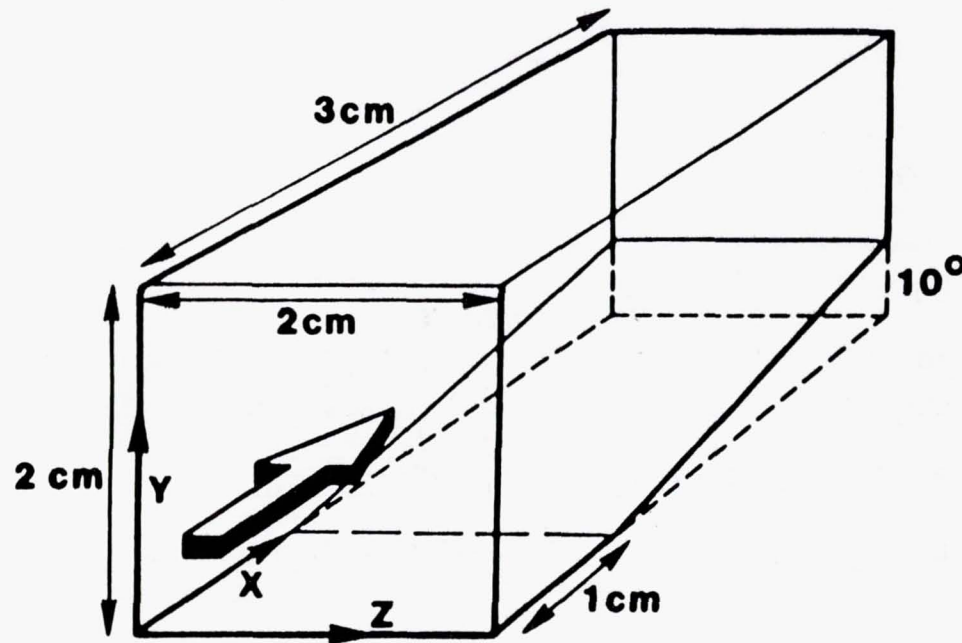
Inflow conditions: Mach = 4, T = 900K, P = 1 atm, Equivalence ratio = 1

FLOW FIELD AT THE MIDPLANE
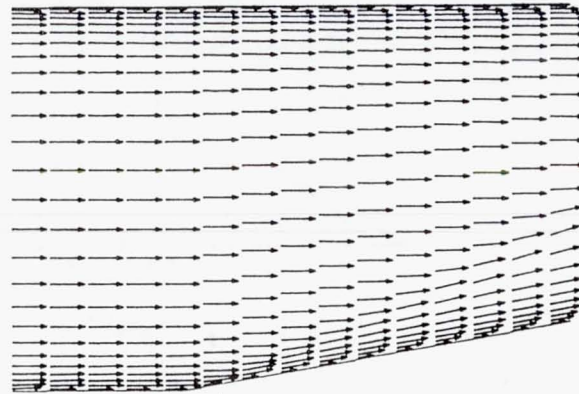
Velocity vectors

Pressure contours

Water mass fraction contours

CONCLUDING REMARKS

- Computer codes are being developed and validated at HPB, FMD, NASA-LaRC

- Results so far have shown that MacCormack algorithm, despite some drawbacks, can give good physical results

- Simple Prandtl mixing length scheme is both viable and economical

- More sophisticated combustion and turbulence models can be used at the expense of computer time which is very costly for any 3D-reacting flow simulation

- 3D-PNS code is an economical alternative to the costly elliptic code provided that certain conditions are met

- Need to make the PNS algorithm more robust

HYPERSONIC CFD APPLICATIONS AT NASA LANGLEY

USING CFL3D AND CFL3DE

Pamela F. Richardson
NASA Langley Research Center
Hampton, Virginia

N91-10874

CFL3D/CFL3DE

- Time-dependent conservation law form of compressible Euler and Navier-Stokes equations

  Upwind-biased spatial differencing (Flux Vector Splitting - FVS and Flux Difference Splitting - FDS)

- Thin-layer, finite-volume implementation with algebraic turbulence model

  Zonal grids - longitudinally patched (for hypersonic flows)

  - CFL3D

    - 3-factor implicit time advancement algorithm
    - Thin-layer viscous in 3 directions - two wall corner model

  - CFL3DE

    - Streamwise-relaxation crossflow-AF, space-marching Euler or PNS, first or second order
    - Perfect gas or equilibrium air

INDUSTRY USE STATUS OF CODES

● NASP prime contractors - all instructed in code use at workshop August 2-3, 1988.

  - Production code for NASP for McDonnell Aircraft Company

  - Some use at General Dynamics

● Other industry use

  - Boeing

  - Northrup

  - United Technologies Research Center

● University use

  - Iowa State University

● Other government use

  - Naval Surface Warfare Center

SR71 - GEOMETRY DEFINITION
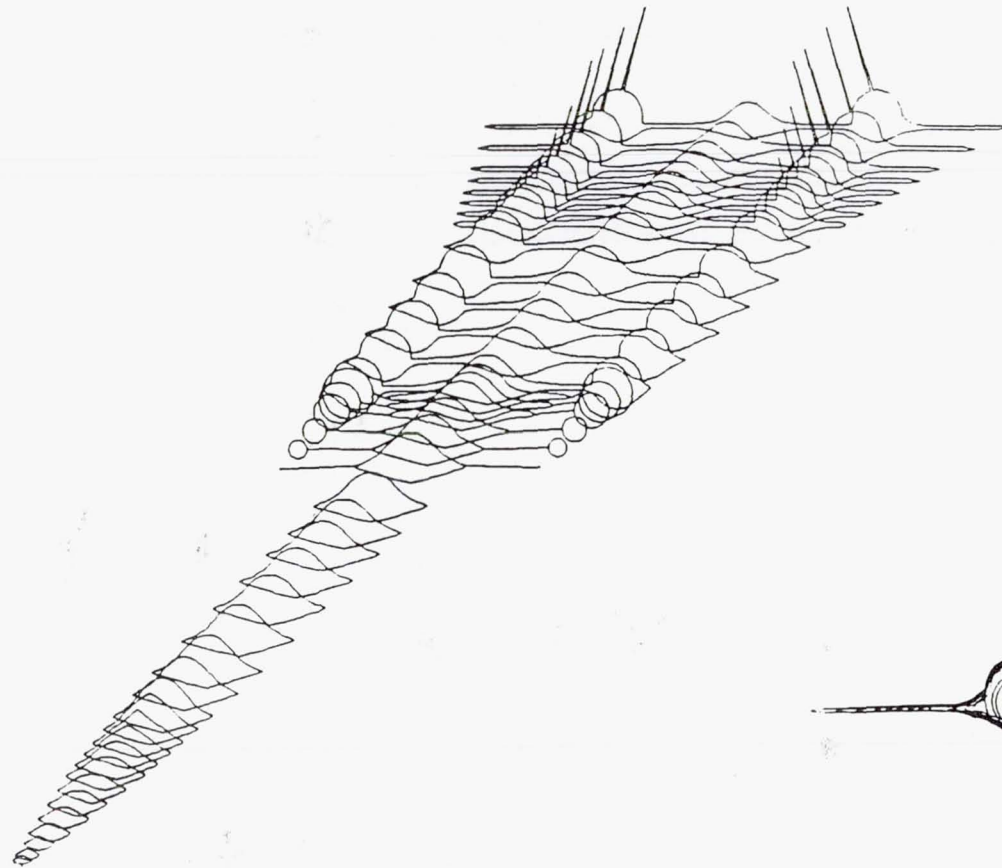
FOUR ZONES:
- 51X51X23
- 71X51X8
- 71X51X7
- 91X51X4

$$M_\infty = 3.0 \qquad \alpha = 0^o$$
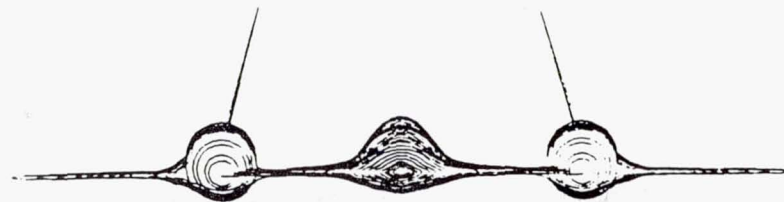
$$\rho_\infty = 0.088 kg/m^3 \qquad p_\infty = 5460 N/m^2$$

SR71 - EQUILIBRIUM AIR EULER SOLUTION

CROSS-SECTION PRESSURE DISTRIBUTIONS AND GRID DEFINITIONS
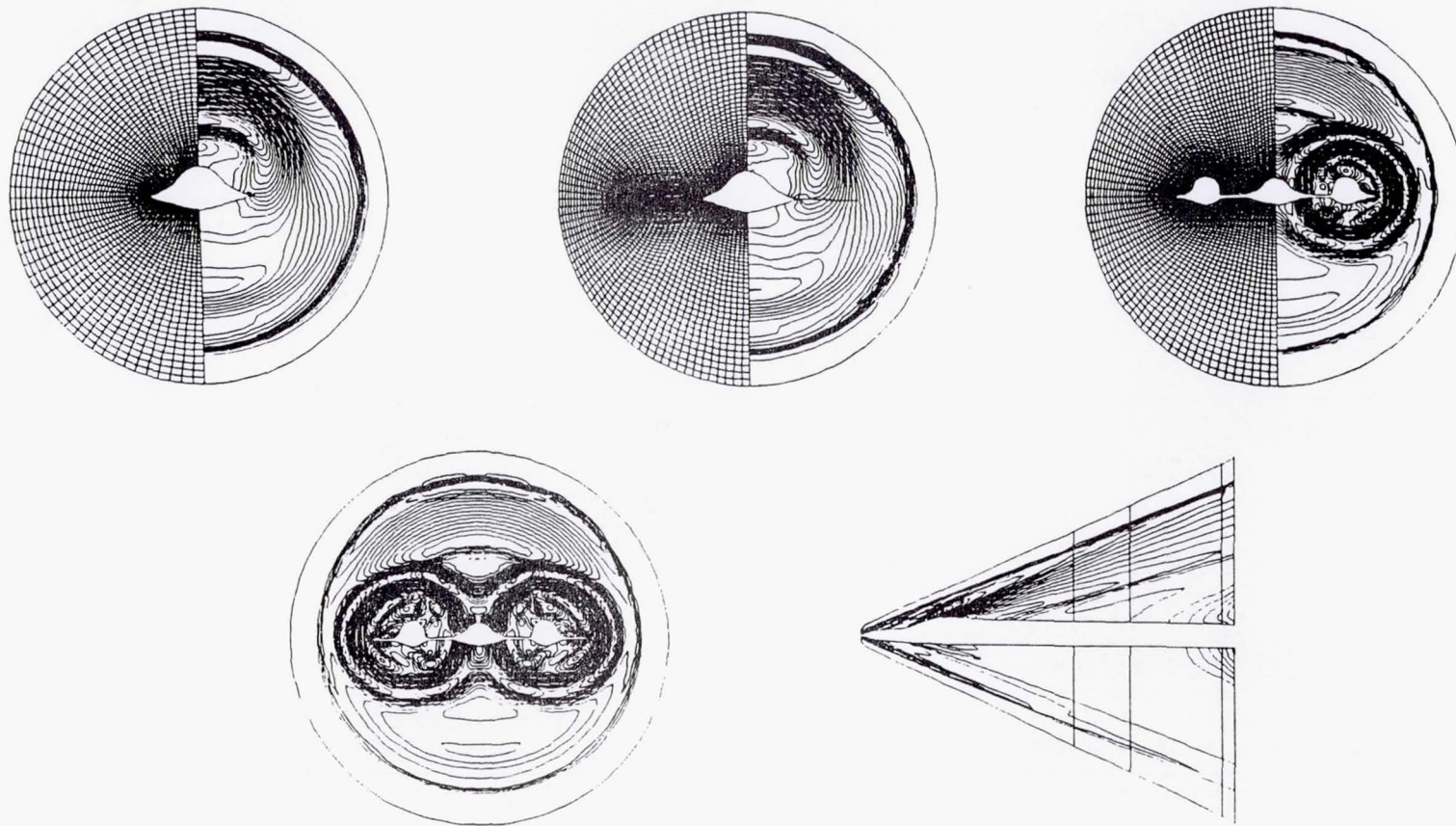
GOVERNMENT BASELINE

Pressure
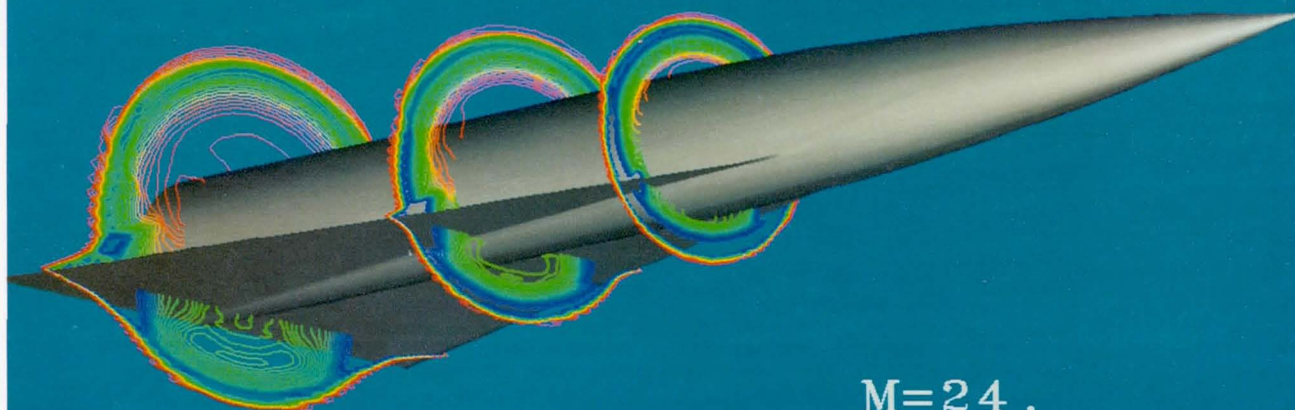
M=24.

AOA=1.

Re=9000./in

HYPERSONIC LIFTING BODY

TEMPERATURE
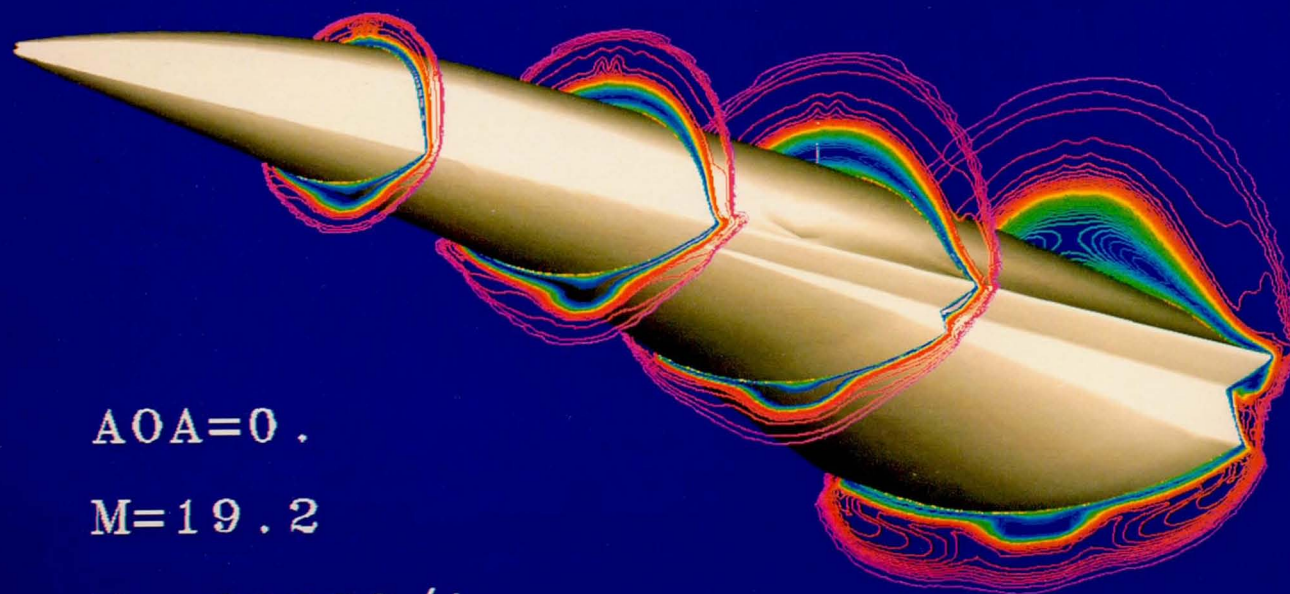
AOA=0.

M=19.2

Re=30000/in

PARTICLE TRACES

19.200	MACH
0.00 DEG	ALPHA
3.00×10**4	Re
65×65×46	GRID
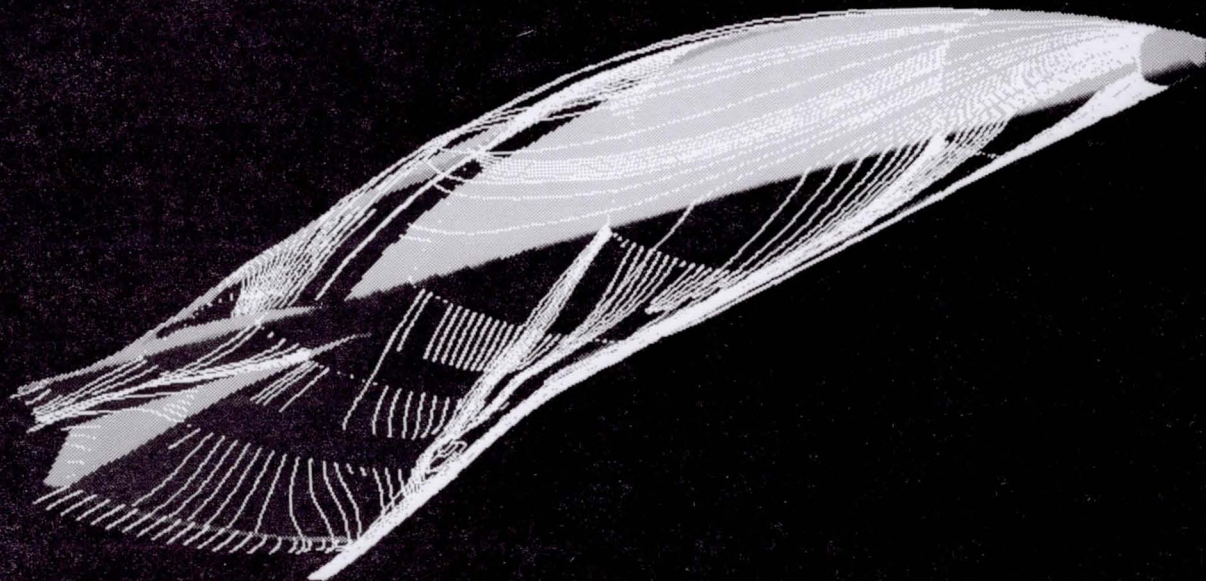
GRID DENSITY COMPARISON

CROSS-SECTION 45 (COWL PLANE)
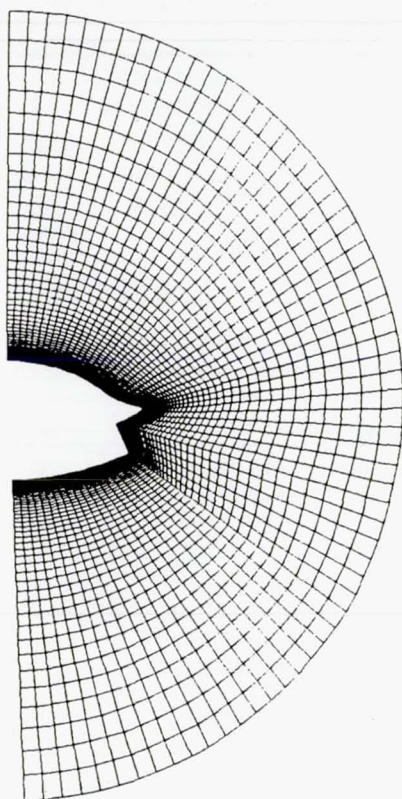
65 X 65 X 46 GRID
Y-PLUS ORDER 1.
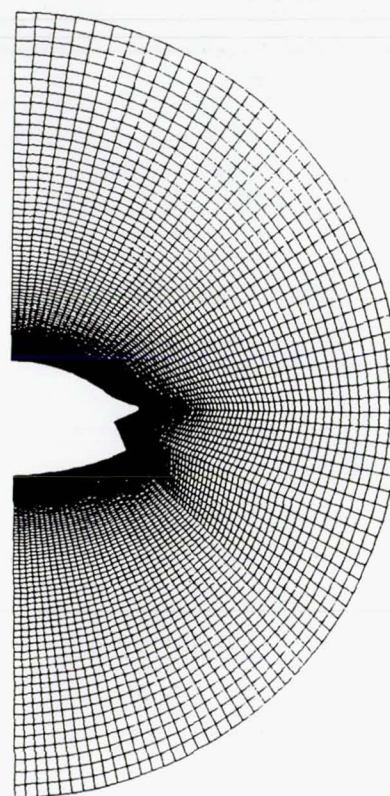
80 X 130 X 56 GRID
Y-PLUS ORDER .001

PRESSURE COMPARISONS

M = 12.55
Re = 2.7 million/ft.
Zero degrees angle of attack
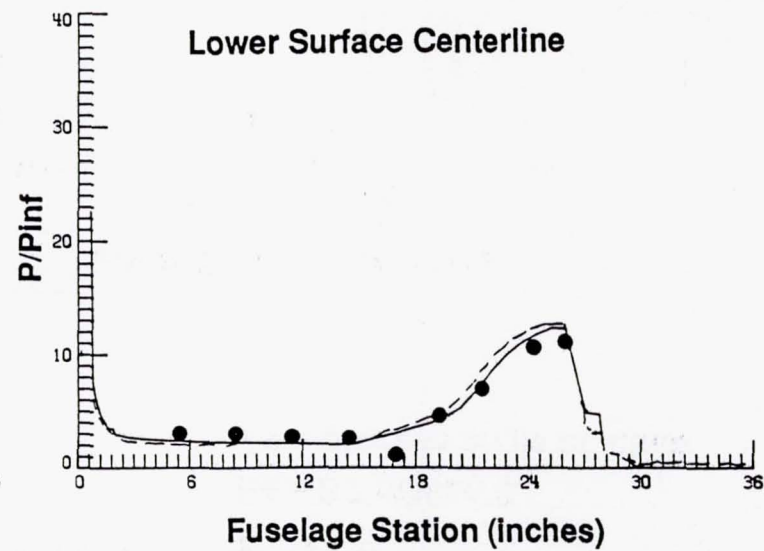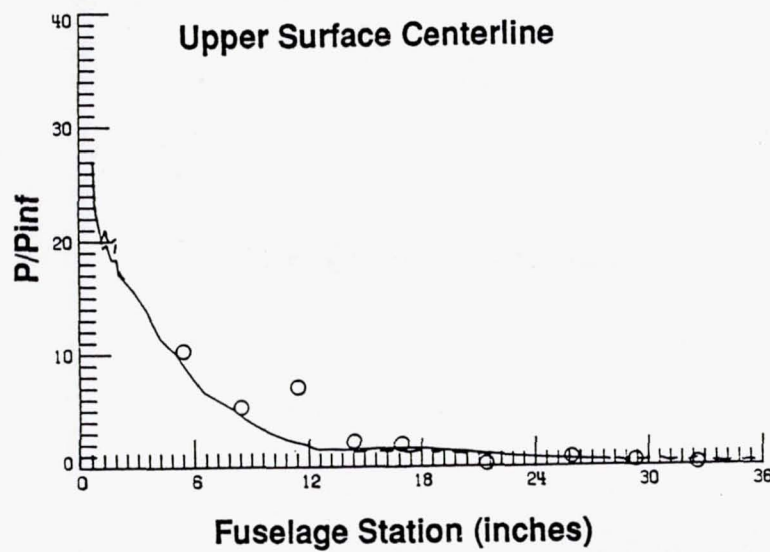
Open symbols - upper surface
Closed symbols - lower surface

HEET TRANSFER COMPARISONS

M = 12.55
Re = 2.7 million/ft.
Zero degrees angle of attack

104

AERODYNAMIC COEFFICIENTS COMPARISON MCDONNELL BLENDED WING BODY CFD AND EXPERIMENT

$M = 12.4, \alpha = 6^{o}, Re/L = 930,000/ft$

	CN	%ERROR	CA	%ERROR
AFWAL PNS	0.07154	3.1	0.02002	.9
MDC CFL3D	0.06956	5.8	0.01949	3.5
LARC CFL3D	0.07247	1.8	0.02154	6.6
Experiment	0.07382		0.02020	
Experimental Uncertainty		7.5		6.4

DENSITY

GENERIC NOZZLE AFTERBODY

COMPUTATIONAL METHODS BRANCH NASA LANGLY

CONTOUR LEVELS
0.00000
0.02500
0.05000
0.07500
0.10000
0.12500
0.15000
0.17500
0.20000
0.22500
0.25000
0.27500
0.30000
0.32500
0.35000
0.37500
0.40000
0.42500
0.45000
0.47500
0.50000
0.52500
0.55000
0.57500
0.60000
0.62500
0.65000
0.67500
0.70000
0.72500
0.75000
0.77500
0.80000
0.82500

3.987	MACH
0.00 DEG	ALPHA
2.34×10**5	Re
63×12×40	GRID 1
28×12×40	GRID 2

113

FUTURE PLANS RELATED TO THE NATIONAL AERO-SPACE PLANE PROGRAM

Continue to expand the envelope of capabilities for the code to include calculations of an entire NASP-like configuration

- Improved zonal capabilities for inlets with sweep and combustors

- Addition of non-equilibrium chemistry for combustor and nozzle/afterbody calculations

- All capabilities scheduled for production code by 1/90 (NASP Technology Maturation Program)

SESSION VIII

SPACE SHUTTLE

Chairman:
Luke A. Schutzenhofer
Chief, Computational Fluid Dynamics Branch
NASA Marshall Space Flight Center

NUMERICAL AERODYNAMIC SIMULATION OF THE SPACE SHUTTLE ASCENT ENVIRONMENT

J.P. Slotnick
Lockheed Engineering and Sciences Company, Houston, TX
F.W. Martin, Jr.
NASA Lyndon B. Johnson Space Center, Houston, TX

in collaboration with the

NASA Ames Space Shuttle Flow Simulation Group
P.G. Buning, I.T. Chiu, R.L. Meakin, S. Obayashi, Y.M. Rizk
S. Ben-Shmuel, J.L. Steger, and M. Yarrow
NASA Ames Research Center, Moffett Field, CA

ABSTRACT

After the STS 51-L accident, an extensive review of the Space Shuttle Orbiter's ascent aerodynamic loads uncovered several questionable areas that required further analysis. The insight gained by comparing the Shuttle ascent CFD numerical simulations, obtained by the NASA Ames Space Shuttle Flow Simulation Group led by Dr. J.L. Steger, to the current IVBC-3 aerodynamic loads database was instrumental in resolving uncertainties on the Orbiter payload bay doors and fuselage. Initial confidence in the numerical simulations was gained by comparing them with the limited flight data that had been obtained during the Orbiter Flight Test (OFT) program. Current CFD results exist for Mach numbers 0.6, 0.9, 1.05, 1.55, 2.0, and 2.5. Since the pre STS-1 wind tunnel test program (IA-105) often yields considerable differences when compared to STS-5 flight data, the $M_\infty = 1.05$ transonic case is the most investigated. The IA308 mated-vehicle hot gas plume wind tunnel test, recently completed at AEDC 16T (transonic) and Lewis (hypersonic), is also used to compare with the computation where applicable.

Objective

○ *Joint* effort between the ARC team led by J.L. Steger and P.G. Buning and a JSC team led by F.W. Martin, Jr.

○ ARC Team : Develop the technology to numerically simulate the complex launch vehicle (SSLV) geometry in a time accurate manner to
- compute SSLV flowfield data
- support Fast Separation Abort study
- assist JSC with Orbiter problematic issues:
  - Crew Escape flowfield
  - STS-27 Debris Study flowfields

○ JSC Team : Apply the CFD technology to gain insight into the ascent aerodynamic loads environment
- SSLV payload bay pressure distribution
- Orbiter Wing Loads

Jeff P. Slotnick / *March 8, 1989*

Scope

o ARC Team

- Model the Orbiter ascent configuration with the *Chimera* composite grid discretization approach.
- Overset body-conforming grids for each major component (CALSPAN *Pegasus* code).
- Apply *F3D*, an implicit approximately factored finite-difference procedure, to solve the three-dimensional thin-layer Navier-Stokes equations.
- Employ the NAS Cray 2 and Cray Y-MP.

o JSC Team

- Provide technical guidance and evaluate ARC results with respect to existing databases:
  - ▷ IA-105 WTT, high resolution model.
  - ▷ IA-308 WTT, hot gas plume simulation.
  - ▷ *Limited* flight data from STS-1 through STS-5.
  - ▷ IVBC-3 operational database.

Jeff P. Slotnick / *March 8, 1989*

Justification

The Orbiter's modest structural capability, coupled with a complex launch vehicle configuration and severe ascent environment, places unprecendented demands on the aerodynamacist.

- ○ Orbiter structure was designed to civil transport specifications.

    - • Consistent with entry flight envelope.
    - • $\bar{q} \approx 350$ psf, $g_z=2.5$ ($g_z=2.25$ as weight increases).

- ○ Ascent environment is considerably more severe, $\bar{q}=750\text{-}819$ psf, with the simultaneous occurance of:

    - • maximum $\bar{q}$
    - • jet stream penetration (perturbates α, β and $\bar{q}$)
    - • transonic flow field
    - • maximum differential pressure, inside-outside, as the vehicle vents
    - • plume/flow field interactions
    - • High R_e ($\sim$ 100 million) at maximum load condition

○ Discrepancies exist between aerodynamic predictions and flight experience.
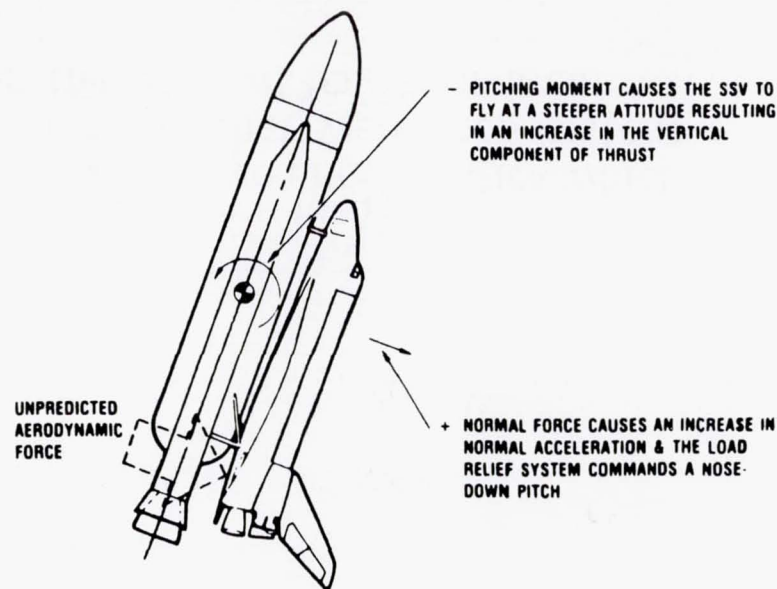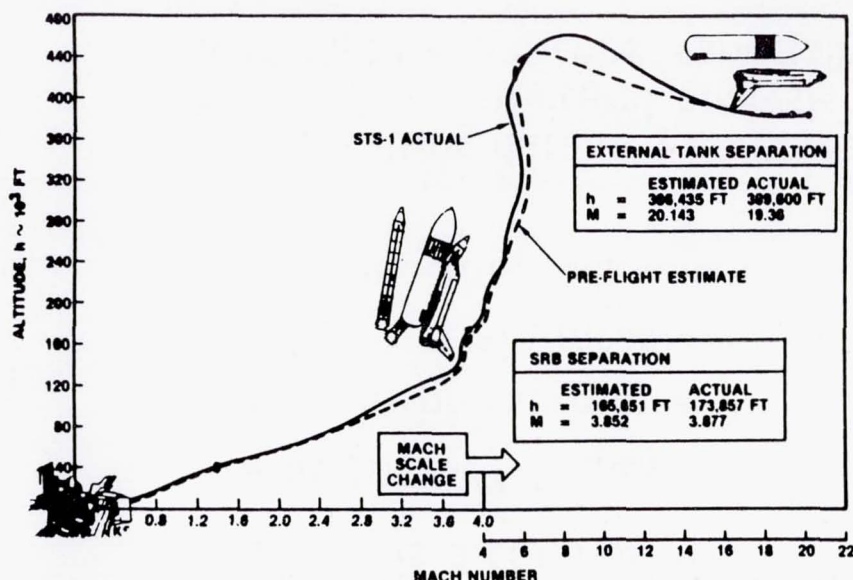
○ Force and moment data was easily corrected **with flight derived** aerodynamic increments.

○ Aerodynamic loads (pressure distribution) cannot be readily corrected because of *limited* flight pressure measurements.

Jeff P. Slotnick / *March 8, 1989*

121

Current Database

○ The *Integrated Vehicle Baseline Configuration* (IVBC) - 3 aero loads database is a composite of

- IA-105 WTT data
- Flight pressure measurements
- Flight strain measurements
- Engineering judgement

○ This resulting database contains relatively large uncertainties which have led to structural analysis predictions that were inconsistent with flight experience, especially in the payload bay door area.

Jeff P. Slotnick / *March 8, 1989*

Selected STS-5 Tap Points

V07P9484

V07P9495

V07P9126

V07P9108

V07P9132

V07P9860

V07P9128

123
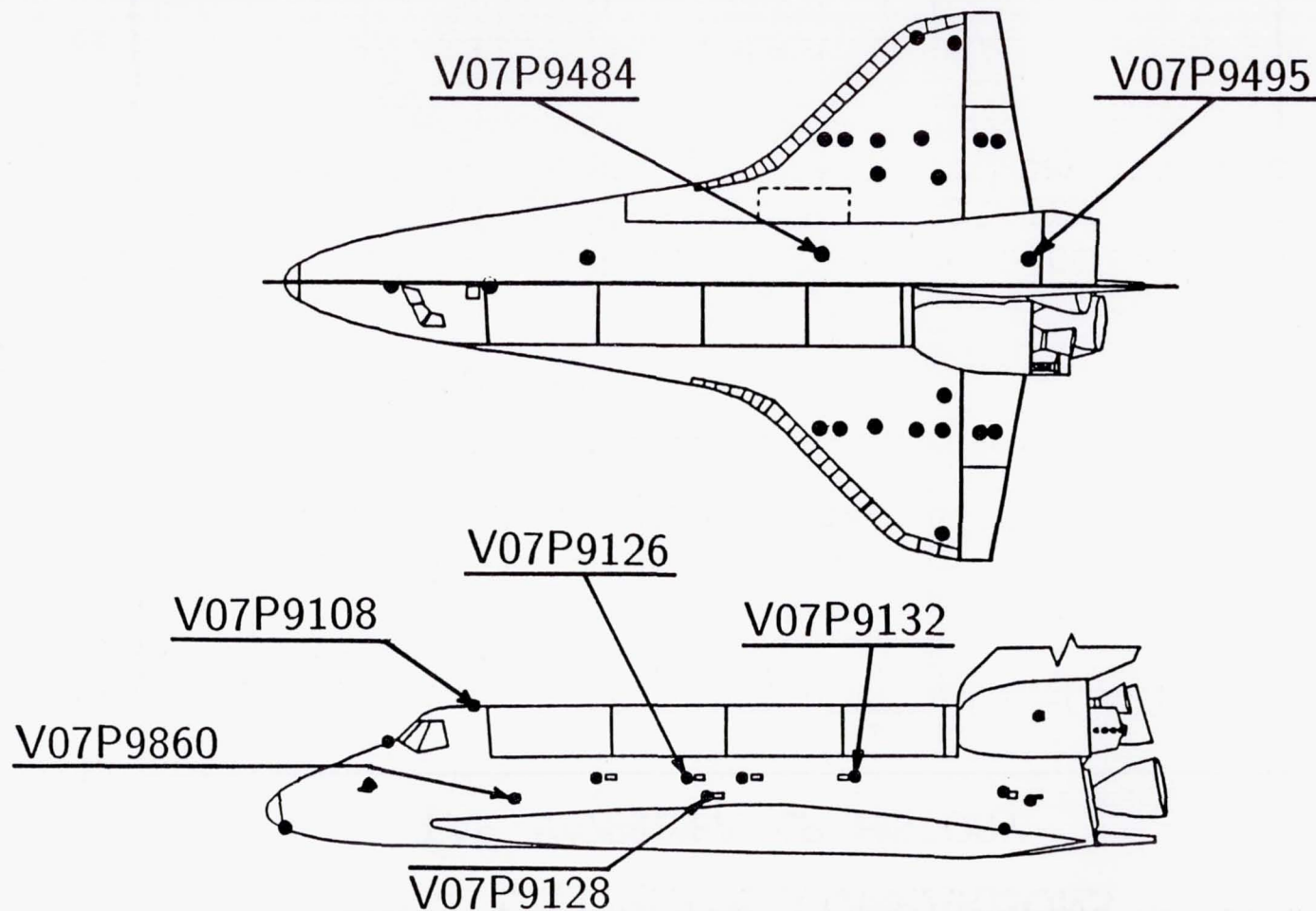
Jeff P. Slotnick / March 8, 1989

AERO DATABASE COMPARISONS
TAP V07P9108A CP HISTORY
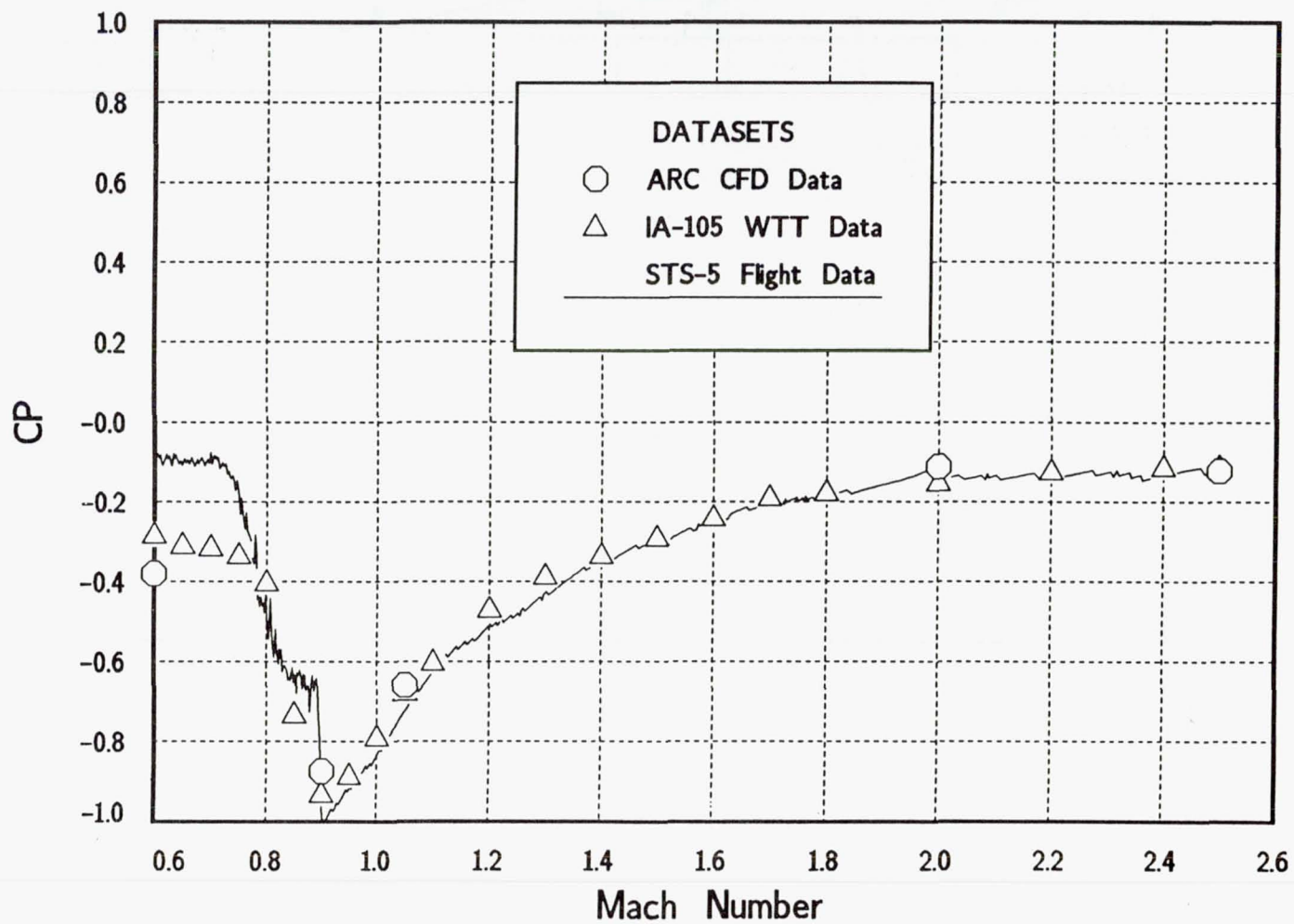
AERO DATABASE COMPARISONS

TAP V07P9495A CP HISTORY
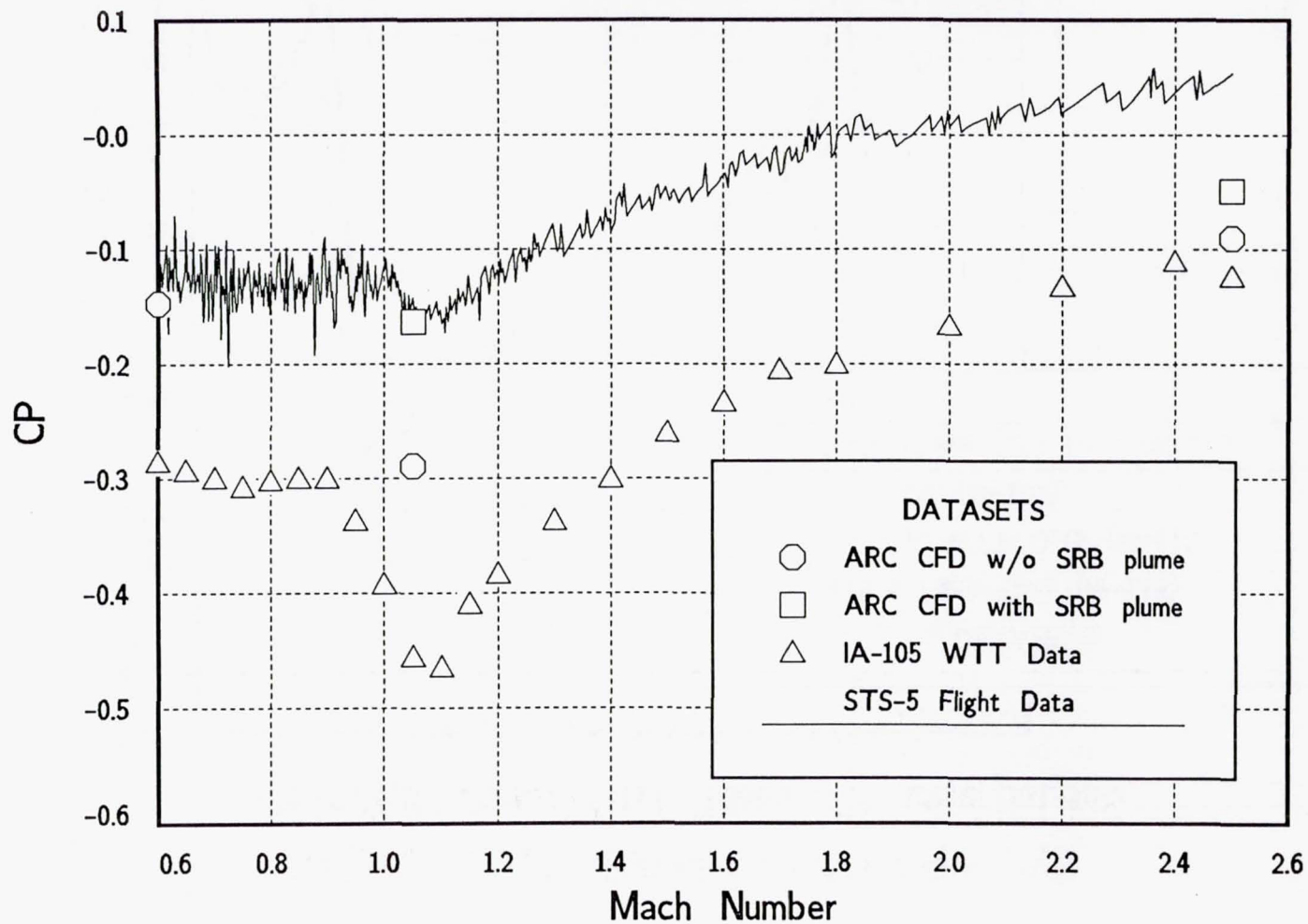
AERO DATABASE COMPARISONS
ORBITER Upper Pitch Plane CP Distributions
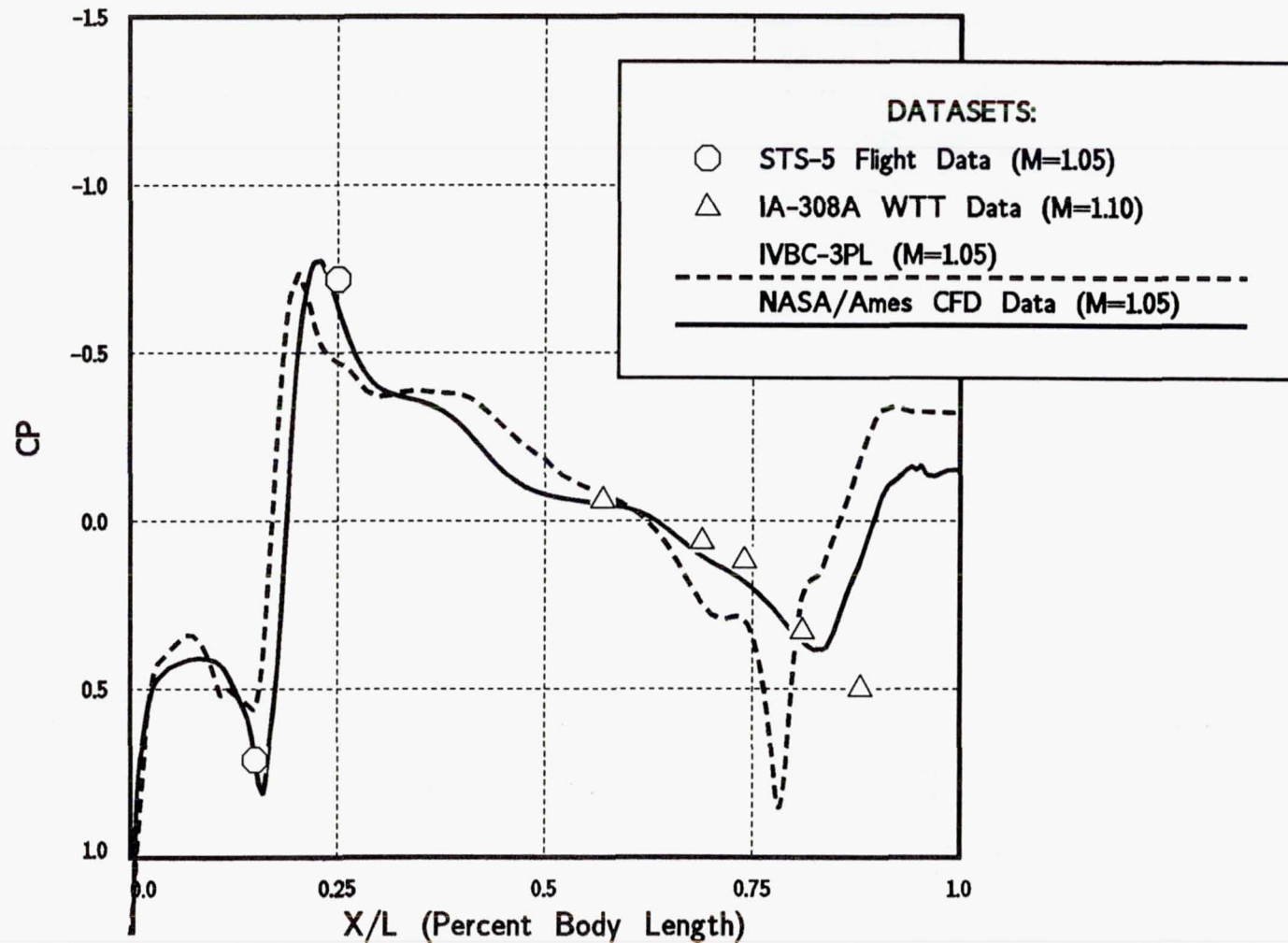
AERO DATABASE COMPARISONS
ORBITER Mid-Fuselage Region CP Distributions

DATASETS:

○ STS-5 Flight Data (M=1.05)

△ IA308A WTT Data (M=1.10)

-- -- IVBC-3PL Data (M=1.05)

—— NASA/Ames CFD Data (M=1.05)

CP

X/L (Percent Body Length)
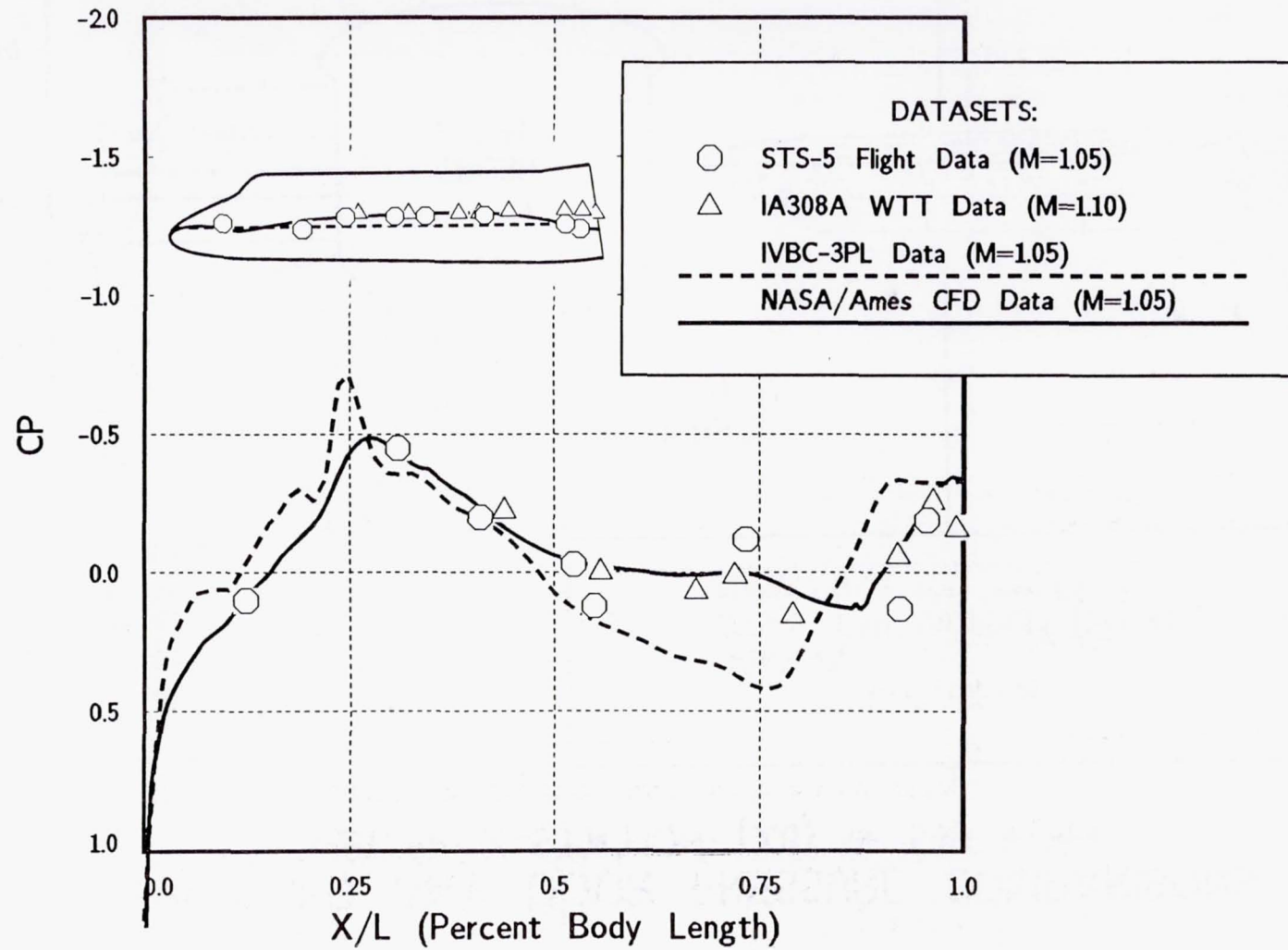
PAYLOAD BAY DOOR PRESSURE COMPARISONS
ORBITER X-STATION (X0) = 590 inches
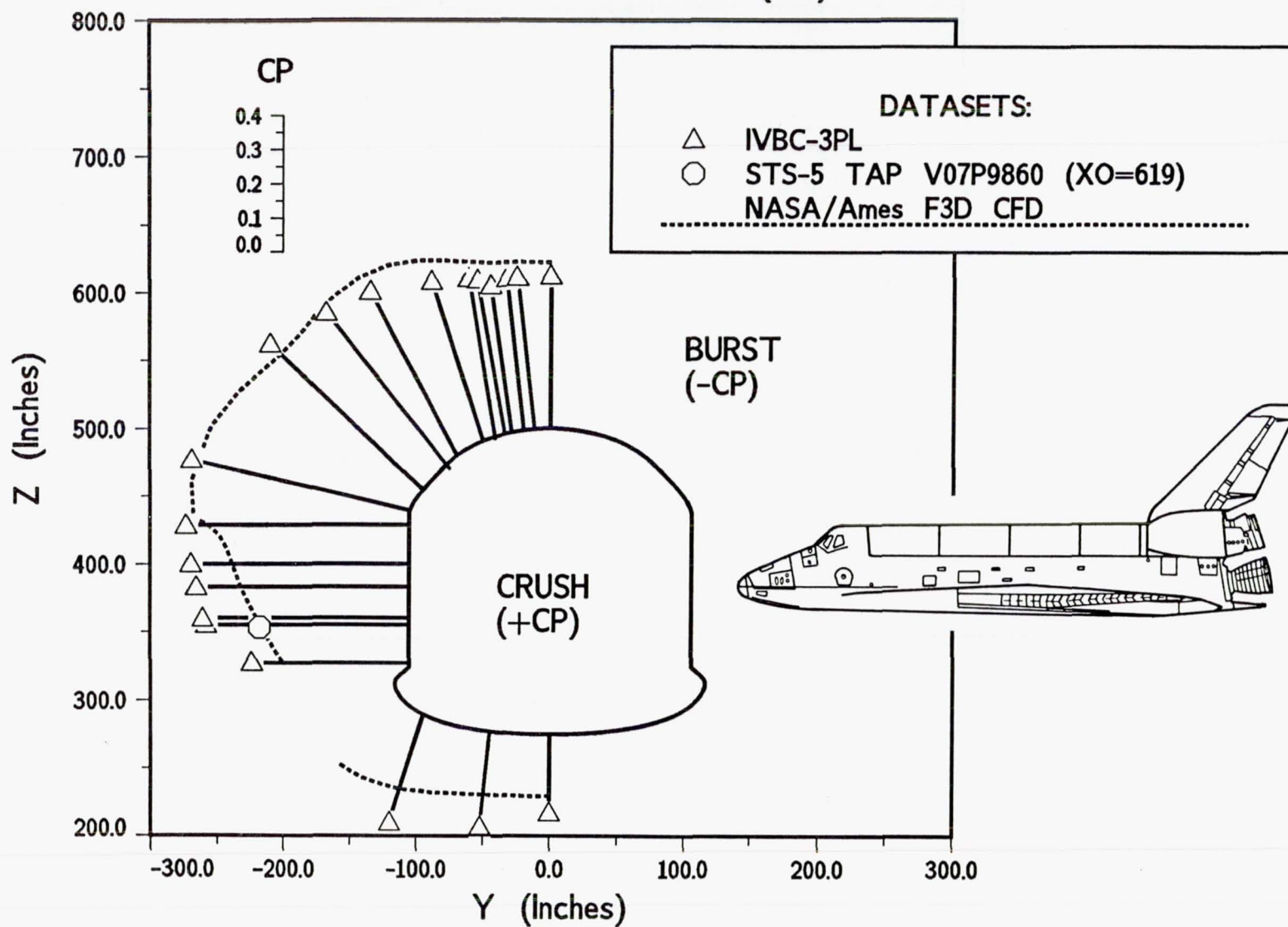
PAYLOAD BAY DOOR PRESSURE COMPARISONS
ORBITER X-STATION (X0) = 905 inches

CP

0.4
0.3
0.2
0.1
0.0

DATASETS:
△ IVBC–3PL
○ STS–5 TAP V07P9126 (XO=885)
◇ STS–5 TAP V07P9128 (XO=915)
NASA/Ames CFD

BURST
(–CP)

CRUSH
(+CP)

Z (Inches)

Y (Inches)

800.0
700.0
600.0
500.0
400.0
300.0
200.0

-300.0 -200.0 -100.0 0.0 100.0 200.0 300.0

129
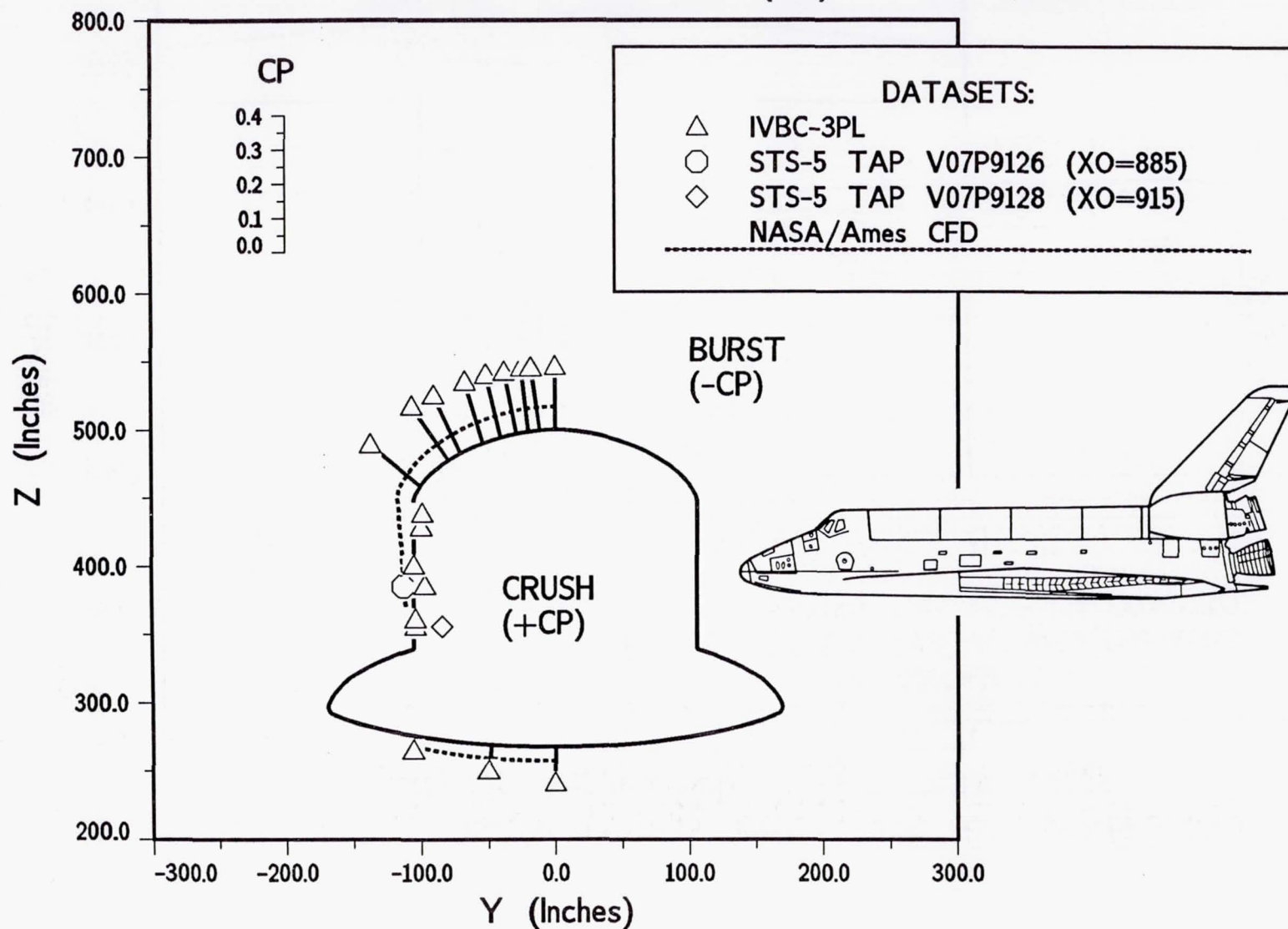
PAYLOAD BAY DOOR PRESSURE COMPARISONS
ORBITER X-STATION (X0) = 1214 inches
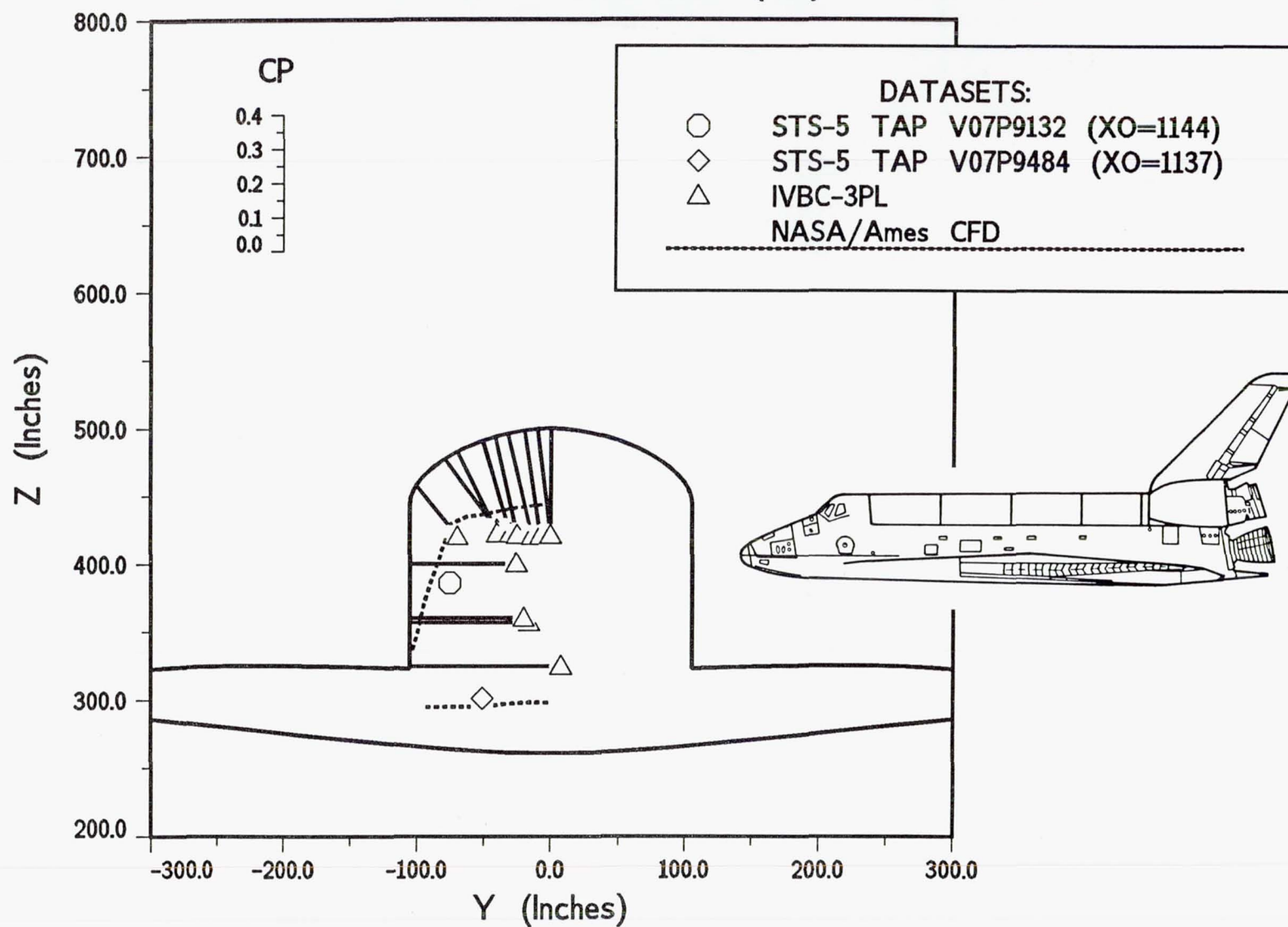
$$\boxed{\text{Status}}$$

○ Preliminary CFD results have been instrumental in gaining insight into the present design aero database. Even with the large advances in SSLV geometry modelling, all three aero data sources (flight, wind tunnel, and CFD) are required to completely understand Shuttle ascent aerodynamics and structural loads.

○ On-going CFD Activities:

- Add the SRB attach ring and IEA box protuberances into the SSLV grid system.
- Add more realistic aft attach hardware to the geometry model to better simulate blockage effects.
- Add $\gamma = \gamma(T)$ to the F3D flow solver.
- Grid the vertical tail and include in the geometry model.
- Grid the SSMEs and incorporate the SSME plumes into the solution.

Jeff P. Slotnick / March 8, 1989

COMPUTATIONAL FLUID DYNAMICS ANALYSIS OF SPACE SHUTTLE MAIN PROPULSION FEED LINE 17-INCH DISCONNECT VALVES

Max Kandula* and Daniel Pearce**
Lockheed Engineering and Sciences Company
Houston,Texas

ABSTRACT

A steady incompressible three-dimensional (3-D) viscous flow analysis has been conducted for the Space Shuttle Main Propulsion External Tank (ET)/Orbiter (ORB) propellant feed line quick separable 17-inch disconnect flapper valves for liquid oxygen (LO_2) and liquid hydrogen (LH_2). The main objectives of the analyís were to predict and correlate the hydrodynamic stability of the flappers and pressure drop with available water test data.

Computational Fluid Dynamics (CFD) computer codes were procured at no cost from the public domain, and were modified and extended to carry out the disconnect flow analysis. The grid generator codes SVTGD3D and INGRID, developed by Sverdrup Technology Inc., were obtained from Arnold Air Force Station, Tennessee. NASA Ames Research Center supplied the flow solution code INS3D, and the color graphics code PLOT3D. A driver routine was developed to automate the grid generation process. Components such as pipes, elbows and flappers can be generated with simple commands, and flapper angles can be varied easily. The flow solver INS3D code was modified to treat interior flappers, and other interfacing routines were developed, which include a turbulence model, a force/moment routine, a time-step routine, and initial and boundary conditions. In particular, an under-relaxation scheme was implemented to enhance the solution stability.

Major physical assumptions and simplifications made in the analysis include the neglect of linkages (drive/follower arms), slightly reduced flapper diameter, and smooth solid surfaces. A grid size of 54x21x25 was employed for both the LO_2 and LH_2 units. Mixing length theory applied to turbulent shear flow in pipes formed the basis for the simple turbulence model.

Results of the analysis are presented for LO_2 and LH_2 disconnects. The predicted stop loads, hydrodynamic stability boundaries of the ET and orbiter flappers, and pressure drop across the valve compare well with the water test data, covering a tube Reynolds number of 3.5E06 for LO_2 unit and 2.4E06 for LH_2 unit. The ability to predict the valve performance and flapper stability over a wide range of flow rates and flapper angle combinations demonstrates the validity of the CFD model.

---

* Advanced Systems Engineering Specialist
** Engineer

LO$_2$ DISCONNECT VALVE

	WATER	FLIGHT
Re =	3.5E06	20E06

EXTERNAL TANK

SEPARATION INTERFACE

ORBITER

FOLLOWER ARM

STOP LOAD

FLOW

STOP LOAD

17 IN.

4.5° ±0.25°   CLOSE

CLOSE 3.0° ±0.25°

90° INLET BEND

11.50 IN.

DRIVE ARM

LH$_2$ DISCONNECT VALVE

26^0 INLET BEND   0.750 $\pm$ 0.250   FLOW   2.40 $\pm$ 0.250

4.0 IN.
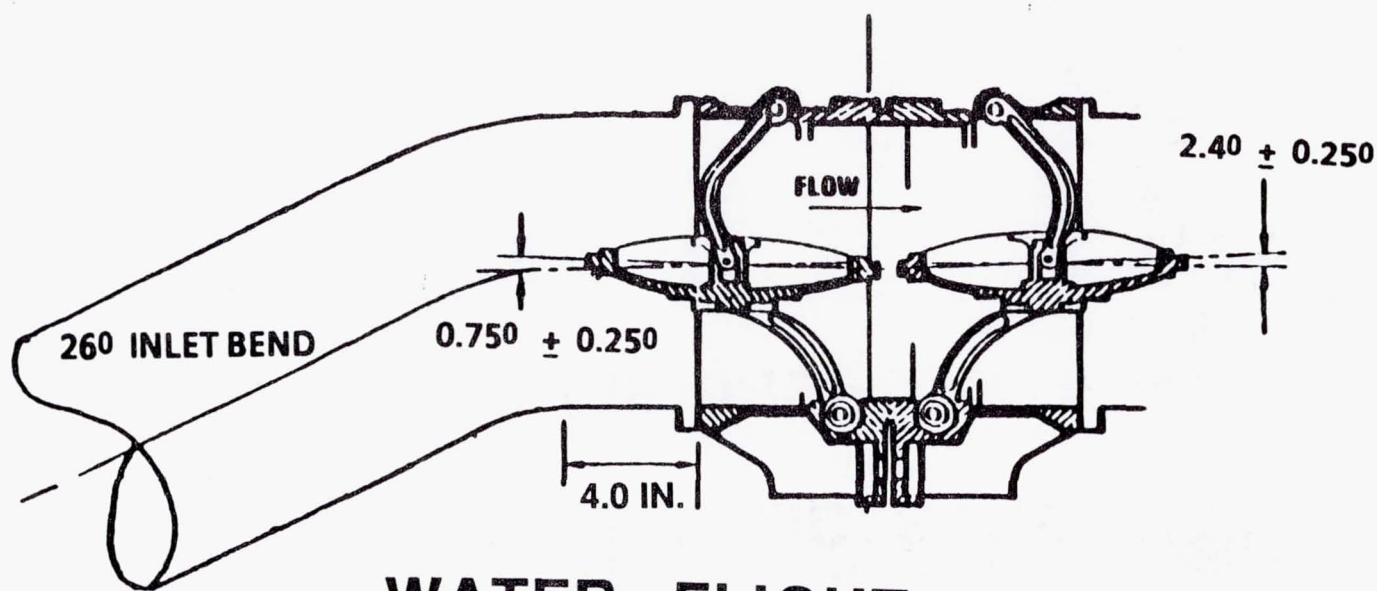
	WATER	FLIGHT
Re =	2.7E06	50E06

OBJECTIVES

- **PREDICT**

    - **HYDRODYNAMIC STABILITY**

    - **PRESSURE DROP**

    - **CAVITATION**

136

COMPUTATIONAL GRID

CODE : SVTGD3D (SONI ET AL. 1986)
ORG   : SVERDRUP / AIR FORCE
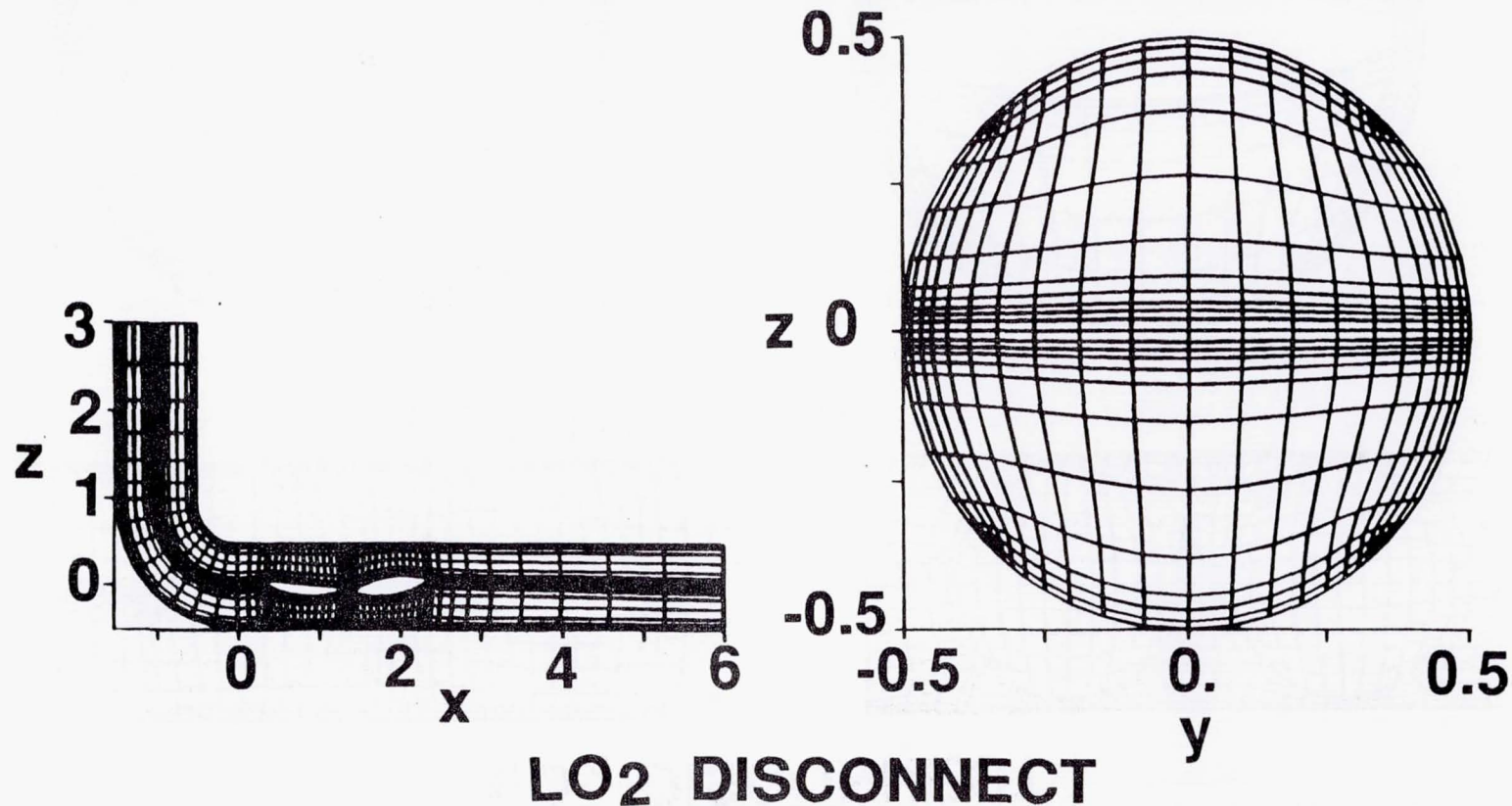
LO2 DISCONNECT

COMPUTATIONAL GRID
LO$_2$ DISCONNECT
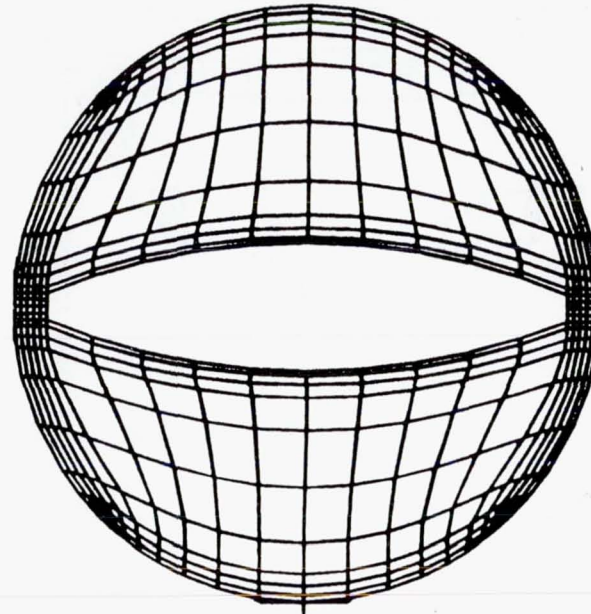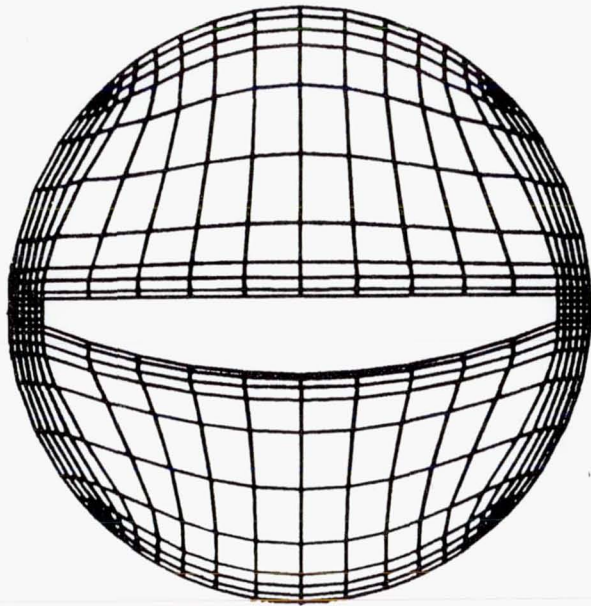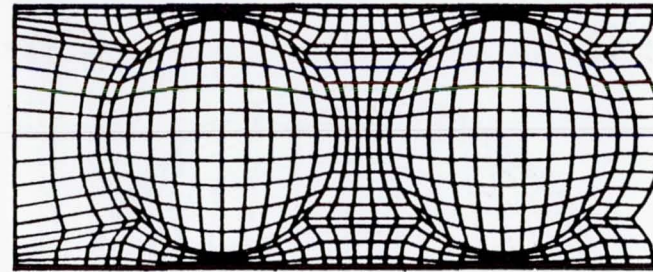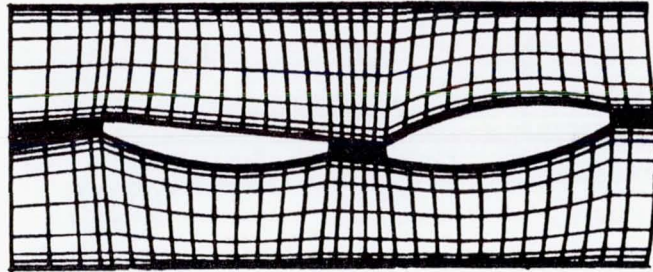
FLOW SOLUTION DEVELOPMENT

CODE : INS3D (KWAK ET AL. , 1985)
ORG : NASA AMES

- INTERNAL OBSTACLES
- TURBULENCE MODEL
- UNDER-RELAXATION

ANGLE CORRECTIONS

LO_2 : $\begin{cases} ET & : FA = (PA+1) \text{ deg} \\ ORB : & FA = (PA-5) \text{ deg} \\ PA = PRELOAD \text{ ANGLE} \\ FA = FLIGHT \text{ ANGLE} \end{cases}$

LH_2 : NONE

UNDER-RELAXATION

- **ENHANCED STABILITY**

$$Q_i^{n+1} = Q_i^n + \alpha r \, \Delta Q_i^n$$

$$Q_i = [\, p, u, v, w \,]^T$$

$$\alpha r = \text{RELAXATION FACTOR}$$

CONVERGENCE HISTORY
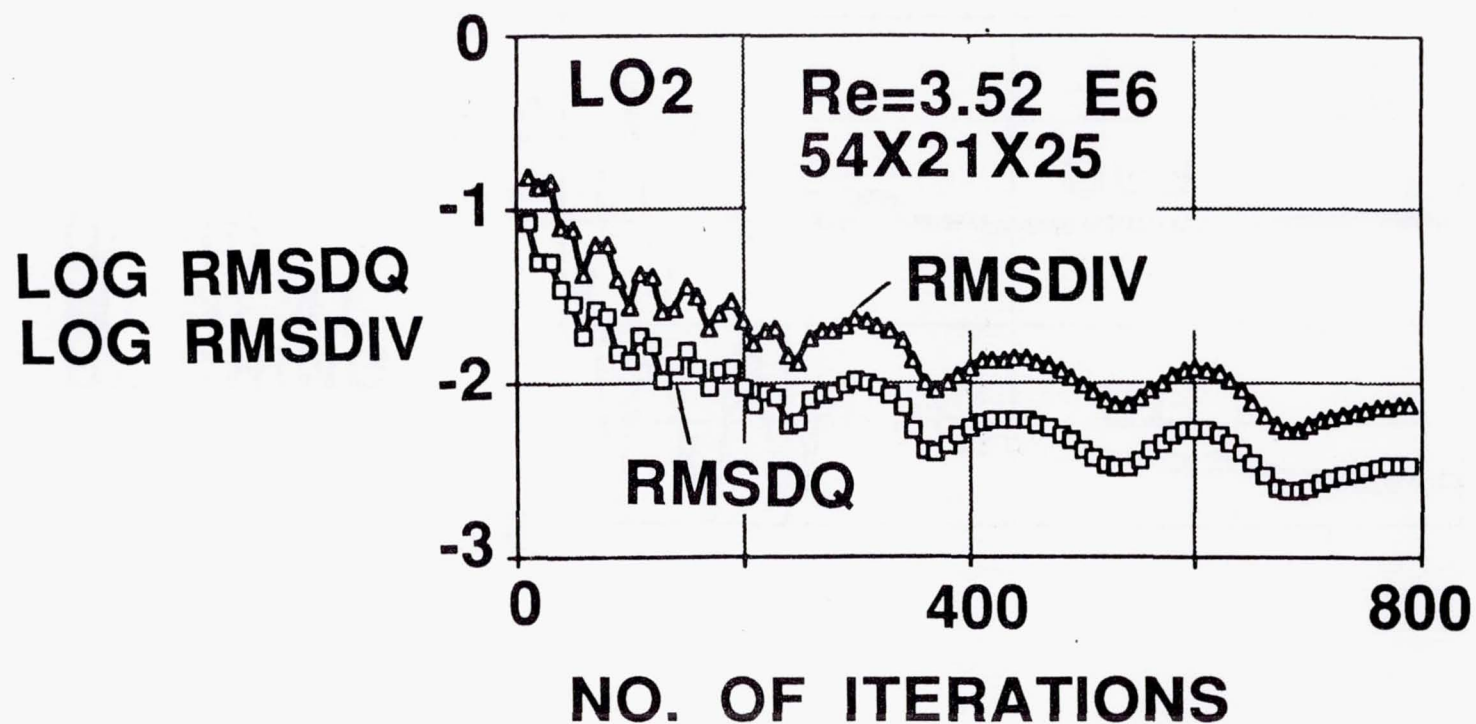
CONVERGENCE HISTORY

FLOW FIELD

LO$_2$

STATIC PRESSURE

SEPARATION   WAKE

VELOCITY
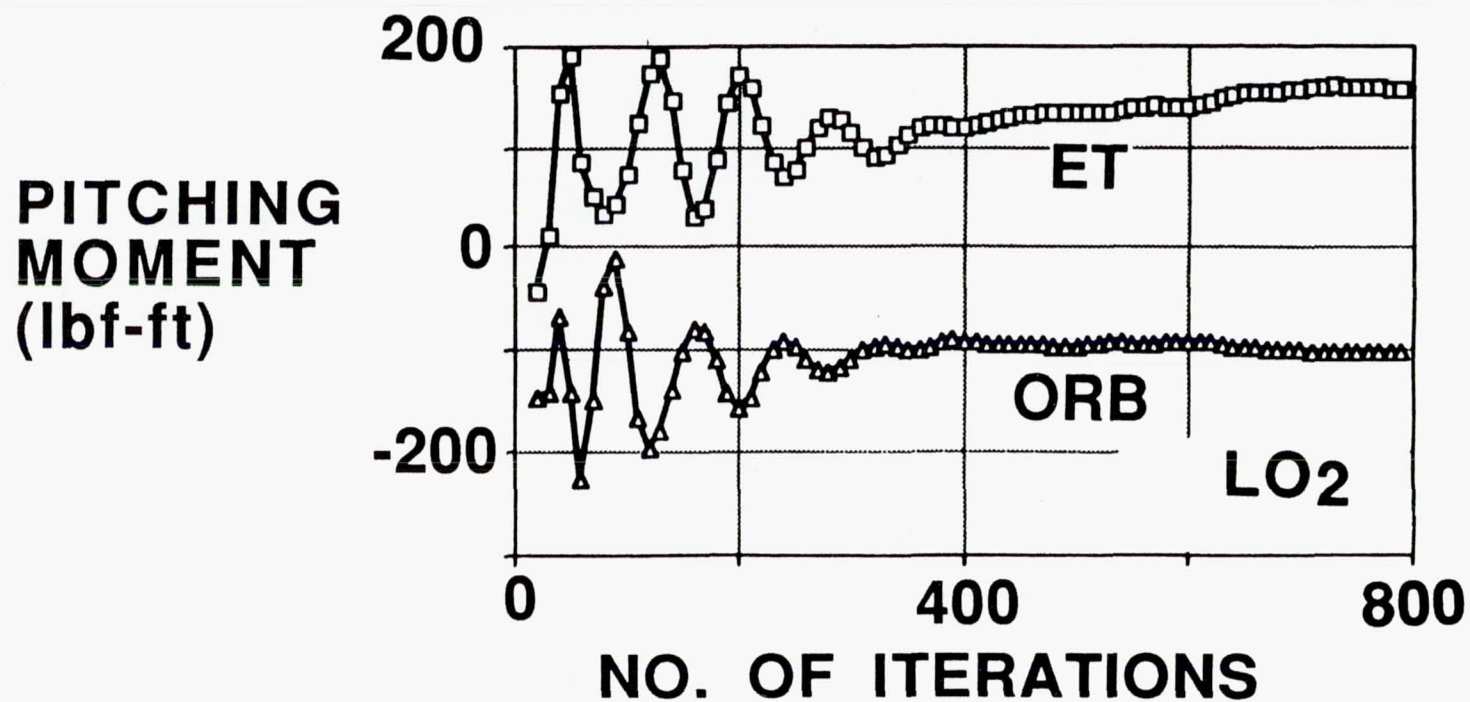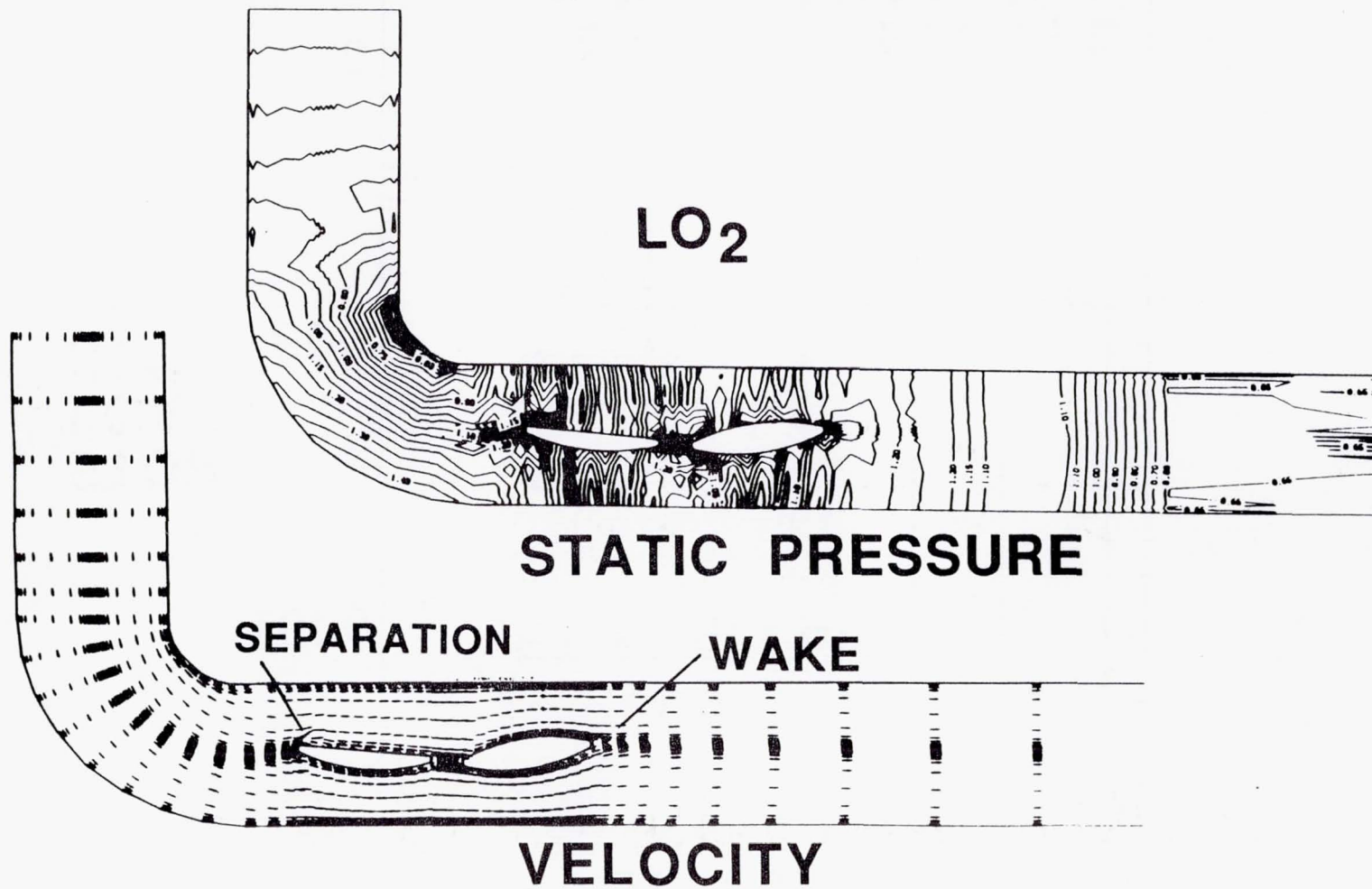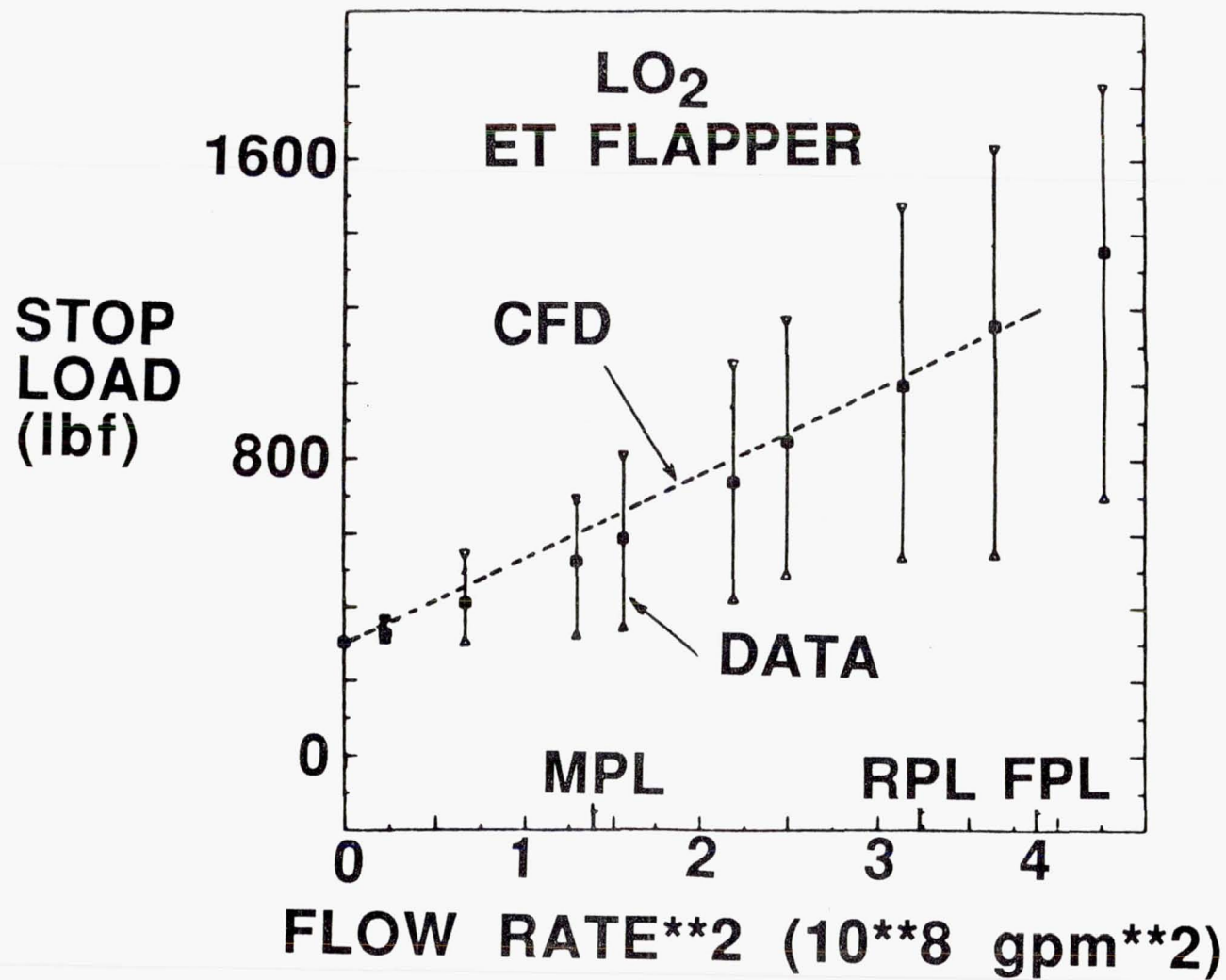
EFFECT OF FLOW RATE

EFFECT OF FLAPPER ANGLE
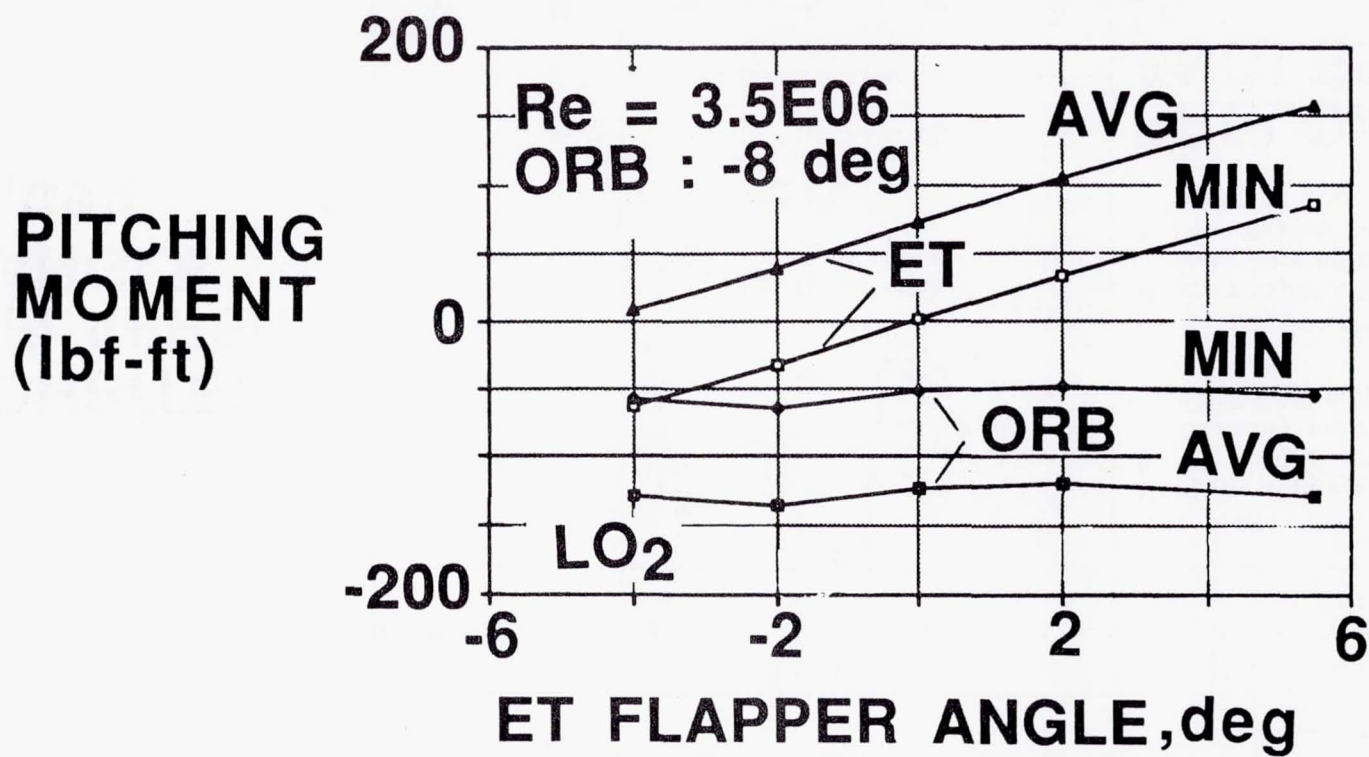
STABILITY BOUNDARIES
LO$_2$ DISCONNECT
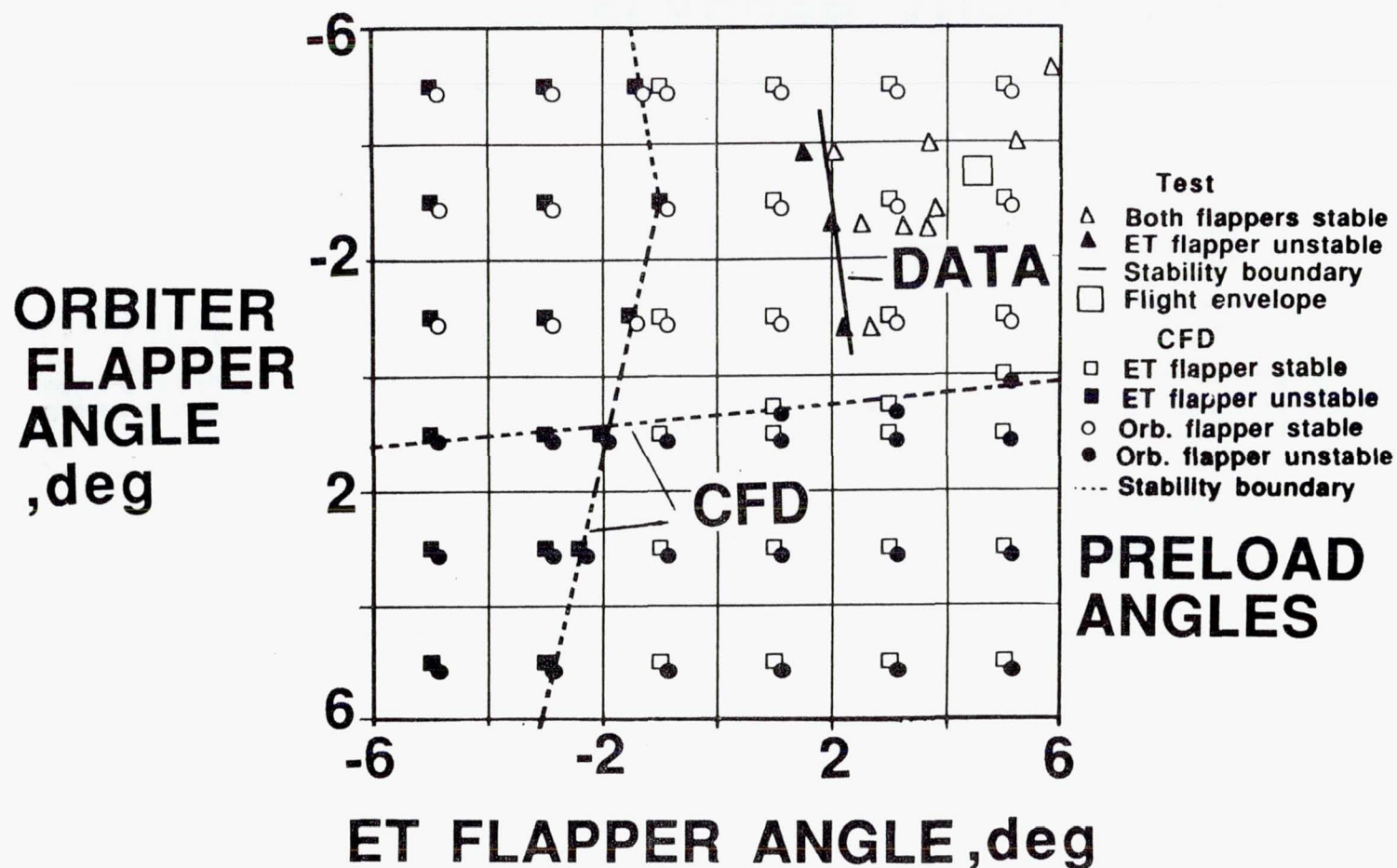
STABILITY BOUNDARIES
LH$_2$ DISCONNECT
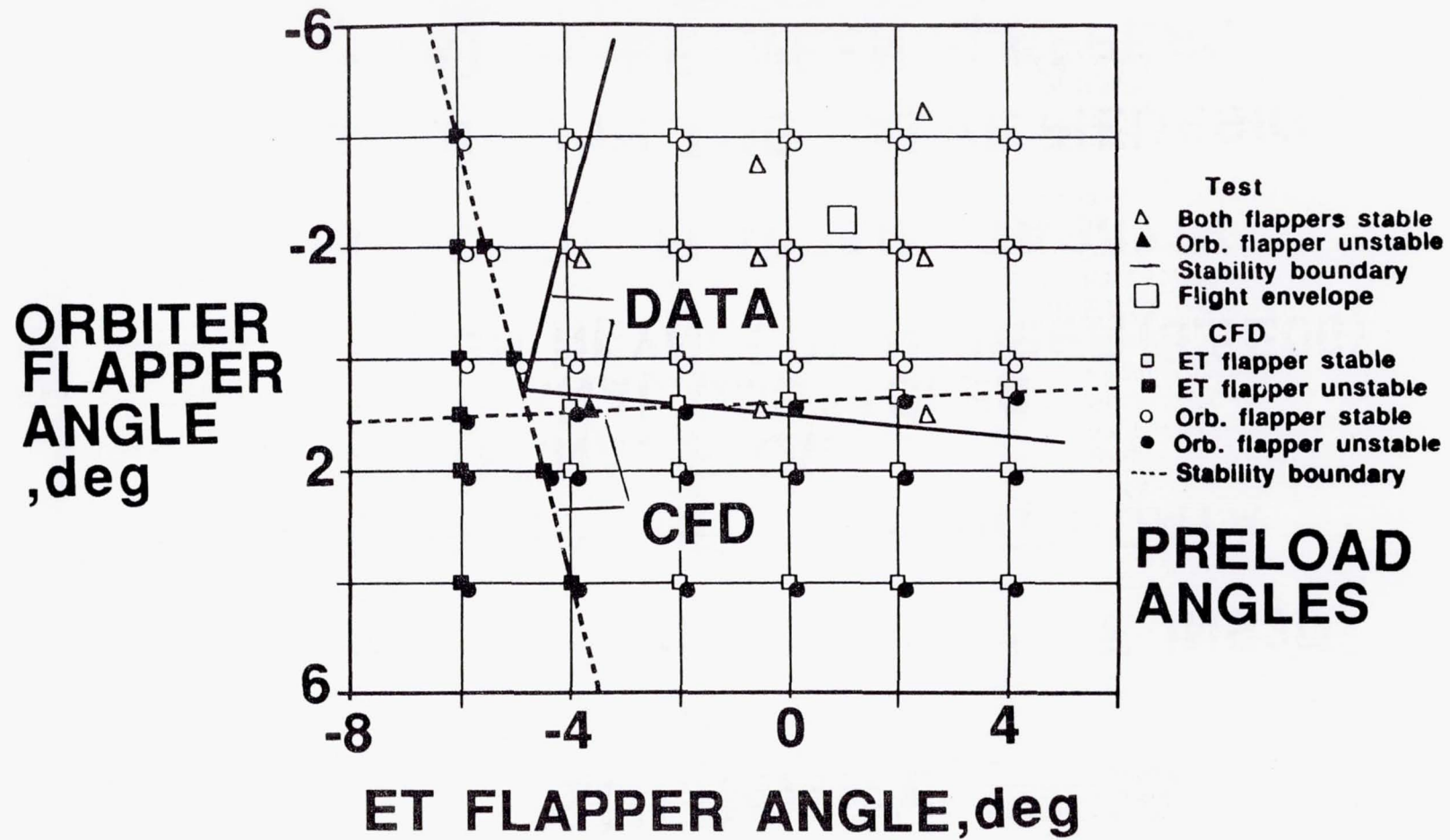
SUMMARY

- ENHACED THE STABILITY OF INS3D

- VALIDATED THE CODE WITH DATA
  - INTERNAL FLOW
  - INTERNAL OBSTACLES
  - HIGH REYNOLDS NUMBER (3.5E06)

- PREDICTED FLAPPER STABILITY

- ASSISTED IN THE VALVE REDESIGN
  - LATCH BETWEEN FLAPPERS

Analysis of the SSME HPOTP Bearing Inlet Cavity

P. McConnaughey, NASA/MSFC

Analysis of the flow in the Space Shuttle Main Engine (SSME) high pressure oxygen turbopump (HPOTP) bearing #1 inlet cavity has been completed in support of return-to-flight. With the incorporation of several design changes in the Phase II turbopump, rotordynamic stability of the pumps has been enhanced, but the durability and life of the LOX-cooled bearings has decreased. During the post-Challenger SSME recertification, the MSFC bearing team investigated the causes of limited bearing durability. One topic addressed by this team was the flow environment upstream of the pump-end bearing and the effect of seal exit swirl (Phase I labyrinth seal vs. Phase II damping seal) and a cavity anti-vortex rib on the bearing environment and life. The objective of the present work was to define the hydrodynamic environment upstream of the pump-end bearing and determine the effect of seal exit swirl and the anti-vortex rib on bearing inlet swirl.

The problem was posed as an axisymmetric cavity flow with the computational domain extending from the seal exit to the bearing inlet. This domain was discretized with 22800 grid points. Boundary conditions were obtained from a 1-D model of the SSME coolant path. These resulted in an axial Reynolds number of 297000 and with a seal tip speed of 29,200 rpm. The inlet Mach number was 0.19 and the problem was solved with the CMINT code utilizing the Briley-McDonald/Beam-Warming algorithm with preconditioning to speed convergence at low Mach numbers. Three parametric cases with inlet swirl of 50% shaft speed (labyrinth seal), 20% shaft speed (damping seal) and no inlet swirl were considered. Total CPU time for all analyses was 9 hours on a Cray X-MP with memory requirements of 1.7 million words.

Computational results indicate large vortical flow structures in the cavity, with the labyrinth, damping, and no-swirl cases yielding bearing inlet swirl rates of 14, 10, and 9 percent of shaft speed, respectively. These small differences are due to fluid spin-up on the shaft and inner race and indicate that upstream influences (either inlet swirl or anti-vortex ribs) have little effect on bearing inlet conditions. When these results were used as input to the SHABRETH bearing model, limited durability could not be explained by these small differences in swirl. Also, based on these results, a proposed design change for the cavity anti-vortex rib was not implemented by the SSME chief engineer.

OVERVIEW

- OBJECTIVE
- JUSTIFICATION
- APPROACH
- RESULTS
- SUMMARY AND CONCLUSIONS
- PROGRAM IMPACT

OBJECTIVES (IN SUPPORT OF RETURN-TO-FLIGHT)

- DEFINE THE HYDRODYNAMIC ENVIRONMENT FOR THE LOX
  BEARING #1 INLET CAVITY
  - UNDERSTAND THE SEAL EXIT/CAVITY/BEARING INLET FLOW PATH
  - QUANTIFY THE PRESSURE DROP IN THE CAVITY

- EVALUATE THE EFFECT OF SEAL EXIT SWIRL ON BEARING INLET SWIRL
  - INLET SWIRL AFFECTS VISCOUS HEAT GENERATION IN BEARING, CAGE
    DRAG AND PRESSURE DROP ACROSS BEARINGS

- EVALUATE EFFICACY OF THE BEARING CAVITY ANTI-VORTEX RIB

150

5-1631-9-104

JUSTIFICATION

- DURABILITY OF HPOTP PUMP-END BEARINGS (2000 SECOND LIMIT)
    - LOWER LIFE IN PHASE II DESIGN RELATIVE TO PHASE I DESIGN
    - CONFIGURATION CHANGES
        - DAMPING SEALS (PHASE II) VS. LABYRINTH SEALS (PHASE I)
        - INCREASED DEADBAND, INTERNAL CLEARENCES
        - ELONGATED CAGE POCKETS

- PROPOSED DESIGN CHANGE TO REMOVE ANTI-VORTEX RIB IN CAVITY

5-1619-9-104
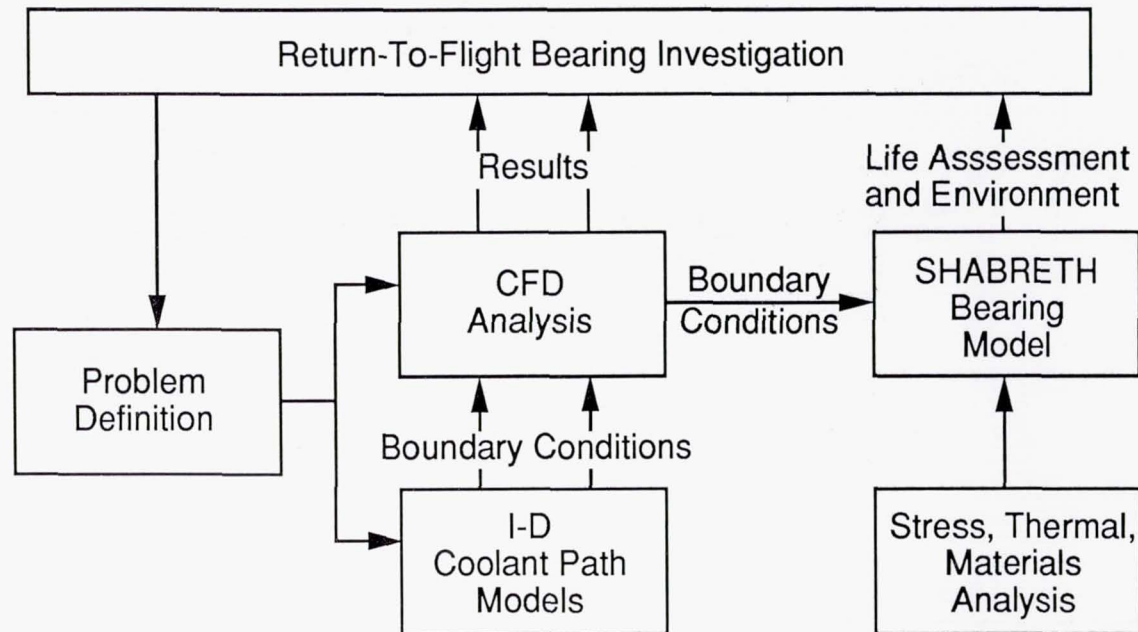
BEARING INLET CAVITY ANALYSIS

PHASE I

PHASE II

ANTI-VORTEX
RIB

THIN ISOLATOR

LABYRINTH
SEAL

THICK ISOLATOR

DAMPING
SEAL

INNER
RACE

5-1616-9-98
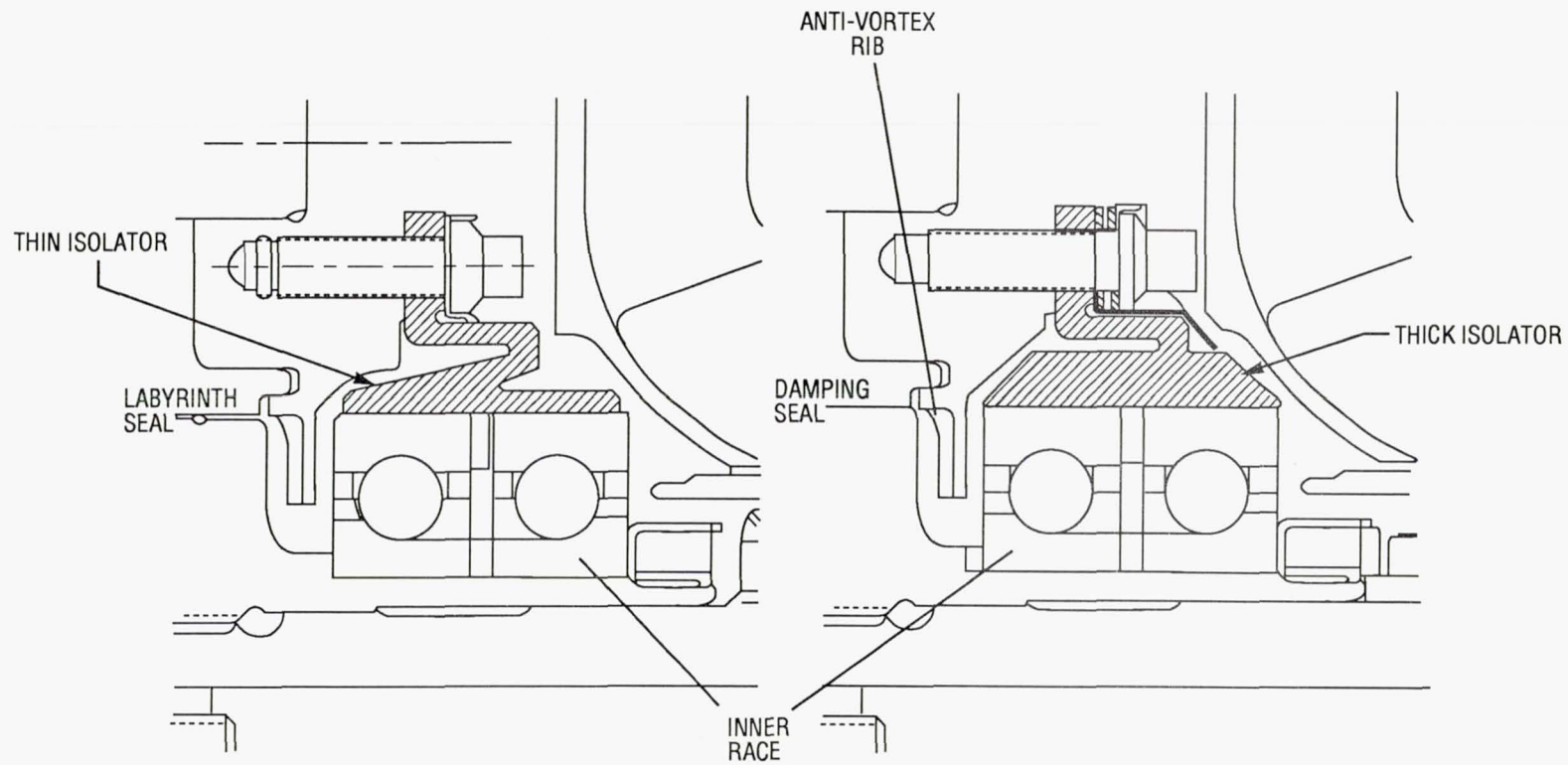
APPROACH

PROBLEM DEFINITION

- DOMAIN FROM SEAL EXIT TO BEARING INLET

  - AXISYMMETRIC ANALYSIS (NO ANTI-VORTEX RIB)
  - LEAKAGE PATH IGNORED (1% OF FLOW)
  - ALL FLOW TO BEARING GOES BETWEEN INNER RACE AND CAGE

- Re_{ax} = 297000, Ω = 29200 rpm, M_{in} = 0.19 (109% POWER LEVEL)

METHOD OF ANALYSIS

- COMPRESSIBLE NAVIER-STOKES EQUATIONS (2-D AXISYMMETRIC WITH SWIRL)

- BRILEY-McDONALD/BEAM-WARMING WITH PRECONDITIONING

- CMINT CODE

- LOW, Re K-ε TURBULENCE MODEL

- 22800 GRID POINTS

- SOFT-START ON DOWNSTREAM STATIC PRESSURE

- 9 HOURS, 1.7×10^6 WORDS ON MSFC CRAY X-MP

VALIDATION OF DISK CAVITY ANALYSES

- OWEN AND PINCOMBE (JFM, 1980)

- DAILY AND NECE (1960)

153

5-2134-8-39

SSME HPOTP BEARING #1 INLET CAVITY ANALYSIS

120x190 Grid

Seal Exit
(Cavity Inlet)

Stationary
Wall

Bearing
Cage

Rotating Shaft

Stationary
Wall

Bearing
Cage

Bearing Inlet
(Cavity Exit)

Rotating Shaft

SSME HPOTP BEARING #1 INLET CAVITY ANALYSIS

120x190 Grid
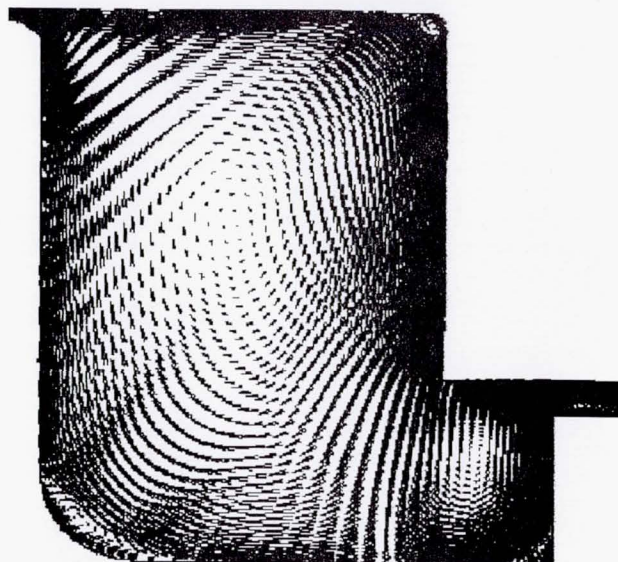
Velocity Vectors Colored
by Velocity Magnitude
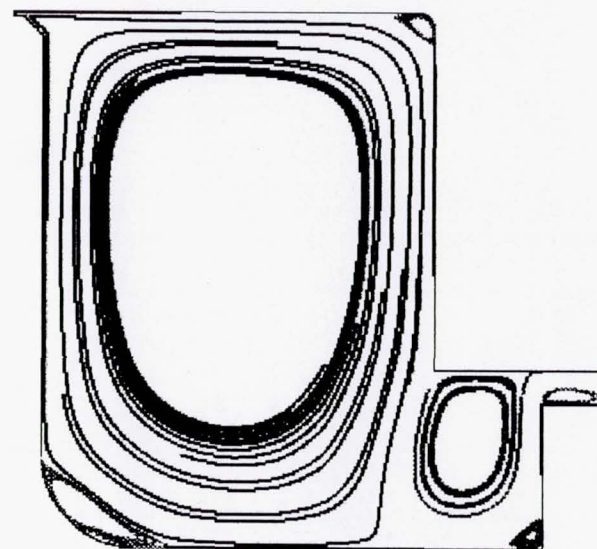
Particle Traces

CONTOUR LEVELS
SWIRL VELOCITY IN HPOTP BEARING #1 INLET CAVITY

0.000 MACH
0.00 DEG ALPHA
120x1x190 GRID

0.000010 ...
10.00000
20.00000
30.00000
40.00000
50.00000
60.00000
70.00000
80.00000
90.00000
100.000
110.000
120.000
130.000
140.000
150.000
160.000
170.000
180.000
190.000
200.000
210.000
220.000
230.000
240.000
250.000
260.000
270.000
280.000
290.000
300.000

Labyrinth Seal Inlet Conditions (50% Swirl)
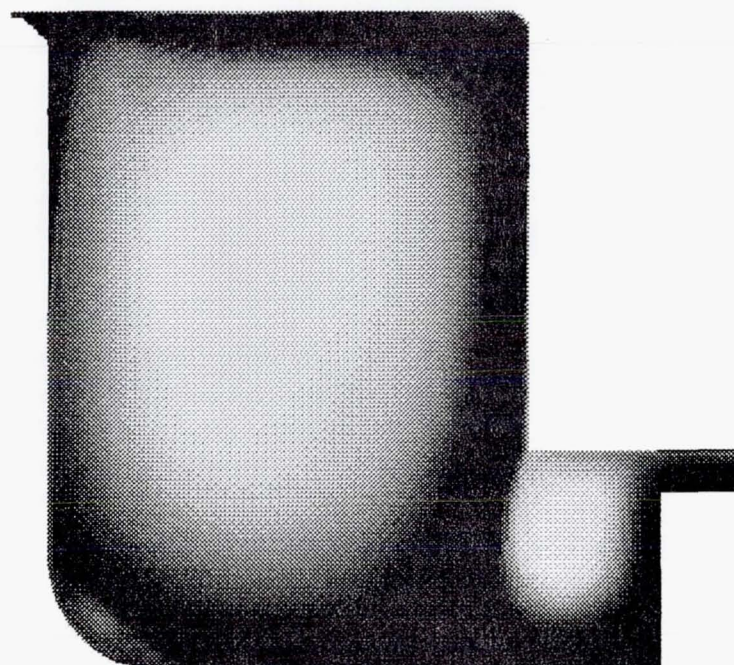
Damping Seal Inlet Conditions (20% Swirl)

156

Computational Fluid Dynamics Branch, ED32

NASA / Marshall Space Flight Center
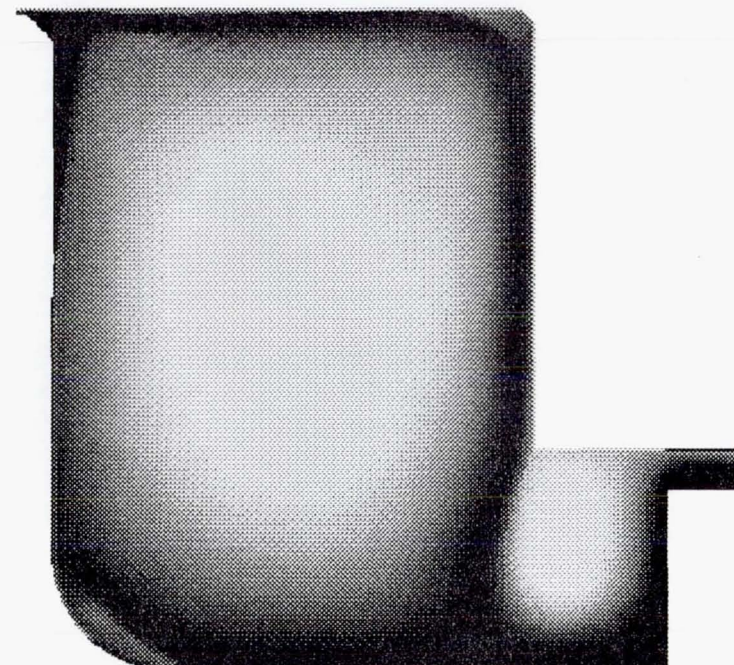
BEARING INLET CAVITY ANALYSIS

LOX SWIRL PROFILES AT BEARING CAGE INLET

SEAL EXIT SWIRL	BEARING INLET SWIRL
50 %	14%
20%	10%
0%	9%

INNER RACE SPEED

LABY. SEAL (50% SWIRL)

● CAGE SPEED

● DAMPING SEAL (20% SWIRL)

0% SWIRL

SWIRL VELOCITY AT BEARING INLET (FT/SEC)

INCHES FROM SHAFT CENTERLINE
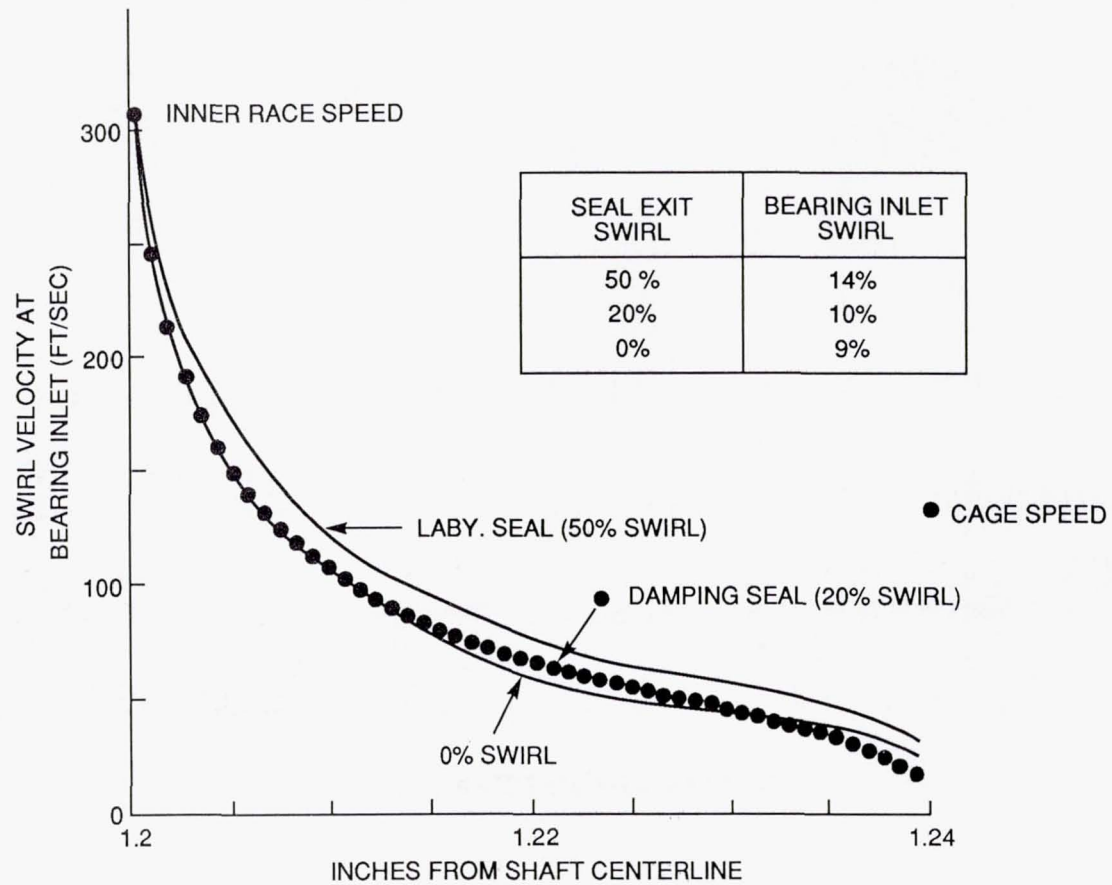
5-1615-9-98

BEARING INLET CAVITY ANALYSIS

SUMMARY AND CONCLUSIONS

- HYDRODYNAMIC ENVIRONMENT FOR THE SSME HPOTP BEARING #1 INLET CAVITY HAS BEEN DEFINED FOR PHASE I AND PHASE II DESIGNS

- SMALL DIFFERENCE (4%) IN BEARING INLET SWIRL BETWEEN PHASE I AND PHASE II PUMPS

- CFD RESULTS WERE USED AS INPUT INTO SHABRETH BEARING MODEL IN SUPPORT OF RETURN-TO-FLIGHT

158

5-1617-9-104

BEARING INLET CAVITY ANALYSIS

PROGRAM IMPACT

- DETERMINED THAT THE LIMITED DURABILITIY OF THE HPOTP PUMP-END BEARINGS IS NOT CAUSED BY CHANGES IN SWIRL ASSOCIATED WITH THE PHASE II DESIGN DAMPING SEALS

- DETERMINED THAT THE PROPOSED MODIFICATION OF THE CAVITY ANTI-VORTEX RIB WOULD HAVE LITTLE EFFECT ON SWIRL ENTERING THE BEARING. PROPOSED DESIGN CHANGE WAS NOT IMPLEMENTED BY CHIEF ENGINEERS OFFICE

159

5-1618-9-104

o DISK CAVITY ANALYSIS AT NASA-MSFC

PROBLEM	CODE	TURNAROUND TIME
- HPFTP TURBINE AFT CAVITY	PHOENICS	-
- HPOTP BEARING # 1 INLET CAVITY	CMINT	3 MOS
- HPFTP TURBINE FORE CAVITY	CMINT	6 MOS
- TEST BED ENGINE CABLE CAVITY	INS3D*	3 WKS

*   CODE WILL BE SET UP FOR GENERALIZED DISK CAVITY
        ANALYSIS

N91-10878

A COMBINED EULERIAN-LAGRANGIAN TWO-PHASE ANALYSIS OF THE SSME HPOTP NOZZLE PLUG TRAJECTORIES

R. Garcia, P. K. McConnaughey, NASA/MSFC
F. de Jong, J. Sabnis, Scientific Research Associates
D. Pribik, Rocketdyne Division, Rockwell International

Abstract

As a result of high cycle fatigue, hydrogen embrittlement, and extended engine use, it was observed in testing that the trailing edge on the first stage nozzle plug in the High Pressure Oxygen Turbopump (HPOTP) could detach. The objective of this study was to predict the trajectories followed by particles exiting the turbine. Experiments had shown that the heat exchanger coils, which lie downstream of the turbine, would be ruptured by particles traveling in the order of 360 ft/sec. An axisymmetric solution of the flow was obtained from the work of Lin et al [1] who used INS3D to obtain his solution. The particle trajectories were obtained using the method of de Jong et al [2] which employs Lagrangian tracking of the particle through the Eulerian flow field. The collision parameters were obtained from experiments conducted by Rocketdyne using problem specific alloys, speeds, and projectile geometries. A complete 3-D analysis using the most likely collision parameters shows maximum particle velocities of 200 ft/sec. in the heat exchanger region. Subsequent to this analysis, an engine level test was conducted in which seven particles passed through the turbine but no damage was observed on the heat exchanger coils.

References

1) Lin, S.-J. and Chang, J.L.C.: "Numerical Study of Laminar and Turbulent Flow Inside a Turnaround Duct With and Without Guide Vanes," AIAA Paper 87-0365, 1987.

2) de Jong, F.J., Sabnis, J.S., and McConnaughey, P.K.: "A Combined Eulerian-Lagrangian Two-Phase Flow Analysis of SSME HPOTP Nozzle Plug Trajectories; Part I- Methodology," To be presented at the AIAA Joint Propulsion Conference, 1989.

HIERARCHY OF ANALYSIS

- 2–D: PARTICLE EXITS TURBINE WITH NO SWIRL

- 3–D: PARTICLE WITH SWIRL, NO RADIAL STRUTS

- 3–D: PARTICLE WITH SWIRL, RADIAL STRUTS INCLUDED

PARAMETERS OF ANALYSIS

- 15 DIFFERENT PARTICLE RADIAL POSITIONS AT THE INLET TO THE DOMAIN FOR EACH RUN. (INNER TO OUTER WALL)

- DRAG COEFFICIENT OF PARTICLES – 0.4, 0.6, 0.8
    - TURBINE EXIT AXIAL VELOCITY OF PARTICLE FROM 180 TO 255 FT/SEC.

- SWIRL VELOCITY OF PARTICLE VARIED FROM ZERO TO BLADE SPEED

- LOSS OF NORMAL MOMENTUM AT THE WALLS:
    - COEFFICIENT OF RESTITUTION – 0.2, 0.4, 0.6, 0.8

- LOSS OF TANGENTIAL MOMENTUM AT THE WALLS:
    - COEFFICIENT OF SLIDING FRICTION – 0.0, 0.1, 0.2, 0.3

Main Combustion Chamber

High Pressure Oxygen Turbopump Preburner

Heat Exchanger Coils

Turbine Discharge Manifold

Two Stage Turbine

High Pressure Oxygen Pump

First Stage Turbine Blade

First Stage Nozzle Plug

Heat Exchange Coils

Turning Vanes and Struts

Second Stage Turbine Blade
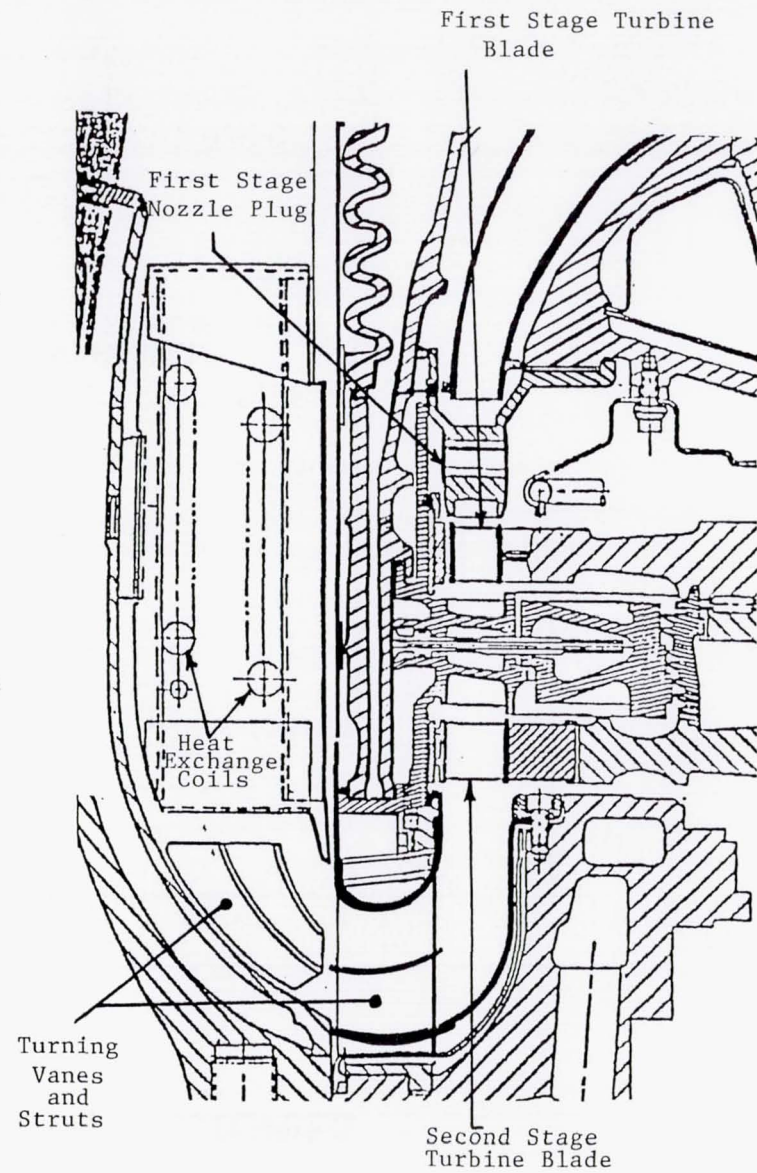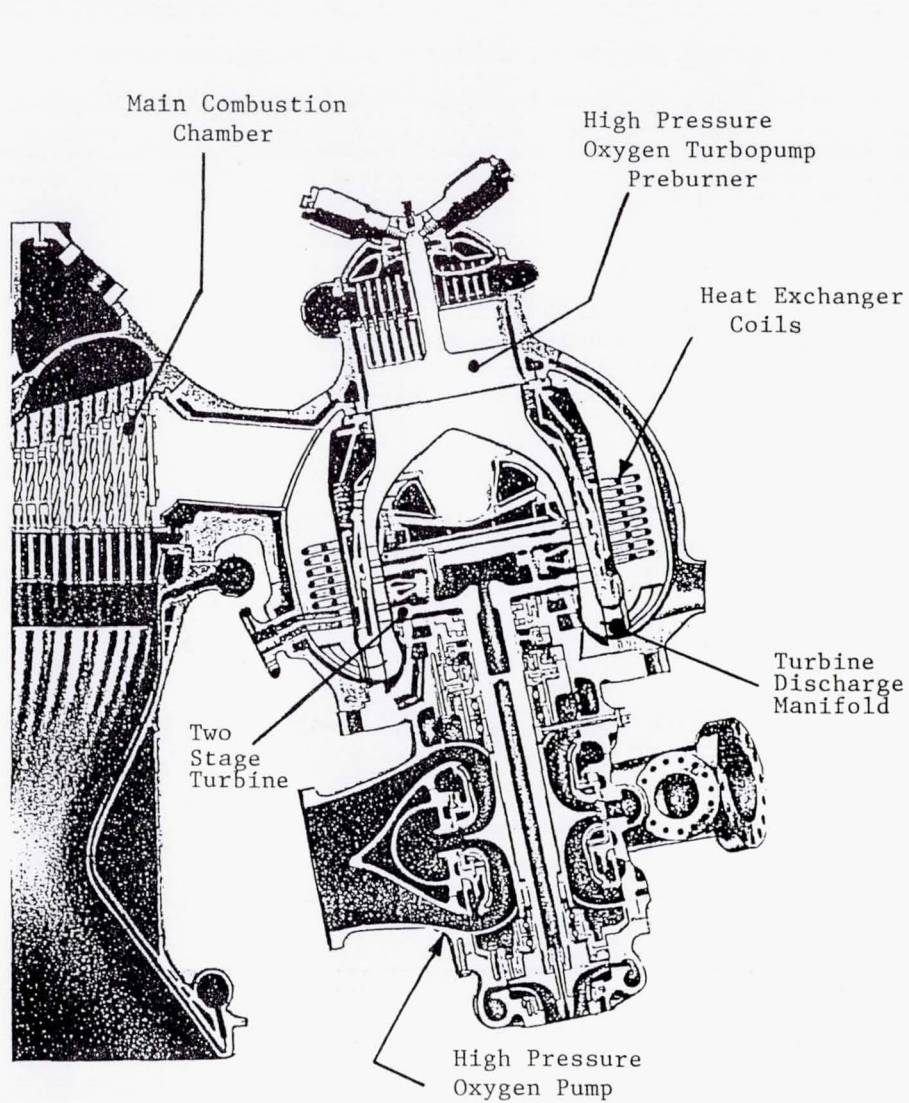
SSME HPOTP NOZZLE PLUG TRAJECTORIES
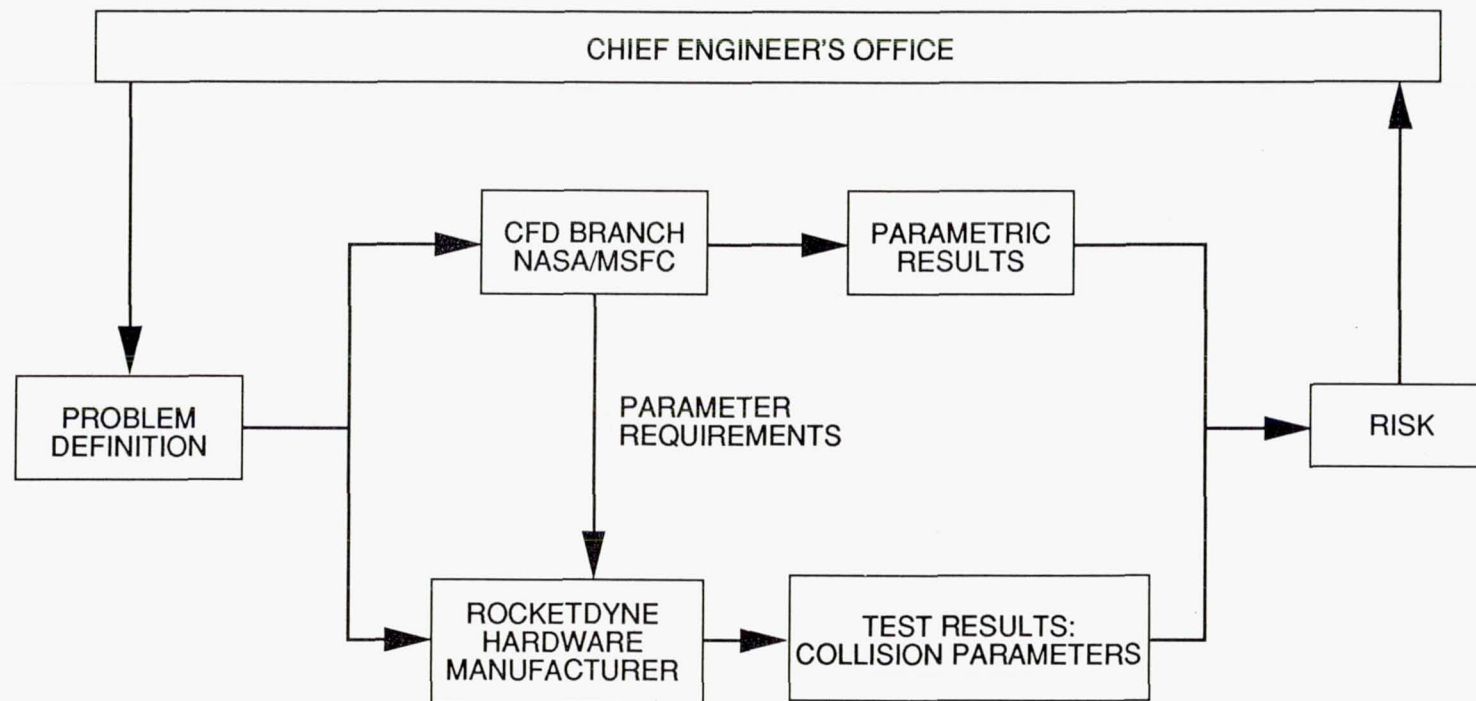
OBJECTIVE

- TO DETERMINE THE LOCATIONS AND VELOCITIES OF NOZZLE PLUG IMPACTS ON

  THE HPOTP LOX HEAT EXCHANGER. TEST DATA INDICATED IMPACT VELOCITIES OF

  360 FT/SEC WOULD CAUSE HEAT EXCHANGER COIL RUPTURE.

JUSTIFICATION

- RESULTS REQUESTED BY SSME CHIEF ENGINEER TO ASSESS:

  - RISK OF FULL SCALE ENGINE TEST.

  - RISK OF RETURN TO FLIGHT OF THE SPACE SHUTTLE WITH CURRENT DESIGN.

165

5-1580-9-99

TECHNICAL APPROACH

- USED LIN's AND CHANG's (ROCKETDYNE) AXISYMMETRIC SOLUTION OF THE FLOW IN THE HPOTP HOT GAS MANIFOLD

  - SOLUTION OBTAINED USING INS3D:

  - INCOMPRESSIBLE M = 0.1

  - Re $\cong 3 \times 10^6$, 588 FT/SEC AXIAL VELOCITY

- TRAJECTORIES CALCULATED USING LAGRANGIAN TRACKING OF THE PARTICLES THROUGH THE EULERIAN FLOW FIELD

  - METHOD OF F. J. de JONG AND J. S. SABNIS OF SRA

  - $\vec{F} = m\vec{a}$ ON THE PARTICLE THROUGH THE FLOW FIELD

  - COLLISION MODEL AT THE WALLS.

- VALIDATION

  - INS3D: COMPARED TO EXPERIMENTAL MEASUREMENTS FOR VARIOUS INCOMPRESSIBLE INTERNAL FLOWS.

  - LAGRANGIAN TRACKER: COMPARED AGAINST EXPERIMENTAL MEASUREMENTS IN A TWO-PHASE MIXING LAYER FLOW.

5-1581-9-99

166

SSME HPOTP NOZZLE PLUG TRAJECTORIES

OVERVIEW

- INTRODUCTION TO THE PROBLEM

- OBJECTIVES

- TECHNICAL APPROACH

- RESULTS

- CONCLUSION/IMPACT

HPOTP Nozzle Plug Trajectories

Drag Coefficient = 0.6
Coeff. of Restitution = 0.6
Coeff. of Sliding Friction = 0.0

2-D

Swirl = 0%
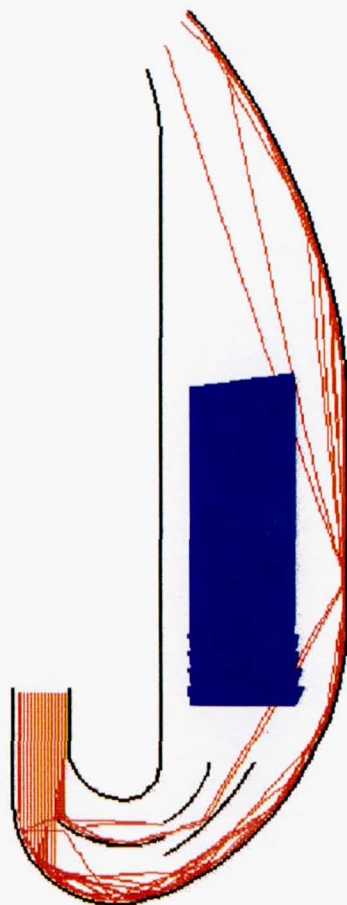
3-D

Swirl = 100%
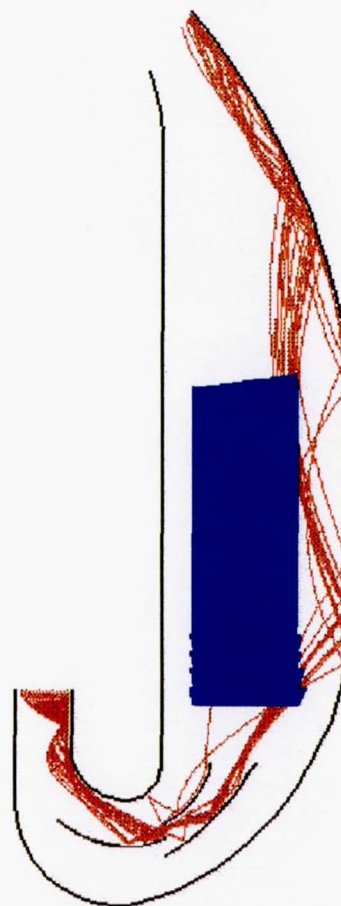
PARTICLE VELOCITIES* AT THE HEAT EXCHANGER (FT/SEC)

FOR ALL CASES SHOWN: $C_D = 0.6$; $\mu = 0.0$

	2–D $V_{SWIRL} = 0.0$			3–D, NO RADIAL STRUTS $V_{SWIRL} = 1310$ ft/sec	
0.4	192 – 152	V_{MAX} V_{MEAN} V_{MIN}	0.4	635 610 572	V_{MAX} V_{MEAN} V_{MIN}
C_{RES} 0.6	204 – 200	V_{MAX} V_{MEAN} V_{MIN}	0.6	672 611 435	V_{MAX} V_{MEAN} V_{MIN}
0.8	224 – 167	V_{MAX} V_{MEAN} V_{MIN}	0.8	765 683 465	V_{MAX} V_{MEAN} V_{MIN}

*SWIRL COMPONENT NOT INCLUDED (NOT NORMAL TO COILS)

5-1583-9-99

3-D HPOTP Nozzle Plug Trajectories
Complete Geometry
Drag Coefficient = 0.6
Coefficient of Restitution = 0.6
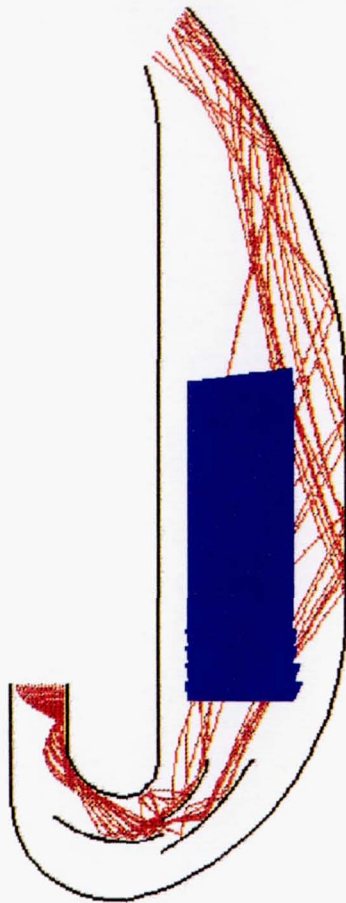
Coeff. of Sliding
Friction = 0.0

Coeff. of Sliding
Friction = 0.1
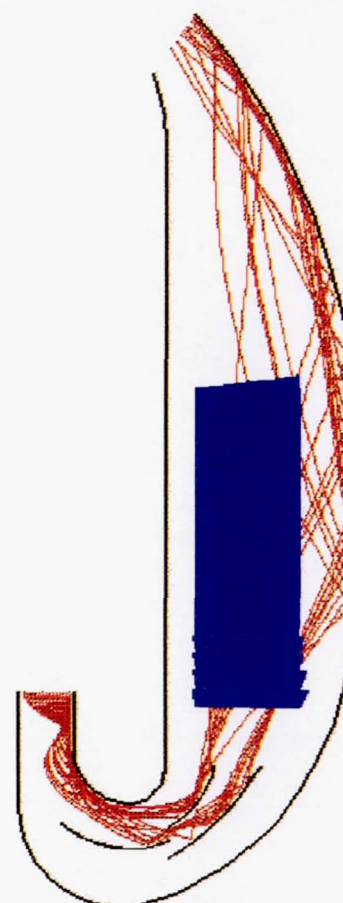
Coeff. of Sliding
Friction = 0.2
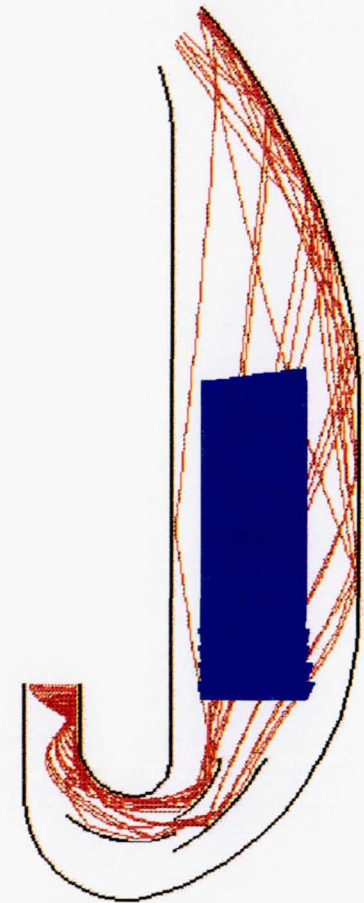
Coeff. of Sliding
Friction = 0.3

175

3-D ANALYSIS WITH RADIAL STRUTS (COMPLETE GEOMETRY)

PARTICLE VELOCITIES* AT HEAT EXCHANGER (FT/SEC)

$C_D = 0.6$ V_{SWIRL} = BLADE SPEED

$C_{RESTITUTION}$

		0.2	** 0.4	0.6	0.8	
	** 0.1	150.9 141.1 161.1	130.0 61.5 176.7	156.3 82.3 302.5	210.1 61.7 328.6	$\bar{V}$ V_{MIN} V_{MAX}
μ (COEFF. OF SLIDING FRICTION)	0.2	82.4 76.9 86.3	65.2 49.5 110.2	75.4 42.4 161.8	96.4 38.2 150.7	$\bar{V}$ V_{MIN} V_{MAX}
	0.3	49.5 43.3 56.0	60.5 51.9 66.4	54.6 26.8 94.3	55.2 21.4 69.0	$\bar{V}$ V_{MIN} V_{MAX}

*SWIRL COMPONENT NOT INCLUDED (NOT NORMAL TO COIL)
**EXPECTED MEAN VALUE FOR COEFFICIENT BASED ON TEST DATA

5-717-9-83

IMPACT

- DECISION MADE TO CONDUCT FULL SCALE TEST WITH PURPOSELY CUT NOZZLE PLUGS:
  NO DAMAGE TO THE HEAT EXCHANGER

- DECISION MADE TO USE CURRENT DESIGN ON RETURN TO FLIGHT

176

CONCLUSIONS

- PARTICLE MOTION DOMINATED BY COLLISION PARAMETERS

- MOST PARTICLES WILL HIT THE HEAT EXCHANGER DUE TO "FOCUSING" OF THE TURNING VANES.

- MEAN COLLISION PARAMETERS (C_{RES} = 0.6, μ = 0.1) YIELD MAXIMUM PARTICLE IMPACT VELOCITIES OF 180 FT/S

- WORST CASE STACK OF COLLISION PARAMETERS YIELDS MAXIMUM IMPACT VELOCITIES OF 300 FT/S (RUPTURE VELOCITY IS 360 FT/S).

177

Conjugate (Solid/Fluid) Computational Fluid Dynamics
Analysis of the Space Shuttle Solid Rocket Motor
Nozzle/Case and Case Field Joints

D. Doran, NASA/MSFC, L. W. Keeton, P. J. Dionne,
and A. K. Singhal, CFD Research Corporation

This work describes three-dimensional, conjugate
(solid/fluid) heat transfer analyses of new designs of the
Solid Rocket Motor (SRM) nozzle/case and case field joints.

The main focus of the study has been to predict the
consequences of multiple "rips" (or debonds) in the ambient
cure adhesive packed between the nozzle/case joint surfaces
and the bond line between the mating field joint surfaces.'
The models calculate the transient temperature responses of
the various materials neighboring postulated flow/leakpaths
into, past and out from the nozzle/case primary O-ring cavity
and case field capture O-ring cavity. These results were
used to assess if the design was failsafe (i.e. no potential
O-ring erosion) and reusable (i.e. no excessive steel
temperatures).

The models are adaptions and extensions of the general
purpose PHOENICS fluid dynamics code.

A non-orthogonal coordinate system was employed and 11,592
control cells for the nozzle/case and 20,088 for the case
field joints are used with non-uniform distribution.
Physical properties of both fluid and solids are temperature
dependent.

A number of parametric studies were run for both joints with
results showing temperature limits for reuse for the steel
case on the nozzle joint being exceeded while the steel case
temperatures for the field joint were not. O-ring
temperatures for the nozzle joint predicted erosion while for
the field joint they did not.

SRB NOZZLE/CASE AND CASE FIELD JOINT
FLOW AND THERMAL ANALYSIS

OVERVIEW

- PROBLEM DEFINITION

- OBJECTIVES

- TECHNICAL APPROACH

- RESULTS

- PROGRAM IMPACT AND CONCLUSIONS

SPACE SHUTTLE SRM

CASE FIELD JOINTS

FLAP

CF/EPDM

FLAP GAP

BOND REGION

CAPTURE O-RING

NBR →

← NBR

TANG

CLEVIS

ARCTIC NITRILE O-RINGS

NOZZLE/CASE JOINTS

GLASS PHENOLIC

CARBON PHENOLIC

CIRCUMFERENTIAL FLOW BAFFLE

CARBON FIBER FILLED EPDM

INTERFERENCE FIT BONDLINE

AMBIENT CURE ADHESIVE

NOZZLE FIXED HOUSING (D6AC STEEL)

WIPER (O-RING)

AFT DOME (D6AC STEEL)

0.100 NOMINAL BONDLINE

ASBESTOS/SILICA FILLED NBR

ED6613
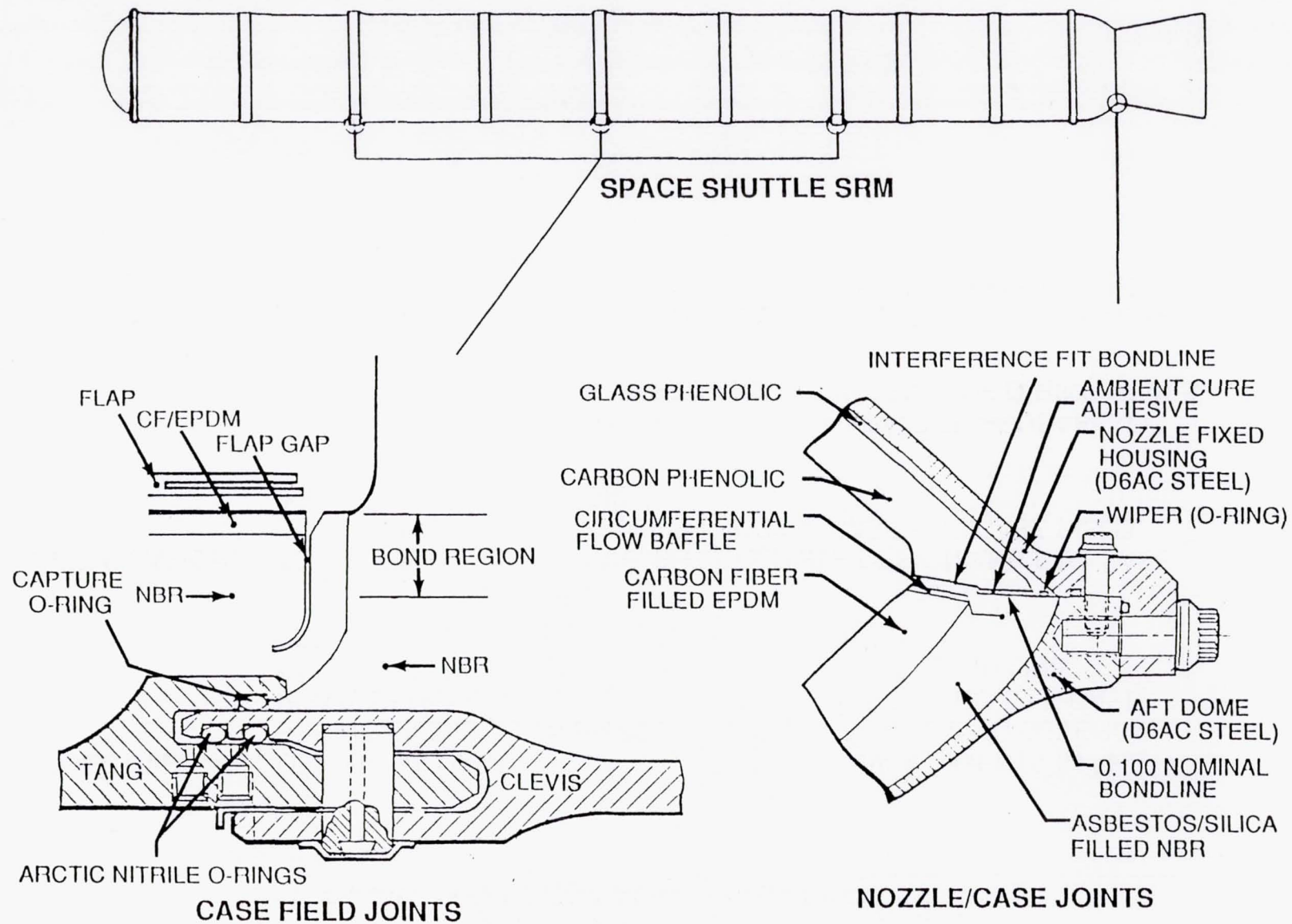
SRB NOZZLE/CASE AND CASE FIELD JOINT
FLOW AND THERMAL ANALYSIS

OBJECTIVE: DEFINITION OF THE FLOW AND THERMAL ENVIRONMENTS IN THE
SRB NOZZLE/CASE AND CASE FIELD JOINTS ASSUMING SEVERAL
POSTULATED DOUBLE LEAKPATHS THROUGH THE NOZZLE/CASE
AMBIENT CURE ADHESIVE AND THE CASE FIELD BOND LINE
BETWEEN THE MATING FIELD JOINT SURFACES

JUSTIFICATION: TO DEFINE CONSERVATIVE, BUT CREDIBLE DESIGN AND FAIL-SAFE
CONDITIONS AND CRITERIA FOR NOZZLE/CASE AND CASE FIELD
JOINT THERMAL ANALYSIS

     DESIGN -   TEMPERATURES WHICH GUARANTEE REUSABILITY
OF METAL PARTS AND NO EROSION OF O-RING SEALS

     FAIL-SAFE - TEMPERATURES WHICH GUARANTEE A STRUCTURAL
SAFETY FACTOR OF 1.0 ON METAL PARTS AND NO
EROSION OF ONE SEAL

5-1572-9-102

RETURN-TO-FLIGHT RSRM JOINT INVESTIGATION

RESULTS

ASSESSMENT FOR
FAIL-SAFE AND REUSEABILITY
CONDITIONS

CFD
FLOW/THERMAL
ANALYSIS

TEMPERATURES
&
VELOCITIES

RSRM
GAS DYNAMICS
TEAM

BOUNDARY
CONDITIONS

PROBLEM
DEFINITION

MORTON THIOKOL
TEST DATA

183

5-1624-9-103
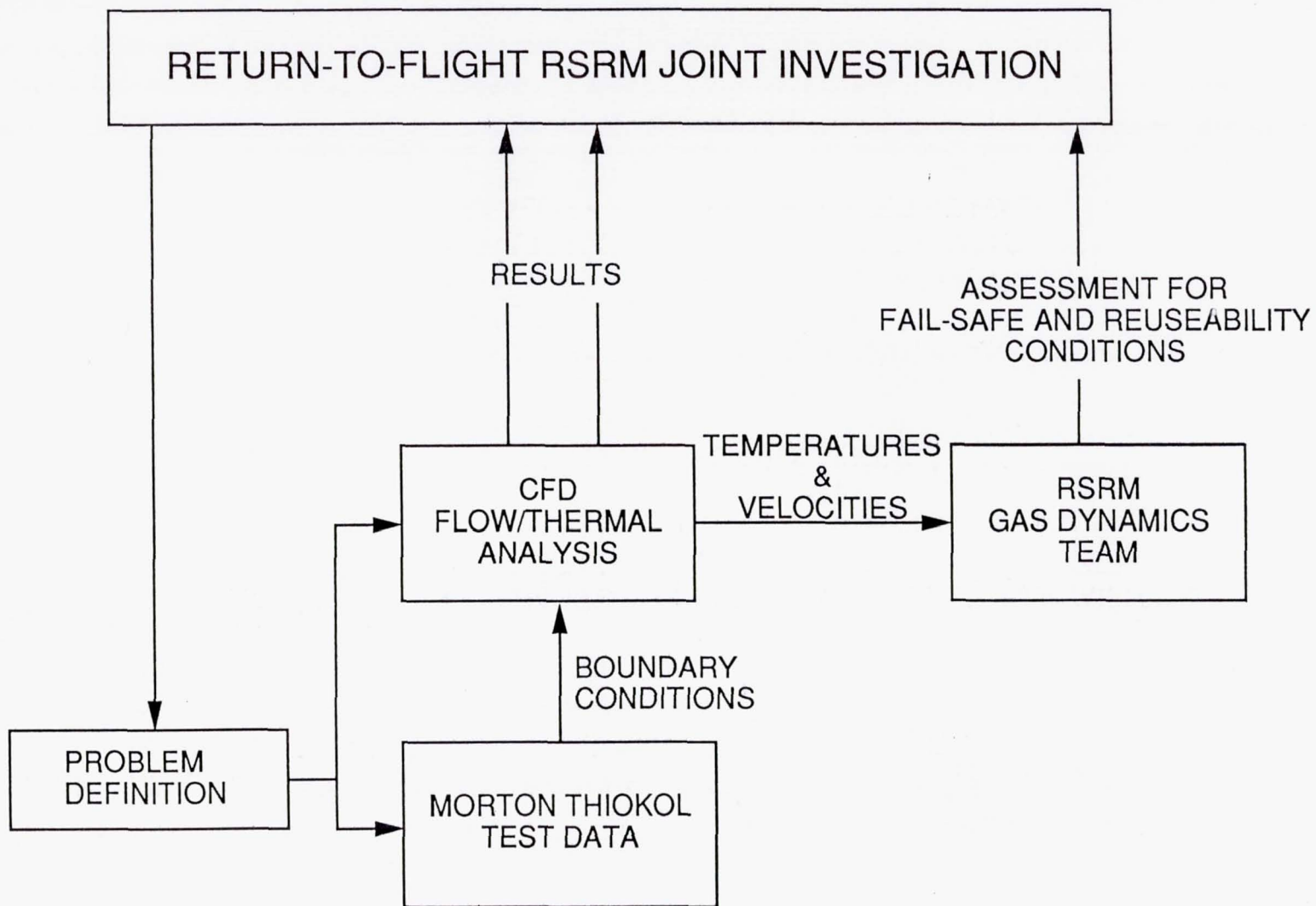
SRB NOZZLE/CASE AND CASE FIELD JOINT
FLOW AND THERMAL ANALYSIS

APPROACH: APPLICATION OF 3-D NAVIER-STOKES CODE (PHOENICS) TO FLOW
IN THE DEBOND GAP AND O-RING REGIONS COUPLED WITH
HEAT CONDUCTION OF THE FLUID AND NEIGHBORING "SOLIDS"
(NOZZLE/CASE 11592 CELLS; CASE FIELD 20088 CELLS)

PHOENICS
- (PARABOLIC, HYPERBOLIC, OR ELLIPTIC NUMERICAL INTEGRATION CODE SERIES)

MODEL USES:
- BODY-FITTED COORDINATES
- FINITE-VOLUME FORMULATION
- 3-D TRANSIENT
- K-EPSILON TURBULENCE MODEL
- TEMPERATURE DEPENDENT SOLID AND FLUID PROPERTIES
- WALL FUNCTIONS (LOG LAW OF THE WALL)
- CHILTON-COLBURN FORM OF REYNOLDS ANALOGY FOR HEAT TRANSFER AT WALL

GRID

Glass Phenolic

Carbon Phenolic

Debond

EPDM

NBR

Steel

Primary O-ring

Y

X

Primary O-Ring

x
z
Inlet

Primary O-Ring

X

Z

Inlet

Outlet

NX = 23
NY = 28
NZ = 18

185
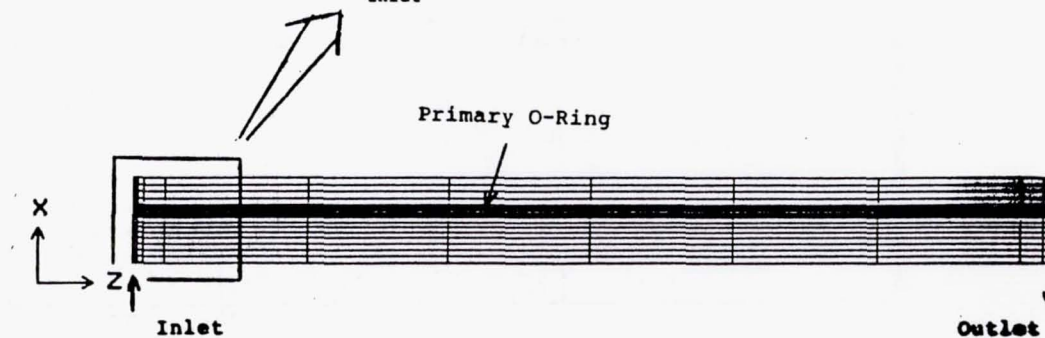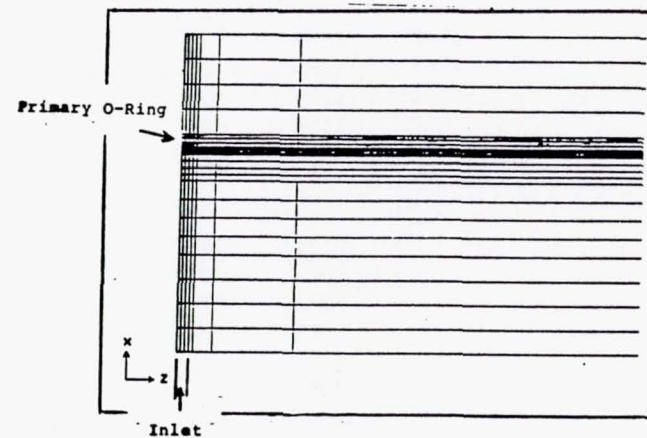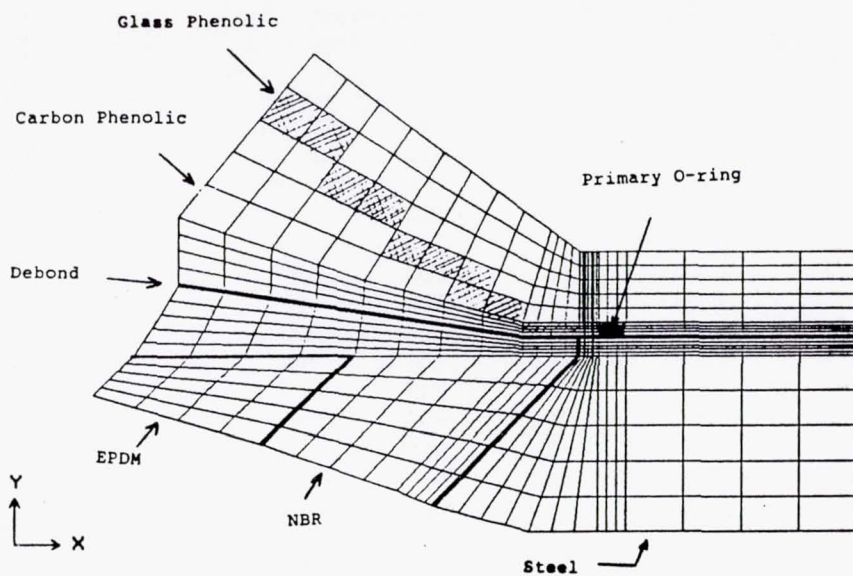
SUMMARY OF MAXIMUM TEMPERATURES FOR
NOZZLE/CASE JOINT MODEL

Run No.	Insul. Gap (in.)	Steel Gap (in.)	Debond Width (5) (in.)	Diff. P (psi)	Diff. P Angle (deg)	T max Gas (deg F)	T max Steel (deg F)	T max O-ring (deg F)	Notes
1	.024	.004	F.O.	1.08	0 – 180	142	180	105	
2	.024	.010	F.O.	1.08	0 – 180	295	230	170	
3	.024	.004	3.5	1.08	0 – 180	1120	1092	769	
4	.024	.010	3.5	1.08	0 – 180	2071	1432	1423	
5	.024	.015	F.O.	envelope	0 – 180	258	132	129	
6	.100	.050	F.O.	envelope	0 – 180	1125	659	607	
7	.024	.008	3.5	envelope	0 – 180	1628	1117	885	
8	.024	.008	3.5	QM–4	0 – 180	1103	742	582	
9	.024	.008	3.5	QM–4	0 – 180	1153	769	601	1
10	.024	.008	3.5	QM–4	0 – 120	1256	852	667	1
11	.024	.008	3.5	QM–4	0 – 120	1643	1380	909	1,2
12	.050	.010	0.4	QM–4	0 – 120	2898	2320	1510	1,2
13	.050	.010	0.4	QM–4	0 – 120				1,2,3
14	.024	.008	3.5	QM–4	0 – 120	1502	1304		1,2,3
15	.046	.008	0.75	QM–4	0 – 120	2276	2352	1856	1,2,3
16	.090	.008	0.75	QM–4	0 – 120	2834	2846	2341	1,2,3
17	.046	.008	0.75	QM–4	0 – 120	2278	2359	1859	1,2,3,4
18	.046	.008	0.75	QM–4	0 – 120	2278	2351	1858	1,2,3,6
19	.046	.008	0.75	QM–4	0 – 120	2211	2252	1847	1,2,3,7
20	.046	.008	0.75	QM–4	0 – 120	2083	2353	1691	1,2,3,8
21	.046/.020	.008	0.75	QM–4	0 – 120	2089	2178	1588	1,2,3,9
22	.046/.020	.008	0.75	QM–4	0 – 120	2059	2187	1568	1,2,3,9,10
23	.046/.020	.008	0.75	QM–4	0 – 120	2053	2272	1543	1,2,3,9, 11
24	.046/.020	.008	0.75	QM–4	0 – 120	1866	2255	1509	1,2,3,9,11,12,13
25	.046/.020	.008	0.75	DM–8	0 – 120	1610	1818	1274	2, 3, 9, 11

Notes:
1. Improved modeling of QM–4 duty cycle
2. Model revised to open NBR/glass phenolic area 360 deg. and improve average material properties
3. Material properties computed as function of temperature
4. Same as Run 15 but with number of time steps doubled
5. One-half of values listed input to model due to symmetry
6. 2 X nominal number of grid nodes in Z direction
7. Increased number of grid nodes in X direction (<2 X nominal)
8. 2 X nominal number of grid nodes in X direction
9. Model regrided to provide two insulation gap width capability
10. Y grid sensitivity. Number of insulation cells increased
11. K-Epsilon turbulence model
12. Y grid sensitivity. Number of fluid cells increased by factor of 2
13. Calculation of O-ring wall temperature corrected

186

5-1576-9-102

QM-4

DM-8

STEEL TEMP
GAS TEMP
O-RING TEMP

187

C-3
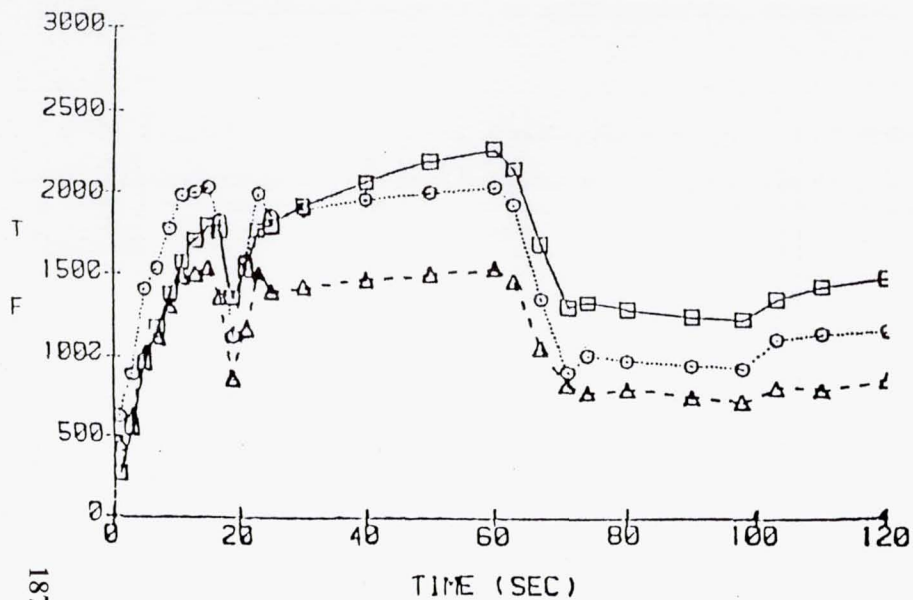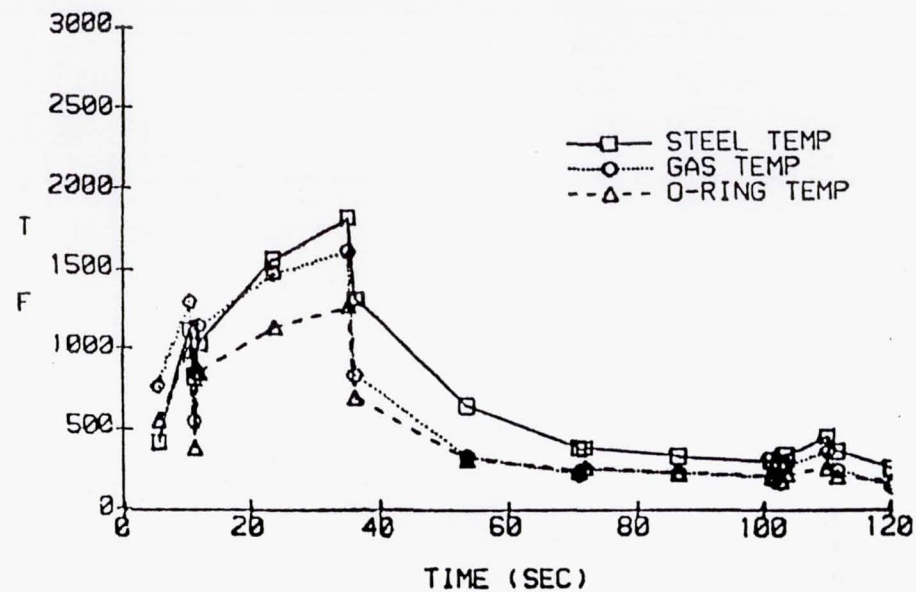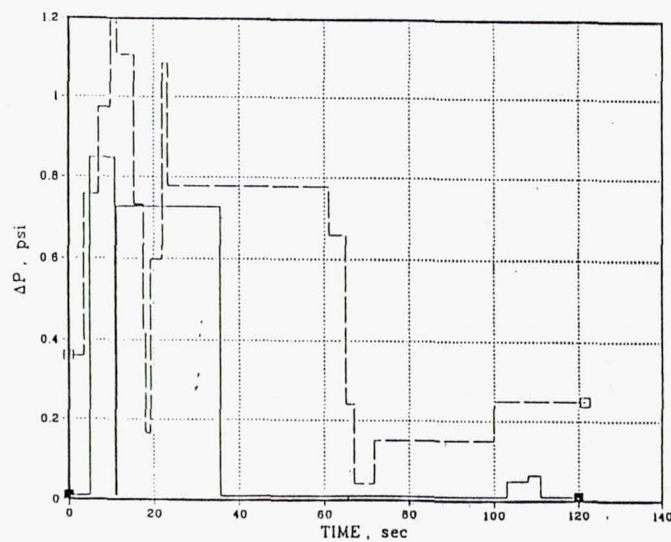
Legend
■ ΔP FOR DM-8
□ ΔP FOR QM-4

TIME, sec

GRID   37×32×19   GRID   GRID
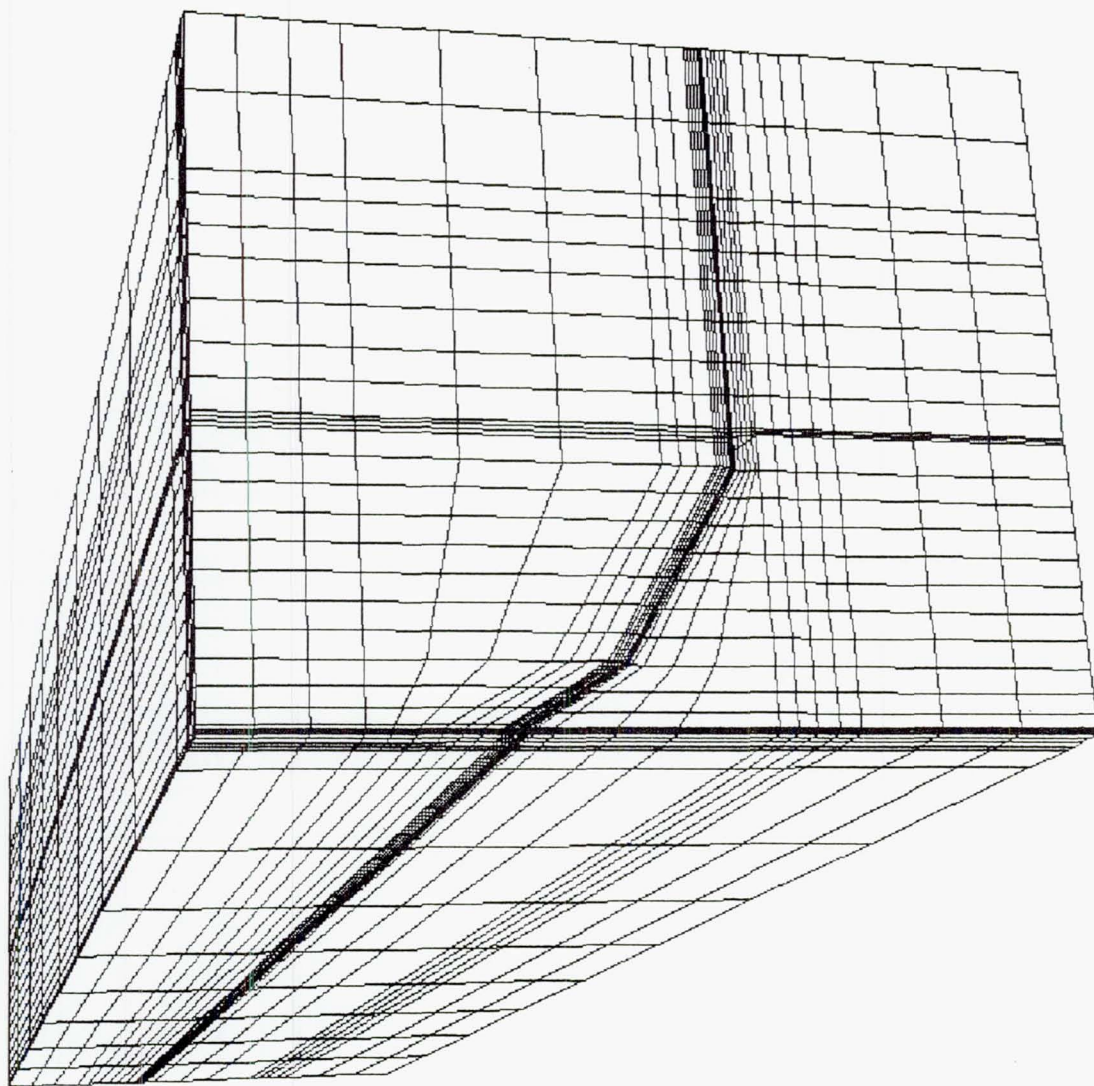
SUMMARY OF MAXIMUM TEMPERATURES
FOR FIELD JOINT MODEL

RUN	SPECIFICATION				CALCULATED RESULTS		
NO.	G1 (IN)	CIRCUM. DEBOND WIDTH (IN)	CIRCUM. DEBOND ANGLE (DEG)	Δp PSI	TMAX STEEL (DEG C)	TMAX GAS (DEG C)	TMAX O-RING (DEG C)
1	0.002	2.8	120	0.5	16.1	13.9	13.6
2	0.002	2.8	15	0.5	16.2	14.1	13.7
3	0.016	0.25	120	0.5	16.5	23.3	14.2
4	0.016	0.25	15	0.5	161.7	746.6	607.4
5	0.016	0.25	15	0.1	21.0	65.4	42.3

NOTE: FOR ALL CASES G2 = 0.0264", AND G3 = 0.0241"

189

5-1569-9-105

CONTOUR LEVELS

TEMPERATURE (DEG C)

0.010	MACH
0.00 DEG	ALPHA
5.00x10 2	Re
37x32x19	GRID

0.000×10 0
100.000
200.000
300.000
400.000
500.000
600.000
700.000
800.000
900.000
1000.000
1100.000
1200.000
1300.000
1400.000
1500.000
1600.000
1700.000
1800.000
1900.000
2000.000
2100.000
2200.000
2300.000
2400.000
2500.000
2600.000
2700.000
2800.000
2900.000
3000.000
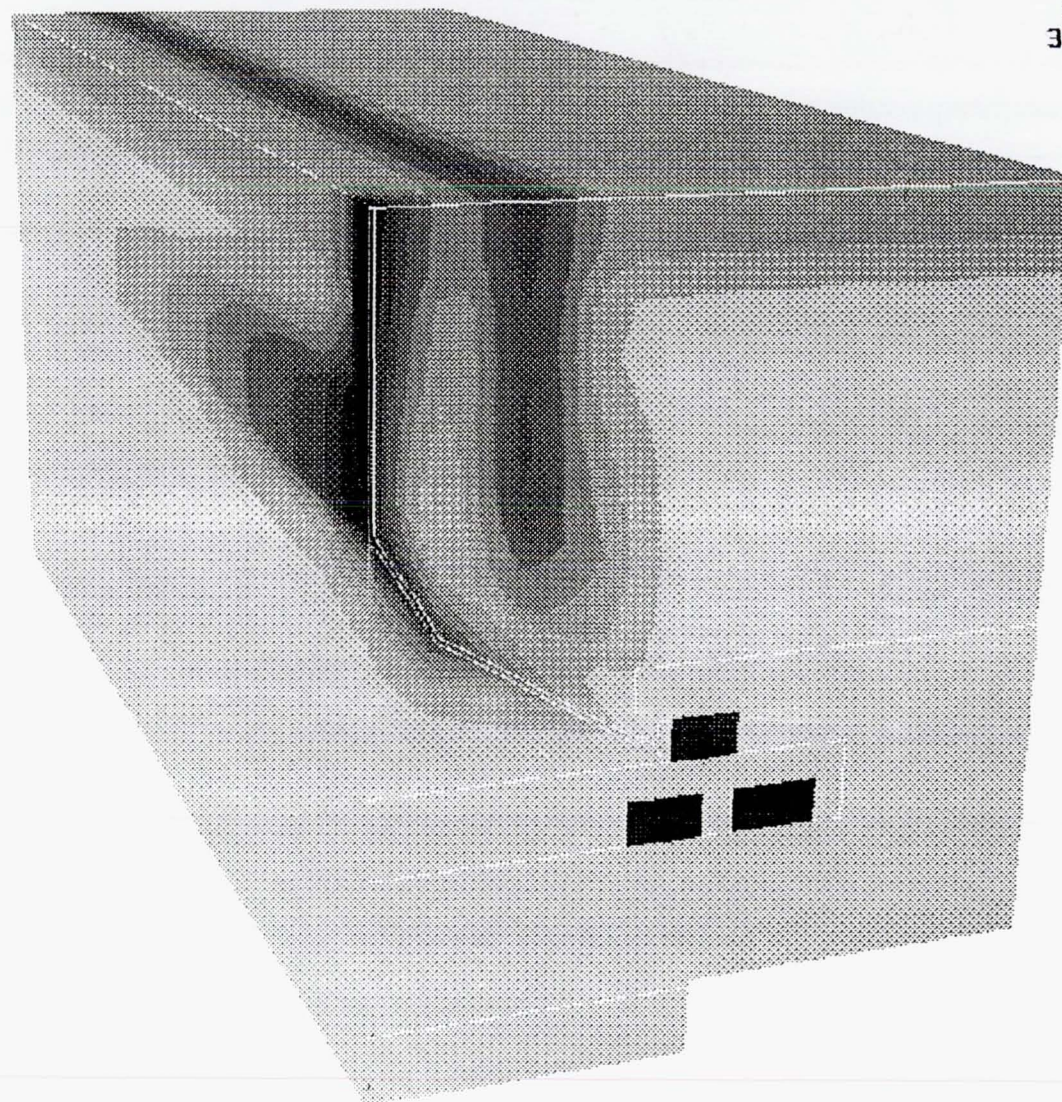
SRB NOZZLE/CASE AND CASE FIELD JOINT
FLOW AND THERMAL ANALYSIS

PROGRAM IMPACT:
- STEEL CASE TEMPERATURE LIMIT FOR REUSE (1000°F)
  - EXCEEDED FOR NOZZLE/CASE JOINT (IF 2 LEAKPATHS OCCUR WHICH IS VERY UNLIKELY)
  - WITHIN LIMIT FOR CASE FIELD JOINT

- ABLATION TEMPERATURE LIMIT FOR O-RINGS (700°F)
  - EXCEEDED FOR NOZZLE/CASE JOINT (IF 2 LEAKPATHS OCCUR WHICH IS AGAIN UNLIKELY)
  - WITHIN LIMIT FOR CASE FIELD JOINT (EXCEPT ONE CASE WHERE FLOW PATH IS ONLY OVER 15°)

CONCLUSIONS:
- ANALYSIS CONSIDERED CONSERVATIVE, DUE TO WORST CASE SCENARIOS BEING ANALYZED

- ANALYSIS PERFORMED TO VERIFY OTHER ANALYSIS BEING DONE IN PARALLEL, AT MORTON THIOKOL TO SUPPORT RETURN-TO-FLIGHT STATUS

- PROBABILITY OF TWO LEAKPATHS OCCURING IS ONE IN ONE-THOUSAND SO DESIGN MEETS FAIL-SAFE AND REUSEABILITY CONDITIONS.

5-1623-9-103

SESSION IX

TURBOMACHINERY

Chairman:
Robert M. Stubbs
Chief, Computational Methods Branch
NASA Lewis Research Center

SIMULATION OF TURBOMACHINERY FLOWS

by

John J. Adamczyk
NASA Lewis Research Center

ABSTRACT

Significant advancements have been made in the last five years in the abil-
ity to model turbomachinery flows of engineering interest. This advance-
ment can be directly attributed to the second generation of supercomputers
like the Cray XMP and Cray II and advanced instrumentation techniques.
Early on, the National Aeronautics and Space Administration Lewis Research
Center recognized the potential gains in turbomachinery performance and
life that could be achieved by taking advantage of this technology and
instituted a comprehensive research program in turbomachinery flow model-
ing. This activity combined the areas of fluid flow analysis, computa-
tional fluid dynamics, and experimental fluid mechanics. As a result of
this activity, Lewis has become an internationally recognized leader in
turbomachinery flow modeling. Many of the research activities conducted
under this progam have been utilized by industry. The presentation will
give an overview of this program and provide sample illustration of simu-
lation performed to date.

HIGH BY PASS TURBOFAN ENGINE

FOUR-STAGE L. P. COMPRESSOR

TWO-ZONE COMBUSTOR

SINGLE-STAGE FAN

FOUR-STAGE L. P. TURBINE

MIXER

TEN-STAGE H. P. COMPRESSOR

SINGLE-STAGE H. P. TURBINE
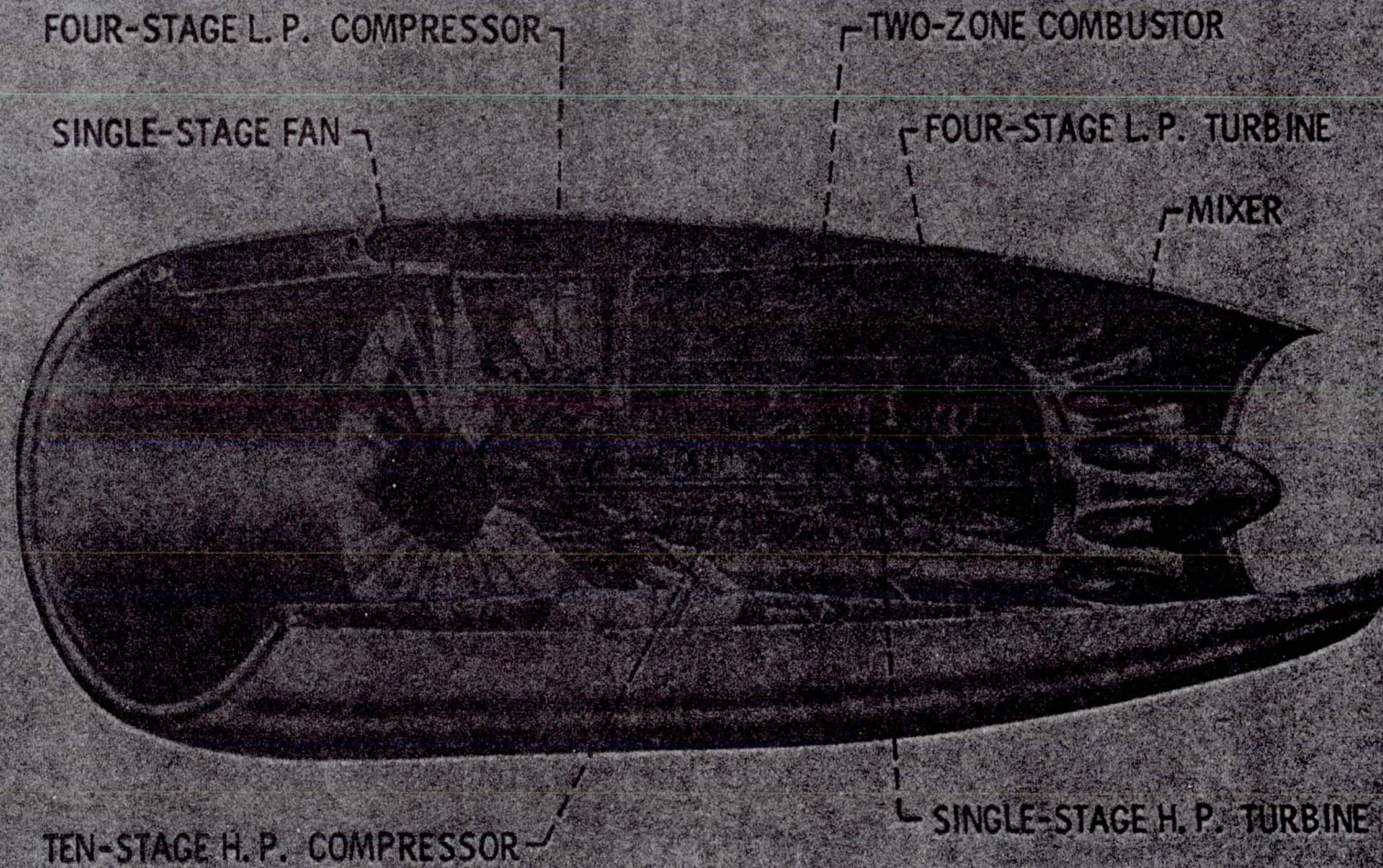
CLOSELY COUPLED EXPERIMENTAL
AND COMPUTATIONAL RESEARCH

**NUMERICAL
CODE DEVELOPMENT**

EXPERIMENTATION

**MODELING OF PHYSICS
VALIDATION OF COMPUTATIONS**
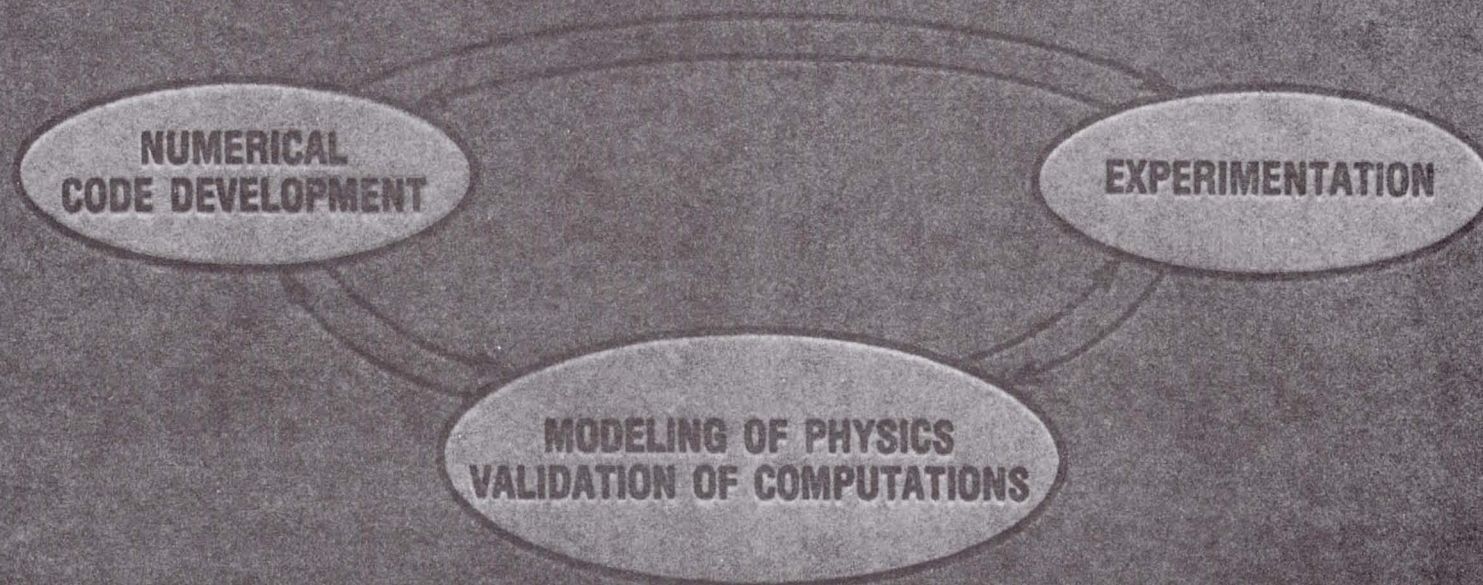
**UNDERSTANDING OF FLOW PHYSICS
ACCURATE PREDICTIVE CODES**

CD-87-28477

CFD IN THE PROBLEM SOLVING PROCESS

PHYSICAL PHENOMENA
(eg. FLUID MOTION)

EXPERIMENTS

COMPUTATIONS

COMPONENT

FUNDAMENTAL

GOVERNING EQUATIONS

SIMPLIFYING ASSUMPTIONS

SOLVABLE EQUATION SET

VALIDATION DATA

ANALYTICAL SOLUTION

NUMERICAL SOLUTION

CALIBRATION DATA

ALGORITHMS
GRIDS
COMPUTERS

IMPROVED PREDICTIVE CAPABILITY
IDENTIFICATION OF NEW CONCEPTS
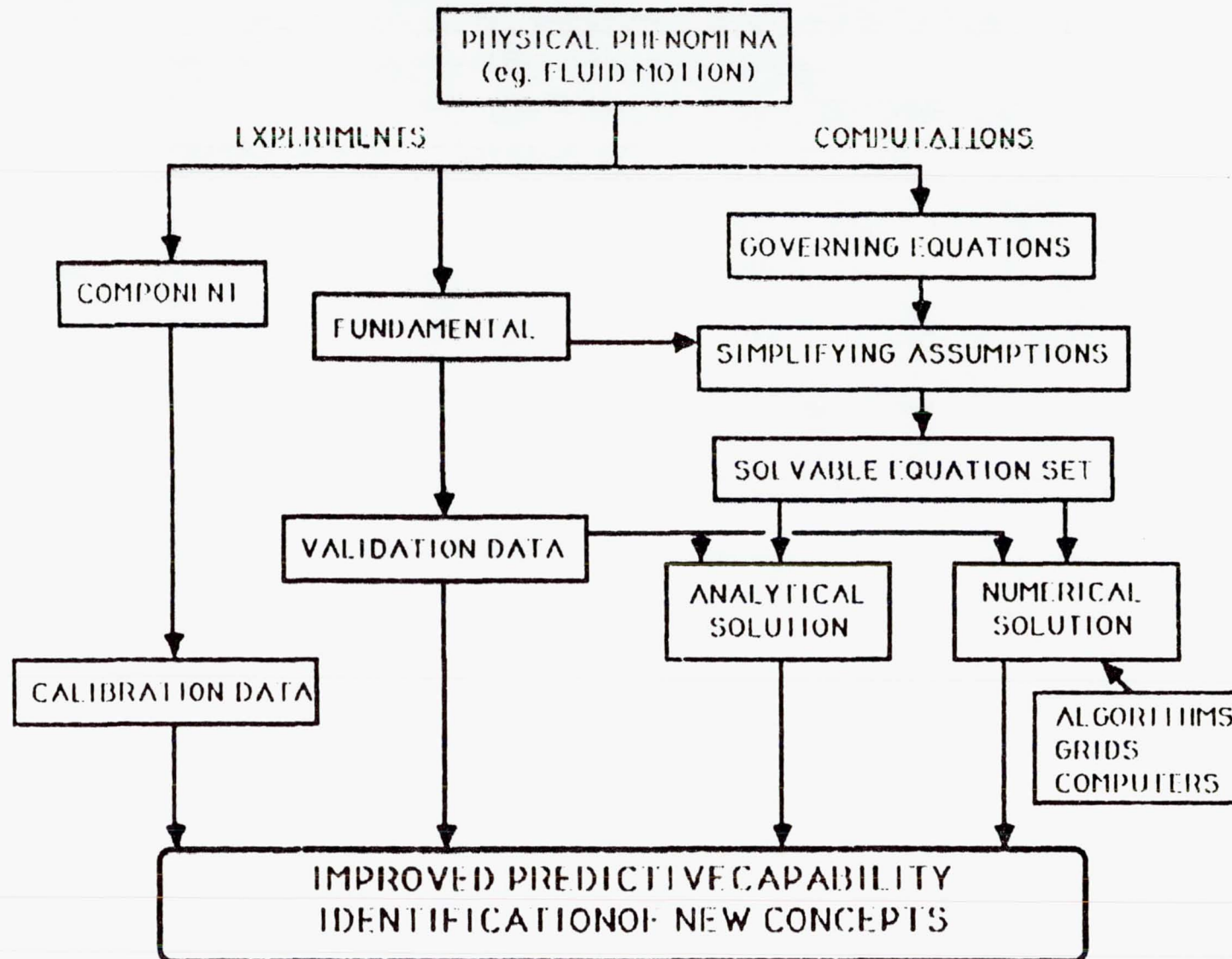
EQUATIONS HIERARCHY

199
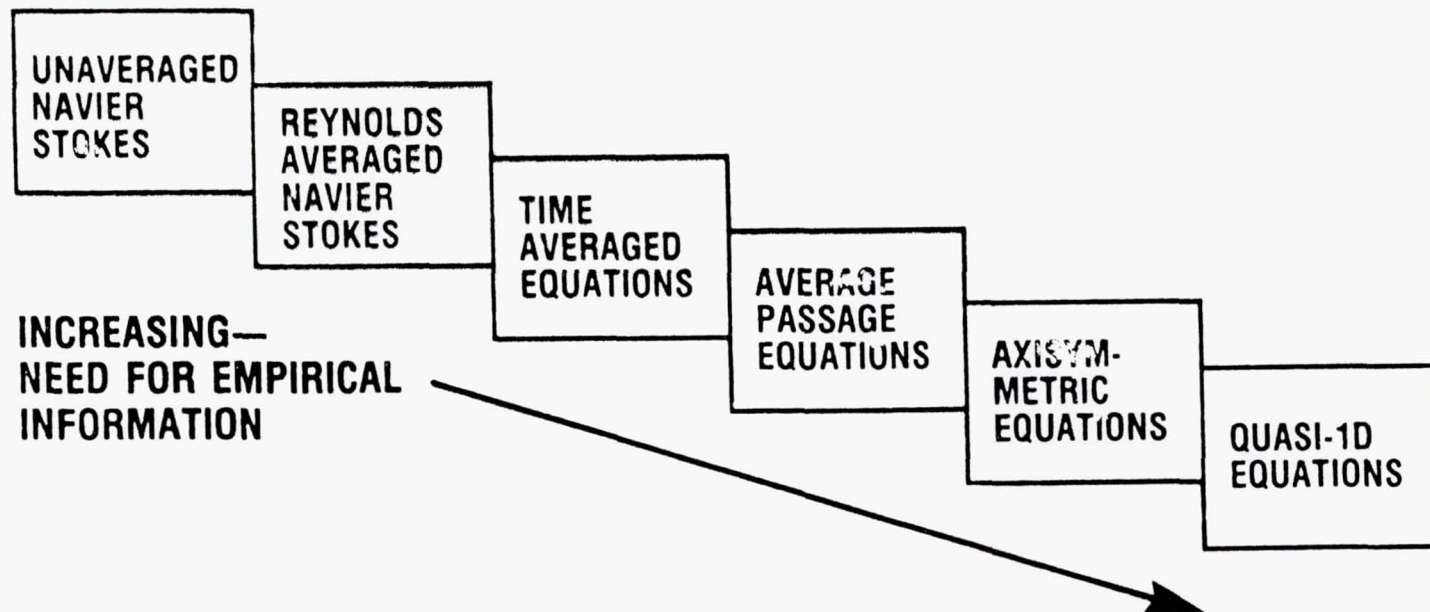
CASCADE ENDWALL FLOW STRUCTURE
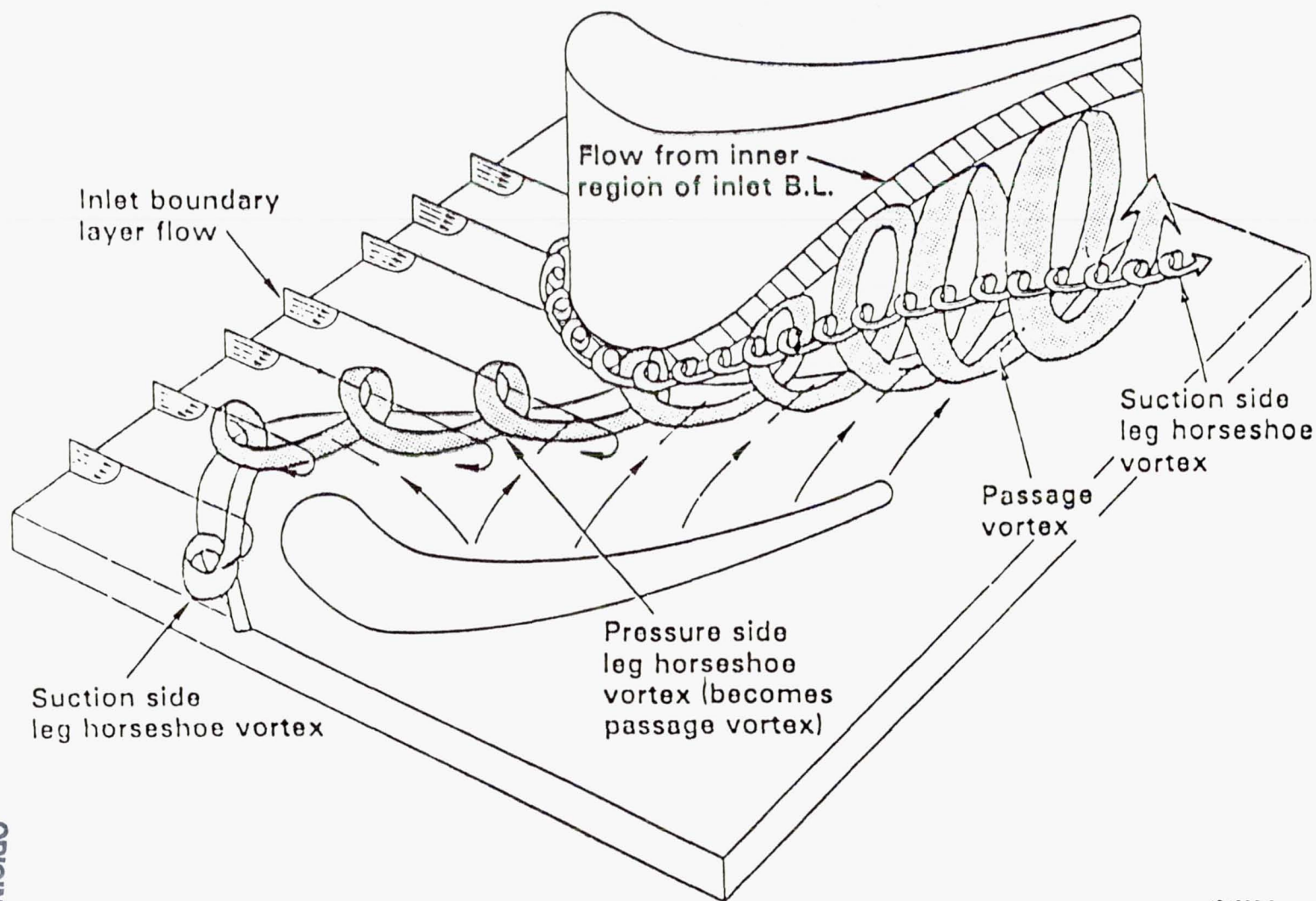
Inlet boundary
layer flow

Flow from inner
region of inlet B.L.

Suction side
leg horseshoe
vortex

Passage
vortex

Pressure side
leg horseshoe
vortex (becomes
passage vortex)

Suction side
leg horseshoe vortex

JJ4507-5
860606
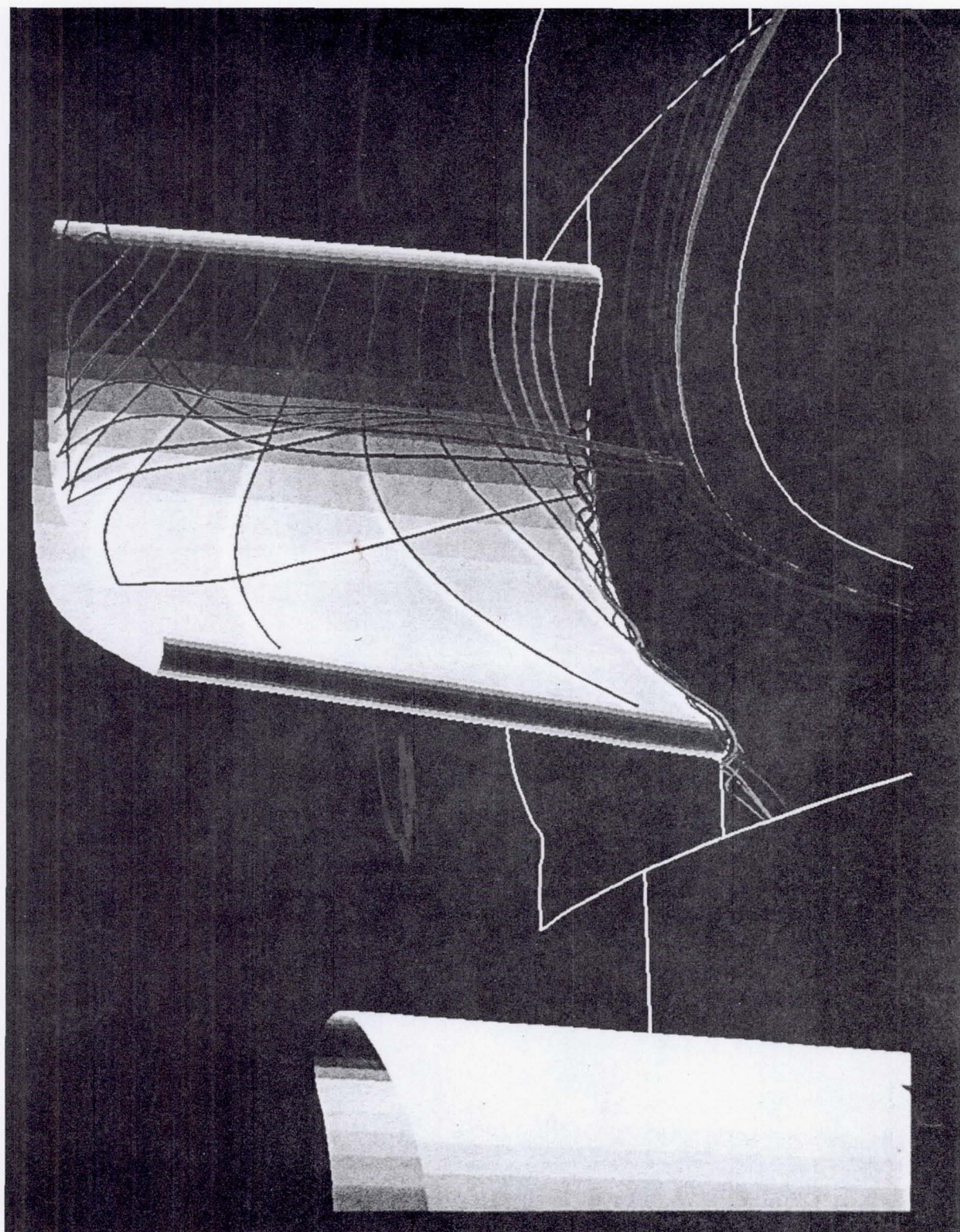
EVOLUTION OF THE TOTAL TEMPERATURE
FIELD WITHIN THE S.S.M.E. FUEL TURBINE
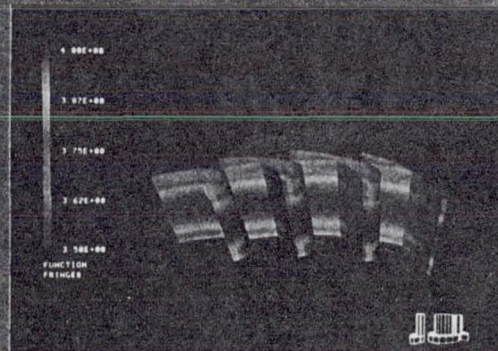
1st VANE
MID PASSAGE
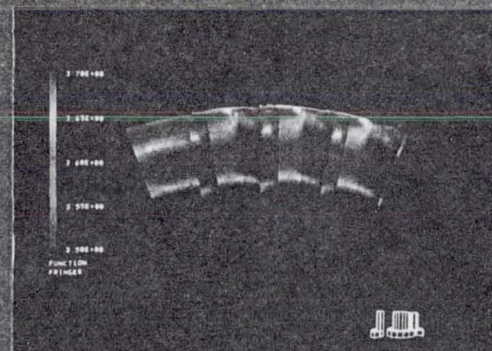
2nd VANE
MID PASSAGE

1st ROTOR
MID PASSAGE
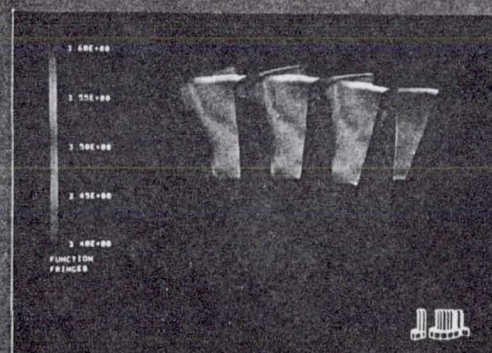
2nd ROTOR
MID PASSAGE

SIMULATION PERFORMED ON LEWIS CRAY XMP 24

CD-87-24839
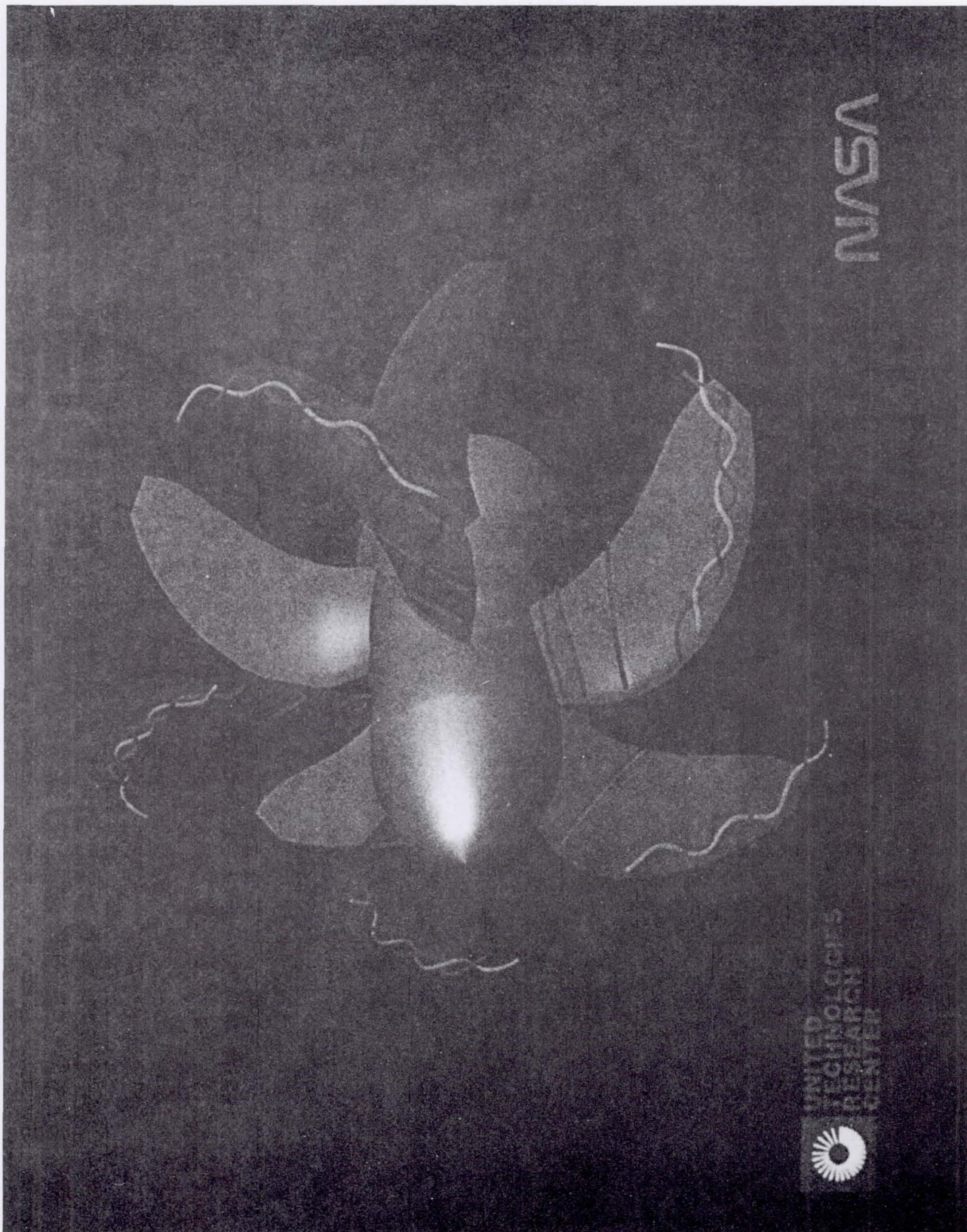
ADVANCED CONTRA-ROTATING PROPELLER NOISE PREDICTION

2' GE F7/A7, LeRC 8x6 WIND TUNNEL, DESIGN CONDITION (M=0.72)
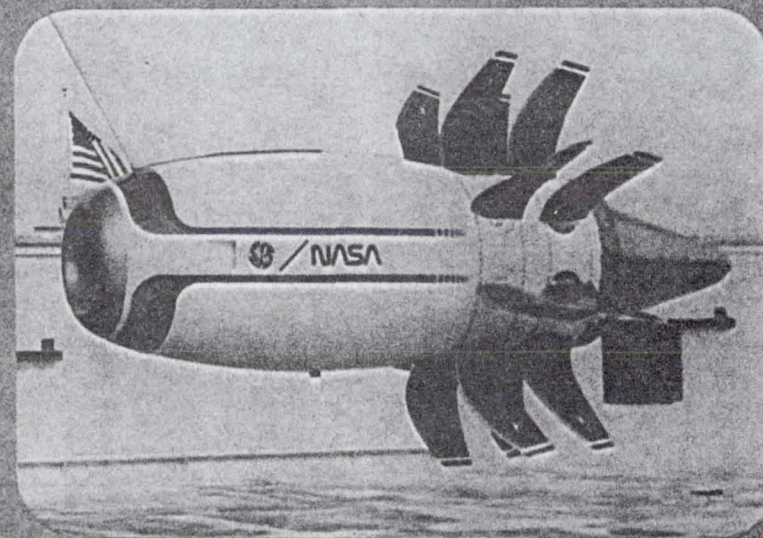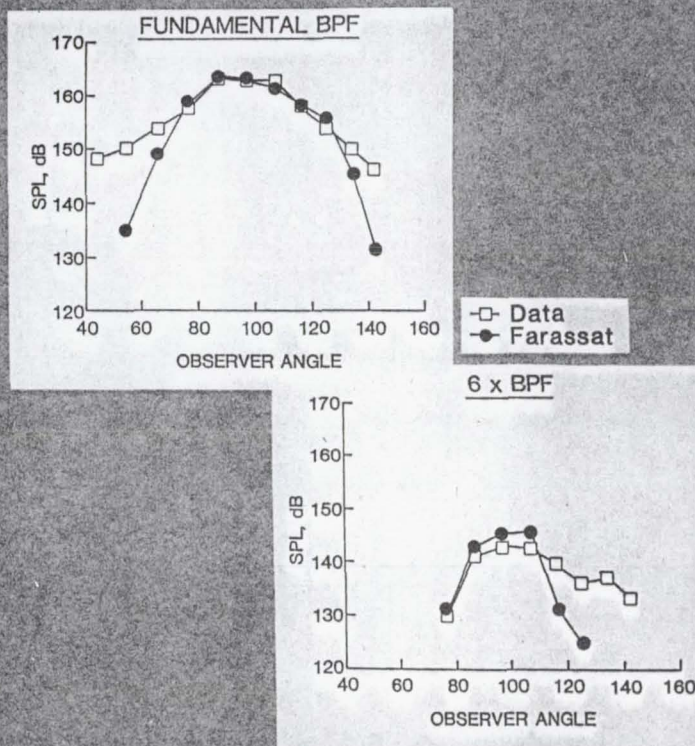
PREDICTION OF TURBINE ROTOR-STATOR INTERACTION
USING NAVIER-STOKES METHODS

N. K. Madavan and M. M. Rai
NASA Ames Research Center
Moffett Field, CA 94035

and

S. Gavali
Amdahl Corporation
Sunnyvale, CA 94088

Abstract

Flows in turbomachinery are generally complex and do not easily lend themselves to numerical computation. The flows are three-dimensional and inherently unsteady. The unsteadiness arises from the interaction of the downstream airfoils with the wakes and passage vortices generated upstream, from the motion of the rotors relative to the stators and from vortex shedding at blunt airfoil trailing edges. Complicated blade geometries and flow phenomena such as separation and periodic transition from laminar to turbulent flow add to the numerical complexity. Nevertheless, the accurate numerical analysis of such flows is a problem of considerable interest and practical importance to the turbomachinery community.

Much of the early work in turbomachinery flow prediction focussed on airfoil cascades. While such analyses of flows in isolated airfoil rows have helped improve our understanding of the flow phenomena and have gained widespread acceptance in the industrial community as a design tool, they do not yield any information regarding the unsteady effects arising out of rotor-stator aerodynamic interaction. These interaction effects become increasingly important as the distance between successive stator and rotor rows is decreased. Thus, the need exists for analytical tools that treat the rotor and stator airfoils as a system and provide information regarding the magnitude and the impact of the unsteady effects.

The focus of this presentation is a three-dimensional, time-accurate, thin-layer Navier-Stokes code that has been recently developed to study rotor-stator interaction problems. A system of patched and overlaid grids that move relative to each other is used to discretize the flow field and the governing equations are integrated using a third-order upwind scheme set in an iterative, implicit framework. The code has been used to simulate subsonic flow through an axial turbine configuration for which considerable experimental data exists. Grid refinement studies have also been conducted as part of the code validation process. The current status of the research, along with planned future directions, are also discussed.

INTRODUCTION

- THE PREDICTION OF FLOWS IN TURBOMACHINERY IS A PROBLEM OF CONSIDERABLE INTEREST

- THE FLOWFIELDS ARE INHERENTLY UNSTEADY DUE TO :

  MOTION OF ROTORS RELATIVE TO THE STATORS

  INTERACTION OF DOWNSTREAM AIRFOILS WITH WAKES OF UPSTREAM AIRFOILS

  VORTEX SHEDDING AT BLUNT TRAILING EDGES

- UNSTEADY (OR INTERACTION) EFFECTS PRESENT EVEN FOR AXIAL GAPS USED IN CURRENT DESIGNS (50% TO 25% CHORD)

INTRODUCTION.....CONTD.

- COMPLEX BLADE GEOMETRIES, PERIODIC TRANSITION FROM LAMINAR TO TURBULENT FLOW, FLOW SEPARATION, ETC. PRESENT ADDITIONAL COMPUTATIONAL DIFFICULTIES

- NEED EXISTS FOR A COMPUTATIONAL TOOL THAT TREATS THE COMPLETE TURBINE STAGE AS A SYSTEM AND PROVIDES INFORMATION REGARDING THE UNSTEADY EFFECTS

POSSIBLE GAINS

- IMPROVED PERFORMANCE (LOWER LOSSES, ETC.)

- IMPROVED STRUCTURAL DESIGN (STRUCTURES THAT BETTER WITHSTAND THE DYNAMIC STRESSES ASSOCIATED WITH THE UNSTEADY NATURE OF THE FLOW)

- AN UNDERSTANDING OF THE ACOUSTICS (MINIMIZATION OF ENGINE NOISE)

- PREDICTION OF UNSTEADY HEAT TRANSFER (IMPROVED COOLING TECHNOLOGY)

CURRENT STATUS

- COMPUTER CODES CAPABLE OF PREDICTING UNSTEADY FLOWFIELDS IN SINGLE-STAGE TURBOMACHINERY DEVELOPED

    ROTOR-2 .... 2D, NAVIER-STOKES CODE

    ROTOR-3 .... 3D, NAVIER-STOKES CODE

CURRENT STATUS.....CONTD.

- CODE CAPABILITIES DEMONSTRATED BY SIMULATING AN EXPERIMENTAL SINGLE—STAGE AXIAL TURBINE CONFIGURATION

    2D COMPUTATIONS

    3D COMPUTATIONS FULLY ACCOUNTING FOR HUB, CASING AND ROTOR TIP CLEARANCE EFFECTS

    GRID—REFINEMENT STUDIES IN 3D

- STATE—OF—THE—ART COMPUTER GRAPHICS TECHNIQUES USED FOR VISUALIZATION OF COMPUTED RESULTS

    "STEREO ANIMATION" TECHNIQUES

COMPUTATIONAL DETAILS

- HIGH—ORDER UPWIND FINITE—DIFFERENCE ALGORITHM FOR TIME—ACCURATE SOLUTION OF THE THIN—LAYER NAVIER—STOKES EQUATIONS

- ALGORITHM SET IN AN ITERATIVE, FACTORED AND IMPLICIT FRAMEWORK

- SYSTEM OF PATCHED AND OVERLAID GRIDS FOR FLOWFIELD DISCRETIZATION

- ROTOR GRIDS MOVE RELATIVE TO THE STATOR GRIDS

- BALDWIN—LOMAX TYPE TURBULENCE MODEL USED

COMPUTATIONAL GRID
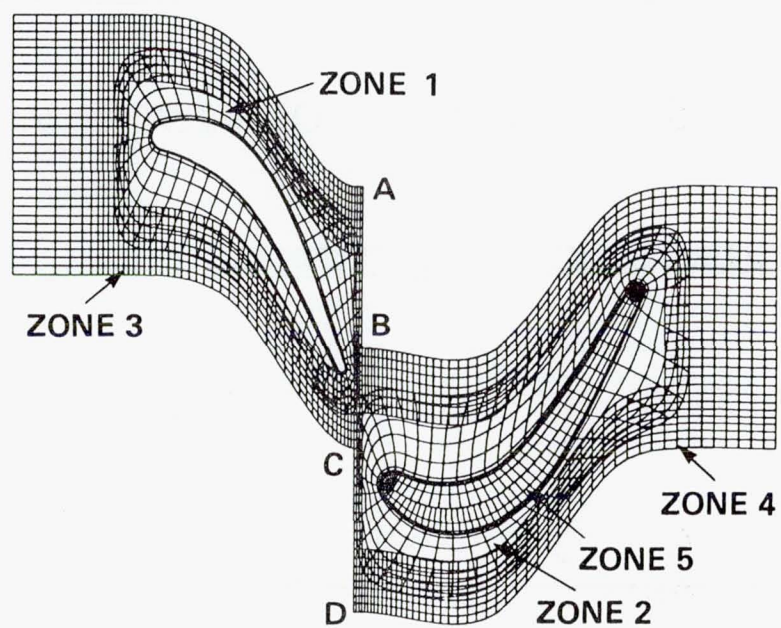
SPANWISE VARIATION OF STATOR TIME-AVERAGED PRESSURE
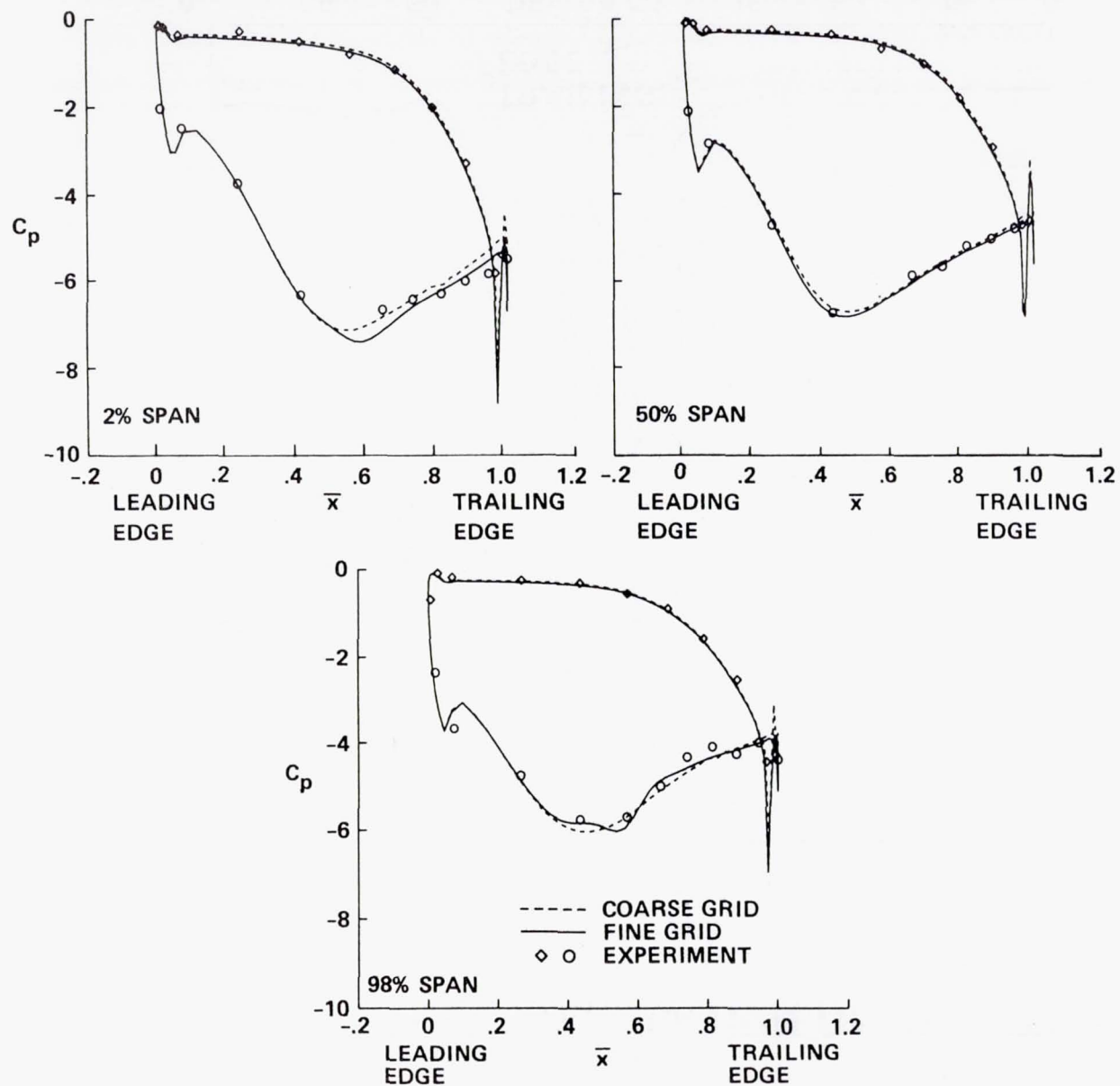
PRESSURE AMPLITUDE DISTRIBUTION ON THE STATOR
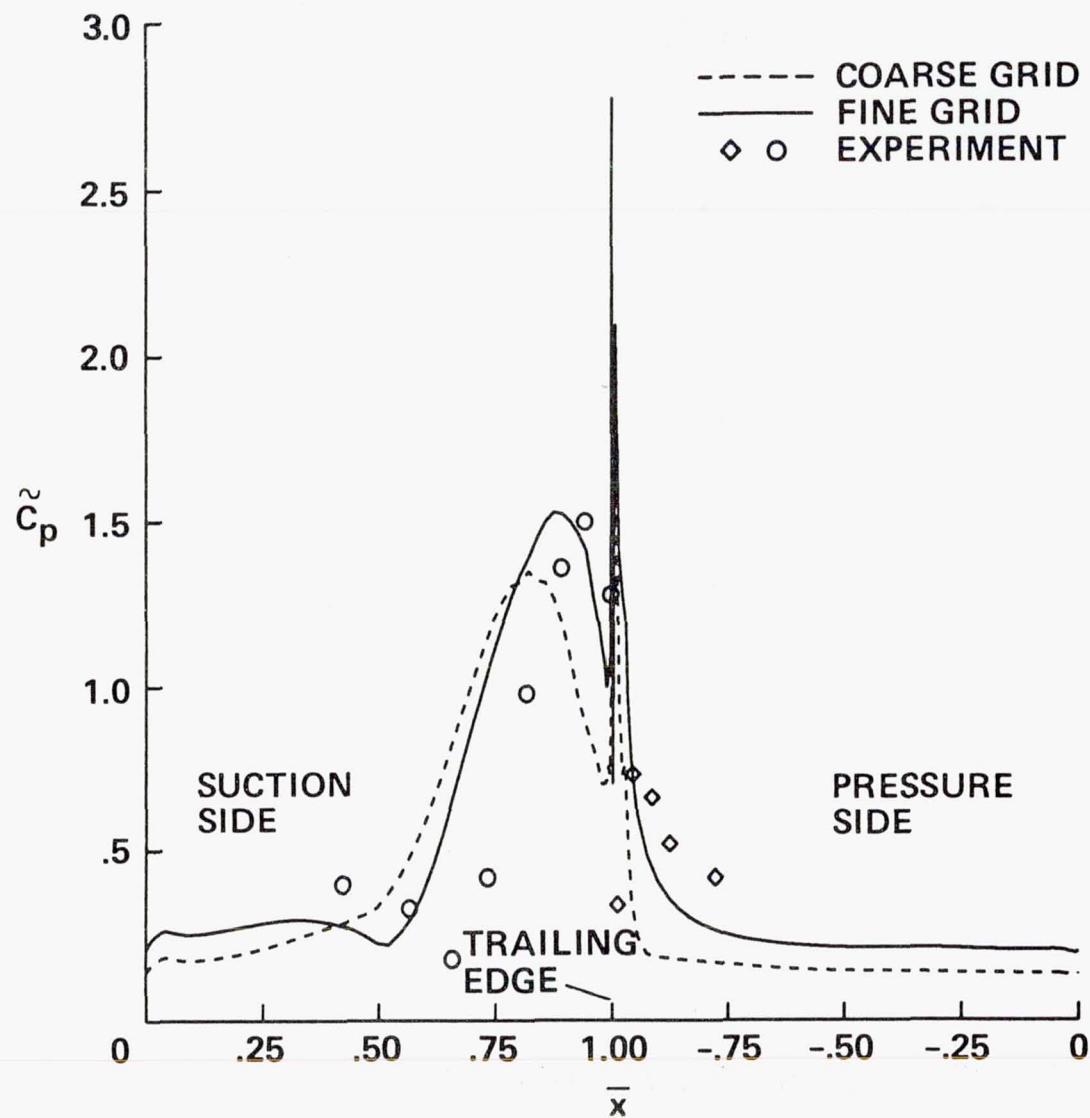
TIME-AVERAGED LIMITING STREAMLINES
ROTOR SUCTION SURFACE

FINE GRID
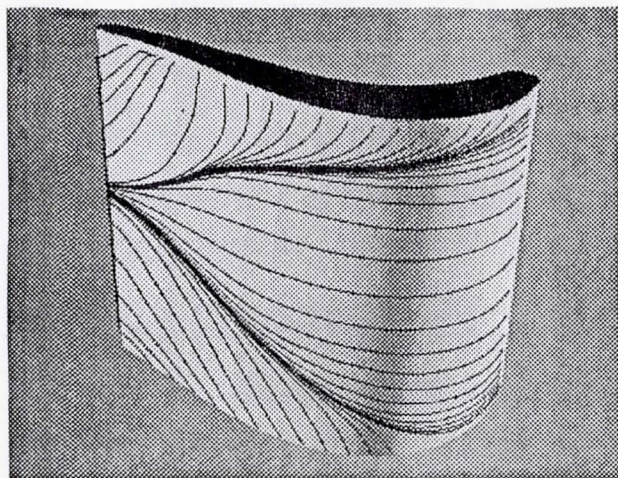
EXPERIMENTAL VISUALIZATION
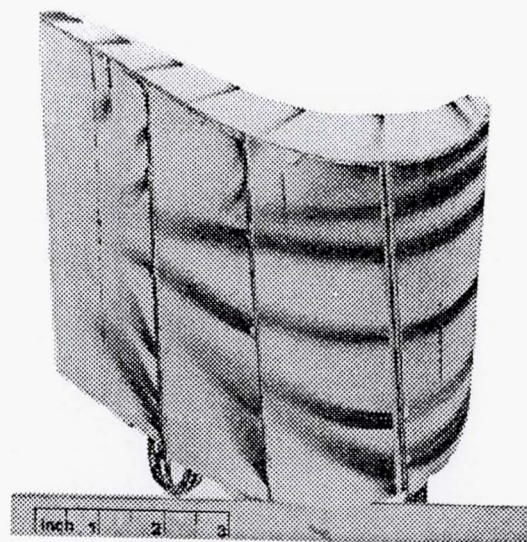
SUMMARY AND FUTURE DIRECTIONS

- 2D AND 3D UNSTEADY, THIN—LAYER NAVIER—STOKES CODES DEVELOPED TO SIMULATE ROTOR/STATOR INTERACTION IN TURBOMACHINERY

- CURRENT RESEARCH EFFORTS AND FUTURE DIRECTIONS INCLUDE :

    MULTI—BLADE COMPUTATIONS

    MULTI—STAGE COMPUTATIONS

    BOUNDARY CONDITIONS

    TURBULENCE MODELING

    CODE ACCELERATION TECHNIQUES

    GRAPHICS

Turbine Stage Aerodynamics
And Heat Transfer Prediction

L. W. Griffin and H. V. McConnaughey
NASA/MSFC

A numerical study of the aerodynamic and thermal environment
associated with axial turbine stages is presented.
Computations were performed using a modification of the
unsteady NASA Ames viscous code, ROTOR1, and an improved
version of the NASA Lewis steady inviscid cascade system
MERIDL-TSONIC coupled with boundary layer codes BLAYER and
STAN5. Two different turbine stages were analyzed: the
first stage of the United Technologies Research Center Large
Scale Rotating Rig (LSRR) and the first stage of the Space
Shuttle Main Engine (SSME) high pressure fuel turbopump
turbine. The time-averaged airfoil midspan pressure and heat
transfer profiles were predicted for numerous thermal
boundary conditions including adiabatic wall, prescribed
surface temperature, and prescribed heat flux. Computed
solutions are compared with each other and with experimental
data in the case of the LSRR calculations. Modified ROTOR1
predictions of unsteady pressure envelopes and instantaneous
contour plots are also presented for the SSME geometry.
Relative merits of the two computational approaches are
discussed.

OVERVIEW

- **OBJECTIVES**

- **MOTIVATION**

- **APPROACH**

    - CODES

    - APPLICATIONS

- **RESULTS**

    - AERODYNAMIC

    - HEAT TRANSFER

- **COMPUTER RESOURCES REQUIREMENTS**

- **IMPACT**

- **SUMMARY AND CONCLUSIONS**

5-1556-9-105

OBJECTIVES

- DEFINITION OF STEADY AND UNSTEADY AEROTHERMAL ENVIRONMENTS FOR THE SPACE SHUTTLE MAIN ENGINE (SSME) HIGH PRESSURE FUEL TURBOPUMP (HPFTP) TURBINE

- CALIBRATION OF TURBINE ANALYSIS CODES VIA COMPARISON OF PREDICTED AND EXPERIMENTALLY MEASURED AIRFOIL LOADS IN UNITED TECHNOLOGIES RESEARCH CENTER LARGE SCALE ROTATING RIG (LSRR)

5-1557-9-105

MOTIVATION

RETURN-TO-FLIGHT TURBINE BLADE CRACKING INVESTIGATION

PROBLEM DEFINITION

1-D TURBINE MODELS: GAS PATH AND COOLANT PATH

LEAKAGE

CFD ANALYSIS

B. C.

THERMAL ANALYSIS (SINDA)

STRESS ANALYSIS (ANSYS)

FLIGHT ACCEPTABILITY VERIFIED

ASSESSMENT OF HARDWARE FIXES

IDENTIFICATION OF CRITICALLY STRESSED REGIONS

220

5-1629-9-103
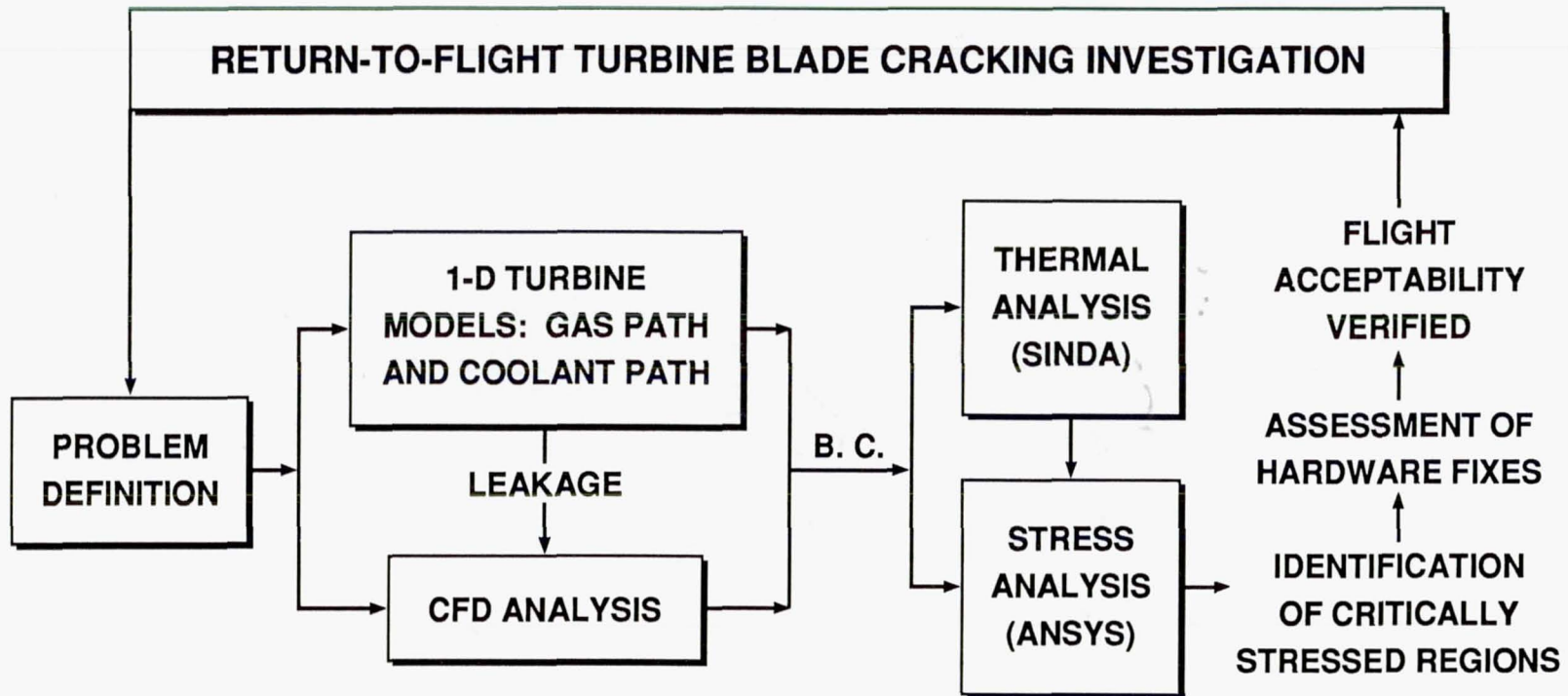
APPROACH

CODES:

- MTSBL-
  STAN5
  — STEADY INVISCID QUASI-3D SYSTEM MERIDL-
  TSONIC COUPLED WITH BOUNDARY LAYER CODES
  BLAYER AND STAN5. DEVELOPED AT NASA/LEWIS.

- ROTOR1
  — UNSTEADY 2D SINGLE-STAGE CODE DEVELOPED AT
  NASA/AMES. ASSUMES EQUAL BLADE COUNT.
  MODIFIED TO INCORPORATE HEAT TRANSFER
  PREDICTION CAPABILITY

APPLICATIONS:

- LSRR
  — CODE CALIBRATION

- SSME HPFTP
  — ENVIRONMENT DEFINITION

221

5-1558-9-105

PRESSURE DISTRIBUTIONS FOR THE LSRR

Stator

Rotor

5-1562-9-105
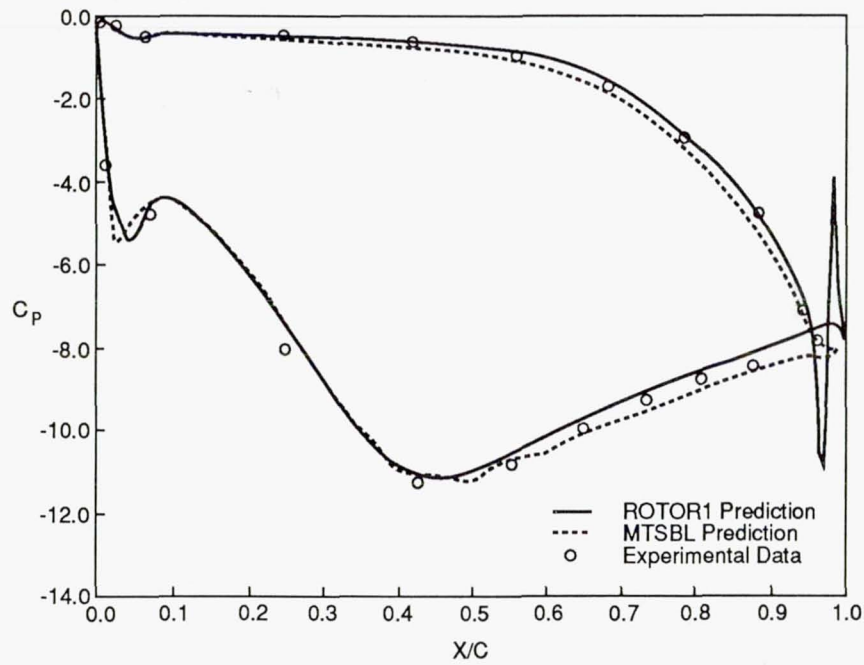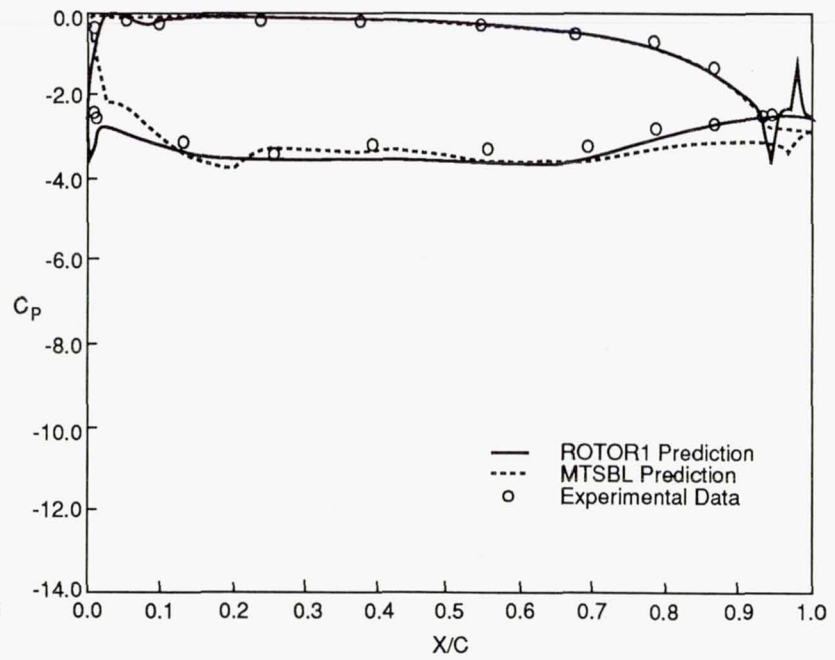
PRESSURE DISTRIBUTIONS FOR
THE SSME HPFTP

Stator

Rotor

5-1563-9-105
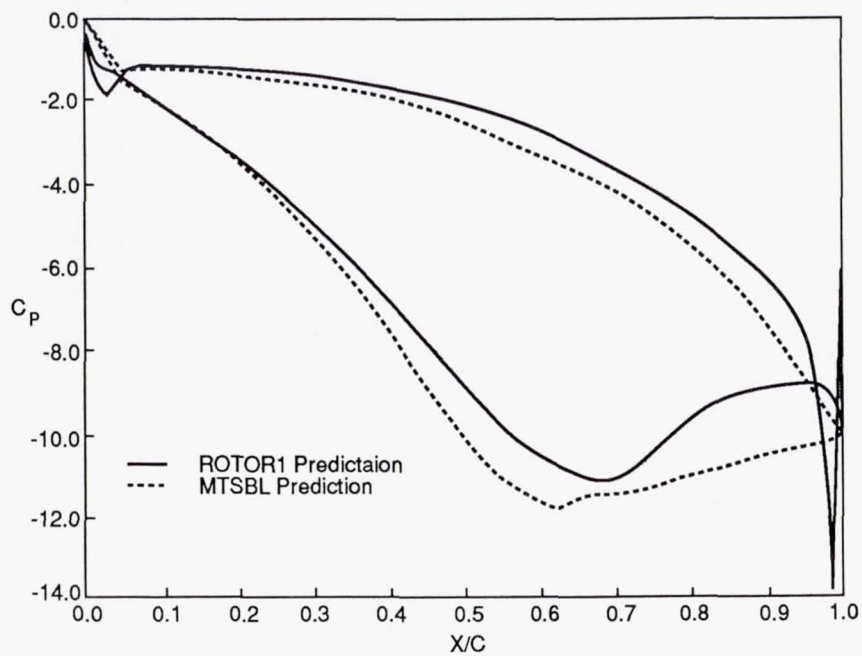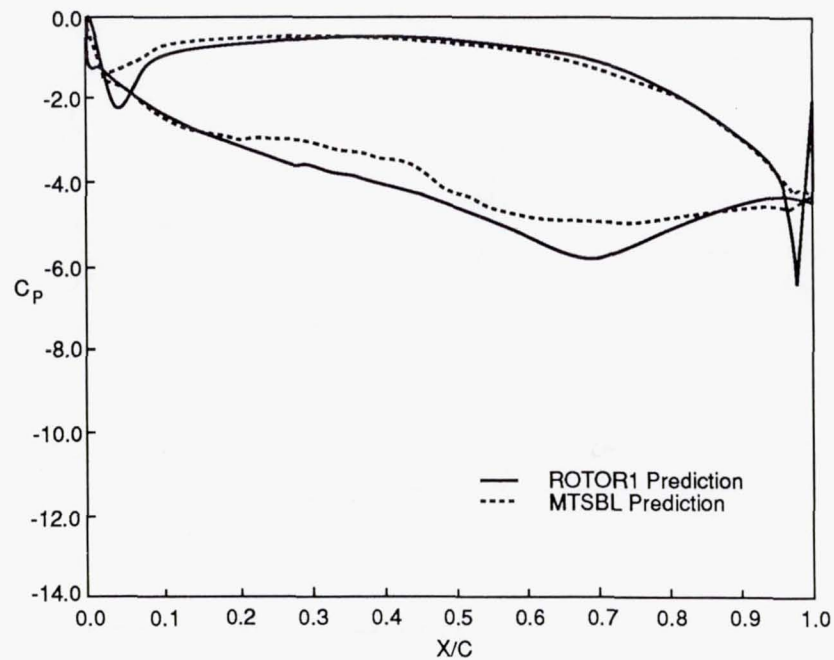
UNSTEADY PRESSURE DISTRIBUTIONS ON
THE SSME HPFTP ROTOR

5-1592-9-105
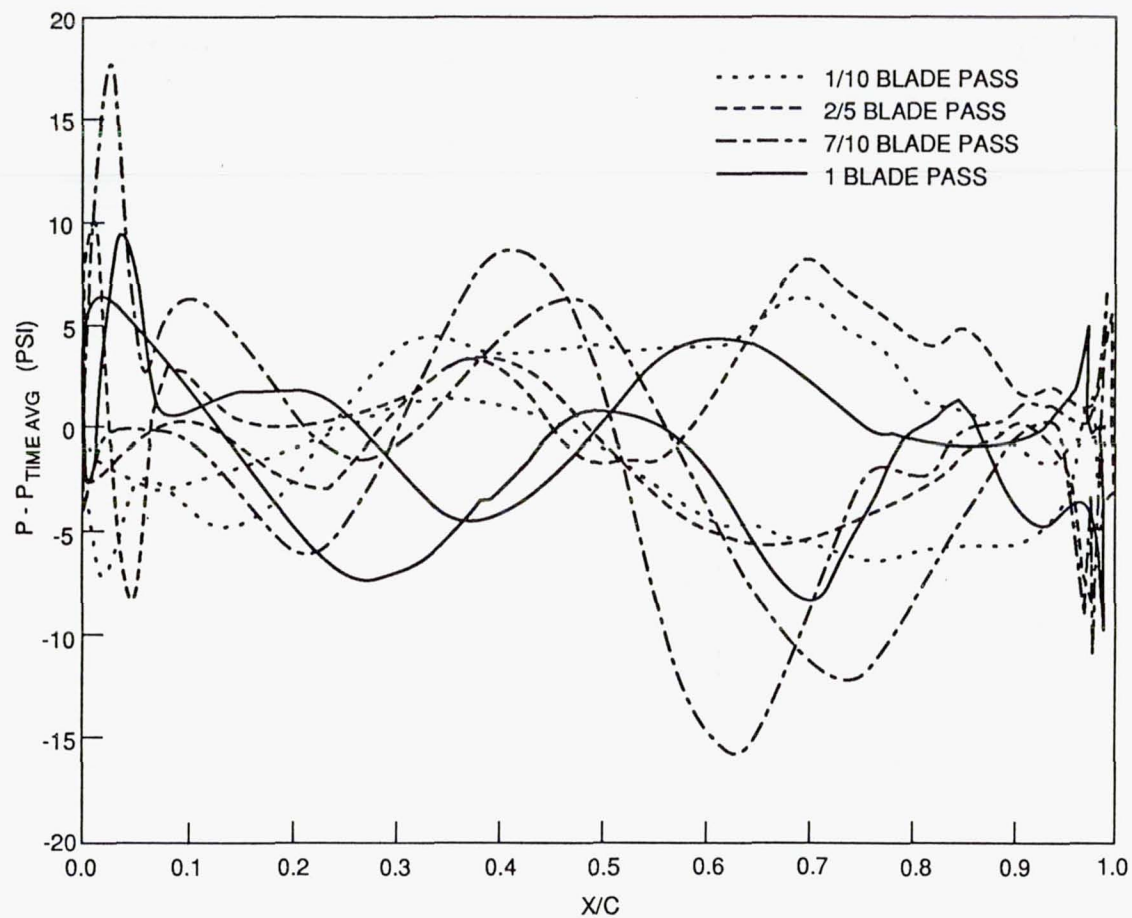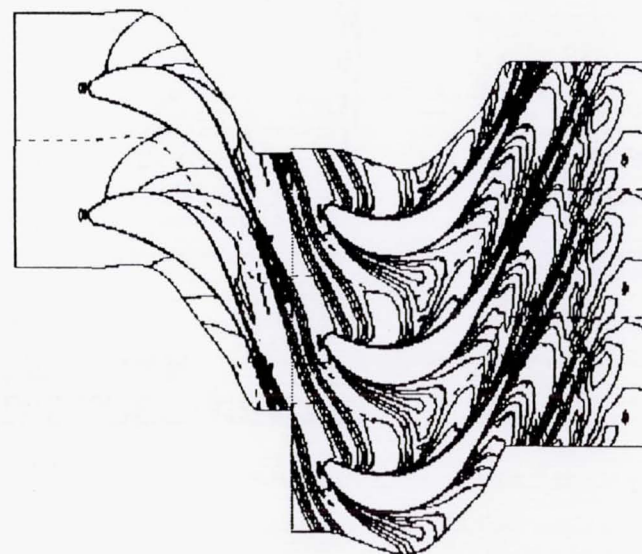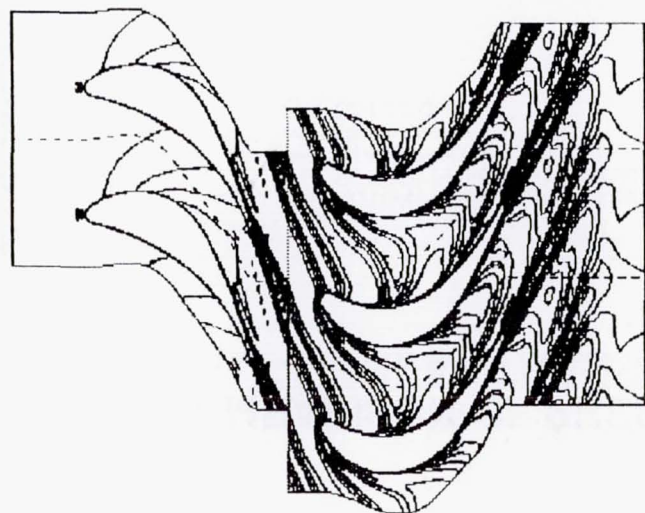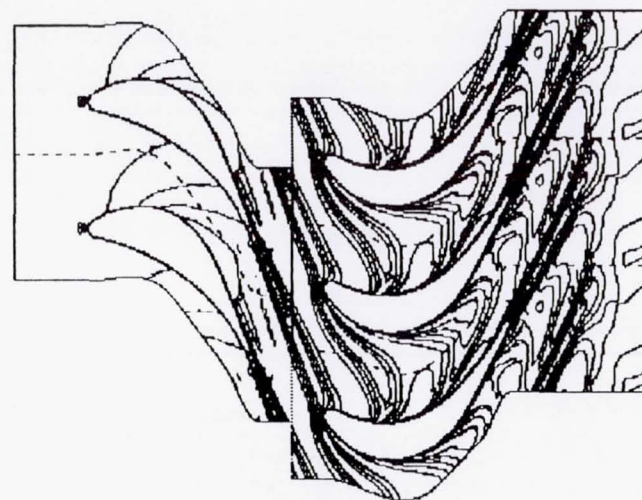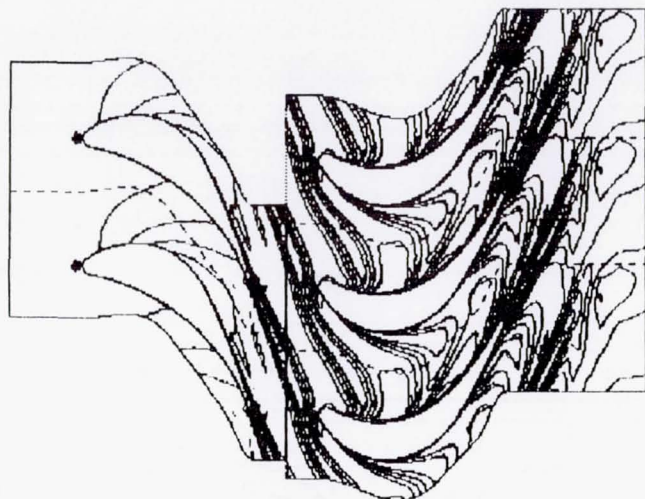
COMPARISON OF PREDICTED AND EXPERIMENTAL
HEAT TRANSFER FOR THE LSRR
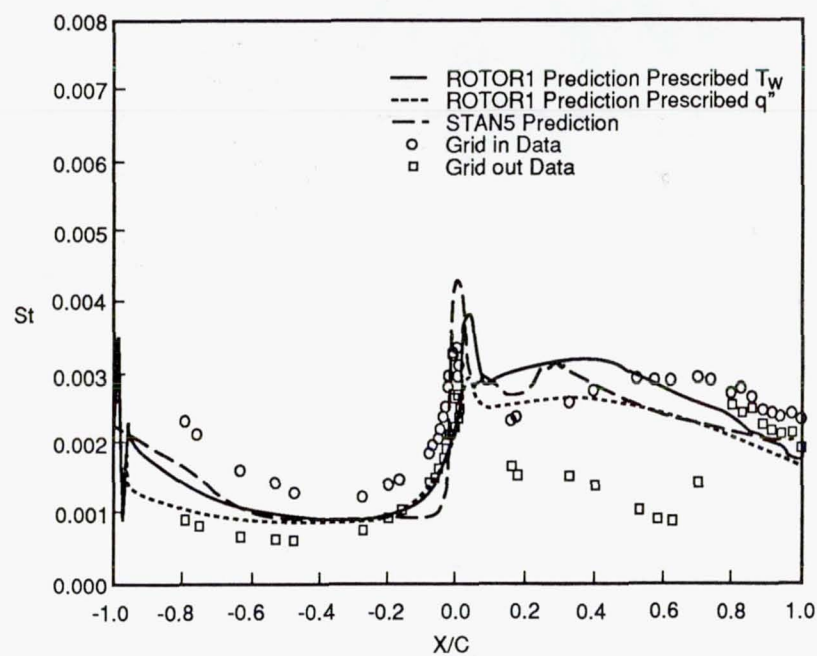
Stator
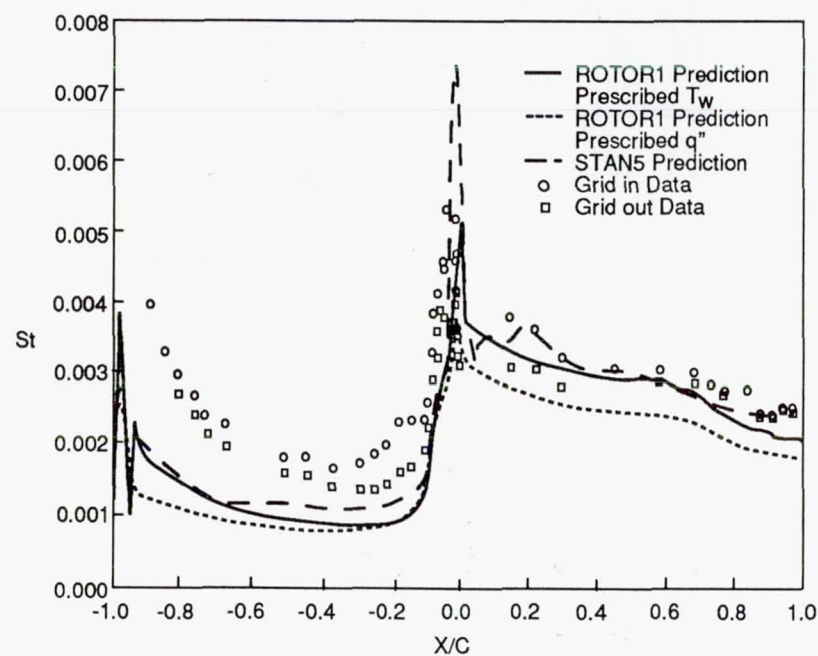
Rotor

COMPUTER RESOURCES REQUIREMENTS

MTSBL - STAN5   — 6 CPU MINUTES, 0.9×10^6 WORDS MEMORY

ROTOR1   — 6 CPU HOURS, 2.1×10^6 WORDS MEMORY +
                                  4.1×10^6 WORDS SSD

IMPACT

- MSFC BENCHMARKING OF QUASI-3D TURBINE ANALYSIS SYSTEM AND UNSTEADY STAGE CODE; ASSESSMENT OF RELATIVE MERITS OF THE TWO APPROACHES.

- STEADY 3D FIRST AND SECOND STAGE BLADE LOADS WERE USED IN STRESS ANALYSIS OF HPFTP TURBINE BLADES IN SUPPORT OF <u>RETURN TO FLIGHT</u>; INTEGRATED LOADS PREDICT CORRECT TORQUE WITHIN 1%.

- UNSTEADY MIDSPAN PRESSURES WERE USED IN STRUCTURAL DYNAMICS ANALYSIS OF HPFTP FIRST STAGE BLADES.

228

SUMMARY AND CONCLUSION

- SUPPORTED MSFC SSME PROGRAMS THROUGH CHARACTERIZATION OF THE STEADY AND UNSTEADY AEROTHERMAL ENVIRONMENTS OF THE HPFTP.

- BOTH APPROACHES YIELDED COMPARABLE STEADY OR TIME-AVERAGED AERODYNAMIC AND THERMAL RESULTS.

- AERODYNAMIC RESULTS FROM BOTH APPROACHES COMPARE WELL WITH DATA; THERMAL RESULTS EXHIBIT FAIR AGREEMENT WITH DATA.

229

5-1561-9-105

AUTOMATED DESIGN OF CONTROLLED DIFFUSION BLADES

Jose M. Sanz

NASA Lewis Research Center

ABSTRACT

A numerical automation procedure has been developed to be used in conjuction with an inverse hodograph method for the design of controlled diffusion blades.
With this procedure a cascade of airfoils with a prescribed solidity, inlet Mach No., inlet air flow angle and air flow turning can be produced automatically.
The trailing edge thickness of the airfoil, an important quantity in inverse methods, is also prescribed.

The automation procedure consists of a multi-dimensional Newton iteration in which the objective design conditions are achieved by acting on the hodograph input parameters of the underlying inverse code.

The method, although more general in scope, is applied in this paper to the design of axial flow turbomachinery blade sections, both compressors and turbines. A collaborative effort with U.S. Engine Companies to identify designs of interest to the industry will be described.

CURRENT APPROACH

- **GUESS GEOMETRY**

  - SINGLE CIRCULAR ARC
  - MULTIPLE CIRCULAR ARC
  - POLYNOMIAL SHAPES
  - NACA AIRFOILS SERIES

- **ANALYZE SHAPE WITH FLOW SOLVER**

  - 2-D, QUASI 3-D OR 3-D CODES
  - POTENTIAL, EULER OR NAVIER-STOKES SOLVERS

- **BUILDS IN EMPIRICISM**

AUTOMATION PROCEDURE

- ITERATION OF INVERSE HODOGRAPH METHOD

- PRODUCES BLADE WITH PRESCRIBED
    - SOLIDITY
    - INLET MACH NUMBER
    - INLET AIR ANGLE
    - AIR FLOW TURNING
    - TRAILING EDGE THICKNESS

BENEFITS

- REPLACE TRIAL AND ERROR PROCESS BY EXACT 2-D SOLUTION

- GREATLY REDUCES MANPOWER AND TURN AROUND TIME

- INITIALLY OPTIMIZED BLADE SECTIONS

- INNOVATIVE DESIGNS

- MAJOR IMPACT FOR DESIGNS PROBLEMS WITH NO DATA BASE

TO IMPLEMENT AUTOMATION

EQUATION $\quad u = \mathscr{F} (R, M_0, \theta, q(s))$

IS REPLACED BY

$$\bar{y} = \bar{F}(\bar{x})$$

WHERE

$$\bar{x} = (R, M_0, \theta, Q_M, Q_{te}, S_{te})$$

$$\bar{y} = \bar{y}(\sigma, M_1, \beta_1, \Delta\beta, dn_{te}, ds_{te})$$

NEWTON ITERATION TO SOLVE VECTOR EQUATION

$$\bar{F}(x) - \bar{y}_0 = 0,$$

$$\bar{y}_0 = (\sigma, \ M_1, \ \beta_1, \ \Delta\beta, \ dn_{te}, \ ds_{te})_0$$

IS OBJECTIVE FUNCTION.

ITERATION

$$\bar{x}_{n+1} = \bar{x}_n - J^{-1} (\bar{x}_n) (\bar{y}_n - \bar{y}_0)$$

JACOBIAN: $\quad J = \left(\dfrac{\partial F_i}{\partial x_j} \right)$

APPLICATIONS

- ARC 40X80X120 WIND TUNNEL TURNING VANES

- SUBSONIC AND TRANSONIC (SHOCK-FREE) TURBOMACHINERY AND PROPELLER SECTIONS

- INLET GUIDE VANES FOR LARGE RANGE OF INLET AIR FLOW ANGLE - EXPERIMENTAL VERIFICATION 3/88

ARC 40X80X120 WIND TUNNEL TURNING VANES

SCHEMATIC OF THE JUNCTION OF THE NASA AMES
40 x 80/80 x 120 FOOT WIND TUNNEL

PLANE OF
DRIVE FANS

25° STAGGER

40 x 80

45°

80 x 120

LOCUS OF LEADING
EDGES OF INLET GUIDE
VANES (AXIS OF
CASCADE)

SURFACE
MACH
NUMBER

UPPER SURFACE

LOWER SURFACE

CHORD, PERCENT

UPPER SURFACE

LOWER SURFACE

CHORD
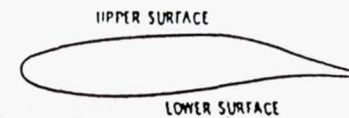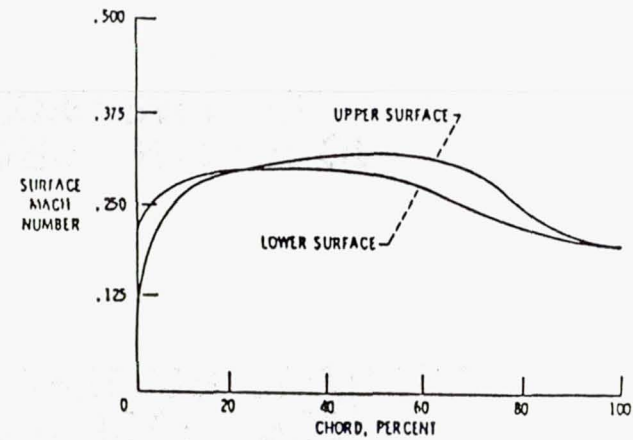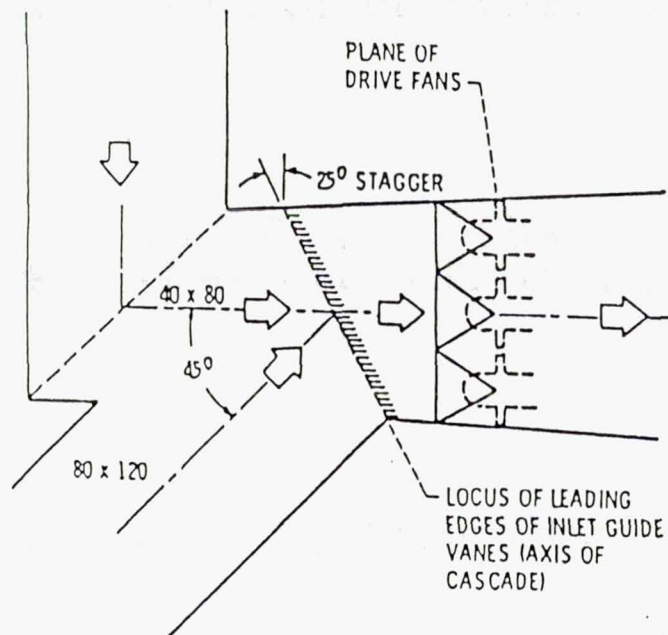
VARIABLE INLET GUIDE VANES
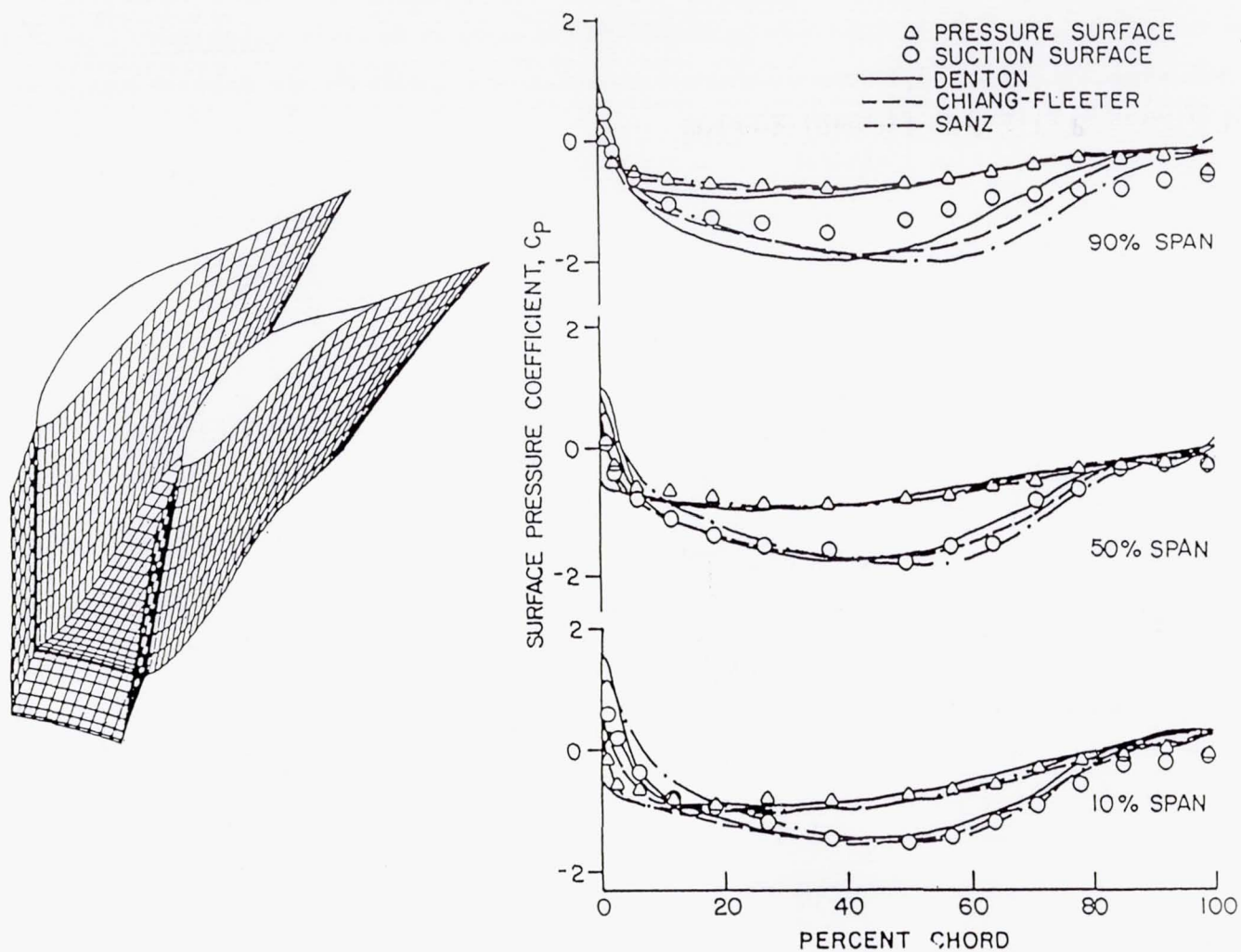
AWT TURNING VANES

$$M_{in} = .352 \quad M_{out} = .389$$
$$\beta_{in} = 44.9° \quad \beta_{out} = 45.6°$$
$$\sigma = 1.89 \quad max.\ thick/C = .196$$
$$C = 10.668\ cm \quad T.E.\ thick/C = .018$$

(a)

$$C_{p_v} = \frac{p_v - p_{in}}{q_{in}}$$

(b)

(b₁) A-LOCATION

TAILS ARE B-LOCATION

SANZ DESIGN (REF. 14, 15)

(b₂) B AND C-LOCATIONS

FRACTION OF CHORD FROM L.E., c/C

TDC

OUTSIDE CORNER

VANE TAP LOCATIONS

(b₃) D-LOCATION

AXIAL DISTANCE TO CHORD RATIO, X/C

TRUNNION ABOUT WHICH VANES CAN BE ROTATED TO DIFFERENT SETTING ANGLES

DESIGN SETTING ANGLE
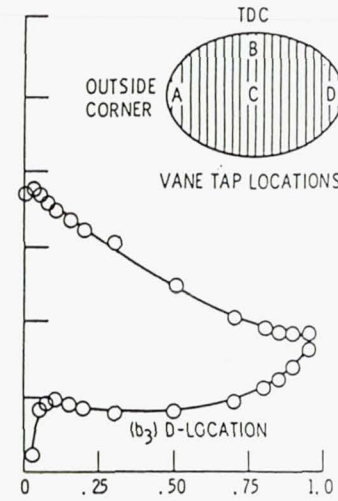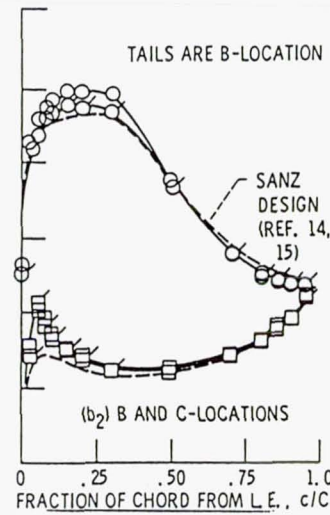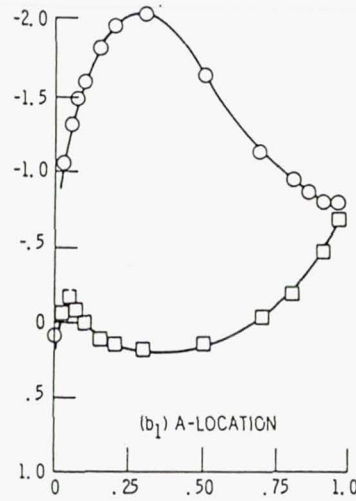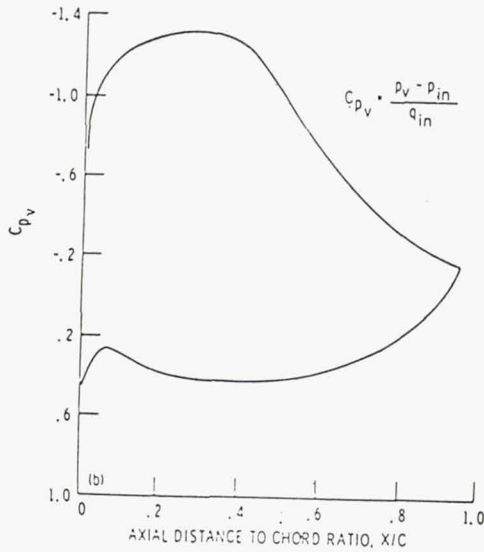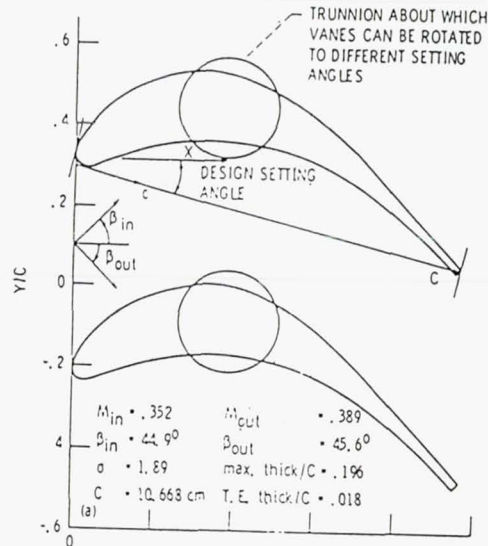
AUTOMATED DESIGN OF COMPRESSOR STATOR BLADE
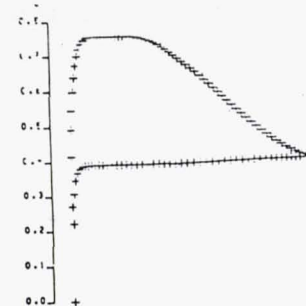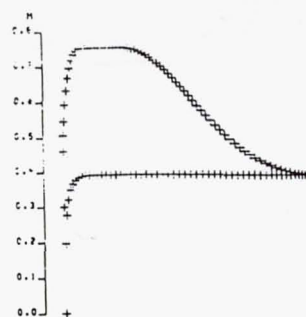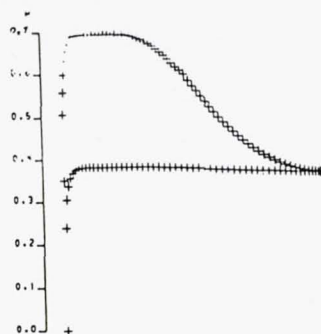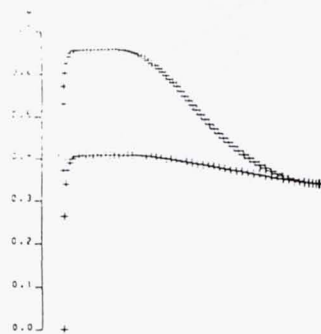
HUB SECTION   MID-HUB SECTION   MID-TIP SECTION   TIP SECTION

MID SPEED STATOR

AUTOMATED DESIGN OF TURBINE BLADE SECTIONS
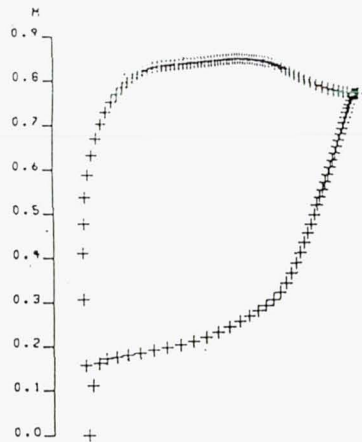
M1	0.337
BET1	36.39
M2	0.782
BET2	-61.06
DELB	97.44
SOL	1.45
THCR	0.224
DNTE	0.018
OSTE	-0.000
TEV	0.014
LOSS	0.005
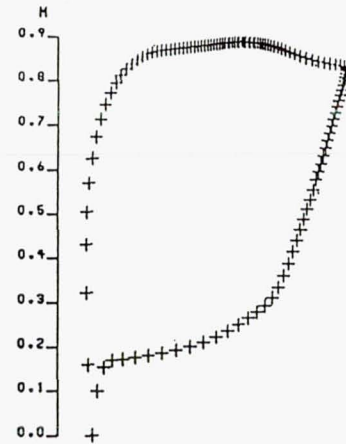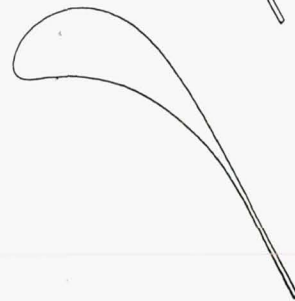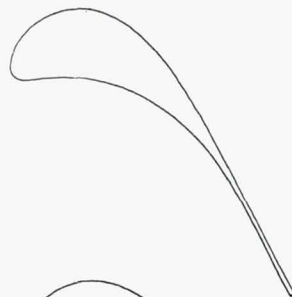
M1	0.337
BET1	36.38
M2	0.839
BET2	-61.01
DELB	97.38
SOL	1.45
THCR	0.224
DNTE	0.025
OSTE	-0.000
TEV	0.021
LOSS	0.005
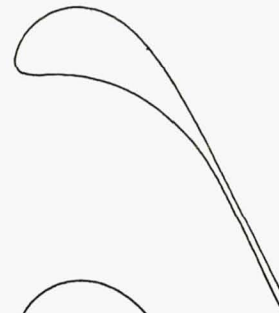
AUTOMATED DESIGN OF TURBINE BLADE SECTIONS
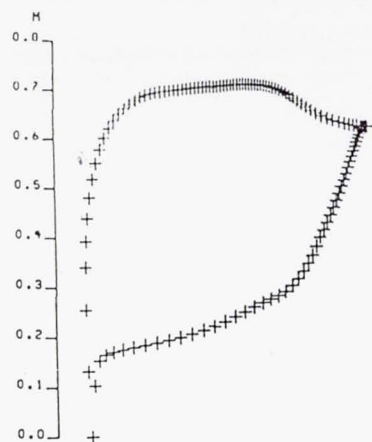
M1	0.301
BET1	36.41
M2	0.629
BET2	-61.14
DELB	97.55
SOL	1.45
THCR	0.239
ONTE	0.017
OSTE	-0.000
TEV	0.013
LOSS	0.006
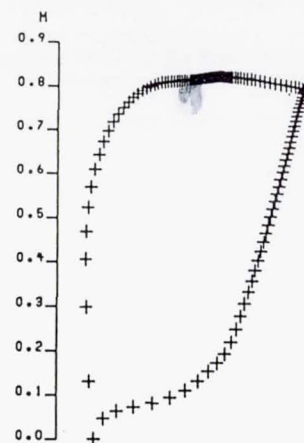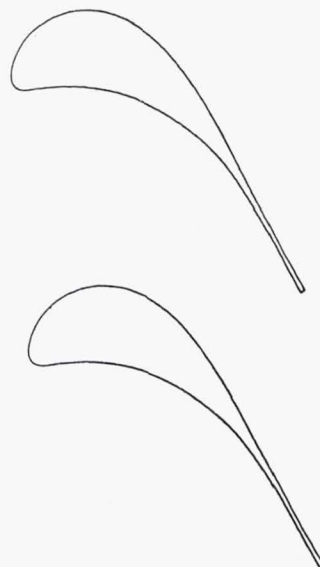
M1	0.253
BET1	32.49
M2	0.805
BET2	-66.74
DELB	99.23
SOL	1.43
THCR	0.186
ONTE	0.019
OSTE	-0.000
TEV	0.016
LOSS	0.003
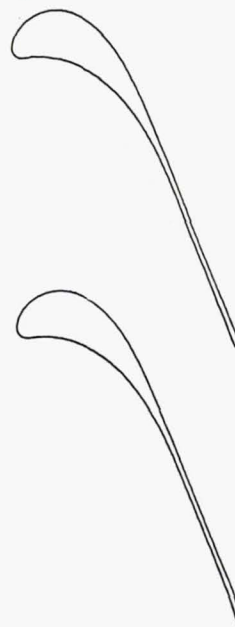
AUTOMATED DESIGN OF COMPRESSOR BLADE SECTIONS
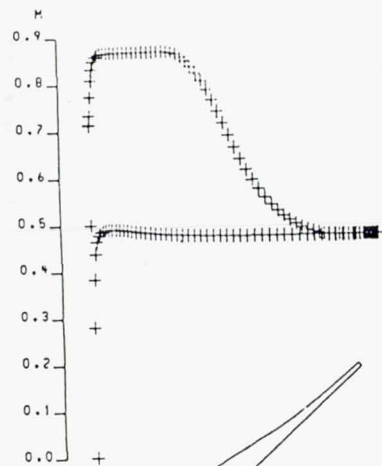
M1	0.670
BET1	52.02
M2	0.476
BET2	38.23
DELB	13.79
SOL	1.04
THCR	0.083
DNTE	0.020
DSTE	-0.000
TEV	0.012
LOSS	0.026
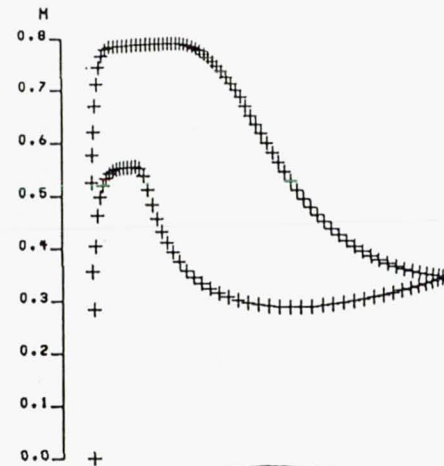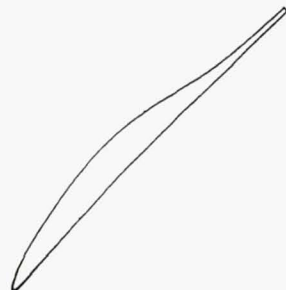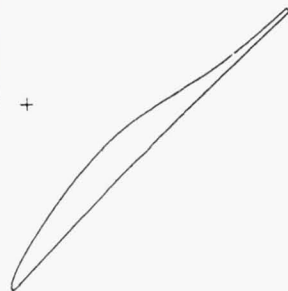
M1	0.600
BET1	51.01
M2	0.344
BET2	-3.95
DELB	54.96
SOL	1.70
THCR	0.112
DNTE	0.025
DSTE	-0.001
TEV	0.016
LOSS	0.055
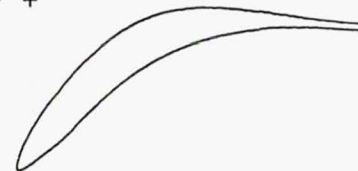
Numerical Analysis of Flow Through Oscillating
Cascade Sections

by Dennis L. Huff

NASA Lewis Research Center

The design of turbomachinery blades requires the prevention
of flutter for all operating conditions. However, flow field
predictions used for aeroelastic analysis are not well understood
for all flow regimes. The present research focuses on numerical
solutions of the Euler and Navier-Stokes equations using an ADI
procedure to model two-dimensional, transonic flow through
oscillating cascades. The model prescribes harmonic pitching
motions for the blade sections for both zero and non-zero
inter-blade phase angles. The code introduces the use of a
deforming grid technique for convenient specification of the
periodic boundary conditions. Approximate nonreflecting boundary
conditions have been coded for the inlet and exit boundary
conditions. Sample unsteady solutions have been performed for an
oscillating cascade and compared to experimental data. Also,
test cases were run for a flat plate cascade to compare with an
unsteady, small-perturbation, subsonic analysis.
The predictions for oscillating cascades with non-zero
inter-blade phase angles are in good agreement with experimental
data and small-perturbation theory. The zero degree inter-blade
phase angle cases, which were near a resonant condition, differ
from the experiment and theory. Studies on reflecting versus
non-reflecting inlet and exit boundary conditions show that the
treatment of the boundary can have a significant effect on the
first harmonic, unsteady pressure distributions for certain flow
conditions. This code is expected to be used as a tool for
reviewing simpler models that do not include the full non-linear
aerodynamics or as a final check for designs against flutter in
turbomachinery.

OBJECTIVE:

- DEVELOP AN UNSTEADY, VISCOUS, TRANSONIC FLOW ANALYSIS METHOD
  FOR CASCADED AIRFOILS WITH PITCHING MOTIONS

TECHNIQUE:

- A COMPRESSIBLE, FULL NAVIER-STOKES, FINITE DIFFERENCE CODE IS
  DEVELOPED TO MODEL OSCILLATING CASCADES FOR BOTH ZERO AND NON-
  ZERO INTER-BLADE PHASE ANGLES

- A UNIQUE DEFORMING GRID TECHNIQUE IS INTRODUCED TO CAPTURE
  BLADE MOTIONS

- APPROXIMATE NON-REFLECTING BOUNDARY CONDITIONS ARE USED TO
  MINIMIZE WAVE REFLECTIONS FROM THE OUTER BOUNDARIES

CD-88-38197

DEFORMING GRID TECHNIQUE, SIMPLIFIED GRID WITH EXAGGERATED MOTION
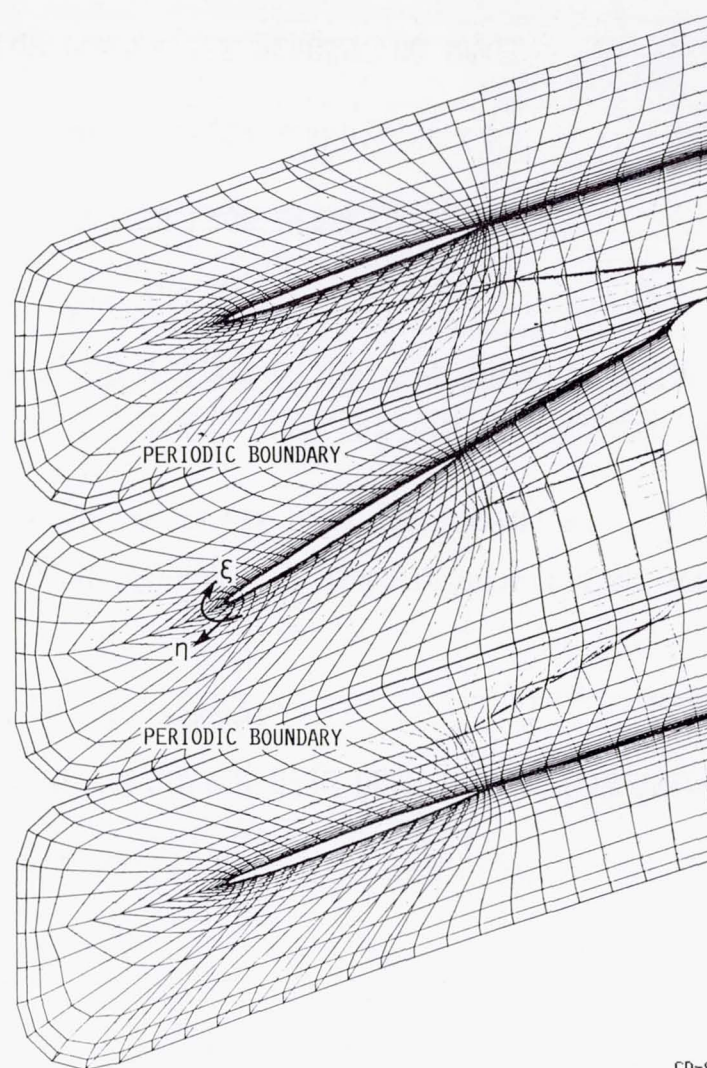
BOUNDARY CONDITIONS

INLET:

- SPECIFY DENSITY, VELOCITY, AND FLOW ANGLE

- SOLVE THE CHARACTERISTIC FORM OF THE GOVERNING EQUATIONS TO DETERMINE THE ENERGY

EXIT:

- FOR VISCOUS FLOWS, SPECIFY STATIC PRESSURE AND EXTRAPOLATE DENSITY AND VELOCITY FROM THE INTERIOR

- FOR INVISCID FLOWS, SPECIFY STATIC PRESSURE AND SOLVE THE CHARACTERISTIC FORM OF THE GOVERNING EQUATIONS TO DETERMINE DENSITY AND VELOCITY

PERIODIC BOUNDARIES FROM BLADE-TO-BLADE

SOLID WALL BOUNDARIES ON AIRFOIL SURFACE

AVERAGE FLOW PROPERTIES ACROSS THE WAKE

CD-88-38198

RESULTS

1. NACA 65-SERIES CASCADE, M = 0.17, TWO INTER-BLADE PHASE ANGLES, COMPARISONS WITH EXPERIMENT

2. FLAT PLATE CASCADE, M = 0.65 AND 0.80, THREE INTER-BLADE PHASE ANGLES, COMPARISONS WITH SMALL-PERTURBATION THEORY

3. NASA LEWIS CASCADE, M = 0.65 AND 0.80, THREE INTER-BLADE PHASE ANGLES, BOUNDARY CONDITION STUDY, NUMERICAL TIME ACCURACY STUDY, COMPARISONS WITH EXPERIMENT.

CD-88-38200

MEAN FLOW PRESSURE DISTRIBUTION FOR NACA 65-SERIES CASCADE

$M_1 = 0.17, \gamma = 55^0, g/c = 0.75, \tau' = 0.06$
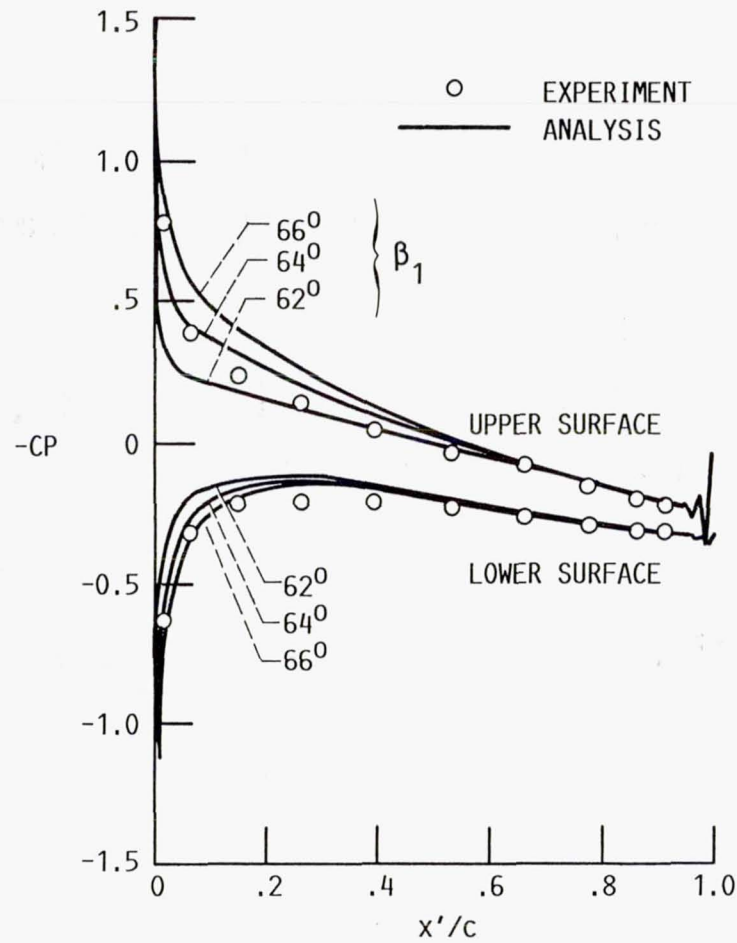
CD-88-38204

FIRST HARMONIC PRESSURE DISTRIBUTION FOR NACA 65-SERIES OSCILLATING CASCADE

$$M_1 = 0.17, \beta_1 = 64^0 \pm 2^0, k = 0.123$$
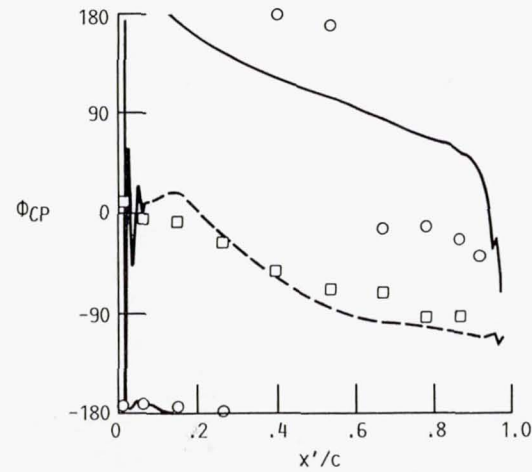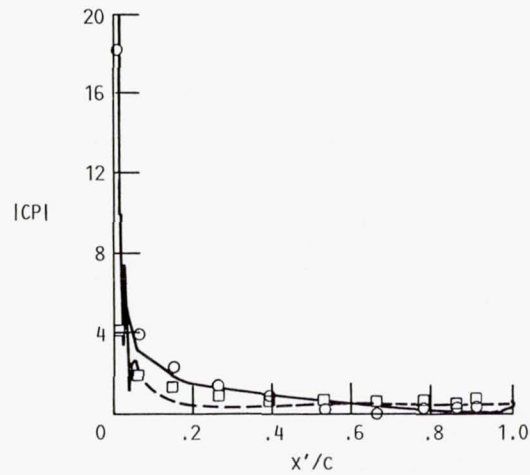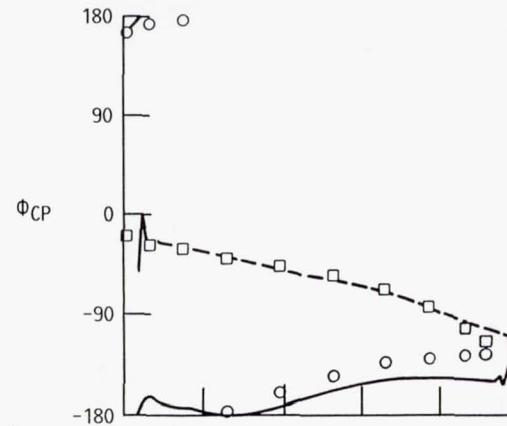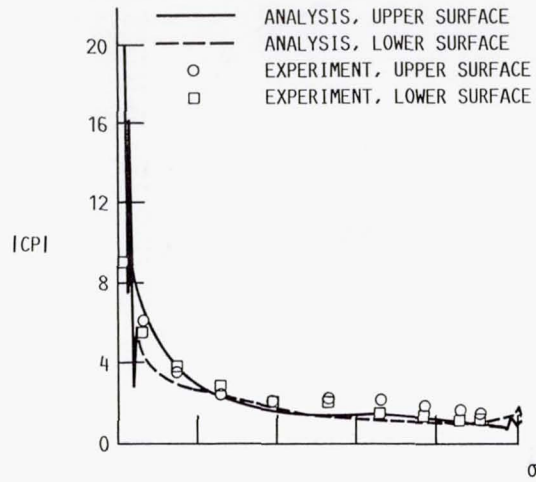
CD-88-38205

BOUNDARY CONDITION AND THEORY COMPARISON FOR
FLAT PLATE CASCADE

$M_1 = 0.65$, $\beta_1 = 53^0 \pm 0.10^0$, $k = 0.221$
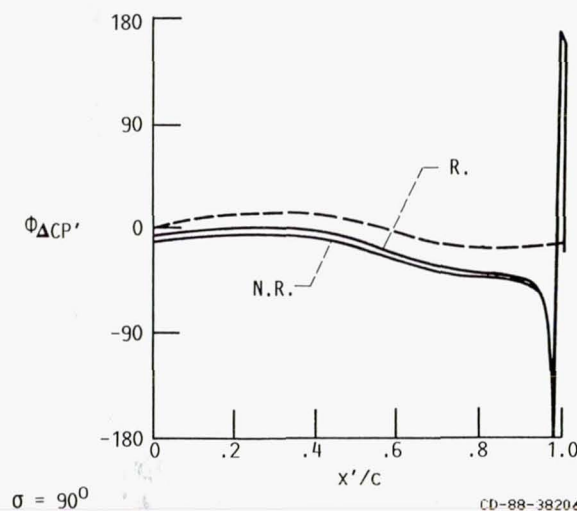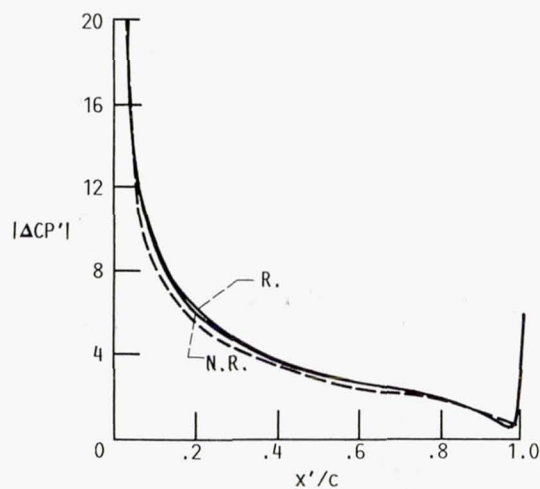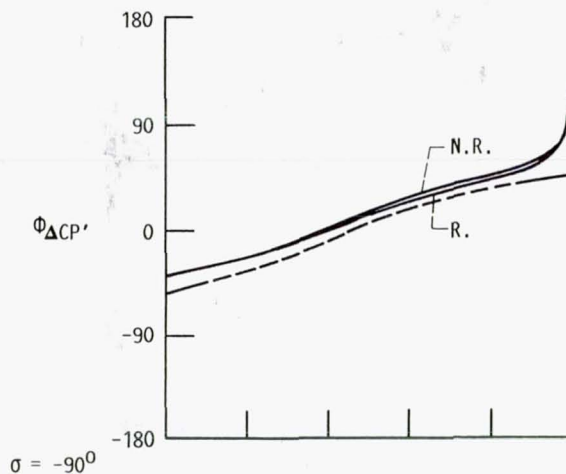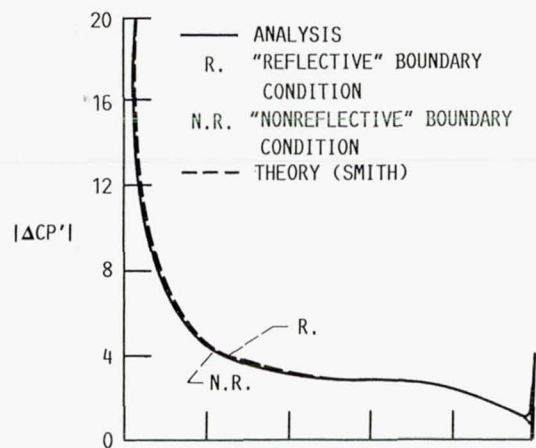
CD-88-38206

BOUNDARY CONDITION AND THEORY COMPARISON FOR
FLAT PLATE CASCADE

$M_1 = 0.65$, $\beta_1 = 53^0 \pm 0.10^0$, k $= 0.221$
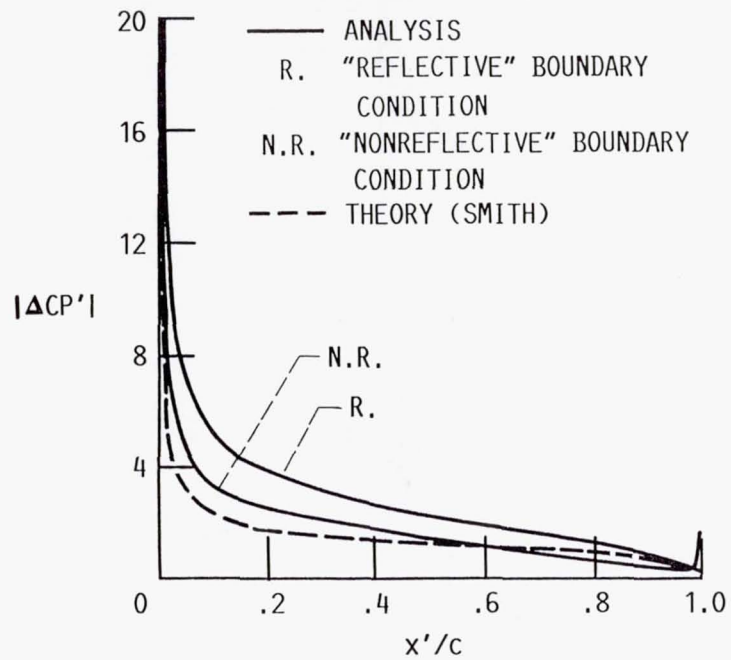
σ = 0^0
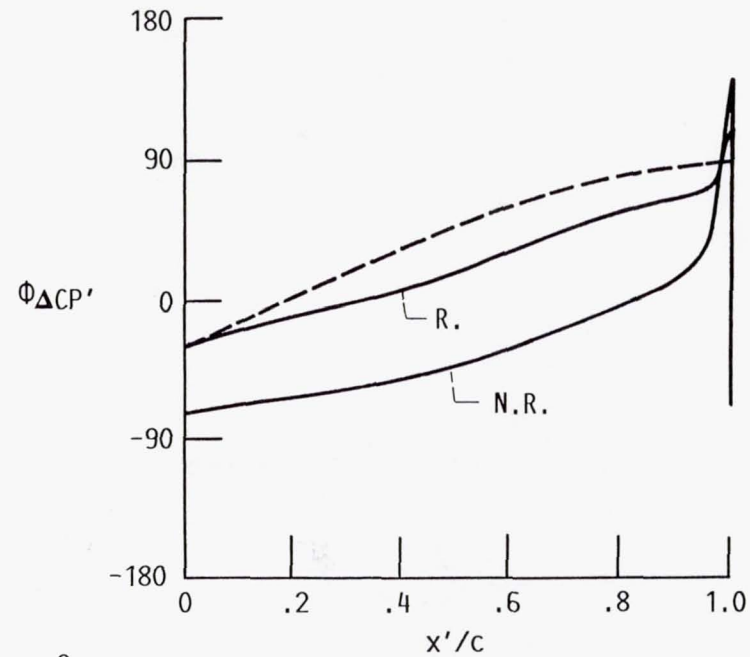
CD-88-38207

MEAN FLOW PRESSURE DISTRIBUTION FOR BICONVEX AIRFOIL CASCADE

$\beta_1 = 60^0$, $\gamma = 53^0$, g/c = 0.767, $\tau' = 0.07$
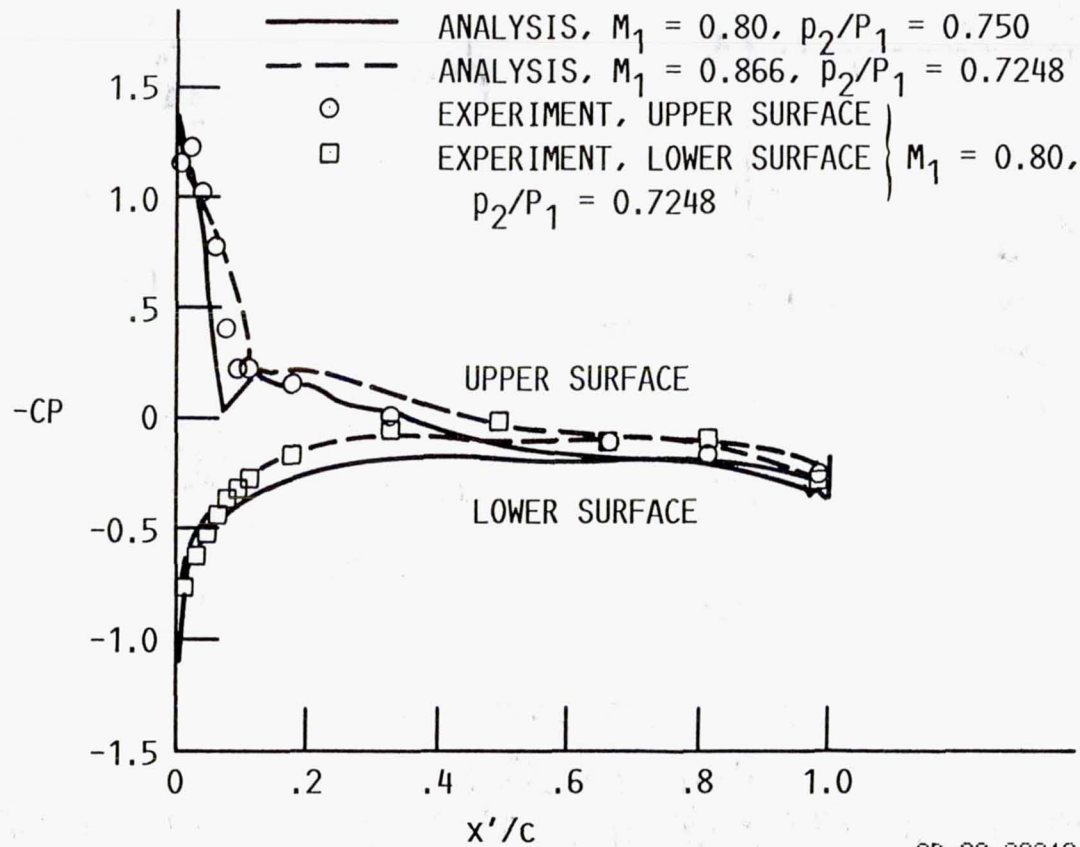
CD-88-38218

FIRST HARMONIC PRESSURE DISTRIBUTION FOR BICONVEX AIRFOIL CASCADE
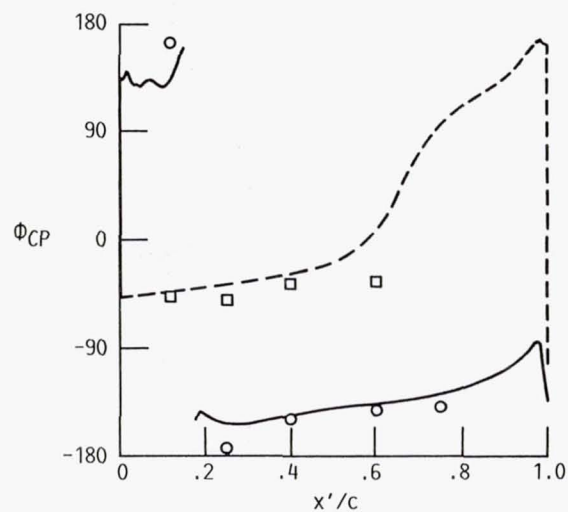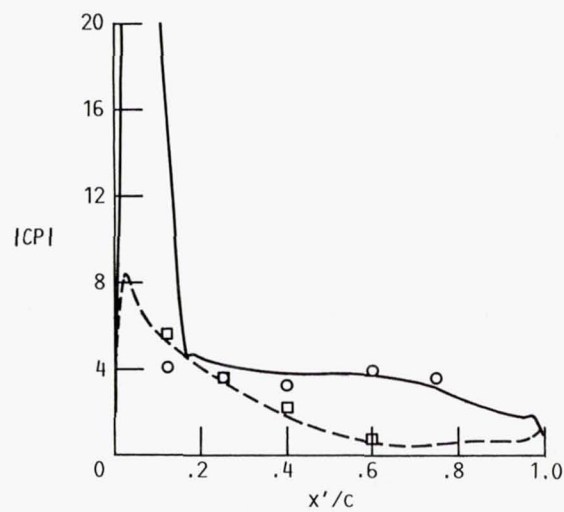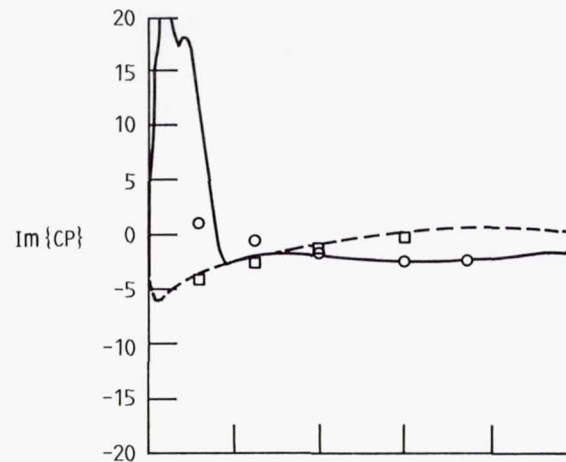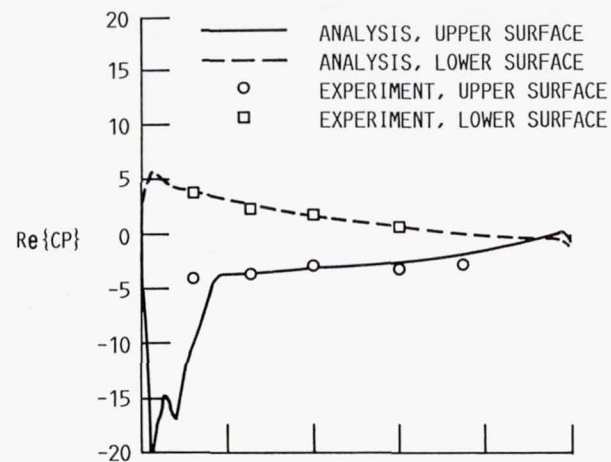
$M_1 = 0.80$, $\beta_1 = 60^0 \pm 1.2^0$, $k = 0.185$, $\sigma = -90^0$

FIRST HARMONIC PRESSURE DISTRIBUTION FOR
BICONVEX AIRFOIL CASCADE

$M_1 = 0.80$, $\beta_1 = 60^0 \pm 1.2^0$, k = 0.185, $\sigma = 0^0$
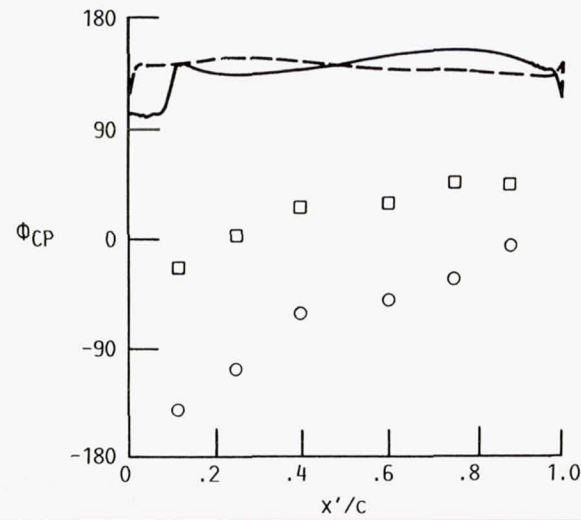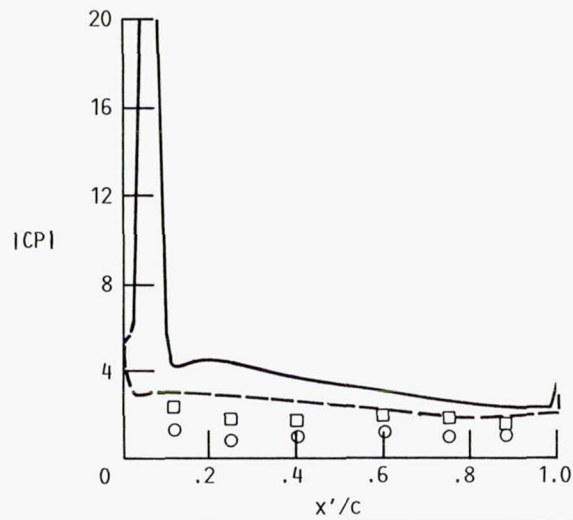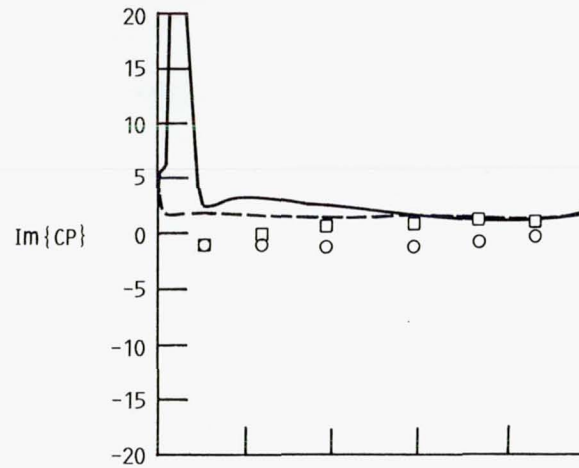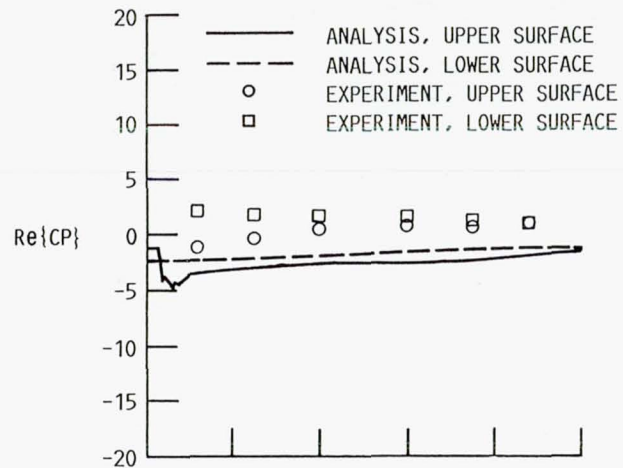
CD-88-38223

CONCLUSIONS

- A COMPRESSIBLE EULER OR NAVIER-STOKES, FINITE-DIFFERENCE CODE HAS BEEN DEVELOPED FOR THE ANALYSIS OF OSCILLATING CASCADES

- A DEFORMING GRID TECHNIQUE IS USED TO CAPTURE THE MOTION OF THE AIRFOILS FOR BOTH ZERO AND NON-ZERO INTER-BLADE PHASE ANGLES

- APPROXIMATE TWO-DIMENSIONAL, UNSTEADY CHARACTERISTIC BOUNDARY CONDITIONS ARE USED AT THE INLET AND EXIT TO MINIMIZE WAVE REFLECTIONS

- IN GENERAL, PREDICTIONS WITH NON-ZERO-INTER-BLADE PHASE ANGLES ARE IN GOOD AGREEMENT WITH THE EXPERIMENTAL DATA AND SMALL-PERTURBATION THEORY

- PREDICTIONS FOR ZERO DEGREE INTER-BLADE PHASE ANGLE CASES, WHICH WERE NEAR AN ACOUSTIC RESONANT CONDITION, DIFFER FROM THE EXPERIMENT AND THEORY

- THE TYPE OF BOUNDARY CONDITION USED AT THE INLET AND EXIT CAN HAVE A SIG-NIFICANT EFFECT ON THE FIRST HARMONIC, UNSTEADY PRESSURE DISTRIBUTIONS

- FIRST-ORDER AND SECOND-ORDER TEMPORAL ACCURACY RESULTS DO NOT SHOW SIGNIF-ICANT DIFFERENCES IN THE UNSTEADY PRESSURE DISTRIBUTIONS

CD-88-38199

ANALYSIS OF THREE-DIMENSIONAL VISCOUS FLOW IN A SUPERSONIC THROUGHFLOW FAN

by

Dr. Rodrick V. Chima
NASA Lewis Research Center
Cleveland, OH 44135

Abstract

A three-dimensional Navier-Stokes code has been developed for analysis of turbomachinery blade rows and other internal flows. The Navier-Stokes equations are written in a Cartesian coordinate system rotating about the x-axis, and then mapped to a general body-fitted coordinate system. Streamwise viscous terms are neglected using the thin-layer assumption, and turbulence effects are modelled using the Baldwin-Lomax turbulence model. The equations are discretized using finite differences on stacked C-type grids and are solved using a multistage Runge-Kutta algorithm with a spatially-varying time step and implicit residual smoothing.

Calculations were made of the flow around a supersonic throughflow fan blade. The fan was designed at NASA Lewis Research Center as a key component in a supersonic cruise engine. It was designed to produce a total pressure ratio of 2.7 at an axial Mach number of 2.0. The midspan section of the blade is being tested in a supersonic linear cascade at Virginia Polytechnic Institute and will be tested in a rotating rig at Lewis in the near future. Comparisons between earlier quasi-3-D calculations and the VPI data show excellent agreement between shock locations and wake traverses.

The 3-D calculations were done on a 129 * 29 * 33 grid and took 50 minutes of cpu time on a Cray X-MP. Comparisons with the quasi-3-D results show minor differences in loading due to 3-D effects. Particle traces show nearly 2-D flows near the pressure surface, but large secondary flows within the suction surface boundary layer. The horseshoe vortex ahead of the leading edge is clearly seen.

References

1. Chima, R. V., and Yokota, J. W. "Numerical Analysis of Three- Dimensional Viscous Internal Flows," NASA TM-100878, July, 1988.
2. Schmidt, J. F., Moore, R. D., and Wood, J. R. "Supersonic Throughflow Fan Design," NASA TM-88908, AIAA-87-1746, June, 1987.

RVC3D (ROTOR VISCOUS CODE 3-D)

BY R. V. CHIMA

DESCRIPTION

- EULER OR NAVIER-STOKES ANALYSIS FOR STEADY
  3-D FLOWS IN TURBOMACHINERY BLADE PASSAGES

FEATURES

- STACKED C-TYPE GRIDS FOR AXIAL OR CENTRIFUGAL MACHINES

- CARTESIAN FORMULATION ROTATING ABOUT X-AXIS
  RECTANGULAR OR ANNULAR GEOMETRIES

- SOLVES NAVIER-STOKES EQUATIONS IN FINITE-DIFFERENCE FORM
  THIN-LAYER FORMULATION NEGLECTS STREAMWISE VISCOUS TERMS
  RETAINS HUB-TO-TIP & BLADE-TO-BLADE VISCOUS TERMS
  BALDWIN-LOMAX TURBULENCE MODEL

- EXPLICIT 4-STAGE RUNGE-KUTTA TIME-MARCHING SCHEME
  VARIABLE $\Delta t_{i,j}$ & IMPLICIT RESIDUAL SMOOTHING
  HIGHLY VECTORIZED FOR CRAY X-MP

RESULTS

- SUPERSONIC THROUGHFLOW FAN

GOVERNING EQUATIONS

$$\partial_t q + J[\partial_\xi \hat{E} + \partial_\eta \hat{F} + \partial_\varsigma \hat{G} - Re^{-1}(\partial_\eta \hat{F}_V + \partial_\varsigma \hat{G}_V)] = H$$

WHERE:

$$q = [\,\rho, \quad \rho u, \quad \rho v, \quad \rho w, \quad e\,]^T$$

$$H = [\,0, \quad 0, \quad -\Omega\rho w, \quad \Omega\rho v, \quad 0\,]^T$$

$$\hat{E} = J^{-1}[\,\rho U', \ \rho u U' + \xi_x p, \ \rho v U' + \xi_y p, \ \rho w U' + \xi_z p, \ eU' + pU\,]^T$$

$$\hat{F} = J^{-1}[\,\rho V', \ \rho u V' + \eta_x p, \ \rho v V' + \eta_y p, \ \rho w V' + \eta_z p, \ eV' + pV\,]^T$$

$$\hat{G} = J^{-1}[\,\rho W', \ \rho u W' + \varsigma_x p, \ \rho v W' + \varsigma_y p, \ \rho w W' + \varsigma_z p, \ eW' + pW\,]^T$$

RELATIVE VELOCITIES:

$$u' = u$$

$$v = v - \Omega z$$

$$w' = w + \Omega y$$

RELATIVE CONTRAVARIANT VELOCITIES:

$$U' = \xi_x u + \xi_y v' + \xi_z w'$$

$$V' = \eta_x u + \eta_y v' + \eta_z w'$$

$$W' = \varsigma_x u + \varsigma_y v' + \varsigma_z w'$$

ENERGY AND STATIC PRESSURE:

$$e = \rho\left[C_v T + (u^2 + v^2 + w^2)/2\right]$$

$$p = (\gamma - 1)\left[e - \rho(u^2 + v^2 + w^2)/2\right]$$

MULTISTAGE RUNGE-KUTTA ALGORITHM

GOVERNING EQUATIONS

$$\partial_t q = -J \left[R_I - (R_V + D) \right]$$

$R_I = $ INVISCID RESIDUAL

$R_V = $ VISCOUS RESIDUAL

$D \quad = $ ARTIFICIAL DISSIPATION TERM

MULTISTAGE SCHEME

$$q_0 = q_n$$

$$q_1 = q_0 - \alpha_1 J \Delta t \left[R_I \, q_0 - (R_V + D) \, q_0 \right]$$

$$\vdots$$

$$q_k = q_0 - \alpha_k J \Delta t \left[R_I \, q_{k-1} - (R_V + D) \, q_0 \right]$$

$$q_{n+1} = q_k$$

R_V & D EVALUATED AT FIRST STAGE ONLY

ARTIFICIAL DISSIPATION

NONCONSERVATIVE VERSION OF JAMESON FORMULATION

$$Dq = (D_\xi + D_\eta + D_\varsigma)\, q$$

ξ-DIRECTION OPERATOR

$$D_\xi q = C_\xi \left(V_2 q_{\xi\xi} - V_4 q_{\xi\xi\xi\xi} \right)$$

WHERE:

$$C_\xi = \frac{1}{J}\left(\frac{1}{\Delta t_\eta} + \frac{1}{\Delta t_\varsigma} \right) \simeq \frac{a}{J}\left(\frac{1}{\Delta s_\eta} + \frac{1}{\Delta s_\varsigma} \right)$$

$$V_2 = \mu_2 \max\left(\nu_{i+1}, \nu_i, \nu_{i-1} \right)$$

$$V_4 = \max\left(0, \mu_4 - V_2 \right)$$

AND

$$\nu_{i,j} = \frac{\left| P_{i+1,j} - 2P_{i,j} + P_{i-1,j} \right|}{\left| P_{i+1,j} + 2P_{i,j} + P_{i-1,j} \right|}$$

$$\mu_2 = O(1)$$

$$\mu_4 = O\!\left(\tfrac{1}{16}\right)$$

IMPLICIT RESIDUAL SMOOTHING

USE A TIME STEP GREATER THAN THE STABILITY LIMIT
MAINTAIN STABILITY BY SMOOTHING THE RESIDUAL IMPLICITLY

$$(1 - \epsilon_\xi \delta_{\xi\xi})(1 - \epsilon_\eta \delta_{\eta\eta})(1 - \epsilon_\varsigma \delta_{\varsigma\varsigma})\bar{R} = R$$

UNCONDITIONALLY STABLE IF

$$\epsilon \geq \frac{1}{4}\left[\left(\frac{\lambda}{\lambda^*}\right)^2 - 1\right]$$

WHERE
λ^* IS COURANT LIMIT OF THE UNSMOOTHED SCHEME
λ IS THE LARGER OPERATING COURANT NUMBER

SUPERSONIC FAN

(NASA LeRC ASSESSMENT STUDY)

SUPERSONIC
DIFFUSER ⋯

⌐⋅3 STAGE CONVENTIONAL FAN

SUBSONIC
DIFFUSER ⋯⋯⋯⋯

CONVENTIONAL TURBOFAN

⌐⋅SINGLE STAGE SUPERSONIC FAN

⌐⋅DUCT NOZZLE

SUPERSONIC
DIFFUSER ⋯⋯⌡

SUPERSONIC FAN ENGINE
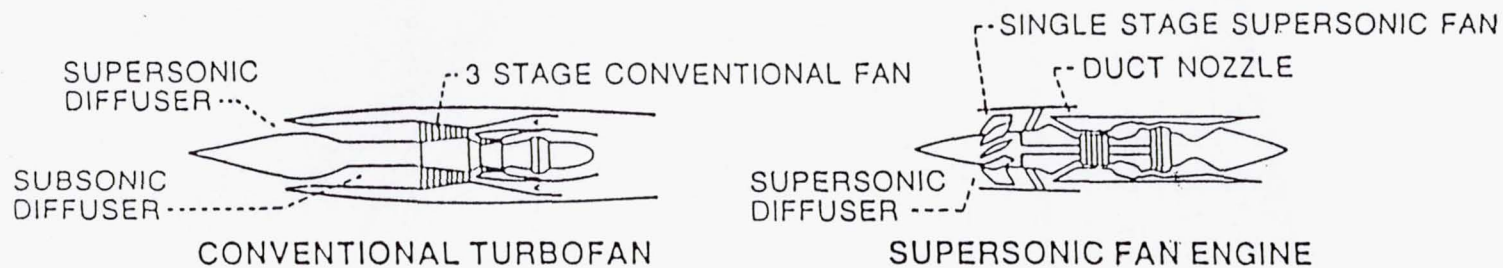
SUPERSONIC FAN ENGINE FEATURES
- SHORT, ALL SUPERSONIC INLET
- SINGLE STAGE SUPERSONIC FAN
- BPR DECREASES WITH M_0

IMPLICATIONS
- LOWER WEIGHT, LOWER INLET DRAG
- LOWER WEIGHT AND COST, RUGGED BLADING
- HIGHER CRUISE THRUST

WEIGHT 15 TO 20% LOWER   CRUISE SFC-10 TO 20% LOWER

CD-86-19471
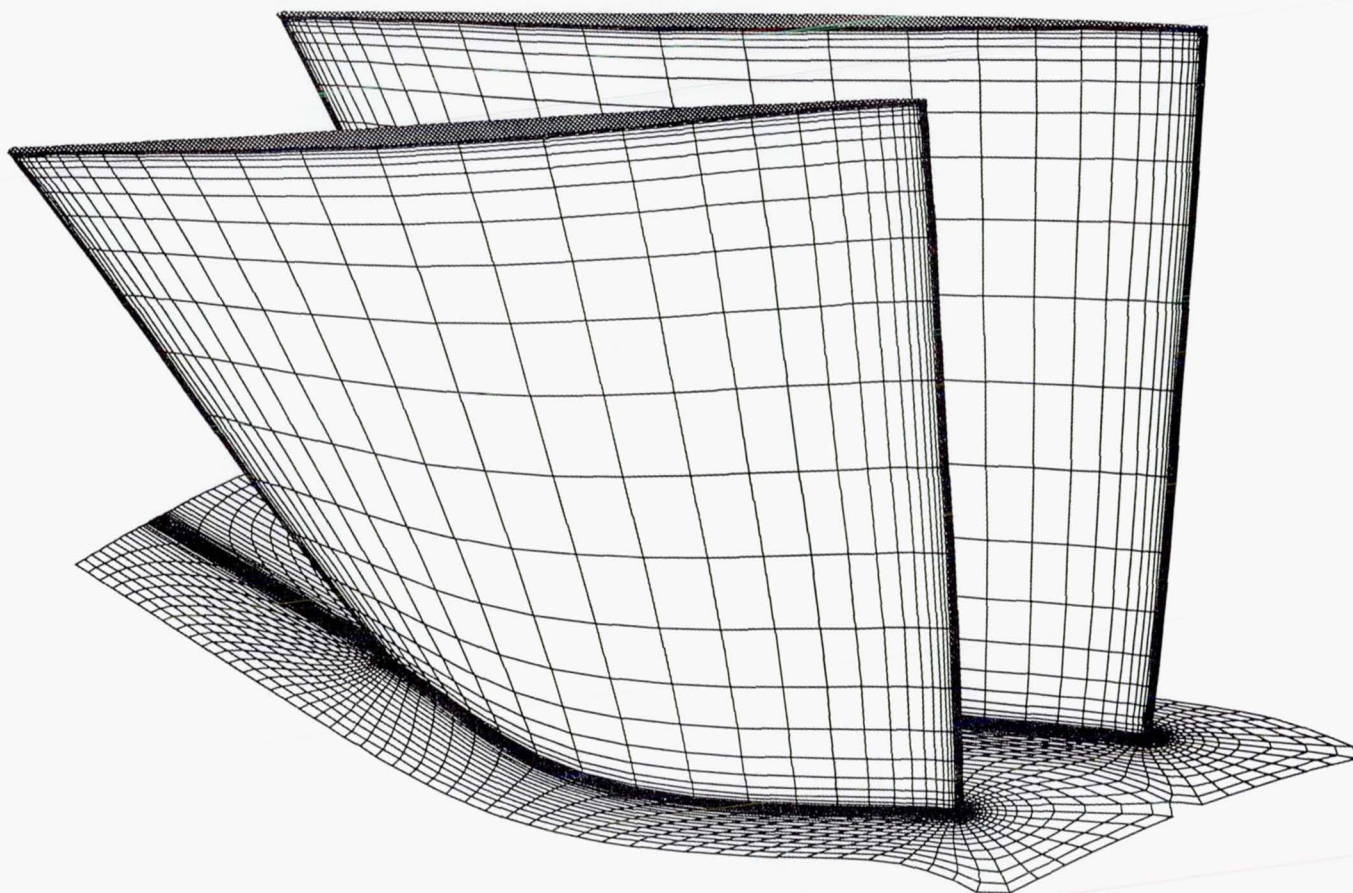
PRESSURE

SUPERSONIC THROUGHFLOW FAN, Mrel = 2.5

COMPARISON OF MIDSPAN PRESSURES

Q-3-D (161 POINTS, 121 ON BLADE)

3-D (129 POINTS, 103 ON BLADE)
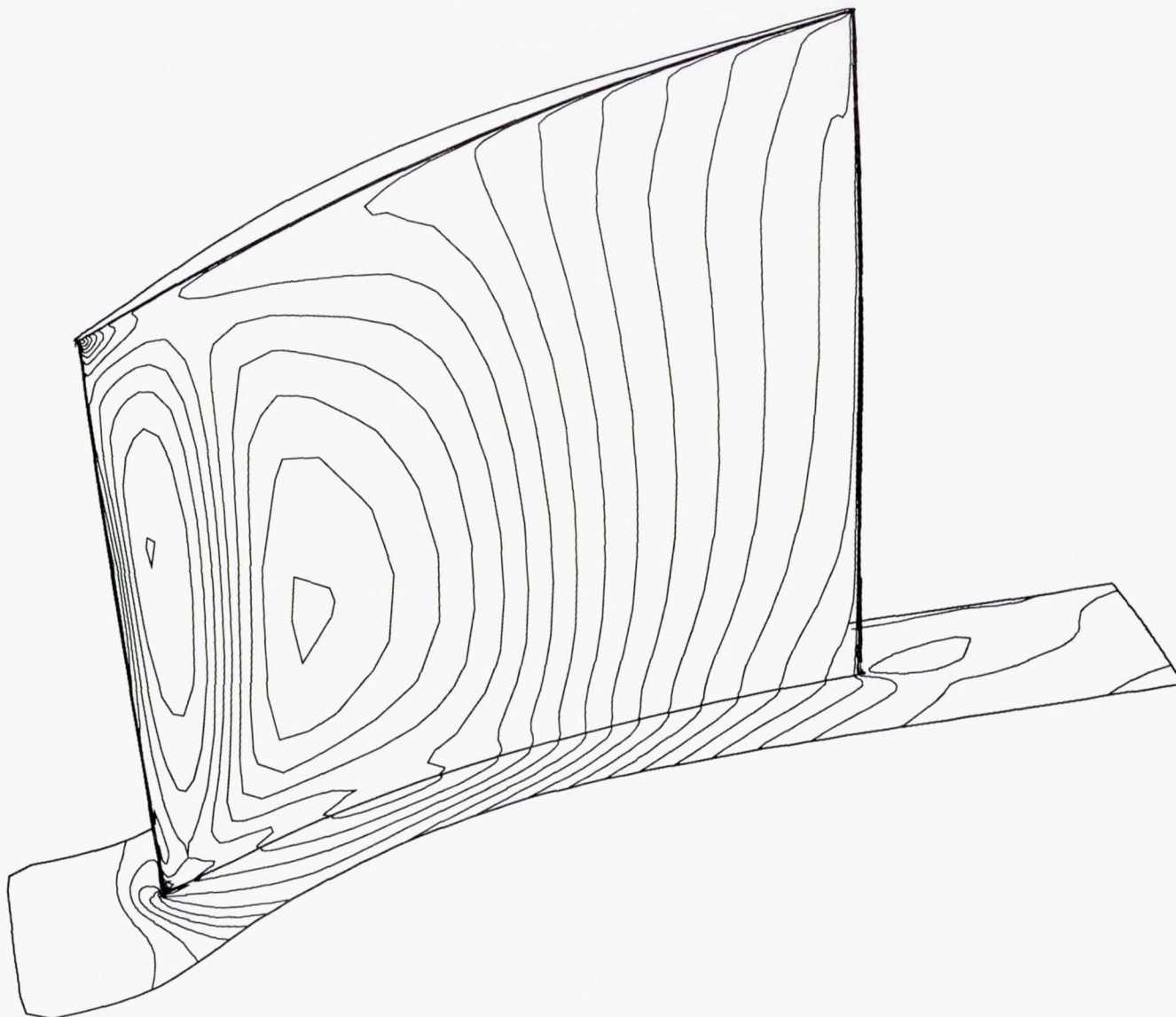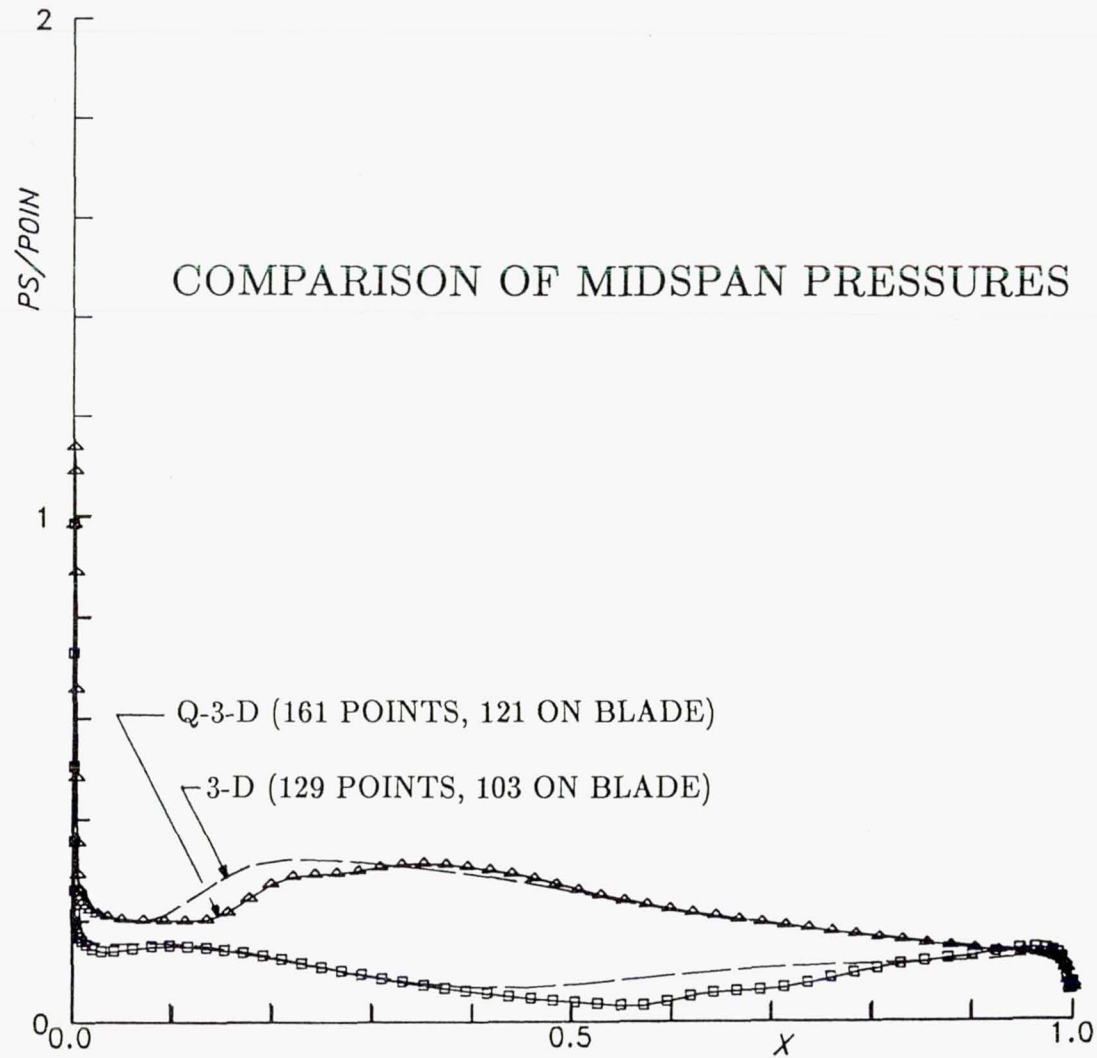
SUPERSONIC THROUGHFLOW FAN 3-D   K=17
MACH 2.000   RE   554500.   ALPHA 0.00   ITER   1000

DENSITY

SUPERSONIC THROUGHFLOW FAN, Mrel = 2.5
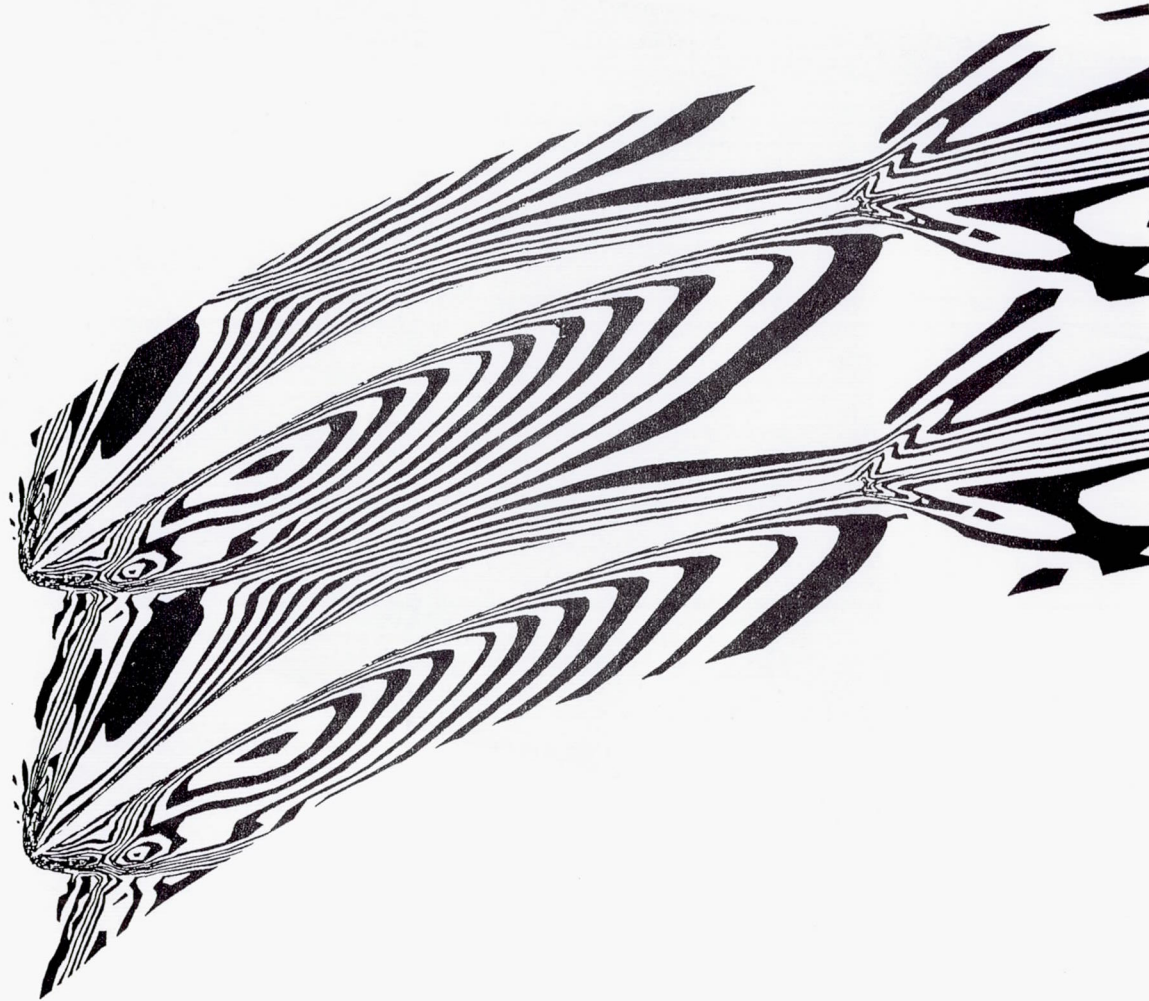
PARTICLE TRACES

SUPERSONIC THROUGHFLOW FAN, Mrel = 2.5
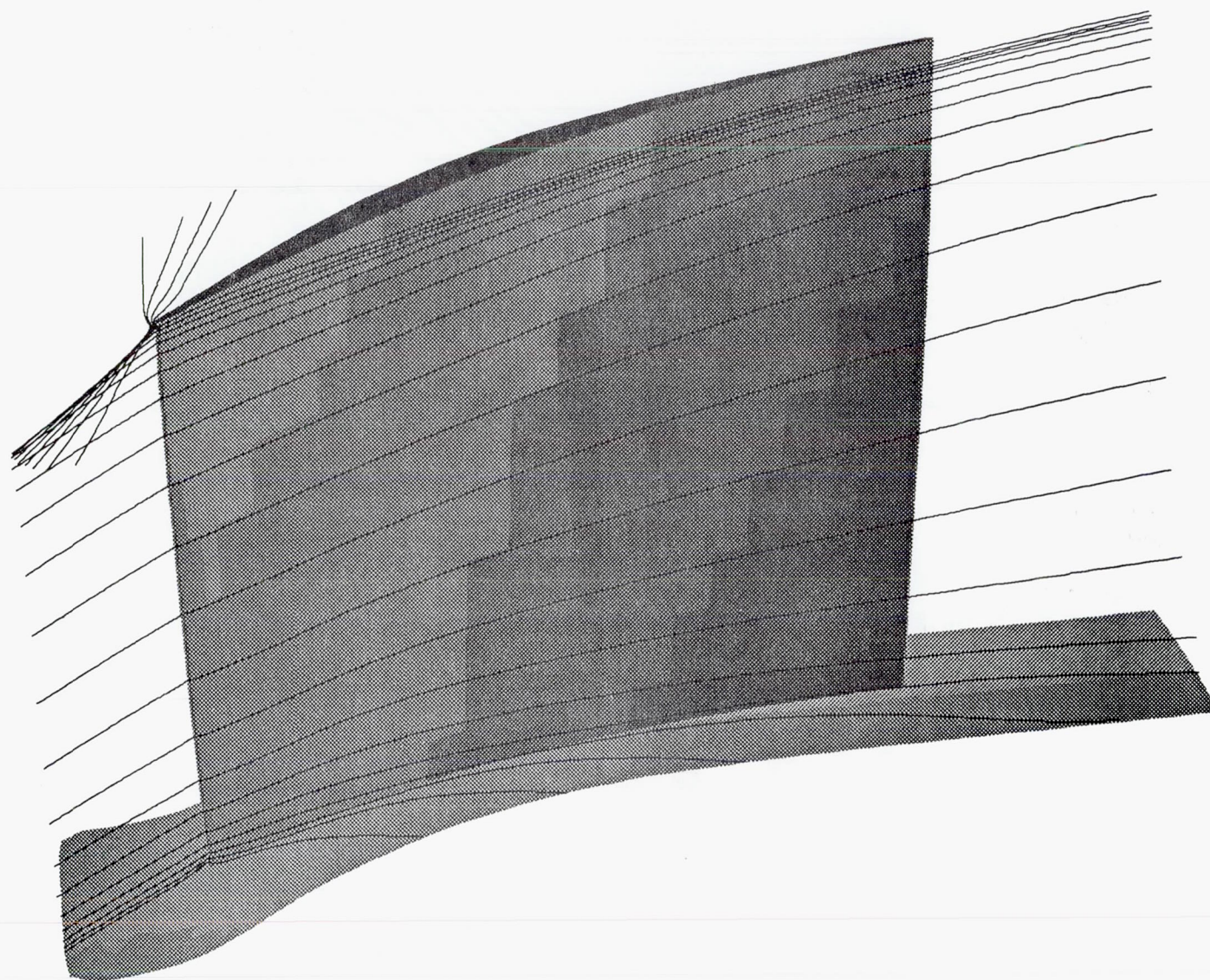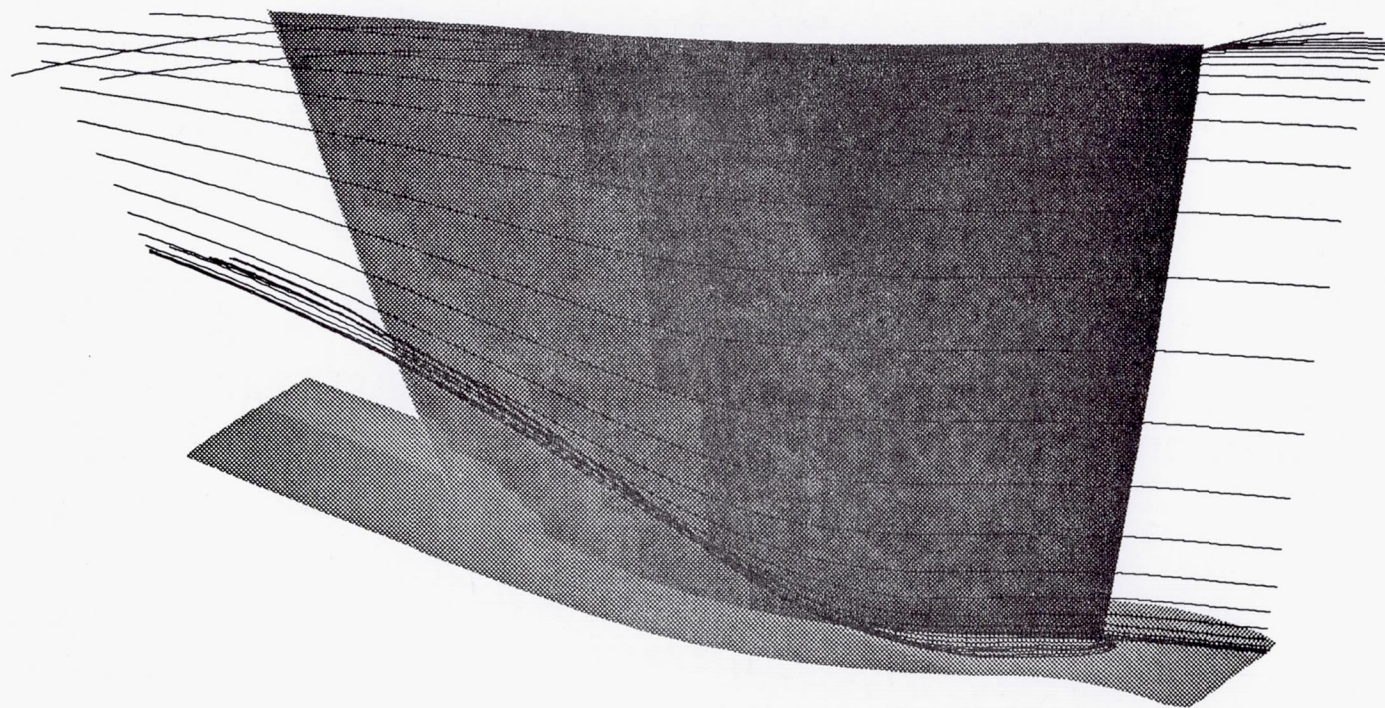
SUMMARY

PHYSICS

- 3-D NAVIER-STOKES ANALYSIS FOR STEADY INTERNAL FLOWS
- CARTESIAN FORMULATION ROTATING ABOUT X-AXIS
- THIN LAYER IN STREAMWISE DIRECTION, FULL N-S IN OTHERS
- BALDWIN-LOMAX TURBULENCE MODEL

NUMERICS

- FINITE-DIFFERENCE FORM ON GENERAL BODY FITTED GRID
- EXPLICIT MULTISTAGE RUNGE-KUTTA SCHEME
- VARIABLE $\Delta t_{i,j}$ & IMPLICIT RESIDUAL SMOOTHING

RESULTS

- SUPERSONIC THROUGHFLOW FAN
- HORSESHOE VORTEX AHEAD OF CYLINDER
- ANNULAR TURBINE CASCADE

FUTURE

- NEW FAN DESIGN WITH CONVERGING HUB, HIGH TURNING
- FINER GRIDS ON NAS
- TIP CLEARANCE
- MULTIGRID

SESSION X

STOVL

Chairman:
Meng-Sing Liou
Chief, Computational Fluid Dynamics Branch
NASA Lewis Research Center

SIMULATION OF POWERED-LIFT FLOWS

William R. Van Dalsem
Kalpana Chawla
Karlin R. Roth
Merritt H. Smith
Kuditipudi V. Rao

NASA Ames Research Center, Moffett Field, CA

Thomas C. Blum

BOEING Advanced Systems, Seattle, WA

The primary objective of this presentation is to expose government, industry, and academic scientists to work underway at NASA-Ames towards the application of CFD to the powered lift area. One goal of our research is to produce the technologies which will be required in the application of numerical techniques to, for example, the Supersonic STOVL program.

In the presentation, we will summarize our progress to date on the following specific projects:

Jet in ground effect with crossflow

Jet in a crossflow

Delta planform with multiple jets in ground effect

Integration of CFD with thermal and acoustic analyses

Improved flow visualization techniques for unsteady flows

YAV-8B Harrier simulation program

E-7 simulation program

Additional work is underway at NASA-Ames in the development of turbulence models and solution adaptive grid techniques suitable for the powered lift area, and the simulation of USB configurations. However, this work is not included here due to space constraints.

POWERED-LIFT CFD PROGRAM

OBJECTIVE

Develop and validate CFD technologies for the V/STOL field, with particular emphasis on the requirements of the supersonic STOVL program.

TECHNICAL APPROACH

Time-accurate Navier-Stokes solutions on overlapped adapting grids, coupled to thermal, propulsive, controls, and acoustic analyses.

STRATEGY

- Starting from the RFA CFD technology base, develop in-depth expertise in the most critical components of the flow about V/STOL aircraft.

- As required, improve the computational techniques to allow the accurate simulation of these flows.

- Simultaneously, begin complete V/STOL aircraft simulation efforts (e.g., VSRA and E-7), with above "component" efforts contributing required technologies and expertise.

IN A TIMELY MANNER, DEVELOP BOTH IN-DEPTH EXPERTISE AND THE ABILITY TO TREAT COMPLETE V/STOL CONFIGURATIONS.

POWERED-LIFT CHALLENGES & CFD REQUIREMENTS

FUNDAMENTAL FLUID MECHANICS

| JETS IN GROUND EFFECT | JETS EXITING FROM A SURFACE | IMPACT OF BODY DYNAMICS | MULTIPLE JETS/ FOUNTAIN EFFECTS | EJECTORS |

THERMAL LOADS — VEHICLE — LANDING SURFACE

TURBULENCE — COHERENT STRUCTURE MOTION

ACOUSTIC LOADS

POWERED-LIFT DESIGN PROBLEMS
- SUCK DOWN
- FOUNTAIN EFFECTS
- LIDS AND LOWER SURFACE CONTOURS
- GROUND VORTEX
- INDUCED LIFT AND PITCHING MOMENTS
- LATERAL AND DIRECTIONAL CHARACTERISTICS
- HOT GAS INGESTION
- LANDING GEAR AND LANDING ENVIRONMENT
- LOWER SURFACE HEATING
- ACOUSTIC LOADS
- ETC ...

| COMPLEX GEOMETRIES | SOLUTION ADAPTIVE | MOVING GRID TECHNOLOGY | UNSTEADY GRAPHICS | JET | GROUND VORTEX | FOUNTAIN |

| GRID GENERATION | DYNAMICS | TURBULENCE MODELING |

CFD TECHNOLOGY REQUIREMENTS

277

JET IN GROUND EFFECT WITH CROSSFLOW

A fundamental component of STOVL take-off/landing flow physics

- To date, CFD has proved capable of resolving the salient features, and adding to previous understanding:

  ○ Computed correct ground vortex formation and extent over a range of jet to freestream velocity ratios and jet heights.

  ○ Allowed a systematic study of the impact of a variety of flow conditions, including jet shape, moving ground board, etc...

  ○ Simulated ring vortex and shock disc motion, which may be important sources of unexplained intense noise levels

- In the future, will focus on improving our understanding of jet unsteadiness and the existing discrepancies between experimental and full-scale studies.

IMPACT OF TURBULENCE MODELING
C_p ALONG CENTERLINE OF JET
$V_e = 0.223, h/D = 3$

BASE BALDWIN/LOMAX
ADD A+
ADD A+ AND GVLS
ADD SGS
□ EXP— STEWART/KUHN/WALTERS
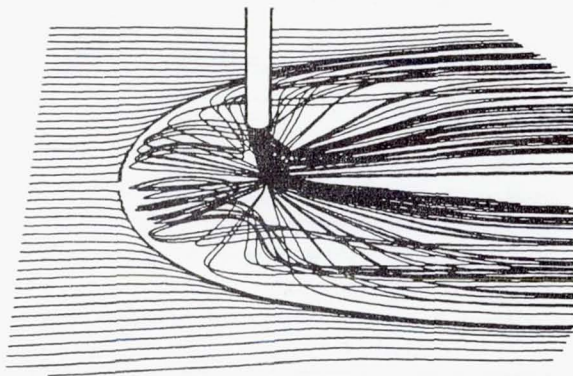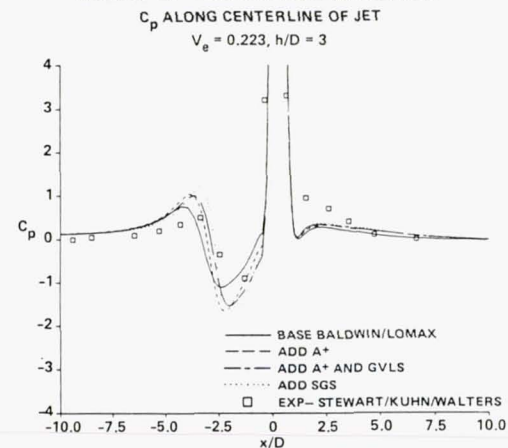
JET IN GROUND EFFECT SIMULATION
(Ve=0.10, h/D=3, turbulent jet)
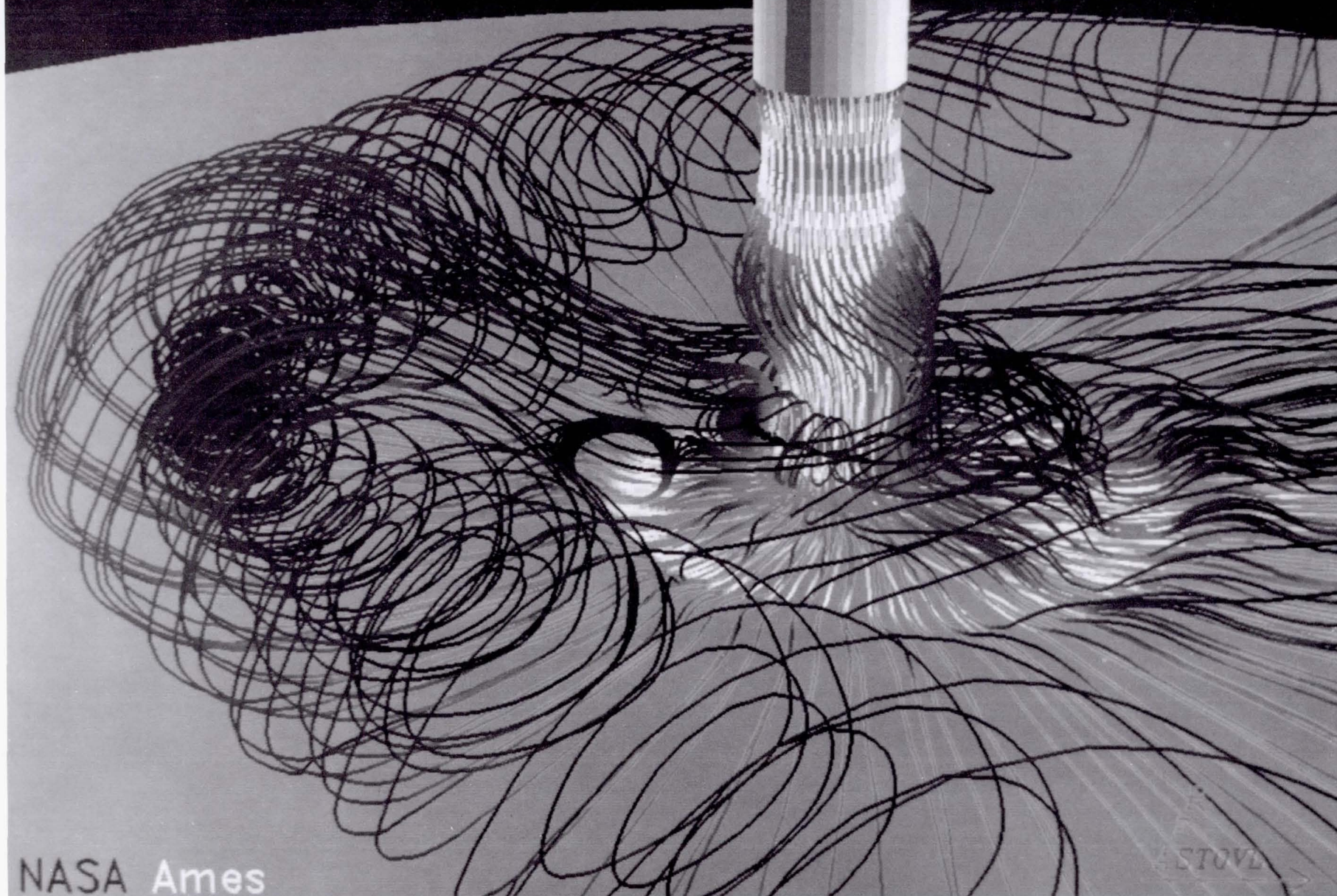
NASA Ames

UNSTEADY FLOW ANALYSIS

BACKGROUND   The unsteady flow about powered-lift vehicles induces significant unsteady loads, hence must be accurately predicted.

Require significant software improvements to deal with unsteady flows on a routine basis.

APPROACH   Develop techniques which allow the rapid yet indepth analysis and validation of unsteady flow simulations.

PLOT4D
An "upgraded" version of PLOT3D program which allows the interactive animation and analysis of unsteady data sets.

STREAKER
Produces time-accurate numerical streaklines (smoke) suitable for direct comparison with experimental unsteady flow visualizations.
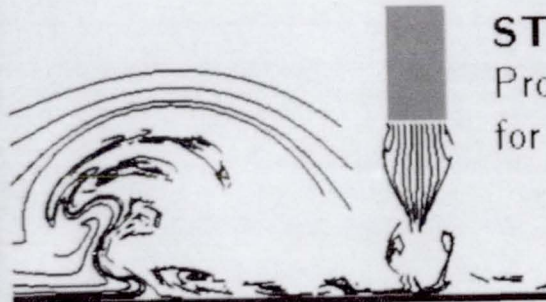
NUMERICAL STREAKLINES
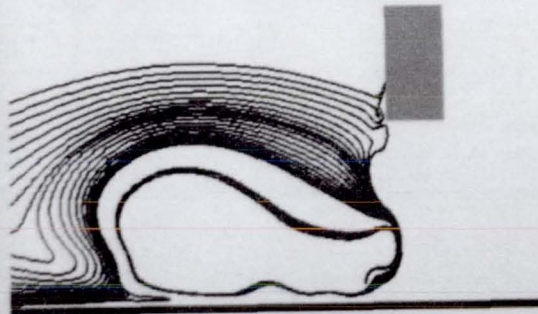
NUMERICAL STREAMLINES
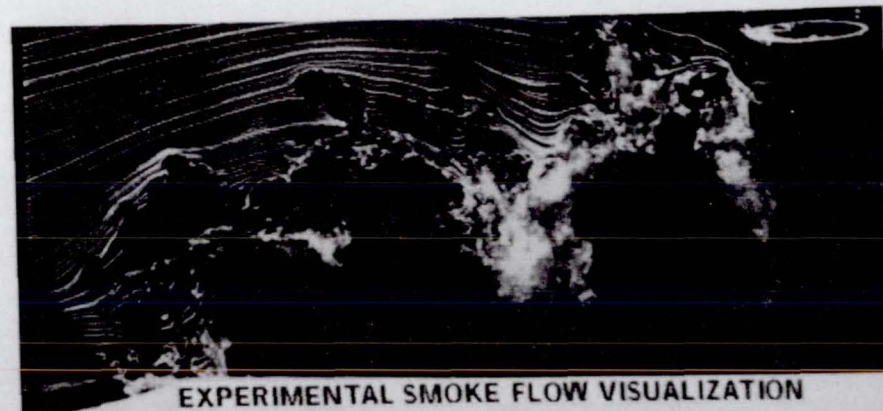
EXPERIMENTAL SMOKE FLOW VISUALIZATION

THERMAL LOADS

PROVEN RISK OF VEHICLE AND LANDING SURFACE DAMAGE (e.g., LPH TRIPOLI DECK BUCKLING) DURING TAKE-OFF/LANDING, AND VEHICLE DAMAGE DURING TRANSITION

• AT PRESENT, EXPENSIVE FULL-SCALE JET ENGINE/MATERIALS TEST (FLUK) ARE ONLY METHOD OF TESTING UNSTEADY THERMAL RESPONSE OF MATERIALS TO ENGINE EXHAUST

• COUPLED UNSTEADY JET FLOW CFD/THERMAL ANALYSIS OF SURFACES MADE OF A VARIETY OF MATERIALS (FROM ALUMINUM AND COMPOSITES, TO CONCRETE) WOULD ALLOW DETAILED ANALYSIS OF V/STOL THERMAL DAMAGE

NAVIER-STOKES EQS.

$$Q_t + E_x + F_y + G_z = Re^{-1}(Ev_x + Fv_y + Gv_z)$$

JET TEMPERATURE PROFILE

THERMAL CONDUCTION EQ.

$$(kT_x)_x + (kT_y)_y + (kT_z)_z + \dot{q} = \rho c T_t$$

SIDE VIEW
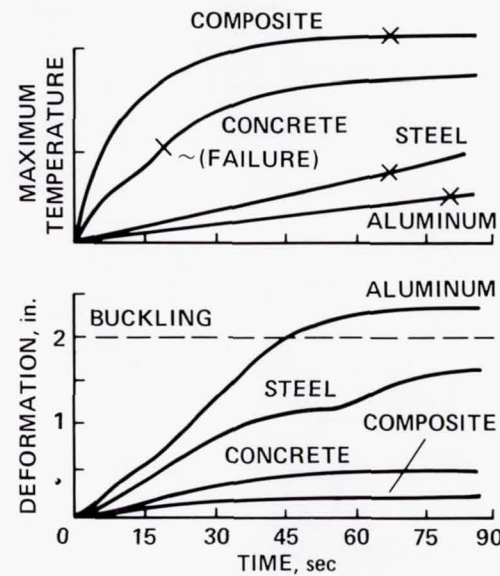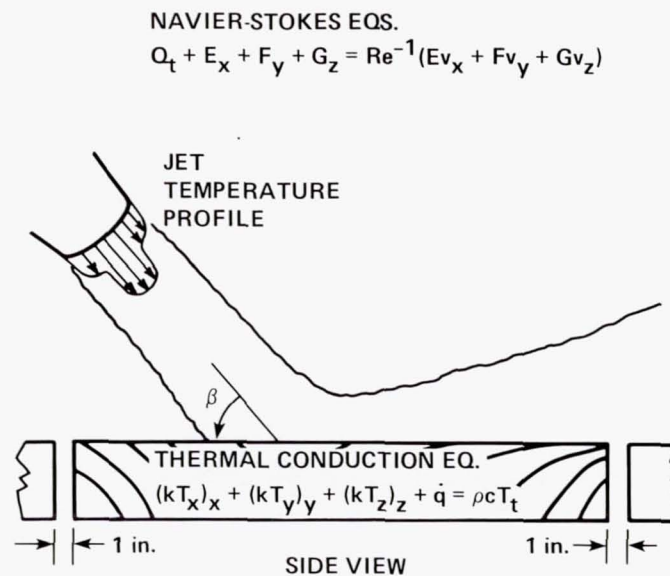
HOT JET THERMAL LOAD
(Ve=0.10, h/D=3, turbulent jet)

NAVIER–STOKES EQS.
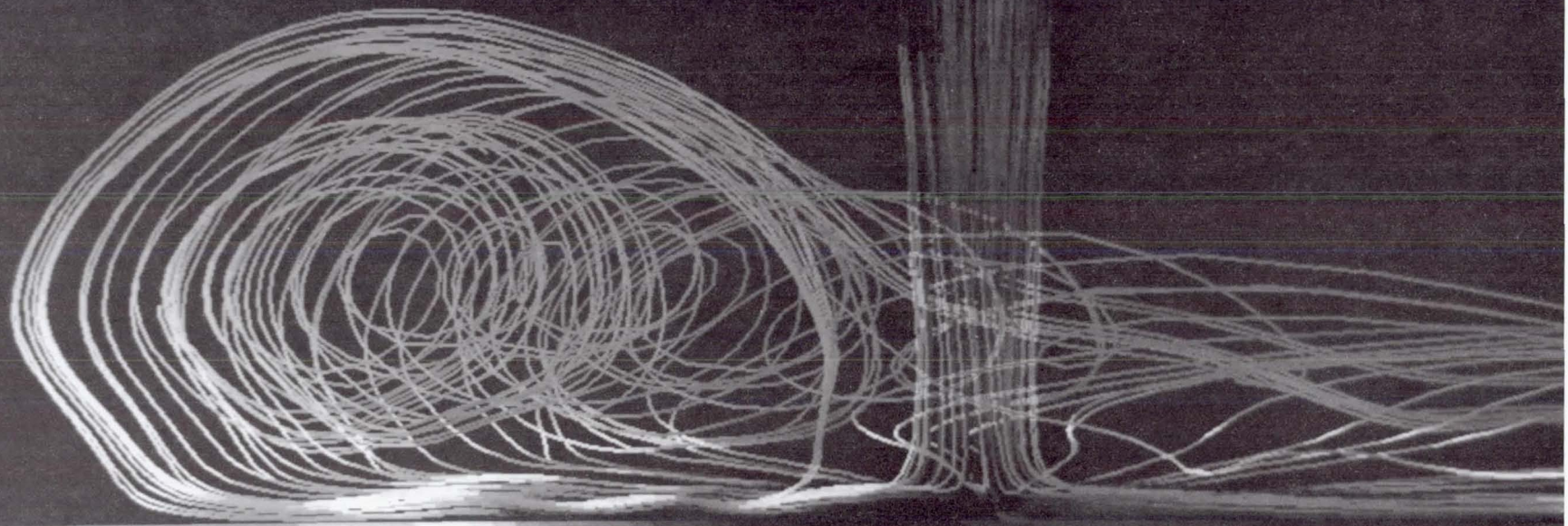
THERMAL CONDUCTION EQ.

NASA Ames

JET IN A CROSSFLOW

- Isolates physics of aero/propulsive interaction region during transition.

- Navier-Stokes solution captures all critical flow features.

- Quantitative correlation with existing database demonstrated.

- Current efforts focus on computing realistic STOVL geometries.

FLOW PHYSICS
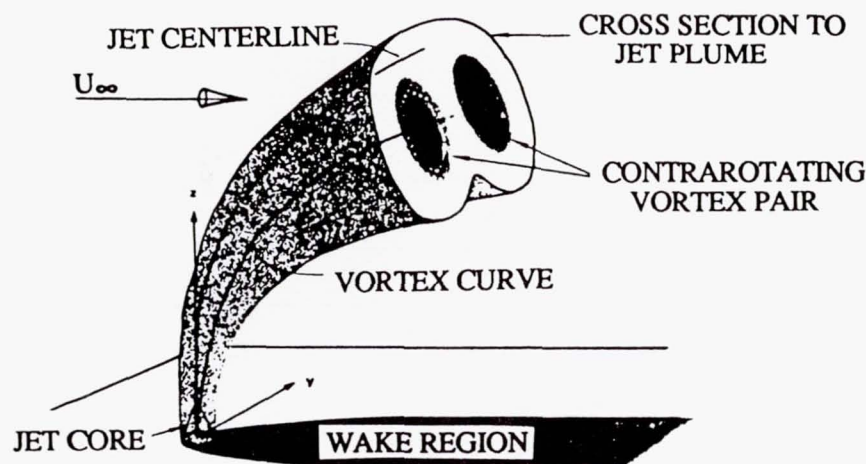
JET CENTERLINE
$M_j/M_\infty = 4.0$, $M_\infty = 0.19$
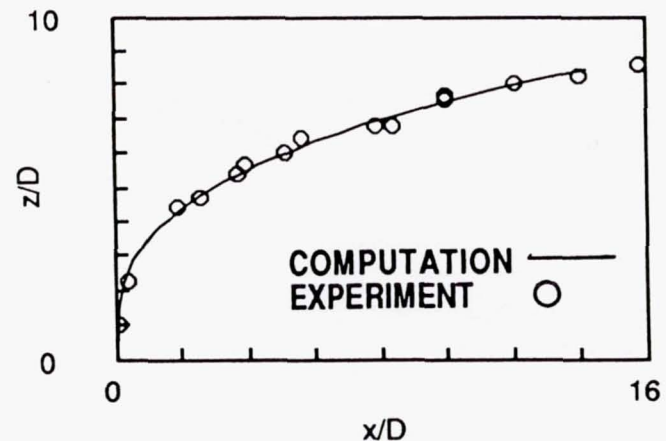
K. Roth, **FFF**

JET IN A CROSSFLOW
R = 6.0, Mj = 0.76
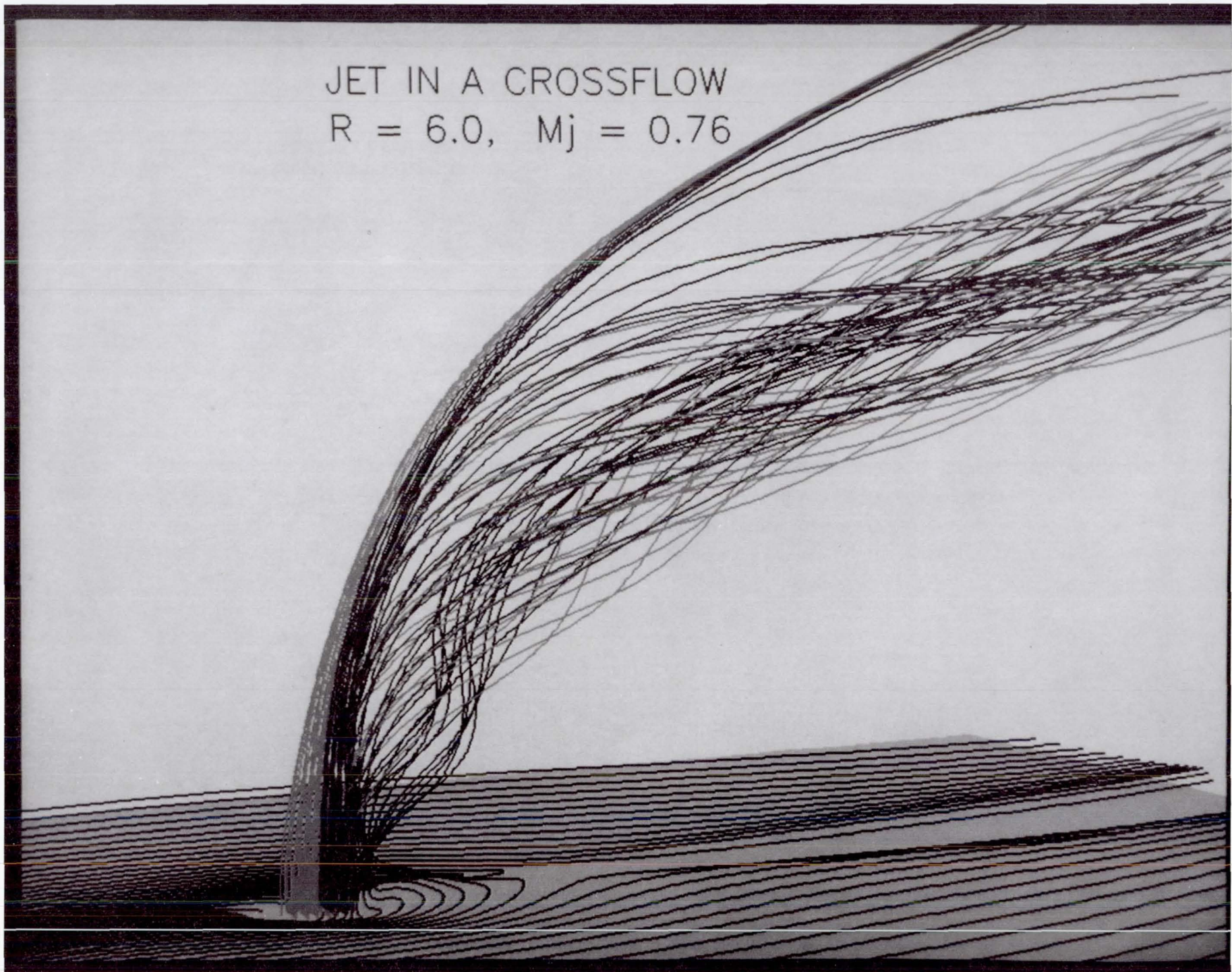
GROUND EFFECTS

C_l AND C_m OF V/STOL VEHICLES IN GROUND-EFFECT ARE STRONGLY INFLUENCED BY HEIGHT ABOVE GROUND AND RATE OF ASCENT/DESCENT

- DIFFICULT TO STUDY EXPERIMENTALLY, AT PRESENT GOVERNING FLOW PHYSICS IS NOT UNDERSTOOD

- TO DATE, CFD HAS SHED INSIGHT IN TO FLOW PHYSICS OF NEGATIVE C_l AT LOW HEIGHTS, AND WORK IS IN PROGRESS TO STUDY DYNAMIC CASE

$\beta(\alpha, \dot{h}, V_e)$ = EFFECTIVE ANGLE OF ATTACK
α = ANGLE OF ATTACK
$\dot{h}$ = RATE OF DESCENT
$V_e = V_\infty/V_{jet}$
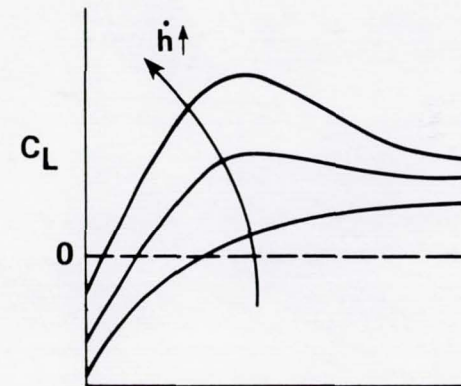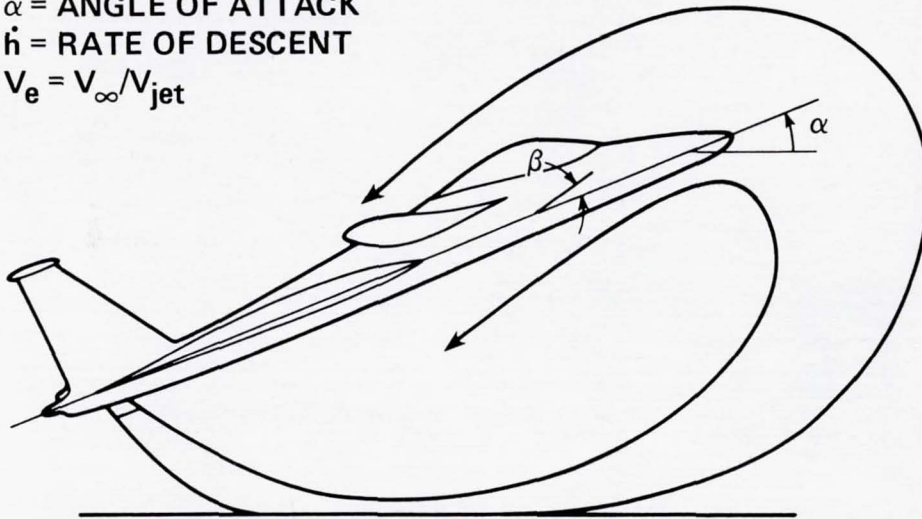
V/STOL SIMULATION
(60° Delta, Ve=0.064, h/B=0.25)
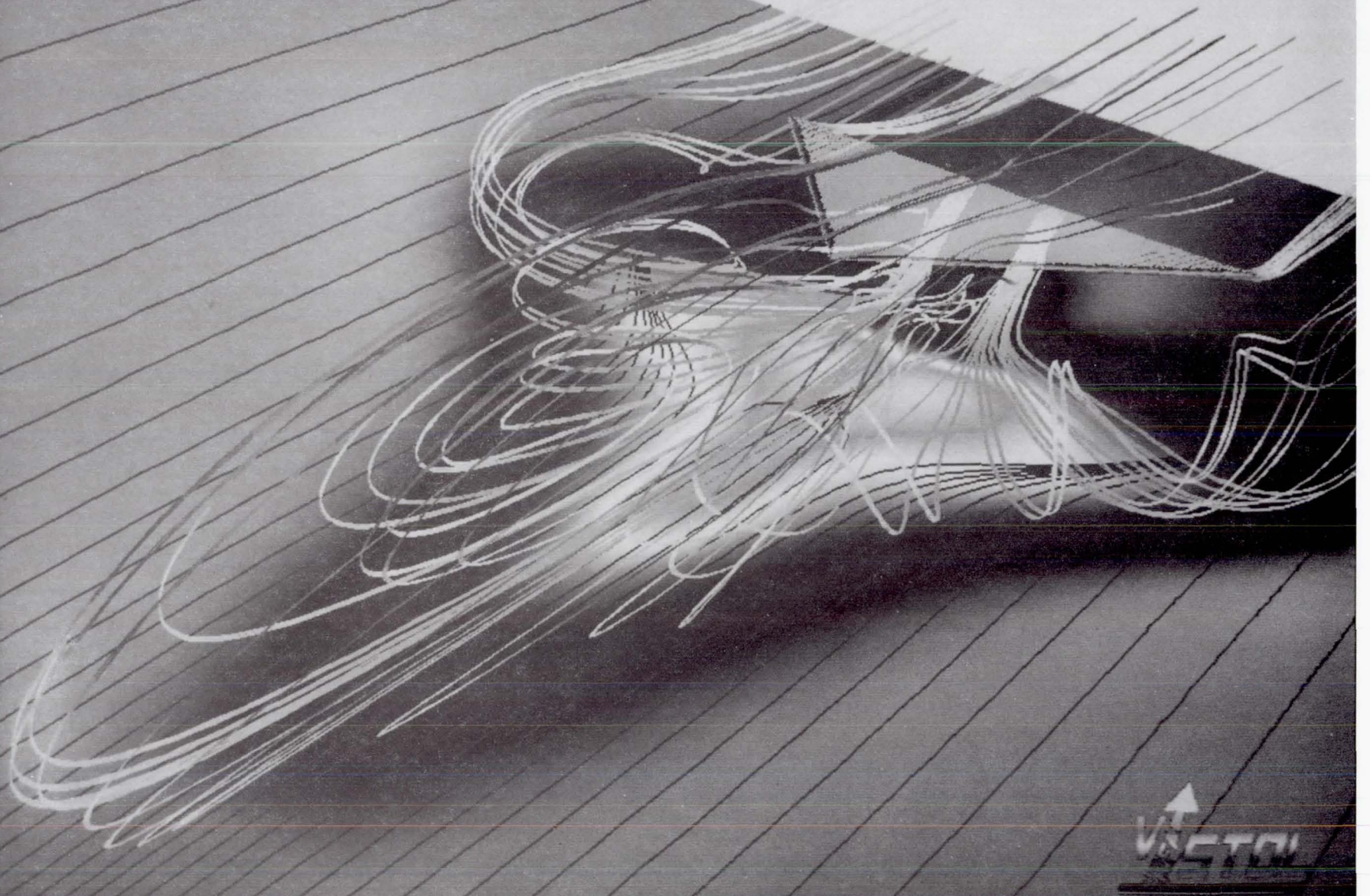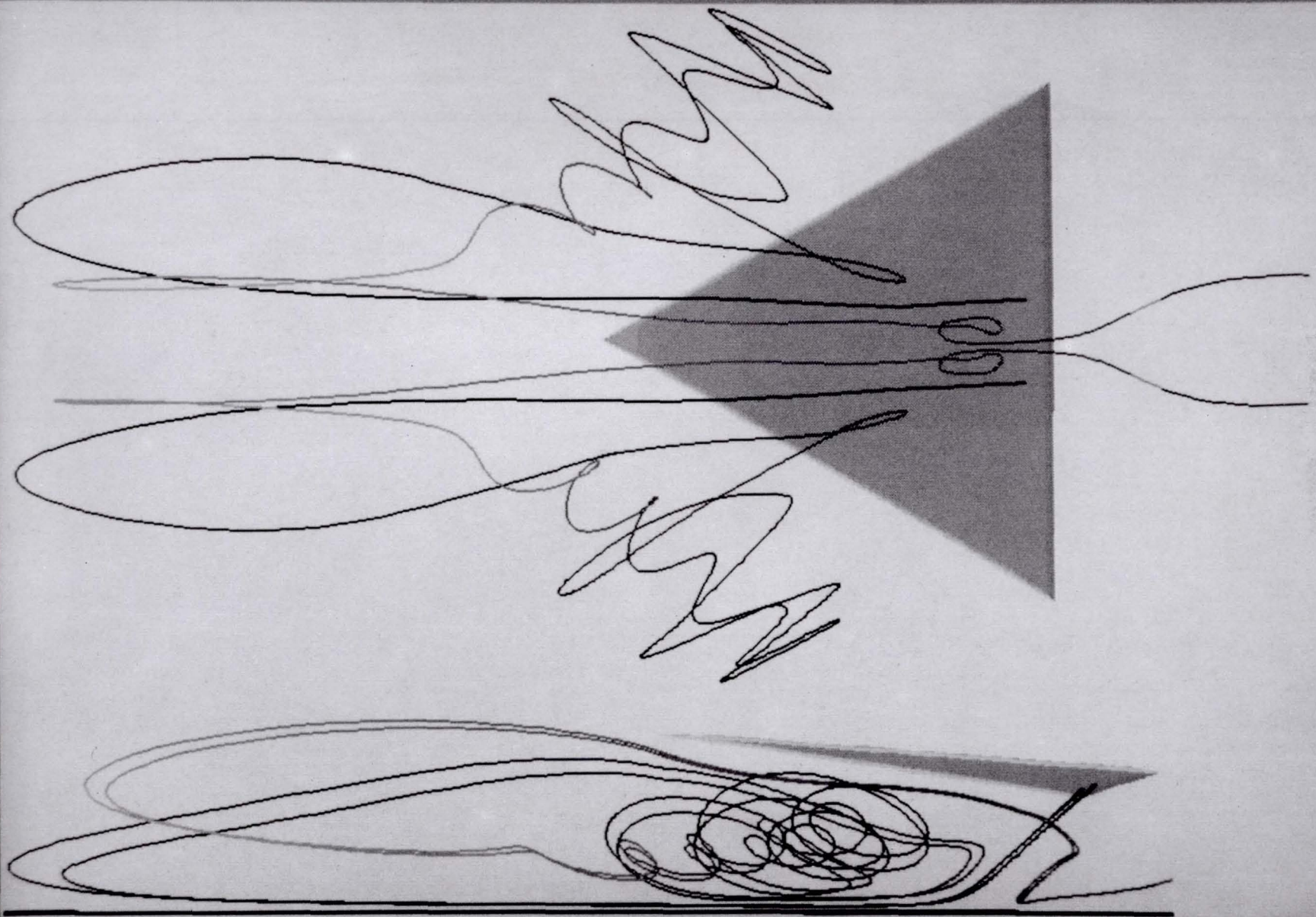
VSRA COMPUTATION TO FLIGHT PROGRAM
(Preliminary Harrier YAV-8B Surface Definition)
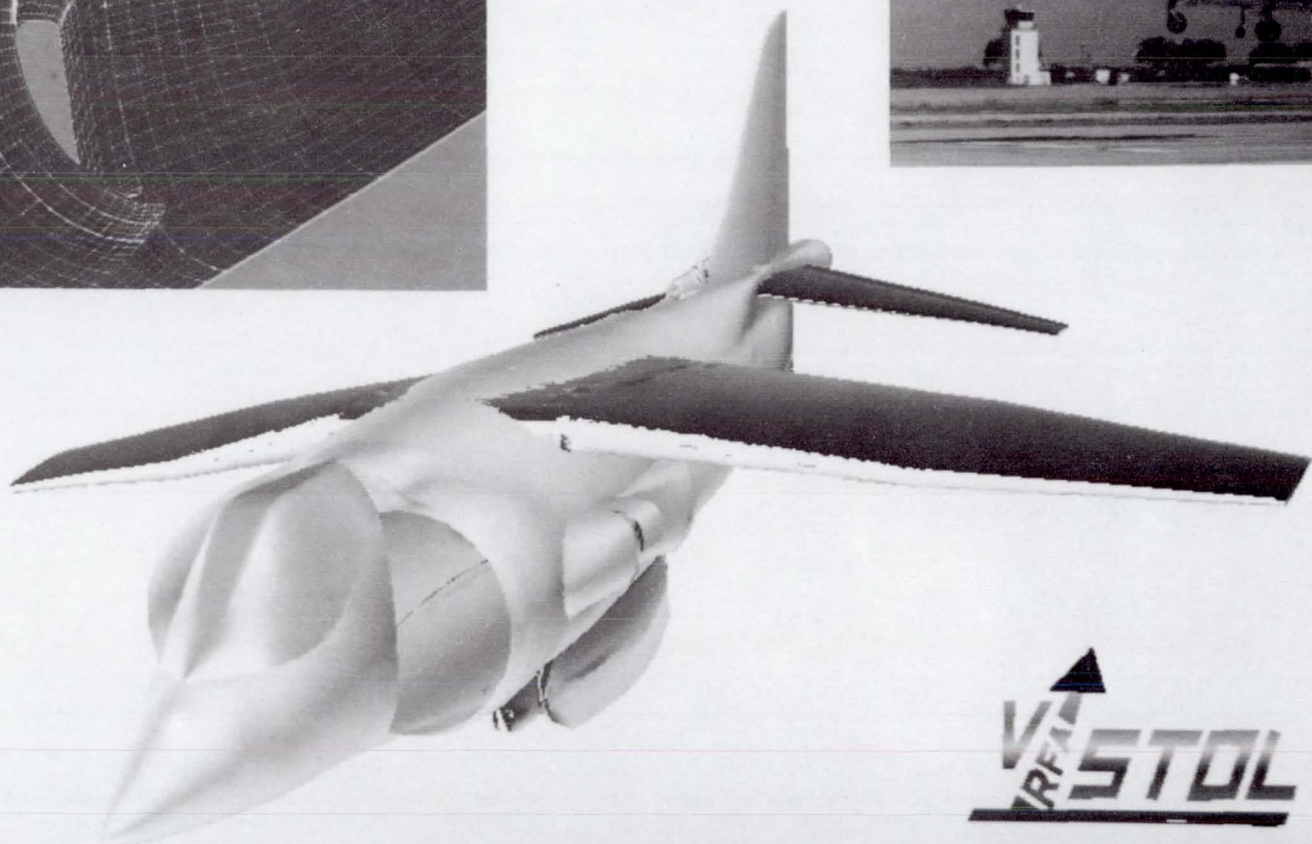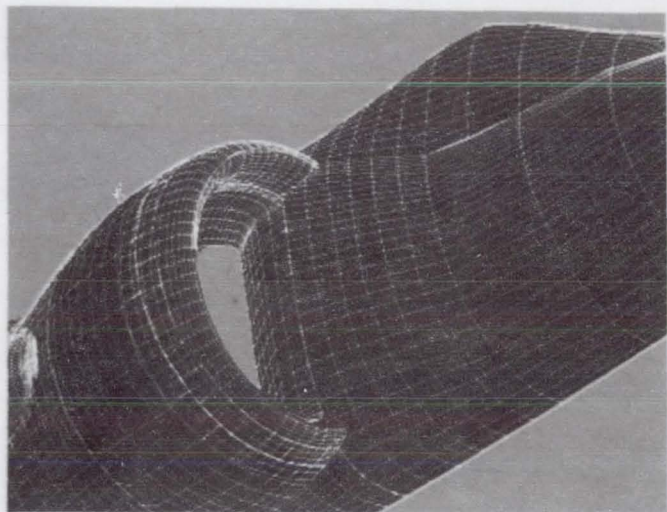
E-7 COMPUTATION THROUGH FULL-SCALE EXPERIMENT PROGRAM
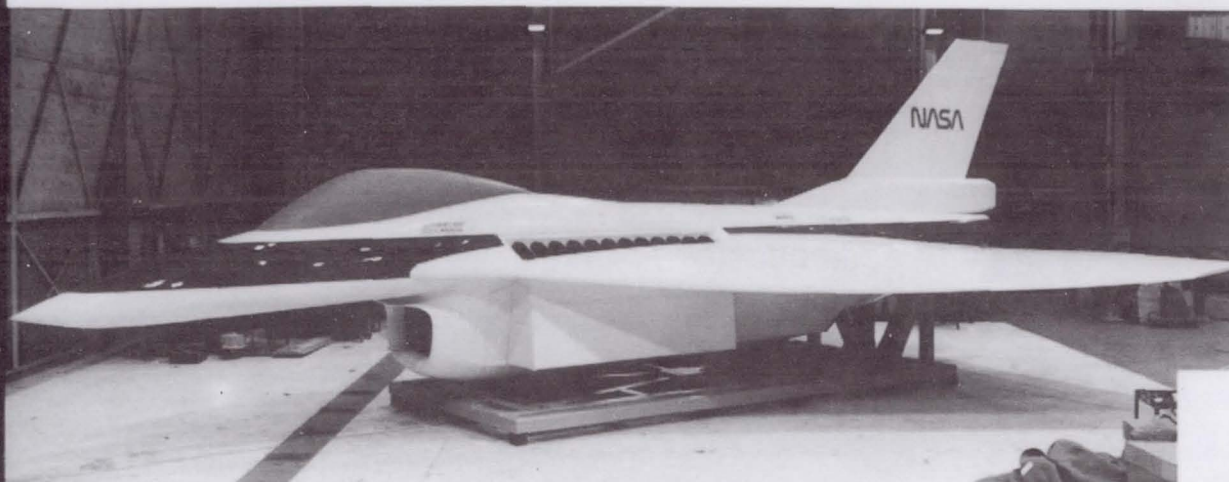
- GRIDS GENERATED BY BOEING

- COMPUTATIONS A JOINT BOEING/NASA-AMES EFFORT
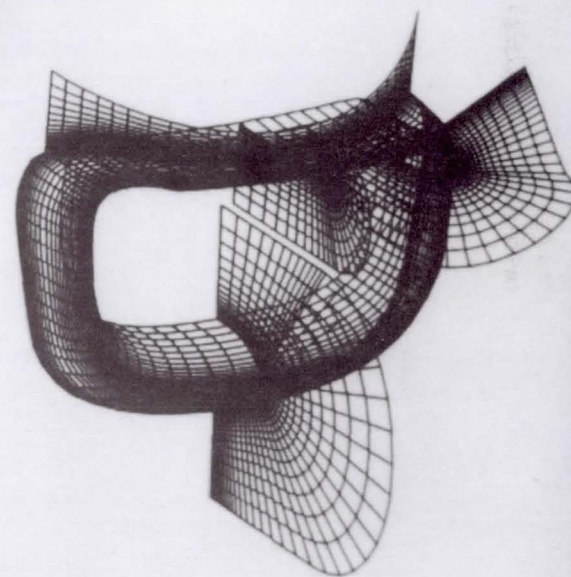
SUMMARY

- To date, have studied the numerical simulation of the following powered-lift flows:
  - Jet in ground effect with crossflow (including thermal loads)
  - Jet in crossflow
  - Delta with multiple jets in ground effect with crossflow

  Comparison with data indicates that these simulations predict the fundamental flow phenomena and yield quantitative results for many of the observed trends.

- This experience has motivated us towards additional R&D in the following areas:
  - Adaptive gridding
  - Improved turbulence modeling
  - Unsteady flow simulation and analysis

- Presently also working towards simulation of the following "complete" configurations:
  - STOVL CFD Validation model (In cooperation with FFF)
  - YAV-8B Harrier (" FAP to obtain data)
  - E-7 (" Boeing)
  - USB configuration (" FAP)
  - Tiltrotor configuration (" RFA Rotorcraft group)

290

A Numerical Study of the Hot Gas Environment
Around a STOVL Aircraft in Ground Proximity

by

Thomas J. VanOverbeke

and

James D. Holdeman

of

NASA Lewis Research Center

ABSTRACT

    The development of Short Take-off Vertical Landing (STOVL) aircraft
has been based on empiricism. In this study, a 3-D flow code was used to
calculate the hot gas environment around a STOVL aircraft in ground
proximity. Preliminary calculations are reported to identify key
features of the flowfield, and to demonstrate the capability of a CFD
code to calculate the temperature of the gases ingested at the engine
inlet for typical flow and geometric conditions.

CALCULATIONS WERE DONE WITH A 3-D TEACH-TYPE CODE
TO SOLVE THE TIME-AVERAGED NAVIER-STOKES EQUATIONS

EQUATIONS ARE SOLVED SEQUENTIALLY

A PRESSURE CORRECTION EQUATION IS SOLVED USING
THE SIMPLE ALGORITM OF PATANKAR

HYBRID DIFFERENCING WAS USED TO SAVE MEMORY

A TWO EQUATION TURBULENCE MODEL WAS USED

CODE WAS USED FOR COMBUSTORS AND DID NOT INCLUDE
A DENSITY CORRECTION TERM FOR RAPIDLY VARYING
PRESSURE

EXIT BOUNDARY CONDITIONS WERE CHANGED FOR
MODELING THE HOT GAS INGESTION PROBLEM

SCHEMATIC OF COMPUTATIONAL DOMAIN
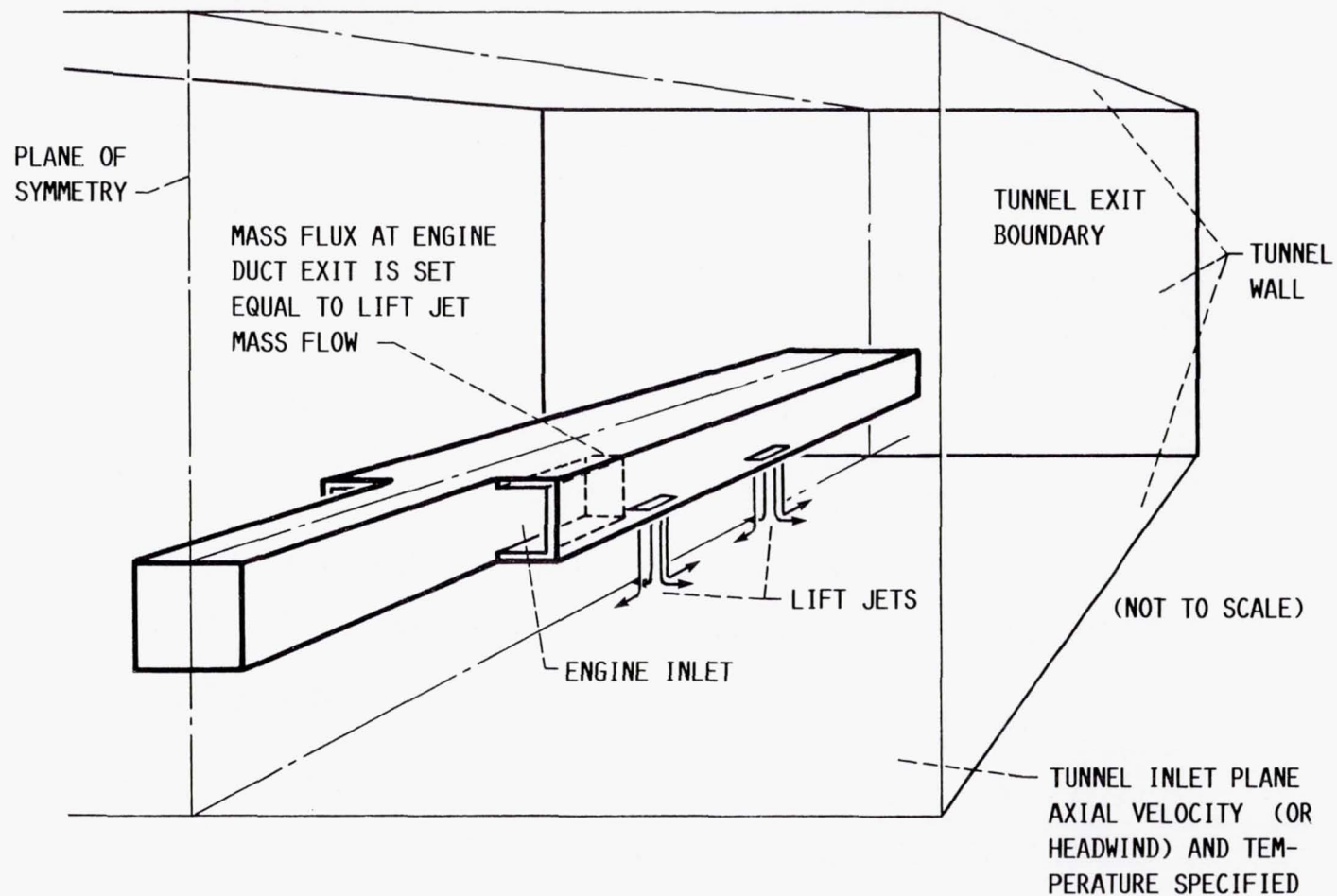
PLANE OF
SYMMETRY

MASS FLUX AT ENGINE
DUCT EXIT IS SET
EQUAL TO LIFT JET
MASS FLOW

TUNNEL EXIT
BOUNDARY

TUNNEL
WALL

LIFT JETS

(NOT TO SCALE)

ENGINE INLET

TUNNEL INLET PLANE
AXIAL VELOCITY (OR
HEADWIND) AND TEM-
PERATURE SPECIFIED

CD-88-34774

NEAR-GROUND PLANE VELOCITY AND TEMPERATURE DISTRIBUTIONS

$(H/D_j = 4)$

$U_\infty/V_j = 0.03$

1100 °F

0 °F

CD-88-34776

NEAR-GROUND PLANE VELOCITY AND TEMPERATURE DISTRIBUTIONS

(H/Dj=4)

U∞/Vj = 0.09

1100 °F

0 °F
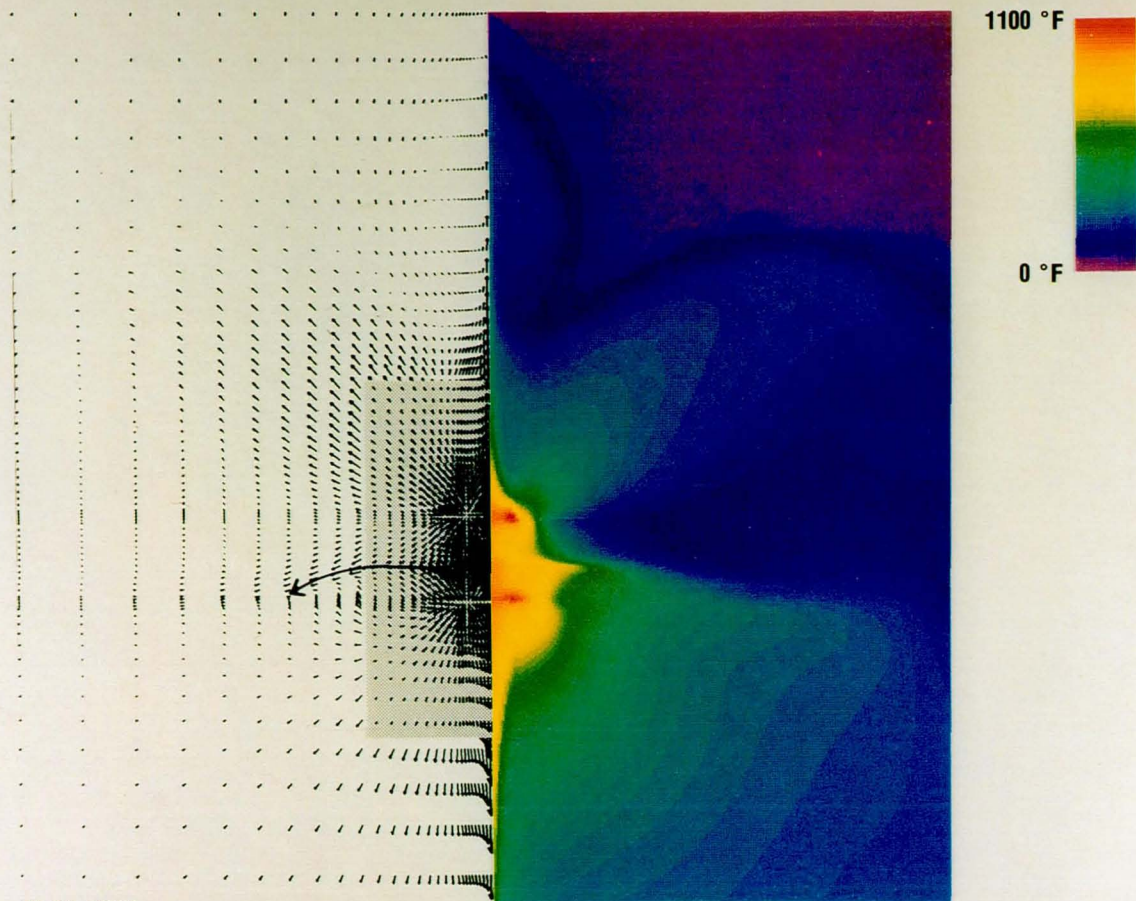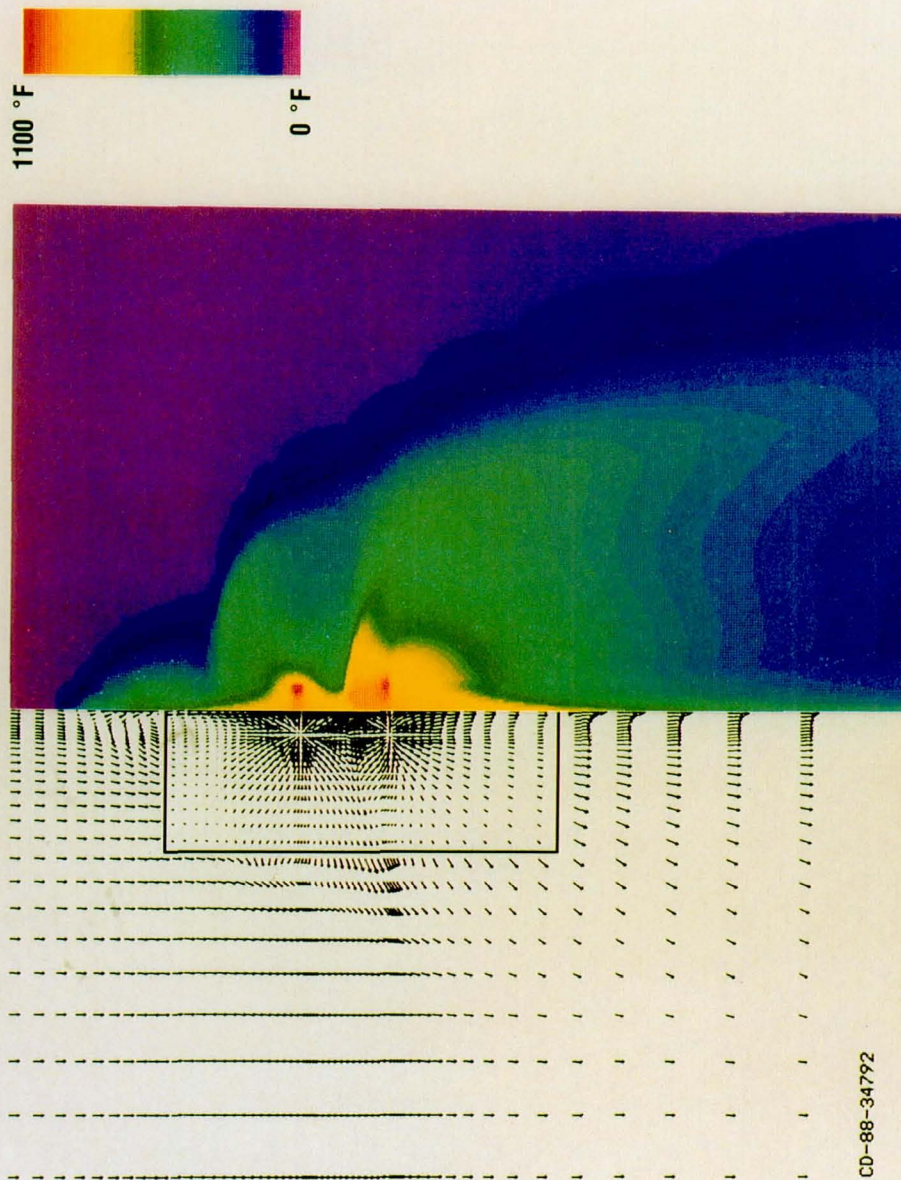
CALCULATED VELOCITY AND TEMPERATURE DISTRIBUTIONS IN VERTICAL X-Y PLANE THROUGH ENGINE INLET

$(H/Dj=4; U\infty/Vj=0.03)$
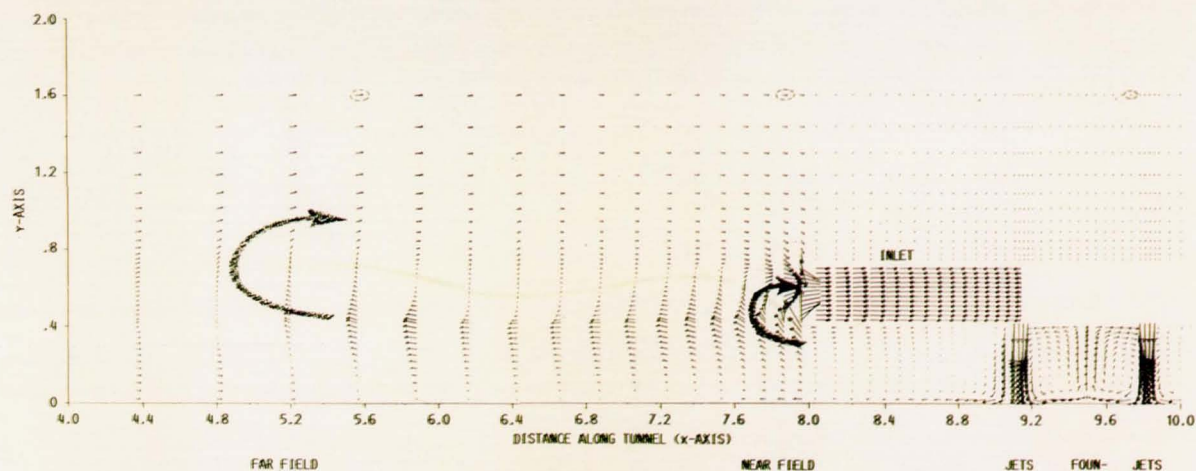
A) VELOCITY
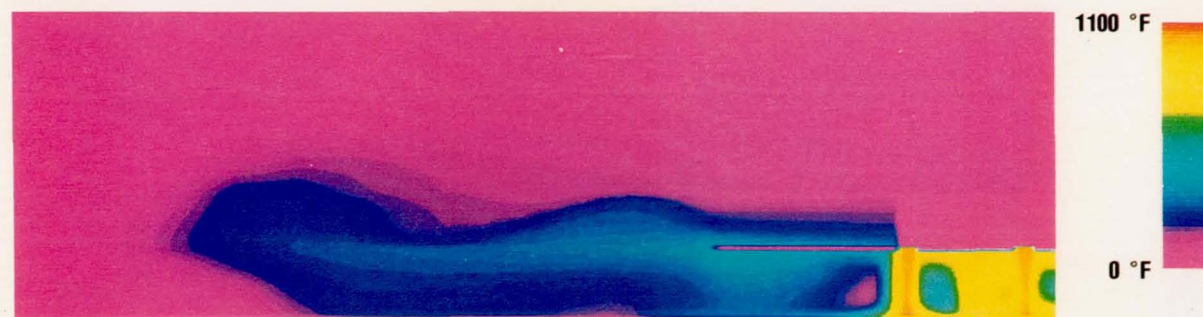
CD-88-34777

B) TEMPERATURE

TEMPERATURE DISTRIBUTIONS IN VERTICAL PLANES FROM AIRCRAFT CENTERPLANE TO OUTBOARD OF FUSELAGE

$(H/Dj = 4)$

$U\infty/Vj = 0.03$ 0.09
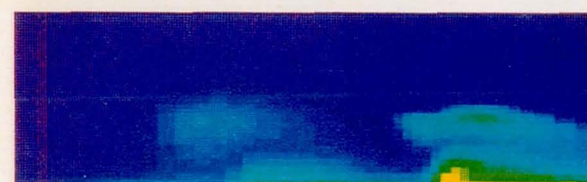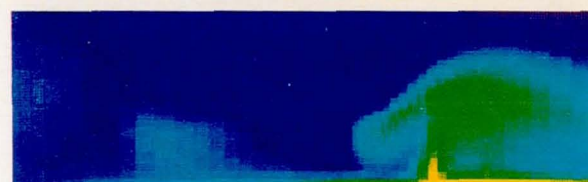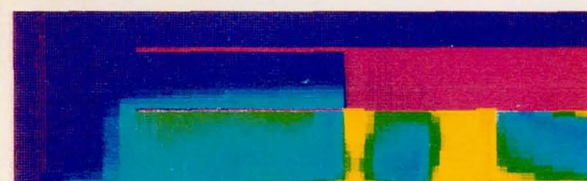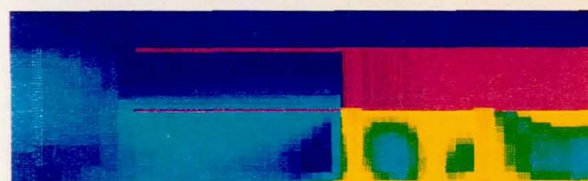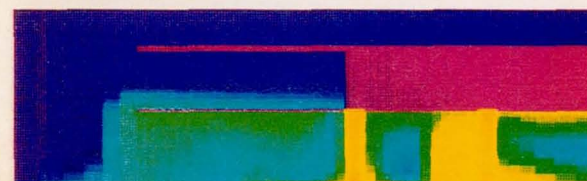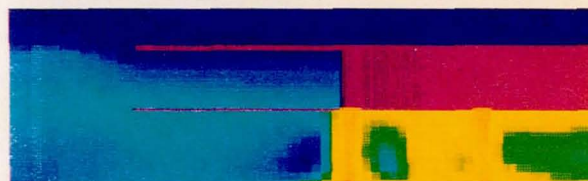
1100 °F

0 °F

TEMPERATURE DISTRIBUTIONS IN VERTICAL PLANES FROM AIRCRAFT CENTERPLANE TO OUTBOARD OF FUSELAGE

$(U_\infty/V_j = 0.09)$
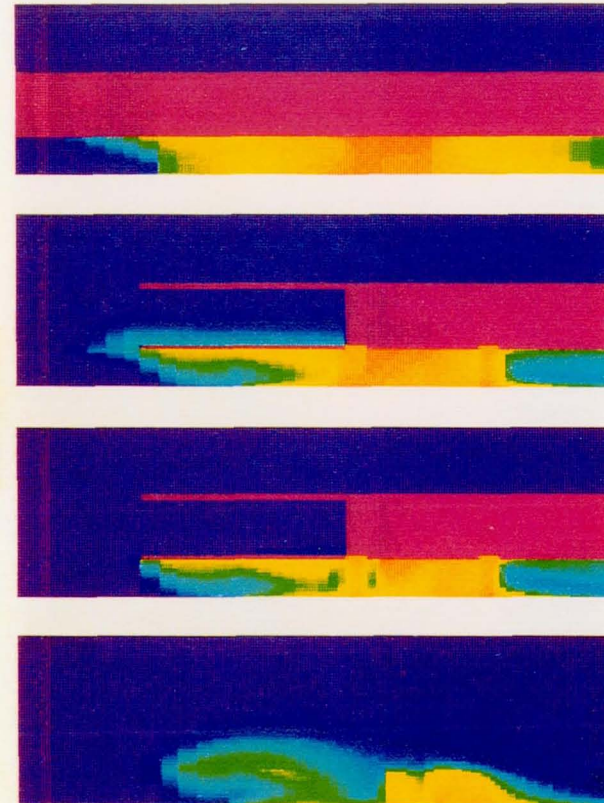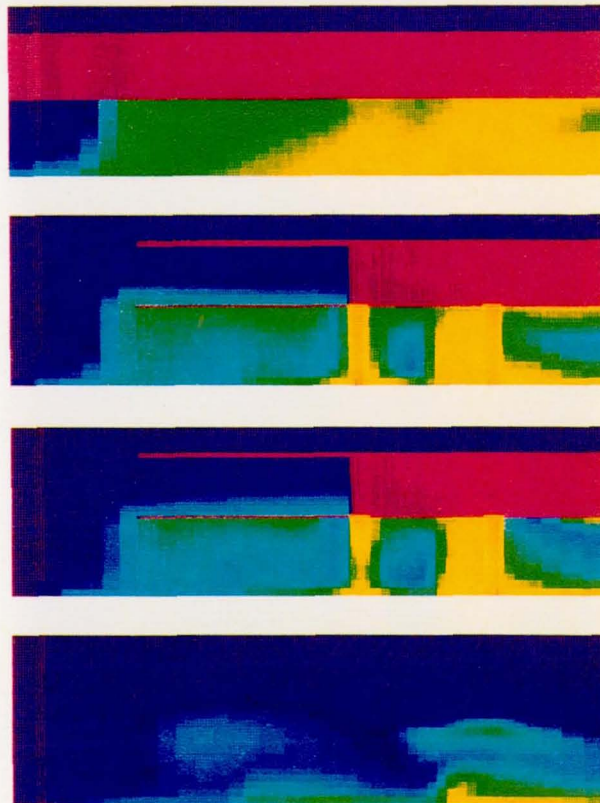
TEMPERATURE DISTRIBUTION IN HORIZONTAL PLANES
EFFECT OF CHANGING HEIGHT
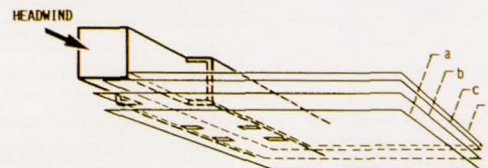
$U\infty/Vj = 0.09$
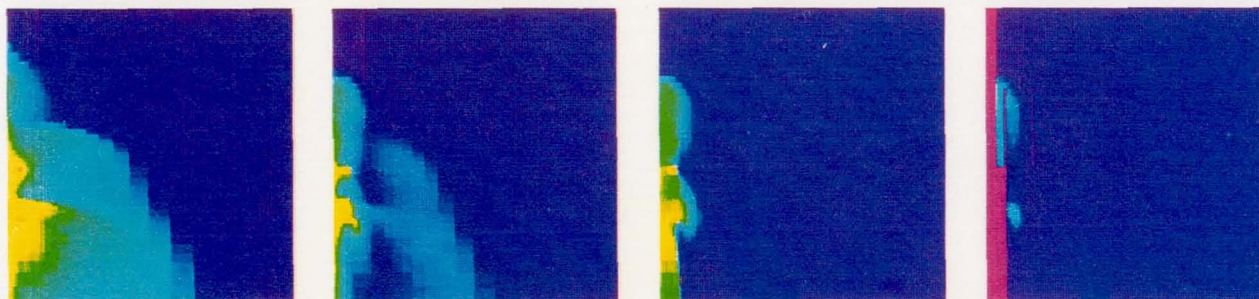
H/Dj = 4
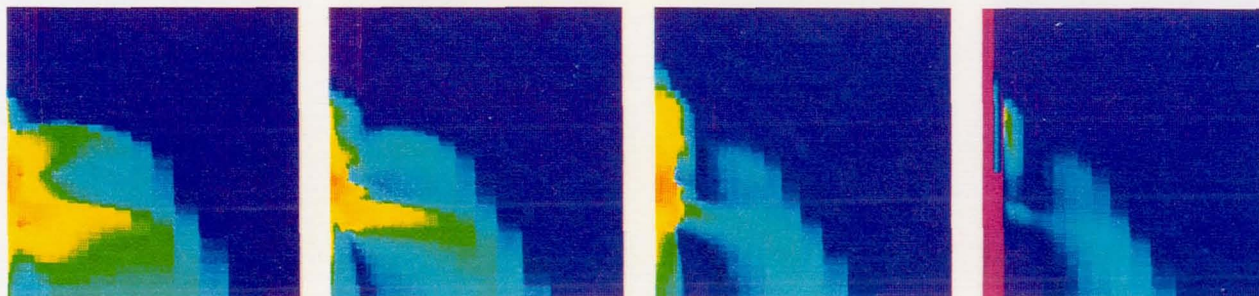
H/Dj = 2

CD-88-34790

TEMPERATURE DISTRIBUTIONS IN VERTICAL
(Y-Z) PLANES THROUGH ENGINE INLET

$U\infty/Vj = 0.03$

0.09

$H/Dj = 4$

$H/Dj = 2$

500 °F

0 °F
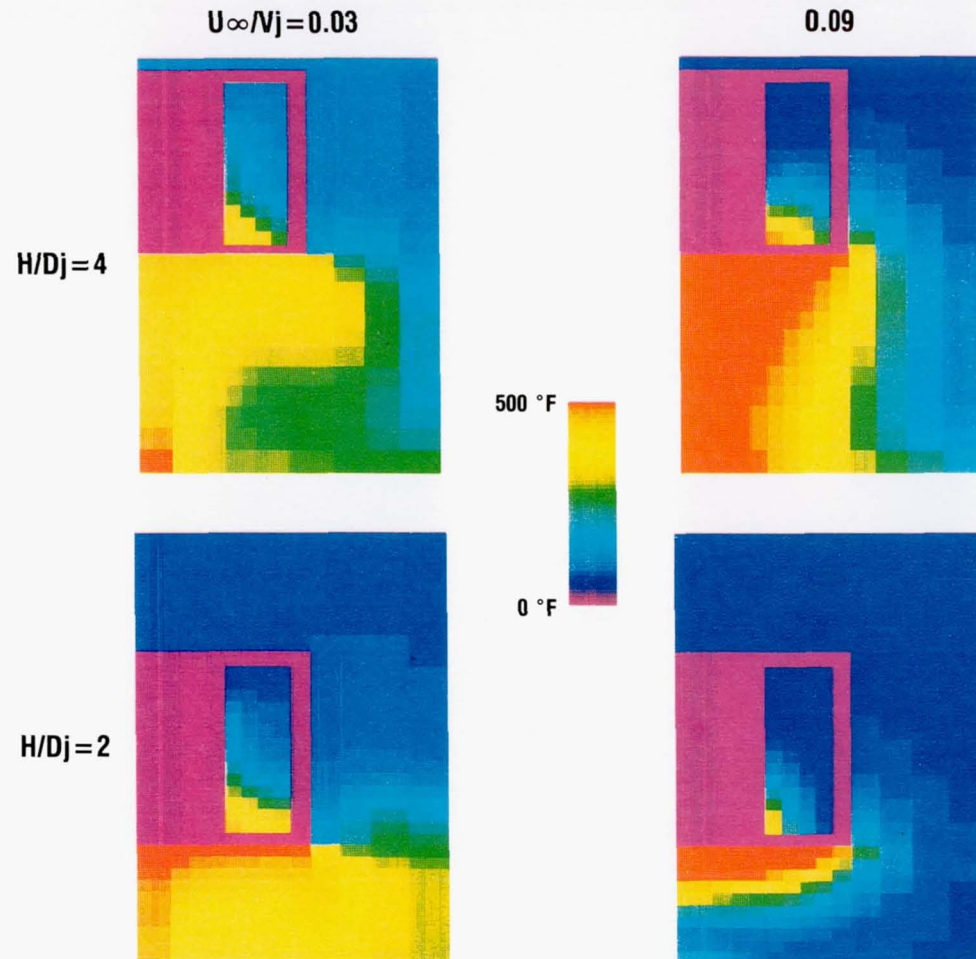
CD-88-34791

Jet, Ambient, and Inlet
Temperatures for Cases Calculated[a]

U_∞/V_j	H/D_j	U_∞, kn	T_{avg}	T_{max}	T_{min}
0.03	4	17.8	187.7	388.2	109.8
.03	2	17.8	173.5	429.6	72.0
.09	4	53.6	145.1	469.9	61.6
.09	2	53.6	97.6	375.3	62.3

[a]At nozzle pressure ratio of 1.21; $T_j = 1000$; $T_\infty = 70$ (all temperatures are degrees F).

Average Inlet Temperatures[a]

Distance from exhaust lift jets to ground plane, H/D_j	Ratio of forward speed of aircraft (or strength of headwind) to exhaust jet velocity, U_∞/V_j	
	0.03	0.09
4	0.13	0.08
2	.11	.03

[a]$(T_{avg} - T_\infty)/(T_j - T_\infty)$

Inlet Temperature Distortion[a]

Distance from exhaust lift jets to ground plane, H/D_j	Ratio of forward speed of aircraft (or strength of headwind) to exhaust jet velocity, U_∞/V_j	
	0.03	0.09
4	0.30	0.44
2	.38	.34

[a]$(T_{max} - T_{min})/(T_j - T_\infty)$

CD-88-34961

SUMMARY

INTERNAL FLOW CODE CAN BE USED IN PREDICTING STOVL FLOWFIELDS

SIGNIFICANT INGESTION WAS PREDICTED IN ALL CASES CALCULATED

ALL CASES PREDICTED NEAR FIELD INGESTION

WEAKER HEADWINDS ALSO PREDICTED INGESTION BY GROUND VORTEX FLOW

CFD ANALYSIS FOR HIGH SPEED INLETS

Tom Benson

NASA Lewis Research Center

ABSTRACT

The increased national interest in high speed flight has increased research for high speed propulsion components. The highly three-dimensional flows present in supersonic/hypersonic inlets are currently being studied at NASA Lewis both experimentally and computationally using a family of steady PNS and NS solvers and unsteady NS solvers. This paper presents some of the results of these efforts with an emphasis on the comparison of the computational and experimental results.

The flow in high speed inlets typically involves the interaction of compression shock waves and boundary layers on the internal surfaces. The fundamentals of these interactions have been studied experimentally for many years, while more recently, computations have been used to study these complex three dimensional flow fields. Attempts to control the flow through boundary layer bleed are being investigated computationally prior to wind tunnel experiments. The ultimate goal of this research will be the higher performing inlets required for high speed flight.

CFD FOR HIGH SPEED INLETS
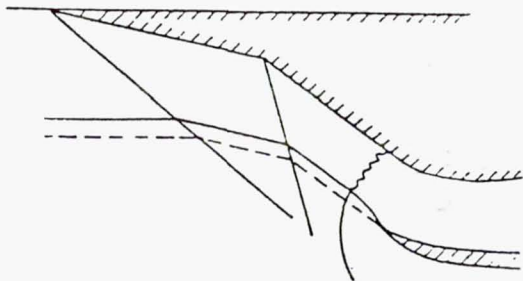
MIXED COMPRESSION

EXTERNAL COMPRESSION

AXI-SYMMETRIC

313
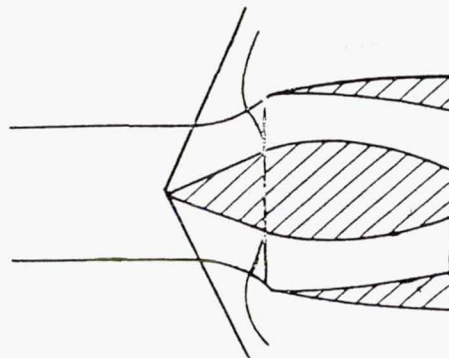
THRUST DISTRIBUTION FOR SR-71

MACH NO	INLET	ENGINE	EJECTOR
2.2	13%	73%	14%
3. ✛	54%	18%	28%

CFD FOR HIGH SPEED INLETS

$1.3 < MACH < 5.0$

PHENOMENA

BUZZ
UNSTART
SHOCK/SHOCK INTERACTION
OBLIQUE SHOCK/BOUNDARY LAYER
NORMAL SHOCK/BOUNDARY LAYER
GLANCING SHOCK/BOUNDARY LAYER
CORNER FLOWS

All of the above with
BOUNDARY LAYER BLEED

CODES

3D PNS (PEPSIS)
   -BRILEY/MCDONALD LBI SCHEME
3D-STEADY NS (PARC)
   -BEAM/WARMING ADI
3D-UNSTEADY NS (PROTEUS)
   -BEAM/WARMING ADI
   -2nd ORDER TIME ACCURATE

CFD FOR HIGH SPEED INLETS
OBLIQUE SHOCK BOUNDARY LAYER INTERACTION
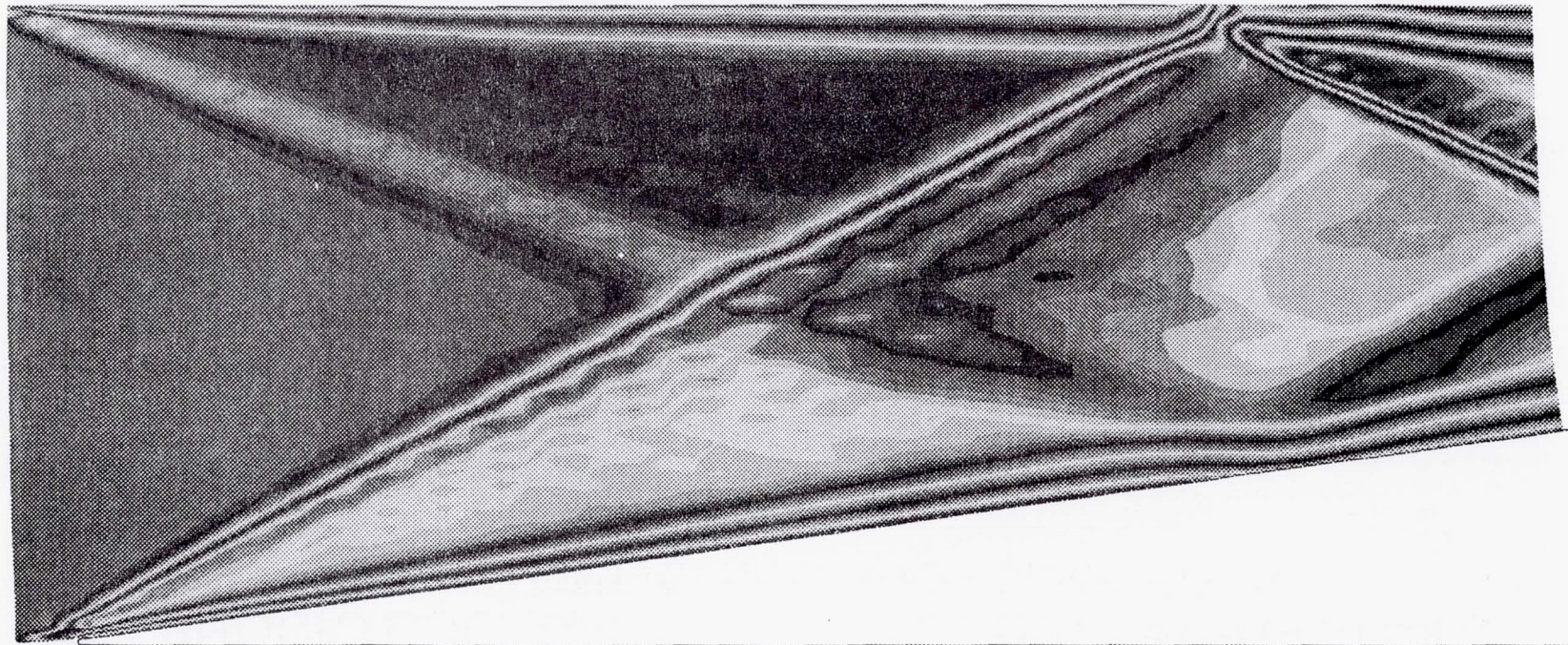
DENSITY GRADIENTS

SHOCK/BOUNDARY LAYER/BLEED INTERACTION
EXPERIMENT/COMPUTATION COMPARISON
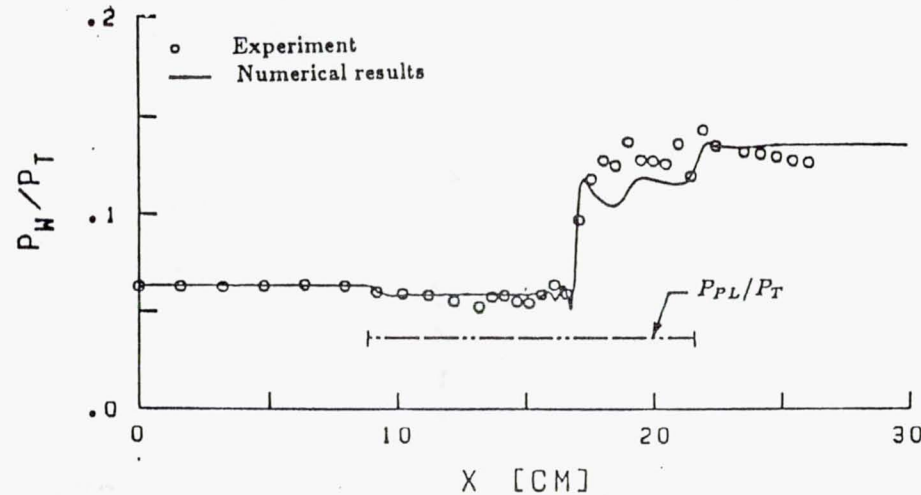
WALL PRESSURE DISTRIBUTION

M=2.46

Ang=6.5 deg
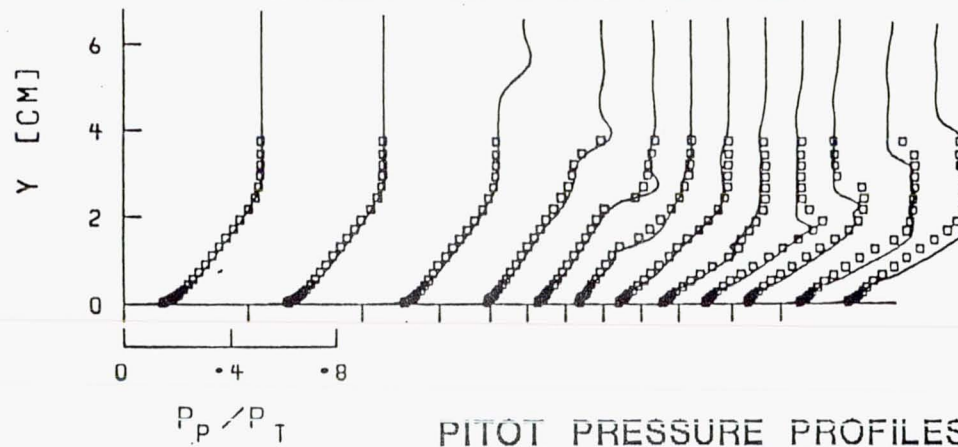
PITOT PRESSURE PROFILES

INTERNAL FLUID MECHANICS DIVISION

NASA
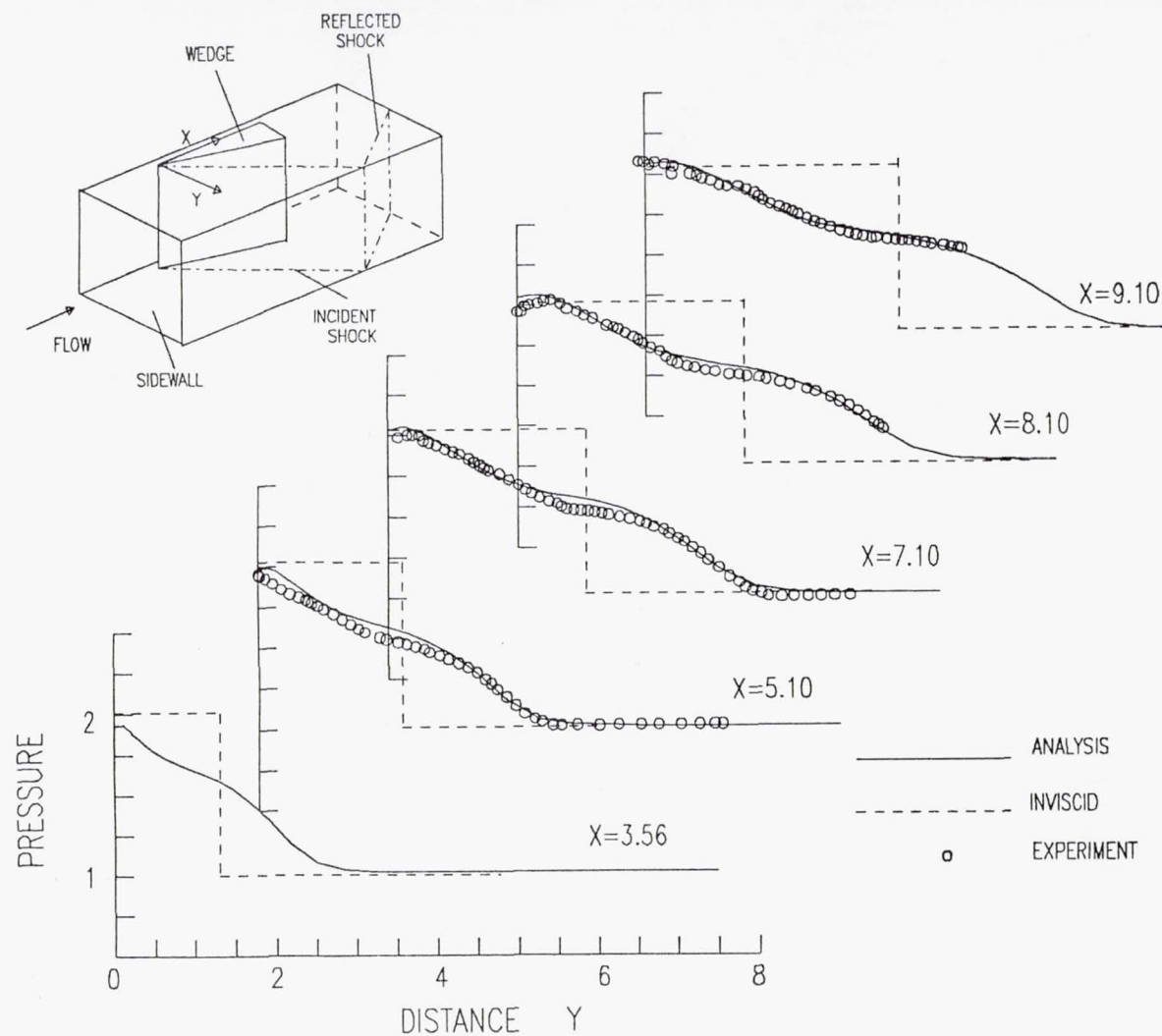
CFD FOR HIGH SPEED INLETS

MACH 5.0 INLET
STREAMLINE TRACES
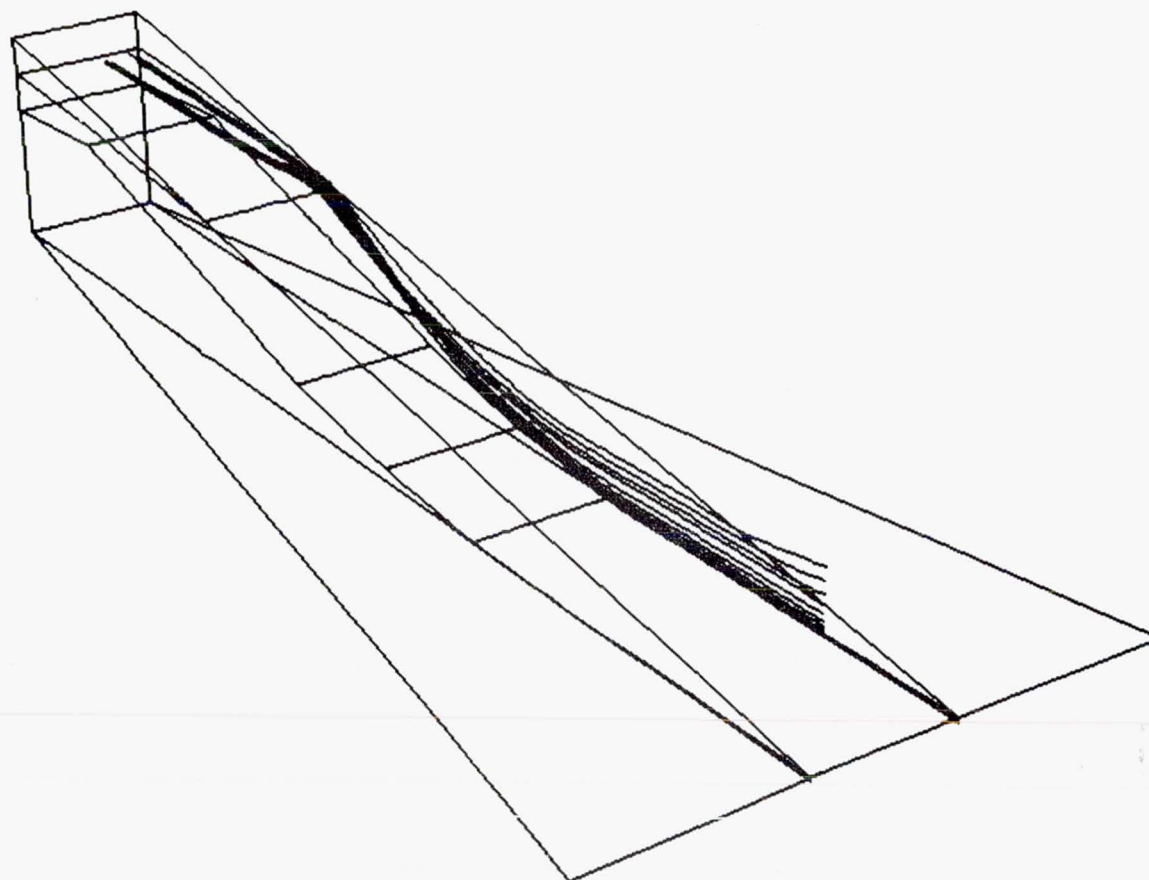
CFD FOR HIGH SPEED INLETS

SUMMARY

Combined computational/experimental investigation has identified importance of 3D shock/boundary layer interactions for rectangular inlets at high speeds

Possible control of glancing shock/boundary layer interaction through bleed now being explored. Little success to date.

Understanding of three dimensional interactions may lead to better methods of flow control in inlets.

N91-10889

THE USE OF A NAVIER-STOKES CODE IN THE WING DESIGN PROCESS

S. Naomi McMillin
NASA Langley Research Center
Hampton, Virginia 23665-5225

An ongoing investigation is being conducted in the Supersonic/Hypersonic
Aerodynamics Branch at NASA Langley Research Center to determine the
feasibility of incorporating the Navier-Stokes computational code, CFL3D, into
the supersonic wing design process. The approach taken in this investigation
is of two steps.

The first step was to calibrate CFL3D against existing experimental data
sets obtained on thin sharp-edged delta wings. The experimental data
identified six flow types which are dependent on the similarity parameters of
Mach number and angle of attack normal to the leading edge. The calibration
showed CFL3D capable of simulating these various separated and attached-flow
conditions.

The second step was to use CFL3D to study the initial formation of
leading-edge separation over delta wings at supersonic speeds. This study
consisted of examining solutions obtained on a 65° delta wing at Mach number
of 1.6 with varying cross-sectional shapes. Reynolds number was held constant
at 1000000 and the Baldwin-Lomax turbulence model was used. The study showed
that through the use of leading-edge radius and/or camber, the onset of
leading-edge separation can be delayed to a higher angle of attack than
observed on a flat sharp-edged wing.

Based on the geometries studied, three wind-tunnel models are being
designed to verify these results. These models are to be tested over a
Reynolds number range of 2×10^6/foot to 8.5×10^6/foot.

Fig. 1   The objective and approach for the present investigation.

Fig. 2   CFL3D code characteristics.

Fig. 3   Sketches of the wind-tunnel models tested by Miller and Wood in the Langley Unitary Plan Wind Tunnel (NASA TP-2430).

Fig. 4   The types of flow classified from the Miller and Wood experimental test (NASA TP-2430).

Fig. 5   The computational test matrix at $M = 2.8$ superimposed on the chart which defines the flow types as functions of α and M normal to the leading edge.

Fig. 6   A comparison of computational results with experimental data for the 75° delta wing at $\alpha = 8^\circ$ and $M = 2.80$ (AIAA 87-2270).

Fig. 7   The major elements of the incipient separation study (second step of approach).

Fig. 8   Computational results which quantify the effects of leading-edge radius at $\alpha = 4^\circ$.

Fig. 9   Computational results which quantify the effects of leading-edge radius at $\alpha = 8^\circ$.

Fig. 10   Computational results which quantify the effects of camber at $\alpha = 8^\circ$.

Fig. 11   A summary on the effects of leading-edge radius and camber on a 65° delta wing at $M = 1.6$.

Fig. 12   Major element of proposed wind-tunnel test.

Fig. 13   Concluding remarks.

OBJECTIVE

- To determine the feasibility of incorporating
the Navier - Stokes computational code,
CFL3D, into the supersonic wing design process.

APPROACH

- Calibrate CFL3D with experimental data
obtained on flat sharp-edged delta wings
at supersonic speeds (AIAA 87-2270).
Parameters:

    - leading edge sweep
    - angle of attack
    - Mach number

- Use CFL3D to study the initial formation of
leading edge separation on delta wings.
Geometric parameters:

    - leading edge radius
    - camber

CFL3D CODE CHARACTERISTICS

- Developed at NASA-LaRC by Jim Thomas

- Unsteady conservation-law form of compressible Navier-Stokes equations (thin layer laminar viscous model)

- Laminar viscous model or Baldwin-Lomax eddy viscosity turbulence model

- Upwind-biased spacial differencing implemented in finite volume form

  - Upwind (flux split) for convective terms and pressure
  - Central for shear stress/heat transfer
  - 2nd order accurate

- Implicit time differencing

  - Streamwise relaxation/cross-flow ADI
  - 1st order accurate

- Conical solutions obtained by 3-D solution

  - Single array of conically constructed volumes
  - Inflow equal outflow

- Grids generated using an elliptic grid generation method, 121 x 93 grid required to resolve details of flow patterns

LEE-SIDE FLOW FLAT DELTA MODELS
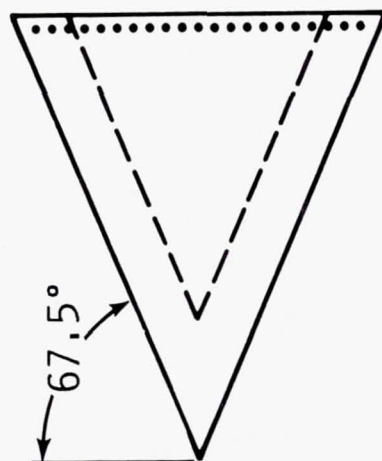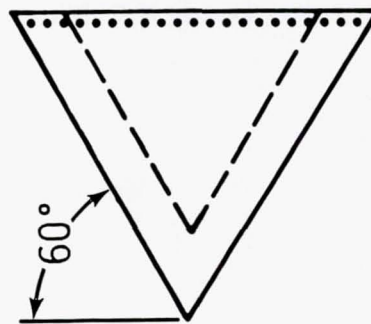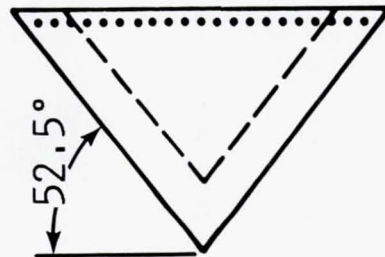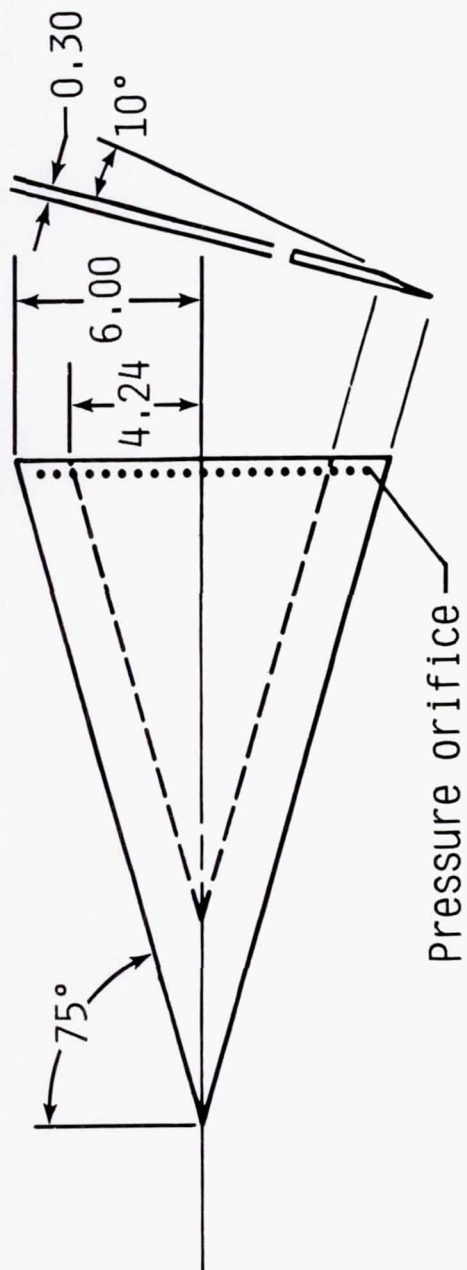
FLOW CLASSIFICATIONS

CLASSICAL VORTEX

SHOCK-INDUCED
SEPARATION
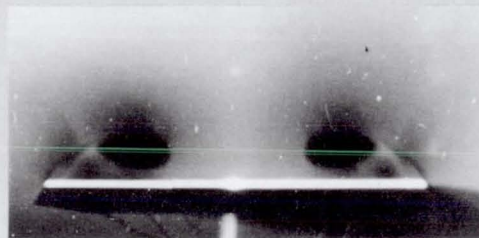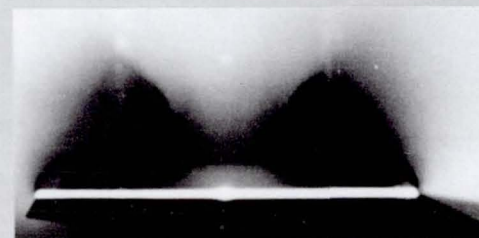
NO SHOCK/NO SEPARATION

VORTEX WITH SHOCK
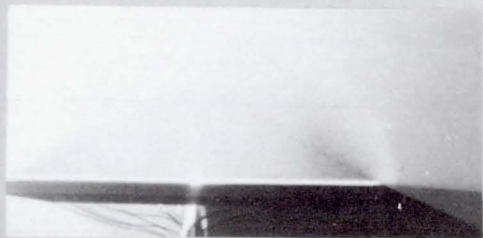
SHOCK WITH NO
SEPARATION
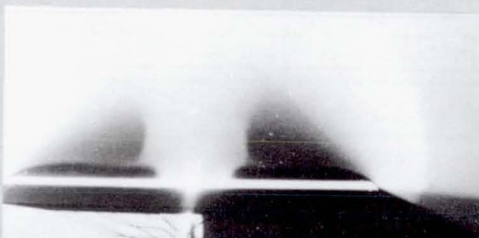
SEPARATION BUBBLE
WITH NO SHOCK

SEPARATION BUBBLE
WITH SHOCK

THEORETICAL TEST MATRIX
M = 2.8
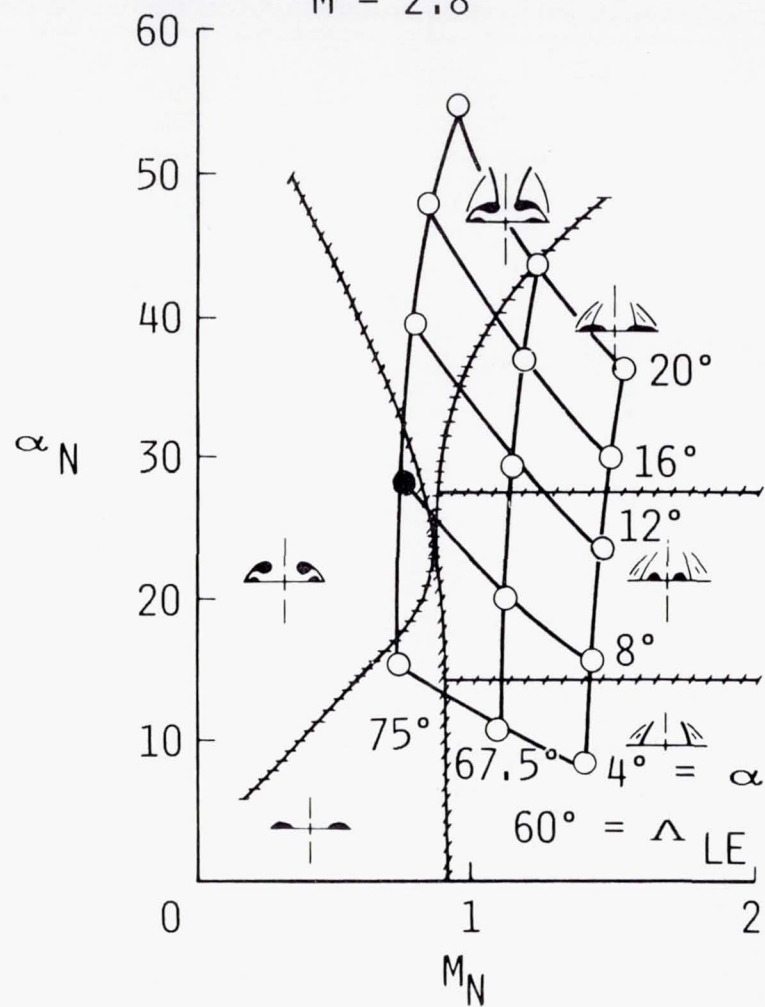
PRECEDING PAGE BLANK NOT FILMED

INCIPIENT SEPARATION STUDY

Attached flow

α_N

Stanbrook-Squire boundary

Separated flow $\longleftarrow$

$\alpha = 2°$

M_N
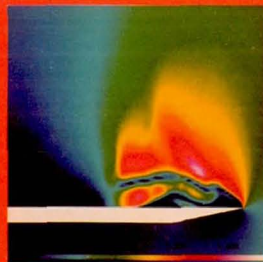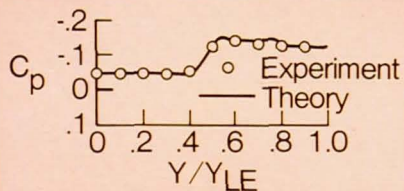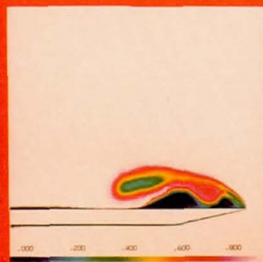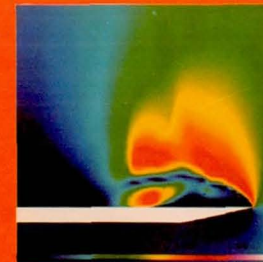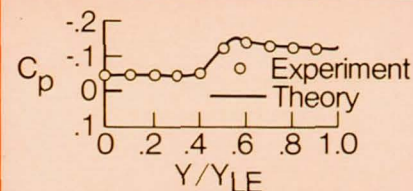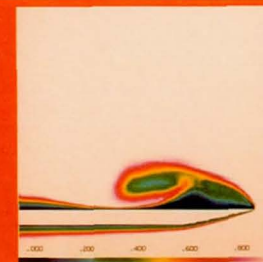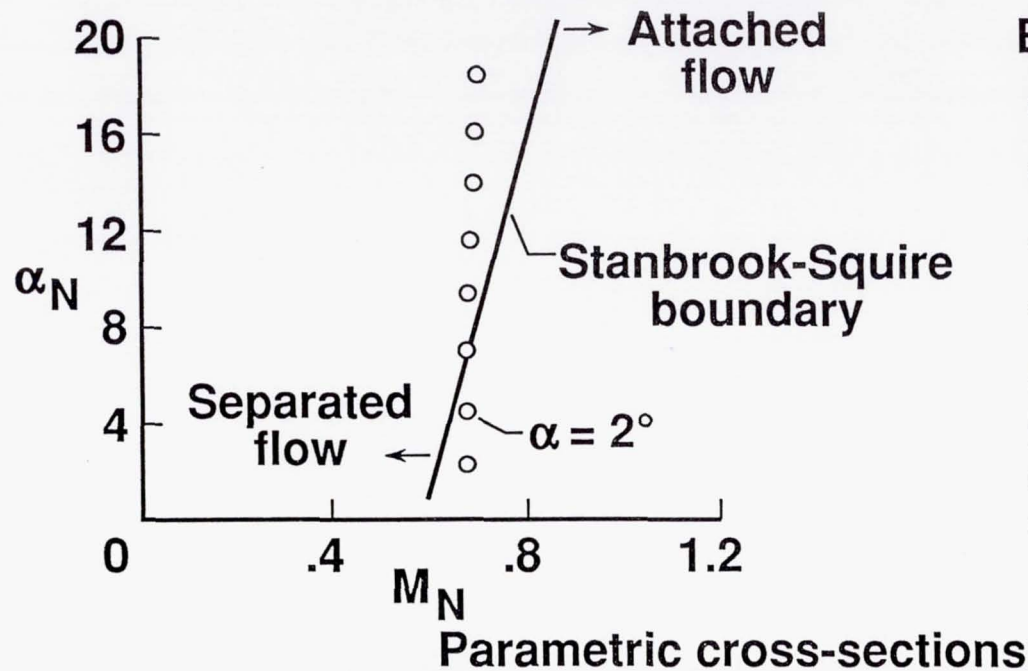
Examine effects of
- Leading edge radius
- Camber
- Angle of attack
- Reynolds number

On the formation of leading edge separation on a conical 65° delta wing at M = 1.6

Parametric cross-sections

Leading edge radius:
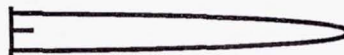
| Sharp | r/(b/2) = 0.0025 (20:1 ellipse) | r/(b/2) = 0.0100 |
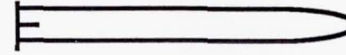
Camber (20:1 ellipse)
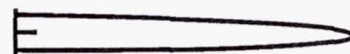
| 4° camber | 8° camber | 10° camber |
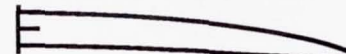
EFFECT OF LEADING EDGE RADIUS

$\alpha = 4°$

M = 1.6 $\Lambda = 65°$ Re = 1 000 000
Turbulent boundary layer

Sharp

$\frac{r}{b/2} = 0.0025$
(20:1 ellipse)

$\frac{r}{b/2} = 0.01$

Total pressure:
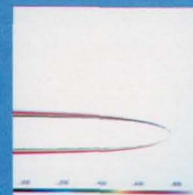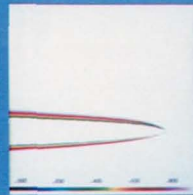
Crossflow Mach number:
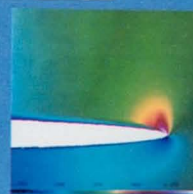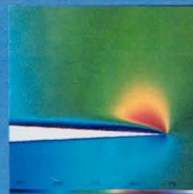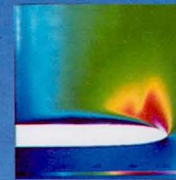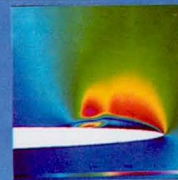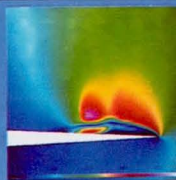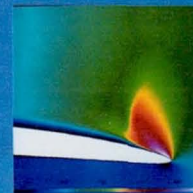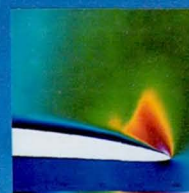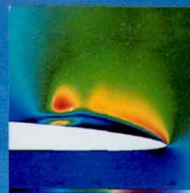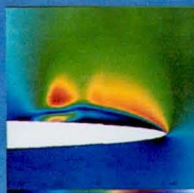
Surface pressure:
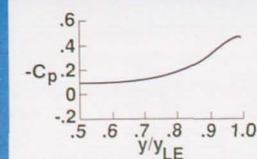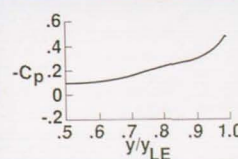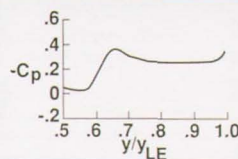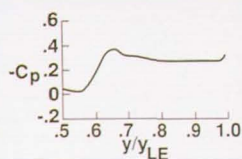
EFFECT OF LEADING EDGE RADIUS

$\alpha = 8°$

$M = 1.6 \quad \Lambda = 65° \quad Re = 1\ 000\ 000$
Turbulent boundary layer

EFFECT OF CAMBER

$\alpha = 8°$
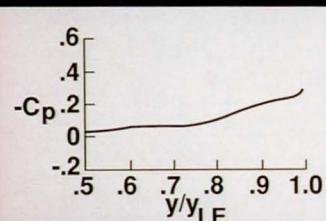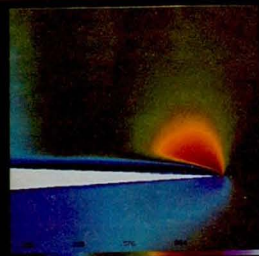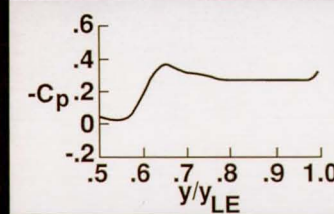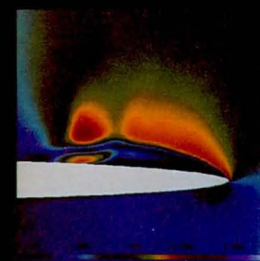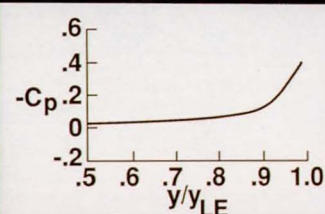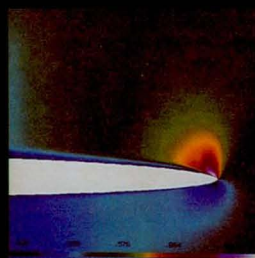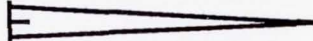
$M = 1.6$ $\Lambda = 65°$ $Re = 1\ 000\ 000$
Turbulent boundary layer
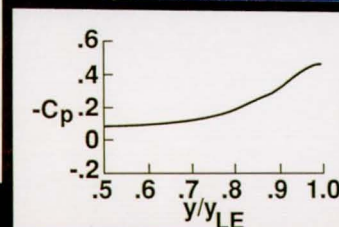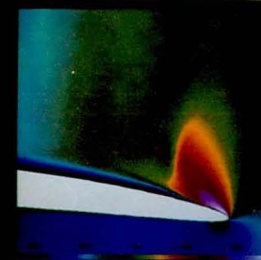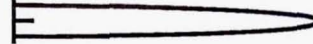
WIND TUNNEL MODELS
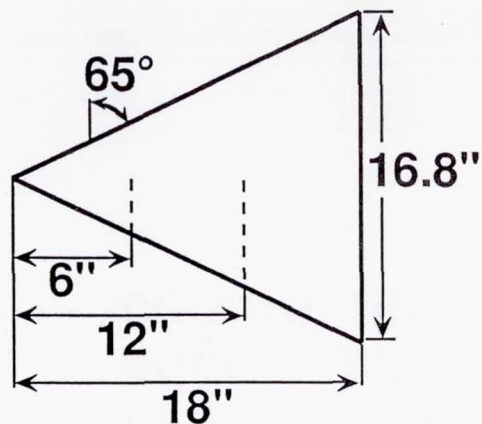
Cross-sections:

Sharp

20:1 ellipse

20:1 ellipse
with 10° camber

(Diagram labels: 65°, 16.8", 6", 12", 18")

Wind Tunnel Test Description

- M = 1.6; α = 0° to 8° (initial conditions)
- Surface pressure data (~100 ports)
- Vapor screen photographs
- Oil flows
- Unitary Plan Wind Tunnel
  $Re = 2 \times 10^6$ /foot, 5×10^6 /foot
- 20" Supersonic Wind Tunnel
  $Re = 2 \times 10^6$ /foot, 8.5×10^6 /foot

CLOSING REMARKS

- The six distinct flow types observed over delta wings at supersonic speeds have been computationally reproduced using CFL3D (AIAA 87-2270)

- CFL3D has been used to quantify the effects of leading edge radius and camber on leading edge separation. Wind tunnel test designed to confirm these results.

342

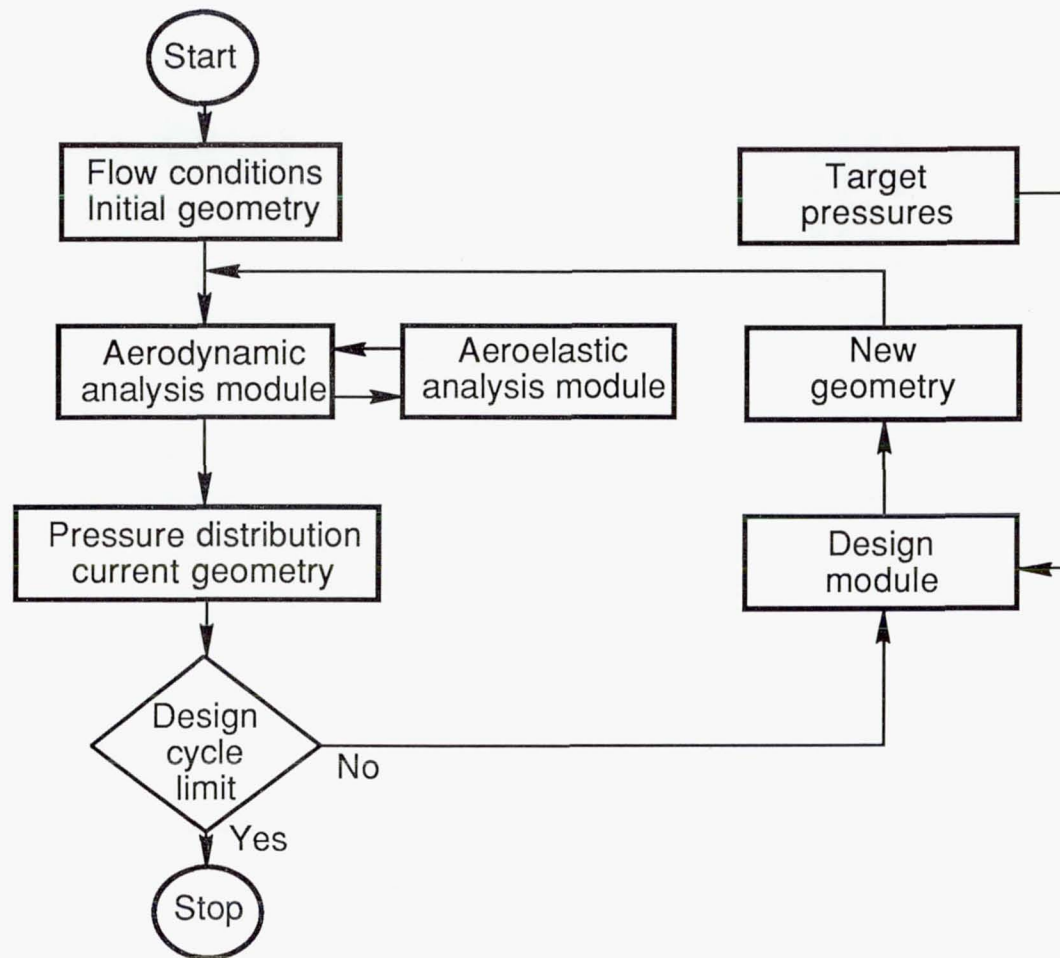# APPLICATIONS OF A TRANSONIC WING DESIGN METHOD

by

Richard L. Campbell and Leigh A. Smith
NASA Langley Research Center

ABSTRACT

The development of transonic computational fluid dynamic methods over the last fifteen years has had a tremendous impact on the design of airfoils and wings. A variety of approaches to automated design have been developed, such as the hodograph and fictitious gas methods for shock-free design, and inverse, numerical optimization, and predictor/corrector methods for the more general cases. Each of these techniques has advantages as well as limitations, and the designer must choose the one that best suits his specific task.

A method for designing wings and airfoils at transonic speeds using a predictor/corrector approach has been developed. The procedure iterates between an aerodynamic code, which predicts the flow about a given geometry, and the design module, which compares the calculated and target pressure distributions and modifies the geometry using an algorithm that relates differences in pressure to a change in surface curvature. The modular nature of the design method makes it relatively simple to couple it to any analysis method. The iterative approach allows the design process and aerodynamic analysis to converge in parallel, significantly reducing the time required to reach a final design. Viscous and static aeroelastic effects can also be accounted for during the design or as a post-design correction.

Results from several pilot design codes indicated that the method accurately reproduced pressure distributions as well as the coordinates of a given airfoil or wing by modifying an initial contour. The codes were applied to supercritical as well as conventional airfoils, forward- and aft-swept transport wings, and moderate-to-highly swept fighter wings. The design method was found to be robust and efficient, even for cases having fairly strong shocks. Comments from a user in industry indicated that for a specific design problem, this design method was about 25 times faster than a numerical optimization approach that utilized the same aerodynamic analysis code.

```
                    ┌─────────┐
                    │  Start  │
                    └────┬────┘
                         │
                         ▼
              ┌─────────────────────┐          ┌──────────────┐
              │  Flow conditions    │          │    Target    │
              │  Initial geometry   │          │   pressures  │
              └──────────┬──────────┘          └──────────────┘
                         │◄──────────────────────────────┐
                         ▼
              ┌─────────────────┐    ┌──────────────────┐   ┌──────────────┐
              │   Aerodynamic   │◄───│    Aeroelastic   │   │     New      │
              │ analysis module │───►│  analysis module │   │   geometry   │
              └────────┬────────┘    └──────────────────┘   └──────┬───────┘
                       │                                           ▲
                       ▼                                           │
              ┌─────────────────────┐              ┌──────────────────┐
              │Pressure distribution│              │      Design      │
              │  current geometry   │              │      module      │
              └──────────┬──────────┘              └──────────┬───────┘
                         │                                    ▲
                         ▼                                    │
                      ╱─────╲                                 │
                     ╱ Design ╲          No                   │
                    ◄  cycle   ►──────────────────────────────┘
                     ╲ limit  ╱
                      ╲─────╱
                         │ Yes
                         ▼
                    ┌─────────┐
                    │  Stop   │
                    └─────────┘
```

HYBRID DESIGN ALGORITHM

- Subsonic regions

$$\Delta C = \Delta C_P \; A \, (1 + C^2)^B$$

- Supersonic regions   (M > 1.15)

$$\Delta C = \frac{0.05 \, A}{(1 + (y')^2)^{1.5}} \; \frac{d}{dx} \, (\Delta C_P)$$

SUPERCRITICAL AIRFOIL DESIGN
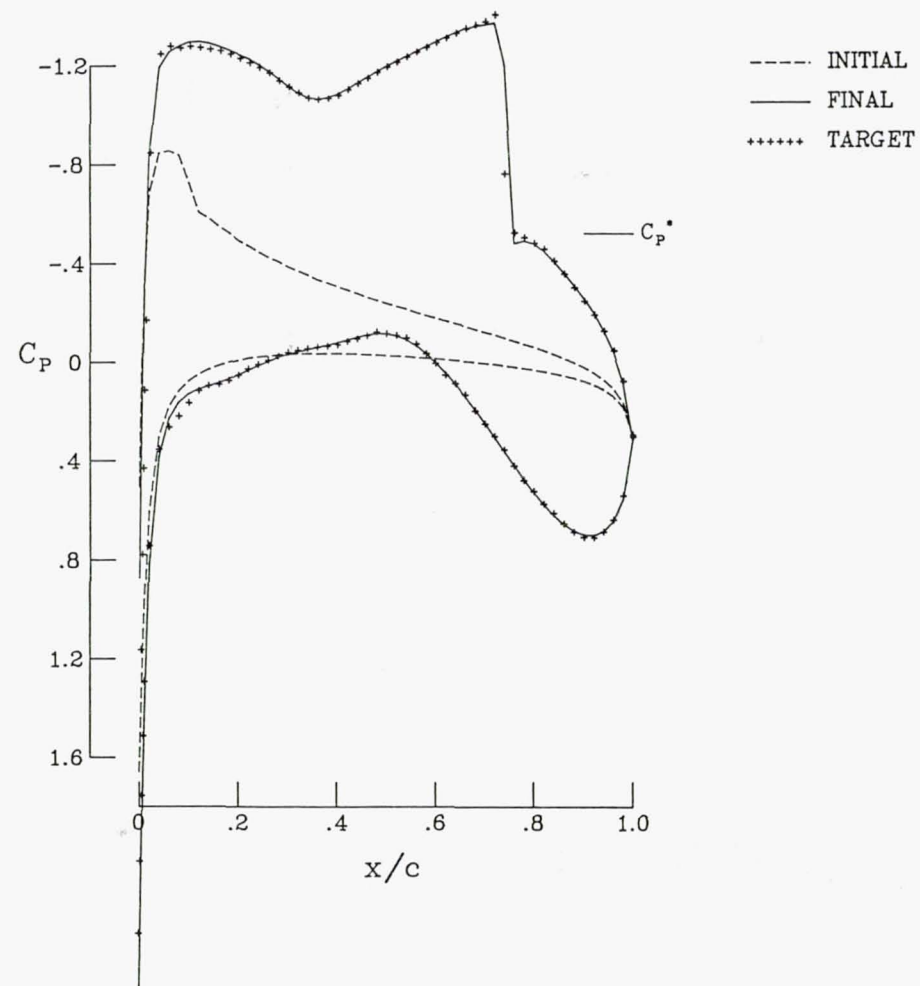
SUPERCRITICAL AIRFOIL DESIGN
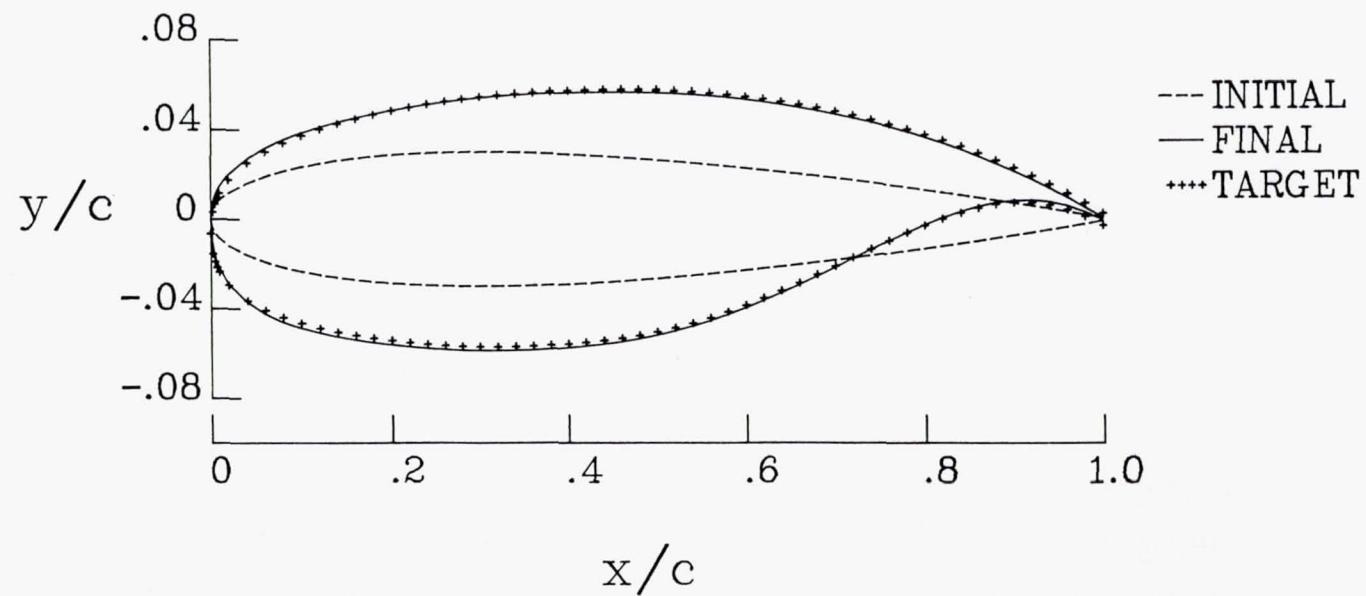
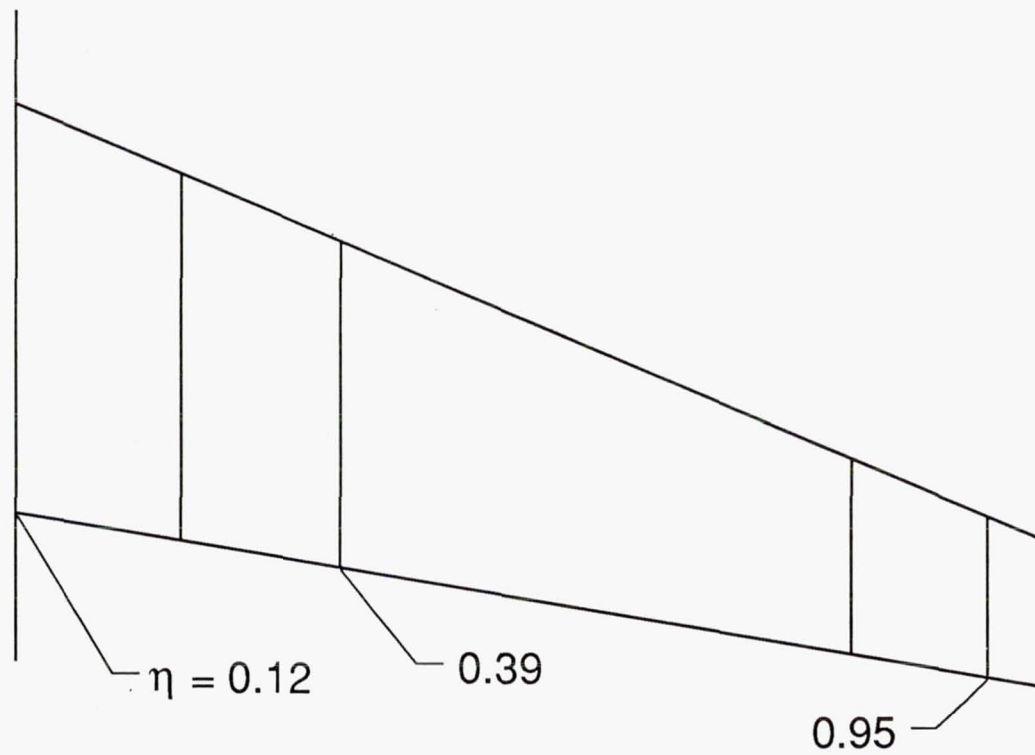# NYU CODE- PARTIAL AIRFOIL MODIFICATION
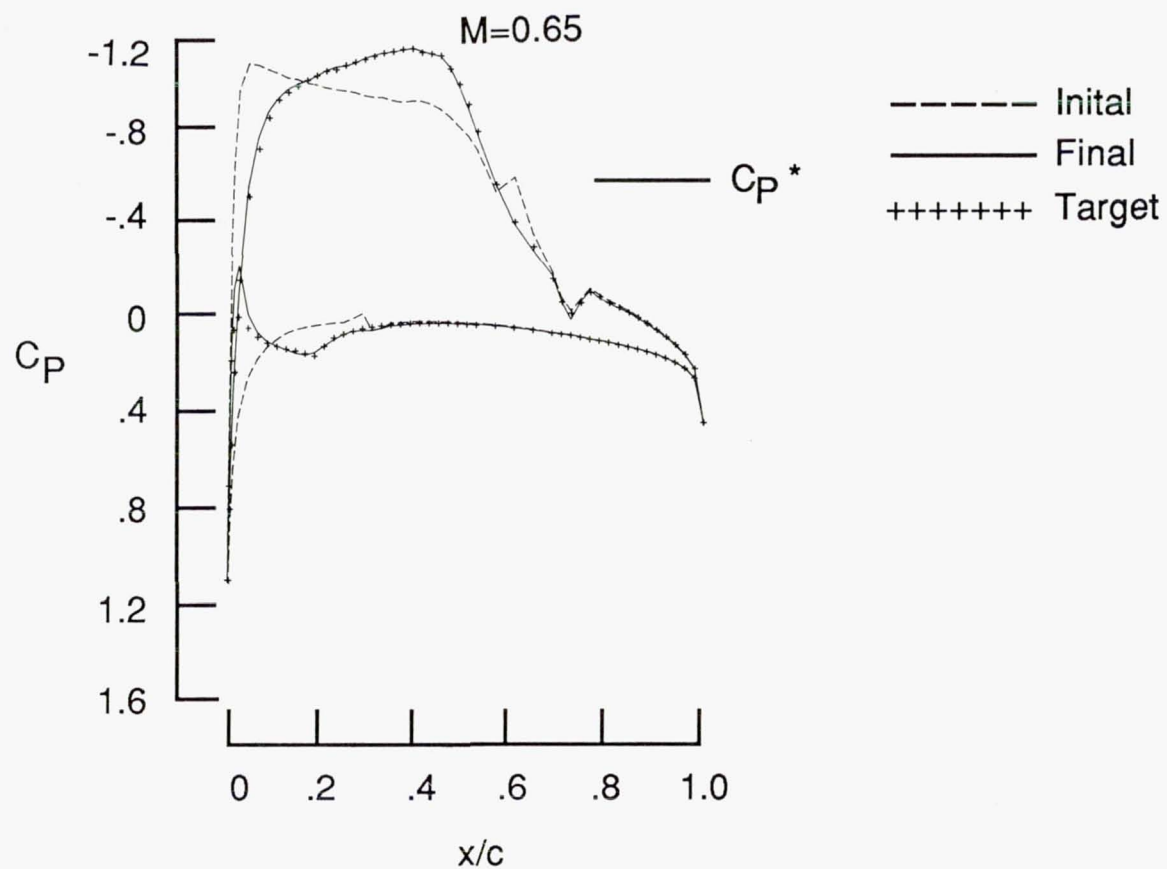
NYU CODE- PARTIAL AIRFOIL MODIFICATION

EXECUTIVE JET DESIGN

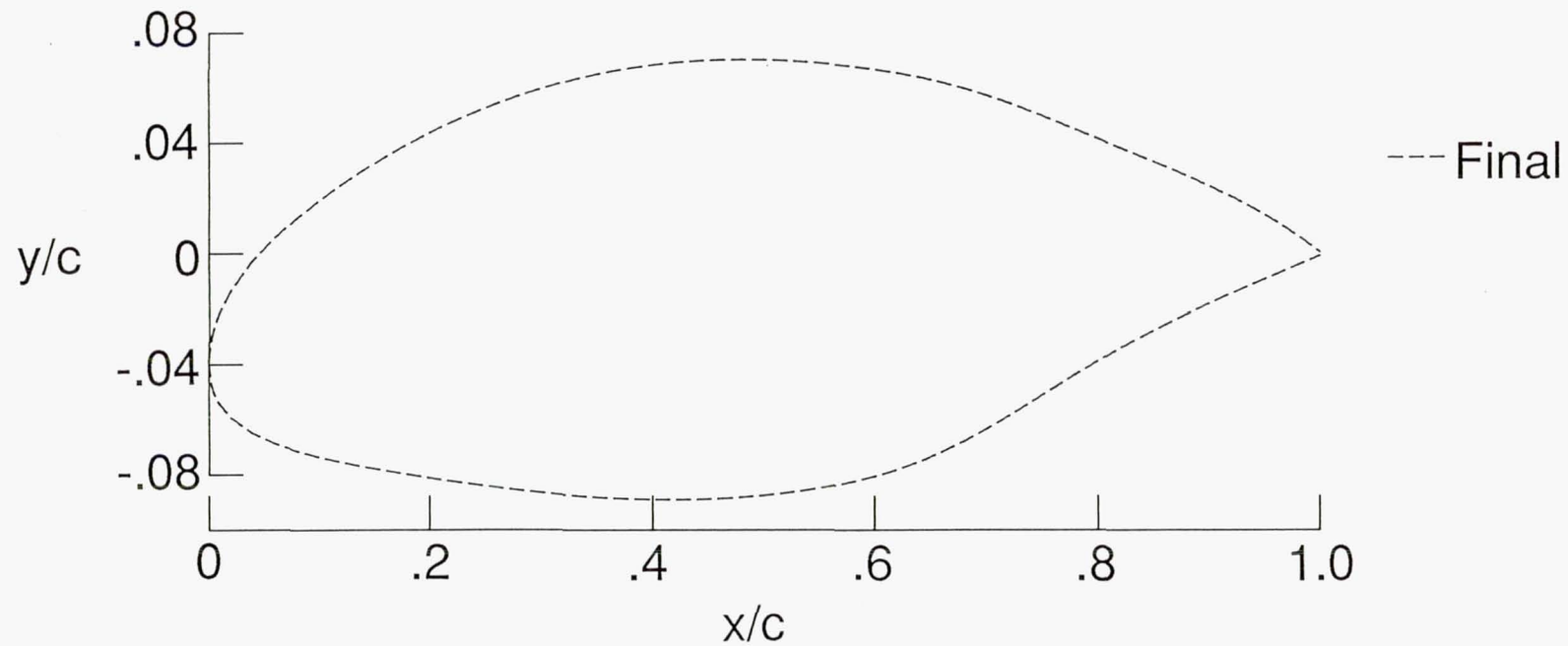$\eta = 0.12$ 0.39

0.95
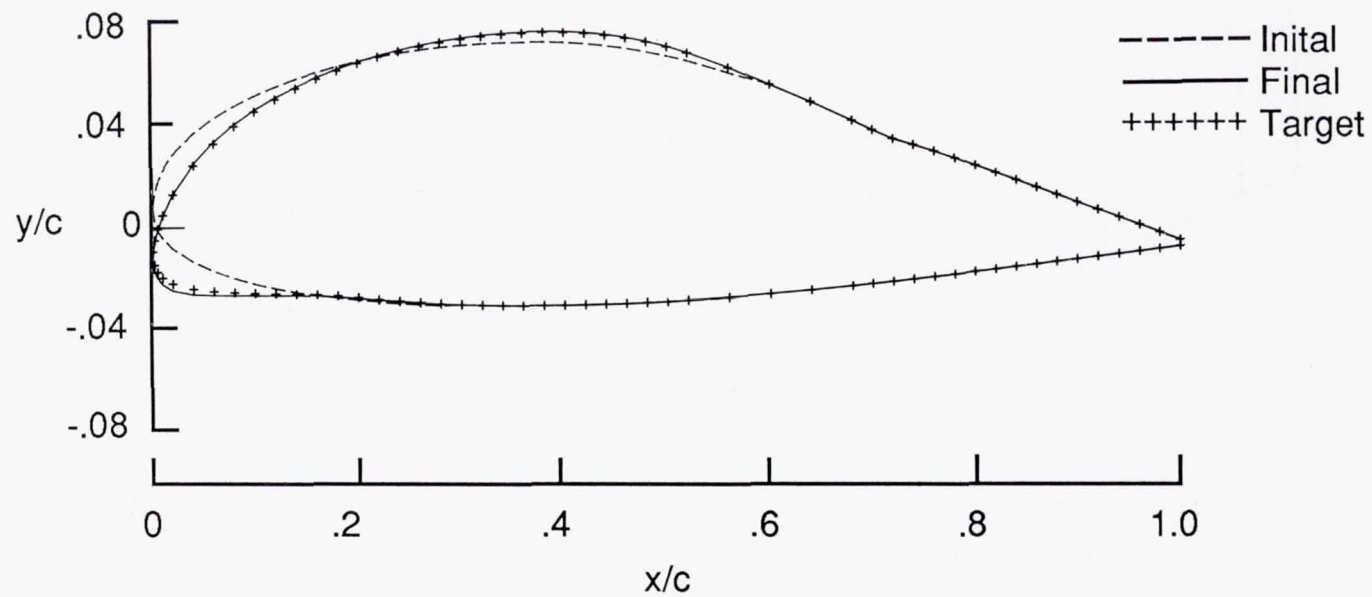
EXECUTIVE JET DESIGN

M = 0.78

η = .12
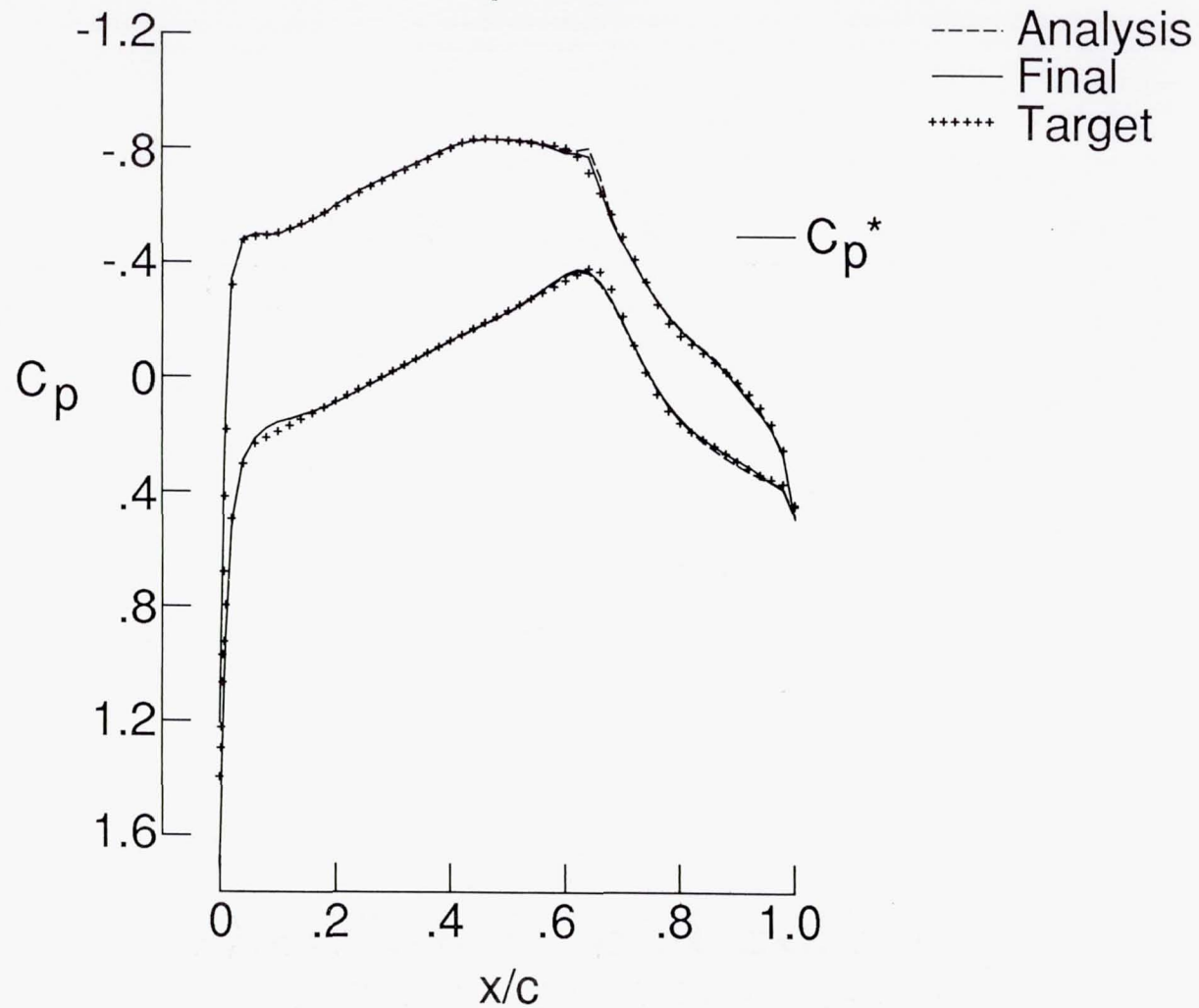
EXECUTIVE JET DESIGN
M = 0.78
η = .12

HIGHLY SWEPT FIGHTER WING GEOMETRY

HIGHLY-SWEPT FIGHTER WING CASE

M = 0.85

η = 0.77

C_P

C_P*

-1.2

-.8

-.4

0

.4

.8

1.2

1.6

0   .2   .4   .6   .8   1.0

x/c

----- Initial
—— Final
+++++ Target
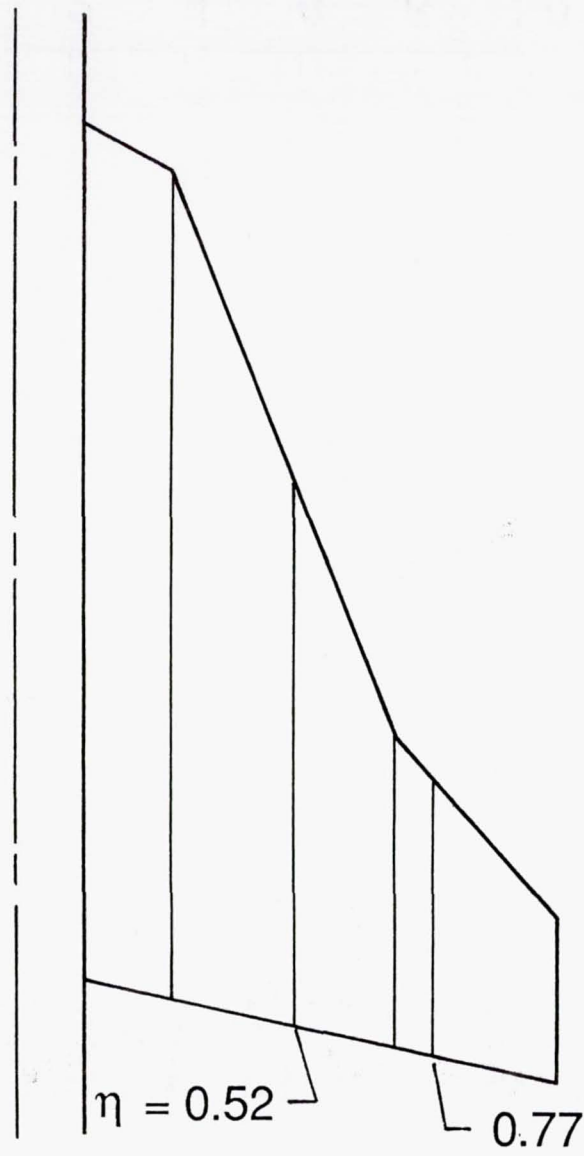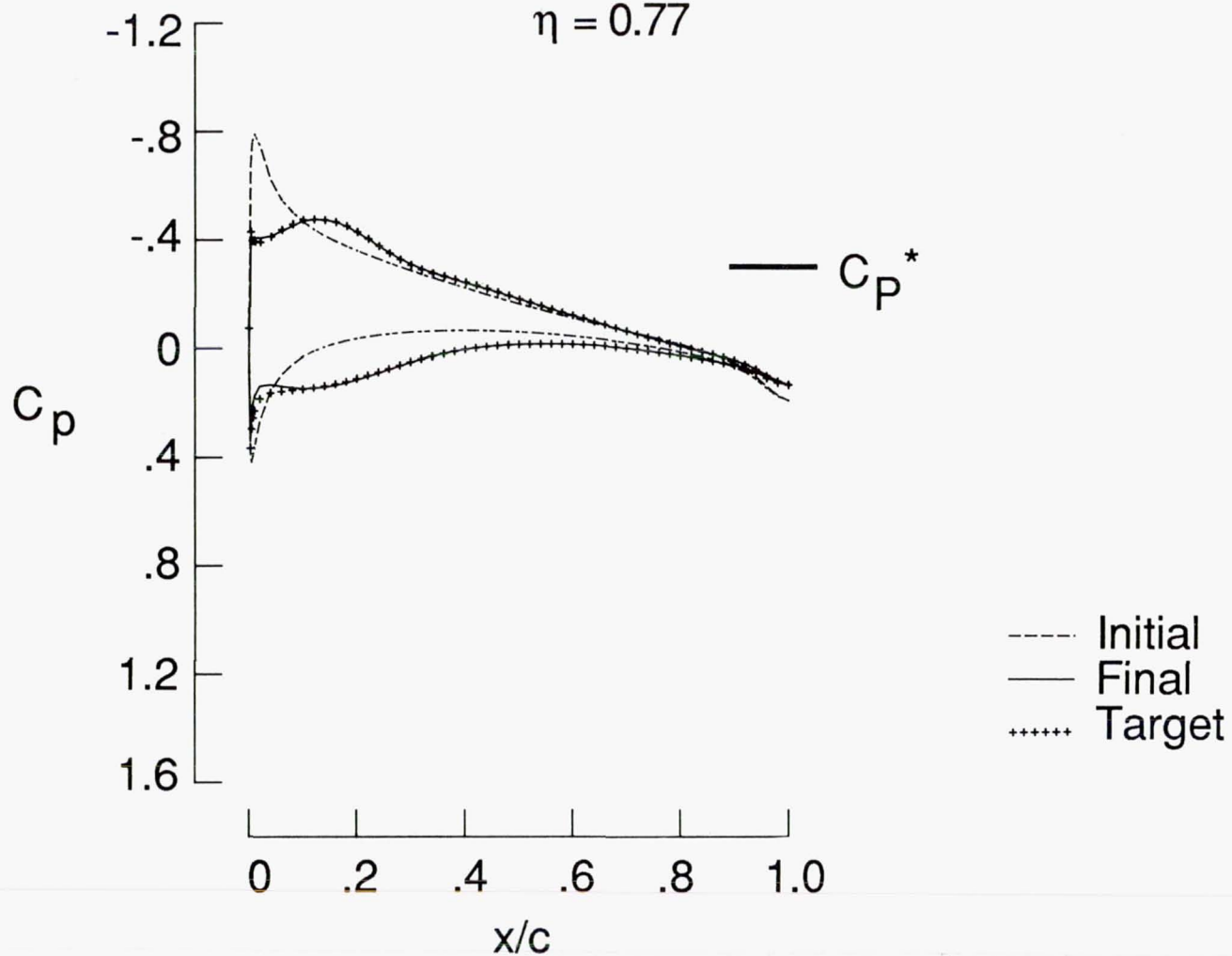
HIGHLY-SWEPT FIGHTER WING CASE

$M = 0.85$

$\eta = 0.52$
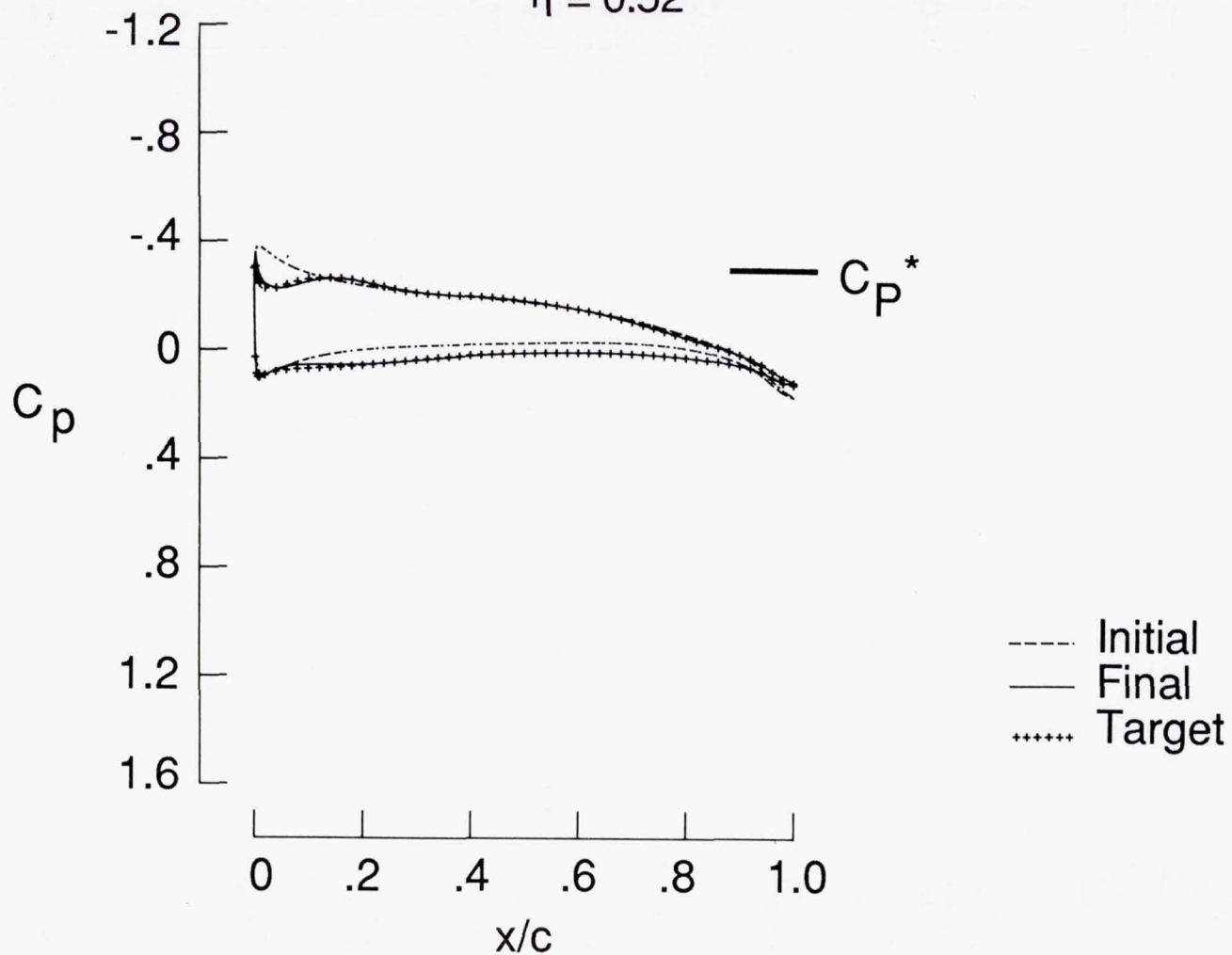
HIGHLY-SWEPT FIGHTER WING CASE

$\eta = 0.77$
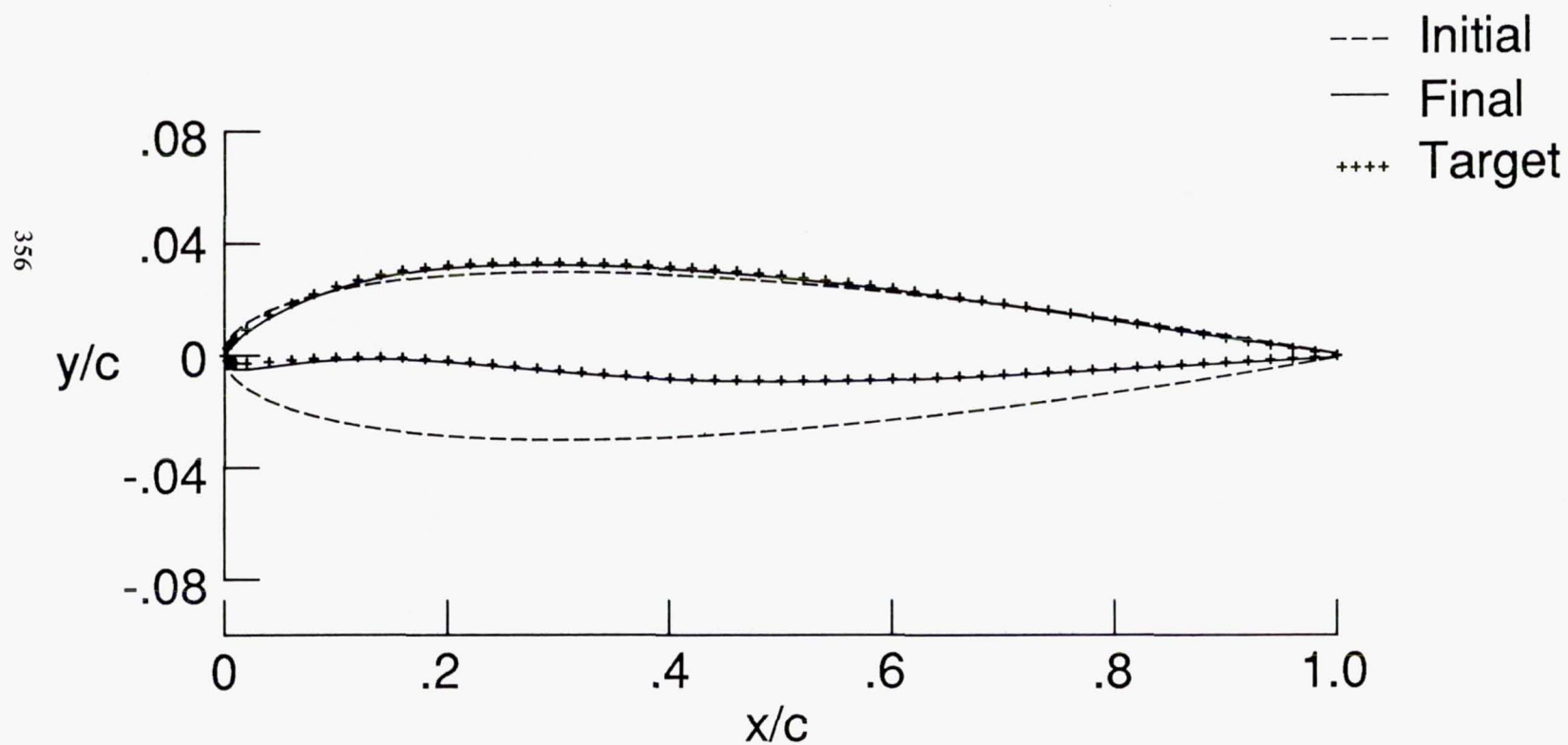
HIGHLY-SWEPT FIGHTER WING CASE

$\eta = 0.52$

- - - Initial
— Final
++++ Target
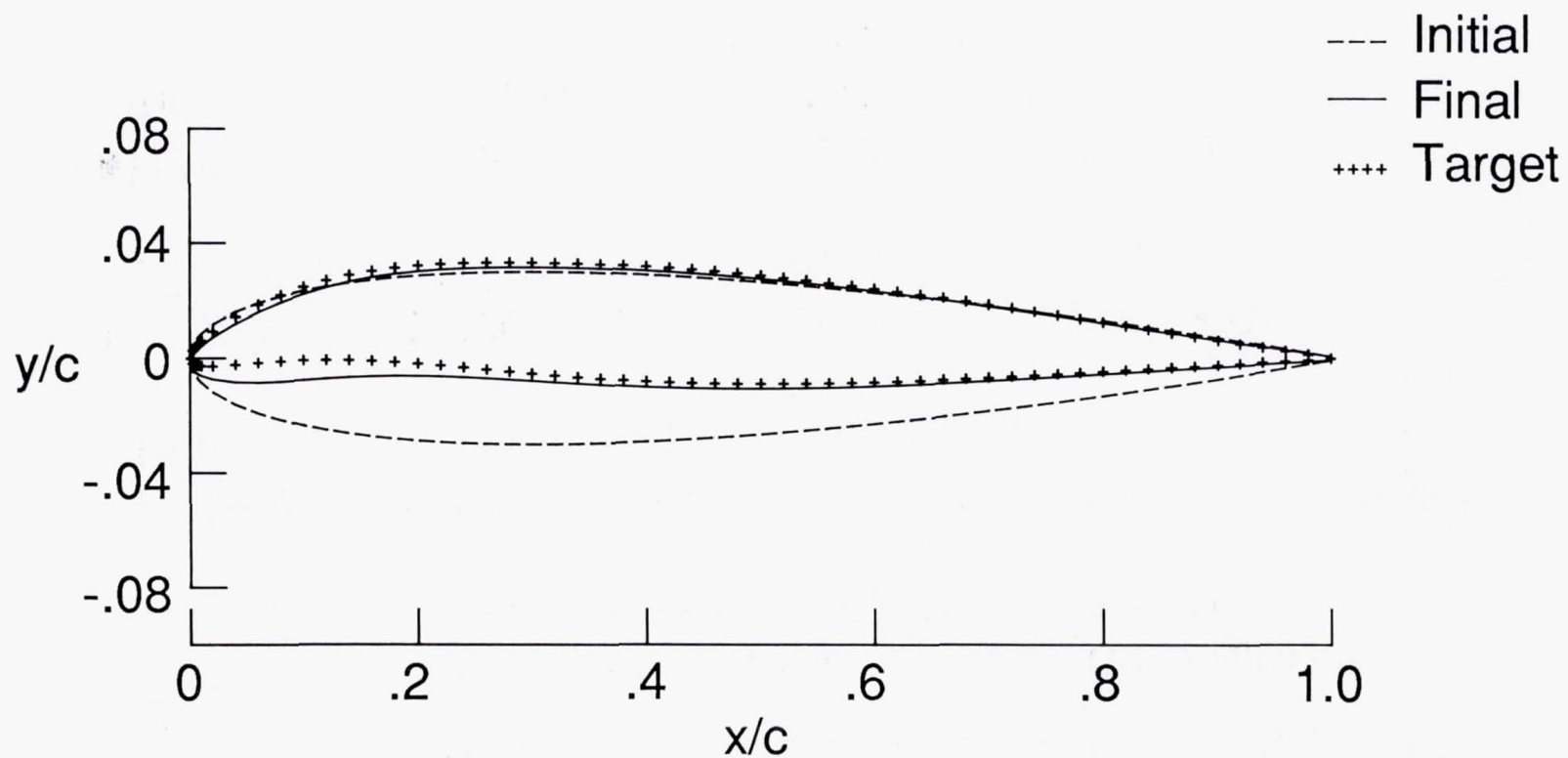
CONCLUDING REMARKS

- A predictor/corrector method for designing airfoils and wings at transonic speeds has been developed

- Hybrid algorithm used in strongly supercritical regions to improve convergence of design process

- Predictor/corrector approach allows geometry constraints to be easily included

- Results from airfoil and wing design pilot codes indicate that the method is robust, efficient, and accurate for a wide variety of configurations

- Techniques for accounting for viscous and aeroelastic effects have been included

SESSION XI

ALGORITHMS AND TOOLS

Chairman:
Joseph L. Steger
Senior Staff Scientist
Fluid Dynamics Division
NASA Ames Research Center

361

An Embedded Grid Formulation
Applied to Delta Wings

James L. Thomas
NASA Langley Research Center, Hampton, Virginia
Sherrie L. Krist
Vigyan Research Associates, Inc., Hampton, Virginia

An embedded-grid algorithm for the Euler/Navier-Stokes equations is developed and applied to delta wings at high angles of attack in low-speed flow. The Navier-Stokes code is an implicit, finite-volume algorithm, using flux-difference-splitting for the convective and pressure terms and central differencing for the viscous and heat transfer terms. Calculations are compared with detailed experimental results over an angle of attack range up to and beyond the maximum lift coefficient, corresponding to vortex breakdown at the trailing edge, for a delta wing nominally of unit aspect ratio. The results indicate that the overall flowfield, including surface pressures, surface streamlines, and vortex trajectories, can be simulated accurately with the global grid version of the present algorithm. However, comparison of computed velocities and vorticity with experimentally measured off-body values at an angle of attack of 20.5 degree indicates the core region is substantially more diffuse in the computations than that measured with either a five-hole probe or a laser velocimeter.

Embedded grids, used in the present work to improve the numerical discretization in the core region, are formulated within the framework of the implicit, upwind-biased multi-grid algorithm. Structured levels of local nested refinements are made. The refinements, which should be based on the local truncation error of the solution, are currently based on the location of the vortex core trajectory. The embedded grid boundary data are determined through linear interpolation of the coarser underlying grid. The values of flow variables in the coarser grid cells underlying finer grids are determined by a volume-weighted restriction of the finer grid values. To compensate for the limited extent of the implicit operators in the embedded grids, each level of grid refinement uses corrections from coarser grids, which can be either embedded or global grids, to accelerate the convergence to the steady state of the embedded blocks.

Three-dimensional results for both Euler and Navier-Stokes calculations are shown, with up to 3 levels of embedded refinement. The embedding procedure was effective in eliminating a crossflow secondary separation produced in the Euler solutions on coarse grids. The core velocities in the Euler solutions are substantially higher than in the viscous solutions and in both, the embedded grids can efficiently reduce the numerical diffusion in the flowfield. The computed core velocities in the viscous calculations are increased on the embedded grids but are lower than the measured values with the grids used in the present study.

LIST OF CHARTS

Chart 1. Introduction.

Chart 2. Outline of presentation.

Chart 3. Global grid algorithm.

Chart 4. Comparisons with experiments.

Chart 5. Secondary and tertiary separation lines.

Chart 6. AR=1 delta wing, Cl vs. alpha plot.

Chart 7. Embedded grid scheme.

Chart 8. Embedded grid scheme with V-cycle.

Chart 9. Crossflow embedded grids.

Chart 10. Particle traces.

Chart 11. Euler solution for 76 degree delta wing; U-velocity.

Chart 12. Grid refinement effect plot.

Chart 13. 3-D Navier-Stokes results.

Chart 14. Streamwise U-velocity contours.

Chart 15. Concluding remarks.

INTRODUCTION

Motivation :

Performance and stability of aircraft at high angles of attack
are dominated by the nonlinear interaction of shed vortices

Present objective :

Compare predictions of Navier-Stokes code with detailed
experimental data for delta wings with both global and
embedded grid schemes
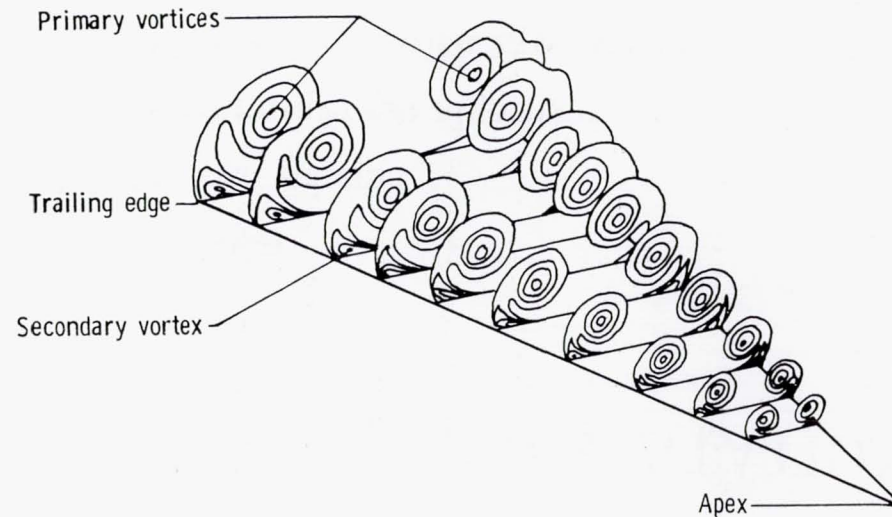
OUTLINE OF PRESENTATION

- Introduction
- Global grid scheme
    - Computational algorithm
    - Comparisons with experiment
- Embedded grid scheme
    - Spatial differencing
    - Time advancement
- Computational results
    - Euler
    - Navier-Stokes
- Concluding remarks

GLOBAL GRID ALGORITHM

Upwind-biased Navier-Stokes code CFL3D

$$\frac{\partial \widehat{Q}}{\partial t} + \frac{\partial \widehat{F}}{\partial \xi} + \frac{\partial \widehat{G}}{\partial \eta} + \frac{\partial (\widehat{H} - \widehat{H}_v)}{\partial \zeta} = 0$$
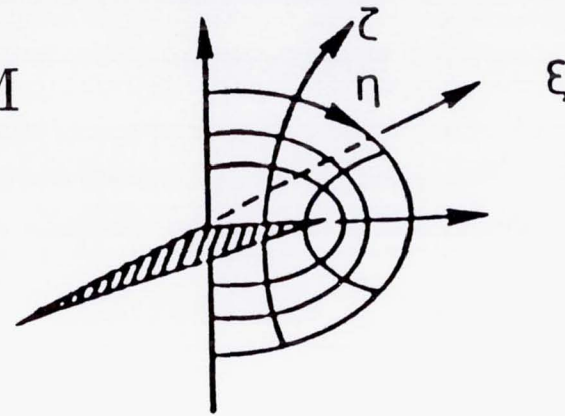
- Time-dependent conservation law form of compressible Navier-Stokes equations
- Implicit (diagonalized) time advancement algorithm
- Upwind-biased spatial differencing
  - Flux difference splitting for convective/pressure terms
  - Central differencing for shear stress/heat transfer terms
- Thin-layer with algebraic turbulence model
- Semi-discrete finite-volume implementation
- Zonal (patched) grids

COMPARISONS WITH EXPERIMENTS

Delta wings at high alpha in low speed flow

- Hummel (DFVLR) AR=1 wing

  - $R_L = 0.95 \times 10^6$

  - Force and moment

  - Surface oil flows

- Kjelgaard and Sellers (BART) $\Lambda = 75°$wing

  - $R_L = 0.5 - 1.5 \times 10^6$

  - Surface oil flows

  - Flowfield measurements (5-hole probe / LDV)

SECONDARY AND TERTIARY SEPARATION LINES

Apex

Experiment

Computation

Semispan Location of Separation Lines

	Secondary	Tertiary
Computation	.69	.87
Experiment	.69	.88

Primary attachment line

Primary separation line

Secondary attachment line

Secondary separation line

Tertiary attachment line

Tertiary separation line

Trailing edge
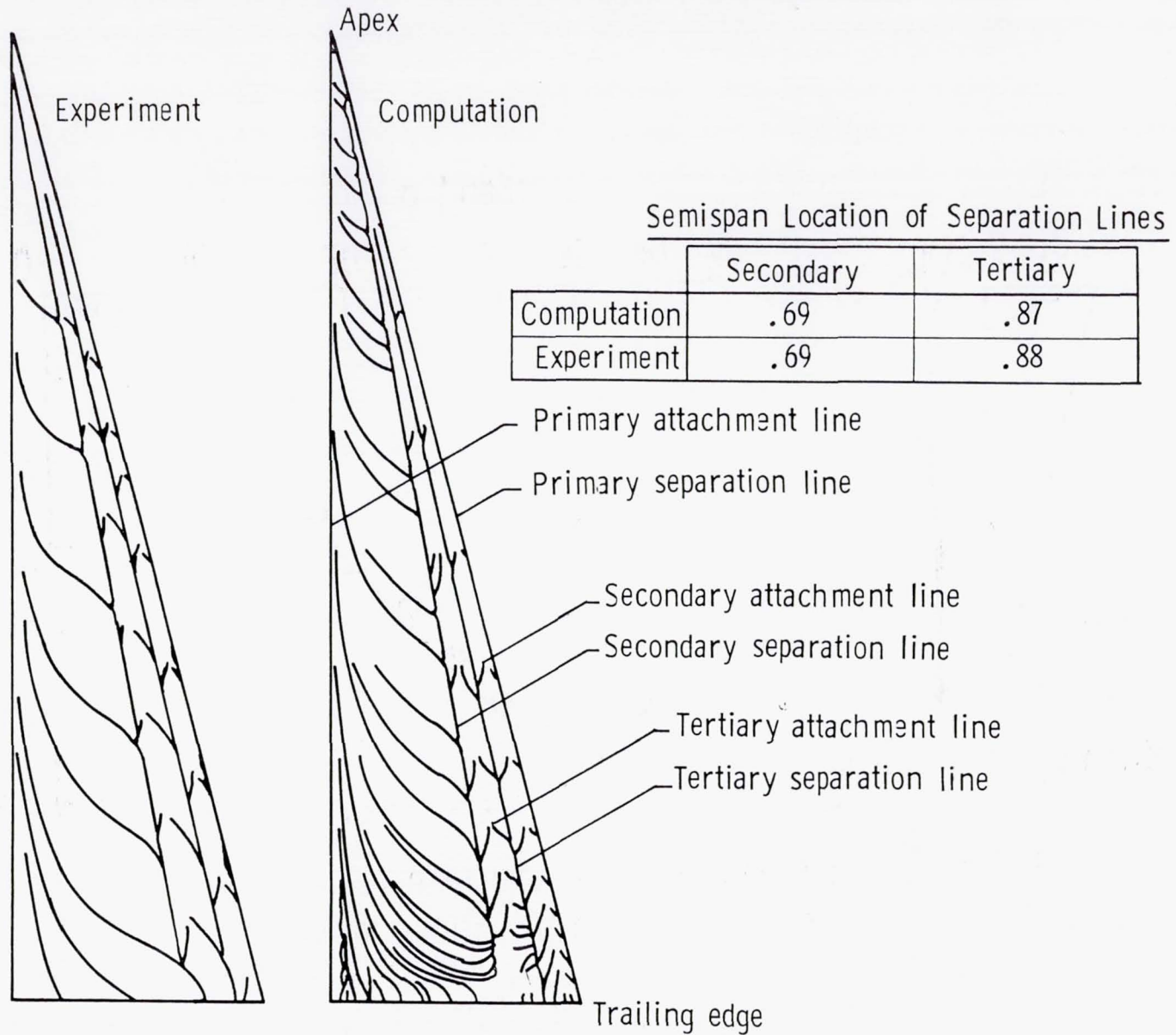
AR = 1   DELTA WING

$$Re_L = 0.95 \times 10^6$$

○   Experiment (Hummel) $M_\infty = 0.1$

—   Thin-layer Navier-Stokes (CFL3D) $M_\infty = 0.3$

C_L

Hummel Delta wing

75.96°

AR=1

$\delta = 12°$

α , deg.
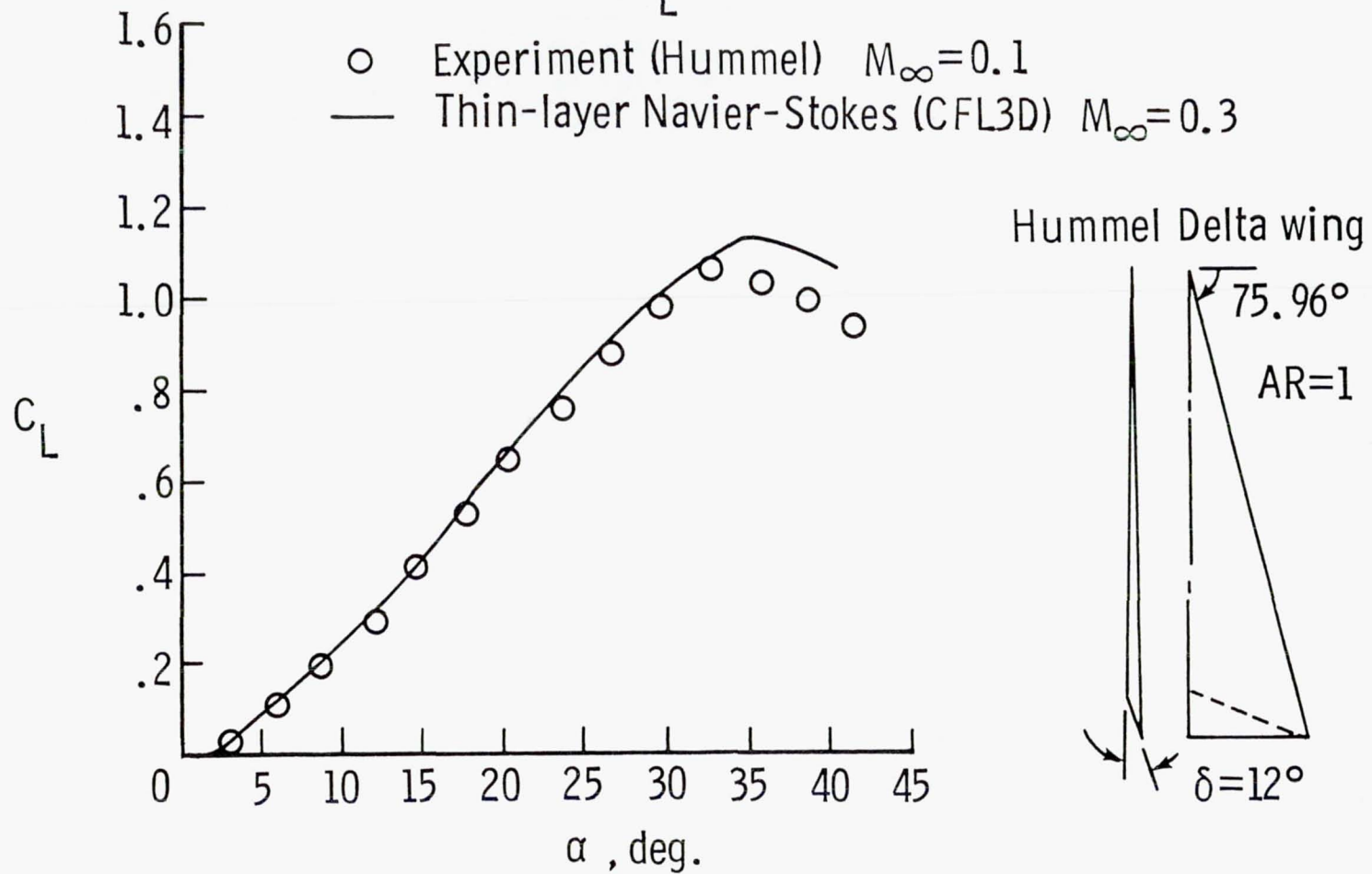
Embedded Grid Scheme
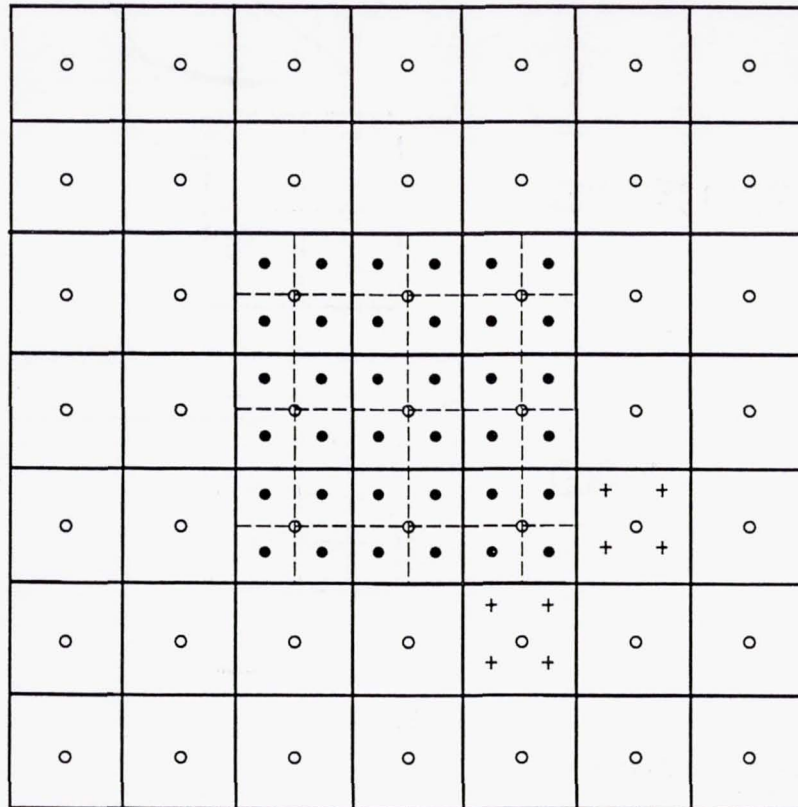
Coarse grid

Fine grid

- Volume-weighted restriction of finer grid to coarser grid cells

- Linear interpolation for projections of finer grid cells into coarse grid

Embedded Grid Scheme
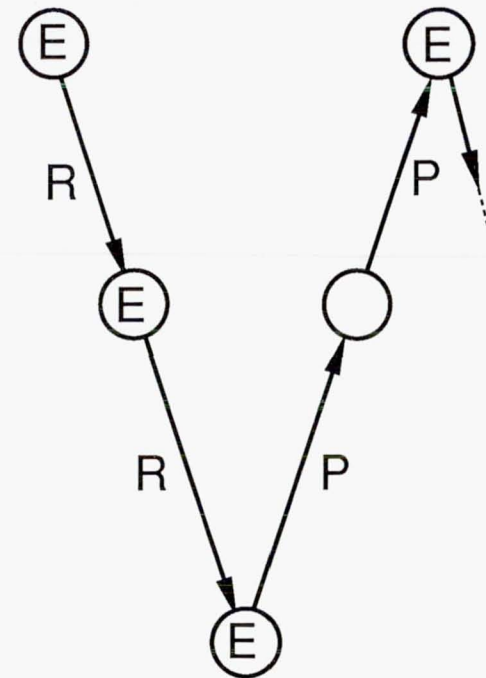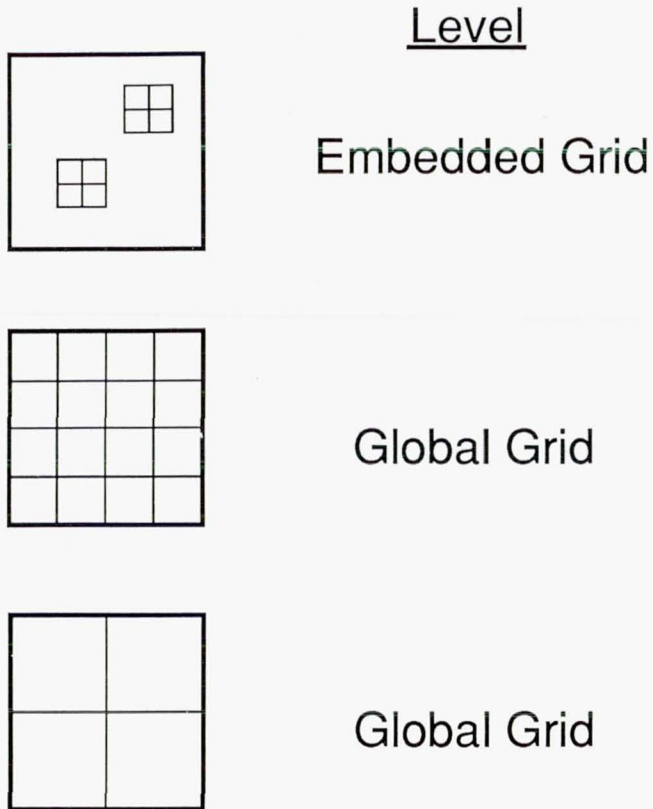
E: Navier-Stokes Calculation
R: Restriction of Residual and Q
P: Prolongation of Correction

CROSSFLOW EMBEDDED GRIDS

19×33×33	GRID 1
21×45×53	GRID 2
33×49×37	GRID 3
53×43×45	GRID 4

PARTICLE TRACES

33x33x19 Mesh
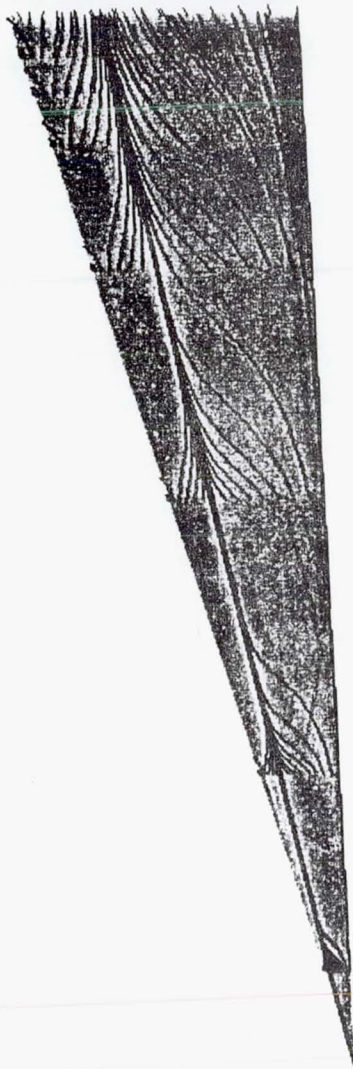
w/Grid Embedding
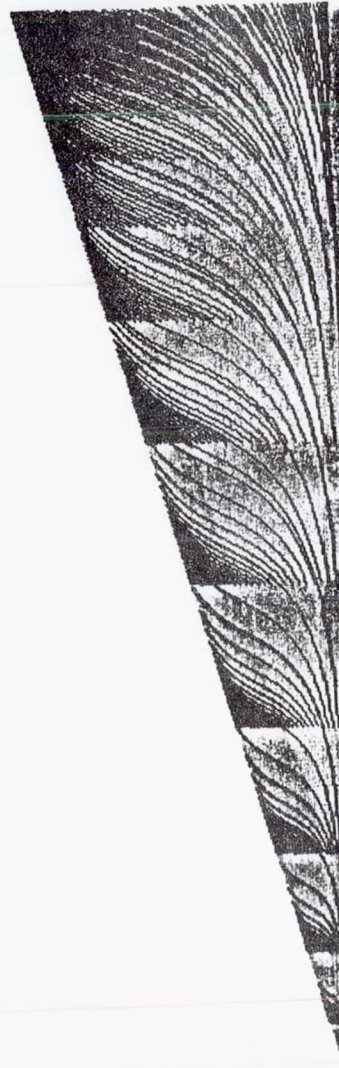
EULER SOLUTION FOR 76 DEGREE DELTA WING
u velocity component

$$\frac{u_{max}}{U_{inf}} = 2.5$$
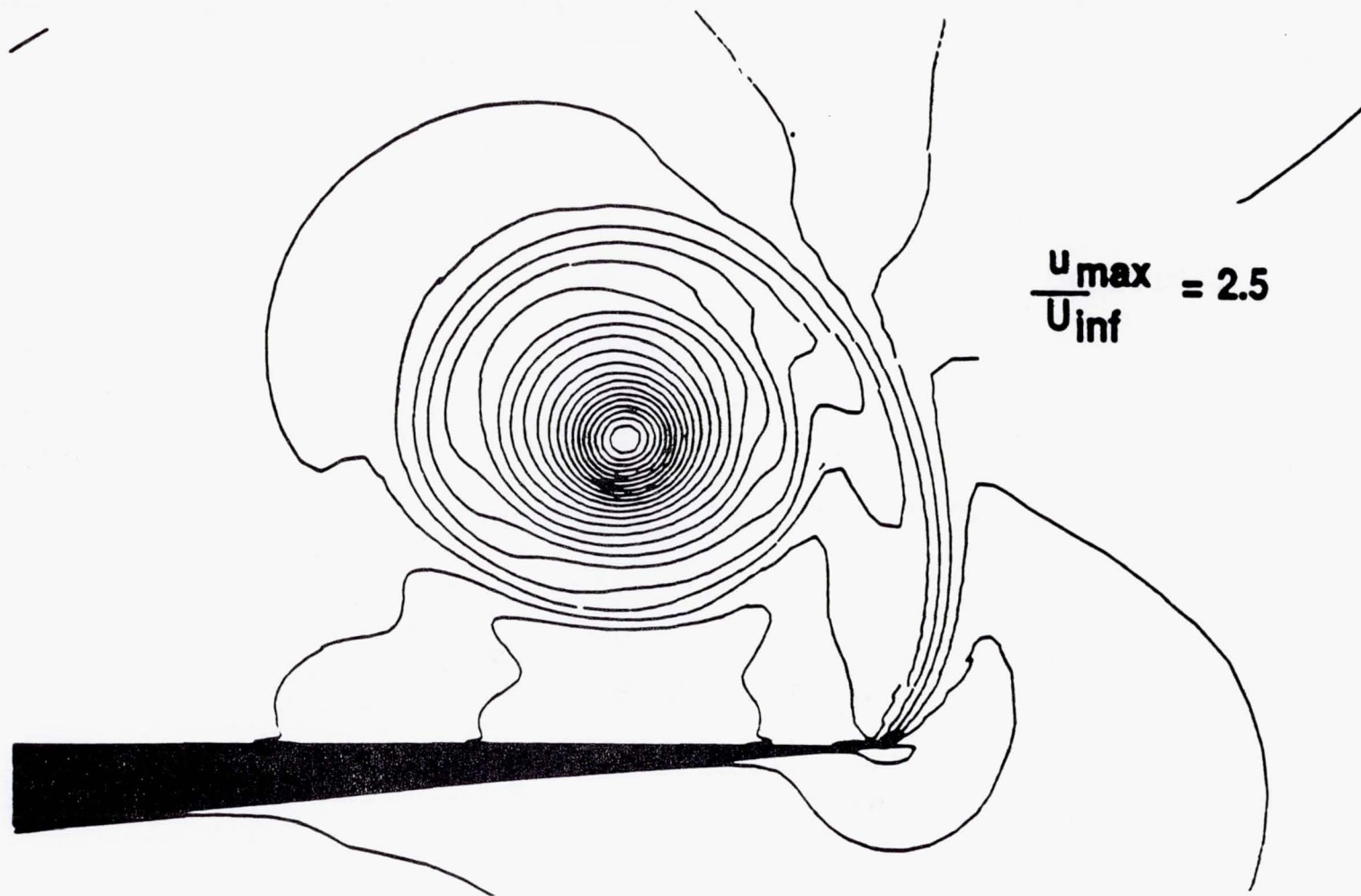
GRID REFINEMENT EFFECT
x/L = 0.7
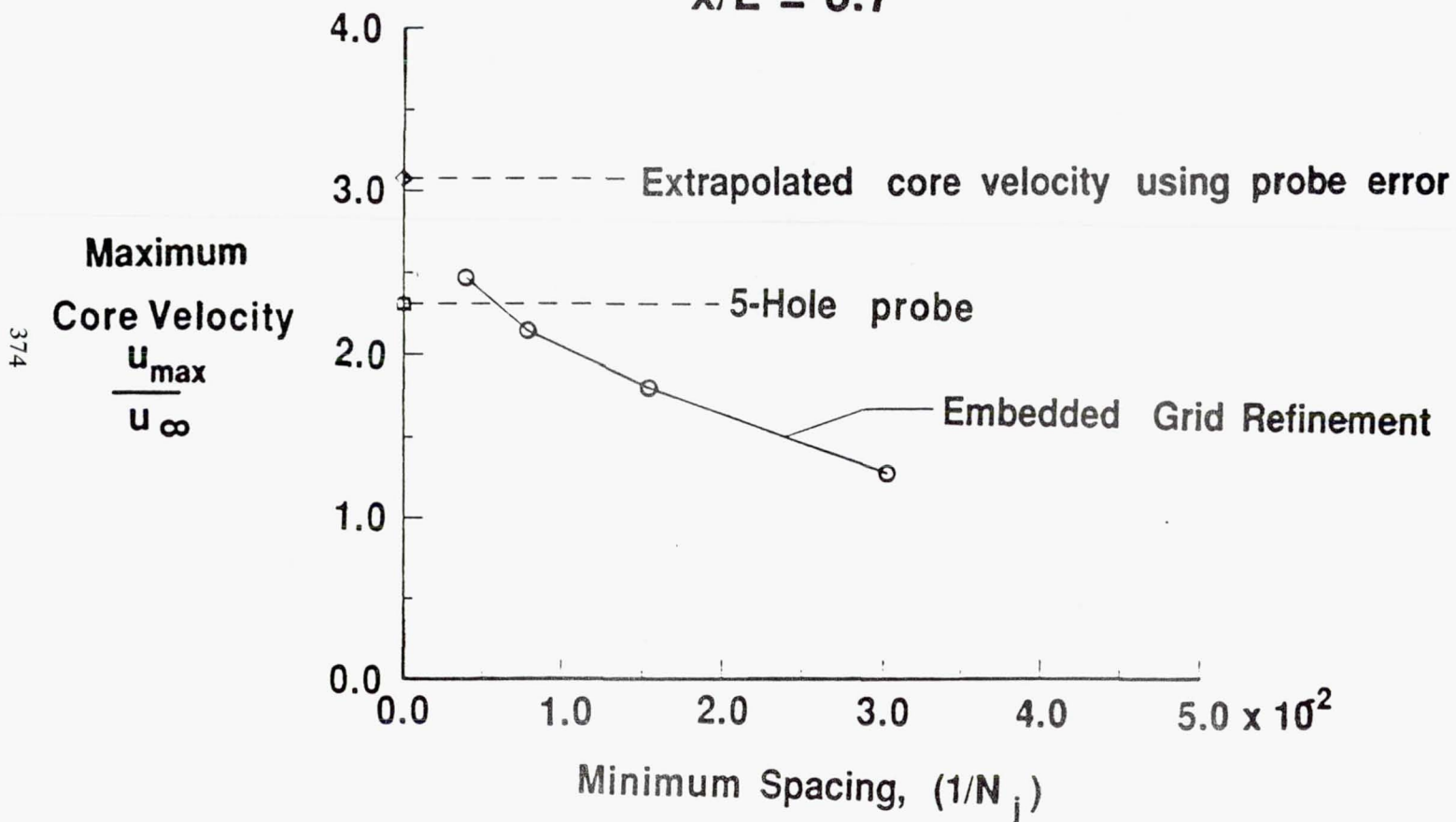
3-D NAVIER STOKES RESULTS

$\alpha = 20.5$ °; $\Lambda = 75$ °; $R_L = 0.5$ x 10^6

Mesh	Grid points	u_{max}/u_∞ @ x/L = 0.7
33x33x19 global	20,691	1.20
33x33x19 global w/ 3 embedded levels	233,160	1.80
65x65x37 global	156,325	1.55
65x65x37 global w/ 1 embedded level	512,770	1.92

STREAMWISE VELOCITY CONTOURS

$x/L = 0.7$; $\alpha = 20.5$

Experiment

$u_{max}/u_{\infty} = 2.25$
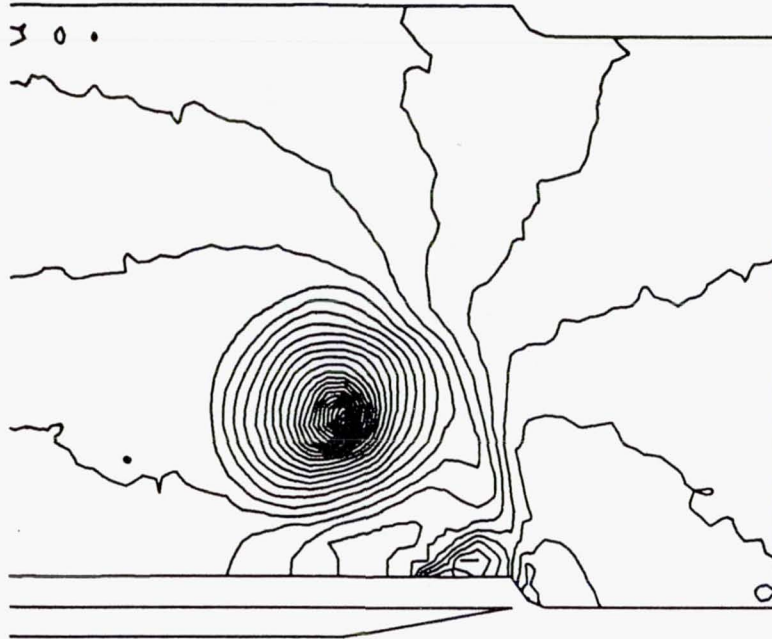
Navier-Stokes

$u_{max}/u_{\infty} = 1.92$
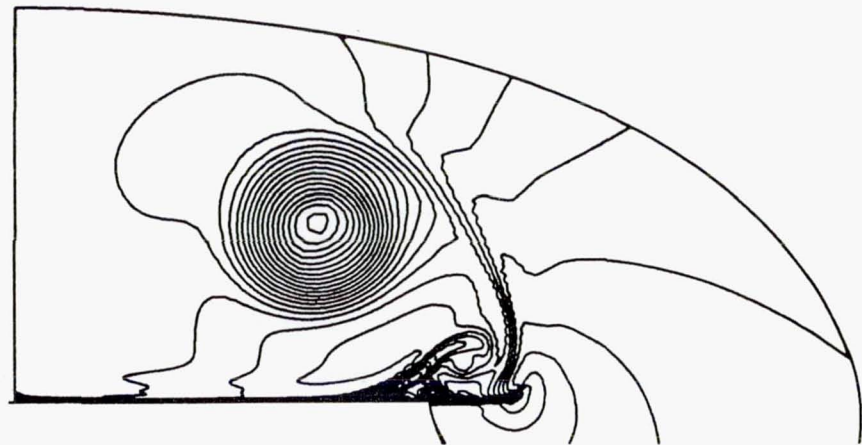
CONCLUDING REMARKS

• Global grid algorithm predicts overall flow topology
and surface characteristics of delta wings in good
agreement with experiment

- Force and moment

- Surface oil flows

- Vortex trajectories

• Embedded grid algorithm provides efficient way to predict
local off-surface flows

- Vortex core velocities

- Downstream interactions

Unstructured Mesh Solution
of the Euler and Navier-Stokes Equations

Timothy J. Barth

CFD Branch
NASA Ames Research Center
Moffett Field, CA 94035

Mesh generation procedures as well as solution algorithms for solving the Euler and Navier-Stokes equations on unstructured meshes are presented. The solution algorithms discussed utilize approximate Riemann solver, upwind differencing to achieve high spatial accuracy. Numerical results for Euler flow over single and multi-element airfoils are presented.

Motivation/Requirements

- Generality
  - Mesh Generation of Complex Geometries
  - Inviscid/Viscous, Subsonic/Transonic Flows
- Accuracy
  - High Spatial Accuracy for Smooth Flows
    - Mesh Adaptation
  - Shock Capturing for Discontinuous Flows
    - Generalized Upwind Scheme
- Efficiency
  - Edge Data Structure
    - Edge and Face "Coloring"

Mesh Generation

- Structured

  - Algebraic, Elliptic, Hyperbolic, Parabolic, ...

- Delaunay Triangulation

  - $O(n \log n)$

  - Maximize Minimum Angle

- Advancing Front

  - Probably $O(n \log n)$

"Random" Mesh (Delaunay Triangulation)
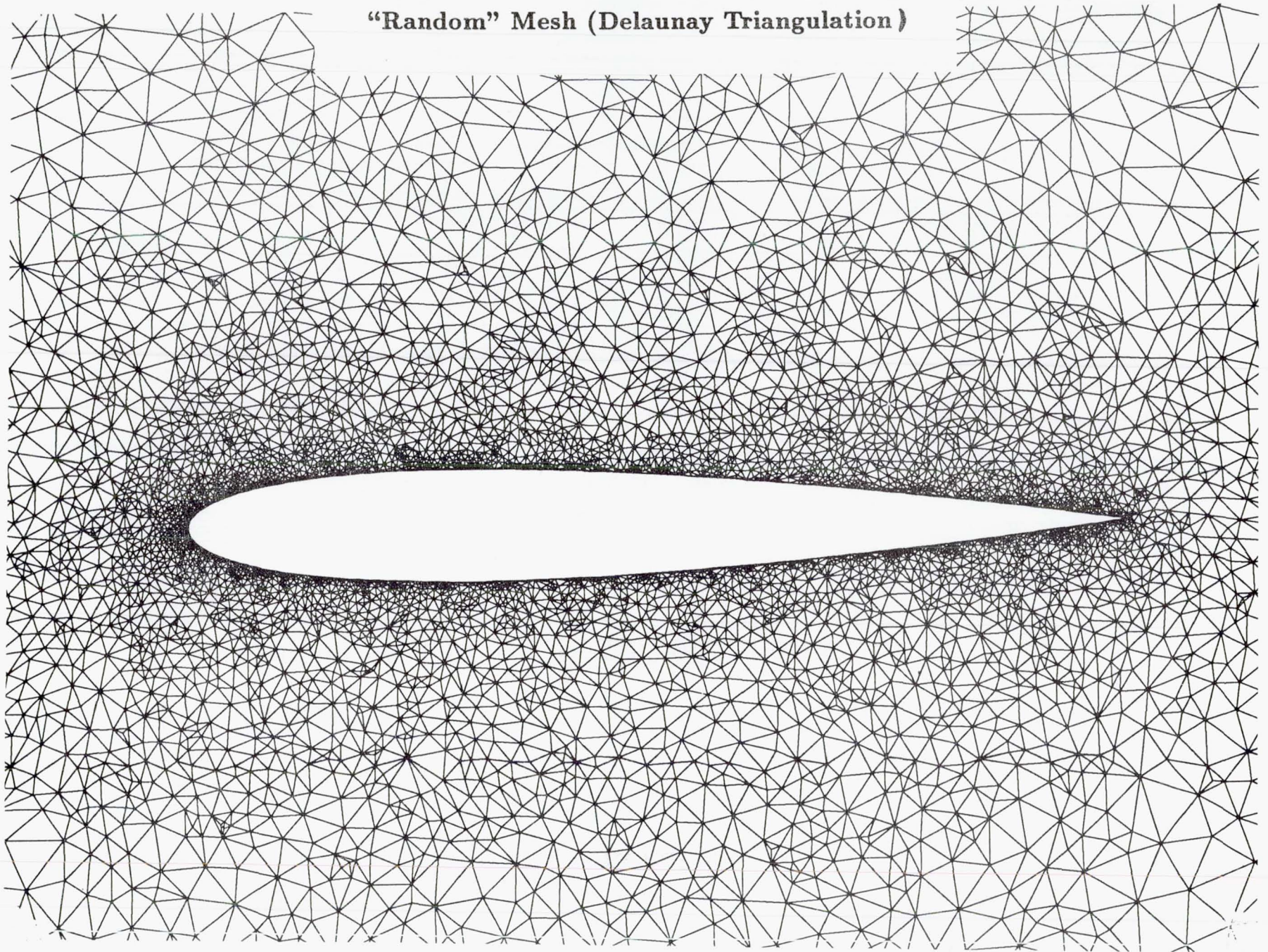
Advancing Front Mesh
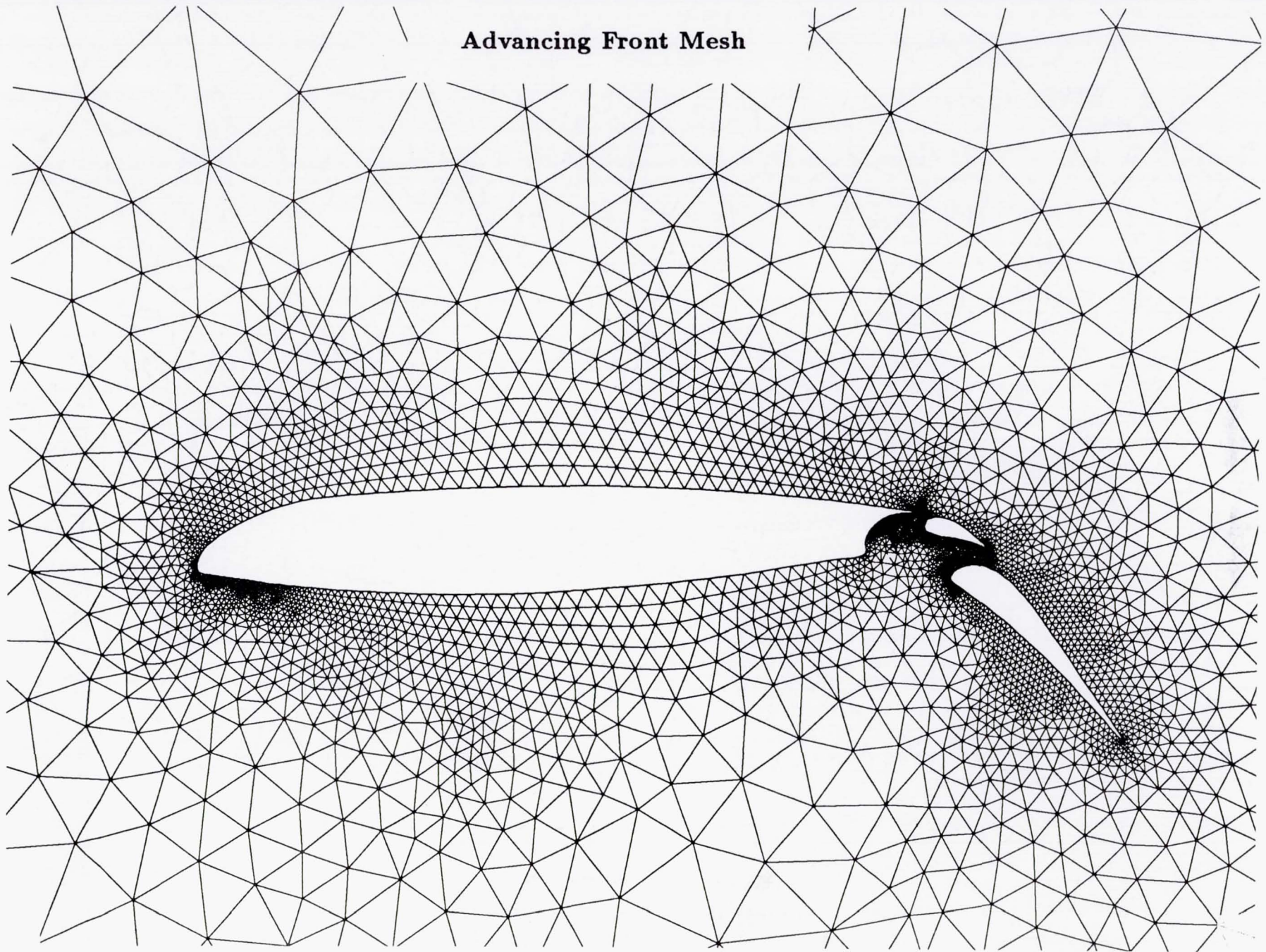
Advancing Front Mesh (Dual)
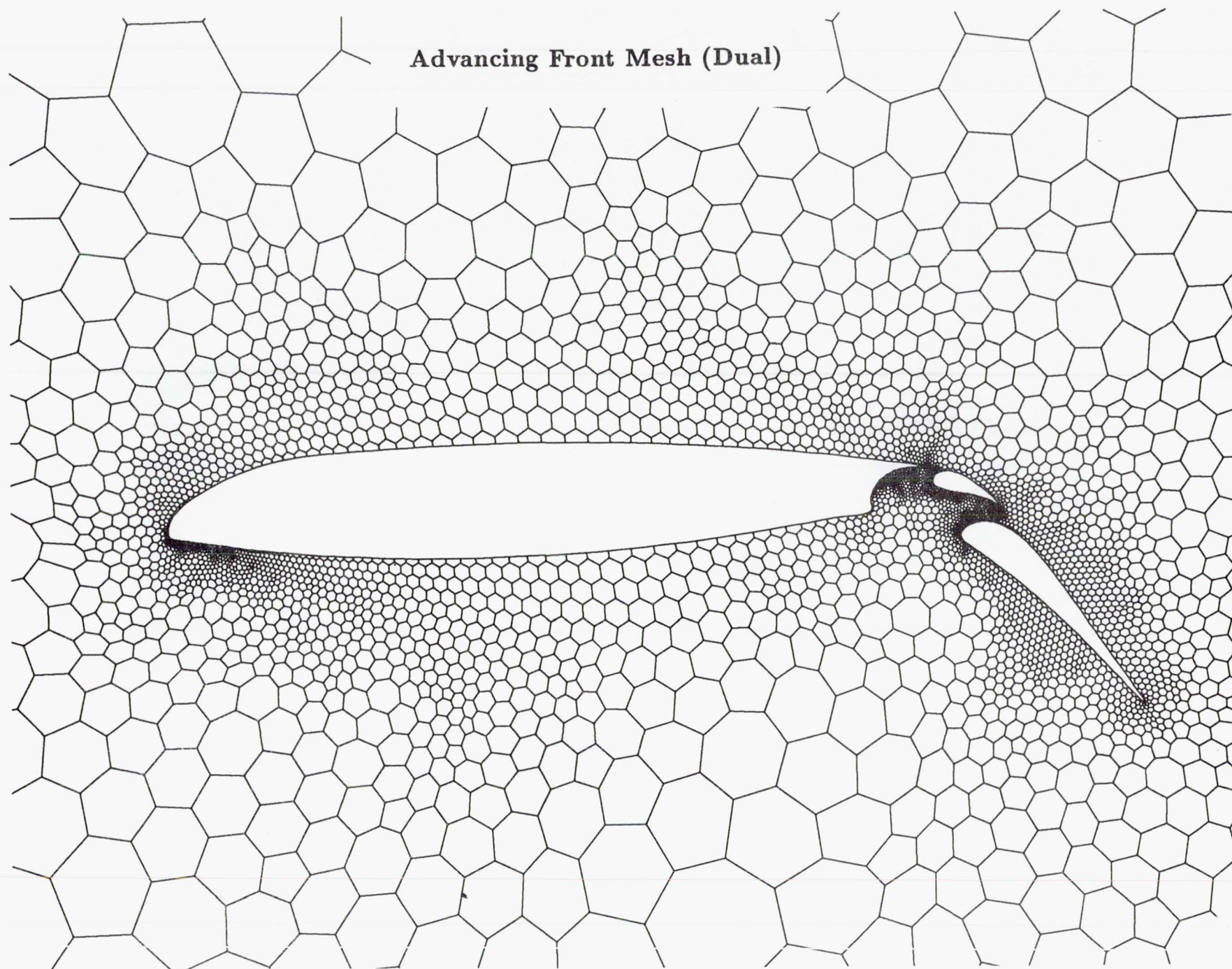
Fig. 2.1a) Three-component configuration.
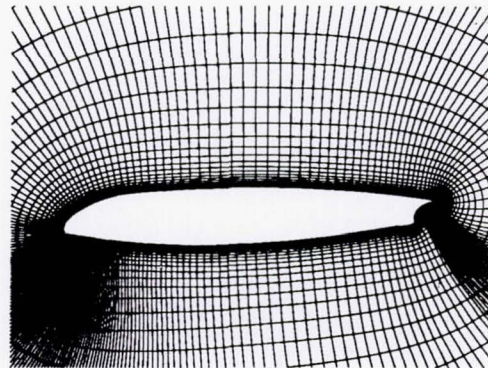
Fig. 2.1b) Grid about main element.
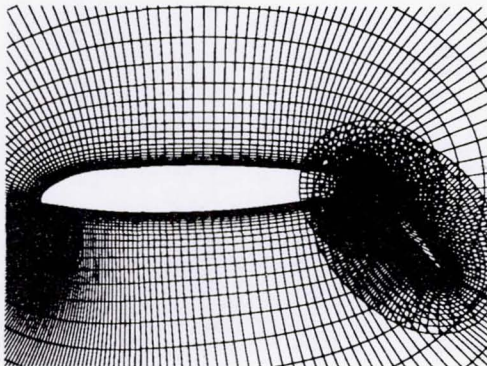
Fig. 2.1c) Grids plotted atop one another.
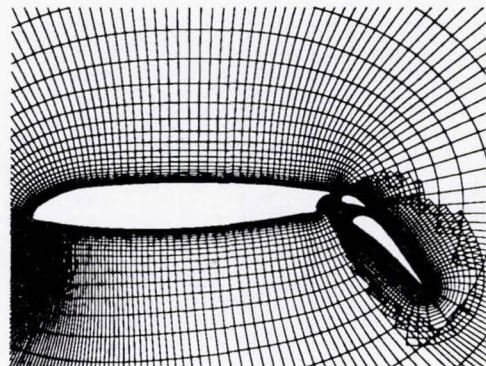
Fig. 2.1d) Grid after elimination of unwanted pts.
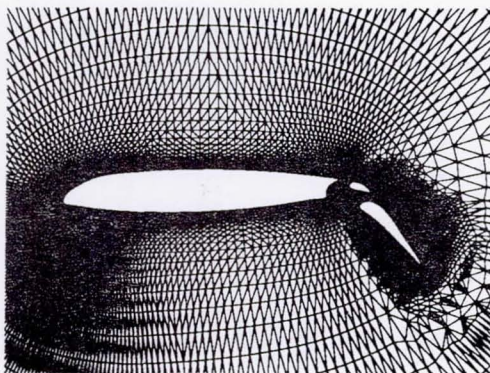
Fig. 2.1e) Grid after reconnection of points.
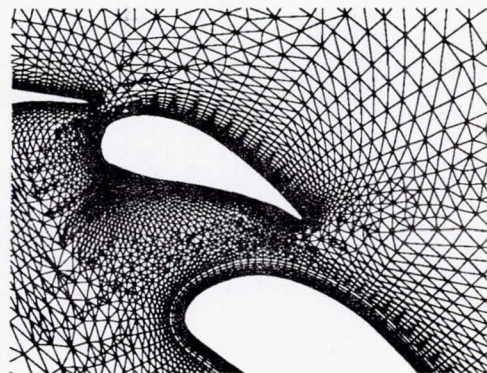
Fig. 2.1f) Grid after reconnection, detail.

Figure (2.1) Mesh generation synthesis of 3 element airfoil.

Finite-Volume Spatial Scheme

Euler equations in integral form:

$$\frac{\partial}{\partial t} \int_\Omega \mathbf{u}\, da + \oint_{\partial\Omega} \bar{\mathbf{f}}(\mathbf{n})\, dl = 0$$

where $\bar{\mathbf{f}}(\mathbf{n}) = n_x \mathbf{f} + n_y \mathbf{g}$

Numerical approximation about polygonal face:

$$\frac{\partial}{\partial t} \int_{\Omega_{f_j}} \mathbf{u}\, da = -\sum_{i=1}^{d(f_j)} \Delta l_i\, \mathbf{h}(\bar{\mathbf{u}}_i^+, \bar{\mathbf{u}}_i^-; \mathbf{n}_i), \quad j = 1, n(f)$$

Roe Flux Function:

$$\mathbf{h}(\mathbf{u}^+, \mathbf{u}^-; \mathbf{n}) = \frac{1}{2}(\bar{\mathbf{f}}(\mathbf{u}^+; \mathbf{n}) + \bar{\mathbf{f}}(\mathbf{u}^-; \mathbf{n}))$$

$$-\frac{1}{2}|A(\mathbf{u}^+, \mathbf{u}^-; \mathbf{n})|(\mathbf{u}^+ - \mathbf{u}^-)$$

Reconstruction - Evolution

- Solution Reconstructions

  - Piecewise Constant

  - Piecewise Linear $\quad \overline{u}(x, y) = u(x_0, y_0) + \Phi \nabla u \cdot \Delta \mathbf{r}$

    - Gradient Estimation in each face, $\quad \nabla u = \frac{1}{a_\Omega} \int_{\partial \Omega} u \mathbf{n} \, d l$

    - Monotonicity Enforcement

      - Limiting (Multidimensional), $\Phi \in [0, 1]$

- Solution Evolution

  - Three Stage Runge-Kutta Time-Stepping

Numerical Examples

- NACA 0012 airfoil $(M_\infty = .8, \alpha = 1.25°)$

  - Subdivided Structured Mesh (193x33)

  - Irregular Mesh

- 3 Element Airfoil $(M_\infty = .2, \alpha = 0.0°)$

Mach Contours on Random Mesh
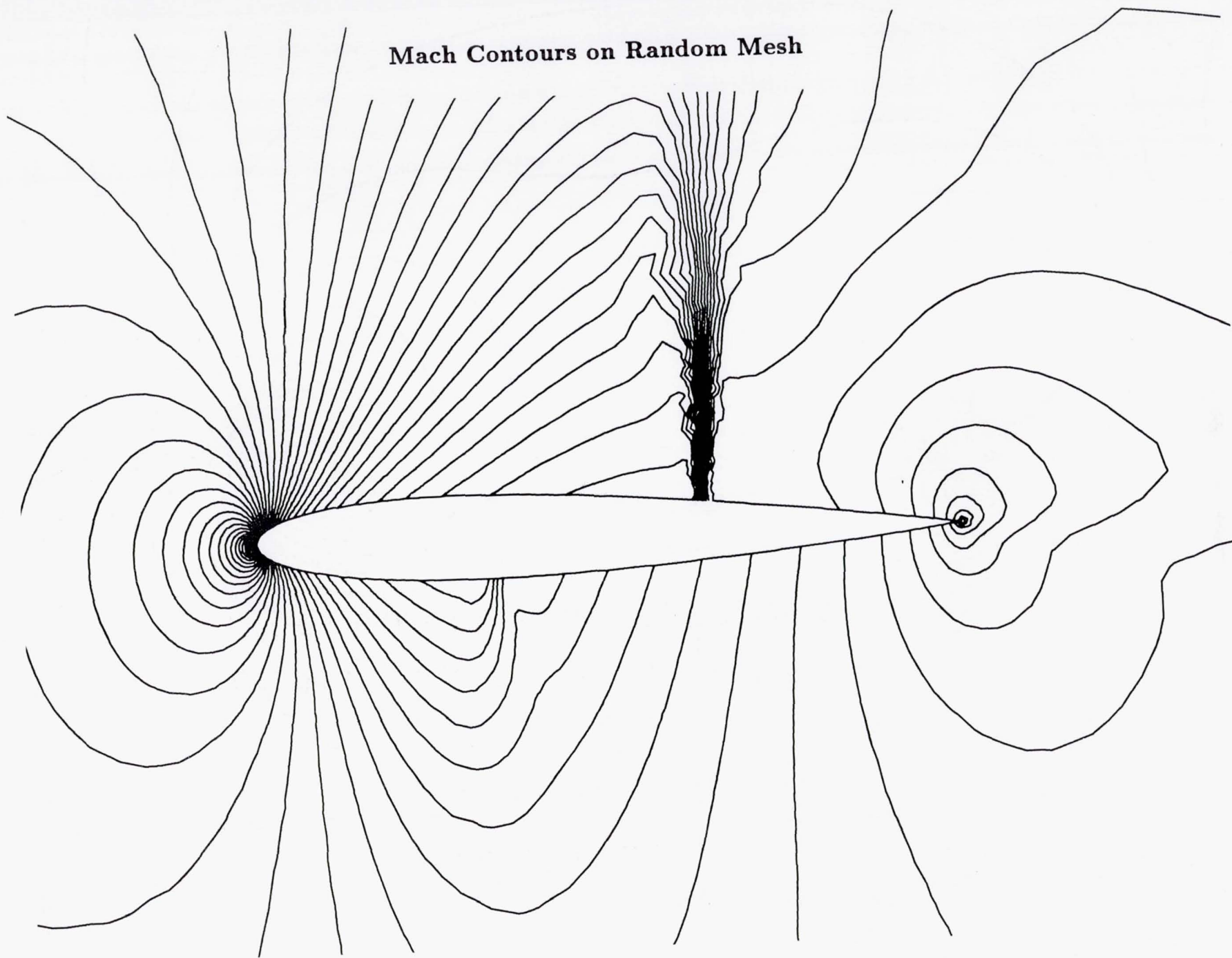
Mach Contours on 3-Element Airfoil
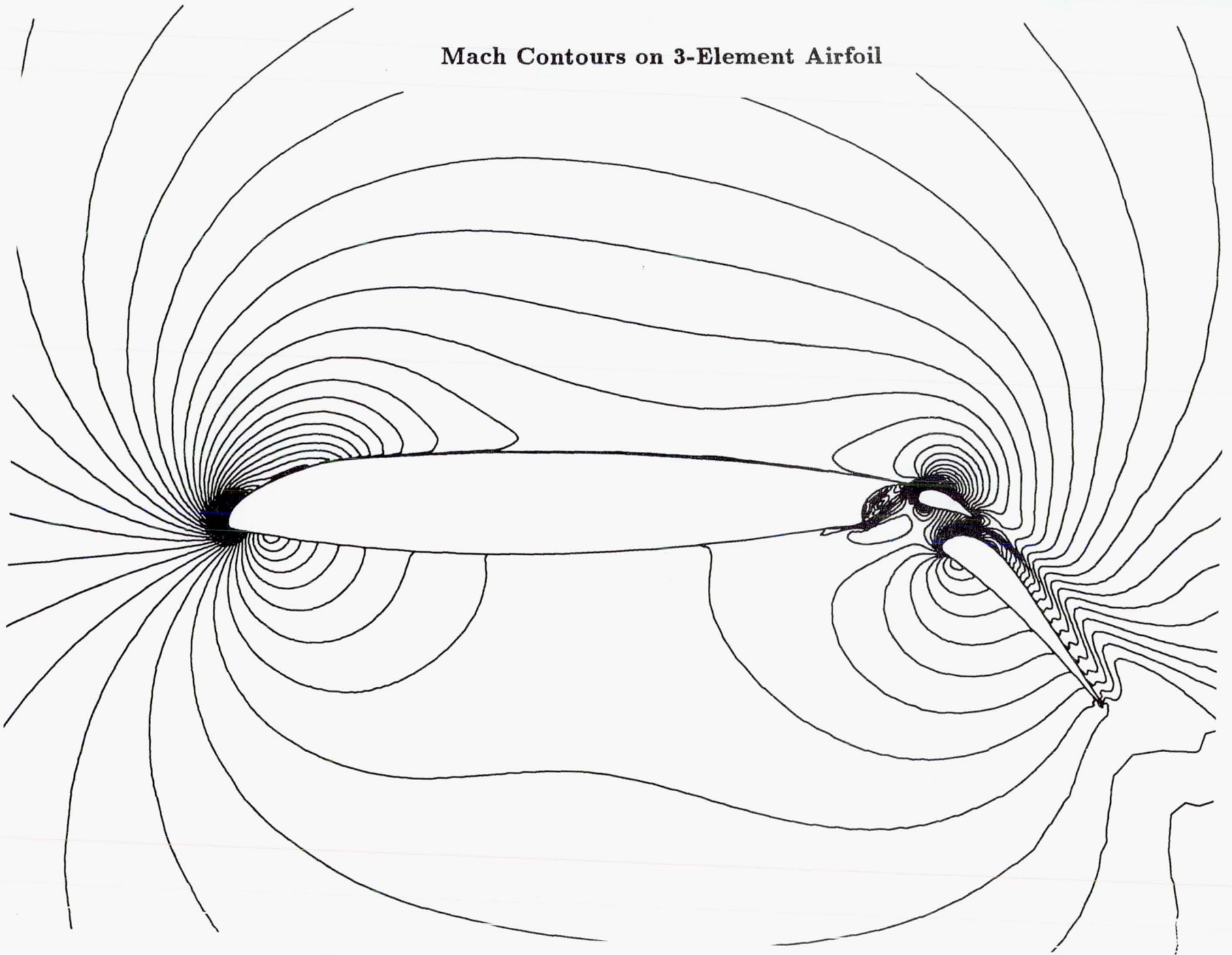
Pressure Contours on 3-Element Airfoil

C-5
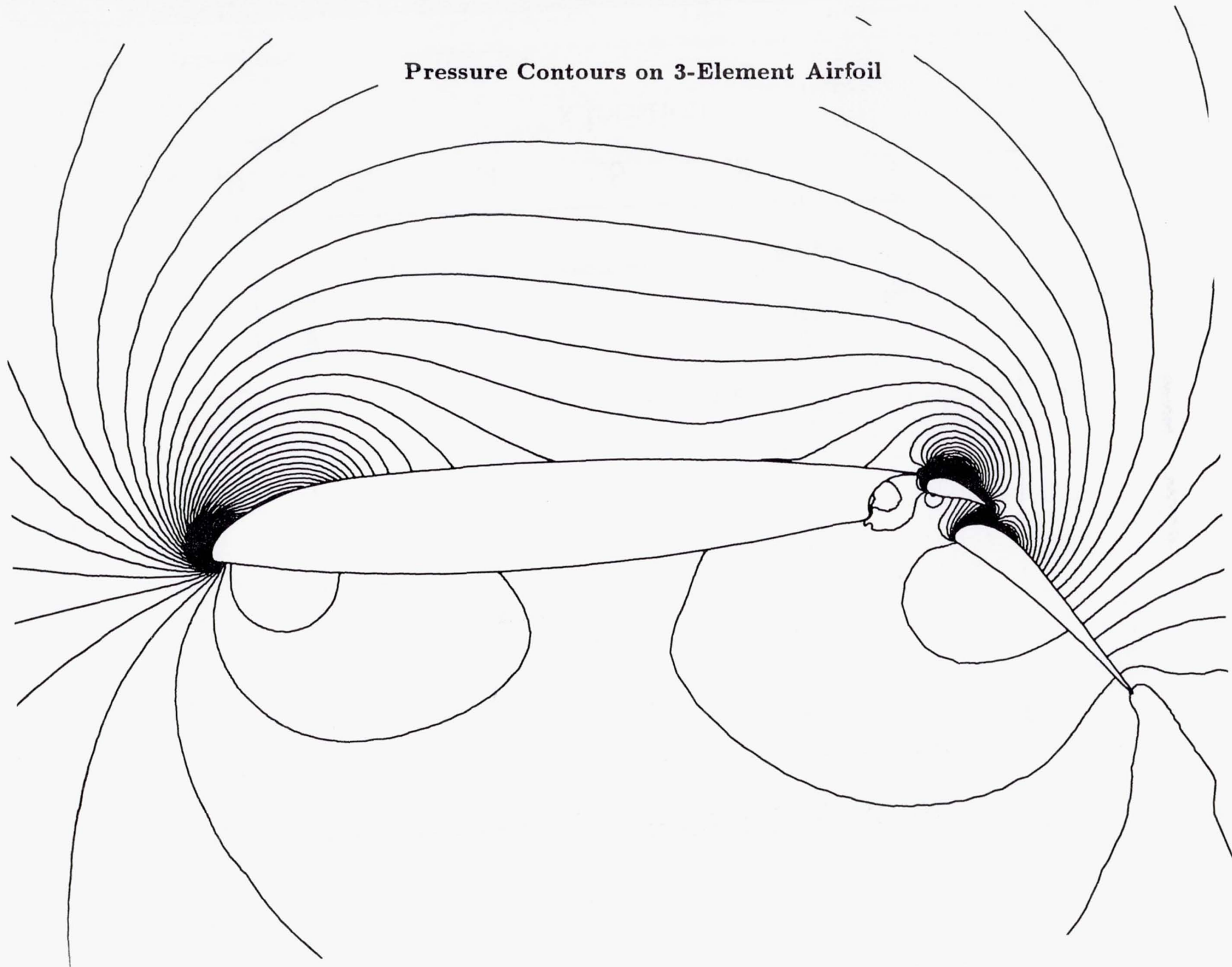
3-Element Airfoil Cp Distribution
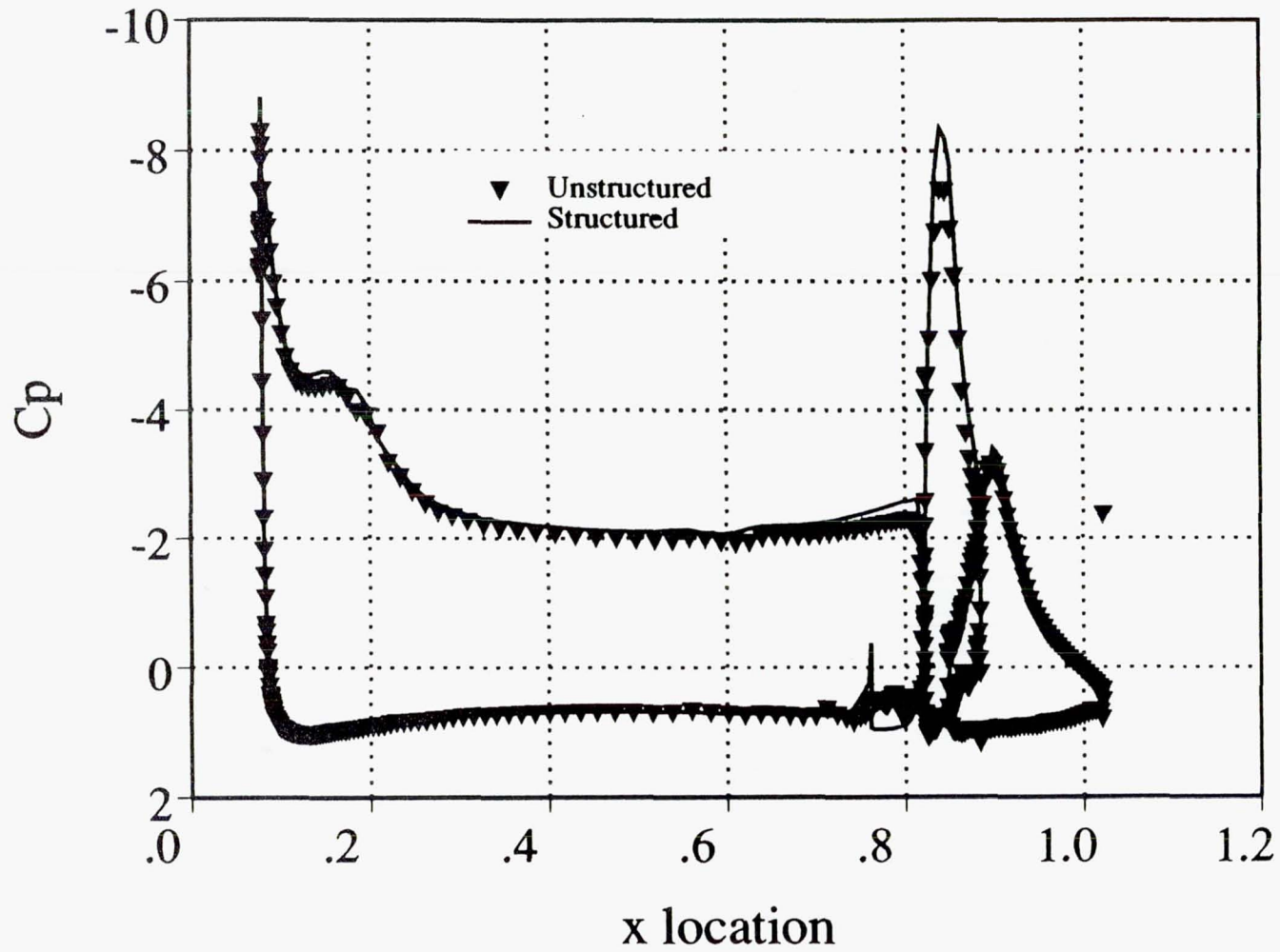
Current and Future Directions

- Quadratic Reconstructions

- Viscous Calculations with Turbulence Modelling

- Adaptive Mesh Refinement

3–D UNSTRUCTURED GRIDS FOR THE SOLUTION OF THE EULER EQUATIONS

C. Gumbert

NASA Langley Research Center

P. Parikh, S. Pirzadeh

Vigyan Research Associates

R. Löhner

George Washington University

Advancing Front Grid Generator

The advancing front technique is being used to develop a code to generate grids around complex three dimensional configurations for use in computing the invisid flow solutions by the Euler equations. By the advancing front technique points are introduced concurrently with the connectivity information so that a separate library is not required. The generation of a 3–D grid is accomplished in several steps. First the boundaries of the domain to be gridded must be described by two-, three– or four-sided surface patches. Next, a background mesh is required to control the grid spacing and stretching throughout the domain. This coarse tetrahedral grid is not required to conform to any of the boundaries. Next, each of the patches is mapped to 2–D, triangulated by the advancing front technique and mapped back to 3–D. These triangles form the initial front for the generation of the final tetrahedral mesh.

ADVANCING FRONT GRID GENERATOR

- The field points are introduced *while* grid is generated.

  - Does not require a separate library to introduce points before grid generation.

  - Allows adaptive regeneration of grids easily.

- Generation Steps:

  - Define boundaries of the domain using surface patches.

  - Set up background grid to control local grid characteristics.

  - 2-D triangulation of patches

  ⇒ Initial Front

  - Advancing front in 3-D to fill region with tetrahedra.

Advancing Front in 2–D

The figure is a schematic showing the advancing front technique in 2–D. The initial front is a set of line segments called faces. In 3–D a face is a triangle. In succession, each face of the front is deleted and a new point in the field is introduced. As in the center figure, if the new point is close to an existing point, then the existing one is used instead. The front advances until it closes in on itself at which point the region is fully gridded.

ADVANCING FRONT IN 2-D

initial front

deleted face
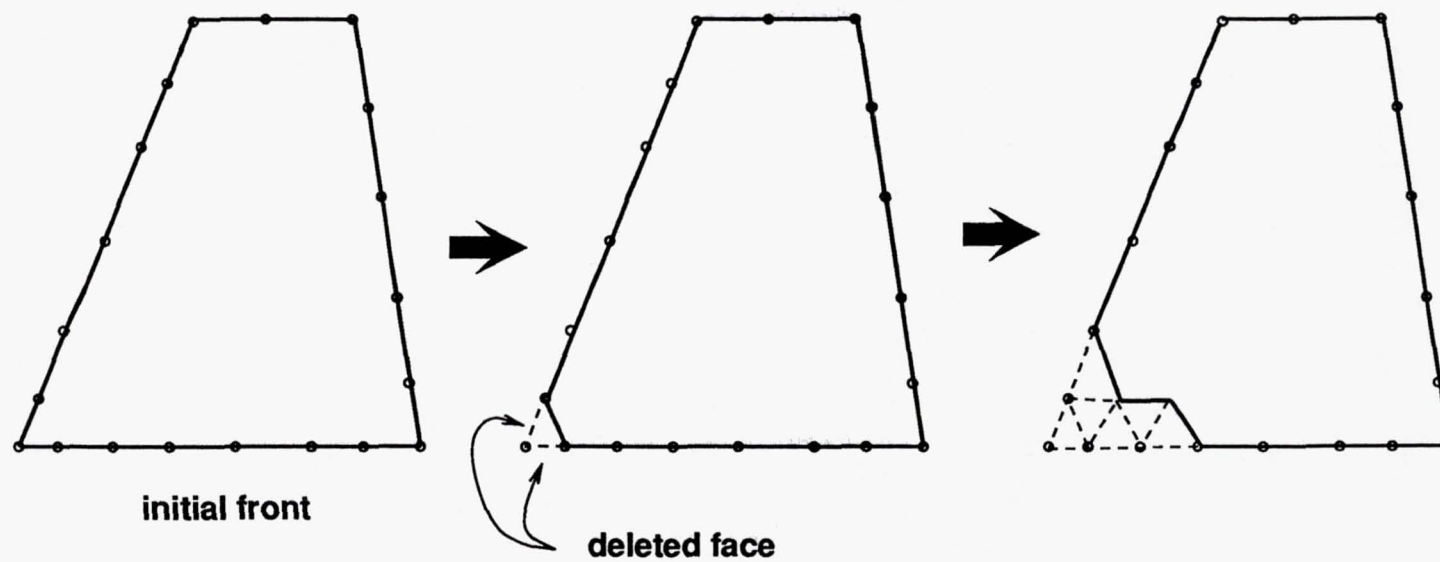
Surface Grid for F-18 Configuration

The figure shows the surface grid for an F-18 fighter configuration. The grid was generated for only one half of the configuration but it has been mirrored in the picture. The grid consists of 367,000 tetrahedrons using nearly 66,000 points of which 10,000 lie on the 75 surface patches defining the airplane and the computational box. It required about 400 seconds on the NAS CRAY-2 computer.
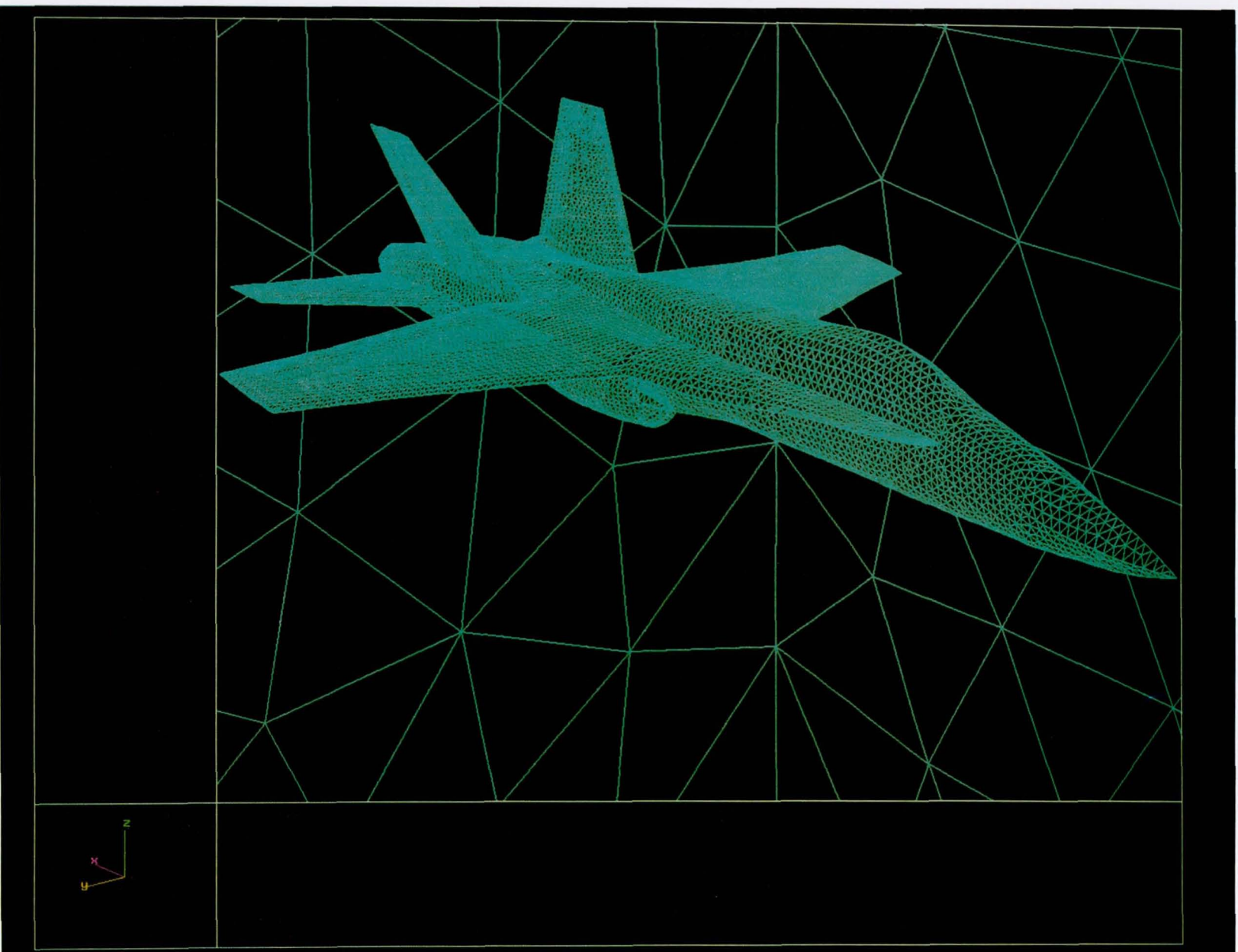
Finite Element Flow Solver

The flow solver developed in conjunction with the grid generator uses a two-step Taylor Galerkin finite element method for the Euler equations cast in Arbitrary Lagrangian-Eulerian (ALE) form. The Galerkin weighted residual method is used to perform the spatial discretization. Timestepping options are available for steady-state or transient problems. Accurate solutions without spurious over/undershoots can be obtained using Flux Corrected Transport (FCT) techniques. Second order pressure or Lapidus damping is used near shocks. Adaptive mesh refinement is used to better capture sharp gradients. This technique has not been fully implemented in 3–D.

403

FINITE ELEMENT FLOW SOLVER

- **Two-step Taylor-Galerkin scheme**

- **Spatial discretization performed via Galerkin weighted residual method using linear elements**

- **Options for:**

    Global/local timestepping

    Second order pressure or Lapidus damping

    Flux Corrected Transport (FCT)

    Adaptive H-refinement

Results In 2-D

As a means of determining the accuracy of this code, results are presented for two 2-D flow calculations. The first case is the transonic flow calculation for an NACA 0012 airfoil at $M_\infty = .80$ and $\alpha = 1.25°$. Comparison is made with results from FLO52, a finite volume method calculated on an O-type grid.

The second case is the flow field around a 20° ramp at $M_\infty = 3.0$. The exact solution is known and can be compared. This case also illustrates the use of adaptive mesh refinement.

RESULTS IN 2–D

- **Comparison of NACA 0012 airfoil**
  at $M_\infty = .80, \quad \alpha = 1.25°$

  FEFLO27 (unstructured mesh, Finite Element solver)

  FLO52 (O-grid, finite volume method)

- **20° ramp flow**
  at $M_\infty = 3.0$

  adaptive mesh refinement

Grid for NACA 0012 Airfoil

The figure shows the unstructured grid used for the calculation. There are nearly 5000 points in the grid of which 266 points lie on the airfoil surface. This is similar to the 193 points in the structured grid of FLO52.
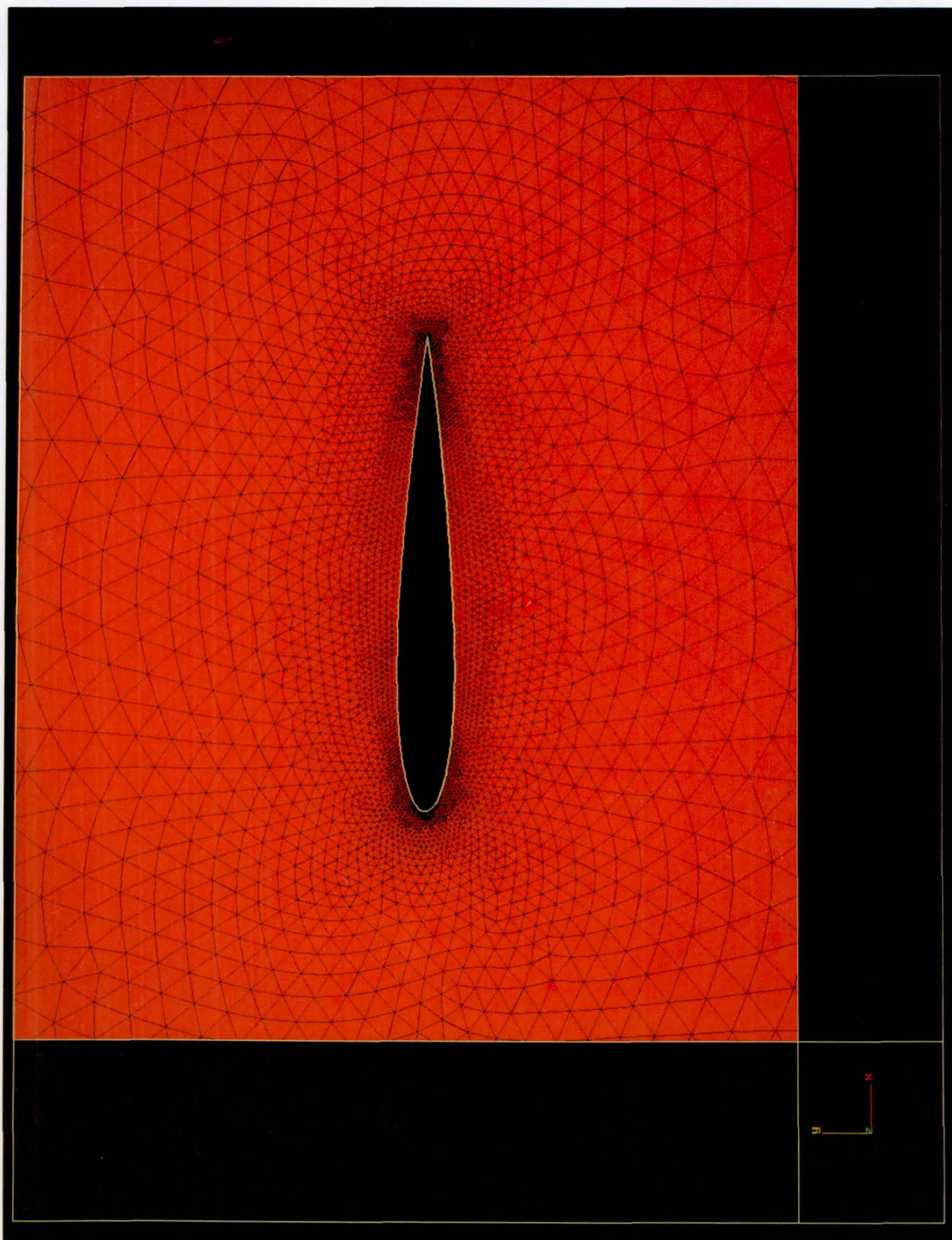
Pressure Coefficient Comparison for NACA 0012 Airfoil

The pressure coefficient distributions are compared in the figure. The results of the calculation made on the structured grid are designated by diamonds connected by straight lines. The results of the calculation on the unstructured grid are designated by filled circles. The solutions are very similar. The location and strength of the normal shock on the upper surface are nearly identical. The finite element solver captured the shock more sharply than did FLO52. The finite element solution shown was obtained in 4000 steps which used 1.9×10^{-3} seconds/point/timestep on a Convex C2 computer.

Comparison of NACA 0012 airfoil
at $M_\infty = .80$, $\alpha = 1.25°$
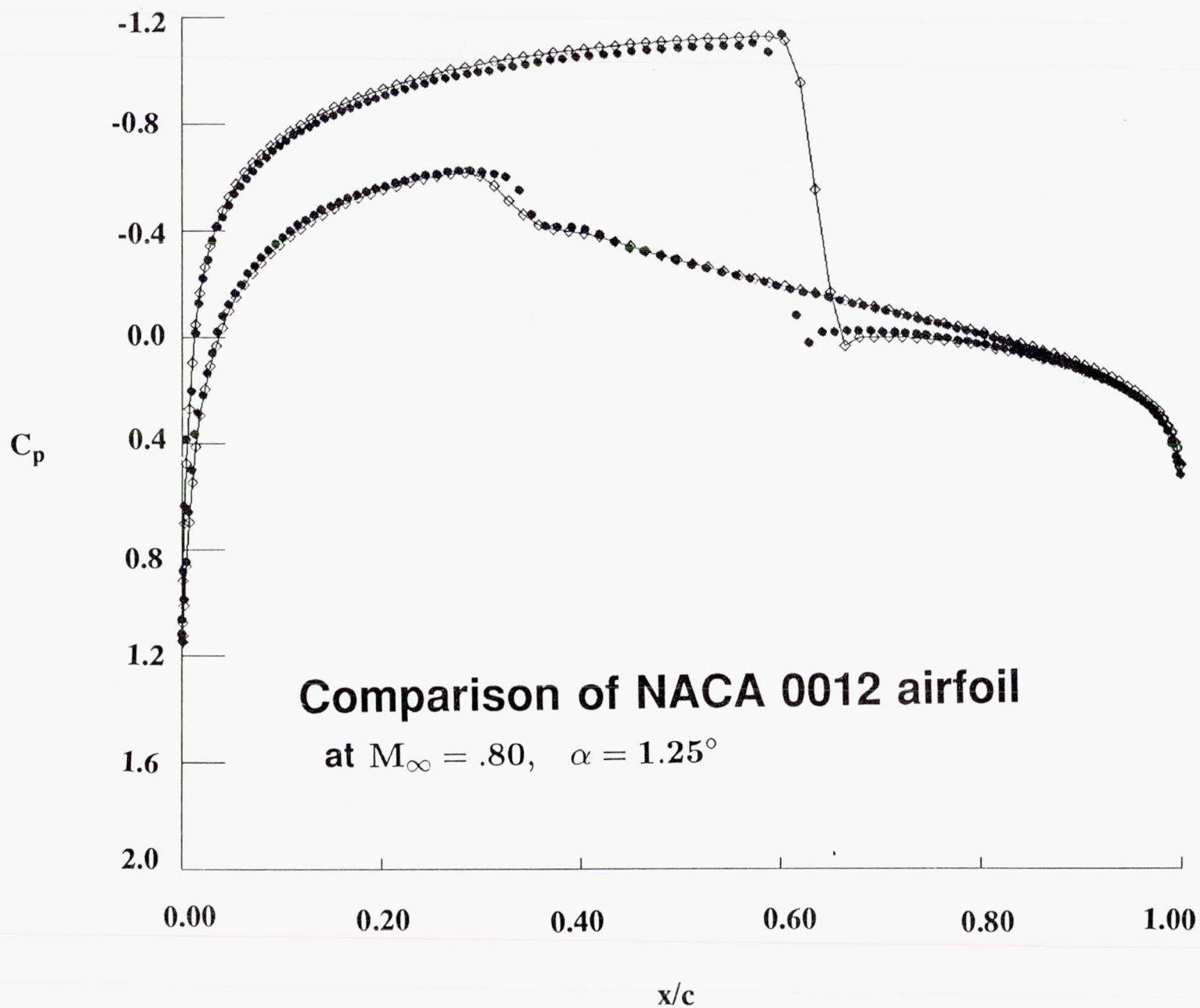
Exact Solution For Supersonic Flow Over A Ramp

This figure shows a schematic of the second case, supersonic flow over a 20° wedge. The exact solution is shown for the regions designated 1, 2, and 3.

EXACT SOLUTION FOR
SUPERSONIC FLOW OVER RAMP

$M_2 = 1.994$

$\dfrac{P_2}{P_1} = 3.77$

$M_3 = 2.823$

$\dfrac{P_3}{P_1} = 1.04$

$M_1 = 3$

2

3

1

$\beta = 37.7°$

$\theta = 20°$
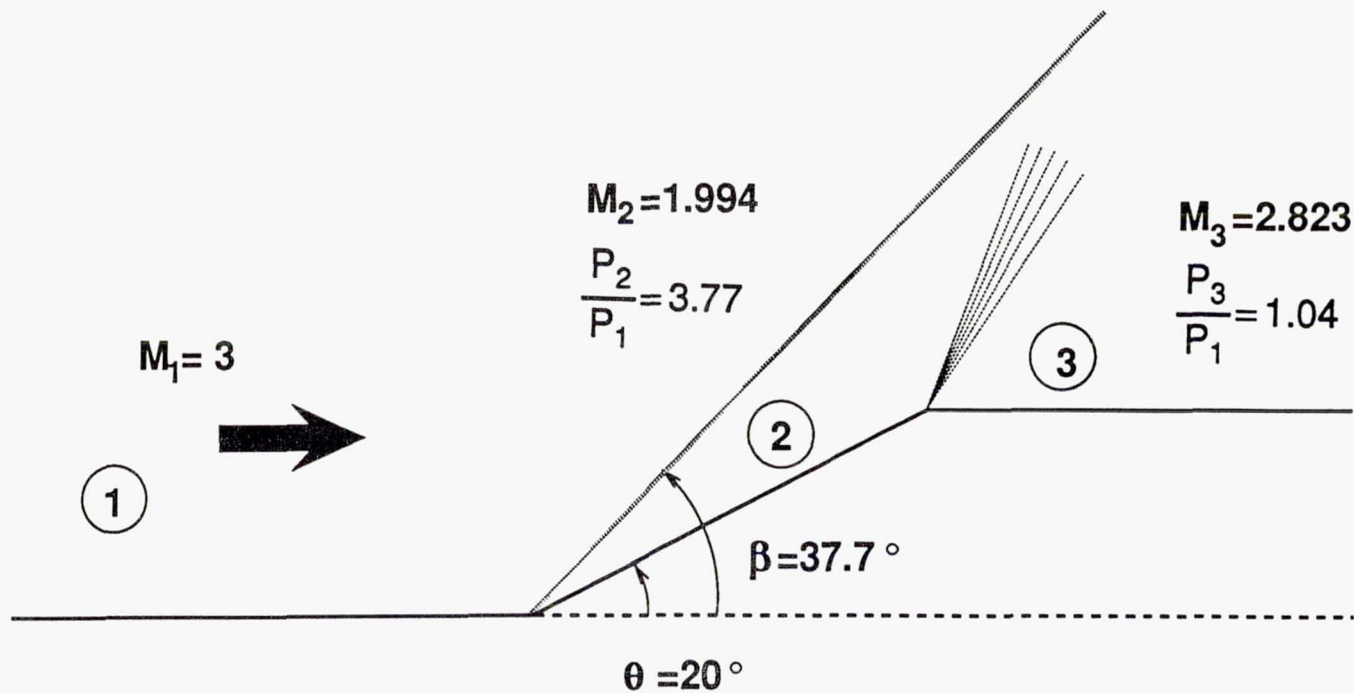
Grid Adaptation for 20° Ramp

This figure shows the final adapted grid for the solution. The levels of adaptation are shown by different colors.

417
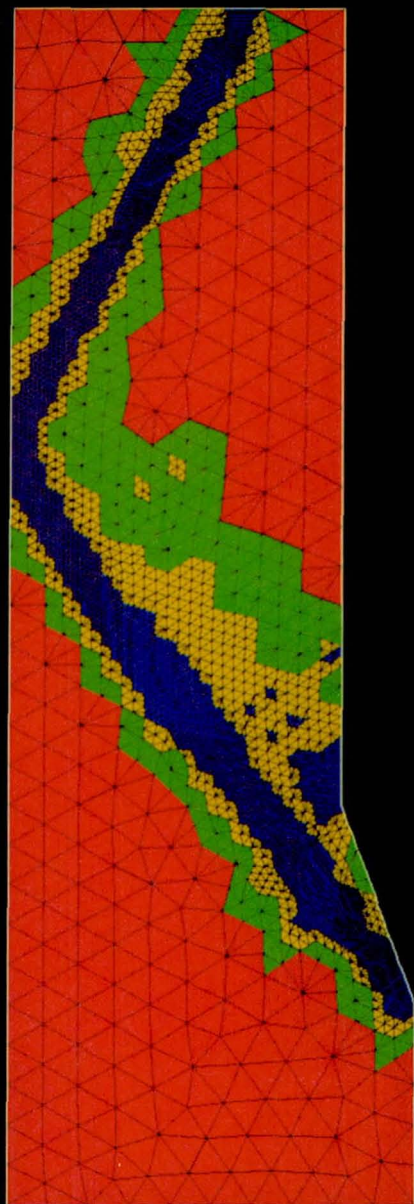
Mach Number and Pressure Contours for 20° Ramp

The calculated Mach number and pressure are shown in the following figures. The shock angle and the conditions in the regions designated 1, 2, and 3 are predicted accurately. The figure also shows the interaction of the oblique shock with the expansion fan and the reflection of the shock off the straight wall.

Surface Pressure Contours on F-18 Aircraft

The figure shows the pressure contours on the surface of an F-18 aircraft configuration at $M_\infty = 0.3$ and $\alpha = 15°$. The solution was calculated on a grid for which the engine inlet and nozzle were blocked. This solution was run 600 iterations in 159 minutes on the NAS CRAY-2 computer to decrease the maximum residual by two orders of magnitude.

PRESSURE

PRESSURE
1.069E+00
1.066E+00
1.063E+00
1.060E+00
1.057E+00
1.054E+00
1.051E+00
1.048E+00
1.045E+00
1.042E+00
1.039E+00
1.036E+00
1.033E+00
1.030E+00
1.027E+00
1.024E+00
1.021E+00
1.018E+00
1.015E+00
1.013E+00
1.010E+00
1.007E+00
1.004E+00
1.001E+00
9.977E-01
9.948E-01
9.918E-01
9.888E-01
9.859E-01
9.829E-01
9.800E-01
9.770E-01
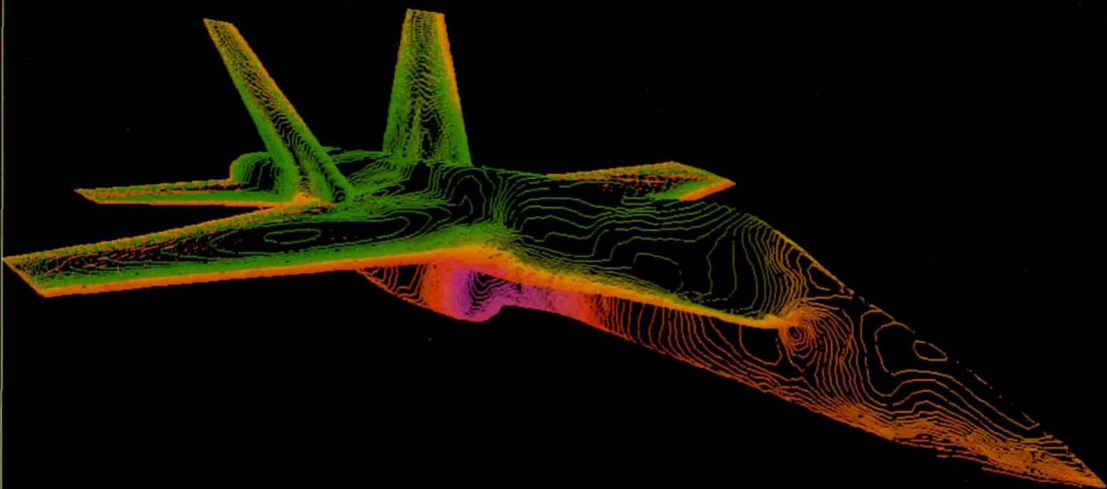
PRESSURE

Pressure Contours For Shock Emanating From A Corner

Sharp gradients in density and pressure were imposed at the intersection of three perpendicular walls as the initial conditions for a transient flow calculation. The figures show the pressure contours on the walls at two different time steps. The grid on the three walls is also shown. Additional grid points were added during the calculation to better capture the sharp gradients. No derefinement was done after the large gradients had passed.
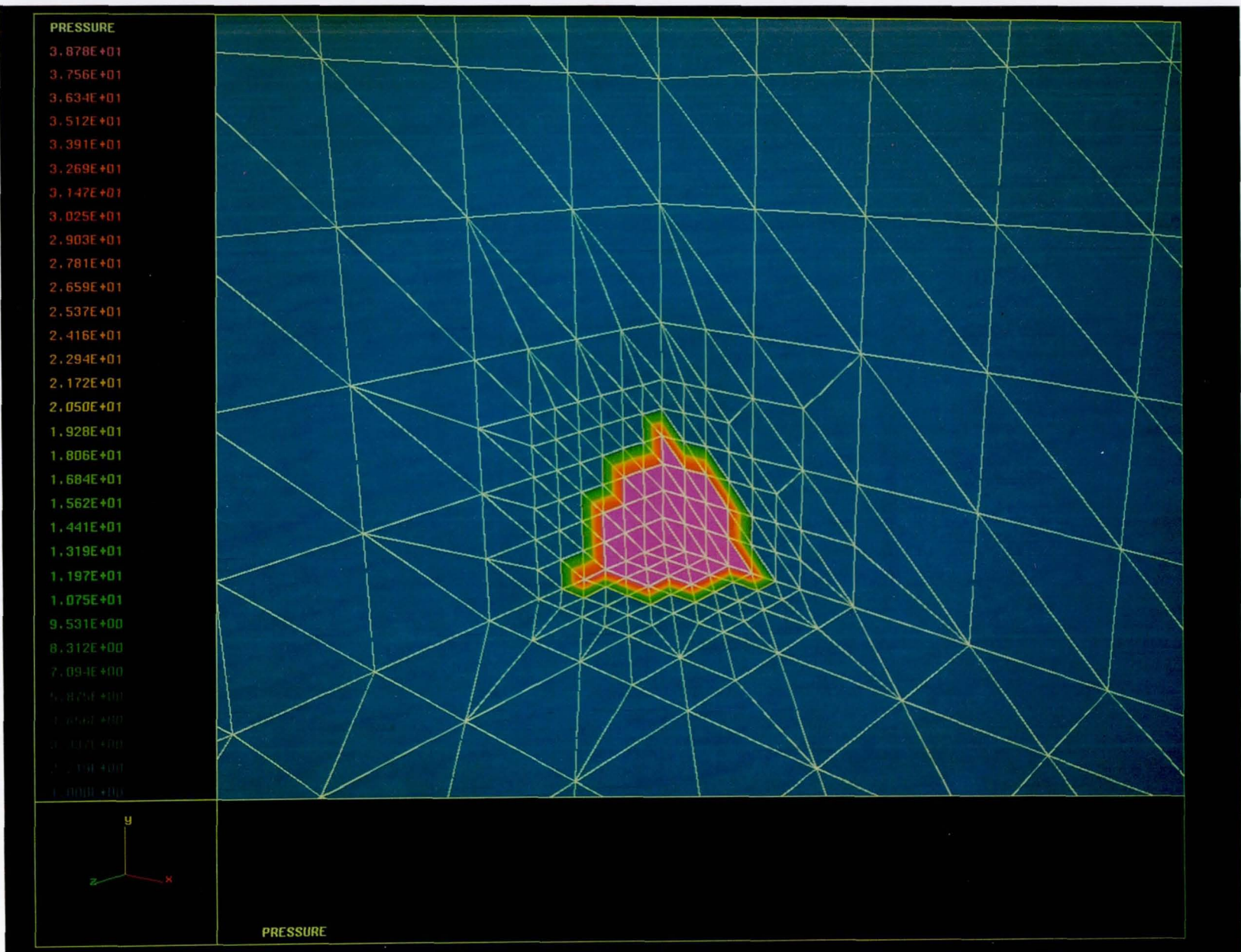
PRESSURE
2.350E+00
2.276E+00
2.201E+00
2.127E+00
2.052E+00
1.978E+00
1.904E+00
1.829E+00
1.755E+00
1.681E+00
1.606E+00
1.532E+00
1.458E+00
1.383E+00
1.309E+00
1.235E+00
1.160E+00
1.086E+00
1.012E+00
9.373E-01
8.629E-01
7.886E-01
7.142E-01
6.399E-01
5.655E-01
4.912E-01
4.168E-01
3.425E-01
2.681E-01
1.938E-01
1.195E-01
4.510E-02

PRESSURE

Future Plans

Further development of the grid generator will tend along three paths: (1) implementation of existing CAD sytem for faster and easier surface definition, (2) enhancement of the surface element library to allow slope continuity across surface patch boundaries and (3) faster and better ways of defining the background grid.

Further development of the flow solver is expected to involve incorporation of the viscous terms into the flow equations, use of implicit or semi-implicit algoriths and implementation on parallel computers.

FUTURE PLANS

- For the grid generator:

    - Link to commercial CAD/CAM systems for faster and
      more accurate surface definition.

    - Faster and better ways to input background grid information.

    - Enhancement of surface element library.

- For the flow solver:

    - Incorporation of viscous terms.

    - Implicit or semi-implicit flow solver for transient problems.

    - Implementation on parallel computers.

FLUX SPLITTING ALGORITHMS FOR TWO-DIMENSIONAL VISCOUS FLOWS WITH FINITE-RATE CHEMISTRY

Jian-Shun Shuen

Sverdrup Technology, Inc.

NASA Lewis Research Center, Cleveland, Ohio 44135

Meng-Sing Liou

NASA Lewis Research Center, Cleveland, Ohio 44135

437

ABSTRACT

The Roe flux-difference splitting method has been extended to treat two-dimensional viscous flows with nonequilibrium chemistry. The derivations have avoided unnecessary assumptions or approximations. For spatial discretization, the second-order Roe upwind differencing is used for the convective terms and central differencing for the viscous terms. An upwind-based TVD scheme is applied to eliminate oscillations and obtain a sharp representation of discontinuities. A two-stage Runge-Kutta method is used to time integrate the discretized Navier-Stokes and species transport equations for the asymptotic steady solutions. The present method is then applied to two types of flows: the shock wave/boundary layer interaction problems and the jet in cross flows.

OBJECTIVES

1. To develop a numerical algorithm for real gases which is robust for high Mach number flows and has the ability to accurately capture strong shocks and other types of discontinuities.

2. To include nonequilibrium chemistry in the formulation.

3. To make the formulation consistent and simple.

GOVERNING EQUATIONS

The 2-D, thin layer Navier-Stokes and species equations for a chemically reacting gas of N species:

$$\frac{\partial \mathbf{U}}{\partial t} + \frac{\partial \mathbf{F}(\mathbf{U})}{\partial x} + \frac{\partial \mathbf{G}(\mathbf{U})}{\partial y} - \frac{\partial \mathbf{W}(\mathbf{U}, \mathbf{U_y})}{\partial y} = \mathbf{S},$$

where

$$\mathbf{U} = \begin{pmatrix} \rho \\ \rho u \\ \rho v \\ \rho E \\ C_1 \\ C_2 \\ \cdot \\ \cdot \\ C_{N-1} \end{pmatrix}, \quad \mathbf{F} = \begin{pmatrix} \rho u \\ \rho u^2 + p \\ \rho u v \\ u(\rho E + p) \\ u C_1 \\ u C_2 \\ \cdot \\ \cdot \\ u C_{N-1} \end{pmatrix}, \quad \mathbf{G} = \begin{pmatrix} \rho v \\ \rho u v \\ \rho v^2 + p \\ v(\rho E + p) \\ v C_1 \\ v C_2 \\ \cdot \\ \cdot \\ v C_{N-1} \end{pmatrix},$$

$$\mathbf{W} = \begin{pmatrix} 0 \\ \mu u_y \\ \frac{4}{3}\mu v_y \\ \mu u u_y + \frac{4}{3}\mu v v_y + k T_y - \sum_{i=1}^{N} C_i h_i \tilde{v}_i \\ -C_1 \tilde{v}_1 \\ -C_2 \tilde{v}_2 \\ \cdot \\ \cdot \\ -C_{N-1}\tilde{v}_{N-1} \end{pmatrix}, \quad \mathbf{S} = \begin{pmatrix} 0 \\ 0 \\ 0 \\ 0 \\ S_1 \\ S_2 \\ \cdot \\ \cdot \\ S_{N-1} \end{pmatrix}.$$

THERMODYNAMIC AND TRANSPORT MODELS

Equation of State

$$p = p(\rho, e, C_1, C_2, \ldots C_{N-1})$$

$$p = R_u T \sum_{i=1}^{N} \frac{C_i}{W_i}$$

Physical Properties

- Mass diffusion is approximated by Fick's law. Binary mass diffusivity obtained from Chapman-Enskog theory.

- For the individual species: C_p, k, and μ are determined by fourth-order polynomials of temperature.

- For the gas mixture: C_p obtained by mass concentration weighting of each species. k and μ obtained using Wilke's mixing rule.

Chemistry Model of Air

- Five (5) species (O_2, N_2, O, N, NO) and eleven (11) elementary reaction steps.

- Neglecting ionization as well as thermal nonequilibrium.

SOLUTION METHOD

1. Two-stage Runge-Kutta method for time integration of the governing equations.

2. Chemical source terms treated implicitly so that the stiffness associated with the source terms will not upset numerical stability.

3. Second-order upwind differencing for convective terms, central differencing for viscous terms.

4. Upwind-based TVD scheme to eliminate oscillations and to obtain a sharp representation of discontinuities.

UPWIND DIFFERENCING

- Good Property for Capturing Discontinuities.

- Flux-Vector Splittings

  ✓ Steger-Warming Splitting

  ✓ Van Leer Splitting

- Flux-Difference Splittings

  ✓ Roe Splitting

  Osher Splitting

ROE FLUX-DIFFERENCE SPLITTING

To construct Roe flux-difference splitting, one usually defines an average state $\hat{U}$ such that

$$\Delta F = \hat{A}\Delta U, \qquad \Delta G = \hat{B}\Delta U, \qquad \Delta(\cdot) = (\cdot)_R - (\cdot)_L,$$

$$\hat{A} = A(\hat{U}), \qquad \hat{B} = B(\hat{U}), \qquad \hat{U} = \hat{U}(U_L, U_R)$$

The eigenvalues of the Jacobian A are (for N=5):

$$\lambda(A) = u, \quad u, \quad u-a, \quad u+a, \quad u, \quad u, \quad u, \quad u$$

A is diagonizable

$$A = S_A \Lambda_A S_A^{-1}, \qquad diag\ \Lambda_A = \lambda(A).$$

Splitting of the diagonal matrix Λ_A results in the splitting of $A^{\pm}$:

$$A = A^+ + A^-, \qquad A^{\pm} = S_A \Lambda_A^{\pm} S_A^{-1}$$

Thus, the splitting of the flux difference ΔF:

$$\Delta F = \Delta F^+ + \Delta F^-, \qquad \Delta F^{\pm} = A^{\pm}(\hat{U})\Delta U.$$

Goal: Find the average state $\hat{U} = \hat{U}(U_L, U_R)$.

ROE'S AVERAGE STATE

- $\Delta F = A(\hat{U})\Delta U$

- **For a calorically perfect gas:** the Roe average state is easily obtained.

- **For a real gas:** the simplicity is lost.

Choose the set of average quantities

$$(\hat{\rho}, \hat{u}, \hat{v}, \hat{e}, \hat{H}, \hat{Y}_{i,i=1,4}, \hat{p}_\rho, \hat{p}_e, \hat{p}_{C_{i,i=1,4}})$$

Define the Roe-average operator μ,

$$\hat{f} = \mu(f) = \frac{f_R + d\,f_L}{1+d}, \qquad d = (\rho_L/\rho_R)^{\frac{1}{2}}, \qquad f = u, v, e, H, Y_i, \qquad \hat{\rho} = \rho_R d.$$

The condition left to be satisfied is:

$$\Delta p = \hat{p}_\rho \Delta \rho + \hat{p}_e \Delta e + \sum_{i=1}^{N-1} \hat{p}_{C_i} \Delta C_i. \tag{A}$$

Condition (A) contains N+1 variables for only one equation.

ROE'S AVERAGE STATE (cont'd)

$$\bar{Q} \equiv (\bar{p}_e, \bar{p}_\rho, \bar{p}_{C_i}), \qquad \bar{p}_\rho = p_\rho(\hat{\rho}, \hat{e}, \hat{C}_i), \quad etc.$$

$$\hat{Q} \equiv (\hat{p}_e, \hat{p}_\rho, \hat{p}_{C_i})$$
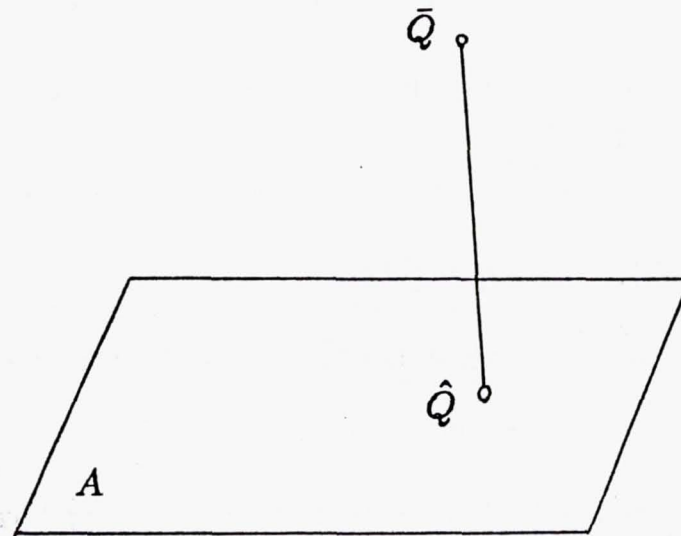
- $(\hat{p}_e, \hat{p}_\rho, \hat{p}_{C_i}) = (\bar{p}_e, \bar{p}_\rho, \bar{p}_{C_i})$ for a calorically perfect gas.

NUMERICAL TEST

- Constituent elements of the present flux-splitting method validated by comparison with exact solutions or experimental data in our previous work on 1-D Euler equations for reacting gases, and 2-D Navier-Stokes equations for ideal gases.

- Direct comparison of the present 2-D reacting flow N-S calculations with experimental data is hindered by the lack of suitable data for high Mach number reacting flows.

Two classes of problems are considered in the following:

(1) shock wave/laminar boundary layer interaction problems.

(2) jet in cross flow problems.

SHOCK WAVE/BOUNDARY LAYER INTERACTION

WALL PRESSURE AND TEMPERATURE

$$M_\infty = 8.0, \quad \beta = 22°, \quad R_e = 1.57 \times 10^6$$
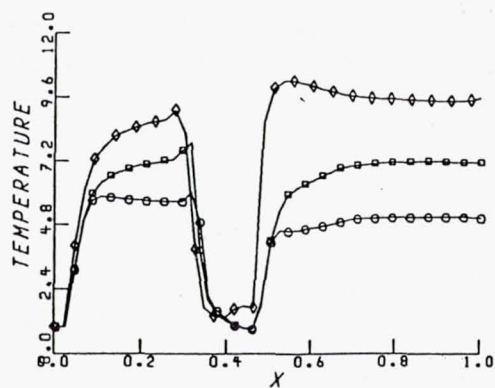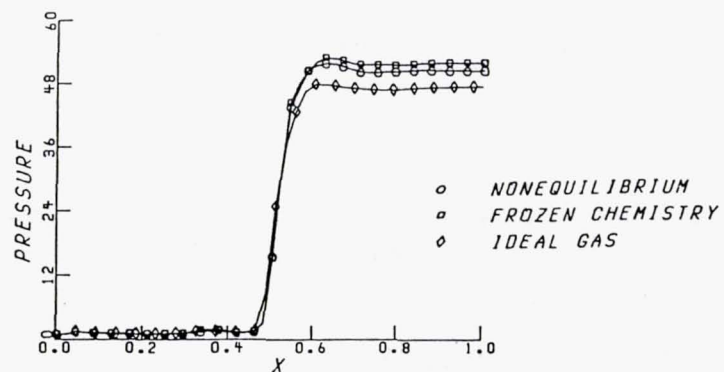
JET-IN-CROSS FLOW

VELOCITY VECTORS AND WALL PRESSURE
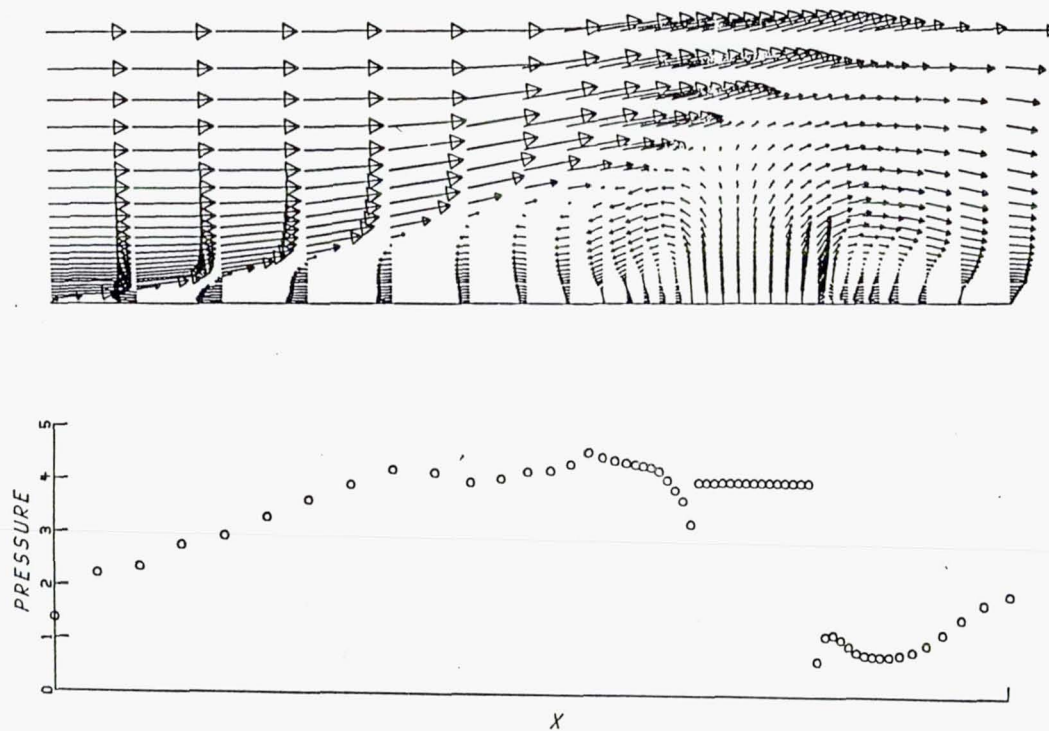
$$M_\infty = 6.0, \quad R_e = 3.21 \times 10^6$$

DUAL JETS-IN-CROSS FLOW

VELOCITY VECTORS AND WALL PRESSURE

$$M_\infty = 6.0, \quad R_e = 3.21 \times 10^6$$
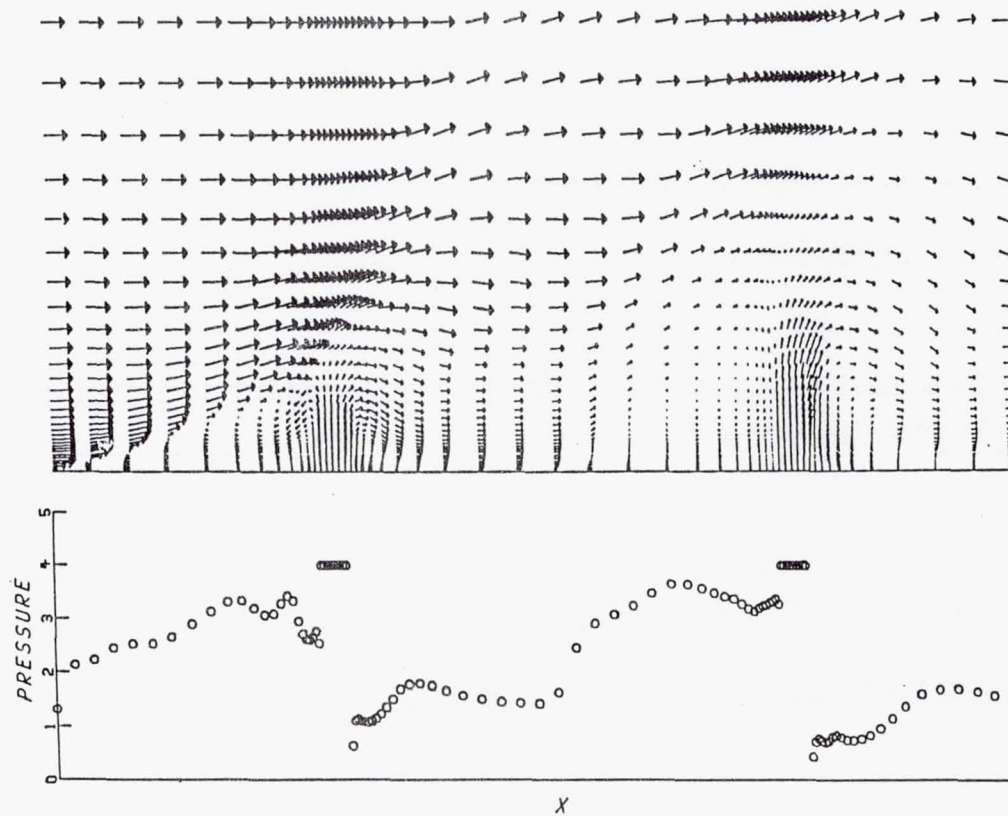
SUMMARY

1. New average state of Roe's splitting for chemical reacting gases is proposed.

2. A numerical method based on Roe flux-splitting for solving the Navier-Stokes and species equations for chemical nonequilibrium gases has been developed.

3. Numerical results show the present method has the potential for calculating high Mach number flows with nonequilibrium chemistry and complex wave structure.

4. Implementation of an implicit time solver is in progress.

5. Thermal nonequilibrium is being considered in the next stage of code development.

6. Work for further code validation is needed.

Visualization of Fluid Dynamics at NASA Ames

Val Watson
NASA Ames Research Center

The hardware and software currently used for visualization of fluid dynamics at NASA Ames is described. The software includes programs to create scenes (for example particle traces representing the flow over an aircraft), programs to interactively view the scenes, and programs to control the creation of video tapes and 16mm movies. The hardware includes high performance graphics workstations, a high speed network, digital video equipment, and film recorders.

With the current workstations, a scientist can interactively view flow over simplified objects, such as the flow over a circular cylinder. For complex objects, such as an aircraft, the workstation creates each picture too slowly to gain a sense of the dynamics of the flow. Therefore, each picture is stored frame by frame on a video tape or 16mm film and then the video or movie is played back at normal speed to illustrate the flow dynamics.

The upgrade in workstations planned for this year is expected to permit moderately complex pictures (pictures that can be represented by 10,000 polygons or less) to be created at a rate of 10 frames per second --- fast enough to gain a sense of the flow dynamics. Therefore, these workstations should permit interactive viewing of the flow over complete aircraft rather than just simple objects. Upgrades planned this year for software should provide a more effective interface for controlling the interactive viewing.

A comparison of the upgrades planned this year with an ideal simulation and visualization environment shows that there is still potential for major improvements in both software and hardware. The greatest potential for improving the environment is the development of software to extract and illustrate the essence of very complex phenomena.

Results presented by other scientists during this conference clearly demonstrate the effectiveness of the current visualization tools for assisting in the understanding of complex simulations, but it is also clear that we are a long way from utilizing visualization tools to their full extent.

<u>Outline</u>

NASA's current visualization tools

Capabilities with the current tools

Upgrades planned for this year

Potential for further improvements

Conclusions

Visualization Hardware

Digital Video System

High Speed

Channel

Supercomputer

Workstation
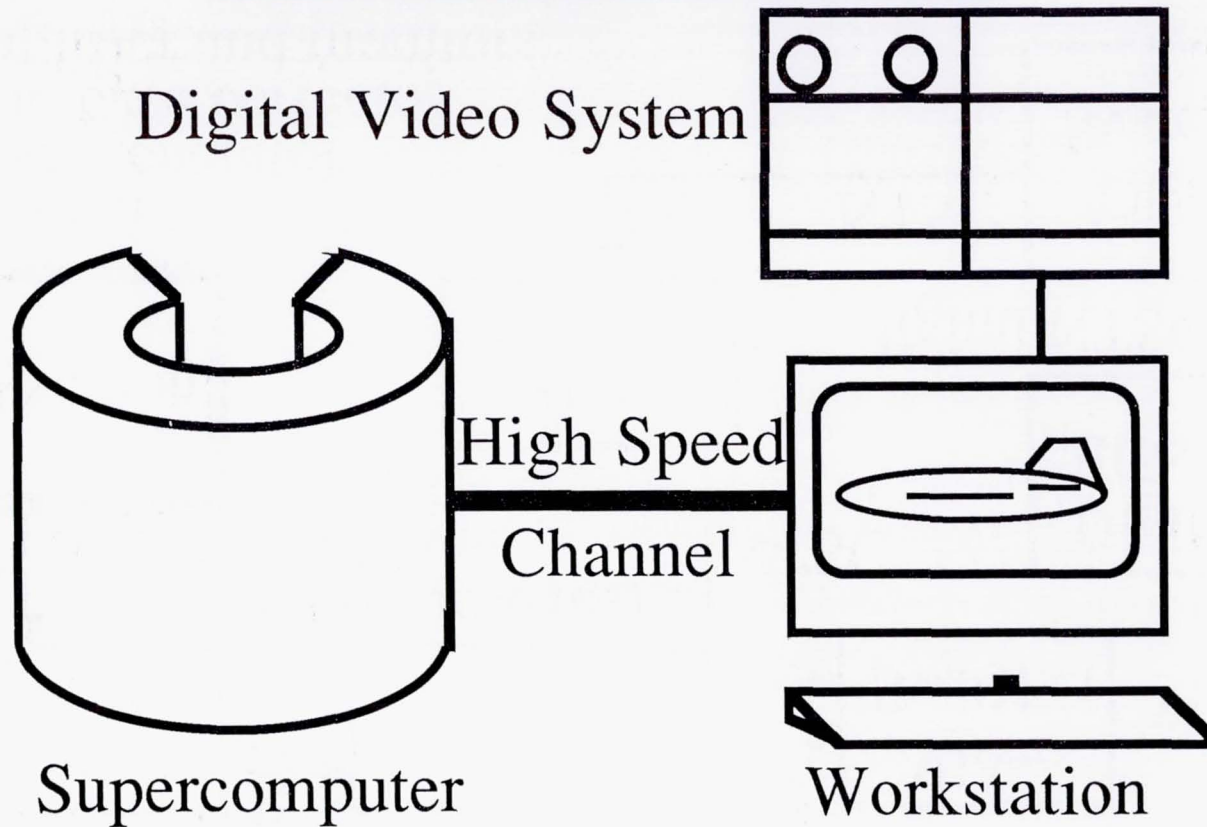
Video Recording System

Scan Converter → R G B → Encoder → NTSC → Video Switcher → NTSC

RS 170 (low res)

R G B high resolution

Workstation

NTSC

Video Recorder

NTSC

Digital Effects

digital NTSC

Disk System

Not shown
Sync. generator
Time base corrector
Amplifier and monitors
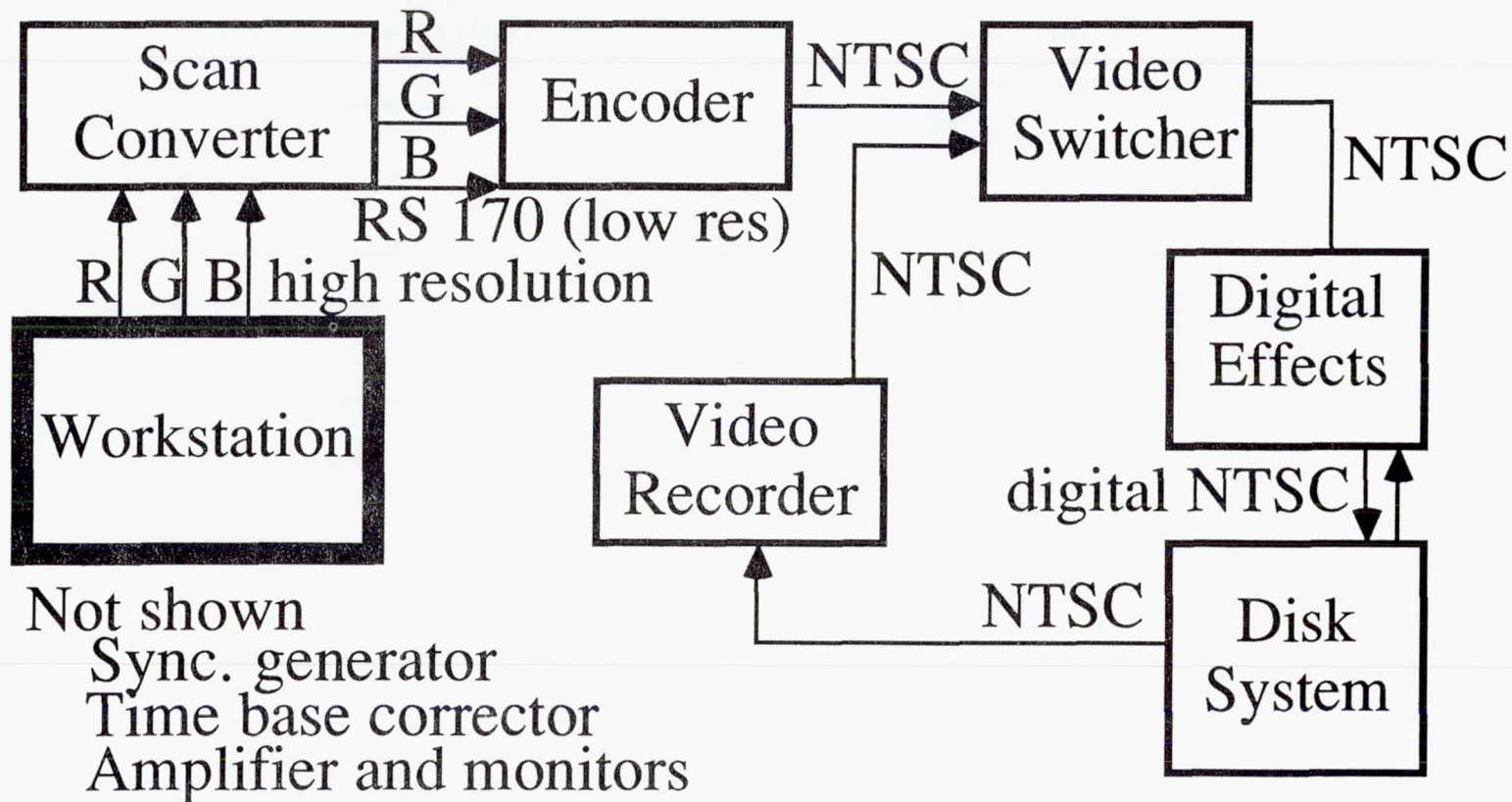
<u>Software</u>

Simulation	Visualization and Recording			
	Scene Creation	Scene Viewing	Animation Sequence Creation	Recording on Film and Video
	← PLOT3D →			
	← SURF →			
	← CPLANE →			
	← RIP →			
	← GAS →			

Current Capabilites in Visualization

Interactive viewing with workstations

    Dynamic illustration of wire frame objects

    Dynamic illustration of simple solid objects

    Static illustration of complex solid objects

Playback viewing with video or film

    Dynamic illustration of complex solid objects

Upgrades in Workstations Planned this Year

Basic Workstation features

  Central processor from 2600 to 2000 Dhrystones
  Arith processor   from 0.1 to 6.0 MFLOPS
  Primary memory   from 4 to 32 MBytes
  Secondary mem.   from 474 to 1000 MBytes

Graphics Features

  3D coord. transf. from 80K to 800K coord./sec
  Solids rendering   from 0.5K to 100K polygons/sec
            (= 10,000 polygons at 10 frames/sec)

Upgrades in Software Planned this Year

Combination of old modules into a single program

Changes to take advantage of new workstations

Changes to make visualization more interactive

Comparison of Current Capabilities with "Ideal" for Vision

Feature	Current	"Ideal"
spatial res.	1 minute of arc	of the same order
color res.	16 million colors	of the same order
freq. resp.	(scene dependent)	15 frames/sec
field of view	1/5 steradian	5 steradians

Comparison of the Ideal vs Current Field of View

Field of view of the human eyes

Field of view of 19" display
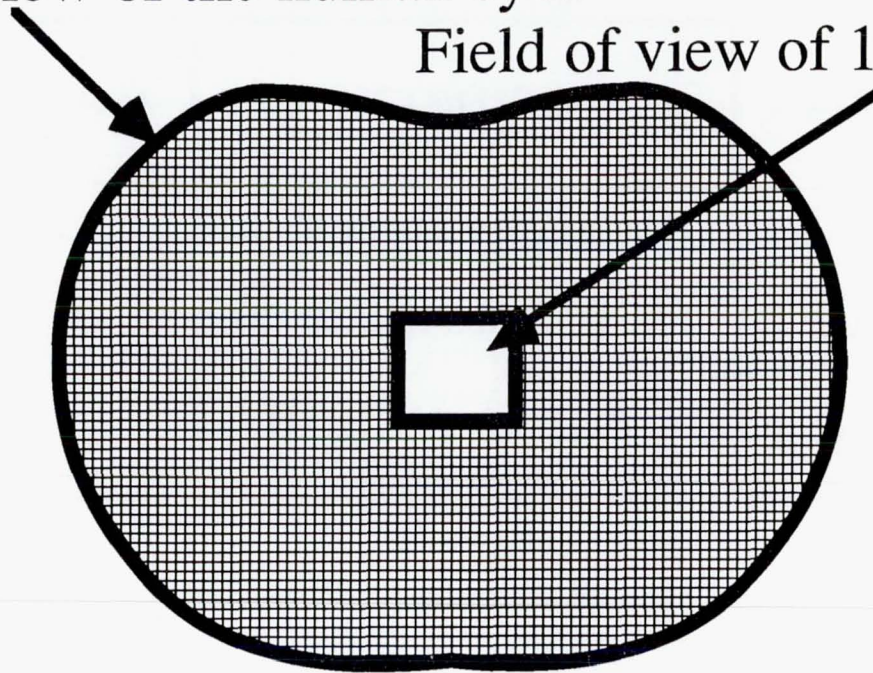
Comparison of Current Capabilities with "Ideal" for Interactive Control

Current

    mouse and keyboard

"Ideal"

    6-degree of freedom control
voice recognition

Potential for Improvements in Software

Tools for extraction of critical features

Tools for highlighting critical features and suppressing less important features

CONCLUSIONS

The NAS decision to invest in visualization tools has been justified by improved analysis capabilities

The most effective use of vis. tools is the *routine* interactive viewing of solutions *and techniques*

Current workstations permit interactive viewing of the flows over simple shapes

Workstations to be procured should permit interactive viewing of flows over complex shapes

CONCLUSIONS (continued)

A new generation of software is being developed
>   to take advantage of new workstation capabilties
>   to make the visual analysis more interactive

The most critical task is overcoming visual clutter
>   developing techniques to extract the "essence"
>   developing techniques to illustrate the "essence"

*We are a long way from utilizing our present
visualization tools completely*

For Further Information

NAS procurement for the new workstations
> Rosemary Buchanan
> Mail Stop 258-6
> NASA Ames Research Center
> Moffett field, CA 94035
> (415) 694-4610

Scientific visualization materials

> Stanford report on automated feature extraction
> 1988 CFD Highlights video
> Stereo slides

>> Pat Mumford Elson
>> Mail Stop 258-2
>> NASA Ames Reseach Center
>> Moffett Field, CA 94035
>> (415) 694-4463

COMPUTATIONAL FLUID DYNAMICS ON A
MASSIVELY PARALLEL COMPUTER

Dennis Jespersen, CFD Branch, NASA/Ames
and
Creon Levit, NAS Applied Research Branch, NASA/Ames

Abstract. We have implemented a finite-difference code for the compressible Navier-Stokes equations on the Connection Machine, a massively parallel computer. The code is based on the ARC2D/ARC3D program and uses the implicit factored algorithm of Beam and Warming. The code uses odd-even elimination to solve linear systems. We give timings and computation rates for the code, and compare with a Cray XMP.

COMPUTATIONAL FLUID DYNAMICS ON A MASSIVELY PARALLEL COMPUTER

Dennis Jespersen, CFD Branch NASA/Ames

and

Creon Levit, NAS Applied Research Branch, NASA/Ames

468

- Goal: implement a real CFD code (ARC2D/ARC3D) on a massively parallel computer, the Connection Machine.
  > Implicit

- Is Connection Machine useful for CFD?

OUTLINE

- CM architecture
- ARC2D
- *Lisp
- Odd-even elimination
- Current status and results
- Problems and prospects

CM ARCHITECTURE

- Very large number of physical processors (up to 64K)
- SIMD
- Single-bit processors
- 2K words (32 bits each) memory per processor
- Floating point accelerator available
- Context bit (each processor on or off)
- Peak performance (computational kernels) 2–4 Gflops

CONNECTIONS

- 16 processors per chip
- Chips wired in 12-dimensional hypercube
  - > If distance=power of 2, communication in 2 hops
- General router
- Nearest-neighbor (NEWS) available and fast
  - > (Reminiscent of ILLIAC)
- Wrap-around at edges

VIRTUAL PROCESSORS

- Each physical processor can be configured as $1, 2, 4, 8, \ldots$ virtual processors.

VP ratio	1	2	4	8	16	32	64
memory/processor (words)	2K	1K	512	256	128	64	32

- Transparent to user.
- Arithmetic slows down (slightly slower than linear)
- Communication relatively faster
  > Memory references that were off-chip may become on-chip.

ARC2D

- 2D Compressible Navier-Stokes

$$\partial_t Q + \partial_\xi E + \partial_\eta F = \text{Re}^{-1}(\partial_\xi E_v + \partial_\eta F_v)$$

- Central space differencing, implicit Euler in time, factored, delta form:

$$(I + \Delta t \delta_\xi A^n - \Delta t \frac{1}{\text{Re}} \delta_\xi R^n)(I + \Delta t \delta_\eta B^n - \Delta t \frac{1}{\text{Re}} \delta_\eta S^n)\Delta Q^n$$

$$= -\Delta t(\delta_\xi E^n + \delta_\eta F^n - \frac{1}{\text{Re}}(\delta_\xi E_v^n + \delta_\eta F_v^n))$$

- Pulliam-Chaussee diagonal form:

$$T_\xi(I + \Delta t \delta_\xi \Lambda_\xi - \Delta t \frac{1}{\text{Re}} \delta_\xi \Lambda_{\xi,v})$$

$$N(I + \Delta t \delta_\eta \Lambda_\eta - \Delta t \frac{1}{\text{Re}} \delta_\eta \Lambda_{\eta,v})T_\xi^{-1}\Delta Q^n = \text{rhs}$$

ARC2D on CM

- One grid point per (virtual) processor.
- Write in *Lisp
    > No line-by-line translation
- Shear-layer
- Cylinder
- Typical size 128×64 (8K processors, VP ratio $= 1$)
- CM well-suited for explicit time-step methods (e.g., Runge-Kutta)

IMPLICIT SOLVER: ODD-EVEN ELIMINATION

- Closely related to cyclic reduction
- One row corresponds to one processor
- Communication is always to processors 2^k distant
- $2^n \times 2^n$ system solvable in n stages
- Algorithm makes no sense on uniprocessor machines
- Stability not a problem in practice
  > Some stability results provable, e.g. $B(-\Delta t, 1, \Delta t)$

ODD-EVEN ELIMINATION: ALGORITHM

$$Ax = y$$

For $k = 0, 1, \ldots, \log_2 n - 1,$

$$
\begin{pmatrix}
b_1 & c_1 & & & & \\
a_2 & b_2 & c_2 & & & \\
& \ddots & \ddots & \ddots & & \\
& & a_{n-1} & b_{n-1} & c_{n-1} \\
& & & a_n & b_n
\end{pmatrix}
$$

$$m = 2^k$$

$$a_i \leftarrow a_i / b_i$$

$$c_i \leftarrow c_i / b_i$$

$$y_i \leftarrow y_i / b_i$$

$$b_i \leftarrow 1 - a_i c_{i-m} - c_i a_{i+m}$$

$$y_i \leftarrow y_i - a_i y_{i-m} - c_i y_{i+m}$$

$$a_i \leftarrow -a_i a_{i-m}$$

$$c_i \leftarrow -c_i c_{i+m}$$

ODD-EVEN ELIMINATION:PERIODIC

- Same code
- Same cost
- Periodic solves no more costly than nonperiodic solves

PROGRESS

- 2D Explicit (Runge-Kutta)
- 2D Implicit (scalar and block tridiagonal)
  - > Shear layer
  - > Cylinder (low Re)
- 3D Explicit (Runge-Kutta)

TIMINGS

- Timings, Mflop rates (16k processors, implicit scalar tridiagonal algorithm)

Grid size	VP ratio	Mflops	sec/step	XMP time/CM time
128×128	1	58	0.43	0.66
256×128	2	86	0.60	0.75
512×512	16	106	4.2	0.86

- Timings, Mflop rates (16k processors, explicit algorithm)

Grid size	VP ratio	Mflops	sec/step	XMP time/CM time
128×128	1	63	0.43	0.69
256×128	2	123	0.44	1.34
512×512	16	241	1.8	2.62

TIMINGS: 2D BLOCK IMPLICIT AND 3D

- 2D Timings, 16k processors, block tridiagonal algorithm

Grid size	VP ratio	sec/step	XMP time/CM time
128 × 128	1	2.61	0.23
256 × 128	2	3.21	0.37
256 × 256	4	4.84	0.49
512 × 256	8	9.66	0.49

- 3D Timings, 8k processors, explicit algorithm

Grid size	VP ratio	sec/step
32 × 32 × 16	2	1.94
64 × 32 × 32	8	3.80
64 × 64 × 32	16	6.53

PROBLEMS AND PROSPECTS

- Memory limitation
- Communication bottleneck?
- Boundary conditions
  - > Complicated boundary conditions – inefficient?
- Future plans:
  - > 3D Implicit

SESSION XII

HYPERSONICS/AFE

Chairman:
Chien P. Li
Advanced Programs Office
NASA Johnson Space Center

Conservation Equations and Physical Models for Hypersonic Air Flows Over the Aeroassist Flight Experiment Vehicle

Peter A. Gnoffo

NASA Langley Research Center
Hampton, VA 23665
Mail Stop 366

Abstract

The code development and application program for the Langley Aerothermodynamic Upwind Relaxation Algorithm (LAURA), with emphasis directed toward support of the Aeroassist Flight Experiment (AFE) in the near term and Aeroassisted Space Transfer Vehicle (ASTV) design in the long term is reviewed. LAURA is an upwind-biased, point-implicit relaxation algorithm for obtaining the numerical solution to the governing equations for three-dimensional, viscous, hypersonic flows in chemical and thermal nonequilibrium. The algorithm is derived using a finite-volume formulation in which the inviscid components of flux across cell walls are described with Roe's averaging and Harten's entropy fix with second-order corrections based on Yee's Symmetric Total Variation Diminishing scheme. Because of the point-implicit relaxation strategy, the algorithm remains stable at large Courant numbers without the necessity of solving large, block tri-diagonal systems. A single relaxation step depends only on information from nearest neighbors. Predictions for pressure distributions, surface heating, and aerodynamic coefficients compare well with experimental data for Mach 10 flow over an AFE wind tunnel model. Predictions for the hypersonic flow of air in chemical and thermal nonequilibrium (velocity = 8917 m/s, altitude = 78 km.) over the full scale AFE configuration obtained on a multi-domain grid are discussed.

SIMULATION CAPABILITIES
PROGRAM LAURA (LANGLEY AEROTHERMODYNAMIC UPWIND RELAXATION ALGORITHM)

I. PHYSICS
Navier -Stokes Or Thin-Layer Navier-Stokes Equations

Steady Or Unsteady

Laminar (Turbulent Boundary Layer)

Chemical Nonequilibrium (11 Species, 2 Chemical Kinetic Models)

Thermal Nonequilibrium (Two-Temperature Model)

Documented In NASA TP 2867

II. NUMERICS
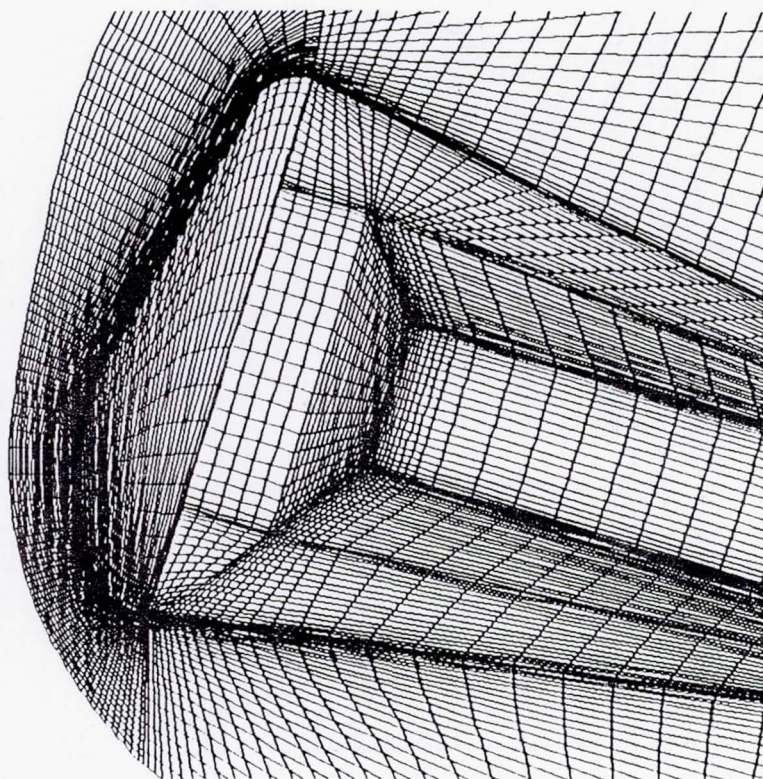Finite Volume, Roe's Averaging, STVD Limiters

Fluid Mechanics And Chemistry Strongly Coupled

Point Implicit Relaxation, Freeze Inverse Jacobian

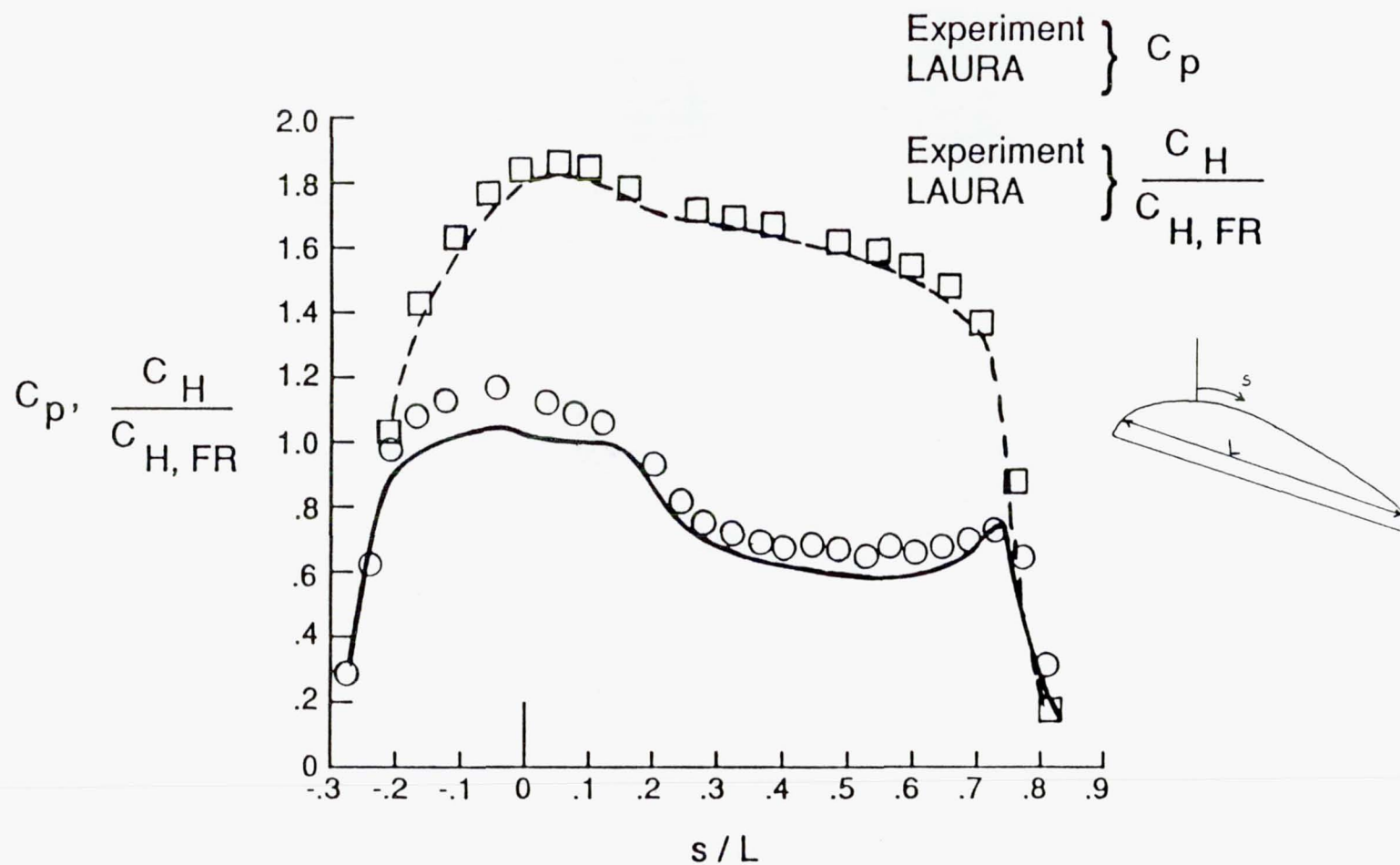Multi-Domain Capability, Structured Grids

Ideally Suited For Parallel, Asynchronous Iteration Using Unstructured Grids

COMPUTATIONAL GRID ON SURFACE AND PLANE
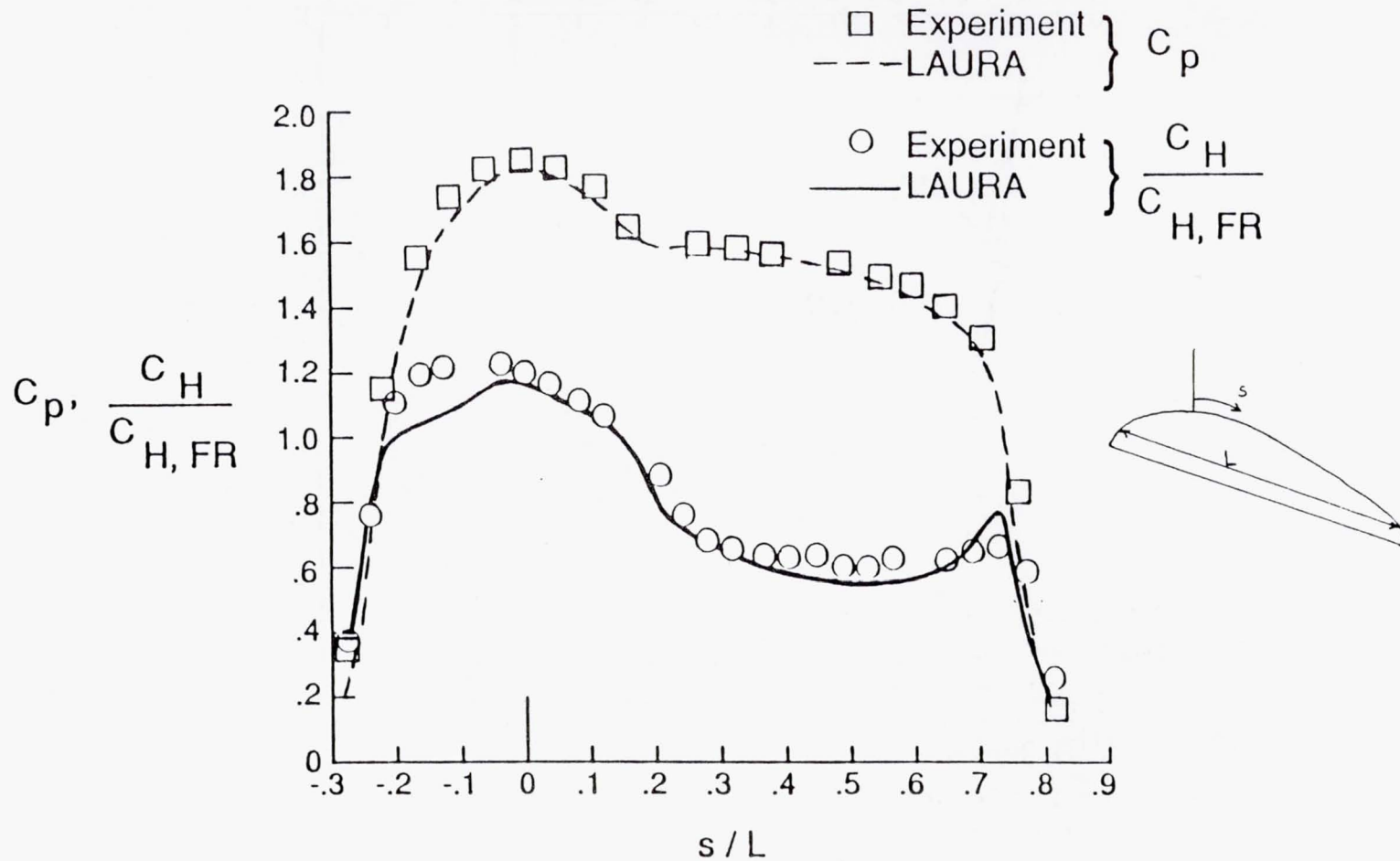OF SYMMETRY FOR AFE WIND TUNNEL MODEL

PRESSURE AND HEATING DISTRIBUTION FOR AFE
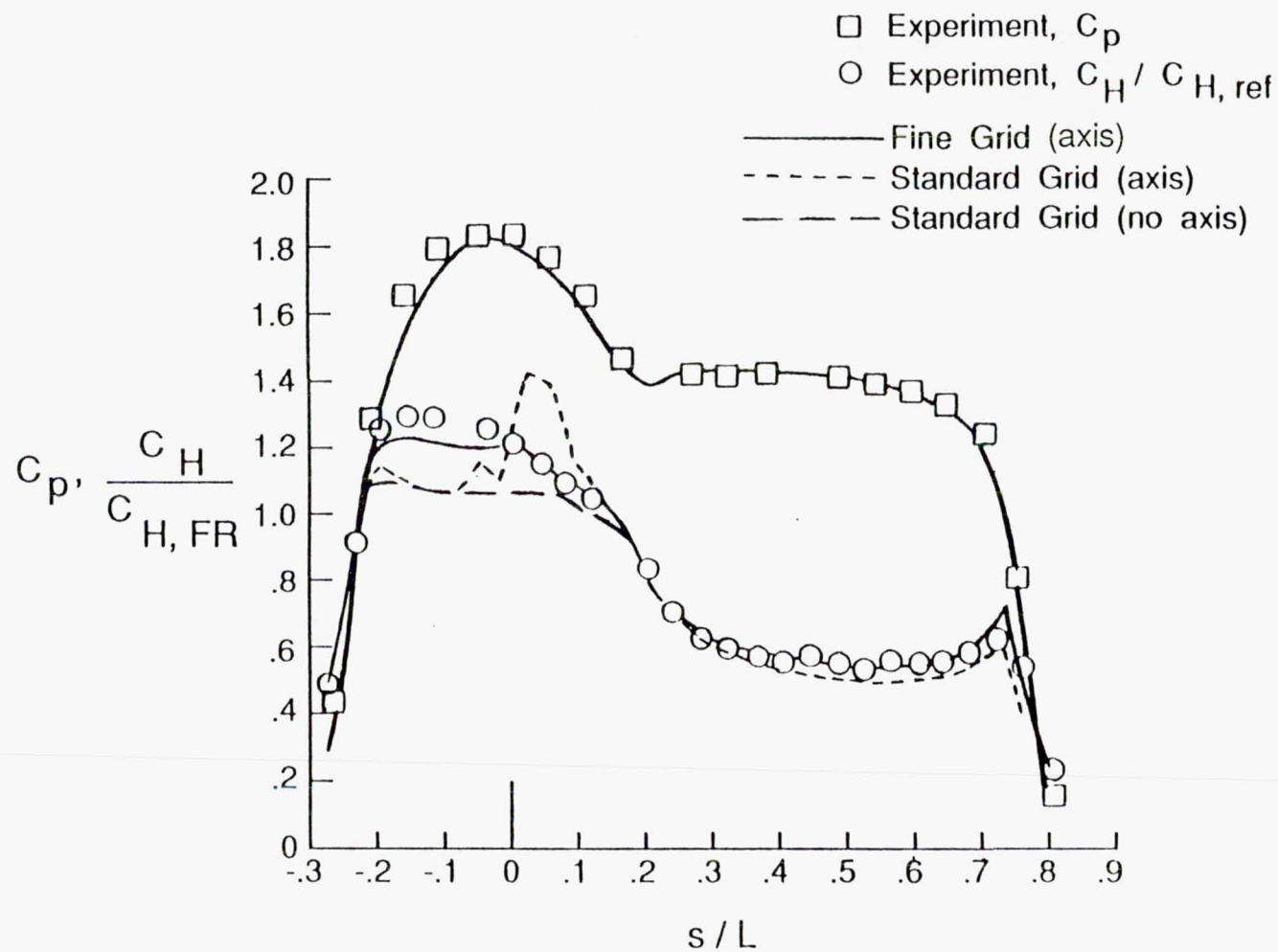Mach 10 $\alpha = 5^o$

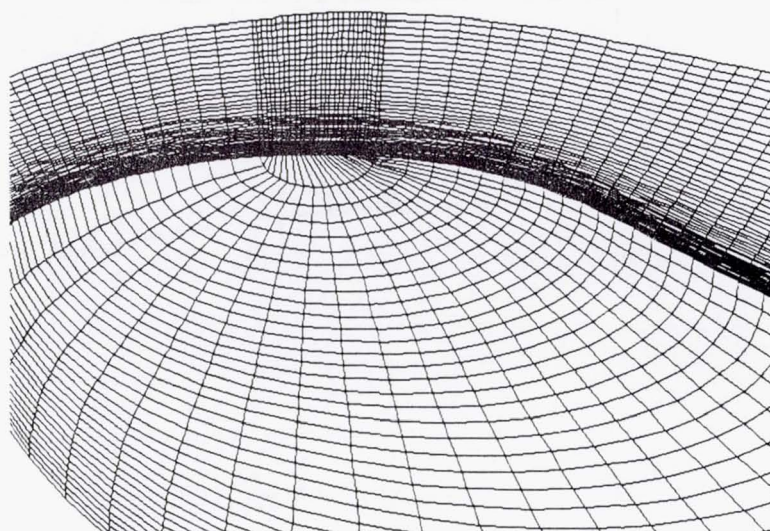PRESSURE AND HEATING DISTRIBUTION FOR AFE
Mach 10 $\alpha = 0^{o}$

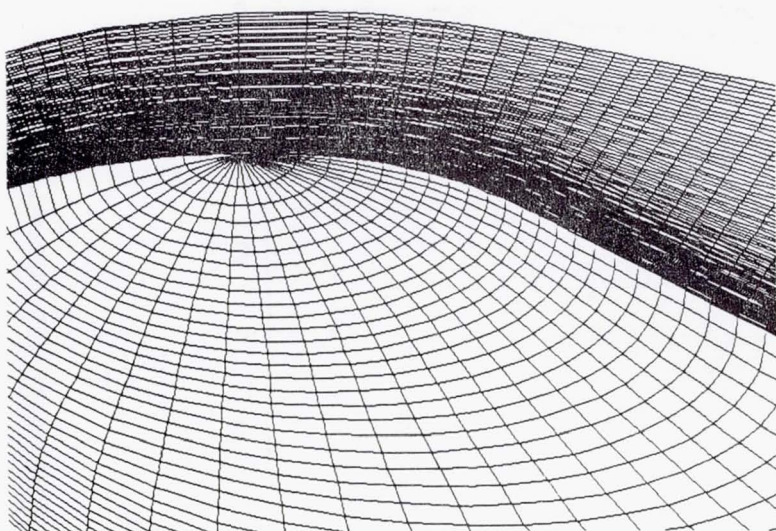PRESSURE AND HEATING DISTRIBUTION FOR AFE
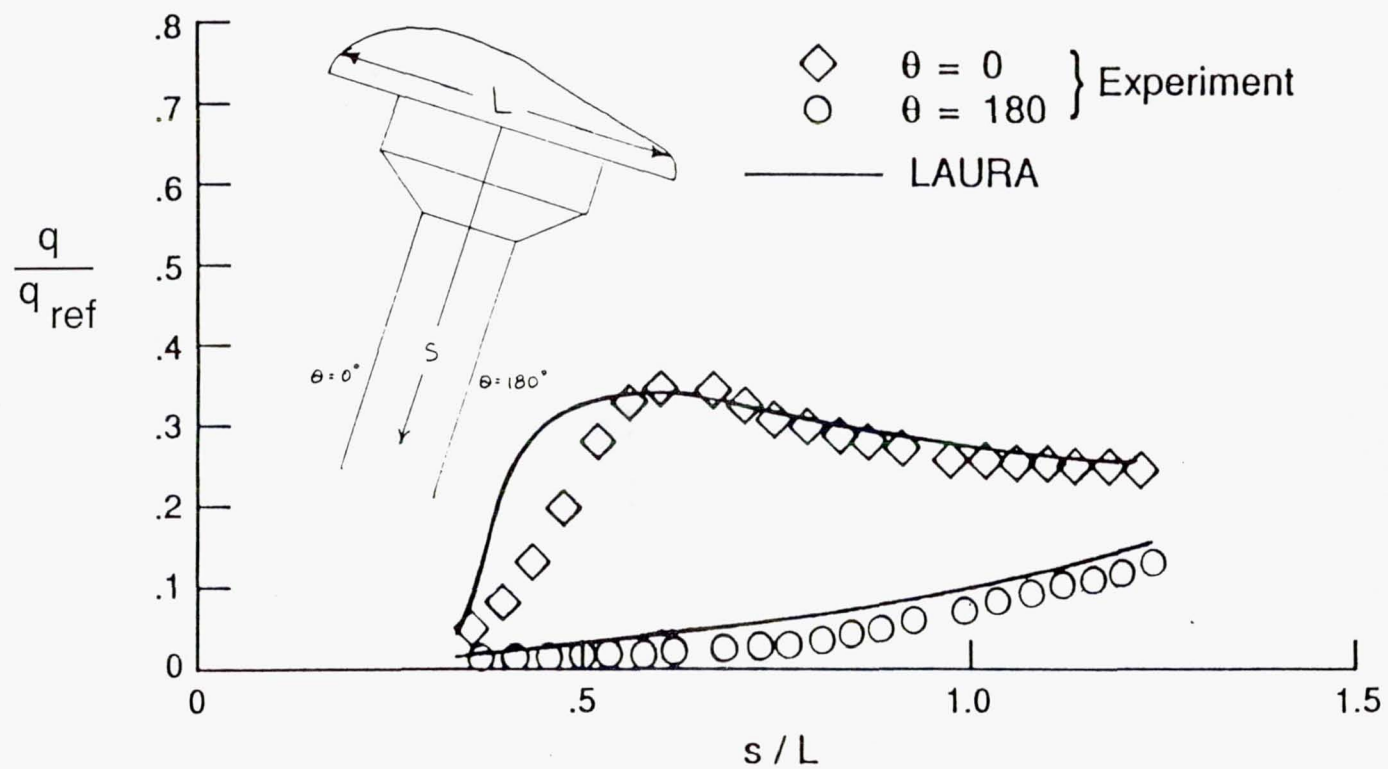
Mach 10 $\alpha = -5^{\circ}$

□ Experiment, C_p
○ Experiment, $C_H / C_{H, ref}$

——— Fine Grid (axis)
- - - - - Standard Grid (axis)
— — — Standard Grid (no axis)

C_p, $\dfrac{C_H}{C_{H, FR}}$

s / L
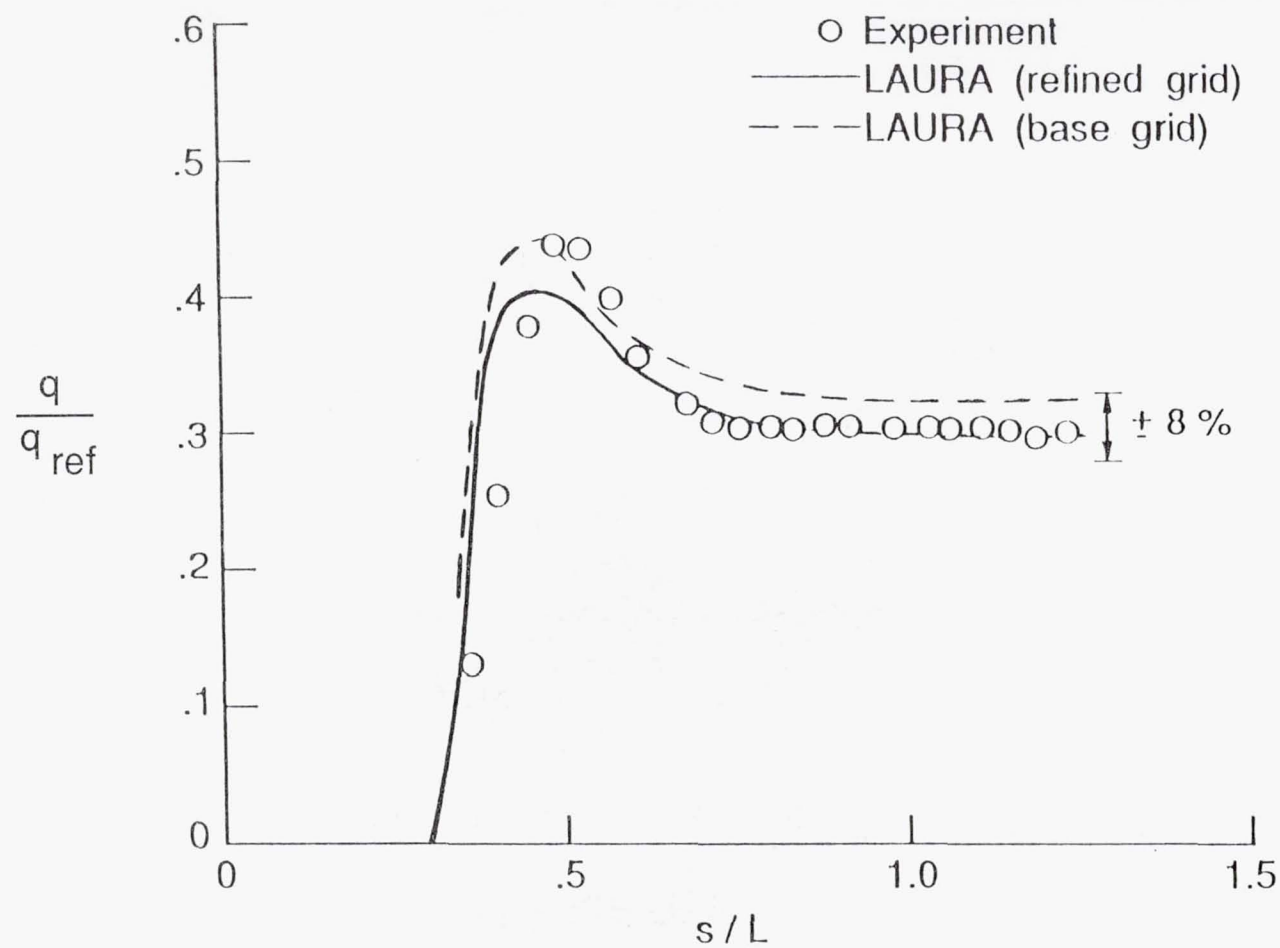
DETAIL OF AXIS AND N0 AXIS GRIDS

HEATING DISTRIBUTIONS FOR AFE STING
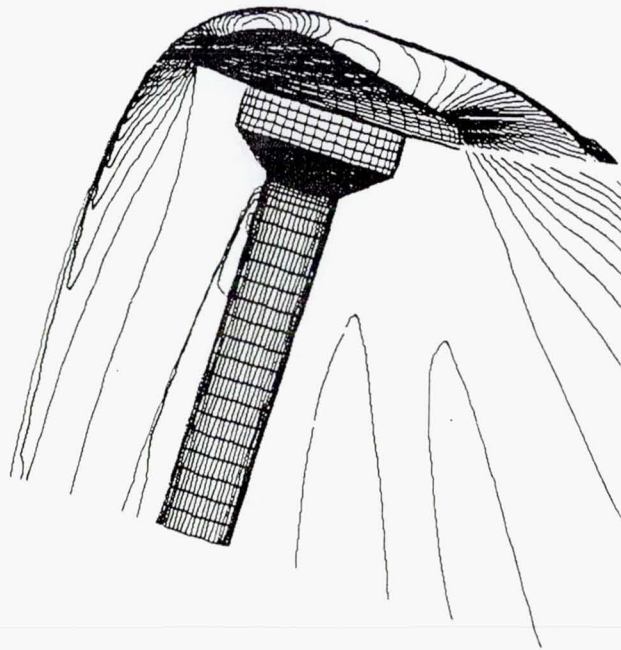## Mach 10 $\quad \alpha = 0^{\circ}$

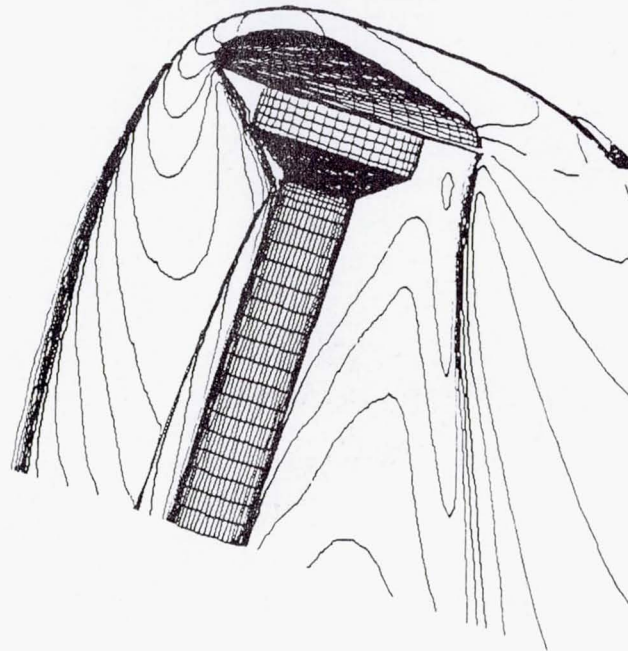# HEATING DISTRIBUTIONS FOR AFE STING

Mach 10 $\alpha = -5^{\circ}$

PRESSURE CONTOURS IN THE PLANE OF SYMMETRY

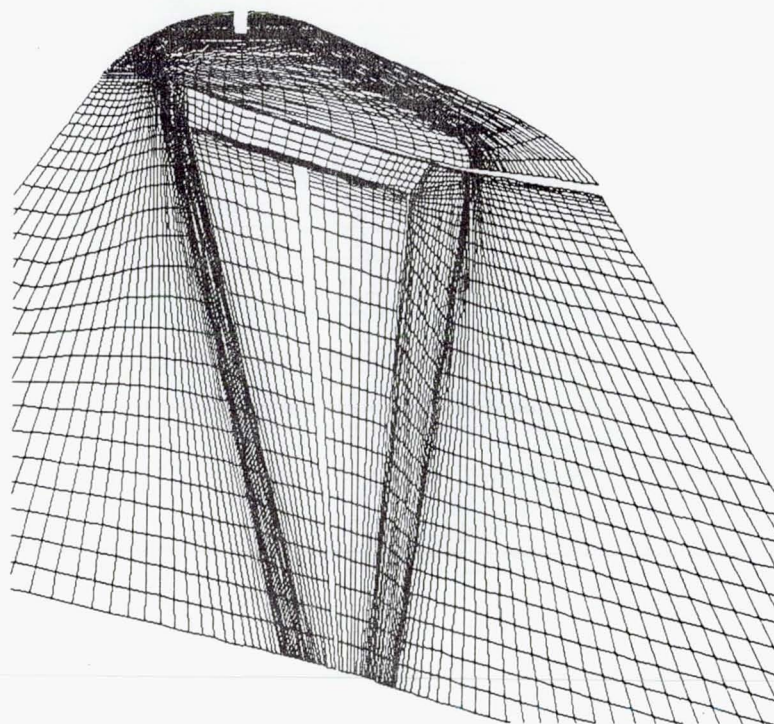## $M_\infty = 10$ $\alpha = -5^\circ$

MACH NUMBER CONTOURS IN THE PLANE OF SYMMETRY

$$M_\infty = 10 \qquad \alpha = -5^\circ$$

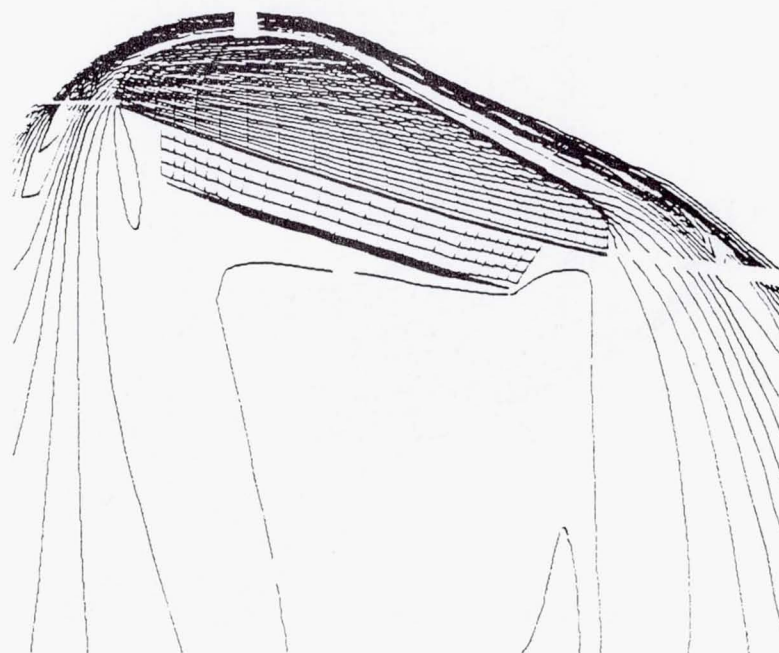# COMPUTATIONAL GRID ON SURFACE AND
PLANE OF SYMMETRY FOR AFE

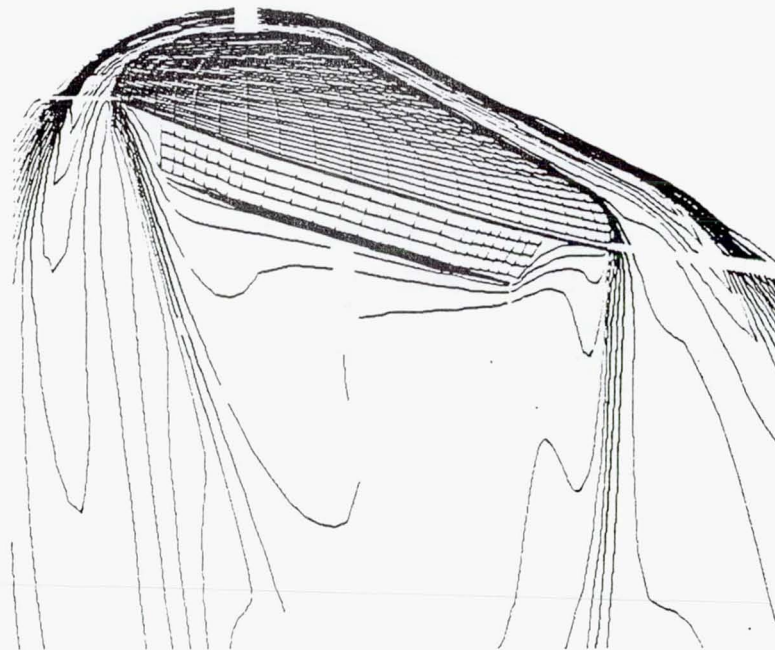# TRANSLATIONAL TEMPERATURE CONTOURS
IN THE PLANE OF SYMMETRY

$$M_\infty = 32 \qquad h = 78 \text{ km}$$

VIBRATIONAL TEMPERATURE CONTOURS
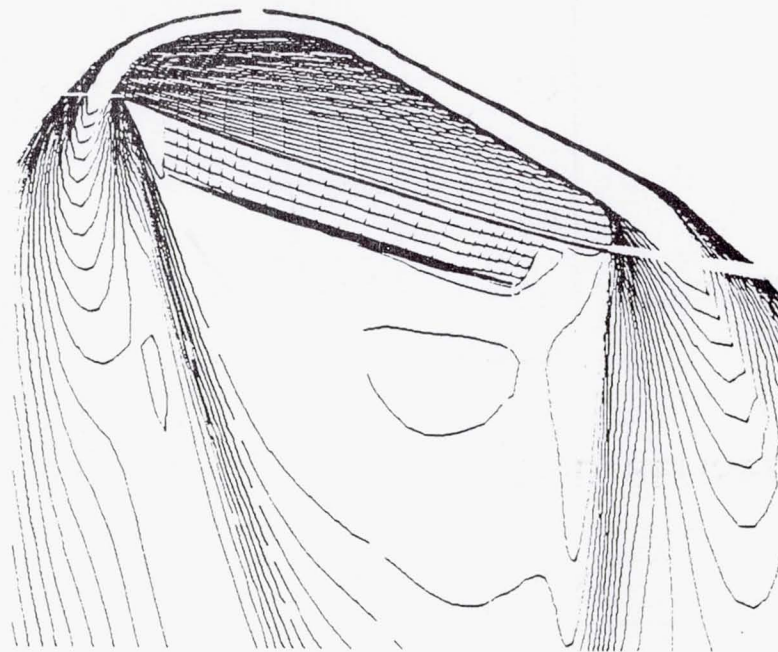IN THE PLANE OF SYMMETRY

$M_\infty = 32 \qquad h = 78$ km

ELECTRON NUMBER DENSITY CONTOURS
IN THE PLANE OF SYMMETRY

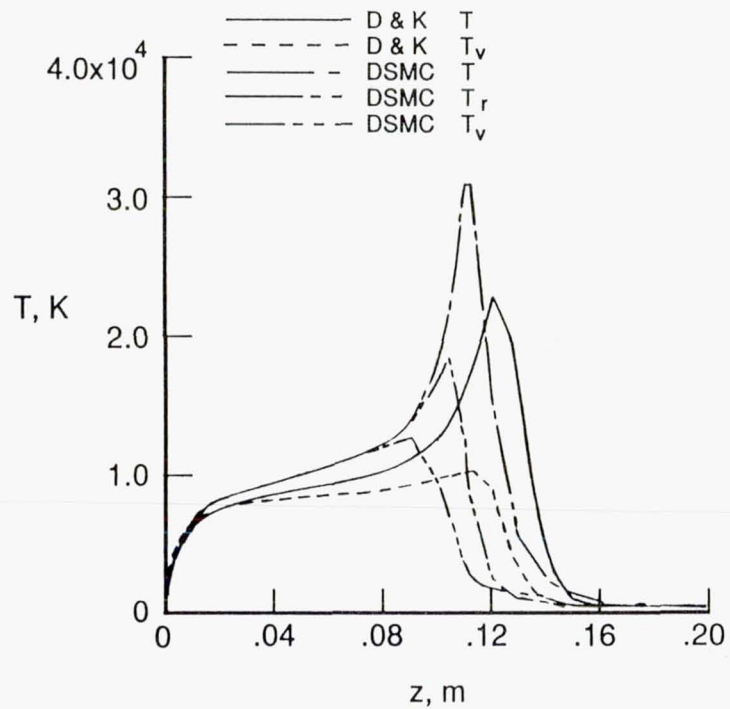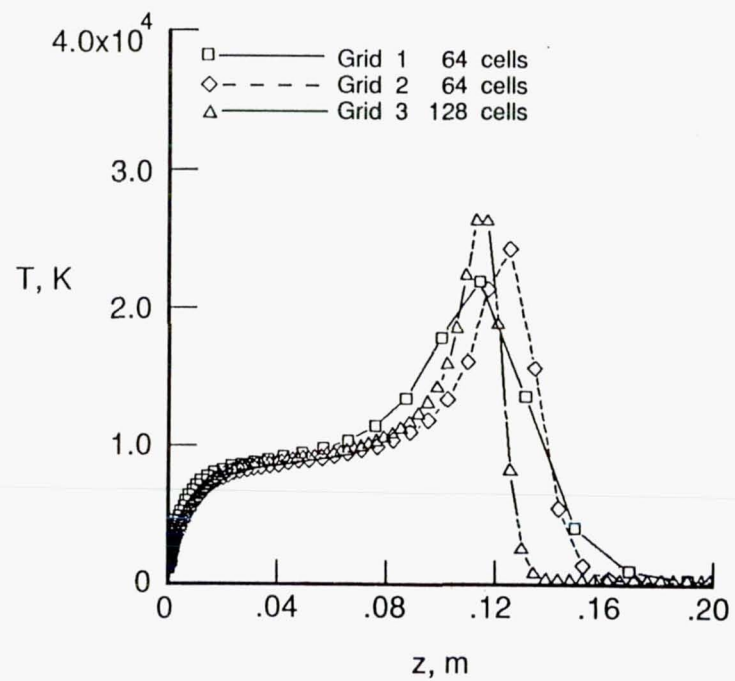$M_\infty = 32$ $h = 78$ km

TEMPERATURE DISTRIBUTION ACROSS THE
SHOCK LAYER

COMPARISON TO DSMC

GRID REFINEMENT STUDY

THE COMPUTATION OF THERMO-CHEMICAL
NONEQUILIBRIUM HYPERSONIC FLOWS

Graham Candler

Aerothermodynamics Branch

MS 230-2, 415-694-4227

NASA Ames Research Center

Moffett Field, CA   94035

Several conceptual designs for vehicles that would fly in the atmosphere at hypersonic speeds have been developed recently. For the proposed flight conditions the air in the shock layer that envelops the body is at a sufficiently high temperature to cause chemical reaction, vibrational excitation, and ionization. However, these processes occur at finite rates which, when coupled with large convection speeds, cause the gas to be removed from thermo-chemical equilibrium. This non-ideal behavior affects the aerothermal loading on the vehicle and has ramifications in its design.

A numerical method to solve the equations that describe these types of flows in two dimensions has been developed. The state of the gas is represented with seven chemical species, a separate vibrational temperature for each diatomic species, an electron translational temperature, and a mass-averaged translational-rotational temperature for the heavy-particles. The equations for this gas model are solved numerically in a fully coupled fashion using an implicit finite volume time-marching technique. Gauss-Seidel line-relaxation is used to reduce the cost of the solution and flux-dependent differencing is employed to maintain stability.

The numerical method has been tested against several experiments. The calculated bow shock wave detachment on a sphere and two cones was compared to those measured in ground testing facilities. The computed peak electron number density on a sphere-cone was compared to that measured in a flight test. In each case the results from the numerical method were in excellent agreement with experiment. The technique has been used to predict the aerothermal loads on an Aeroassisted Orbital Transfer Vehicle including radiative heating. These results indicate that the current physical model of high temperature air is appropriate and that the numerical algorithm is capable of treating this class of flows.

Research Objectives

- Study flows with thermo-chemical nonequilibrium

  - multiple temperatures: $T \neq T_v \neq T_e$

  - chemical state not in equilibrium at local e, ρ

- Primary application to blunt re-entry vehicles in air

  - other nonequilibrium problems are possible, *e.g.* NASP

  - could be used with other gases, *e.g.* $H_2 - Air$

  - steady-state

  - two-dimensional or axisymmetric

  - laminar

- Demonstrate feasibility of numerical solutions to reacting flows

  - stiff equations

  - large source terms

Justifications

- Proposed hypersonic vehicles:

    - AOTV/AFE

    - NASP

    - Mission to Mars

- Ground-based testing is difficult

- Nonequilibrium effects important:

    - force coefficients

    - convective and radiative heating

- Study high-temperature air physics:

    - effects of thermo-chemical nonequilibrium

    - develop new modeling techniques

Technical Approach – Thermodynamic Model

- Translational-rotational equilibrium assumed

- One vibrational temperature for each diatomic species

- Electron-electronic temperature

    o free-electron and electronic temperatures equal

- Model finite-rate energy transfer modes

Technical Approach – Conservation Equations

- Governing equations in two dimensions:

$$\frac{\partial U}{\partial t} + \frac{\partial F}{\partial x} + \frac{\partial G}{\partial y} = W$$

- For a gas with n species, m diatomic:

$$U = \left(\rho_1, \ \rho_2, \ \ldots, \ \rho_n, \ \rho u, \ \rho v, \ E_{v_1}, \ \ldots, \ E_{v_m}, \ E_e, \ E\right)^T$$

Technical Approach – Equations of State

- Pressure and temperature:

$$T = \frac{1}{\rho c_v} \left(E - \sum_{s=1}^{m} E_{v_s} - E_e - \frac{1}{2}\rho(u^2 + v^2) - \sum_{s=1}^{n} \rho_s h_s^\circ - \sum_{s \neq e}^{n} \rho_s e_{\mathrm{el}\,s} \right),$$

$$p = \sum_{s \neq e}^{n} \frac{\rho_s}{M_s} RT + p_e, \qquad c_v = \sum_{s \neq e}^{n} \frac{\rho_s}{\rho} c_{v_s}.$$

- Electron pressure and temperature:

$$T_e = \frac{1}{\rho_e c_{ve}} \left(E_e - \frac{1}{2}\rho_e(u^2 + v^2) \right), \qquad p_e = \rho_e \frac{R}{M_e} T_e.$$
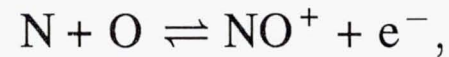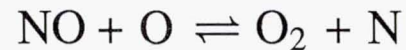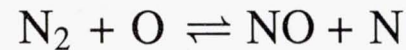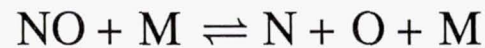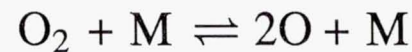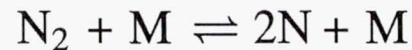
- Vibrational temperature:

$$E_{v_s} = \rho_s \frac{R}{M_s} \frac{\theta_{vs}}{e^{\theta_{vs}/T_{vs}} - 1}.$$

Technical Approach – Chemical Model

- Air is modeled with seven species:

$$N_2, \ O_2, \ NO, \ NO^+, \ N, \ O, \ \text{and} \ e^-.$$

- Possible reactions:

$$N_2 + M \rightleftharpoons 2N + M$$
$$O_2 + M \rightleftharpoons 2O + M$$
$$NO + M \rightleftharpoons N + O + M$$
$$N_2 + O \rightleftharpoons NO + N$$
$$NO + O \rightleftharpoons O_2 + N$$
$$N + O \rightleftharpoons NO^+ + e^-,$$

  - use two-temperature reaction rate (TT_v) model of Park

Technical Approach – Numerical Algorithm _____

- Equations solved in fully coupled fashion:

    - nonequilibrium directly influences solution

- Gauss-Seidel line-relaxation technique of MacCormack (1985)

- Fully implicit:

    - large time steps for rapid convergence

    - rapid reactions do not slow convergence appreciably

    - many computations required per time step

- Gauss-Seidel line-relaxation reduces cost of implicit method

- Flux-splitting:

    - stability in subsonic and supersonic regions

    - capture bow shock wave
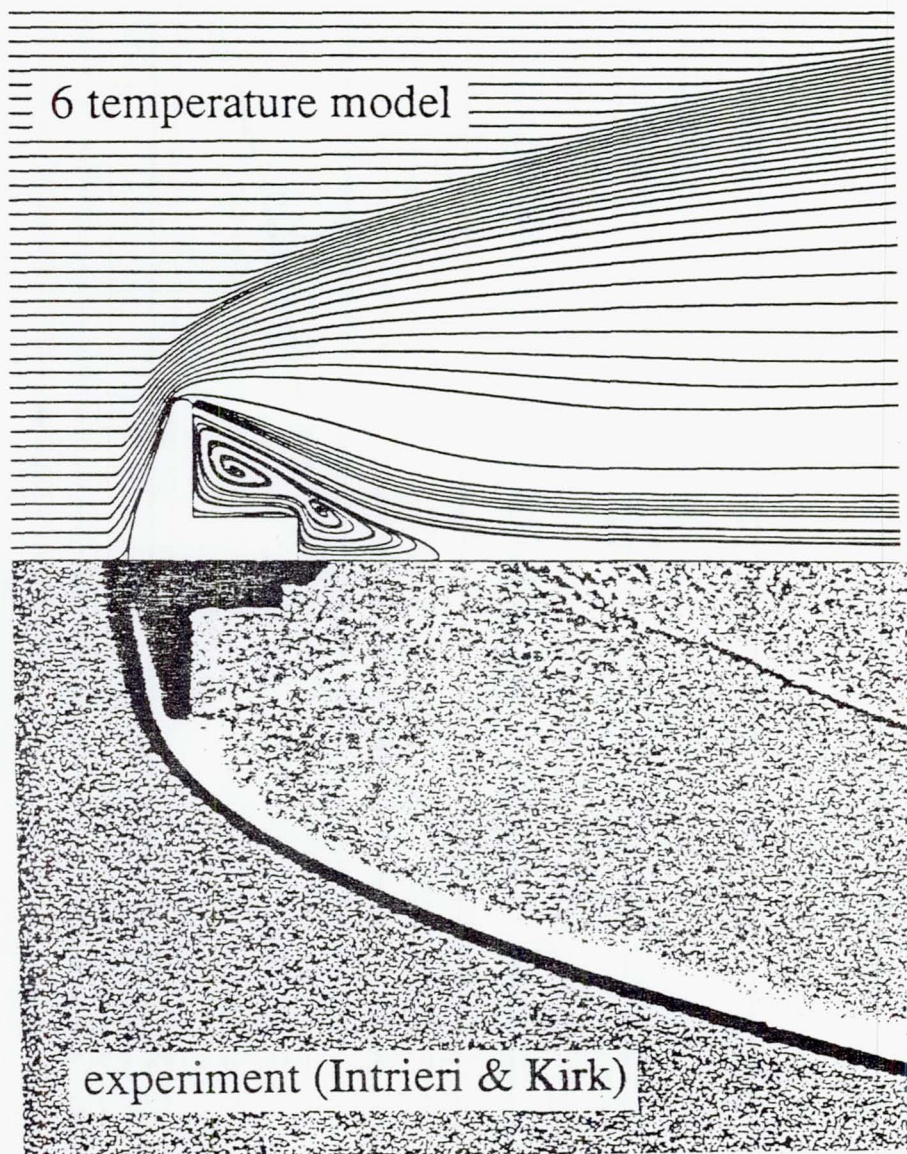
Validation – Peak Electon Number Density

- Sphere–9° Cone in air. $u_\infty = 7.65\,\mathrm{km/s}$, $\mathcal{M}=25.9$, $Re = 6280$.
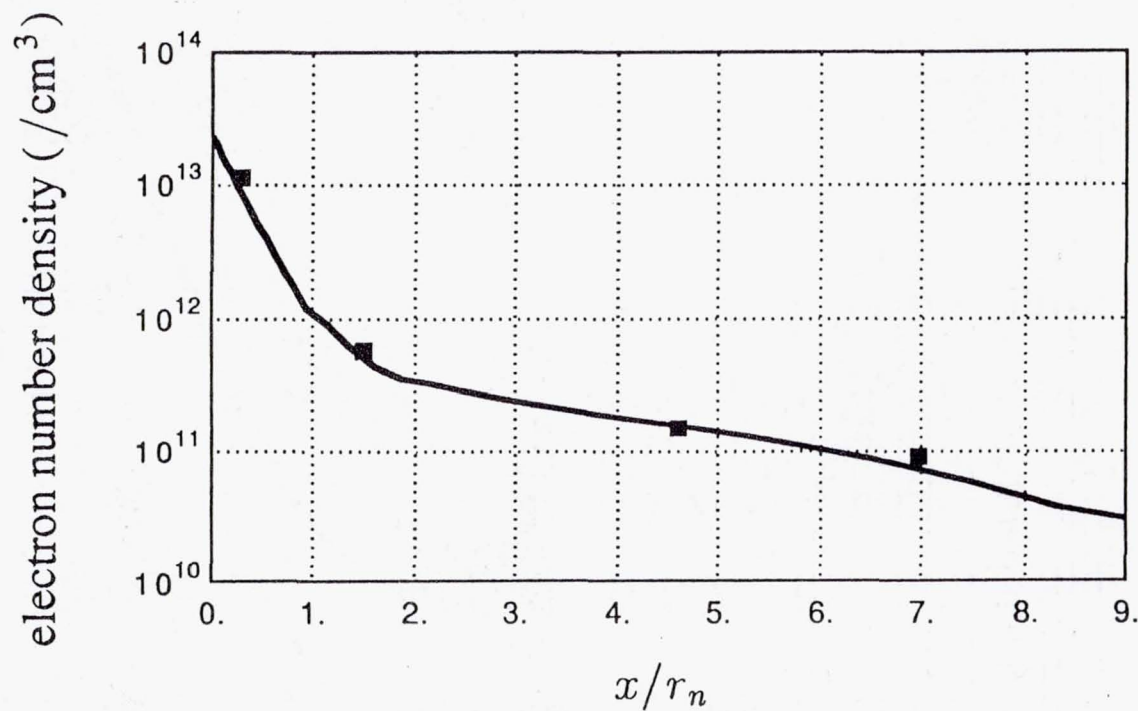
Results – Axisymmetric AOTV

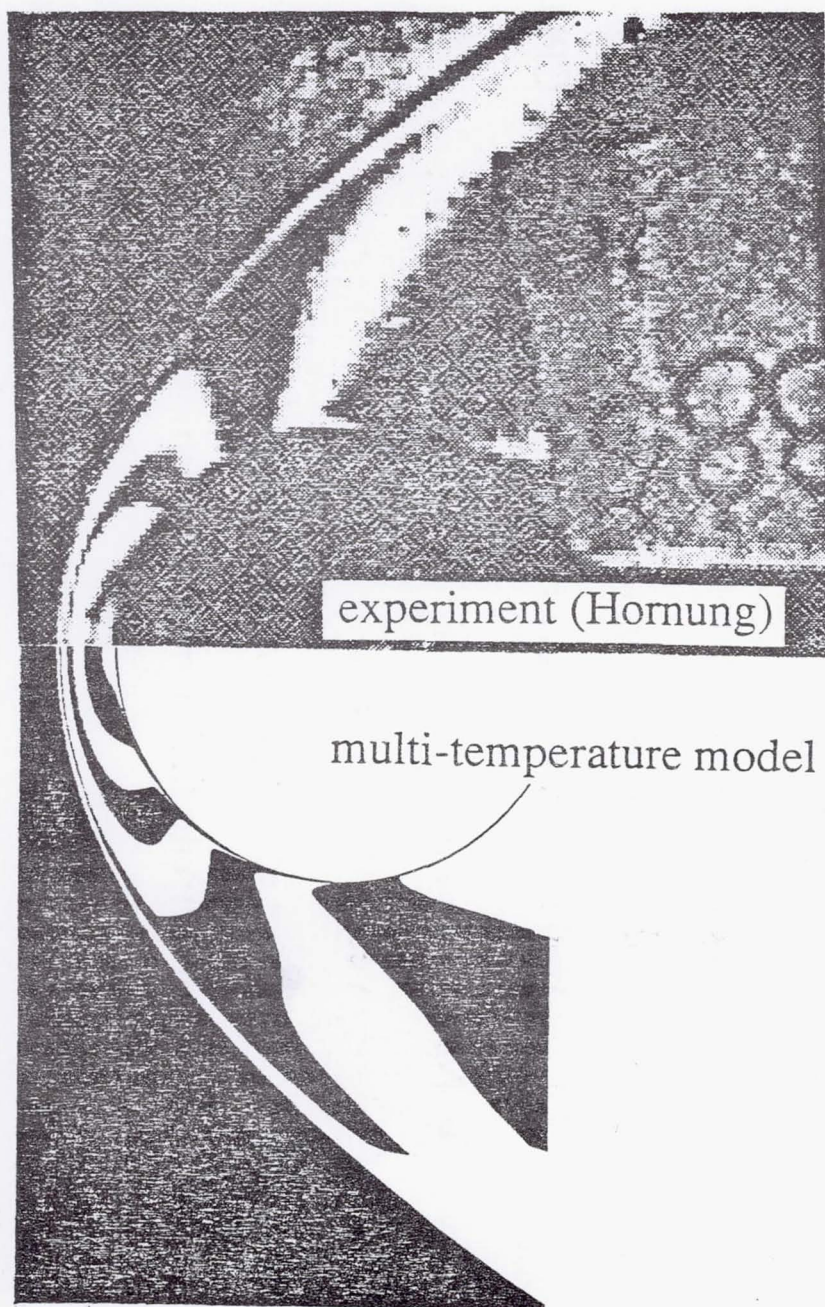- Shadowgraph of an axisymmetric AOTV model in air.
  $u_\infty = 4.02 \, \text{km/s}, \, \mathcal{M}_\infty = 11.6, \, Re = 343000, \, \psi = 180.$

6 temperature model

experiment (Intrieri & Kirk)

Results – Cylinder

- Interferogram of 2 inch diameter cylinder in N_2 and N.
  $u_\infty = 5.59\,\text{km}/\text{s}$, $\mathcal{M}_\infty = 6.1$, $Re = 12000$, $\psi = 5.5$.

experiment (Hornung)

multi-temperature model

Status of Computer Code

- Current status:

  - basically a research code

  - not vectorized (26 mflops on Cray X-MP)

  - code being used outside of Ames

  - typical solution takes 1.5 hours of Cray X-MP CPU

- Near-term improvements:

  - vectorized version

  - more efficient physical modelling

  - anticipate factor of 5 speedup

  - other gas models

Conclusions

- Algorithm for thermo-chemical nonequilibrium flow developed:

    - seven species, six temperatures

    - complete viscous terms (binary diffusion, laminar)

    - implicit numerical method

    - fully coupled equation set

    - results compared to experiment

- Future work:

    - three-dimensions

    - better models for high temperature air

    - larger degree of ionization

Aerodynamic Stability and Heating Analyses for the Aeroassist Flight Experiment Vehicle

J. McGary and C. P. Li
Lockheed Engineering and Science Company, Houston, Tx 77058
Johnson Space Center, Houston, Tx 77058
FTS 525-4684

Since ground based flow simulations are presently unable to model flight conditions expected for AOTVs (Aeroassist Orbital Transfer Vehicle) and other hypersonic space vehicles, computer codes are being developed to provide design parameters necessary for structure, guidance, and control aspects. Over the past four years, VRFLO (Viscous Reactive Flow) has been written to model finite-rate chemistry and viscous effects for a variety of aerobrake bodies. VRFLO includes a number of unique features that are summarized as follows:

1. Grid generation is an integral part of the code for several aerobrake configurations which includes the wake flow region.
2. The formulation is valid for three air chemical models.
3. An ADI central difference technique is used to solve the Navier-Stokes and species continuity equations in split groups.
4. Grid density and numerical damping are minimized by shock-fitting and conformal mapping of body points.

Currently, the AFE (Aeroassist Flight Experiment) project requires critical input parameters for the design development, and to aid its progress, aerodynamic forces and heating rates are calculated at a specified trajectory point of maximum heating. The code was calibrated against Mach 10 measurements taken at the Langley Continuous-Flow Hypersonic Tunnel to determine grid sensitivity and reliability estimates for flight calculations. Aerodynamic forces and moment coefficients (lifts, drags, and pitching moments) were calculated at five angles of attack to determine the basic coefficient behavior as a function of angle for stability analysis. Wind tunnel simulations were modeled by calculating the flowfield about the complete body assuming an inviscid, perfect gas which resolved the non-linear behavior in the pitching moment measured from wind tunnel experiments. Inviscid, reacting air calculations, for flight conditions at Mach 32, show a linear pitching moment that agrees with calculations performed at Langley Research Center which considered inviscid, equilibrium air with forebody geometry. Preliminary, not fully converged, viscous, reacting flow calculations at the same flight conditions reveal a slight non-linear relation between pitching moment and angle of attack. In each case, the base pressure contributions are examined by considering the forebody and complete body separately.

Considering that heat-transfer measurements are accurate within ±7% and an equal amount of uncertainty is associated with CFD results, the convective heat flux calculations are in fairly good agreement with the Langley Mach 10 wind tunnel measurements. While the calculated surface pressure distribution demonstrates excellent agreement with measurement, the heat-transfer coefficient exhibits similar surface behavior to the data but varies in value. Incident angle studies show that the maximum heating decreases with increasing attack angle without modifying the overall distribution shape. Calculations for flight conditions show similar trends observed from wind tunnel simulations but have a more pronounced peak at the stagnation region. Fully catalytic calculations indicate that the heat-transfer coefficients are about 25% larger in general than those in the non-catalytic solutions; the actual fluxes expected for flight conditions will be bounded by the two extremes.

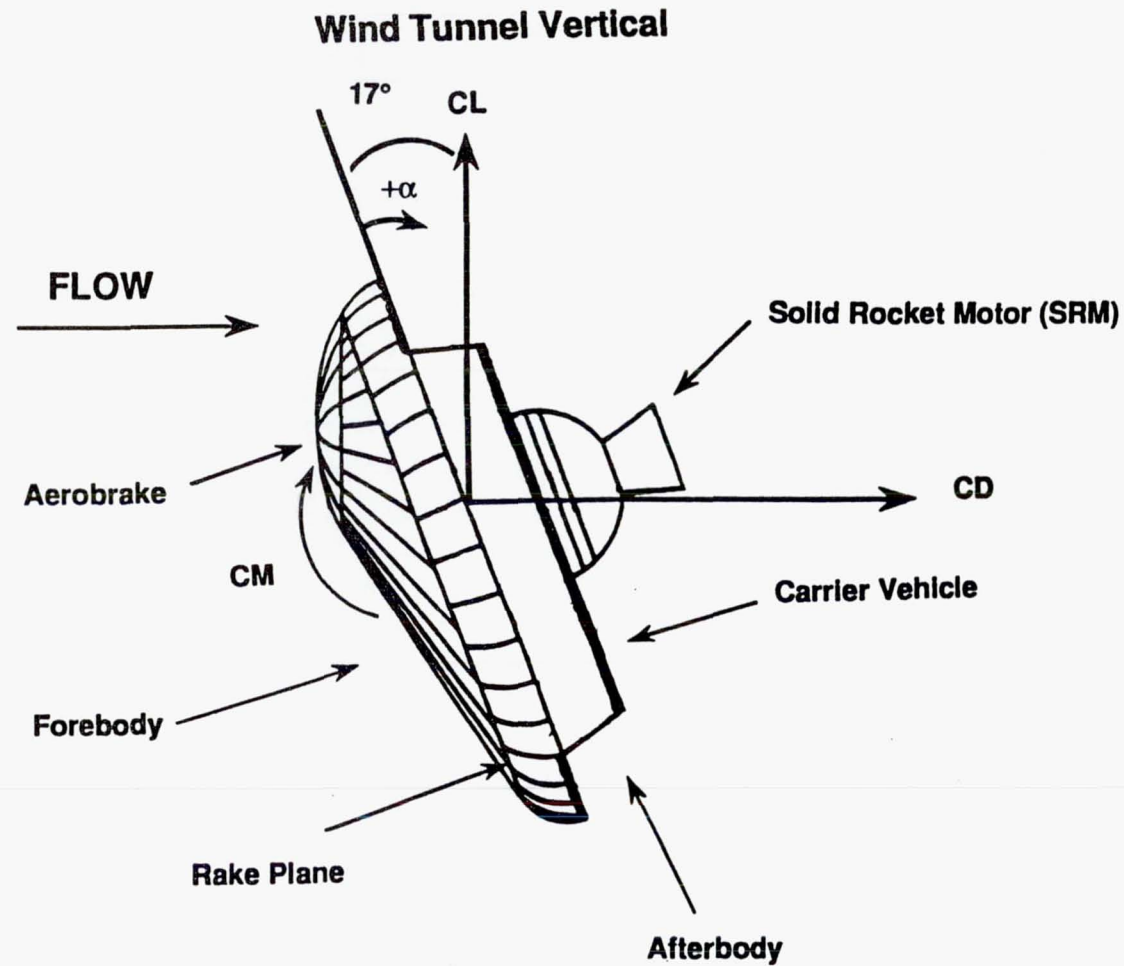# Wind Tunnel Axis System for Aerocoefficients

$$\alpha = 0\,^\circ$$

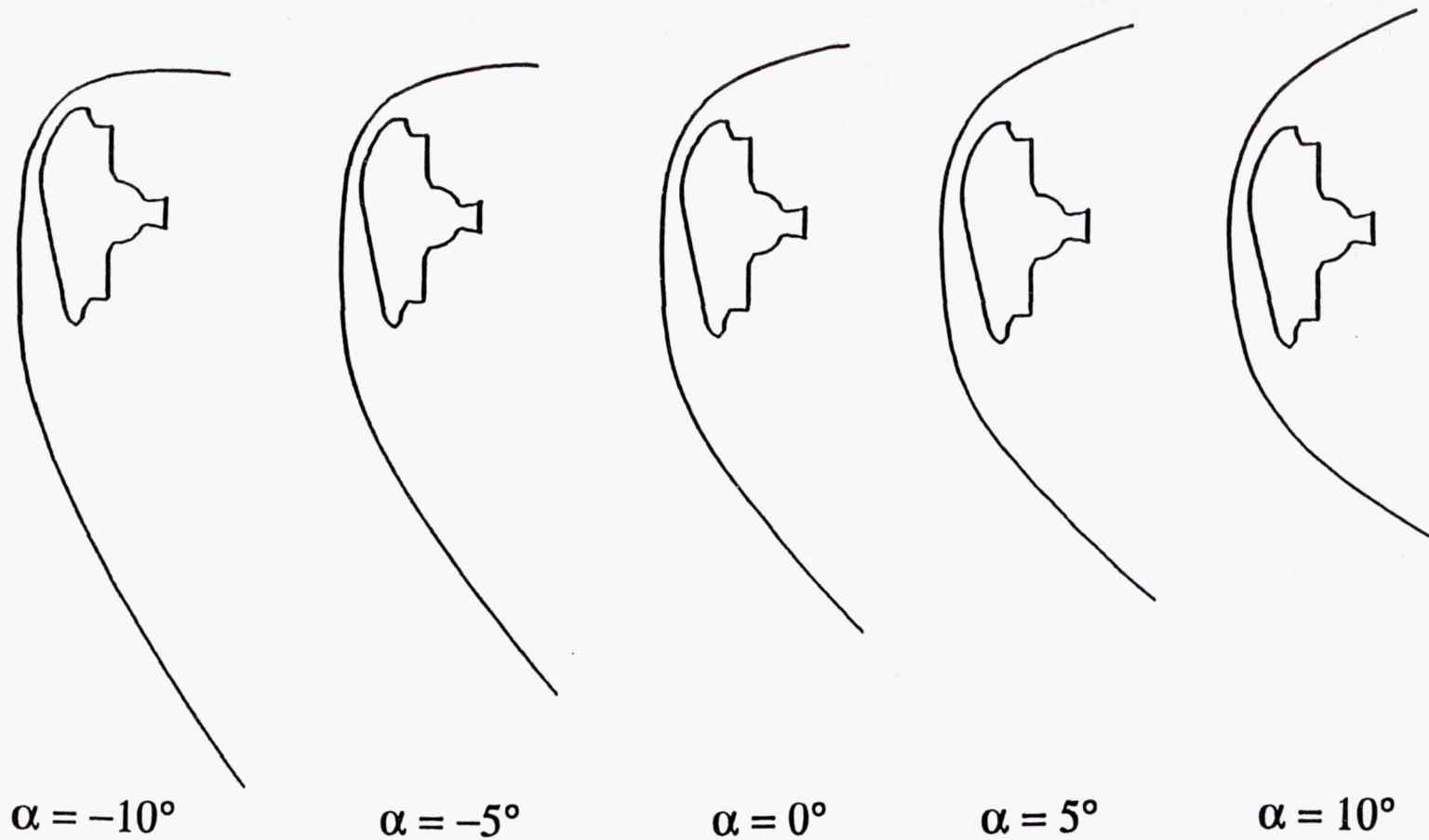$$C_L = \frac{L}{q\,S}$$

$$C_D = \frac{D}{q\,S}$$

$$C_M = \frac{M}{q\,S\,L'}$$

$$S = \frac{\pi\,W\,L'}{4}$$
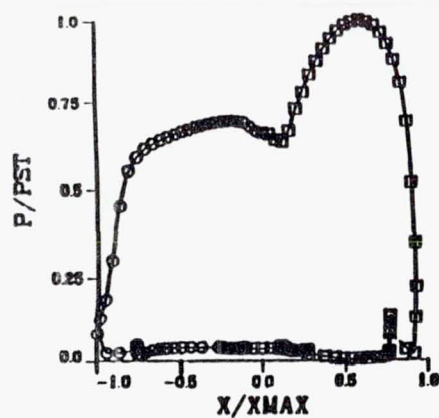
$$q = \frac{1}{2}\rho_\infty V_\infty^2$$

Wind Tunnel Vertical

17°   CL

+α

FLOW

Solid Rocket Motor (SRM)

Aerobrake

CM

CD

Carrier Vehicle

Forebody

Rake Plane

Afterbody

Shock Shape Variations with Angle of Attack

Inviscid, Mach 10

$\alpha = -10°$ $\alpha = -5°$ $\alpha = 0°$ $\alpha = 5°$ $\alpha = 10°$

Pressure Distribution Along AFE Body

Inviscid, Mach 10

PST= 134.836

$\alpha = -10°$

PST= 139.112

$\alpha = 0°$
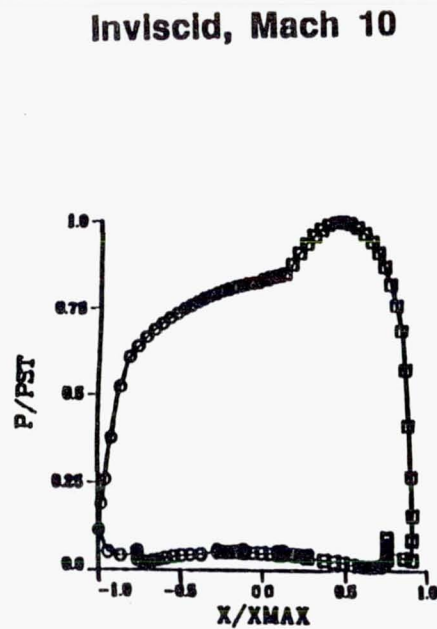
PST= 139.309

$\alpha = -5°$
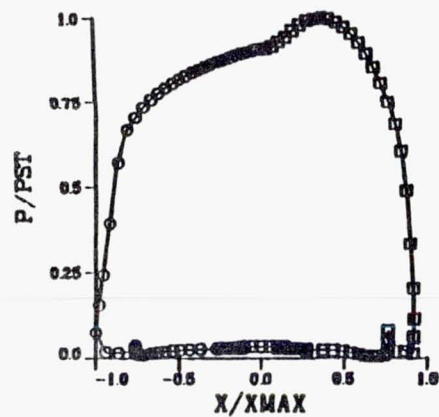
PST= 135.179

$\alpha = 5°$

PST= 132.730

$\alpha = 10°$

518
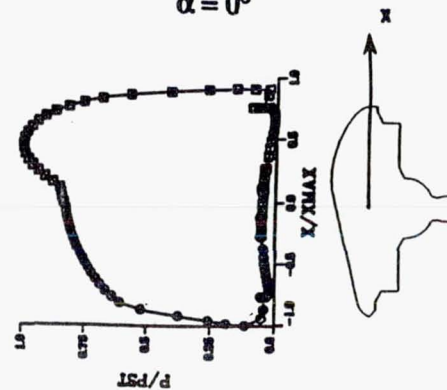
Grid Variations
Inviscid, Mach 10

P/PST vs X/XMAX, α = 0°

12x60x9 PST= 133.579

P/PST vs X/XMAX, α = 0°
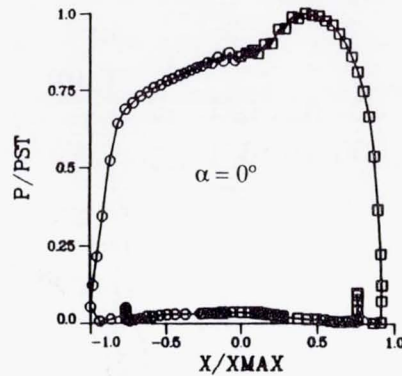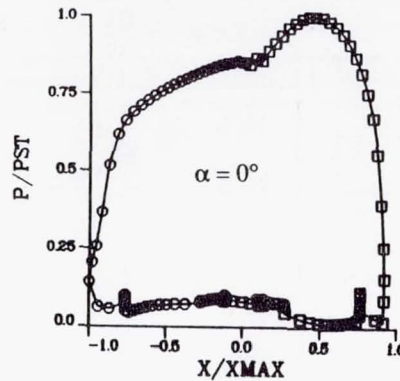
12x60x25 PST= 134.846

P/PST vs X/XMAX, α = 0°
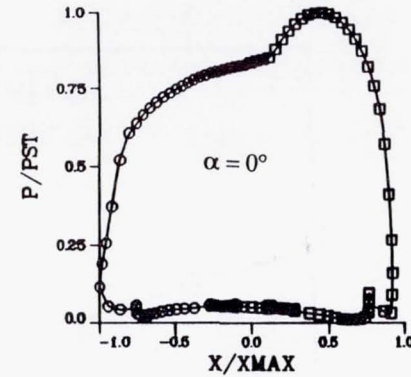
30x60x25 PST= 139.112

CM vs alpha (deg)

- ■ 12x60x9
- ○ 12x60x25
- □ fine grid ~37x60x25
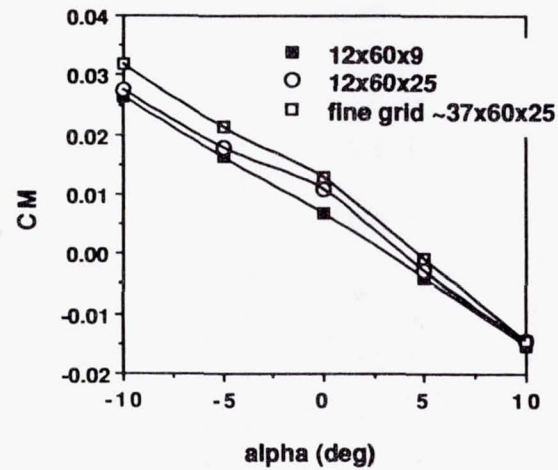
NxMxL , where
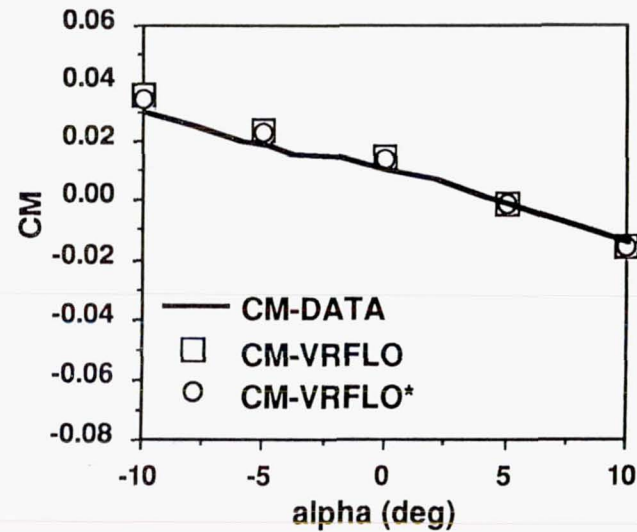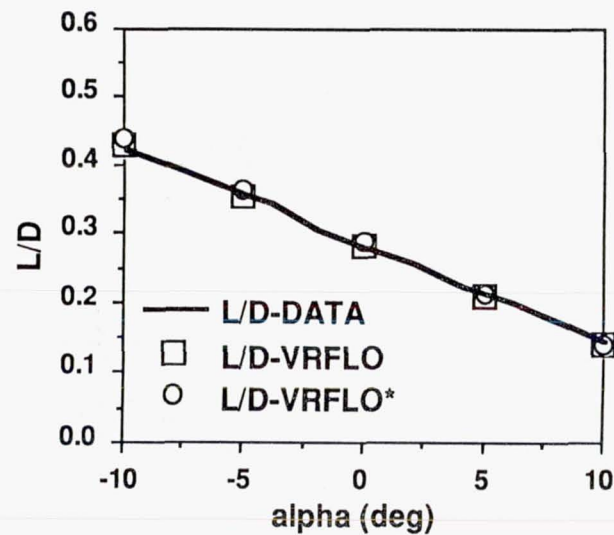
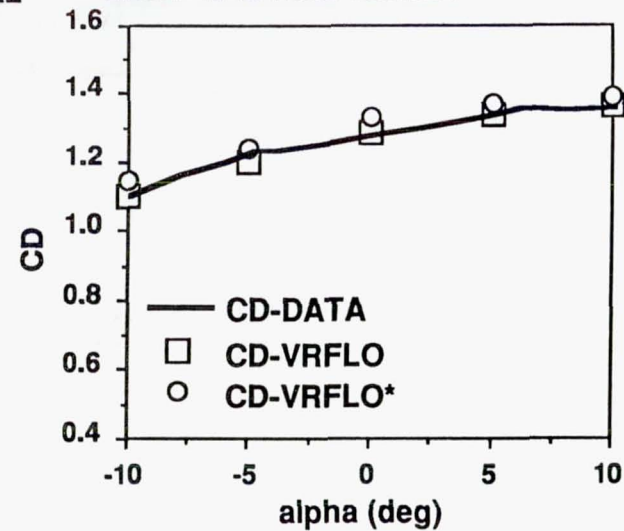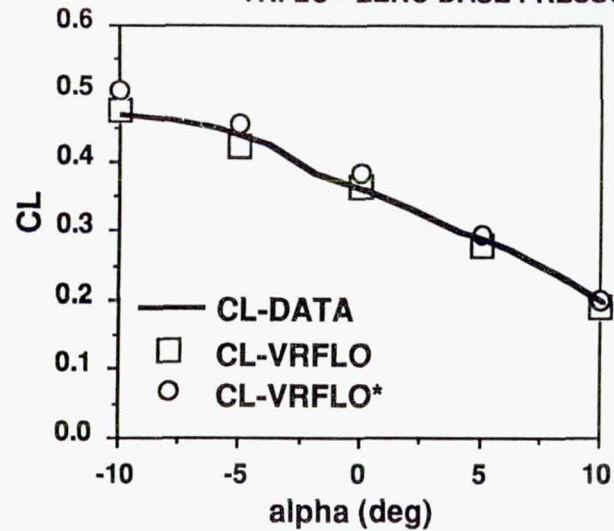N = number of points from AFE body to boundary

M = number of points from forebody to afterbody

L = number of points around body in plane normal to pitch plane

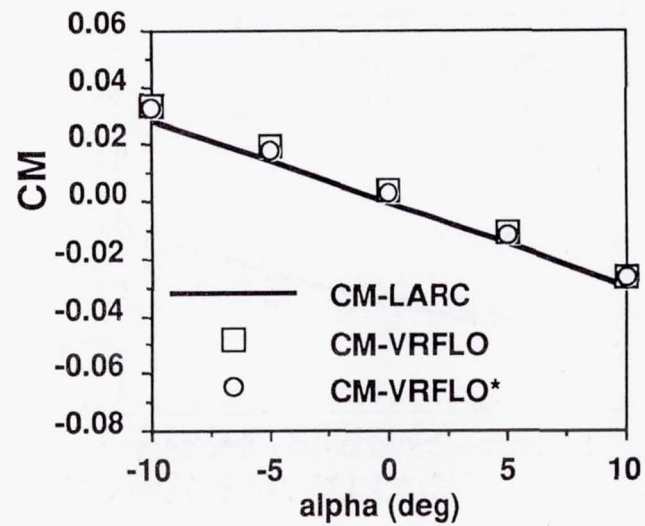INVISCID, MACH 10
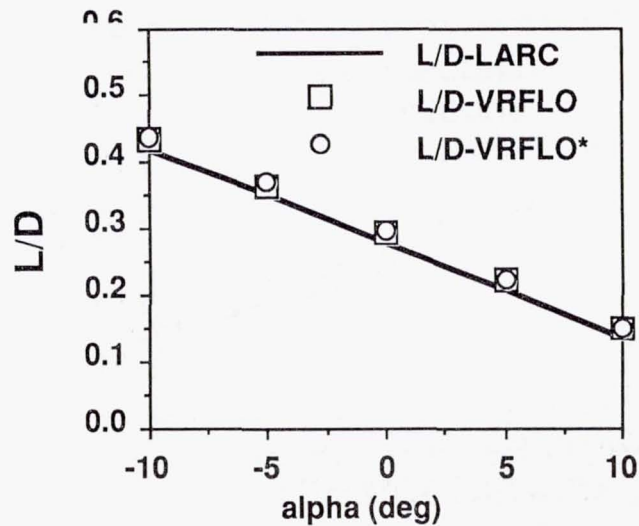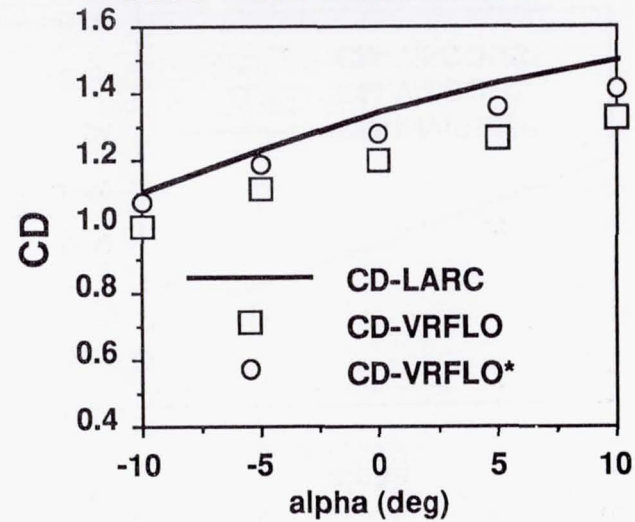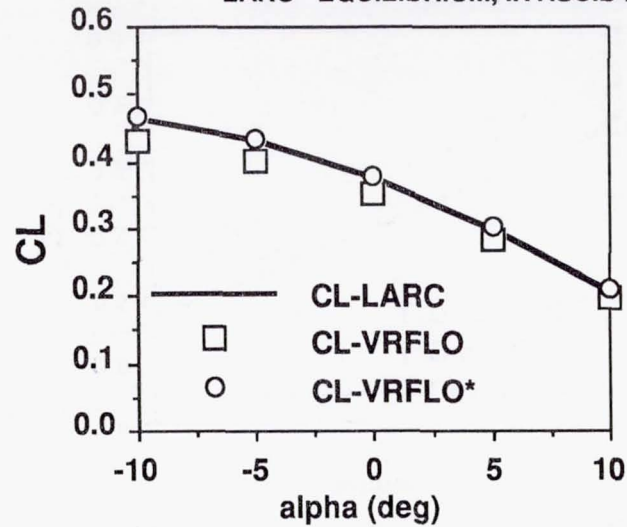AEROCOEFFICIENTS vs ANGLE OF ATTACK

MACH 32
INVISCID, REACTING FLOW
AEROCOEFFICIENTS vs ANGLE OF ATTACK

LARC - EQUILIBRIUM, INVISCID AIR   VRFLO* - ZERO BASE PRESSURE

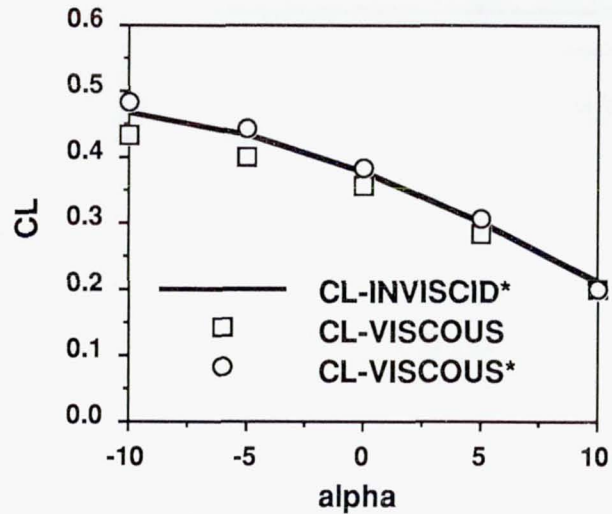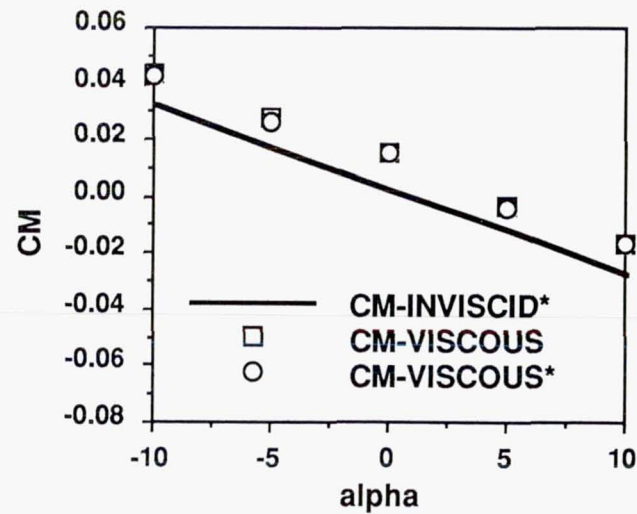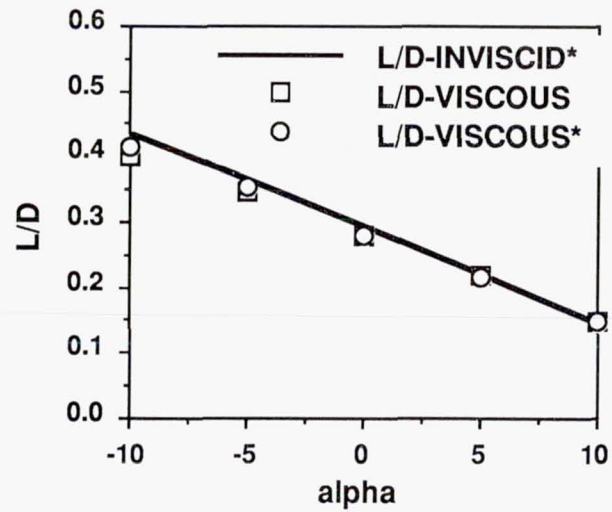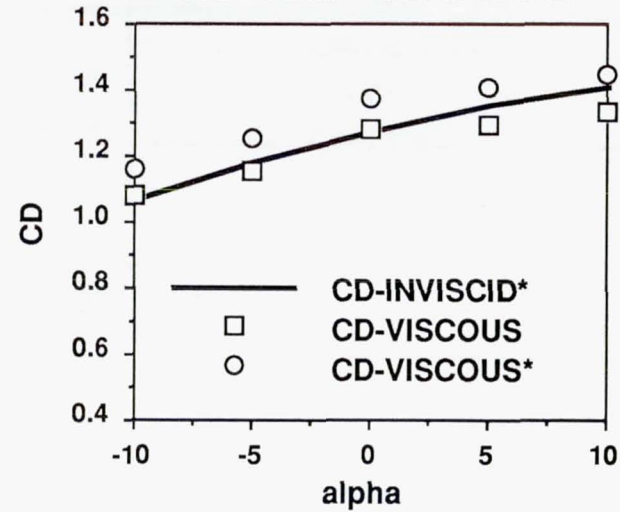# MACH 32
VISCOUS, REACTING FLOW
AEROCOEFFICIENTS vs ANGLE OF ATTACK

NASA
National Aeronautics and
Space Administration

Report Documentation Page

1. Report No. NASA CP-10038	2. Government Accession No.	3. Recipient's Catalog No.
4. Title and Subtitle NASA Computational Fluid Dynamics Conference Volume 2: Sessions VII-XII		5. Report Date September 1989
		6. Performing Organization Code
7. Author(s)		8. Performing Organization Report No. A-89160
		10. Work Unit No. 505-60-01
9. Performing Organization Name and Address Ames Research Center Moffett Field, CA 94035		11. Contract or Grant No.
		13. Type of Report and Period Covered Conference Publication
12. Sponsoring Agency Name and Address National Aeronautics and Space Administration Washington, DC 20546-0001		14. Sponsoring Agency Code

15. Supplementary Notes

Point of Contact: Dale Satran, NASA Headquarters, Code RF, Washington, D.C. 20546
(202) 453-2828 or FTS 453-2828

16. Abstract

This publication is a collection of the presentations given at the NASA Computational Fluid Dynamics (CFD) Conference held at NASA Ames Research Center, Moffett Field, California, March 7-9, 1989. The objectives of the conference were to disseminate CFD research results to industry and university CFD researchers, to promote synergy among NASA CFD researchers, and to permit feedback from researchers outside of NASA on issues pacing the discipline of CFD. The focus of the conference was on the application of CFD technology but also included fundamental activities. The conference was sponsored by the Aerodynamics Division, Office of Aeronautics and Space Technology (OAST), NASA Headquarters, Washington, D.C. 20546.

The conference consisted of twelve sessions of papers representative of CFD research conducted within NASA and three non-NASA panel sessions. For each panel session, the panel membership consisted of industry and university CFD researchers. A summary of the comments made during the panel sessions has been included in this publication.

Volume 1 contains the papers given in Sessions I-VI. Volume 2 covers Sessions VII-XII.

17. Key Words (Suggested by Author(s)) Computational fluid dynamics Numerical methods Computational aerodynamics Supercomputing		18. Distribution Statement Unclassified-Unlimited Subject Category -02	
19. Security Classif. (of this report) Unclassified	20. Security Classif. (of this page) Unclassified	21. No. of Pages 593	22. Price A25

NASA FORM 1626 OCT 86

For sale by the National Technical Information Service, Springfield, Virginia 22161